

THE NATIONAL INSTITUTE
FOR RESEARCH IN NUCLEAR SCIENCE

NIMROD
A 7 GeV PROTON SYNCHROTRON
(Part I)

EDITED BY

B. G. Loach

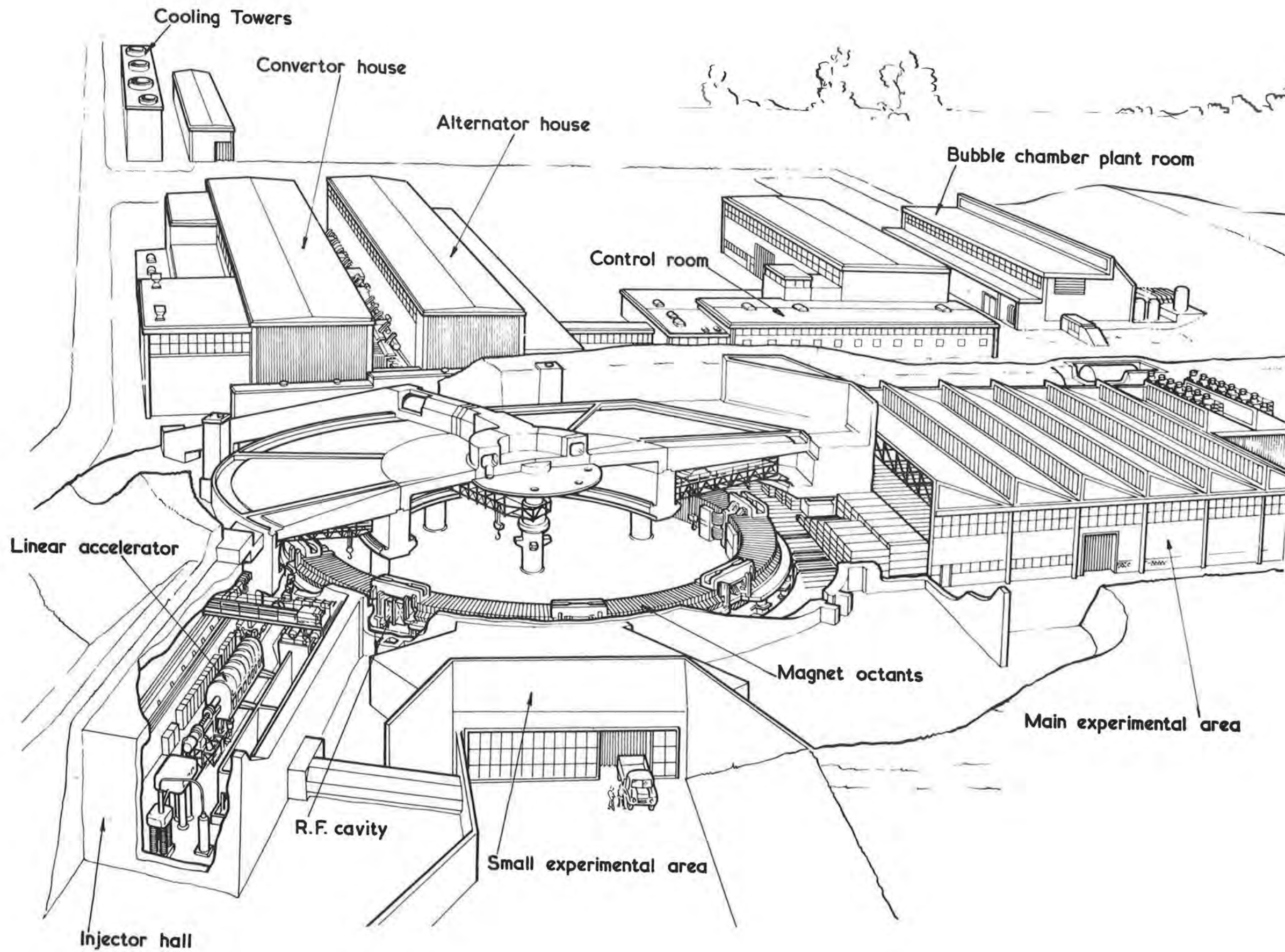
B. Southworth

RUTHERFORD HIGH ENERGY LABORATORY
CHILTON, DIDCOT, BERKSHIRE
1965

Available from H.M. Stationery Office

THIRTY SHILLINGS NET

© THE NATIONAL INSTITUTE FOR RESEARCH IN NUCLEAR SCIENCE, 1965



The 7GeV Proton Synchrotron, NIMROD

NATIONAL INSTITUTE FOR RESEARCH IN NUCLEAR SCIENCE

NIMROD

A 7 GeV Proton Synchrotron

(Part 1)

Edited by

B. G. Loach
B. Southworth

Rutherford High Energy Laboratory,
Chilton,
Didcot, Berkshire.

March 1965.

EDITORS' NOTE

This is the first part of a comprehensive report on the design, construction, commissioning and operation of Nimrod. The amount of information which is worth recording is too extensive to include in one document and also, to publish at least part of the report comparatively quickly, it was necessary for authors of individual sections to make contributions long before the commissioning of the machine was complete.

Work on the report was initially started with the object of producing a "progress report" covering all aspects of the work on Nimrod during the five years from the original decision to build the machine in 1957 up to the end of 1962. It soon became obvious that the report provided an opportunity (possibly the only opportunity) to record the work involved in designing and building the machine in some detail. Consequently it was decided to modify the original conception of a comparatively brief progress report to that of a much more comprehensive and detailed document which would allow the publication of all development, measurement and testing work of a sufficiently interesting or unusual nature, and allow a description of the methods used in overcoming any difficulties peculiar to the construction of Nimrod. (Previously published work, or work about to be published, is generally not recorded in detail but is covered by lists of references.)

This decision meant that the dividing line at the end of 1962 need no longer be strictly adhered to but, in order to complete the first part of the report, writing had to proceed to a conclusion as quickly as possible and the final document is still influenced by the earlier progress report scheme and does mainly describe work on the machine up to the end of 1962.

The second part of the report (to be published later) will cover all aspects of the work on each section of the machine which were not described in the first part; i.e., it will mainly be concerned with the period: January 1962 to October 1964 (including the achievement of the design intensity of 10^{12} protons per pulse in August 1964) and will describe the problems and achievements of the final commissioning of the machine, targetting, the external beam and the experimental area facilities.

B. G. Loach
B. Southworth

Rutherford High Energy Laboratory.
11th March, 1965

ACKNOWLEDGEMENT

It is impossible to acknowledge adequately all individual contributions in the case of a complex project such as Nimrod, which has occupied many years and involved many people at different stages of the work. However, lists of staff who collectively contributed to the various main sections of the project will be given in part 2 of this report. The following had major responsibility for the preparation of part 1 of the report:-

Bennett, R. G. T.
Billinge, R.
Boyd, W.
Brooks, H. C.
Carr, R.
Dunn, P. D.
Edwards, V. W.
Falconer, D. B.
Gray, D. A.
Grossart, G. S.
Hadley, H.
Harold, M. R.
Higgins, E. G.
Hobbis, L. C. W.
Hopes, R. B.
Hyman, J. T.
Jones, E. G.
Jones, P. F.
Kendall, E. W.
Major, J. H.

Moore, D. R.
Morgan, R. H. C.
Mortimer, A. R.
Nevitt, J. H.
Russell, R. G.
Sandels, E. G.
Sheldon, R.
Smith, J. V.
Swain, J. H.
Swales, R. A.
Tarry, K. W. D.
Thompson, D. J.
Walkinshaw, W.
Walsh, T. R.
Ward, B. C. W.
West, N. D.
Whitby, H. C.
Wilde, P.
Wroe, H.

The editors would like to thank all those concerned for their assistance and patience during the long drawn-out task of preparing this report.

FOREWORD

The Nimrod project like all other accelerator projects, was never more than a means to an end. It was specified in 1956 in very simple terms, after much discussion by many physicists who craved for up-to-date facilities for high energy research, as a source of at least 10^{11} protons per second with at least 6.5 GeV kinetic energy. The sights were subsequently raised to 5×10^{11} protons per second, at 7 GeV. Strictly speaking, therefore, the real story began only in February 1964, $6\frac{1}{2}$ years after construction started, when the reliability and intensity of Nimrod justified its scheduled operation for research.

But for the many physicists, engineers, technicians and craftsmen who struggled during those years with the many problems discussed in this report, Nimrod necessarily seemed very much an end in itself. In all work of this kind, done against a ruthless timetable, it is difficult to find time or energy for recording properly the way in which the problems have been tackled. When the job is done, everyone is anxious to adapt himself to his real work of operating, developing, or exploiting the monster he has helped to create. It often happens, therefore, that only brief outlines of the highlights are put on record. This is a pity, because the future exploitation of such a valuable and complicated instrument as a high energy accelerator, eventually by people who played little or no part in its original design or construction, could be greatly aided by full and professionally prepared records. Similarly, there would be much in such records to help engineers and physicists working on similar problems in other projects - not only for high energy physics, because accelerators cover a wide range of engineering and technology.

For these reasons, I am sure that this report will be valuable to many people, and the Editors and contributors deserve our thanks for their hard work in preparing it. I hope that the report will also serve as a tribute to the hundreds of members of the Nimrod project teams who contributed so much during 6 years to the successful completion of a major enterprise.

T. G. Pickavance
Director, Rutherford Laboratory.

C O N T E N T S

	Page No.
Editors Note	(iii)
Acknowledgement	(iv)
Foreword	(v)
List of Illustrations	(xvii)

SECTION 1: INTRODUCTION

Table 1 (I) Nimrod Parameters	1 - 3
-------------------------------	-------

SECTION 2: COMPUTATION AND THEORETICAL WORK

2.1 Linac Injector	2 - 1
2.2 Linacs; General Theory	2 - 1
2.3 Nimrod Dynamics	2 - 2
2.4 Extracted Proton Beam	2 - 2
2.5 Irradiation Studies	2 - 2
2.6 Beam Design	2 - 2

SECTION 3. INJECTION SYSTEM

	Page No.
3.1 Introduction	3 - 1
3.2 Dynamics of the Injector	3 - 3
3.2.1 Dynamical Design of the Linac	3 - 3
3.2.2 Drift Spaces	3 - 4
3.2.3 Buncher and Debuncher	3 - 4
3.3 Pre-injector	3 - 5
3.3.1 R.F. Ion Source	3 - 5
3.3.2 Ion Column	3 - 8
3.3.3 Ion Column Power Supply	3 - 10
3.3.4 Focusing and Ion Source Power Supplies	3 - 10
3.4 Linac	3 - 14
3.4.1 Linac Design	3 - 14
3.4.2 Linac Construction	3 - 15
3.4.3 Installation and Operational Experience	3 - 16
3.4.4 Linac R.F. Drive System	3 - 19
3.4.5 Drive Chain	3 - 21
3.4.6 Modulators	3 - 21
3.4.7 R.F. Commissioning	3 - 21
3.4.8 Linac Quadrupoles	3 - 24
3.4.9 Quadrupole Power Supplies and Gradient Boxes	3 - 26
3.5 Drift Spaces and Inflector	3 - 27
3.5.1 LEEDS and HEDS Quadrupoles	3 - 27
3.5.2 Buncher and Debuncher Cavities	3 - 27
3.5.3 Steering Magnets	3 - 29
3.5.4 Inflector	3 - 30
3.6 Other Injector Facilities	3 - 32
3.6.1 Beam Monitoring System	3 - 32
3.6.2 Timing Facilities	3 - 34
3.6.3 Auxiliary equipment	3 - 35
3.7 Beam Experiments	3 - 36
3.7.1 Emittance Definition in LEEDS	3 - 36
3.7.2 Momentum Analysis	3 - 36
3.7.3 Emittance Measurements	3 - 36
3.7.4 Radiation Survey	3 - 37

SECTION 4: MAGNET AND ASSOCIATED SYSTEMS

	Page No.
4.1 Sector Testing	4 - 1
4.1.1 Results of Tests	4 - 1
4.1.2 Distribution of Sectors Around Magnet	4 - 2
4.2 Main Coils	4 - 3
4.3 Main Polepieces	4 - 4
4.3.1 Design and Measurements	4 - 4
4.3.2 Manufacture	4 - 5
4.4 Straight Sections	4 - 7
4.4.1 Straight Section Boxes	4 - 7
4.4.2 Coil Shielding	4 - 7
4.4.3 End Polepieces	4 - 7
4.4.4 Overall n-correction	4 - 8
4.5 Mechanical Alignment of Sectors and Polepieces	4 - 10
4.5.1 Requirements	4 - 10
4.5.2 Methods	4 - 10
4.5.3 Results	4 - 11
4.5.4 Foundation Movement	4 - 11
4.6 Magnetic Survey	4 - 13
4.6.1 Pulsed Field Measurements	4 - 13
4.6.2 Remanent Measurements	4 - 14
4.6.3 n-measurements	4 - 14
4.6.4 Machine Symmetry Measurements	4 - 14
4.6.5 Effective Length	4 - 15
4.6.6 Median Plane	4 - 15
4.6.7 Other Miscellaneous Measurements	4 - 16
4.6.8 Results of the Survey	4 - 16
4.6.9 n values	4 - 16
4.6.10 Machine Symmetry and Effective Lengths of Octant-ends	4 - 16
4.6.11 Median Plane Results	4 - 16
4.6.12 Miscellaneous Results	4 - 17
4.7 General Characteristics of the Magnet	4 - 18
4.7.1 Field Versus Current	4 - 18
4.7.2 Eddy Current Effects	4 - 18
4.7.3 Transient Effects	4 - 19
4.7.4 Magnet Movements during pulsing	4 - 19
4.8 Pole Face Windings	4 - 21
4.8.1 Overall Adjustment of n and the Median Plané	4 - 21
4.8.2 Aperture at Injection	4 - 22
4.8.3 Aperture at High Fields	4 - 22
4.8.4 B_o Correction	4 - 22
4.8.5 Manufacture of Pole Face Windings	4 - 22

	Page No.
4.9 Pole Face Winding Power Supplies	4 - 24
4.9.1 Control Systems (General)	4 - 24
4.9.2 Integrator Unit	4 - 24
4.9.3 Function Generator	4 - 24
4.9.4 60 Kilowatt Supplies	4 - 24
4.9.5 3.2 Kilowatt Supplies	4 - 25
4.9.6 15 Volt, 5 Amp Supply	4 - 25
4.10 Ripple Filter System	4 - 26
4.10.1 Primary Ripple Filter	4 - 26
4.10.2 Secondary Ripple Filter	4 - 28
4.11 Peaking Strips	4 - 33
4.11.1 Bias Current Source	4 - 33
4.11.2 Pulse Circuitry	4 - 34
4.11.3 Mechanical Construction	4 - 34
4.11.4 Progress	4 - 35

SECTION 5: MAGNET POWER SUPPLY

5.1 Introduction	5 - 1
5.2 Rotating Plant	5 - 3
5.2.1 Brief Note on Commissioning Work Outstanding after 31st December, 1962	5 - 3
5.2.2 The Foundation Block and its Behaviour	5 - 3
5.2.3 Bearing Pedestal Vibration Levels	5 - 5
5.2.4 Machine Bearings	5 - 5
5.2.5 Shaft Eccentricity Levels	5 - 5
5.2.6 Shaft Torsional Stress Monitoring System	5 - 5
5.2.7 Starting and Pre-heating of the Set	5 - 6
5.2.8 Lubrication Oil System	5 - 7
5.2.9 Routine Intrascope Inspections	5 - 7
5.2.10 Flywheels	5 - 8
5.2.11 Alternator Automatic Voltage Regulation System	5 - 8
5.2.12 Brief notes on General Routine Commissioning	5 - 9
5.2.13 Ultrasonic Scanning of the Rotary Plant	5 - 10
5.3 Converter Plant	5 - 13
5.3.1 General Description of Power Circuit	5 - 13
5.3.2 Commissioning Experience	5 - 14
(a) Main Rectifier Transformers	5 - 14
(b) Converter Load Sharing	5 - 15
(c) Power Supply Harmonics	5 - 18
(d) Flat Top Slope Control	5 - 19
(e) Protection Circuits	5 - 19
5.3.3 Further Work	5 - 21

SECTION 6: R.F. SYSTEM

	Page No.
6.1 Introduction to the Synchrotron R.F. System	6 - 1
6.2 Low Power R.F. System	6 - 4
6.2.1 Introduction	6 - 4
6.2.2 Description of System	6 - 4
6.2.3 Component Circuits	6 - 5
6.2.4 Performance of System	6 - 8
6.3 High Power R.F. System	6 - 12
6.3.1 Introduction	6 - 12
6.3.2 Accelerating Cavity	6 - 12
6.3.3 High Power R.F. Amplifier Development	6 - 17
6.3.4 Final Amplifier Design	6 - 21
6.3.5 Automatic Level Control of Gap Voltage	6 - 22
6.3.6 Phase Detector	6 - 24
6.3.7 Mark I (Thermionic) Bias Supply	6 - 27
6.3.8 Mark II (Transistorised) Bias Supply	6 - 30
6.3.9 General Arrangement of High Power R.F. System	6 - 34

SECTION 7: EXTRACTION SYSTEMS AND INTERNAL TARGETS

	Page No.
7.1 Slow Extraction System	7 - 1
7.1.1 Principles of Operation	7 - 1
7.1.2 Practical Considerations	7 - 2
7.1.3 Apparatus	7 - 2
7.1.4 Emergent Beam	7 - 3
7.2 Kicker for Fast Beam Extraction	7 - 4
7.2.1 Principle of Operation	7 - 4
7.2.2 Powering circuits	7 - 5
7.2.3 Model Measurements	7 - 6
7.2.4 Present status	7 - 7
7.3 Plunging Mechanisms for the Extractor Magnets	7 - 8
7.3.1 Description of System	7 - 8
7.3.2 Present Status	7 - 9
7.4 Target Mechanisms	7 - 10

SECTION 8: VACUUM SYSTEM

	Page No.
8.1 Introduction	8 - 1
8.2 Vacuum Vessel Design	8 - 2
8.2.1 Choice of Material	8 - 2
8.2.2 Choice of Design	8 - 2
8.2.3 Design Details	8 - 4
8.2.4 Outer Vessel	8 - 4
8.2.5 Inner Vessel	8 - 4
8.2.6 Header Vessel	8 - 5
8.2.7 Polythene Closing Plate	8 - 6
8.3 Vessel Manufacture	8 - 7
8.3.1 Summary of Method Used	8 - 7
8.3.2 Production Problems	8 - 8
8.4 Inspection at the Manufacturers' Works	8 - 11
8.4.1 Introduction	8 - 11
8.4.2 Flexibility in Inspection	8 - 11
8.4.3 Process Control	8 - 11
8.4.4 Quality Control	8 - 12
8.4.5 Production Tool Inspection	8 - 12
8.4.6 Checking of Lay-Up	8 - 13
8.4.7 Laminate Inspection	8 - 13
8.4.8 Dimensional Accuracy	8 - 14
8.4.9 Dimension Analysis	8 - 15
8.4.10 Repairs and Records	8 - 15
8.5 Handling, Test Equipment and Installation	8 - 16
8.5.1 Transporting the Vessels	8 - 16
8.5.2 Test Equipment	8 - 16
8.5.3 Vessel Installation	8 - 18
8.6 Vacuum Testing	8 - 21
8.6.1 Introduction	8 - 21
8.6.2 Vacuum Vessels	8 - 22
8.6.3 Straight Section Box Proof Tests	8 - 26
8.6.4 Octant Testing	8 - 27
8.6.5 Leak Detectors	8 - 27
8.7 Vessel Repairs	8 - 28
8.8 Radiation Damage	8 - 30
8.9 Main Vacuum Seals	8 - 31
8.9.1 Choice of Materials	8 - 31
8.9.2 Manufacturing Processes	8 - 31
8.9.3 Properties of the Final Material	8 - 32
8.9.4 Conclusions	8 - 33

	Page No.
8.10 Pumping System	8 - 34
8.10.1 Introduction	8 - 34
8.10.2 High Vacuum Pumps	8 - 34
8.10.3 Roughing Pumps	8 - 35
8.10.4 Interlocks and Safety Devices	8 - 36
8.10.5 Straight Section Box Pumping Arrangements	8 - 37
8.10.6 Arrangements for Diagnostic Equipment and Targets	8 - 38
8.10.7 Beam Lines	8 - 39
8.10.8 Pressure Measurement	8 - 40
8.11 Injector Vacuum System	8 - 41
8.11.1 Introduction	8 - 41
8.11.2 Linac Vacuum System	8 - 41
8.11.3 Preinjector and Drift Spaces	8 - 43
8.11.4 Pumping System	8 - 43

SECTION 9: CONTROL SYSTEM

	Page No.
9.1 Injector	9 - 1
9.1.1 Introduction	9 - 1
9.1.2 E.H.T. Supply, E.H.T. Platform and D.C. Gun	9 - 1
9.1.3 R.F. Drive	9 - 2
9.1.4 Tuners and Tilters	9 - 2
9.1.5 Quadrupoles and Steering Magnets	9 - 2
9.1.6 Other Control Facilities	9 - 3
9.2 Vacuum System	9 - 4
9.2.1 Introduction	9 - 4
9.2.2 Injector Vacuum Controls	9 - 4
9.2.3 Main Vacuum Vessel Controls	9 - 4
9.2.4 Vacuum Gauges and Switches	9 - 5
9.3 Cooling Plant, Temperature Monitoring and Flow Monitoring	9 - 7
9.3.1 Introduction	9 - 7
9.3.2 Temperature Monitoring	9 - 7
9.3.3 Coolant Flow Monitoring	9 - 8
9.4 Main Control Room	9 - 10
9.5 Personnel Control and Safety Interlocking	9 - 11

SECTION 10: ANCILLARY PLANT

	Page No.	
10.1	Introduction	10 - 1
10.2	Cooling Towers	10 - 2
10.3	Pump House	10 - 4
	10.3.1 Pumps	10 - 4
	10.3.2 Kennicott Plant	10 - 4
10.4	Permutit Plant House	10 - 6
	10.4.1 Heat Exchanger and Pump Systems	10 - 6
	10.4.2 Permutit Plant	10 - 7
	10.4.3 Demineralised Water Storage Header Tanks	10 - 8
10.5	Water Distribution System	10 - 9
10.6	Air Conditioning Plant House	10 - 10
	10.6.1 Air conditioning Plant	10 - 10
	10.6.2 Chilled Water Storage Tank	10 - 11
10.7	Air Distribution System	10 - 12
10.8	Injector Room	10 - 13
	10.8.1 Injector Cooling System	10 - 13
	10.8.2 Injector Room Ventilation	10 - 15
10.9	R.F. Chilling Equipment	10 - 16
10.10	Sumps and Tunnels	10 - 16
10.11	Miscellaneous Work	10 - 17
	10.11.1 General Access	10 - 17
	10.11.2 Injector	10 - 17
	10.11.3 Diagnostic Equipment	10 - 17
	10.11.4 Remote Handling	10 - 18
10.12	Records Office, Storage and Workshop	10 - 19
	10.12.1 Records Office	10 - 19
	10.12.2 Storage	10 - 19
	10.12.3 Test Area	10 - 19
	10.12.4 Workshop	10 - 19

SECTION 11: OPERATION

11.	Operation	11 - 1
-----	-----------	--------

ILLUSTRATIONS

- Frontispiece
- Fig.1.(i) A simplified plan showing the layout of the NIMROD installation.
- 3.1(i) Injection System.
- 3.3.1(i) RF Ion Source Assembly.
- (ii) Plot of Ion Source Output Current against Extraction Voltage.
- (iii) Ion Source Short Cathode Shield.
- (iv) Measurement of Total Ion Current drawn from Plasma.
- (v) Phase Space Diagram: Horizontal Plane.
- (vi) Phase Space Diagram: Vertical Plane.
- 3.3.2(i) Ion Column Focusing Electrodes.
- (ii) View of the Ion Column.
- 3.3.3(i) Schematic Diagram of 600kV DC Supply System.
- (ii) View of E.H.T. Generator, Condenser and H.T. Platform.
- 3.4.2(i) View of the Linac with the Vacuum Lid raised.
- (ii) Cutaway view of Linac.
- 3.4.4(i) Schematic Diagram of the RS 1041 Valve Circuit.
- (ii) View of RS 1041 Valve prior to Installation.
- 3.4.5(i) Rear view of RF Drive Chain Cubicles.
- 3.4.8(i) Linac Unit Cell.
- (ii) Linac Drift Tubes in Transportation Frames.
- (iii) Linac Drift Tube showing Quadrupole Magnet.
- (iv) Magnetometer used in measurements at the Laboratory.
- 3.4.9(i) Simplified Schematic Diagram of First Gradient Box.
- 3.5.1(i) View of LEDES showing quadrupole triplets, 4 jaw boxes, beam current transformers and probe boxes.
- 3.5.3(i) Steering magnet design.
- (ii) Steering magnet supply circuit.
- 3.5.4(i) Inflector.
- (ii) View of achromatic inflector system.
- 3.6.1(i) Rudimentary Beam Monitoring System.
- (ii) Screening Mount for Beam Current Transformers.
- 3.7.1(i) 15 MeV Momentum Spectra at Various Linac Field Levels.
- (ii) Computed Proton Energy - Phase Distribution at Linac Output for Motion on Axis and 30° Synchronous Phase Angle.
- 3.7.2(i) Map of observed gamma and neutron levels (September 1962).
- 3.7.3(i) Emittance Measuring System.

ILLUSTRATIONS (cont'd)

- Fig.4.1(i) Magnet model IV used for sector comparisons.
- (ii) Variation of remanent field with order of production of sector.
- (iii) Variation of low field properties with remanent field.
- (iv) Variations in gap field at 10 kilogauss.
- (v) Variations in gap field at 14 kilogauss.
- 4.3(i) Polepiece laminations.
- (ii) n values for uncorrected pole.
- (iii) n values at low fields. Production poles on Model V.
- (iv) n values at high fields. Production poles on Model V.
- (v) Polepiece lamination arrangements.
- (vi) n values for Mark II polepieces on Model V.
- (vii) n values at low fields on Nimrod.
- (viii) n values for Mark I polepieces on Nimrod at high fields.
- (ix) n values for Mark II polepieces on Nimrod at high fields.
- 4.4.1(i) Flux densities in straight section box.
- (ii) Straight section box and coil shielding.
- 4.4.2(i) Coil shielding.
- 4.4.3(i) End polepiece.
- 4.4.4(i) Overall n: predicted.
- (ii) Overall n: measured on Nimrod.
- (iii) Correction plate on end polepiece.
- 4.5.3(i) Diagram of heights, showing alignment achieved.
- 4.6.9(i) Average n in Nimrod.
- 4.6.10(i) Effective lengths of octants.
- 4.6.11(i) Magnetic median surface at 300 gauss.
- 4.6.11(ii) Magnetic median surface at 15,000 gauss.
- 4.6.12(i) Radial fringe field.
- (ii) Radial fringe field at large distances.
- (iii) Fringe field into straight section.
- (iv) Field round end of octant at 300 gauss.
- (v) Field round end of octant at 15,000 gauss.
- 4.7.1(i) Sector build-up plates
- (ii) Flux density in build-up plates (Model IV).
- 4.7.2(i) Transient at flat top.
- (ii) Depression of current at flat top with varying rise time.

ILLUSTRATIONS (cont'd)

- Fig.4.7.2(iii) Variation of field within an octant at the beginning of flat top.
- 4.7.3(i) Voltage transients at the beginning of current rise.
(ii) Measured and expected voltage transients.
- 4.8(i) Configuration of pole face windings.
(ii) Diagram for winding calculation.
- 4.8.1(i) Switching of conductors.
(ii) Switching of conductors (detailed).
(iii) Voltage from n windings.
- 4.8.2(i) Connections for aperture correction at injection.
(ii) Current arrangement in windings.
- 4.8.3(i) Aperture correction at high fields.
- 4.9.1(i) Control system for pole face windings.
- 4.9.2(i) Integrator.
- 4.9.3(i) Function generator.
- 4.9.4(i) 60 kW set controller and driver unit.
- 4.9.6(i) 15V, 5A d.c. set.
- 4.10.1(i) Magnet power supply and ripple filter circuits.
(ii) Schematic diagram of ripple filter amplifier.
(iii) Ripple filter frequency response.
- 4.10.2(i) Basic circuit of secondary ripple filter.
(ii) Ripple chain.
(iii) Mechanical arrangement of ripple coils.
(iv) Interconnection of ripple windings.
(v) Basic circuit for secondary ripple filter.
(vi) General circuit for secondary ripple filter.
- 4.11(i) Layout of peaking strip.
(ii) Pulse from peaking strip.
- 4.11.1(i) Basic circuit of current stabiliser for peaking strip.
(ii) Reference potential supply.
- 4.11.4(i) Time between two peaking strip pulses.
(ii) Long term drift of peaking strip.
- 5.1(i) Nimrod power plant schematic diagram.
(ii) View of motor-alternator-flywheel set during final stages of erection.

ILLUSTRATIONS (cont'd)

- Fig.5.2.2(i) Simplified sketch of rotating plant foundation arrangement.
(ii) Typical foundation block profile change in 24 hours.
(iii) Effect of deliberate misalignment between motor and alternator.
- 5.2.6(i) Monitoring of the shaft system.
(ii) Behaviour of the shaft system.
- 5.2.7(i) Charpy - Izod tests on forging steels.
- 5.2.9(i) Pole/rotor dovetail assembly.
- 5.2.11(i) Block schematic diagram of A.V.R. system.
(ii) Aspects of A.V.R. performance (beginning of 12 hour run).
(iii) Aspects of A.V.R. performance (end of 12 hour run).
- 5.2.12(i) Rotating plant protection (simplified).
- 5.3.1(i) View of convertor house.
(ii) Analysis of d.c. output voltage waveform and interphase transformer waveforms (part I).
(iii) Analysis of d.c. output voltage waveform and interphase transformer waveforms (part II).
(iv) Analysis of d.c. output voltage waveform and interphase transformer waveforms (part III).
(v) Pulse shapes from the magnet power plant.
(vi) View of transformer yard.
- 5.3.2(i) General view of rectifier transformer removed from its tank.
(ii) View of rectifier transformer neutral connection showing damaged insulation.
(iii) Effect of current compensation control on inverter operation.
(iv) Degree of phase advance due to current compensation
(v) Circuit diagram showing components contributing to the d.c. input voltage of grid control units.
(vi) Cross connection of current compensation control circuits.
(vii) Interphase transformer waveforms with premagnetisation.
(viii) Polarity of 150 c/s I.P.T. voltage waveforms.
(ix) 300 c/s I.P.T. waveforms showing effect of incorrect grid phasing.
(x) Interphase transformer waveforms with no premagnetisation.
(xi) 300 c/s I.P.T. flux changes.
(xii) Step on grid impulses with capacitor connected to power supply negative terminal.

ILLUSTRATIONS (cont'd)

- Fig.5.3.2(xiii) Sequence of operation of primary protection.
- 5.3.3(i) Power supply control room.
-
- 6.1(i) Simplified block diagram showing the principle of the
planned r.f. accelerating system.
- 6.2.1(i) Relationship of r.f. frequency to magnet guide field.
- 6.2.2(i) Schematic diagram of low power r.f. system.
- 6.2.3(i) Front view of low power r.f. units.
- (ii) Rear view of low power r.f. units.
- (iii) Schematic layout of pick up loop.
- (iv) Circuit diagram of integrator.
- (v) Circuit diagram of integrator switch control unit.
- (vi) Circuit diagram of V/I converter.
- (vii) Circuit diagram of oscillator and gated amplifier.
- (viii) Circuit diagram of comparator.
- (ix) Waveforms at output of converter.
- (x) Block diagram of gate and scaling unit.
- 6.2.4(i) Permissible frequency error during current rise.
- (ii) Frequency determining tank circuit of oscillator.
- (iii) Frequency variation with bias.
- 6.3.1(i) Block diagram of high power r.f. system.
- (ii) Cutaway view of the r.f. cavity.
- 6.3.2(i) View of the accelerating cavity in position in straight
section 8.
- (ii) View of the accelerating cavity.
- (iii) Shape of vacuum vessel insulators.
- (iv) View of a ferrite core 'window frame'.
- (v) The winding configuration of the accelerating cavity.
- (vi) Cavity equivalent circuit diagram.
- 6.3.3(i) Required accelerating voltage v. frequency.
- (ii) Cavity load impedance v. frequency.
- (iii) Power loss v. frequency.
- (iv) Equivalent circuit of the cavities.
- (v) Basic circuit of the output stage.
- (vi) Dummy load for tests on amplifier output stage.
- (vii) Actual load impedance v. frequency.

ILLUSTRATIONS (cont'd)

- Fig.6.3.3(viii) Actual power loss v. frequency.
(ix) Pentode stage circuits.
(x) Response of QY5/3000A (tetrode) driver stage.
(xi) Prototype transmitter - Low power wideband preamplifier.
(xii) Prototype transmitter - High power wideband driver.
(xiii) Prototype transmitter - Final stage power amplifier.
(xiv) Winding arrangement on the driver output transformer.
- 6.3.4(i) Phase splitter/cathode follower driver circuit.
(ii) View of final amplifier cubicle in position.
- 6.3.5(i) Circuit for the automatic level control of gap voltage.
- 6.3.6(i) Block diagrams of the first phase detector circuits.
(ii) Second phase detector circuit.
(iii) Block diagram of final phase detector circuit.
(iv) Waveforms transmitted through the phase lag network.
(v) Diode limiters on the semiconductor phase detector input.
- 6.3.7(i) Mark I thermionic bias supply circuit.
(ii) Arrangement of voltage feedback loop.
(iii) Arrangement of the bias supply in the automatic cavity tuning loop.
(iv) Auxiliary amplifier response.
(v) Plot of closed loop response against frequency.
(vi) Initial transient phase error.
(vii) Plot of open loop d.c. gain against r.f. frequency.
- 6.3.8(i) Transistor voltage-current locus at turnoff.
(ii) Arrangement of control unit, power unit and load.
(iii) Simplified equivalent circuit of phase loop.
- 6.3.9 Layout of high power r.f. equipment in the magnet room.

ILLUSTRATIONS (cont'd)

- Fig.7.1.1(i) Piccioni system.
(ii) Paths of protons, Nimrod extraction system.
- 7.2.1(i) Fast kicker coil.
7.2.2(i) Basic fast kicker circuit.
7.3(i) Plunging mechanism.
- 8.2.2(i) Design of externally supported vessel.
8.2.3(i) Isometric cross section of an octant.
8.2.4(i) End pole piece assembly.
(ii) Vacuum vessel sealing arrangement.
(iii) Pole face windings.
8.2.5(i) Inner vessel crowning and header supports.
8.2.7(i) Closure plate tie rods.
8.3.1(i) Outer vessel splices.
(ii) Curing a section of an outer vessel on a die bed.
(iii) Laying impregnated cloth on a die bed.
(iv) Cross section of vessel and flanges showing "B" stage blocks and "Wet packs".
(v) View of a vessel side.
(vi) Dorsal splicing in progress.
- 8.4.5(i) Diagram of the side moulding bed.
8.4.7(i) Diagrammatic arrangement of the loft plate.
8.5.1(i) View of a transporter carrying a vessel.
8.5.2(i) Vessel test rig.
(ii) Outer vessel stiffening frame.
(iii) Typical section through test seal on front flange.
(iv) Top lifting arrangement for outer vacuum vessel.
(v) View inside an outer vessel. (The wooden jigs are for packing purposes only).
- 8.5.3(i) Inner vessel assembly rig.
8.6.1(i) Leak detection sensitivity.
8.6.2(i) An area of vessel shrouded for test.
(ii) "Top hat" for local testing of a repaired area.
(iii) "Top hat" for vacuum testing inserts.
8.6.4(i) An installed header vessel (octant 6).
(ii) An installed closure plate (octant 4).

ILLUSTRATIONS (cont'd)

- Fig.8.6.4(iii) Pump down of octant 2.
- 8.7(i) An area of a vessel showing resin starvation.
- (ii) Crushing and voids on a vacuum vessel.
- (iii) A cut out repair area showing the half inch steps.
- (iv) Typical repair profile.
- (v) Final stage of repair.
- (vi) A completed repair.
- (vii) Accidental damage to an outer vessel.
- (viii) An enlarged view of the damage.
- 8.9.1(i) Relative outgassing rates of Natural and Synthetic Rubbers.
- (ii) Stability of polyurethane rubber under irradiation.
- (iii) Stability of PVC nitrile under irradiation.
- 8.10.1(i) 24 in oil diffusion pumping unit.
- 8.10.2(i) Pump header and gate valve suspension.
- 8.10.3(i) Inner vessel roughing pump.
- (ii) Refrigerated oil trap.
- (iii) Layout of roughing system.
- 8.10.4(i) Thermistor vacuum switch.
- (ii) Mechanical safety device.
- 8.10.5(i) Assembly of bellows, adaptors & vacuum shut-off valve to vacuum vessel in a long straight section.
- (ii) Shut off valve housing and body sealing plate.
- 8.10.7(i) Schematic layout of a typical beam line vacuum system.
- (ii) 8 in fast shut off valve.
- 8.11.2(i) Machining of the linac vacuum vessel.
- (ii) O-ring corner joint of the linac vacuum vessel.
- (iii) Outer space test sleeves.
- (iv) Linac drift tube.
- (v) 'Top hat' test on conductor tubes.
- 8.11.4(i) An installed 24 in mercury pumping unit.
- (ii) View of d.c. gun 9 in mercury pumping units.
- (iii) View of part of the liquid air system.
- 9.1.1(i) Layout of injector control room.
- (ii) General view of injector control room.
- (iii) Block diagram of injector control system.

ILLUSTRATIONS (cont'd)

- Fig.9.2.2(i) Schematic circuit diagram of 24 in oil diffusion pump unit.
- 9.2.3(i) Vacuum system mimic diagram and control panels
(in main control room).
- (ii) Block diagram of a straight section interlock and roughing
system.
- 9.3.2(i) Temperature monitoring equipment for the injector.
- (ii) Thermistors mounted on pole face winding connections.
- (iii) Transistorised gating and error sensing equipment for
1600 way high speed temperature monitoring system.
- (iv) Temperature monitoring control panel (in main control room).
- 9.3.3(i) Seven-way water flow monitor.
- 9.4(i) Layout of main control room.
- (ii) General view of main control room during installation.
- (iii) Control racks installed in the main control room.
-
- 10.2(i) Diagrammatic arrangement of water cooling system.
- 10.3.2(i) Schematic diagram of Kennicott water treatment plant.
- 10.4.2(i) Permutit water treatment plant.
- 10.6.1(i) Air conditioning system.
- 10.8.1(i) Chilled demineralised water system; circuit No.1.
- (ii) Chilled demineralised water system; circuit No.2.
- 10.9(i) R.F. chilling equipment.

SECTION 1

INTRODUCTION

The preliminary considerations, which lead in 1957 to the decision to build a 7 GeV proton synchrotron in England, took place during the previous two years. The original intention was to produce a proton intensity of at least 10^{11} protons per second at an energy of 6.5 GeV and thus to provide a strong source of all the elementary particles known at that time.

The CERN and Brookhaven machines were then under construction. They embodied a number of new and difficult problems, and estimates of their intensity varied from a few times 10^8 to a few times 10^9 protons per second. On the other hand, the Bevatron was already producing about 10^{10} protons per pulse (once every 6 seconds) and was clearly capable of considerable development along known lines. The large aperture of the weak focusing magnet is costly in steel and power but multi-turn injection allows a strong circulating beam to be set up before acceleration begins. The only sure way to get 10^{11} protons per second, in 1957, was with weak focusing.

A weak focusing machine was therefore chosen and an alternative proposal for a 12 GeV alternating gradient synchrotron was rejected in discussion with future users. Initially, it was intended to increase the strength of vertical focusing significantly by the use of spiral ridges, to give a Q_y of 3 while retaining the main properties of weak focusing machines, but this proposal was abandoned when severe dynamical problems were found to be associated with the presence of the straight sections which are essential. In the subsequent detailed design the energy was raised to 7 GeV and the intensity to about 5×10^{11} protons per second. The main Nimrod parameters are given in Table 1(I).

The magnet was designed with saturable polepieces so as to give a good field region matched to the required radial aperture which shrinks during acceleration, thus yielding considerable economy in magnet weight and power. A double walled vacuum vessel was also chosen with the same economy in mind. An outer vessel is pumped to rough vacuum and contains the magnet poles, which also provide its support. An inner vessel sits in the gap between the poles and is pumped to the necessary degree of fine vacuum. Thus neither vessel has to withstand atmospheric pressure without support and the walls of both can be thin and the maximum possible vertical aperture is thus available for the beam itself.

The magnet ring is divided into eight equal magnet segments or "octants", separated by straight sections which are required for beam injection and extraction systems, the r.f. accelerating cavity and beam control systems.

An injection energy of 15 MeV was chosen as one which could be achieved at reasonable cost while at the same time avoiding serious problems from gas scattering or from too low an initial magnetic field in the synchrotron magnet.

In order to obtain the maximum useful injection interval, the magnet power supply includes a facility for controlling the initial rate of rise of field independently of that during the main acceleration period. Injection intervals up to 1.5 ms are provided, the optimum time being found experimentally.

The synchrotron r.f. system operates with a harmonic order of 4. Although this demands a wide bandwidth in the system, the amplitude of the radial synchrotron oscillations is thereby reduced to half the value produced by operation on the fundamental. Signals from beam induction electrodes are available to give servo control on both the frequency and phase of the accelerating voltage, in addition to the programme control by the main magnet field plus curve correctors.

Besides the use of internal targets, a Piccioni type system will be used for extracting the circulating beam. A second extraction system may be added during subsequent development. Both slow and fast beam spills will be available.

The magnet ring is housed in a large, circular, reinforced concrete building 200 ft in diameter. It is built partly below ground level and covered by 20 ft of earth mounding to serve as an additional radiation shield. The injector section has a separate hall, also covered by earth mounding, which projects almost tangentially from the main building. The magnet is positioned on a large concrete monolith which takes the form of a partly hollow disc, reinforced by radial and circular internal walls to form sixteen cavities which are used to contain auxiliary equipment. An annular trench surrounds the magnet and provides accommodation for the vacuum pumps and for general services. Numerous underground ducts and tunnels are also provided for interconnection of services, power supplies and control systems.

A feature of the Nimrod buildings is a massive concrete shielding bridge, between the magnet room and the main experimental area, which is 60 ft in arc length and 28 ft wide. A small central pillar (1 ft wide, 8 ft long and $2\frac{1}{2}$ ft high) carries 7,500 tons and is the only bridge support which interferes with the positioning of beam lines into the experimental area.

Separate buildings house the magnet power supply (a twin motor/alternator/flywheel set and convertor equipment), ventilation plant and water softening and cooling plant (including a block of four large evaporation coolers). A further building contains the main control room, crew rooms and offices for staff associated with the operation of the machine.

A simplified layout of some of the buildings is shown in Fig. 1(i) and a cut-away view of the complete installation is shown in the frontispiece. More detailed figures showing individual parts of the machine are contained in the appropriate sections of this report.

A list of general articles on Nimrod is presented at the end of the report.

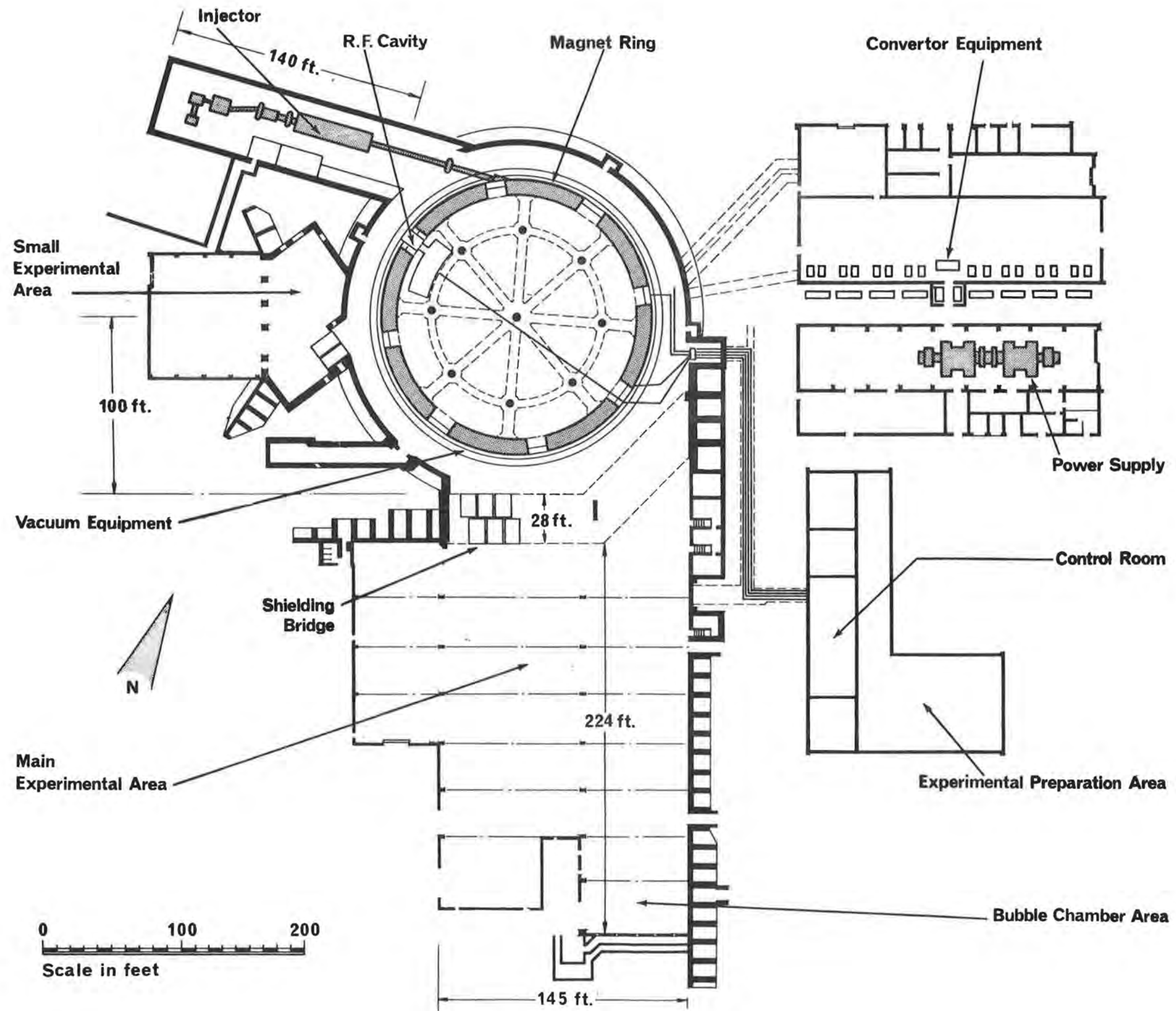


Fig. 1(i) A simplified plan showing the layout of the NIMROD installation.

TABLE 1(I)
Nimrod Parameters

INJECTOR

Ion Source

Extraction potential	5-25 kV
Extracted beam current	25-100 mA
Pulse length	50 μ s - 1.5 ms variable 0.3 μ s and 5 μ s fixed
Pulse repetition frequency	2/s maximum

Pre-Injector

Focusing	Electrostatic
Energy	600 keV
Beam emittance (Area/ π)	Up to 5×10^{-3} cm rad

Low Energy Drift Space

Focusing	Aperture	Maximum gradient
First triplet	8.9 cm	170 gauss/cm
Second triplet	7.6 cm	240 gauss/cm
Third triplet	6.4 cm	480 gauss/cm

Peak r.f. voltage on buncher gap	23 kV maximum
Buncher Q	1500 with external resistive loading
Buncher drift length	1.4 m
Bunching factor (measured)	2.2
Plateau width (theoretical)	6 keV

Linac

Frequency	115 Mc/s
Beam current	10 mA with buncher
Acceptance (area/ π) (+- +-, theoretical)	3.0×10^{-2} cm rad at 600 keV
Synchronous phase	30°
R.F. pulse length	2.5 ms
Pulse repetition frequency	2/s maximum
Quadrupole gradients:	
First drift-tubes	3,700 gauss/cm
Last drift-tube	640 gauss/cm
Tank length	13.45 m
Tank diameter (effective)	1.69 m
No. of drift tubes	$48 + 2 \times \frac{1}{2}$
Drift-tube diameter	28.2 cm

Input aperture	2.1 cm
Output aperture	5.0 cm
Output energy	14.9 MeV
Resonator Q (measured)	80,000
R.F. power at Q = 80,000 (theoretical)	800 kW
Peak r.f. voltage on input gap	140 kV
Peak r.f. voltage on output gap	680 kV
*Energy spread (total)	300 keV
Operating temperature	20°C

High Energy Drift Space

Focusing	Aperture	Maximum gradient
First triplet	7.6 cm	730 gauss/cm
Second triplet)	8.9 cm	430 gauss/cm
Third triplet)		
Fourth triplet)		

Peak r.f. voltage on de-buncher gap	240 kV
De-buncher Q (measured)	20,000
De-buncher drift length	10.7 m

Achromatic Inflector System

Achromatic mode	Single crossover
Total deflection	+ 25°
Number of elements	5

Element	Type	Angle	Radius of Central Orbit	Corresponding Field	Apertures	
					Radial	Vertical
E ₁	'C' magnet	-25°	0.7 m	8 kg	6 cm	9 cm
E ₂	'C' magnet	+50°	0.7 m	8 kg	6 cm	9 cm
E ₃	'C' magnet	-36.5°	0.7 m	8 kg	6 cm	9 cm
E ₄	Shielded 'C' magnet	+26°	1.124 m	5 kg	5 cm	8 cm
E ₅	Electrostatic	+10.5°	6.0 m	50 kV/cm	3 cm	8 cm

MAGNET AND POWER SUPPLY

General

Magnet sector radius, R_o	18.781 m
Mean orbit radius, R_m	23.633 m
Proton kinetic energy: for $B_o = 10$ kilogauss	4.77 GeV
for $B_o = 14$ kilogauss	7.00 GeV
for $B_o = 15.8$ kilogauss	8.00 GeV
Total straight section length (design)	30.480 m
Number of straight sections	8 (4 long, 4 short)
Design length of long straights (each)	4.267 m
Design length of short straights (each)	3.353 m
Magnetic field index, n (design)	0.60
Magnetic length of octant at R_o (design)	14.751 m
Total number of magnet yoke blocks	336
Total number of polepieces	672
Number of pairs of polepieces per octant, type MkI	28 (at centre of octant)
Number of pairs of polepieces per octant, type MkII	12 (6 each side of MkI's)
Number of pairs of polepieces per octant, type end	2

Yoke

Number of yoke blocks per octant	42
Angle between centre lines of extreme blocks	44.03°
Thickness of a yoke block (at R_o)	12.50 in (maximum)
Angle between centre lines of adjacent blocks	1.074°
Block-block spacing at R_o	13.859 in
Block-block spacing at front edges	14.253 in
Block-block spacing at back edges	12.202 in
Thickness of block at back edge	12.10 in (maximum)
Front edges of sectors lie on sector radius	19.355 m
Weight of yoke block	19.5 tons
Total number of laminations per block	47
Steel silicon content	80% minimum, 100% maximum
Vertical yoke gap	23.000 in

Polepieces

Total number of laminations	450 approximately
Thickness of laminations - thin type	0.020 in nominal
Thickness of laminations - thick type	0.030 in nominal
Ratio of thin to thick laminations	1 : 2
Silicon content of thin laminations	3.5%
Silicon content of thick laminations	1.0%
Sector radius of outside edge of magnetic profile of polepieces	63ft 7.9 in
Radial length of magnetic profile of polepieces	45.5 in
Vertical height of polepieces at R_o	5.875 in
Vertical gap between polepieces	10.09 in (minimum)

Magnet Coil

Number of coil turns	42
Peak current (design)	9150
Total copper cross-section	155 in ²
Length of mean turn on an octant	117 ft
Total weight of copper	250 ton
Coil resistance (at 50°C)	0.108 Ω
Magnet inductance (low currents)	1.1 H

Magnet performance under standard pulse conditions

Peak current	9150 A
Rise time	0.72 s
Duration of flat-top	0.115 s
Current decay time	0.80 s
Repetition rate	26/min
Mean voltage during rise	13.9 kV
Assumed voltage variation during rise	16.0 to 11.8 kV
Mean voltage during decay	-11.7 kV
Assumed voltage variation during decay	-11.0 to -13.4 kV
R.M.S. current	4550 A
VI at top of current rise	108 MW
VI during flat-top	9.1 MW

Energy delivered to magnet during current rise:	
Stored energy	39 MJ
Copper loss	1.92 MJ
Eddy current loss	0.07 MJ
Energy delivered during flat-top	1.04 MJ
Energy required during current decay:	
Stored energy	39 MJ
Copper loss	2.03 MJ
Eddy current loss	0.08 MJ
Iron loss (hysteresis)	0.12 MJ
Nett energy loss/pulse	5.26 MJ
Overall average losses	2.22 MW

SECTION 2

COMPUTATION AND THEORETICAL WORK

Computing programs, developed by the Theoretical Physics Group, have been used for the design of the injector and for studying the dynamics of Nimrod, the extracted proton beam and secondary beams. Since most of the work has been fully recorded in reports, only an outline list of these and the computer programs available is given here. Copies of the programs can be obtained from the originators.

2.1 Linac Injector

(a) A.E.R.E./R/3012: 'Calculation of drift-tube dimensions in the linac injector for the 7 GeV Harwell proton synchrotron' by R. Taylor (Sept 1959).

A Mercury Autocode program which computed drift tube dimensions.

(b) A.E.R.E./R/3013: 'Acceptance of axially and radially oscillating particles for the Nimrod injector' by R. Taylor (Oct. 1959).

Several Autocode programs which use the field data from the previous report.

(c) A.E.R.E./R/3096: 'Effect of rotational misalignment for the Nimrod injector' by R. Taylor (Oct. 1959).

A Mercury Autocode program.

(NOTE. Some of the above programs exist in adapted form for tanks 2 and 3, and the redesign of tank 1 of the 50 MeV Proton Linear Accelerator at the Rutherford High Energy Laboratory).

2.2 Linacs; General Theory

The following are more general in application but are included for completeness.

(a) NIRE/M/37: 'Finite-difference computation of parameters of electromagnetic resonant cavities relevant to proton linear accelerators' by R. Taylor and P. Kitching (July 1962).

This report contains a detailed description of a Fortran program for computing dimensions, shunt impedance and field patterns for Alvarez-type cavities, and has been used extensively in accelerating structure studies (e.g. see P.L.A. Progress Report, 1962; NIRE/R/24, p.13).

An Autocode program has been written for the simpler case with sharp corners and no axial hole in the drift tubes. An analytical solution of this was used to test the finite-difference program (See 'Calculation of resonant frequencies of re-entrant cylindrical electromagnetic cavities', J. Nucl. Energy, Part C, 3 (1961), p.129; R.Taylor).

(b) A Fortran program also exists for the calculation of dimensions in an iris-loaded cylindrical waveguide (see 'Calculation of dispersion

of iris-loaded cylindrical electromagnetic waveguides', J. Nuc. Energy, Part C, 4 (1962), p.418; R. Taylor).

2.3 Nimrod Dynamics

A Fortran program is available for studying particle dynamics in Nimrod. The input can be either in the form of directly measured fields or in some simpler form. Straight sections with or without fringe fields are included. The program has been used for studying closed orbits, betatron oscillations and Q-values, and also for extraction studies of the primary protons and secondary particles.

NIRL/R/46: 'Computer program for particle tracking in Nimrod' by D. Whiteside (1963).

NIRL/R/47: 'Trajectories from a Nimrod octant' by D. Whiteside (not yet published).

2.4 Extracted Proton Beam

Early descriptions of the design of the extracted proton beam are contained in:

(a) 'An achromatic modification of the Piccioni extraction system' by R. G. T. Bennett and J. W. Burren (1960). This was originally issued as an internal laboratory note but most of the information, except for some numerical calculations, was published in the Journal of Nuclear Energy (Part C, 3 (1961), p.14; R. G. T. Bennett and J. W. Burren) under the title 'An achromatic system of extraction for proton synchrotrons'.

(b) AERE/M/521: 'The extraction system for Nimrod, Part 1: the Piccioni target and the extraction magnet' by J. W. Burren (November 1959).

(c) NIRL/R/12: 'Design studies for the Nimrod external proton beam' by J. W. Gardner, N. M. King and D. Whiteside (1962).

Detailed design, using more accurate input data, has been carried out recently using the Fortran program described above.

2.5 Irradiation Studies

Orbit calculations were made to estimate the probable distribution of high energy irradiation of the upper and lower walls of the vacuum vessel.

AERE T/M 173: 'High energy irradiation of the vacuum envelope of the 7 GeV Harwell synchrotron' by J. W. Burren and D. Morgan (November 1958).

2.6 Beam Design

Two general purpose programs are available for the design of particle beams. TRAMP (Tracking and matching program) can be used for systems of

quadrupoles, bending magnets and crossed field separators. For a description of the Mercury Autocode version of the program see NIRL/M/21 by J. Gardner and D. Whiteside (1961). The Fortran version by the same authors is described in NIRL/M/44 (1963).

The second program is called OPUS (Optimisation program for unstable secondaries); NIRL/Note (1962) by J.W. Gardner and D. Whiteside.

The principles of separated beam design are contained in the following reports:-

NIRL/R/2: 'Basic concepts in design of electrostatic separators' by N. M. King (1961).

NIRL/R/10: 'Finite separation in electrostatic velocity separator design' by N. M. King and R. G. Cox (1961).

NIRL/R/18: 'Theory of two-stage separated beam systems' by J. W. Gardner (1962).

SECTION 3

INJECTION SYSTEM

3.1. Introduction

If 10^{12} protons per pulse is to be attained in Nimrod it could be necessary to inject about 10^{14} , most of which will, of course, be lost even before acceleration begins. The injection system has accordingly been designed to yield at least 20 mA for a maximum pulse length of 1.5 ms. This injection time corresponds to a lower limit of \dot{B} at injection of 2 kG/s. Optimum injection conditions cannot be predicted since they will depend on phase space current density distribution of the 15 MeV beam and space charge effects in the synchrotron. It is anticipated however that the optimum will be covered by the available range of the parameters concerned.

The injection system is shown in Fig. 3.1(i); it might almost be described as conventional in its functional conception. The main parameters are listed in section 1, Table 1(I).

The 15 MeV linear accelerator is a strong focused Alvarez structure running at 115 Mc/s. Its output energy was determined after consideration of gas scattering losses and remanent field effects in the synchrotron, on the one hand, and complexity, cost and electrostatic inflector breakdowns on the other. Pre-injection energy, initial aperture desired, attainable quadrupole gradient in the first drift tube, and commercially available power valves were all considered in fixing the operating frequency.

An achromatic inflector is necessary for efficient injection of the 15 MeV beam, even assuming the debuncher to be working satisfactorily, and also serves to convey the beam past certain obstructions to a simple inflection arc.

Quadrupoles in the low and high energy drift spaces (LEDS and HEDS) are arranged to transport the beam and match it, over a range of input and output conditions. Beam current transformers (B.C.T.s), fluorescent screens, stops, foils and "Faraday cups" are introduced into the flight tube as required and a "4 jaw box" system allows beam definition by edges, slits, apertures etc. As a general rule, every 4 jaw box has a B.C.T. on either side of it. The B.C.T.s are integral with the flight tube for the most part, other components such as screens and stops are on reciprocating shafts and mounted on standard probe boxes.

Table 3.1(I) summarises the injector history.

TABLE 3.1(I) INJECTOR HISTORY

September 1957	First major contract for the 650 kV installation placed.
March 1959	650 kV equipment received on site.
August 1959	Construction of the pre-injector completed.
December 1959	First accelerated beams achieved from the pre-injector. Vacuum tank for the linac received.

TABLE 3.1(I) INJECTOR HISTORY (Contd.)

January 1960	Main r.f. valve, RS1041, received.
February 1960	Modulator for r.f. drive chain received.
July 1960	Linac cavity received.
March 1961	Last of the linac drift tubes, which were delivered over a period of nine months, received.
May 1961	Last drift tube installed. First vacuum test on the completed linac.
1st July 1961	High r.f. power fed into the linac for the first time.
1st August 1961	First successful acceleration to 15 MeV.

The first 15 MeV beam was obtained on 1st August, 1961, and intermittently during the following six weeks. Some basic measurements, e.g. threshold and trapping efficiency were made and much equipment proved, but operating conditions deteriorated continually, the main difficulties being sparking and multipactoring in the linac and sparking in the main power amplifier circuit. After effecting improvements and repairs to the valve circuit and cleaning up the linac drift tubes, operation was once more attempted in October but multipactoring dominated the situation until February, 1962, when the drift tube faces were lampblackened. This completely stopped multipactoring although a painstaking conditioning phase was now required against sparking. Very satisfactory running conditions obtained until breakdown of the RS1041 anode blocking capacitor in April, 1962, and not until late June was an effective, although temporary repair realised. Since then good running has been experienced with one interruption for cleaning drift tube faces to reduce the incidence of sparking.

Installation in the LEDS and HEDS in anything like final form has been deliberately delayed to allow for as much detailed study as possible of the beam properties. This work though still incomplete, has been of great value in helping to understand the beam physics and in deciding upon a detailed component layout. Measurements are made of, for example, current proton percentage, emittance, and momentum distribution.

This report takes account of events up to the end of 1962.

3.2. Dynamics of the Injector

3.2.1. Dynamical Design of the Linac

(a) Preliminary work

It was decided at an early stage to adopt alternating gradient quadrupoles for the injector as this was the most obvious way of ensuring the highest accelerated currents. A number of experimental quadrupoles were constructed as a guide to magnetic and electrical design. The outcome of this work was the determination of a maximum practicable quadrupole gradient and a corresponding aperture. From an elementary consideration of the dynamical stability of accelerated particles, together with knowledge of the frequency dependence of electrical breakdown it was possible to specify a relationship between initial particle energy and frequency, appropriate to this estimated maximum quadrupole gradient (1).

Subject to this relationship the choices of frequency and injection energy were 115 Mc/s and 600 keV respectively, the latter being consistent with experience of Cockcroft-Walton accelerators and the availability of high voltage power supplies. The output energy of 15 MeV was chosen by weighing the difficulty of producing an inflection system for higher energy particles against their more favourable gas-scattering loss factor. It was also compatible with the minimum useful magnetic field obtainable in the synchrotron.

The effect of misalignment of the quadrupoles was investigated to determine a rate of increase of aperture which would make the probability of particle loss equal at all points through the machine. The maximum initial rate of increase was determined independently by the required quadrupole gradient variation. On this basis the misalignment investigation specified the aperture throughout the machine, together with alignment tolerances for the quadrupoles. As a result of these preliminary calculations it was also possible to specify the approximate length of the machine, the mean accelerating field and the number of unit cells (Fig. 3.4.8(i)). Resonance experiments on scaled unit cells were used to specify the geometry of a unit cell at any point in the machine in terms of the corresponding particle velocity.

(b) Final Dynamical Design

The final stage in the dynamical design was an extensive computation on a Mercury computer, aimed at specifying an actual number of unit cells and then precise dimensions, consistent with the other required features of the design (2). It was assumed that a "reference particle" must cross from the centre of one unit cell to the centre of the next in exactly one r.f. cycle. The r.f. phases at which successive cell centres are passed are thus separated by 2π radians i.e. this occurs at a constant reference phase with respect to each r.f. cycle. The entry and exit phases can be stated with respect to this in terms of the input and output velocities. The computation proceeded by calculating the motion of a particle through a unit cell, its dimensions being appropriate to the input velocity. This established a certain output velocity which was used to define the dimensions of another unit cell for which the particle motion was again computed. In neither of these unit cells was the output phase correctly related to the reference phase and output velocity, but by linear interpolation a unit-cell with the correct relationship could be found. This was used as the starting point for a computation of the following unit cell, and so on throughout the linac. By computing a number

of complete accelerators with differing electrical field-strengths and interpolating, a final design was obtained which incorporated all the requirements to an acceptable accuracy.

On the basis of this design further computation of beam acceptances were made for each of the two planes of symmetry and for a number of input phases and energies (3). Radial and phase motion were also examined in some detail and the effect of a buncher was considered (3). Finally a computation was made of the effect of rotational misalignment of the quadrupoles on beam acceptance (4).

3.2.2. Drift Spaces

The low energy drift space (LEDS) constitutes a matching system between the 600 keV pre-injector and the linac. Provision is made for a "four parameter match" that is the realisation of two required beam conditions, say beam radius and slope, in each of the two planes of symmetry. This necessitates control of four variables in the matching system which in fact are the total and out-of-balance energising currents in each of two quadrupole triplets. There is a third triplet downstream of these two and very close to the linac input, its function being to handle the rather drastic transition between the low gradient matching system and the high gradient linac focusing system. This third triplet must also be compatible with the passing of a fairly small diameter beam through the buncher, the component which is immediately upstream from it. Its energisation is intended to be permanently set at levels which conform to these requirements.

The focusing components of the high energy drift space (HEDS) form essentially two double triplet matching systems in series separated by a fairly long drift space containing the debuncher. The first matching system must be capable of transforming the linac output beam in such a way that it passes with radial and axial symmetry through the debuncher at any position in the central drift space. The second system must be able to transform the symmetrical beam from the debuncher to a variety of conditions dictated ultimately by a range of input radii to the synchrotron which gives a corresponding range of focal properties to the inflector.

3.2.3. Buncher and Debuncher

The buncher imparts an energy modulation to the 600 keV beam at the linac frequency. The position at which the bunch occurs is determined by the axial beam velocity and the depth of the modulation, and when this is fixed, the time at which the bunch occurs relative to the linac field is determined by the buncher phase. The magnitudes and stability of these three quantities have been related to the phase-energy acceptance of the linac in such a way as to ensure a substantial and stable gain in accepted charge.

The debuncher imparts an energy modulation to the 15 MeV beam after the energy spread in the beam has brought about some axial resolution travelling along the HEDS.

Particles of higher energy reach the debuncher before those of lower energy, hence by correct phasing of the debuncher field the early ones may be accelerated and the late ones decelerated, the result being a much narrower energy spectrum.

The post-acceleration drift length and the debuncher field have been chosen to give optimum debunching for estimated energy-phase characteristics of the 15 MeV beam.

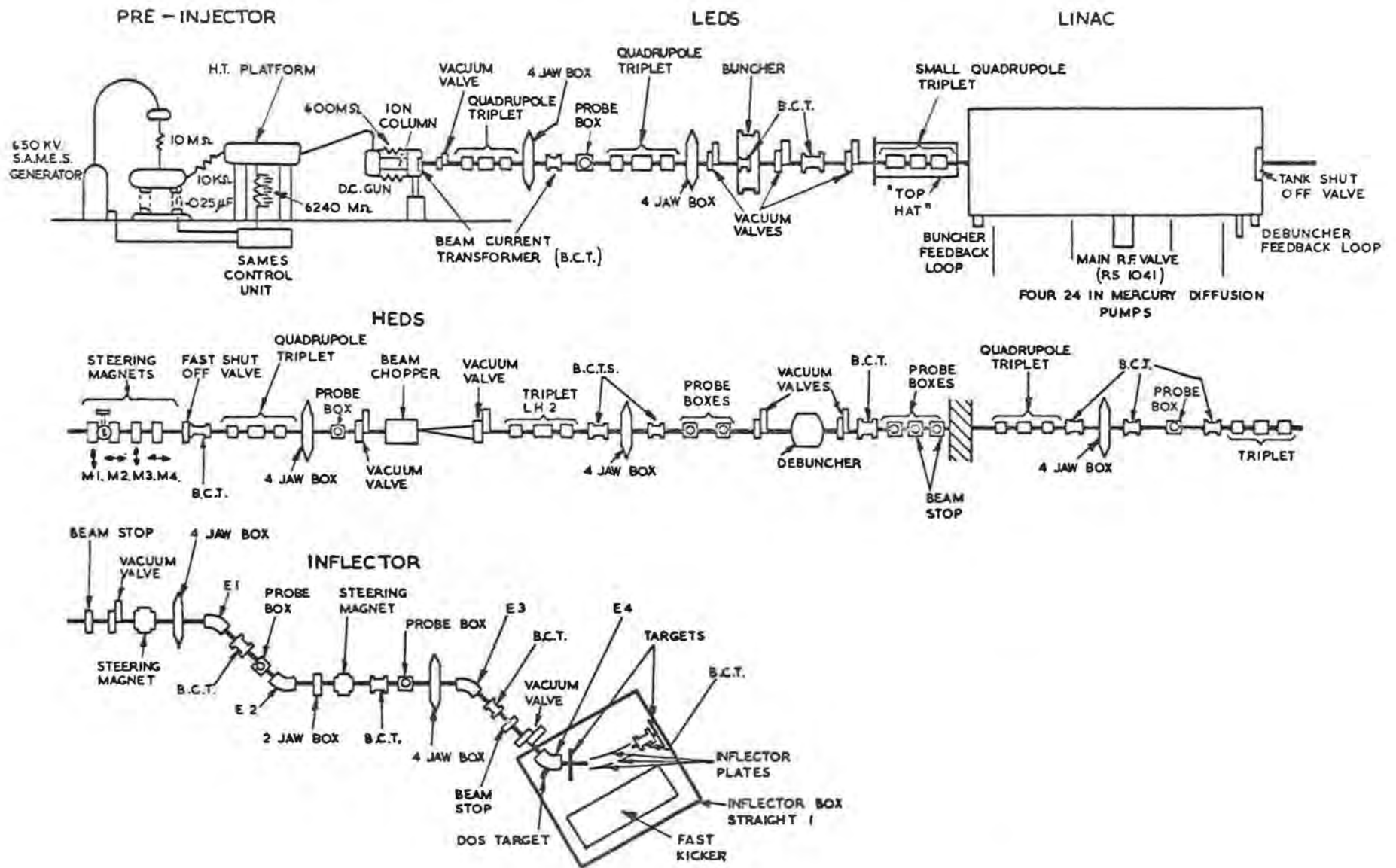


Fig. 3.1(i) Injection System.

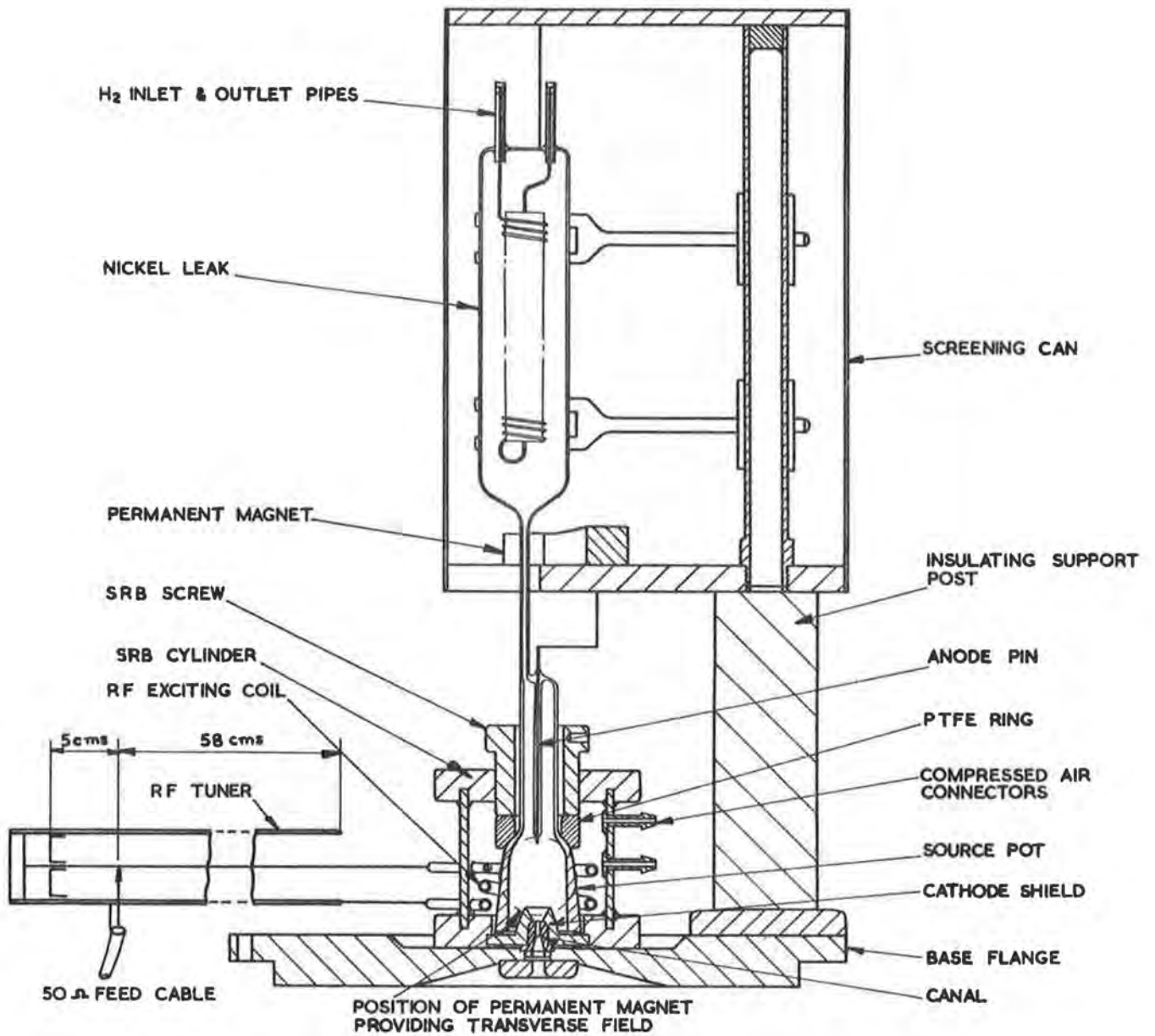


Fig. 3. 3. 1(i) RF Ion Source Assembly

3.3. Pre-injector

3.3.1. R.F. Ion Source

(a) Present Source Assembly

The source is of the radio frequency type and follows closely the design developed by Schneider at CERN (5).

Early work was done with ceramic parts for the source body and cathode shield and the circuit for coupling the r.f. power into the source was that described by Schneider. Results were fairly encouraging, beam currents of 30-40 mA being obtainable at extraction voltage of 10-15 kV. However, arcing took place in the source at higher extraction potentials and the source life was greatly reduced at higher current levels.

The phenomenon of internal breakdown has been by far the most serious problem in development work. It was found convenient to use Pyrex parts for the source body and shield which made for convenience in manufacture and enabled changes to be made without the long delay associated with specially made ceramic parts. No outstanding change in source performance was observed when the change from ceramic to Pyrex was made.

The source is made entirely in Pyrex, mounted on a mild steel flange, (Fig. 3.3.1(i)). The whole assembly is attached to this flange and can be removed from the ion column and replaced as a unit.

The source pot is made from standard 1 in to $\frac{5}{8}$ in QVF reducer. The anode pin is tungsten sheathed in Pyrex glass and the cathode shield is ground from a block of Pyrex to the same dimensions as that used in the CERN source (5). Indium wire (1/64 in dia.) is used as a vacuum seal between the pot and the shield and between the shield and the mounting flange. Some difficulty was experienced in making a good clamping arrangement, but the method shown in Fig. 3.3.1(i) has proved satisfactory.

A PTFE ring presses against the shoulder of the source pot and is clamped down by an SRB screw which is threaded 40 t/in on the outside. This screw is carried by the SRB cylinder which also forms a small pressure vessel, into which the 2 turn r.f. exciting coil is araldited. Compressed air, at about 30 lb/in², is fed to the cylinder through the connectors shown and forms a good insulator between the coil and the source pot. This prevents discharges in this region when the plasma is pulsed up to extraction potential and enables the r.f. matching circuit to be at earth potential, greatly simplifying the circuit. The circuit is a 50 Ω line stretcher and stub connected directly to the coil, shown schematically in Fig. 3.3.1(i); the lengths of the stretcher and stud being typical values for a good match. A reflectometer in the 50 Ω r.f. feed cable records a ratio of forward to reflected wave of ten to one, when the tuner is properly adjusted. A maximum r.f. power of about 15 kW is available.

Hydrogen is fed into the source at extraction potential through a nickel leak connected to the source by a direct glass to glass joint. This avoids any 'O' ring seals. A small permanent magnet provides a strong magnetic field across the hydrogen feed tube and the nickel leak is contained in a screening can. These precautions were intended to suppress discharges in the nickel leak itself but they are not very effective.

The exit canal dimensions are 3.5 mm dia. and 8 mm long in the parallel part and it is located in an accurately turned recess in the base flange. It was accidentally made in mild steel and, since it seems to give no obvious trouble, the material has not been changed. Two permanent magnets provide a transverse magnetic field of about 50 gauss in the source pot which increases the ion density at a given r.f. power.

The maximum output so far obtained from this source in service, is about 100 mA with 20 kV extraction potential, and r.f. power very roughly 10 kW and a pulse length of 170 μ s (r.f. pulse length 700 μ s). This was measured by a beam toroid after acceleration to 600 kV and represents the total beam current. After operation for about half an hour at this level the source failed by arcing internally. The source has operated at 20-30 mA for about 200 h so far without trouble.

The sources are operated on a laboratory rig and their performance checked before being used on the injector. A typical graph of total output current against extraction voltage is shown in Fig. 3.3.1(ii). The r.f. power level is optimised at each value of extraction voltage and the beam current is measured with a collector cup having a transverse magnetic field to suppress secondary electrons.

(b) Operational Experience

Internal Arcing

When the extraction voltage is raised above about 15 kV there is the possibility of internal breakdown leading to an arc discharge. This effect has been by far the most difficult and intractable problem in the development of the source. It has been very difficult to find any parameter which affects the phenomenon in a consistent manner.

The one clear cut result to emerge is the effect of impurities in the discharge in initiating breakdown. In early work with Pyrex sources, they were stuck together with Araldite and suffered very badly from internal arcing. Since then, great care has been taken to clean and dry the glass parts thoroughly and all 'O' rings and Araldite have been eliminated. The arcing has been much less troublesome though the problem is by no means completely solved.

The glass parts are washed in concentrated nitric acid then in dilute hydrofluoric before being thoroughly rinsed in tap water followed by distilled water. They are dried in an oven at about 150°C for several hours. On one or two occasions the hydrofluoric acid has been concentrated enough to etch the glass slightly and this seemed to give a poor source.

There have been two periods when the source performance on the Injector deteriorated for no apparent reason. Eventually in both cases contamination was thought to be the cause. In the first instance the glass parts had not been sufficiently thoroughly dried and in the second, leaks were found which allowed small amounts of air into the discharge. The leaks were never large enough to show up on the ion gauges of the ion column.

Arcing also occurs much more readily on long pulses. A source which is working well with a pulse length of about 100 μ s for example, will often start to breakdown when the pulse length is increased to 1 ms. Persistent arcing can cause

PYREX SOURCE WITH INDIUM SEALS AND MILD STEEL CATHODE

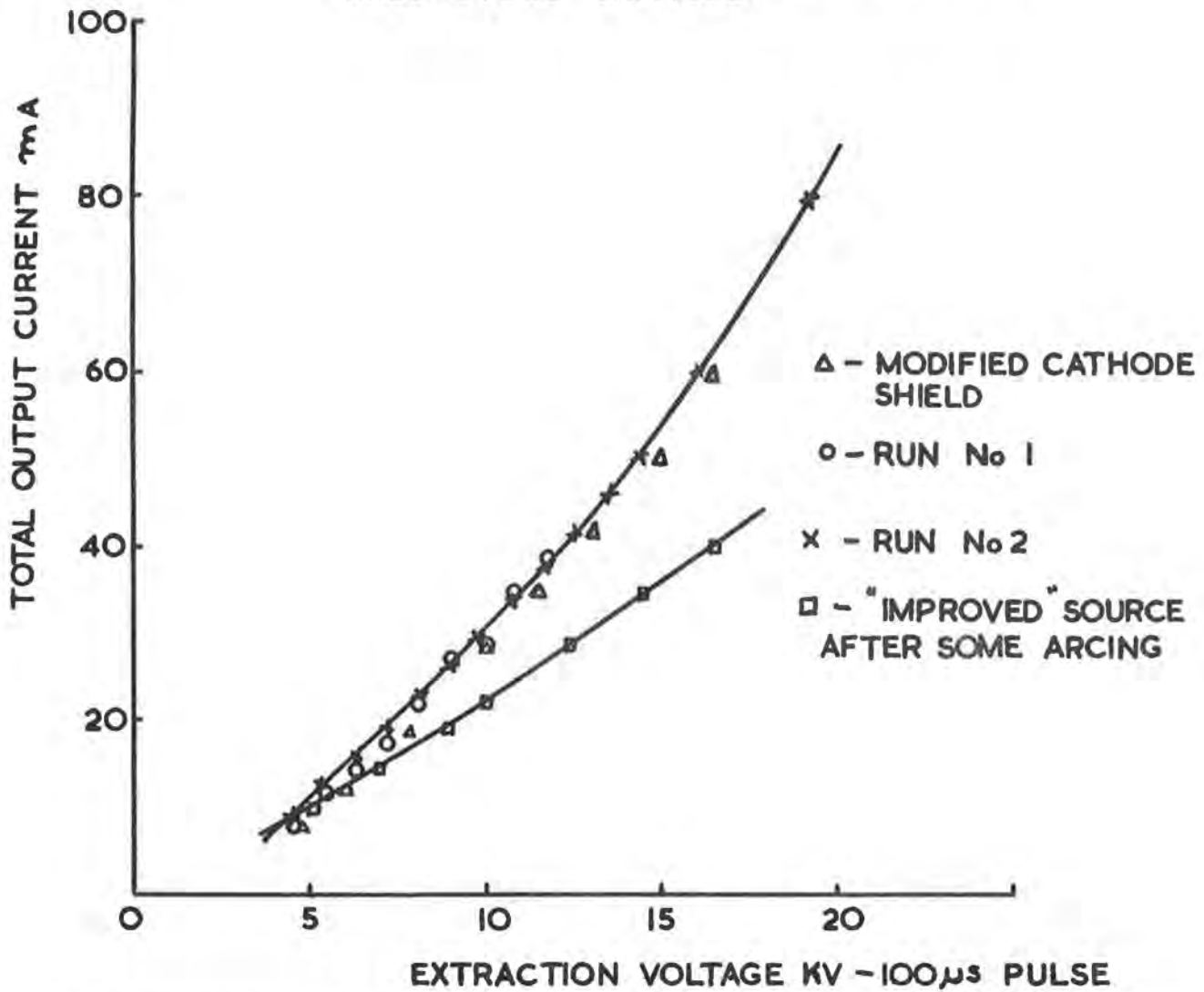


Fig. 3.3.1(ii) Plot of Ion Source Output Current against Extraction Voltage.

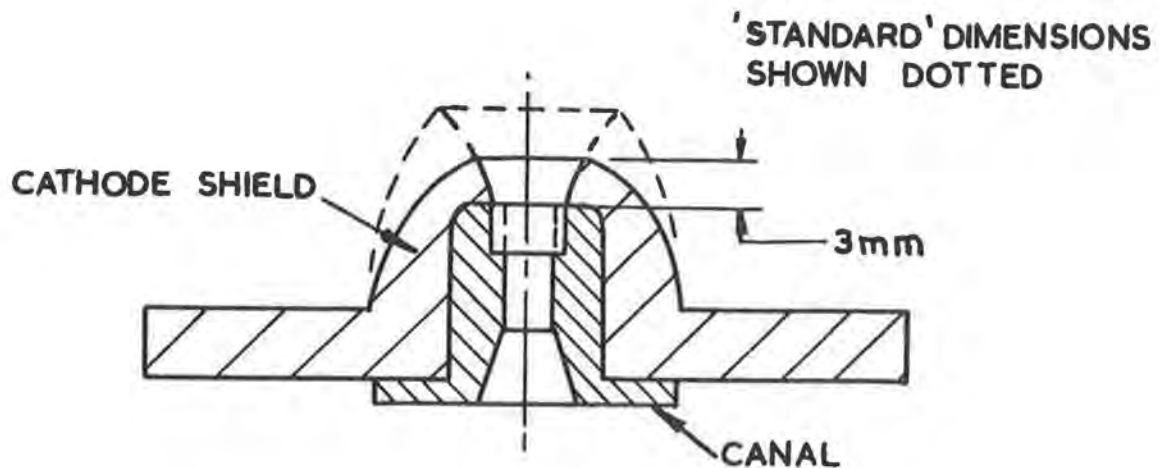


Fig. 3.3.1(iii) Ion Source Short Cathode Shield.

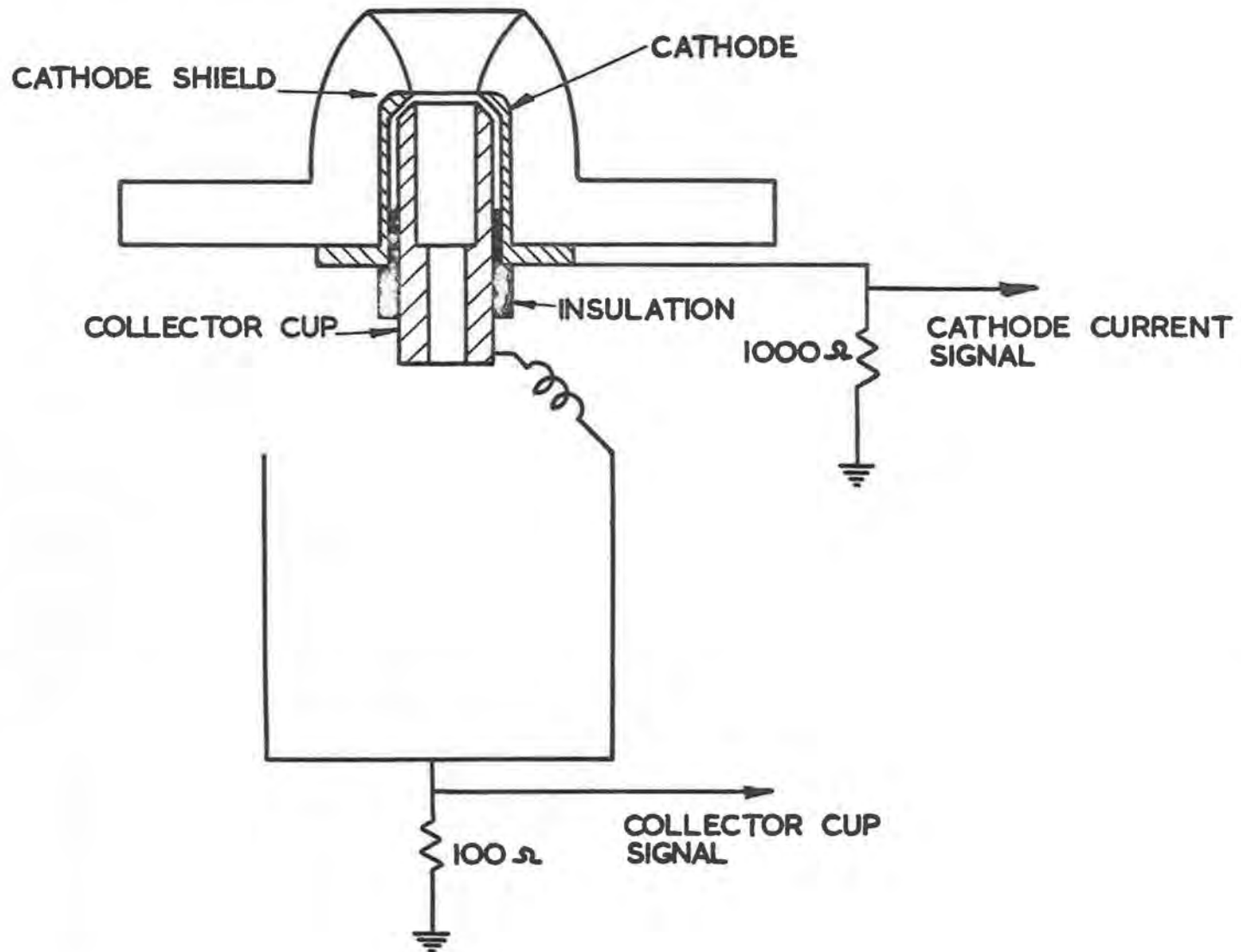


Fig. 3.3.1(iv) Measurement of Total Ion Current drawn from Plasma.

rapid deterioration of the source. In practice if arcing sets in, it almost always ceases if the r.f. power level is reduced.

R.F. Coupling Circuit

The simple circuit already described gives good results as far as matching is concerned but considerable variations in output current can occur if the actual orientation of the tuner, coil or mounting plate are changed. A better arrangement would probably be to enclose the whole source assembly and r.f. circuit in a copper box and this is at present being tried.

There is also some evidence, not very clear cut as yet, that the r.f. circuit may affect the arcing phenomenon. If the exciting coil is fed through two capacitors so as to be isolated from "earth" as far as the extraction voltage is concerned, the latter can be raised to higher values before arcing takes place. The arcing effect is so sensitive to impurities in the discharge, however, that it is difficult to be certain that changing the r.f. circuit was really significant.

Similar effects have been reported by Tallgren at CERN (6).

Extraction Geometry

The perveance of the extraction system actually observed on the machine is about $3.5 \times 10^{-8} \text{ A/(V)}^{3/2}$ which is considerably higher than would be expected from the theory of Pierce (7). This suggests that the position of the plasma boundary is not at the end of the cathode shield, but much closer to the cathode. A second observation supports this view. A special Pyrex shield was made in which the distance between the cathode and the top of the shield was reduced from 6 mm to 3 mm as shown in Fig. 3.3.1(iii) and the total output current remained the same as with a standard shield.

An experiment was set up to measure the total ion current crossing the plasma boundary (Fig. 3.3.1(iv)). The current to the cathode could be measured separately from the current to the collector cup. No effective suppression of secondary electrons could be incorporated so the actual currents recorded are not true ion currents, nevertheless it was found that a current of 500 mA could easily be recorded on the collector cup, with negligible current to the cathode, at an extraction voltage of a few kV.

Thus it seems that ion currents of a few hundred mA can easily be drawn from the plasma. The reason that this current does not appear as useful beam may be that the initial focusing is very poor, the shape of the plasma boundary being far different from the sphere usually assumed.

An interesting effect was the sudden increase in current to the collector cup from 200 mA to 500 mA at a certain r.f. power level. These currents were consistent with the mean current drawn from the extraction power supply, allowing for the duty cycle.

(c) Emittance Measurements

Early, rough measurements of the emittance of the 600 keV beam were done with a "pepper pot" technique; a plate with an array of 1 mm diameter holes was placed in the beam and the resulting image observed on a screen. A few measurements were

made by allowing the beam transmitted by the pepper pot to fall on a copper plate coated with MnO . This was too slow a method, although a clear image could be obtained with a few beam pulses and even a single pulse produced a visible image. Later a quartz screen was used together with a polaroid camera for quick results. The emittance was found to be between 2 and 5 mrad cm for most conditions.

An interesting feature of these measurements was the complexity of the images which could be obtained. Sometimes two or more distinct 'spots' could be seen corresponding to a single pin hole in the pepper pot plate. When a transverse magnetic field was applied (downstream from the pepper pot) the separate 'spots' were deflected equally and resolved into ions of different mass in the same way showing that each spot contained ions of all species.

Later, a much more detailed measurement was performed using two remotely controlled, 4 jaw apertures. The upstream box was set to a 1 mm^2 aperture and for each radial position of this the transmitted beam was scanned by a 1 mm slit in the downstream 4 jaw aperture. The current through this slit was measured by a collector plate having a transverse magnetic field to suppress secondary electrons. Thus a curve of current distribution, in the divergence co-ordinate was found for each radial co-ordinate. Fig. 3.3.1(v) and Fig. 3.3.1(vi) show emittance diagrams for the vertical and horizontal planes.

It is clear that the current distribution in phase space is by no means uniform and that most of the beam is in a smaller phase space area than the 'total' emittance. The emittance boundaries shown in Fig. 3.3.1(v) and Fig. 3.3.1(vi) were obtained by drawing through the points on the current distribution curves at which the current had fallen to 5% of the total.

Some of the current distribution curves have double peaks. A rough mass analysis of the beam downstream from the first 4 jaw aperture showed that the larger peak was made up of protons while the smaller one was due to molecular ions. Thus it seems that the 'double peak' effect is different from the 'double spot' effect mentioned above. The molecular ions may have been separated out by a triplet quadrupole which was used in the experiment.

(d) Proton Percentage

The proton percentage measured in the centre of the 600 keV beam is about 85% with a good source. When the source has been contaminated the percentage has fallen to below 50% and on one source assembly, which had a vacuum leak, the proton percentage was only 40% while about a third of the beam was made up of heavy ions, probably oxygen and nitrogen.

3.3.2. Ion Column

The construction of the column is closely similar to that described in (8), with the electrodes made in stainless steel rather than aluminium. The focusing electrodes are as shown in Fig. 3.3.2(i).

It is pumped by a mercury diffusion pump with a refrigerated chevron baffle and liquid nitrogen cold trap. The normal base pressure measured on an untrapped ion gauge is about 5×10^{-6} torr. With the source in operation this rises to about 2×10^{-5} torr.

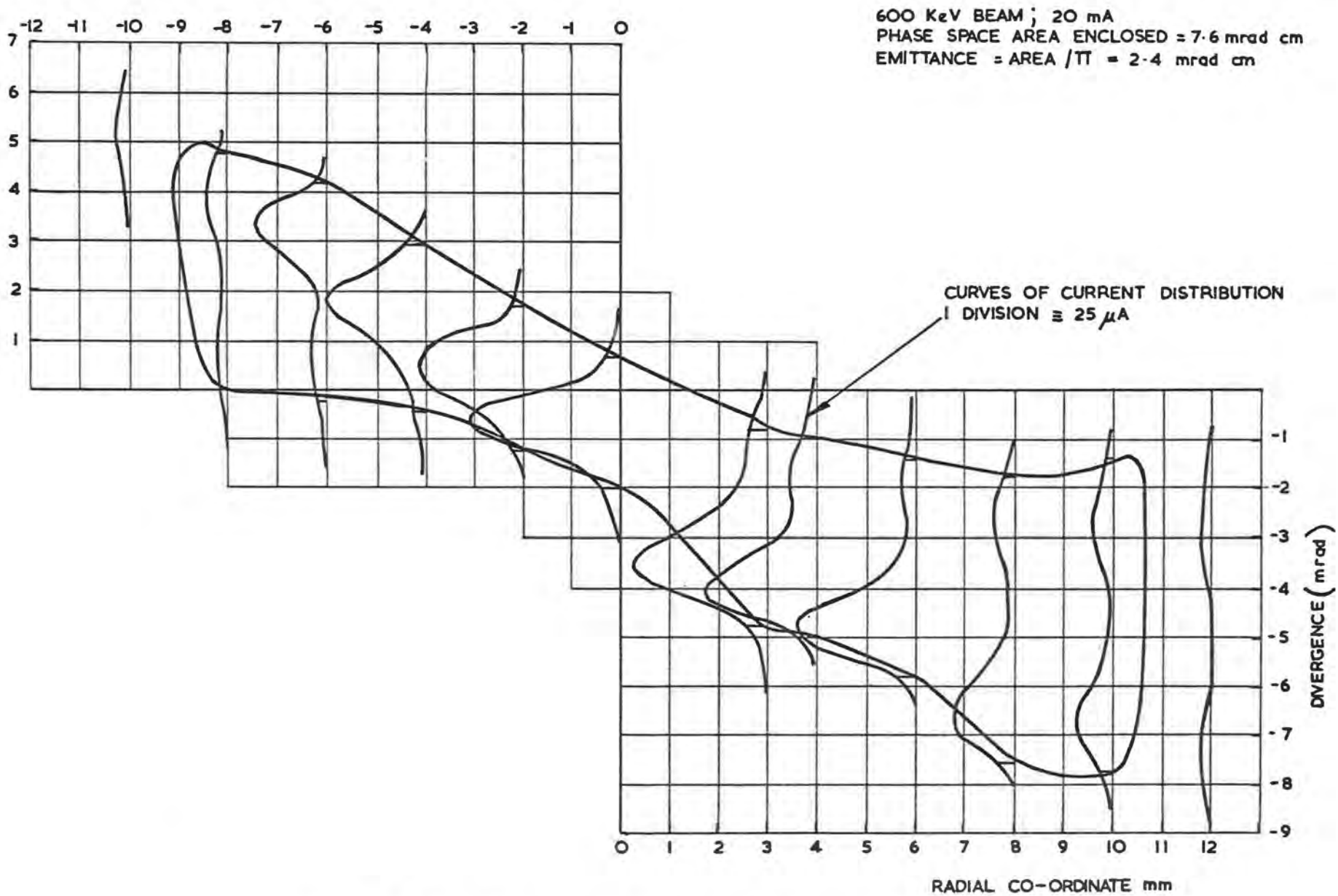


Fig. 3.3.1(v) Phase Space Diagram; Horizontal Plane.

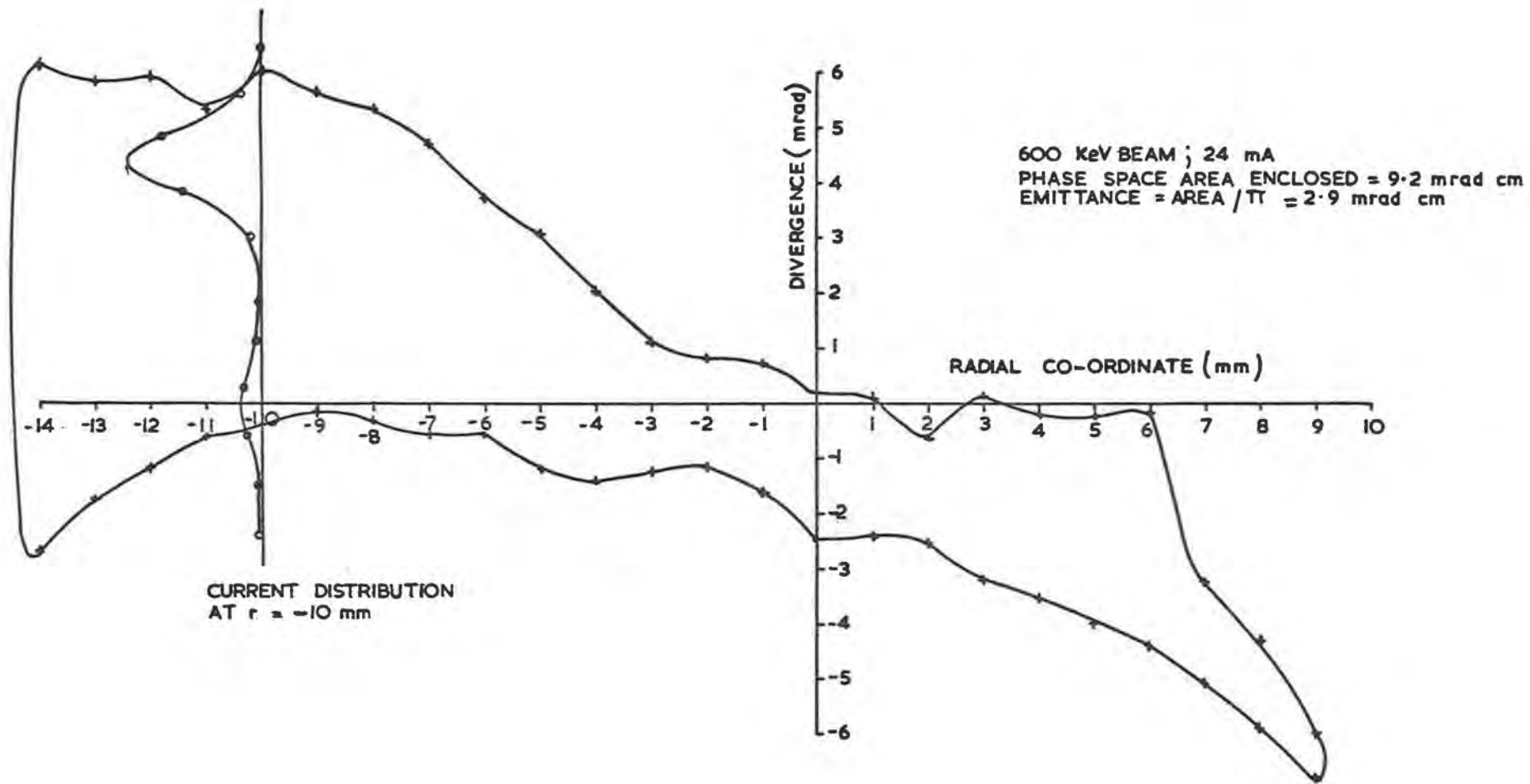


Fig. 3.3.1(vi) Phase Space Diagram: Vertical Plane.

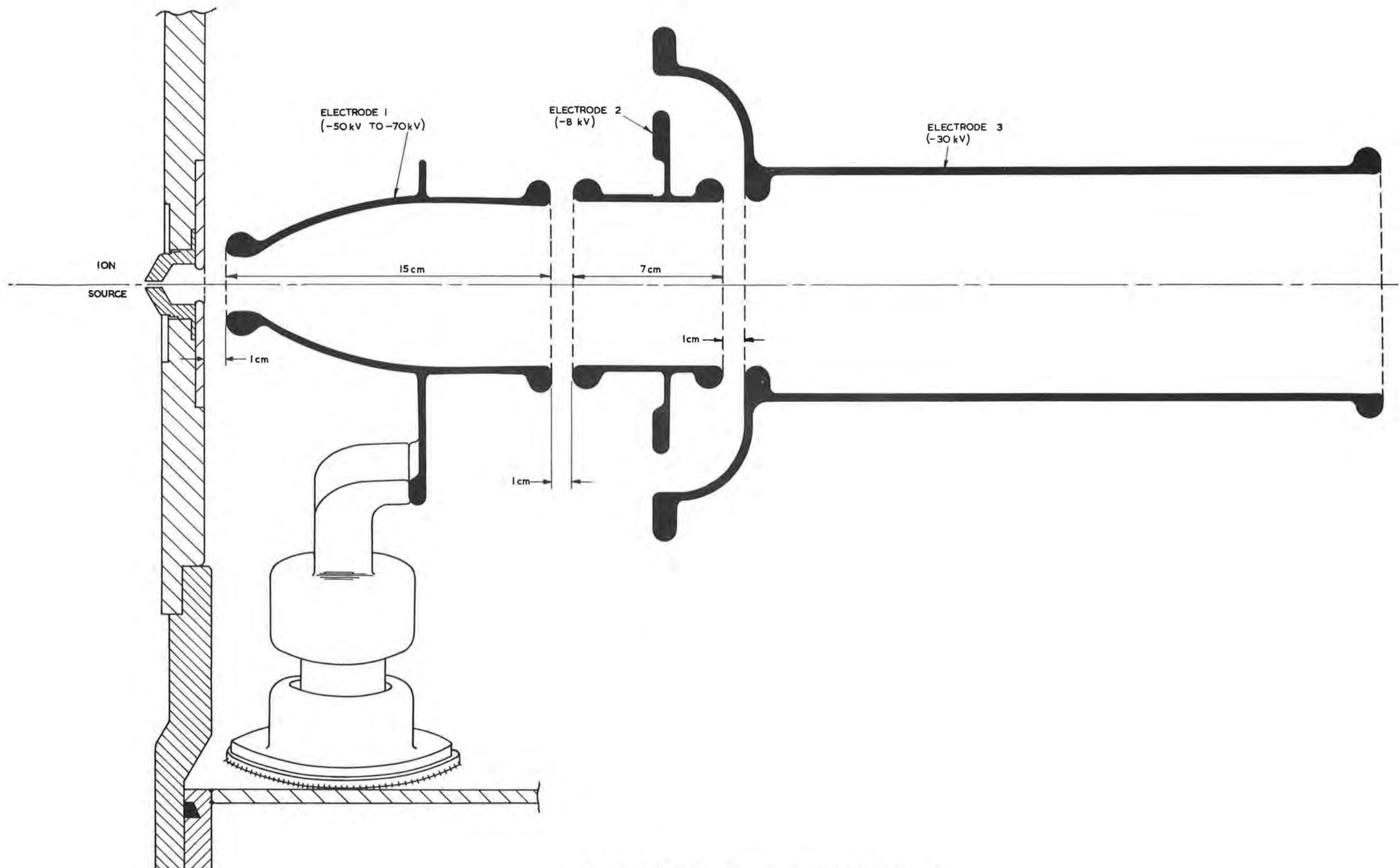


Fig. 3.3.2(i) Ion Column Focusing Electrodes.

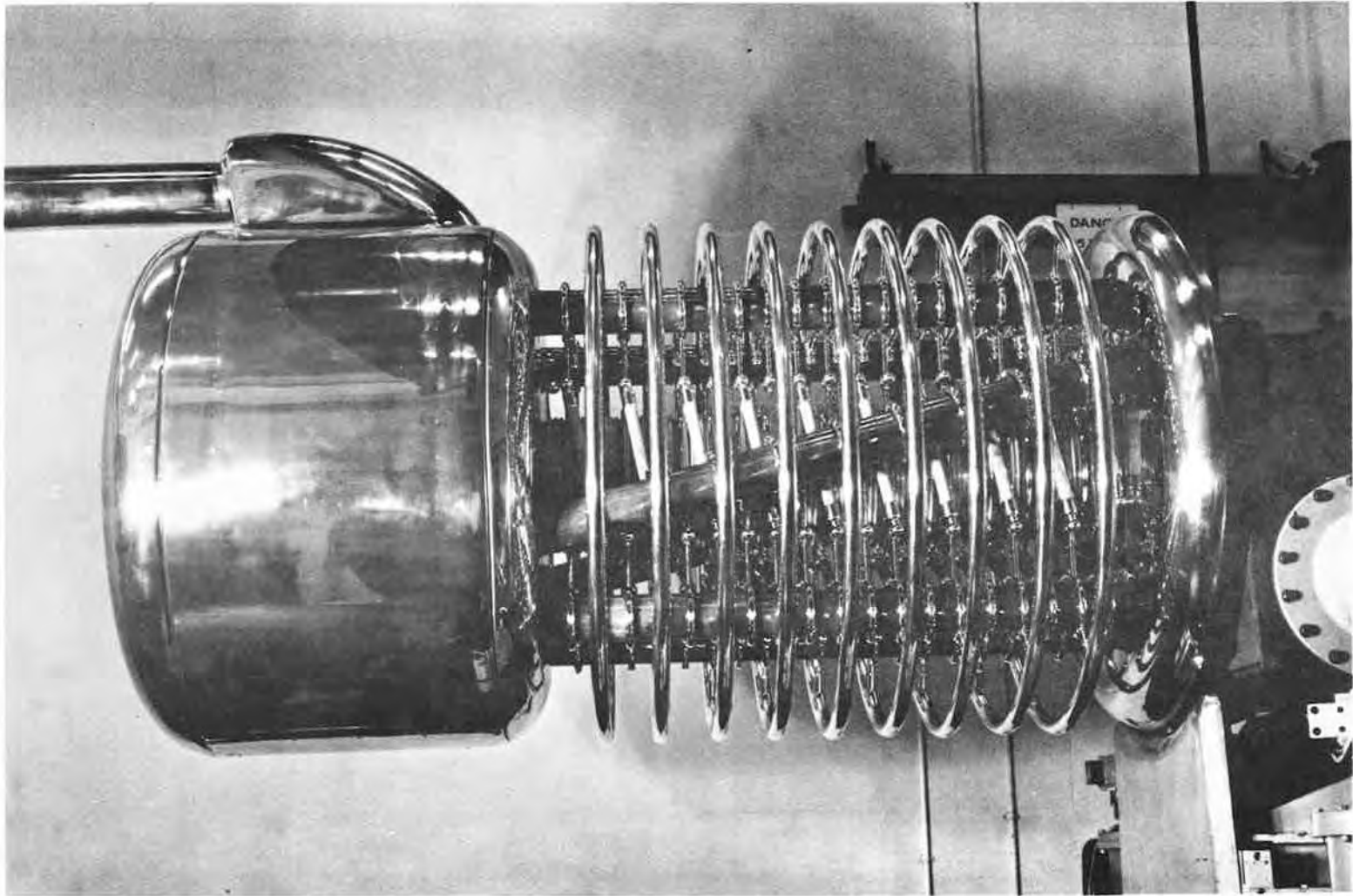


Fig. 3.3.2(ii) View of the Ion Column.

The initial conditioning of the column was a tedious process spread over about two weeks but no trouble is experienced at the present time. When the column has been let up to atmospheric pressure, to change a source unit for example, 600 kV can be applied without trouble immediately after pumping down.

When beams of 20-30 mA at pulse lengths of about 100 μ s are being accelerated, the X-ray production, indicated by a type 1349 hand monitor, is less than 2 mr/h at the nearest point to the column outside the safety screen. With beam currents of about 50 mA for pulse lengths of 1 ms the X-ray level rises sharply to over 50 mr/h.

A large cylindrical electrode in the pumping manifold is biased to -500 V to suppress secondary electrons. No trouble is experienced with 100 μ s pulses, but with higher intensity beams of 1 ms pulse length the column requires an additional chain of 1500 pF capacitors to stabilise the electrode potentials. No extended running has yet been done with long beam pulses.

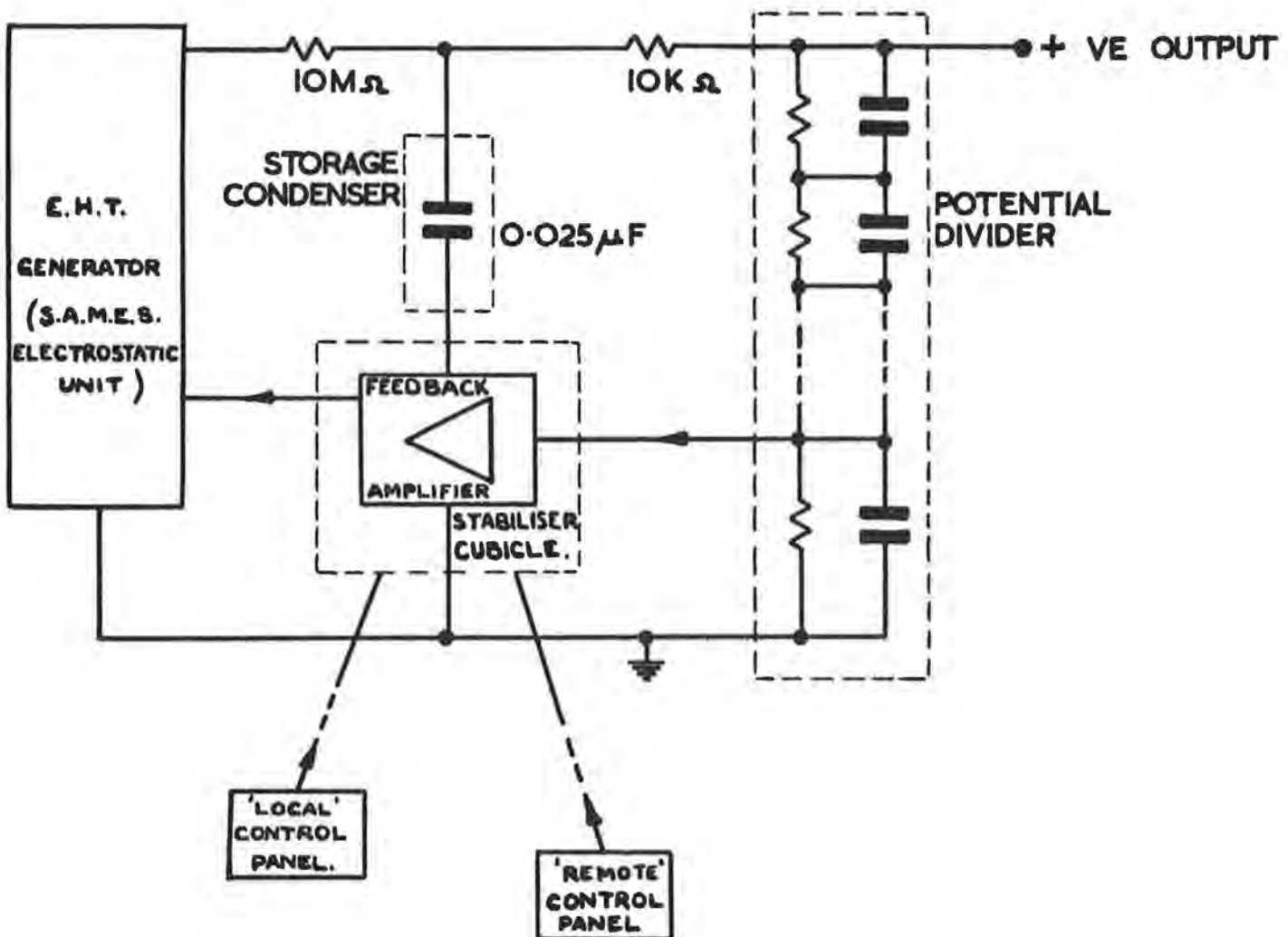


Fig. 3.3.3(i) Schematic Diagram of 600kV DC Supply System.

3.3.3. Ion Column Power Supply

(a) Present System

The requirement was to provide a 650 kV maximum positive polarity output, 4 mA maximum mean D.C. supply capable of remote control. With pulse current loading up to a maximum of 200 mA, 2 ms pulsed at 2 pulses/s, the output voltage was to be within ± 1.5 kV during pulses.

The equipment consists of an electrostatic generator whose output is connected to a 25 nF storage condenser via a charging and surge protecting resistor. The value of this resistor has been changed from an initial 3.5 M Ω to 10 M Ω (Fig. 3.3.3(i)). Connection to the H.T. platform, which houses the focusing and ion source supplies, and to the d.c. accelerator column, is via a 10 K Ω discharge current limiting resistor designed and manufactured locally. The final output voltage is measured by a resistance-capacitance divider connected to the H.T. platform and situated immediately underneath it. The low potential end of the divider is returned to a variable stabilised reference voltage for control of the output voltage. The divider tapping point feeds a wide band d.c. feedback amplifier. The output of the feedback amplifier is connected to the earthy terminal of the 25 nF storage condenser to give fast correction, and to the excitation system of the electrostatic generator to give slow correction and mean output level control.

(b) Operational Experience

The equipment was delivered and installed in April/May 1959. The high voltage generator although working satisfactorily at 600 kV does not at present provide an adequate safety margin and is therefore still under development. The latest generator (installed October, 1962) has delivered 675 kV generator terminal voltage at 4 mA loading on test.

Performance of the stabilising system has been generally satisfactory; re-design of the output stages of the amplifier (a voltage amplifier driving a cathode follower connected to the storage condenser) is in hand. 4PR60A valves are being replaced by type 4PR250C valves which have higher power dissipation and anode voltage capability. Exhaustive measurements of stability have not yet been done but indirect observations, for example during E.H.T. voltage calibration tests and during linac commissioning, indicate that it is adequate.

3.3.4. Focusing and Ion Source Power Supplies

(a) Present arrangement and Operational Experience

With one minor exception (ion source c.w.r.f. 'keep-alive' supply) the supplies are housed on the H.T. platform: Output leads to the ion source and the lens system are run in an alloy tube connecting the platform to the ion source and accelerator column. Mains supplies of 115 V, 2000 c/s single phase, 220 V, 50 c/s three phase and 24 V d.c. (control circuit use) are generated locally on the platform.

The platform is insulated from ground by four 18 in diameter paxolin tubes which also provide mechanical support. The tubes house respectively:-

- i) Insulating shaft drive from a motor at earth potential for the platform generators,

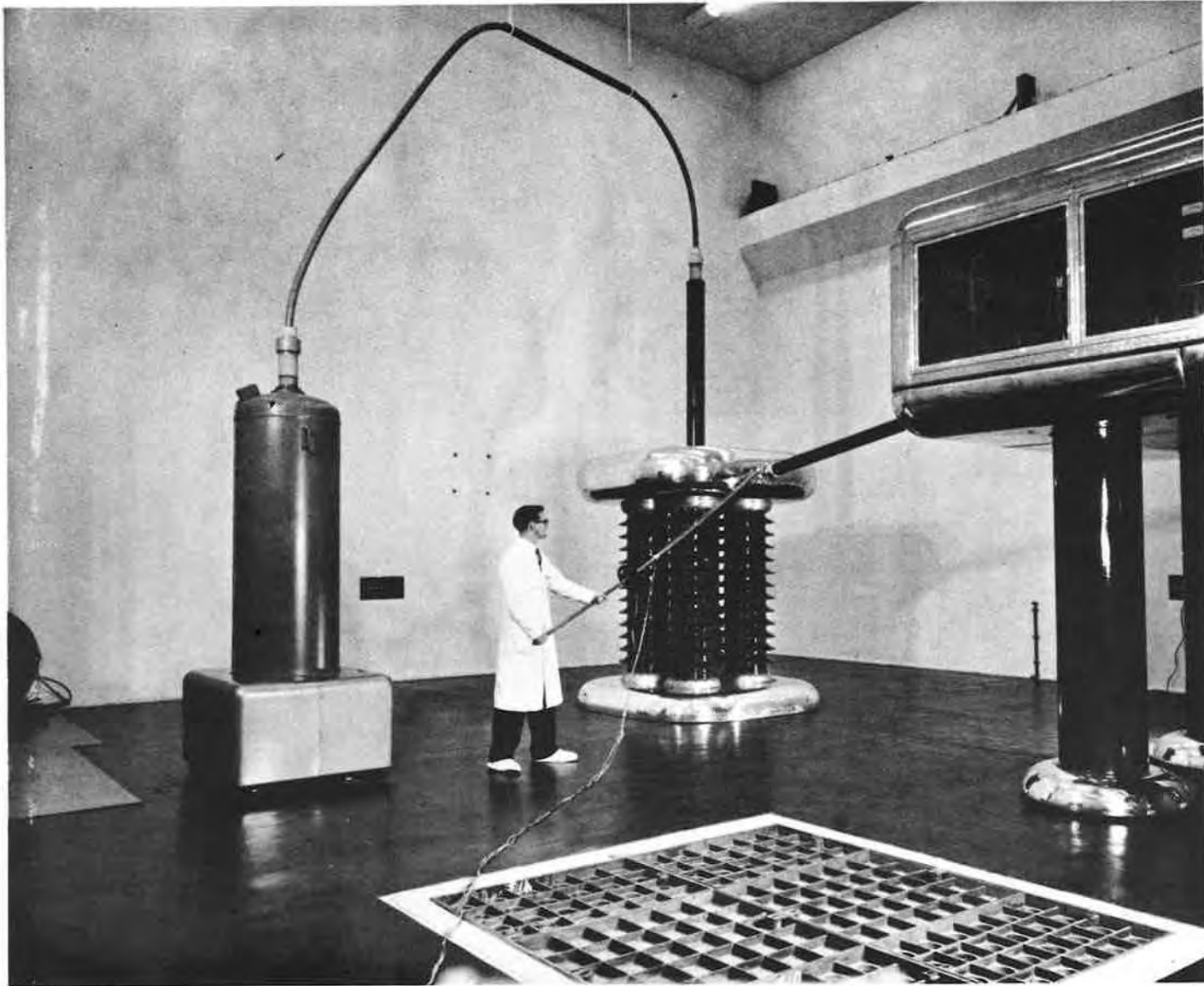


Fig. 3.3.3(ii) View of E. H. T. Generator, Condenser and H. T. Platform.

- ii) Four 1 in dia. perspex rod light guides for timing pulse control and pulse monitoring,
- iii) Polythene tubes for filtered cooling air which is piped to the major units on the platform,
- iv) P.V.C. tubes carrying compressed air which is used for operation of air switches providing unit ON/OFF and signal back circuits; ten paxolin tube rotary drives for Variacs and potentiometers controlling unit output levels. There is also P.V.C. tubing carrying compressed air for ion source cooling and insulation, and polythene tubing for the ion source hydrogen feed. Terminal equipment is housed in a cellar immediately under the platform support legs.

The platform units are as follows:-

R.F. Unit - a pulsed r.f. supply; frequency 125 Mc/s nominal; pulse length 2 ms; output power 10-15 kW into 50 Ω ; 2 pulses/s maximum.

This was designed within the group and uses an ACT 25 triode in a co-axial cavity driving an ACT 28 triode output stage also using a co-axial cavity. Both valves are anode modulated by pulses from a delay modulator using a 5C22 thyatron switch. The variable H.T. supply for the modulator is a voltage doubler using a 250 TH triode valve as the second rectifier. This valve is cut off during and immediately after the output pulse by a signal derived from the output pulse.

Reliability has been generally very good; the output power was increased appreciably above the original level by improving the match between the oscillator/driver and output valves and by altering the delay line impedance. The impedance change used existing components with a consequent reduction in pulse length of 1.2 ms; a line of correct length and impedance is to be provided.

Extraction Unit - a pulsed positive polarity supply; output variable from 1 to 25 kV; pulse length variable from 50 μ s to 2 ms; 2 pulses/s maximum. Maximum output pulse current is 250 mA. Stability during the pulse is better than 0.25% at maximum loading.

The circuit uses a series selected CV2416 valve as the main element in a feedback loop operating only during the pulse period, the reference voltage and feedback amplifier being at the output potential. The series CV2416 valve also acts as a pulse switch using a CRT-photomultiplier light link for isolation from local ground.

During initial commissioning considerable trouble was experienced with pick-up from the r.f. unit causing incorrect output pulses. This was eventually solved by the use of clipping and limiting circuits in the light link switching circuit and by fitting a photo-multiplier valve combination in place of the photo-transistor/transistor circuit. A replacement/spare unit is being developed using similar principles but with two 4PR250C valves. One serves as the series control element; the other acts from ground as the output valve of the feedback amplifier/switch circuits, dispensing with the need for a light link and enabling reference and amplifier circuits to be at local ground level.

Gas Unit - provides a variable 2000 c/s continuous supply to the nickel leak controlling the hydrogen input to the ion source. Maximum output is 20 V r.m.s.,

normal working being some 6 V r.m.s., 4 A; the supply is not specifically stabilised.

P.I.G. Unit - functions so as to switch off all other platform units if the pressure in the column, as monitored by an ion gauge head on the ion column, exceeds a pre-determined level (normally 5×10^{-5} torr).

The gas unit and the PIG unit are housed in the same chassis and the units are similar to those previously used at the Laboratory on the 50 MeV proton linear accelerator. They have been completely reliable.

Light Receiver/Transmitter Pulse Unit - Initially, a unit using a photo transistor with transistor amplifiers was installed; due to its sensitivity to r.f. radiation from the r.f. unit and to thermal variations it was replaced by a photo-multiplier/valve circuit. This circuit is currently being superseded by a more sophisticated photo-multiplier/transistor combination.

Initial trials of this latest unit have shown that to a lesser extent it is susceptible to the same defects. It is now being modified so that where possible only high level signals are used at the platform end of the link, lower level signal processing being done at ground level.

The 'temporary' valve circuit provides two outputs - a 20 V, 20 μ s, trigger pulse for firing the r.f. unit modulator and a 20 V pulse for gating the extraction unit output pulse. The relative timing of these two pulses is variable at ground level.

The system now being installed will provide the following facilities:-

Ground to Platform - two channels (one standby) for transmission of r.f. unit trigger and extraction unit gate (20 μ s to 2.5 ms) pulses; relative timing and duration of extraction gate pulse is variable in the control room. A facility is provided for control of two extraction pulses (pilot and short) for use in injection studies. A current modulated light discharge source is used as transmitter and a photo-multiplier as receiver. Overall timing jitter is 0.1 μ s.

Platform to Ground - for monitoring purposes, two channels are available for transmission of voltage pulses from platform equipment to the control room; pulse widths of 2 μ s to 2 ms and amplitudes of ± 100 mV to ± 10 V can be handled, a standard amplitude calibrating pulse is fed in separately. Light transmission and reception is similar to that above.

High Voltage Focus Units - Output is continuously variable from 20 to 125 kV negative to local earth; maximum mean current is 300 μ A; maximum pulsed current loading is 150 mA, 2 ms pulses. The stability of output during pulses is $\pm 0.25\%$ against input and output variations.

There are two identical units of this type using electrostatic generators. The stabilisation and control systems are similar to those of the 650 kV set. The charging resistor is 7 M Ω , storage condenser 25 nF and discharge limiting resistor 5 K Ω . Fast correction is to the earthy terminal of the condenser, the normally negative going signal being obtained from the anode of a 4PR60A valve.

Initially, the multi-stage rectifier sub-unit, which provides excitation for the electrostatic generator, proved unreliable in its 2000 c/s version. It was redesigned and has since given no trouble.

R.F. pick-up also caused appreciable variation of the output voltage during the pulse. This was cured by fitting an r.f. by-pass condenser directly from grid to cathode of the first stage of the feedback amplifier. Some failures have occurred in inter-electrode insulation on the 4PR60A valves and also with one particular relay.

Low Voltage Focus Unit - A temporary unit was originally installed to determine the requirements for a final supply; this unit is still in use and is an unstabilised negative supply variable up to 10 kV maximum.

At present there is no intention to replace it by a more refined stabilised unit as its behaviour has been satisfactory.

Keep-Alive R.F. Supply - This is situated adjacent to the ion source in the 'bun' on the end of the accelerator column. It is a twin tetrode oscillator giving a c.w. output of a few watts at a frequency of 70-80 Mc/s, coupling to the source via single turn loops around the source hydrogen feed pipe. Its function is to provide a low level continuous discharge to ensure reliable ionisation by the main r.f. pulse.

The unit has given no trouble.

3.4. Linac

3.4.1. Linac Design

The r.f. design of the linear accelerator cavity was strongly influenced by the requirement that the drift tubes, of the Alvarez structure, should contain quadrupole magnets. R.F. defocusing forces dependent on operating frequency, acceleration rate and accepted beam radius, were balanced against the maximum attainable field gradient of a practical quadrupole that can be contained within a drift tube shell. On this basis, the minimum diameter for the drift tubes and the operating frequency, for a given acceleration rate, were determined. Also, in order to utilise the maximum axial length for each quadrupole magnet, drift tubes of a squarish cross section and small gaps between drift tubes, were desirable features.

Published data on re-entrant unit cell cavities (9) supplemented by some exploratory model cavity measurements, was used as the basis for the r.f. design. The chosen system employs constant drift tube and constant cavity diameters with the resonant frequency maintained by an increasing gap to unit cell length ratio. A useful reduction in this ratio at the high energy end of the linac is achieved by allowing a smooth change in the drift tube profile radius along the machine.

The final resonant dimensions were determined by precision model cavity measurements at a model frequency of 1000 Mc/s. (10). The resonant dimensional data was reduced to an algebraic form in which all dimensions were expressed as functions of unit cell length, such that it could be used in the computer programme which computed axial field distributions and the synchronous particle motion (3).

Some of the main r.f. parameters are given in Table 3.4.1(I)

TABLE 3.4.1(I): LINAC CAVITY PARAMETERS

Input energy	600 keV
Output energy	14.9 MeV
Resonant Frequency	115 Mc/s
Cavity length	13.45 m
Cavity diameter (nominal)	1.6945 m
Number of unit cells	49
Drift tube diameter	28.15 cm
D.T. profile radius	3.660 to 6.579 cm
D.T. aperture diameter	2.106 to 4.948 cm
Aperture profile radius	1.27 cm
Unit cell length	9.638 to 45.527 cm
Gap length	1.868 to 13.311 cm
Support stem diameter	4.445 cm
Theoretical Q factor	108,000
Measured Q factor	80,000
Calculated power required for 30° synchronous phase angle at the measured Q	802 kW
Frequency tuner range	± 23 kc/s
Flattener tuner range	± 300 kc/s
End to end field tilt range of tilt tuners	± 20%

3.4.2. Linac Construction

The linac cavity is fabricated from $\frac{1}{8}$ in thick rolled and welded copper sheet, riveted to a stainless steel framework of rings and longitudinal members. It is supported by four legs on the base of a separate mild steel vacuum vessel. Fig. 3.4.2(i) is a view of the linac with the vacuum vessel raised.

Tuning plates are situated in rectangular cut-outs in the cavity wall and are connected to the wall by convoluted flexible copper foil. There are four such frequency tuners which can be operated by push rods passing through the vacuum vessel. Two similar tuning plates are positioned one at each end of the cavity and are used for producing a tilt in the field gradient along the cavity. Two flattener tuners are used to correct for manufacturing errors in the resonant dimensions. Each of these is a continuous convoluted flexible plate, running from end to end of the cavity, with the longitudinal edges soldered to the inside surface of the cavity wall. They can be distorted locally by movement of a number of backing plates.

Two large rectangular cut-outs in the cavity wall form hatches for access to the inside of the cavity which can be blanked off by cover plates using garter spring r.f. joints to the cavity. There are some 350 uniformly distributed $\frac{3}{4}$ in by 5 in pumping slots in the cavity wall and 24 longitudinal water pipes are soldered to the wall to provide cooling and temperature stabilisation.

Each drift tube shell is constructed from a pair of machined copper spinings, joined by a circumferential weld, with an axial tube, which forms the aperture, soft soldered in position at each end. The shell is located on the quadrupole magnet, which in turn is supported by a horizontal and a vertical stem. The end fittings of the stems are carried on the cavity framework and designed to allow alignment of the drift tube in all degrees of freedom. The support stems are sheathed with thin copper tubes, soft soldered into the drift tube shell, and r.f. contact is made between them and the cavity wall via flexible gaters and garter spring joints. A rough vacuum is maintained in the drift tube shells by pumping on the vertical stem. This stem also carries shell water cooling pipes. The horizontal stem carries the quadrupole conductor pipes. The arrangement can be seen in Fig. 3.4.2(ii).

3.4.3. Installation and Operational Experience

Drift tube alignment

The use of quadrupole strong focusing for the linac demanded very accurate alignment of drift tubes on to the axis. This alignment was carried out using a telescope, mounted from the cavity output end face, which could be set on to the line of sight between targets in the input and output end half drift tubes. Alignment was then by viewing targets in the input and output end of each drift tube bore. The targets were of metal having spark eroded V forms to which the telescope cross hairs could be set. A separate target plug was required for each drift tube because of their varying bore diameters. Alignment of the ends of each drift tube was to ± 0.003 in in each plane and the mean of the measured misalignments of the two ends was less than ± 0.002 in in each plane. The misalignment between magnetic and mechanical axes was previously determined and allowed for in the alignment process. (Errors due to all other sources were estimated to be less than ± 0.002 in).

Longitudinal positioning of drift tubes was carried out using a telescope set up on a line of sight external to the cavity and parallel to its axis. This telescope was fitted with a 45° prism so that it could view drift tube faces through appropriate pumping slots, and was mounted on special rails running the length of the cavity. Distances from the input end face of the cavity were measured by referring the telescope position to a calibrated stainless steel tape. With corrections being applied for manufacturing errors in drift tube lengths and for the tolerance error in the overall cavity length allowed in manufacture, the accuracy of drift tube positioning varied between ± 0.002 in at the input end to ± 0.004 in at the output end of the linac.

Field Flattening

The distribution of axial electric field along the length of the cavity was measured by the frequency perturbation technique. The linac was designed to operate with a flat field, that is, all sections of the cavity tuned to the same resonant frequency to give gap voltages directly proportional to unit cell lengths. Since

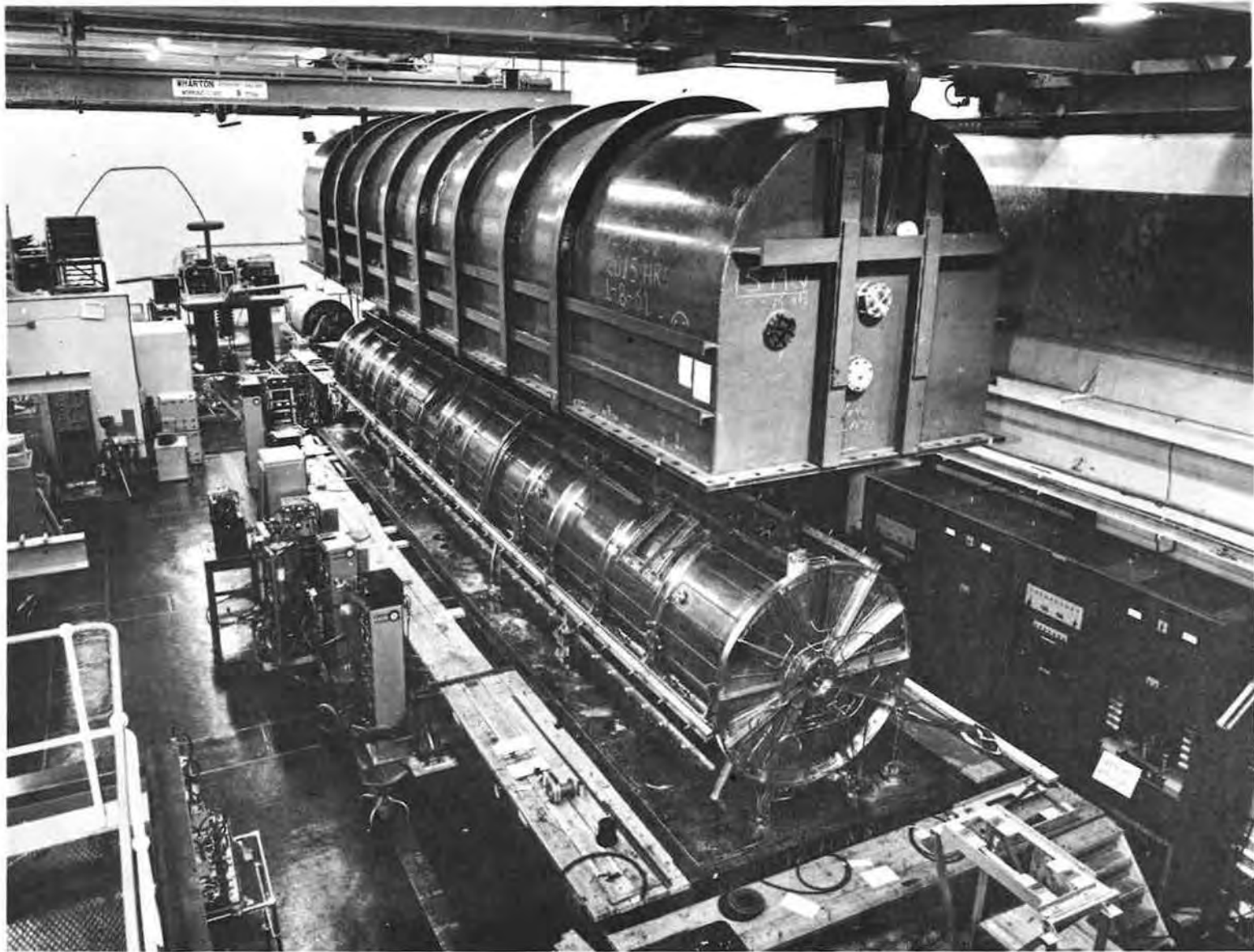


Fig. 3.4.2(i) View of the Linac with the Vacuum Lid raised.

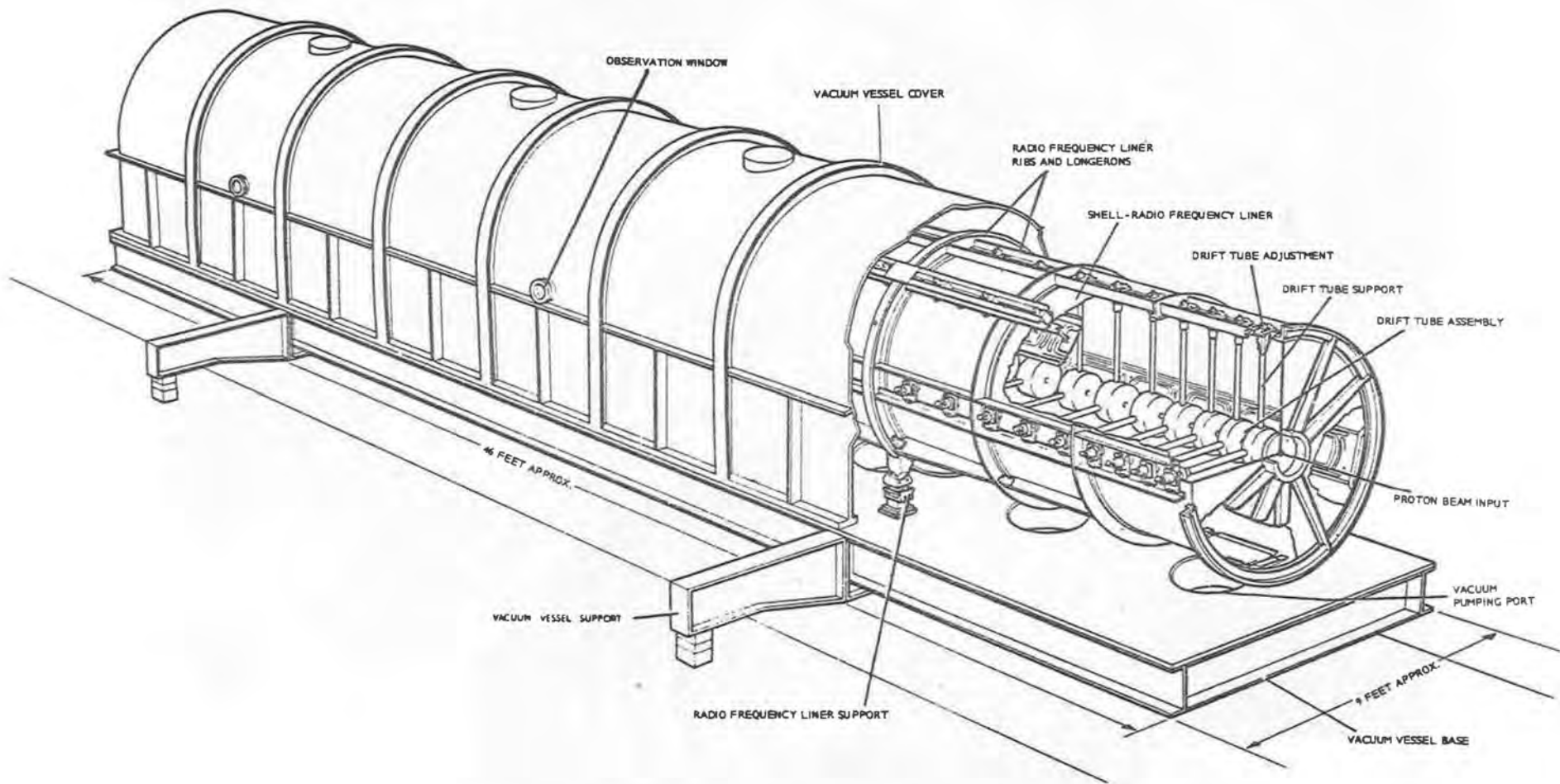


Fig. 3.4.2(ii) Cutaway view of Linac.

the field distribution across each gap was known the mid-gap fields only had to be measured.

A metal sphere of 0.4 in diameter, supported on a nylon cord, was used as the perturbing body, with the cavity excited by a lock-in oscillator. Frequency perturbations of about 100 c/s in 115 Mc/s were measured by a digital frequency meter. In the short gaps at the input end of the linac the sphere was too large in relation to the curvature of the field, and measurements were taken with a sphere placed off axis between the flat faces of the drift tubes. The two methods of measurement were overlapped at a suitable point along the cavity.

The axial electric field was related to the magnet field at the cavity wall, also measured by frequency perturbation using a flat metal plate placed through pumping slots, and in the final stages of the field flattening procedure it was only necessary to measure this magnetic field distribution. The electrical length of the cavity is comparatively short and it was an easy matter to adjust the flattener tuners to give a field flatness of $\pm 1\%$.

R.F. Operation

The first attempt to feed the linac with high r.f. power was made on 1st July 1961 and the first 15 MeV beam was produced on 1st August 1961. Operation in the early months was severely affected by multipactor discharges, the effect of which was to prevent the cavity fields from rising above a very low level. Multipactoring usually occurred on over 20% of all pulses at a pulse repetition frequency of 1 pulse/8s, and the multipactor rate rose sharply as the pulse repetition frequency was increased.

Several methods to overcome multipactoring were tried in addition to careful cleaning of all drift tube surfaces. It has been observed on other machines that the drift tube surfaces become conditioned against multipactoring as the machine is run for a period of time. Accordingly the linac was operated at different pulse rates and under various conditions for long periods, but no tendency to condition was observed. Also, the rate of rise of r.f. drive power to the final amplifier was increased greatly in an attempt to drive through the multipactor level as rapidly as possible. The rise time of the r.f. field in the anode circuit of the final amplifier was reduced to as low as 2 μ s without improving the multipactor breakthrough rate. It is believed that this particular failure may be explained by the existence of a glow discharge, seen at the r.f. feed vacuum window, providing a copious supply of primary electrons.

It was observed that, after only a few hours of multipactoring, the drift tube faces became coated with visible films, the pattern formed being strongly influenced by the quadrupole fringe fields. The secondary emission coefficient of the deposited film therefore determined subsequent multipactoring. Laboratory experiments have since shown that bombardment of a surface by electrons in the presence of oil vapour can produce a carbonised film with a low secondary emission coefficient. The linac vacuum system, however, is thought to be particularly clean and free of oil vapour. The next approach was to provide an artificial film by coating the drift tube faces with a material of known low secondary emission coefficient. Colloidal graphite was unsuccessful, but a mixture of carbon black in alcohol applied to the surfaces by brush has eliminated the multipactoring.

In the first instance all drift tubes were coated in this way with the result that the short gaps at the input of the linac required many hours of spark

conditioning. There was also a considerable increase in X-ray production at high field levels. Subsequently these short gaps have been cleaned of carbon black without reintroduction of multipactoring. As time permits the effect of cleaning off further gaps will be tried, as it is believed that field emission of electrons from these surfaces is a significant source of r.f. power loss.

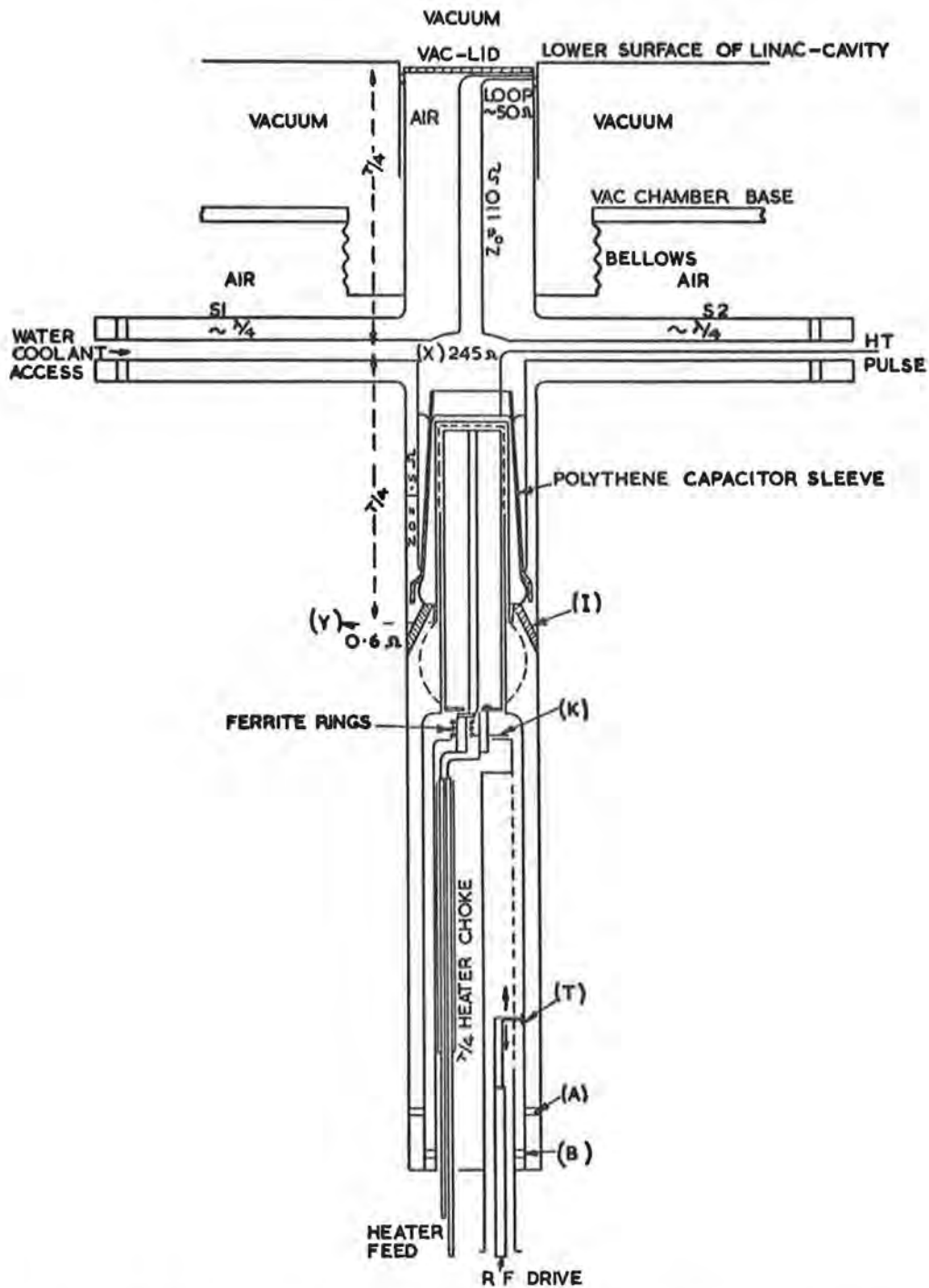


Fig. 3.4.4(i) Schematic Diagram of the RS 1041 Valve Circuit.

3.4.4. Linac R.F. Drive System

Design of Valve Circuit

The system was required to provide r.f. power of 1.5 MW in pulses of 2.5 ms at a repetition rate of up to 2 pulses/s maximum. Provision of this level of power at a frequency of 115 Mc/s, presented the problem of finding a valve (or valves) with suitable geometry, and a cathode equal to the unusually long pulse duration. The original intention, to use six E.E.Co type BW165 in some parallel - push pull arrangement, was abandoned when the use of one Siemens' type RS1041 was confidently advocated by the Siemens Labs.

This valve, designed for 30 Mc/s operation, has a geometry far from ideal for operation at 115 Mc/s in a co-axial type circuit, but its ability to meet the long pulse requirement made the circuit design a worth-while undertaking.

At the outset a decision was taken to couple the anode-circuit of the valve direct to a loop in the linac-cavity via an impedance transformer, and thus avoid the use of a matched coupling line with possible problems of breakdown during the mis-matched 'build-up' period in the cavity. This decision was the result of experience with a type BW165 valve, driving a cavity approximately equivalent to 2 unit cells of the linac. The r.f. arrangement used in this experiment differed considerably from the system designed for the RS1041, but the common factor was the use of direct coupling to the loop via an impedance transformer. The experimental rig performed satisfactorily both as a driven system and as a single valve self-oscillator, producing about 45 kW r.f. in the cavity. A further decision to isolate the anode system and cavity loop from the vacuum system, by the use of an insulating lid, determined in some degree the basic layout of the RS1041 circuit.

Figure 3.4.4(i) shows the circuit in schematic form approximately to scale. The considerable length of the RS1041 elements in relation to the external circuits has a major effect on the external circuit dimensions. This coupled with the design decisions mentioned, had to be arranged to provide impedance transformation from anode to cavity feed-loop, and tuning for resonance of grid-cathode circuit with impedance matching of drive-power input-line.

Anode-Grid Circuit - An anode impedance of $\sim 210 \Omega$ required matching to a loop impedance arbitrarily fixed at 50Ω . The 210Ω is, however, transformed by the long conductors within the valve to the low value of $\sim 0.6 \Omega$ at the output seal, (plus a reactive component which can be tuned out by the outer piston, (A)).

Direct transformation of 0.6Ω to 50Ω by a single quarter-wave section was not possible for various structural reasons, a minimum length of half-wave being unavoidable. The diameter of the valve anode with water-cooling jacket, and the necessary anode-blocking capacitor formed around it, dictated the minimum inner-conductor diameter for the first quarter wave section. Since the end of this section (point X) would be a voltage anti-node the impedance was kept to a value where the peak-voltage would be unlikely to cause troublesome sparking, particularly during mismatch conditions. Allowing some license in considering the geometry around the support insulator (I), the section (Y)-(X) is presumed to have a Z_0 of 12Ω making the impedance at (X) $\sim 245 \Omega$. From this point it was a simple matter to provide a 110Ω

transformer to match the loop impedance of 50Ω . Loop penetration and therefore impedance can be varied readily by raising or lowering the valve-circuit.

The main purpose of the stub-sections S1 and S2 is to provide access for the 30 kV HT pulse-lead from the modulator, and water-cooling to the anode jacket, but the position of the shorting-pistons in conjunction with piston (A) can be optimised for maximum power transfer to the linac-cavity.

Grid-Cathode Circuit - The internal valve-structure necessitates the use of a three quarter wave system, resonance being obtained by the adjustment of piston (B). Drive power is applied via a co-axial line and tapping (T) the setting of (B) and (T) being optimised to obtain input matching.

An unfortunate feature of the RS1041 is the 'two-pin' type heater-cathode connection; although the internal construction of the heater-cathode is co-axial, the axial symmetry is lost in bringing the connection through the seal. Only the pin connecting to the outer heater element is capacity coupled to the r.f. circuit at (K). Originally both pins were so coupled, but in this form the inner heater element is electrically half wave at twice the operating frequency, f , and there exists sufficient $2f$ component of cathode current, to excite a $2f$ resonance to the point of breakdown. The removal of the capacitor resulted in some breakdown in the gland previously occupied by the capacitor; this was eventually stopped when the 'dead' heater line was detuned by fitting a number of 'B' type ferrite rings around the heater pin.

The heater-supply busbars are fitted with a quarter-wave choke to restrict leakage of r.f. power into the power supply.

Operational Experience

Although the RS1041 amplifier has operated from the first trials with much the same performance figures, two major defects showed up after continued pulsing.

The anode-grid circuit piston quickly burned off the 'finger-strip' contact causing considerable erosion of the co-axial tubes. The finger-strip was redesigned and fitted, and no further trouble has been experienced.

More serious has been the breakdown of the polythene sleeve of the anode blocking-capacitor. Several sleeves have failed, in each case due to corona effects at the top end of the capacitor sleeve. A temporary solution has been found in the use of oil to fill the wedge shaped gap in this region. The design of the capacitor was known to be marginal and was limited in design by the size of polythene tube available at the time, but high-density polythene of adequate size is now manufactured, and a redesigned capacitor is under construction.

Sufficient evidence had been obtained that the required loop-impedance would be achieved with the loop withdrawn some distance below the cavity surface. The optimum distance is around 4-5 cms., but is not critical. Vacuum lids of various materials have been tried, with no apparent effect on performance. A fibre-glass epoxy-resin disc, faced on the vacuum side with a thin Pyrex sheet is at present in use.

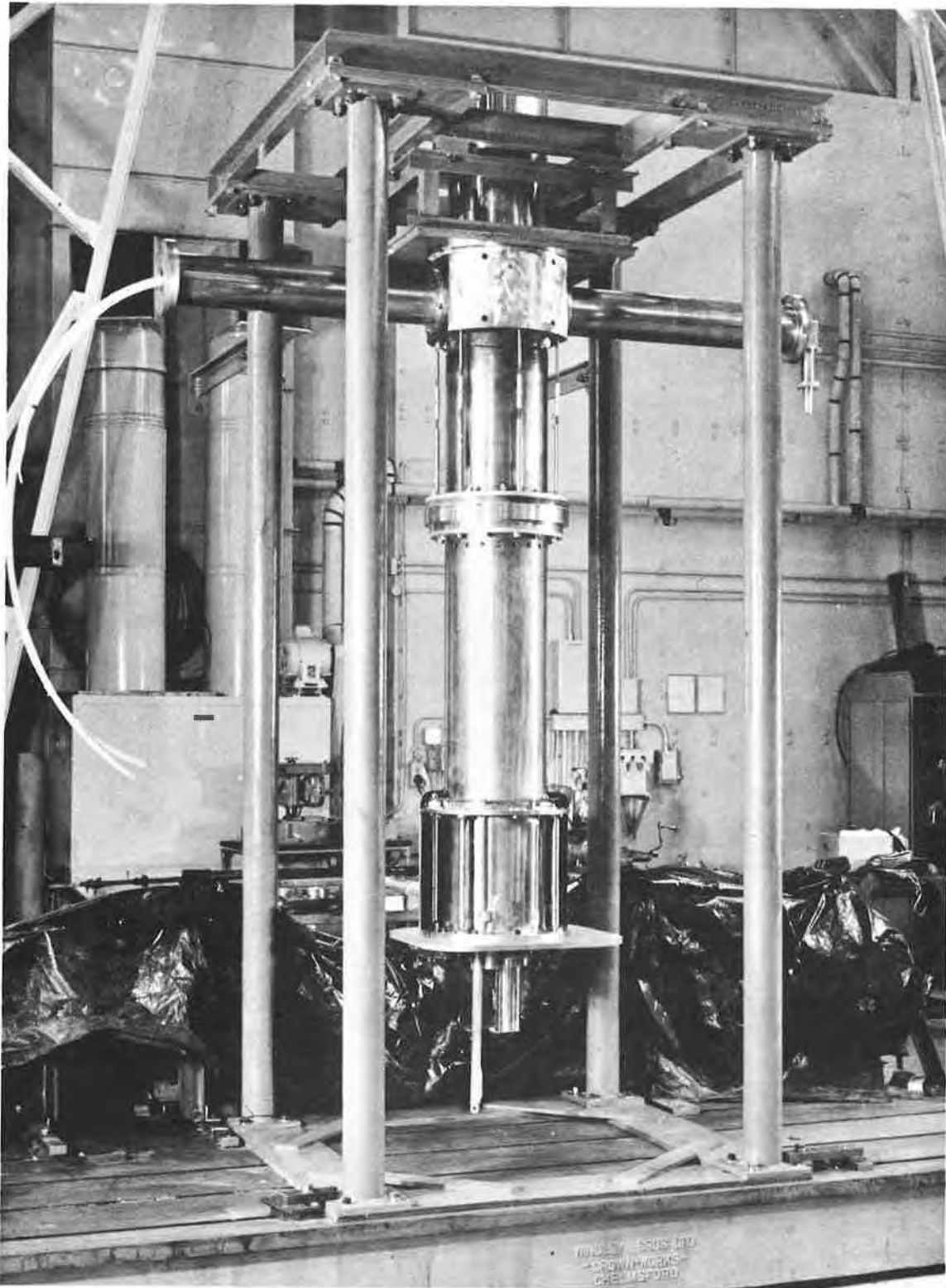


Fig. 3.4.4(ii) View of RS 1041 Valve prior to Installation.

3.4.5. Drive Chain

About 140 kW r.f. power is required to drive the RS1041, in class 'B' operation, to an output of 1.5 MW. The 'drive-chain' amplifies from crystal-oscillator level to 140 kW in a total of 10 stages, the first four low-power stages being used for frequency multiplication from the crystal frequency of 106.481 Kc/s.

The oscillator and a x 10 stage have a short-term stability of ~ 1 or 2 in 10^8 and a long-term of 1 in 10^7 . The three further stages of multiplication are x 6, x 3 to 115 Mc/s at an output power of ~ 3 W c.w.

The remaining five amplifiers are pulsed and are all constructed to a similar r.f. design - a half-wave co-axial anode-line tuned at its open end by a polythene slug, with the HT pulse fed in at the voltage node, and the r.f. output taken via a loop in the same region. The grid is grounded, r.f. drive being applied to the heater-cathode element, a suitable input impedance being provided by chokes in the supply-leads.

This chain of five uses valves in the order:-

3W \rightarrow ACT.25 \rightarrow ACT.25 \rightarrow ACT.27 \rightarrow BR1106 \rightarrow BW165 \rightarrow 144 kW
x 10 x 10 x 6 x 10 x 8

R.F. output from the BW165 is fed to the cathode circuit of the RS1041 via a stub-supported '3 inch' 50Ω co-axial line.

3.4.6. Modulators

Two modulators are used, one to operate the five drive-stages via a suitably tapped pulse-transformer, and a 'main' modulator to supply the RS1041. A tapping on this modulator is also provided to power the BW165 driver, if required.

The main modulator - provides an output pulse to the following specifications:-

Pulse Voltage	30 kV (Tapping at 22.5 kV)
Pulse Current	85 A
Pulse Length	2.5 ms
Pulse Recurrence	2 pulses/s
Pulse Rise-time	100-200 μ s
Pulse Voltage Stability	$\pm 0.5\%$ pulse to pulse
Pulse Voltage drop	0.5% max. into resistive load

These requirements have been very closely met, and except for a few minor faults the modulator has behaved very well.

The drive-chain modulator - is mainly of laboratory manufacture, it is rated at 500 kW. The pulse-network voltage is stabilised to 0.5%. The output pulses are at the levels 1 kV, 2 kV, 5 kV, 8 kV, 22.5 kV and have substantially flat tops.

3.4.7. R.F. Commissioning

No measurement of high-level power output from the RS1041 was made prior to the circuit being assembled in position under the linac. Coupling to a dummy-load

in the absence of the usual anode resonant-circuit and matched out-put line presented a number of difficulties. Tapering from the 12 in dia. co-ax at the loop, to a smaller diameter transmission line and a dummy load could have been constructed, but was not considered justified in view of cost and time-scale. Various disc-shaped loads were tried in place of the 50 Ω loop and powers up to 500 kW were measured in this way, always limited by tracking breakdown or excessive current density at the centre connection.

After installation under the linac, the system was run-up in air until drift-tube breakdown occurred. When everything was optimised this level was reached with a 6 kV pulse to the RS1041, corresponding to about 50 kW in the resonator, if an anode-efficiency of 60% is assumed.

Operation with the linac evacuated, does not affect the drive circuitry except for a slight change of frequency which is well within the bandwidth of the circuits. Once the 'multipactor' effects were eradicated attention was given to the operation of the system under self-oscillatory conditions.

It was known that some system would need to be evolved eventually, to allow for the high reactive loading of the cavity by the high current beams ultimately expected. Automatic control of the source frequency during the pulse was a possibility, but a self-oscillatory system with the resonator the sole frequency determinant was more attractive on the grounds of simplicity.

Such a system has been in operation during most of 1962, and apart from the anode-capacitor troubles mentioned earlier the system is apparently reliable and simple.

Only the two final valves in the chain are used, the BW165 driver and the RS1041. Drive for the cathode of the BW165 is taken from a small loop in the linac resonator. The co-axial line conveying the drive includes a half wave 'line-stretcher' which is adjusted to produce the correct over all phase-relationship for positive feed-back. If necessary a further 180° can be obtained by reversing any coupling loop in the system.

Operation with only two valves, further simplifies matters by eliminating the need for two modulators. The tapping on the 'main' modulator provides pulse power for the one drive-stage.

The acceleration of beams over 3-4 mA places sufficient loading on the resonator to necessitate some arrangement of r.f. power level stabilisation for constant accelerating field.

A simple feed-back arrangement has been in use for some weeks, giving good power level correction during the beam pulse. Advantage was taken of the wide variation of r.f. level in the linac-resonator, obtainable merely by variation of the BW165 H.T. pulse. By feeding the BW165 H.T. via 600 Ω and shunting the valve with one of adequate power capabilities (BR1106), the field level in the linac can be controlled by control of the shunt valve grid-voltage. To complete the feed-back link, some r.f. from the linac cavity is taken via a loop to a diode rectifier and thence to a diode 'gate'. Here the unwanted portion of the pulse is 'clipped' off leaving just the top with its 'loading' signal to be passed on through amplifiers to the grid of the shunt valve, BR1106. The sign of the feed-back is such that a fall in field-level is transmitted to the BR1106 grid as a negative signal, thus

allowing the BW165 H.T. voltage to rise giving increased drive to the RS1041 and higher power in the linac cavity.

A range of approximately 2:1 in power-level will need to be controlled by this device if an accelerated beam of 50 mA is realised.

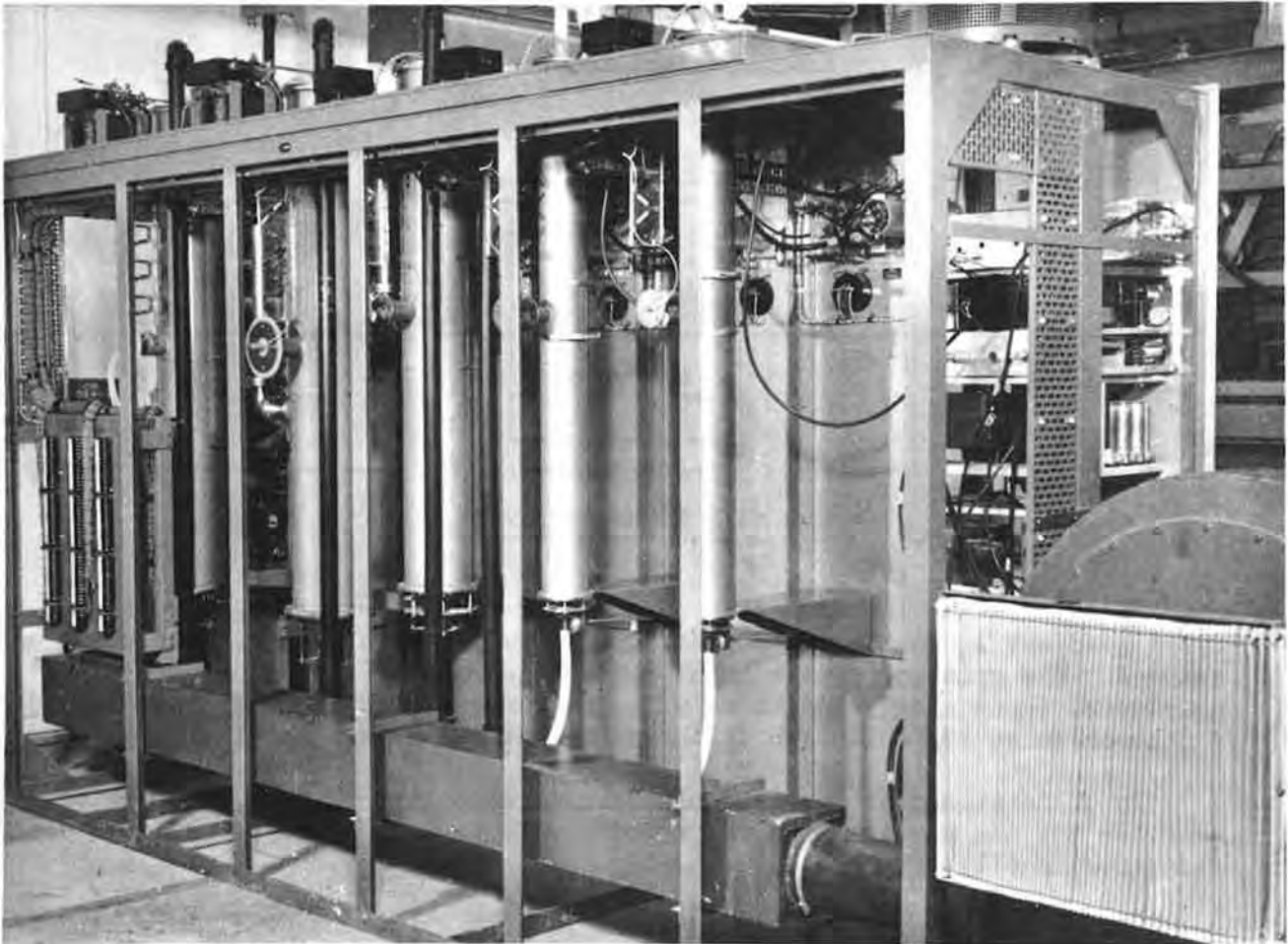


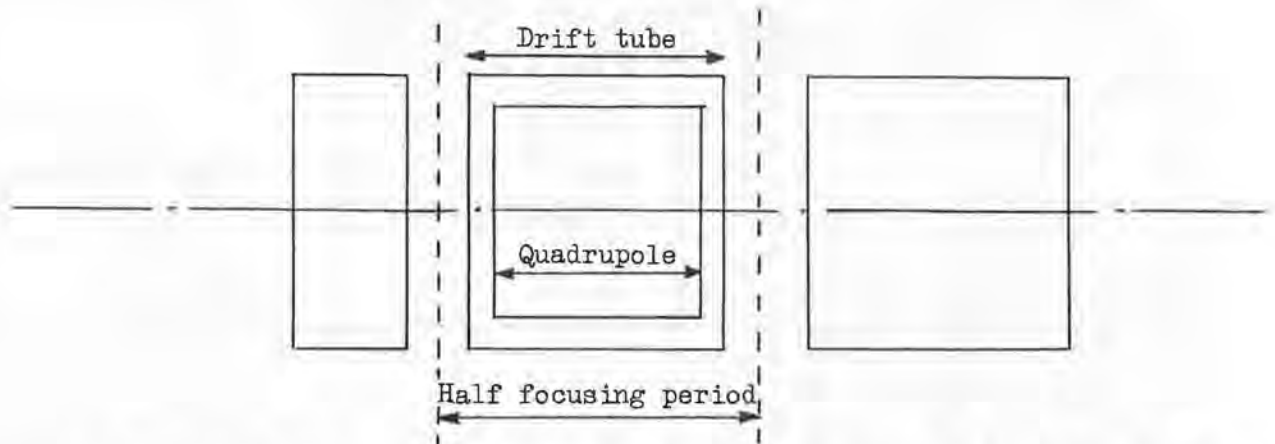
Fig. 3.4.5(i) Rear view of RF Drive Chain Cubicles.

3.4.8. Linac Quadrupoles

(a) Basic design parameters and construction

The quadrupoles, which form part of the linac drift-tube assemblies, were designed to provide a constant focusing or defocusing impulse per half focusing period, along the length of the linac. This means that the effective strength of the quadrupoles follows the law $A_{\text{eff}} \propto \beta^{-1}$, where A_{eff} is the effective field gradient and β is v/c (v - proton velocity). The linac unit cell considered for the calculations was as shown in Fig. 3.4.8(i).

Fig. 3.4.8(i) Linac Unit Cell



In calculating the effective strength of the quadrupole A_{eff} in terms of the field gradient A_0 inside the magnet, hard edged magnets (no fringe fields) were assumed. The gradient of the input quadrupole magnet (and hence drift-tube) apertures, input energy and linac r.f. frequency are all closely interdependent. A discussion on the selection of these parameters appears in (1).

No calculations or detailed experiments were performed on the pole tip profiles and the results of other workers were used. The magnet calculations are described in (11), (12) and (13).

The magnets consist of a mild steel yoke to which the drift-tube support stems are welded, soft iron tapered poles (Low Moor Iron Grade B) and soft iron pole tips (Low Moor Super HiperM). Hollow, low-voltage, high-current conductors are used for the quadrupole windings. These are wound with a number of cross-overs between poles to eliminate unequal heating effects on the poles and to provide a symmetrical array of conductors at the ends of the magnets. The ratio of conductor inner to outer diameters was chosen to give the minimum temperature rise of the magnet cooling water. Each magnet winding was formed from a continuous length of vacuum-tested tube, the conductors entering and leaving the drift-tube via the horizontal support arm. A combined high-pressure water (100 lb/in²) and high current (500 A) coupling is used at the end of each conductor emerging from the drift-tube stem. There have been no vacuum or electrical troubles at this junction.

Extensive use is made of epoxy resin-bonded fibreglass for insulation between the magnet windings and the poles and between winding turns. Steatite sleeves are used for insulation at the junction of the stem to the yoke (to allow an argon-arc

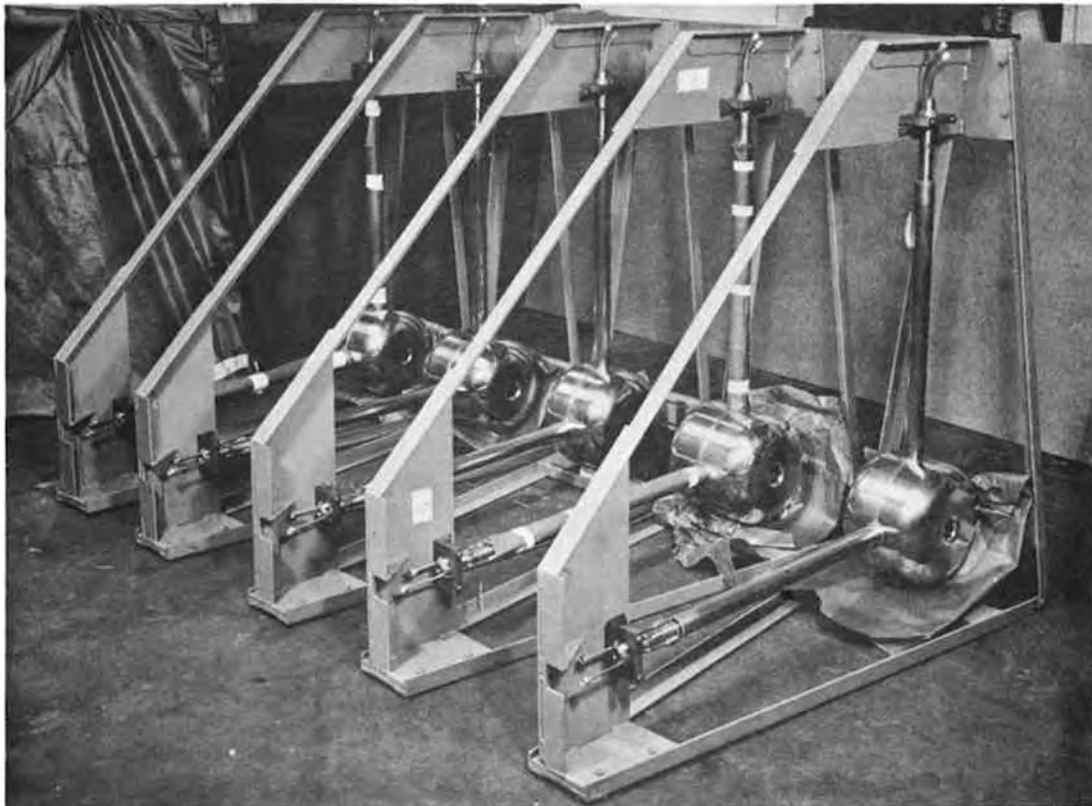


Fig. 3.4.8(ii) Linac Drift Tubes in Transportation Frames.

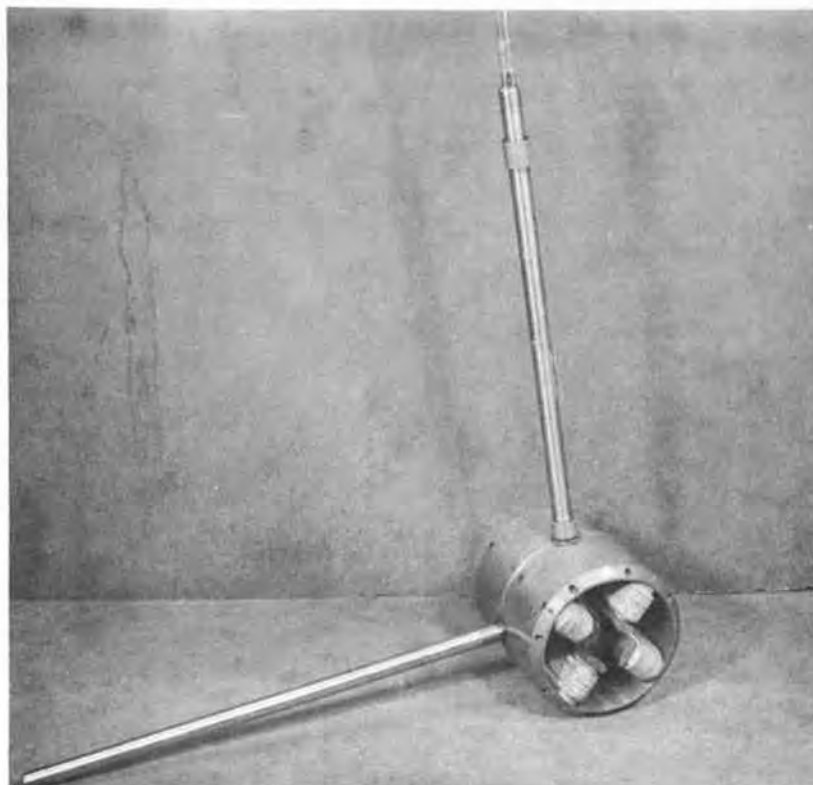


Fig. 3.4.8(iii) Linac Drift Tube showing Quadrupole Magnet.

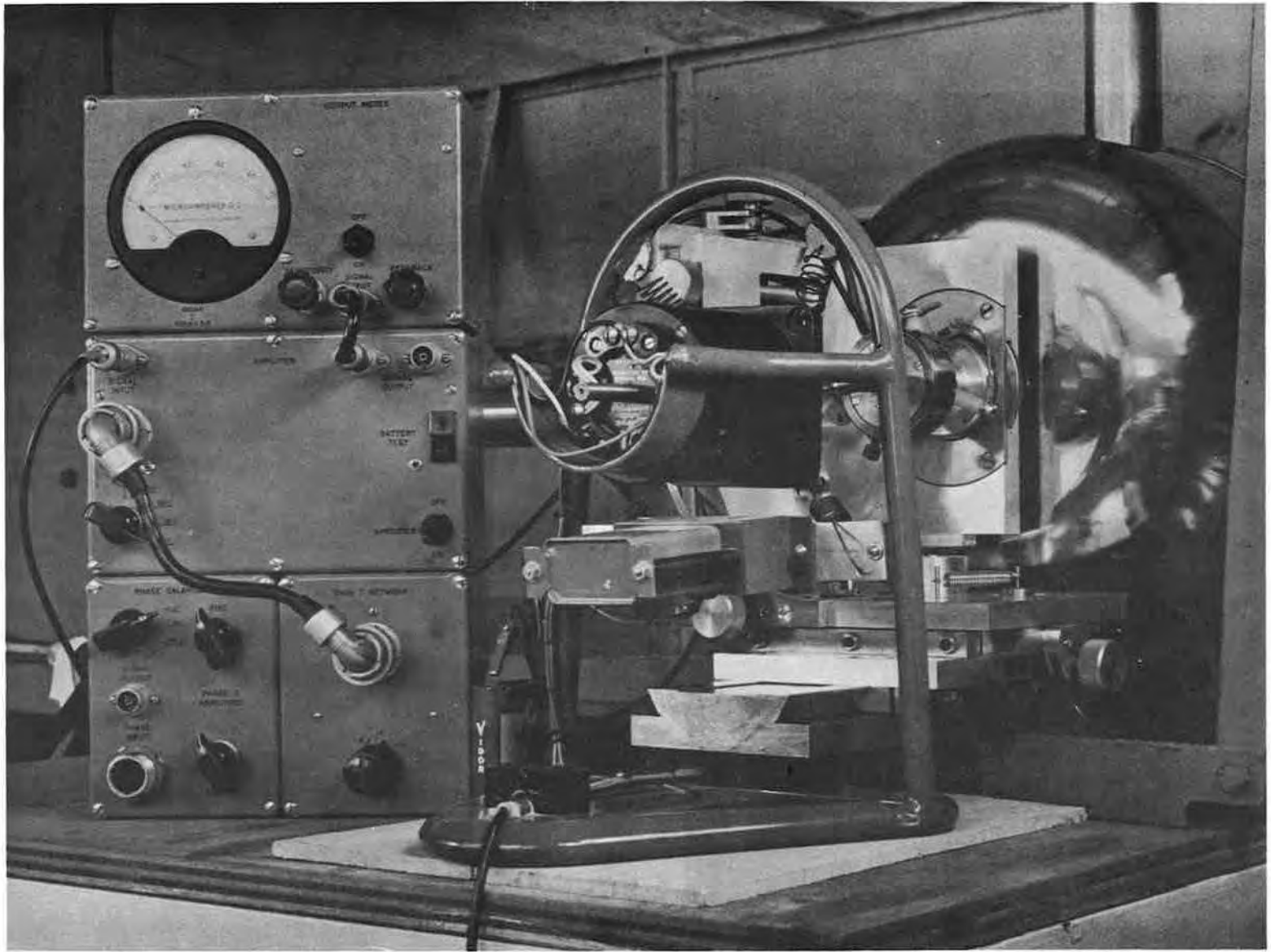


Fig. 3.4.8(iv) Magnetometer used in measurements at the Laboratory.

weld to be made after part assembly of the quadrupole). Insulation inside the drift-tube stem is provided by woven glass sleeving. The two conductors leave the stem via a combined vacuum joint, made of a split neoprene bung.

Insulation resistance to frame in excess of 100 M Ω (500 V Megger test) was measured for all drift-tubes after trouble from "conducting" neoprene (heavily loaded with lampblack) had been eliminated. No vacuum troubles have been experienced at this point.

(b) Magnetic Measurements and Testing

A comprehensive series of mechanical, electrical and magnetic tests was carried out on each quadrupole prior to welding on the drift-tube windings. These tests were carried out at the manufacturer's. A further series of measurements was carried out at the Rutherford Laboratory after delivery of the completed drift-tube assemblies. (The magnetometer used in these measurements is shown in Fig. 3.4.8(iv)).

(i) Sub-assembly tests at the manufacturer's.

Mechanical checks - correct orientation of winding pre-form and yoke; condition of pole tip surfaces, etc.

Electrical checks - measurement of d.c. resistance.

- measurement of $A_0(\text{gradient})/I(\text{current})$.

- checks for shorted turns : two rejects.

- insulation winding/frame : three rejects.

Magnetic checks - position of magnetic axis relative to pole tips : one reject (shorted turns).

- orientation of transverse zero potential planes relative to drift-tube stems.

Every case of failure was investigated fully and corrections made at the source of the trouble. The acceptance limits for these magnetic and electrical tests were as follows:-

Insulation ✦ 10 M Ω (500 V Megger test)

Magnetic Axis ✦ 0.002 in from centre of best tangent circle to the four pole tips.

Transverse planes ✦ 0.25° from correct position (as defined by scratch marks on yoke).

The magnetic tests were based on rotating coil techniques and the magnetometers used were developed specially for the purpose.

(ii) Tests on completed drift-tubes at the Rutherford Laboratory.

Measurements were carried out to determine the position of the magnetic

axis at each end of every drift-tube relative to the optical axis as defined by alignment targets placed in the drift-tube bore. The final optical alignment of the drift tubes in the linac made use of the corrections obtained in these tests. (Due to the method of construction of the drift-tubes, the central tube may not be perfectly aligned with the quadrupole.)

Another specially developed rotating-coil magnetometer was used and the measurement accuracy was estimated to be better than 0.00025 in.

A final check of insulation resistance after drying of the quadrupole (by evacuating the drift-tubes) and after replacement of the neoprene bungs, showed resistances well in excess of 100 M Ω (500 V Megger) for every drift-tube magnet.

3.4.9. Quadrupole Power Supplies and Gradient Boxes

The linac quadrupoles are connected in six series groups, each group having a separate voltage stabilised transformer rectifier set with an LC filter. To enable different current distributions to be obtained along the length of the series connected chain of quadrupoles, difference currents are fed in or led off at the inter-magnet connections.

The purpose of the gradient boxes is to control the feed and bleed currents and allow two pre-set current distributions to be obtained by switch operation and control of supply voltage to the group of quadrupoles only. The two distributions concerned are those appropriate to:-

- (i) Normal "High Law" - $A_{\text{eff}} \propto \beta^{-1}$ (as mentioned in 3.4.8(a))
- (ii) "Low Law" - $A_{\text{eff}} \propto \beta^{-3/2}$

The networks for the gradient boxes (Fig. 3.4.9(i)) were calculated using the results of the d.c. resistance and the A_0/I measurements referred to in 3.4.8(b).

Voltage stabilisation supplies are used in preference to current stabilisation for the power supplies since this facilitates setting up the current distribution network and allows for individual control of the input half quadrupole and the output half quadrupole. The voltage sensing leads for the first and last groups do not include the input half quadrupole and the output half quadrupole. The resistance of the quadrupole windings is maintained constant by the use of temperature stabilised cooling water.

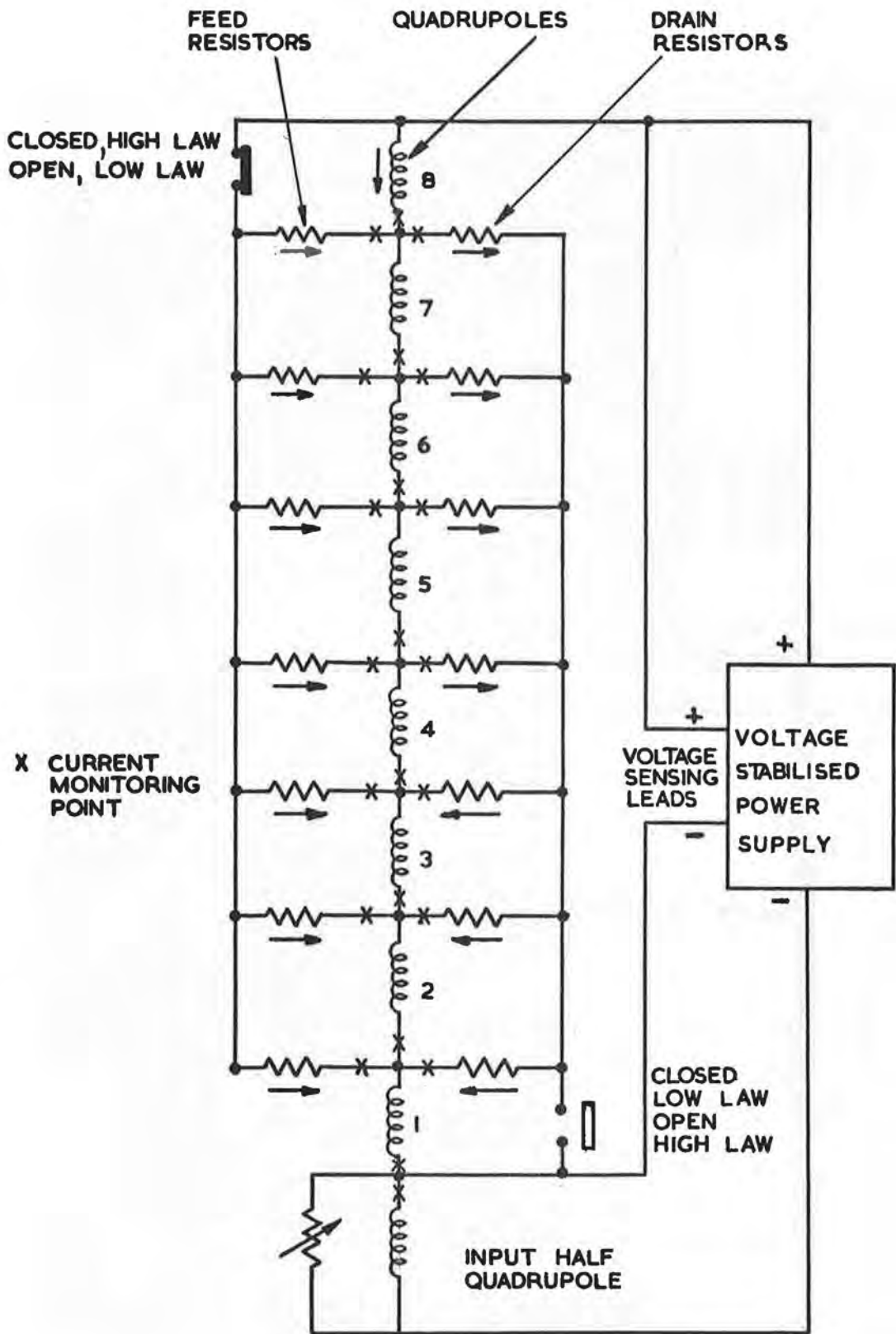


Fig. 3.4.9(i) Simplified Schematic Diagram of First Gradient Box.

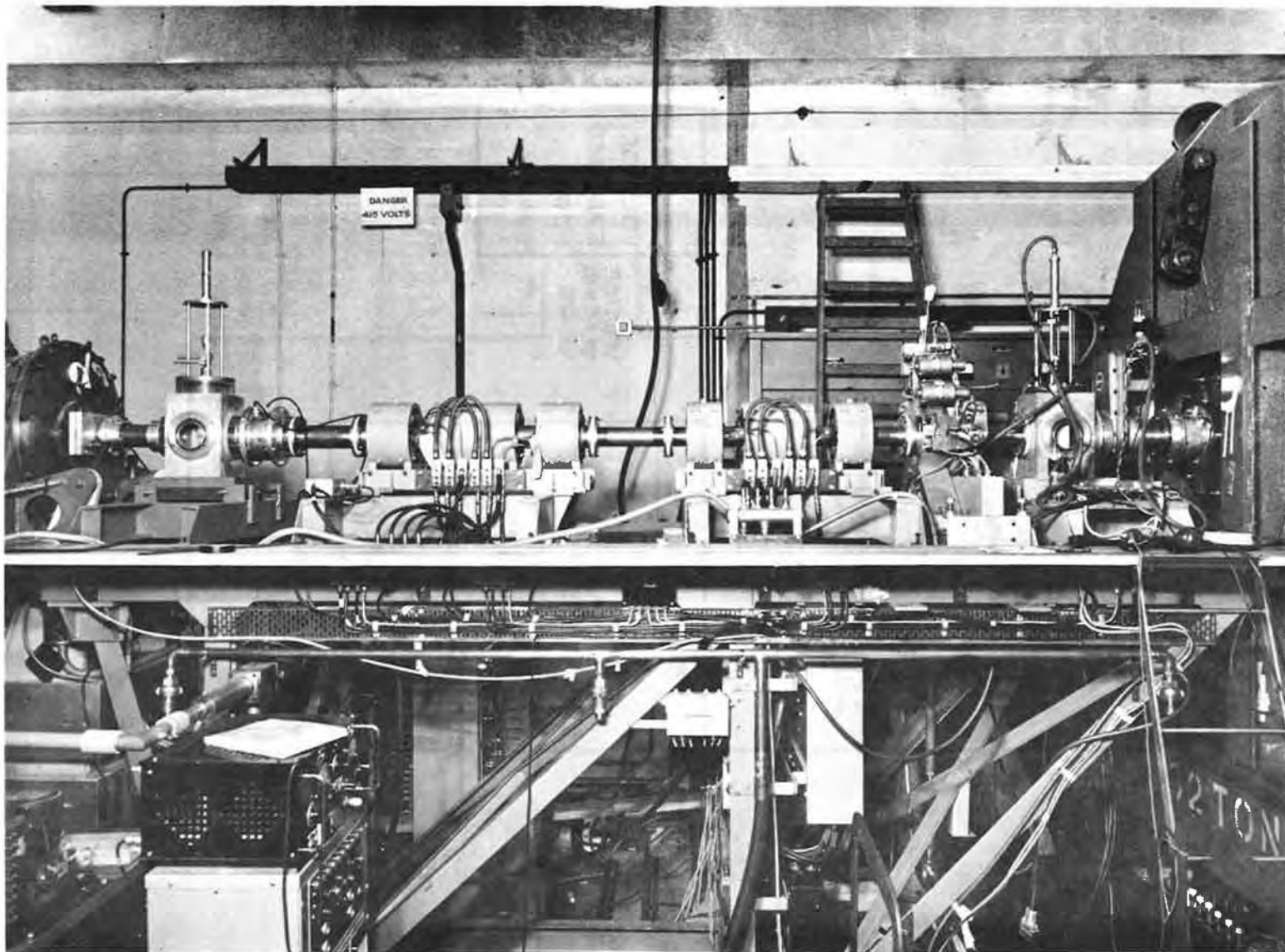


Fig. 3.5.1(i) View of LE DS showing quadrupole triplets, 4 jaw boxes, beam current transformers and probe boxes.

3.5. Drift Spaces and Inflector

3.5.1. LEDS and HEDS Quadrupoles

Quadrupole triplets are used in the low energy drift space (3 triplets) and the high energy drift space (4 triplets) for beam matching purposes. The required values of gradients and apertures were obtained by computation.

The quadrupole magnets were designed in the same way as for the linac quadrupoles (see 3.4.8) and are constructed in a very similar manner. The main differences between the linac quadrupoles and the beam matching quadrupoles are the larger apertures ($2\frac{1}{2}$ in, 3 in and $3\frac{1}{2}$ in diameter) and the smaller gradients of the latter. The beam matching quadrupoles have gradients in the LEDS of 100 to 200 gauss/cm and those in the HEDS of 300 to 400 gauss/cm. The magnetic circuit design is common to the quadrupoles in both drift spaces; the difference between quadrupoles of a particular aperture lies in the number of turns/pole.

Only electrical tests were conducted on the beam matching quadrupoles in view of their relative accessibility and the excellent agreement found between mechanical and magnetic axes with the quadrupoles for the linac. These involved investigation of the number of turns/pole, shorted turns and insulation to frame.

Each triplet is powered by a transformer rectifier set with an output LC filter. All three elements of the triplets are connected in series, with the outer elements adjacent to each other. This enables the outer elements to be shunted relative to the centre element or vice versa. Low resistance, wide-range, adjustable shunts, using transistors, are employed to give $\pm 15\%$ out-of balance control. A description of these shunts can be found in (14).

3.5.2. Buncher and Debuncher Cavities

General R.F. Design

Both buncher and debuncher are single gap cavities of re-entrant geometry, similar to a single unit cell of the linac. Their design was based on published data (9) and accurate resonant dimensions, given in Table 3.5.2(I) were determined by model measurements at 1000 Mc/s.

TABLE 3.5.2(I) BUNCHER AND DEBUNCHER PARAMETERS

	Buncher	Debuncher
Frequency	115 Mc/s	115 Mc/s
Cavity diameter	41.054 in	41.054 in
Drift tube diameter	11.084 in	11.084 in
Drift tube profile radius	2.590 in	2.590 in
Cavity length	11.309 in	25.774 in
Gap length	0.805 in (with grid)	3.290 in (no grid)
Drift tube aperture diameter	2.250 in (aperture through grid)	3.937 in

In the design of the buncher, a high value for the ratio of shunt impedance to Q-factor was sought because the buncher has an artificially loaded Q-factor to give good electrical stability. At the same time a short axial length for the buncher is required because of space restrictions in the LEDES.

The debuncher power requirement is such that it is not practical to reduce its Q-factor artificially and so a high value shunt impedance was chosen. For both cavities a reasonably small diameter was desirable. The theoretical figures for the power requirements are given in Table 3.5.2(II).

TABLE 3.5.2(II) BUNCHER AND DEBUNCHER THEORETICAL
POWER REQUIREMENTS

	Buncher	Debuncher
Peak energy change of proton	21 keV	200 keV
Peak gap voltage	22.8 kV	230 kV
Q-factor (unloaded)	26,200	35,100
Q-factor (loaded)	920	-
Cavity r.f. dissipation	177 W	6,030 W
Total r.f. power required	5,040 W	6,030 W
Proton drift distance from the linac	1.44 m	10.7 m

Tuners

Adjustment of the gap length by moving one of the half drift tubes provides course tuning of each cavity. The r.f. connection of the adjustable half drift tube to the cavity end wall is by a convoluted copper diaphragm. The buncher has two fine tuners, similar in design to those in the linac, one of which can be operated remotely. The debuncher has a single fine tuner which is servo-operated. The servo error signal is derived from the phase comparison of r.f. signals from the cavity and its feed line, in a coaxial cable rat-race phase bridge.

R.F. Feeds

Each cavity is fed with r.f. power from a pick-up loop coupled to the linac. This method of feeding the cavities is preferable to coupling from some point in the linac drive chain, since it ensures that the drive to each cavity maintains a constant phase relationship with the linac fields. The drive level can be adjusted by varying the pick-up loop penetration in the linac and similarly the feed loop to each cavity can be adjusted to give an r.f. match to the feed line. Phase adjustment is achieved by a line stretcher and the r.f. match can be monitored by a reflectometer.

Mechanical Construction

The debuncher cavity is similar in construction to the linac, being fabricated from copper sheet riveted to a framework of stainless steel ribs. The buncher is constructed from $\frac{3}{8}$ in copper plate, rolled and welded with internally machined

surfaces. The end faces are also of copper plate backed by stainless steel ribs.

Both cavities have separate vacuum envelopes; the debuncher has domed end walls but the buncher has flat end walls to minimize the overall length. Both are pumped with single 9 in mercury diffusion pumps.

Operation

Only the buncher cavity has been operated at high power. This cavity is suffering from multipactor troubles at the present time, in spite of the use of a d.c. bias. The bias, of up to 3 kV, is applied to one cavity end wall, which makes r.f. connection to the cylindrical wall through a capacitive joint insulated by 0.010 in polythene sheet.

One cause of the trouble may be r.f. field leakage from this joint into the cavity - vacuum vessel interspace. If the bias suppression of multipactor proves unsuccessful, the buncher surfaces will be coated with carbon black. The debuncher cavity, which is to be commissioned early in 1963, is also designed to have d.c. bias in the same manner.

3.5.3. Steering Magnets

Beam steering facilities are provided at the output end of the linac, (14), using four magnets (M_1 to M_4), and at the inflector using two magnets (M_5 and M_6).

The system consisting of M_1 to M_4 is designed to align any matched output beam from the linac with the theoretical beam line. The requirements of minimum axial length and momentum resolution are self consistent and consequently the system was designed to occupy not more than about 1 m of flight tube. The magnets M_1 and M_3 steer the beam vertically and M_2 and M_4 steer the beam horizontally.

The magnet design can be seen in Fig. 3.5.3(i) and the magnet parameters are given in Table 3.5.3(I).

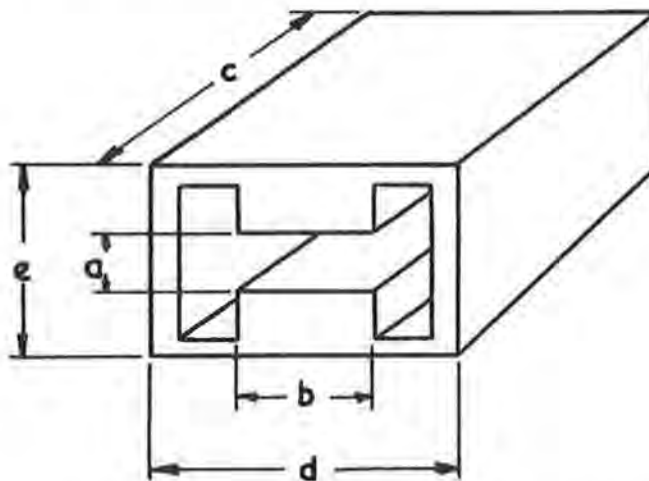


Fig. 3.5.3(i) Steering magnet design.

TABLE 3.5.3(I) STEERING MAGNET PARAMETERS

<u>MAGNET PARAMETER</u>	M_1	M_2	M_3	M_4
<u>Pole Separation: a (cm)</u>	8	8	5	5
<u>Pole Width: b (cm)</u>	16	16	10	10
<u>Pole Length: c (cm)</u>	20	20	15	15
<u>Magnet Width: d (cm)</u>	40	40	25	25
<u>Magnet Height: e (cm)</u>	20	20	15	15
<u>Ampere-Turns</u>	8,210	6,850	6,360	6,140
<u>Flux Density (kgauss)</u>	1.29	1.075	1.6	1.54
<u>Total Coil Area: (cm²)</u>	50.3	44.2	41.0	39.5
<u>Power Consumption (W)</u>	260	200	125	120
<u>Approximate Weight (lb)</u>	240	240	200	200

At the inflector, magnets M5 and M6 allow the beam to be steered vertically. Horizontal steering can be achieved at this point by means of remotely operable shunts on the first two sector magnets of the inflector.

The magnets are constructed from Super Hiper Magnetic Iron which has a low remanent field and they can give field strengths up to 2 kgauss in either direction. A specially developed transistorised power supply, Fig. 3.5.3(ii), is used to power the magnets. The supply is current stabilised at all settings and is continuously variable through zero between +15.A and -15 A.

3.5.4. Inflector

For injection into the synchrotron ring, the 15 MeV beam from the linac must be turned through an angle of 25° onto a line parallel to the central equilibrium orbit (Fig. 3.5.4(i)) without introducing appreciable energy resolution (16). To permit continuous injection of up to 300 turns into the magnet ring and to avoid excessive loss of circulating beam the last part of this deflection is achieved by means of an electrostatic element (E₅ in Figure 3.5.4(i)) with a mean radius of 6 m and a field of 55 kV/cm. To achieve a beam path clear of obstructions on to the required injection radius, the electrostatic element is preceded by a magnet. A suitable magnet has been designed (16), and is shown as E₄ in Fig. 3.5.4(i).

In order to inject the beam using these last two elements, it is necessary to deflect the beam from the linac beam line through an angle of 11.5° towards the

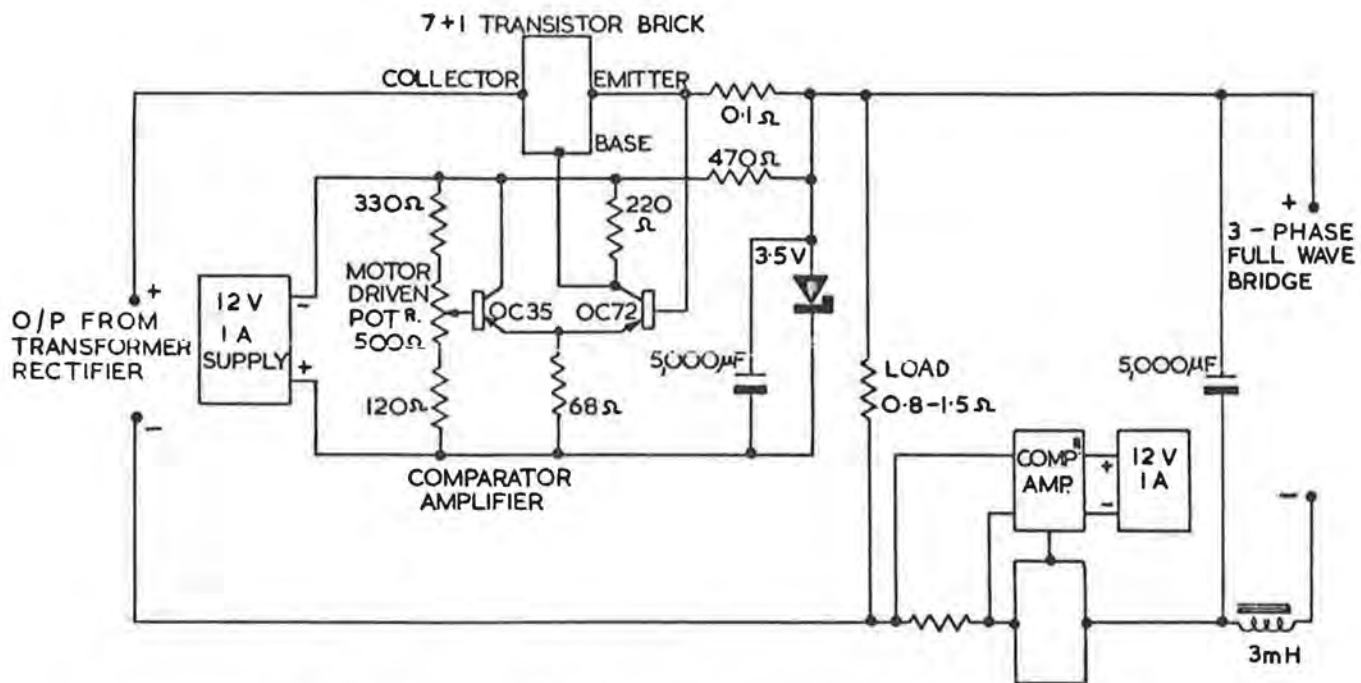


Fig. 3.5.3(ii) Steering magnet supply circuit.

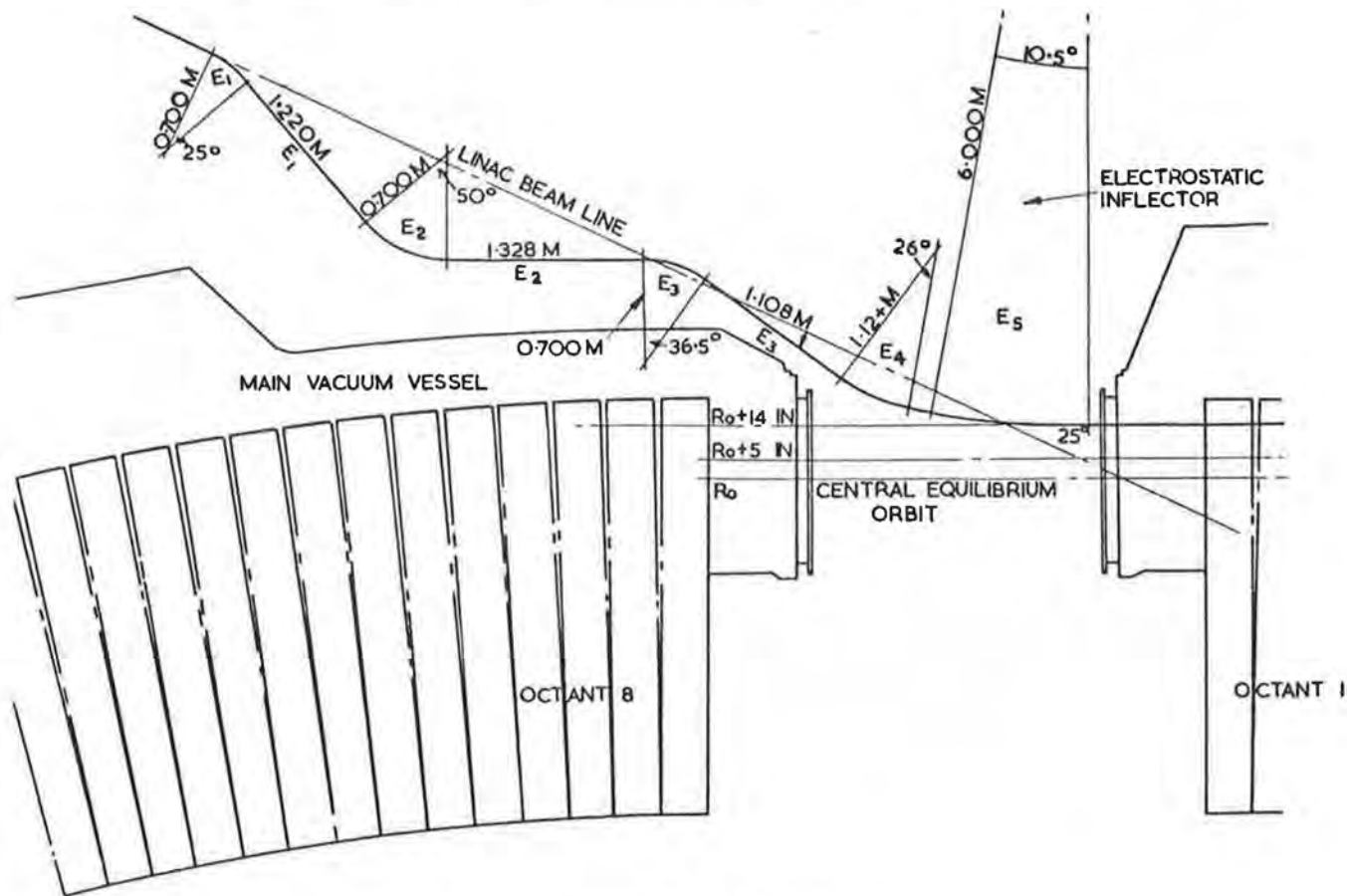


Fig. 3.5.4(i) Inflector

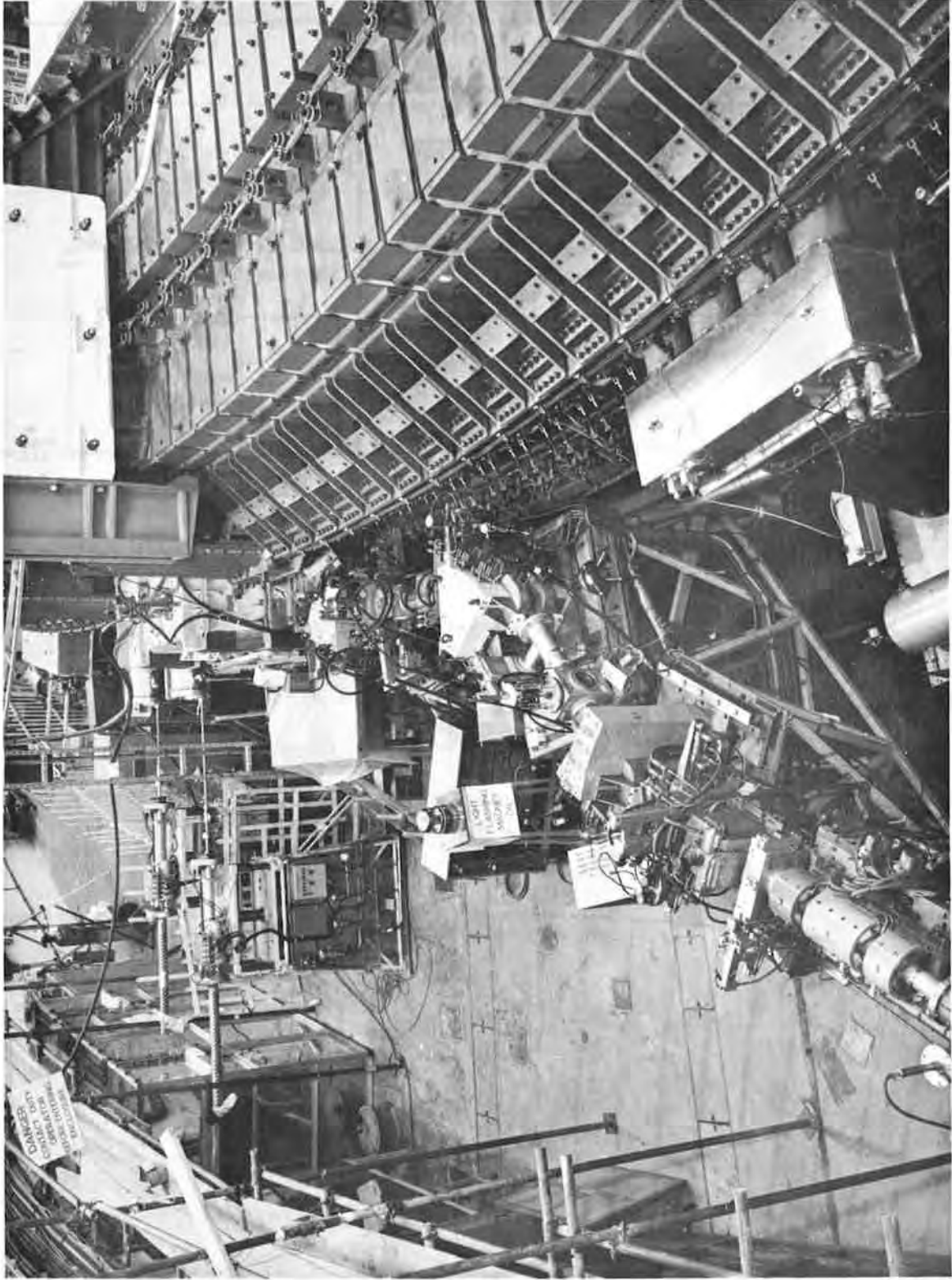


Fig. 3.5.4(ii) View of achromatic inflector system.

synchrotron. The simplest solution would be to produce this deflection by a single element but investigation of the resulting momentum resolution showed that this would result in an effective increase in emittance of about 48%. As this is not acceptable it was decided to design an achromatic system. This consists of four sector magnets followed by the electrostatic element.

The magnets E1, E2, E3 and E4 have apertures 9.25 cm vertically by 14 cm radially and have fields of 8, 8, 8 and 5 kgauss respectively. It was found possible to shim them to give $\int Bdl$ proportional to radius to within $\pm 0.02\%$ over a required good field aperture of 8 cm vertically by 4 cm radially. This was achieved by shimming first to give constant field in the central region of the magnet and then adding end shims to give an effective length proportional to radius.

Since the injection radius is not yet known precisely the system has been made adjustable so that the beam may be injected from any position from the edge of the good field region to up to 4 in inside the good field region.

Investigations of the focal properties of the system showed that emittance and momentum defining facilities could also be incorporated. The defining apertures provided will allow the definition of 'pencil' beams which can be used during the commissioning of the synchrotron and also of matched beams (17) during normal operation.

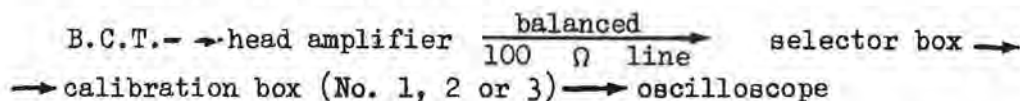
3.6. Other Injector Facilities

3.6.1. Beam Monitoring System

The beam pulse can be monitored at 12 points along the injector by means of toroidal beam current transformers (B.C.T.s) Any three of these may be selected and displayed simultaneously on a suitable oscilloscope either in the injector control room or in the main control room. The system is shown in Fig.3.6.1(i).

The beam intensity is measured by an amplitude reading which is compared with a current pulse (calibration pulse) of known, adjustable, amplitude which can be switched into any of the B.C.T.s.

The monitoring sequence is:-



(a) B.C.T.s

These consists of Selected Grade Mumetal ($\mu_0 > 50,000$) cores 6.5 in o.d., 4.5 in i.d. x 1.5 in x 0.004 in. One type, for long pulses, is wound with 100 turns and a second type, with high sensitivity for short pulses, is wound with 10 turns. The turns are evenly distributed around the core, which also has 1 turn carrying the calibration pulse. Magnadur rings, diametrically magnetised and opposing each other are used each side of the current transformers for electron suppression. (Fig. 3.6.1(ii)).

(b) Head Amplifiers

These are situated near the respective current transformers and provide the necessary low load impedance for the transformers. They have low impedance outputs to feed 100 Ω balanced cable to the injector control room and the main control room. The units are fully transistorised with two switched gain settings:-

Low gain, 1 mA input (100 mA beam current) → 10 V output across
100 Ω

High gain, 0.2 mA input (20 mA beam current) → 10 V output across
100 Ω

A self-contained battery operated version is available for "Faraday-Cup" monitoring with switched settings of 10 μ A, 100 μ A or 1 mA input, with an input impedance of 10 k Ω giving a 10 V output across 100 Ω .

(c) Selector Box

This is situated in the injector control room and contains uniselectors, for selection of transformers and routing of the calibration pulse and also has balance to unbalance pulse transformers. It provides manual control of transformer selection either in the injector control room, using calibration box No.1 or 2, or in the main control room using calibration box No.3.

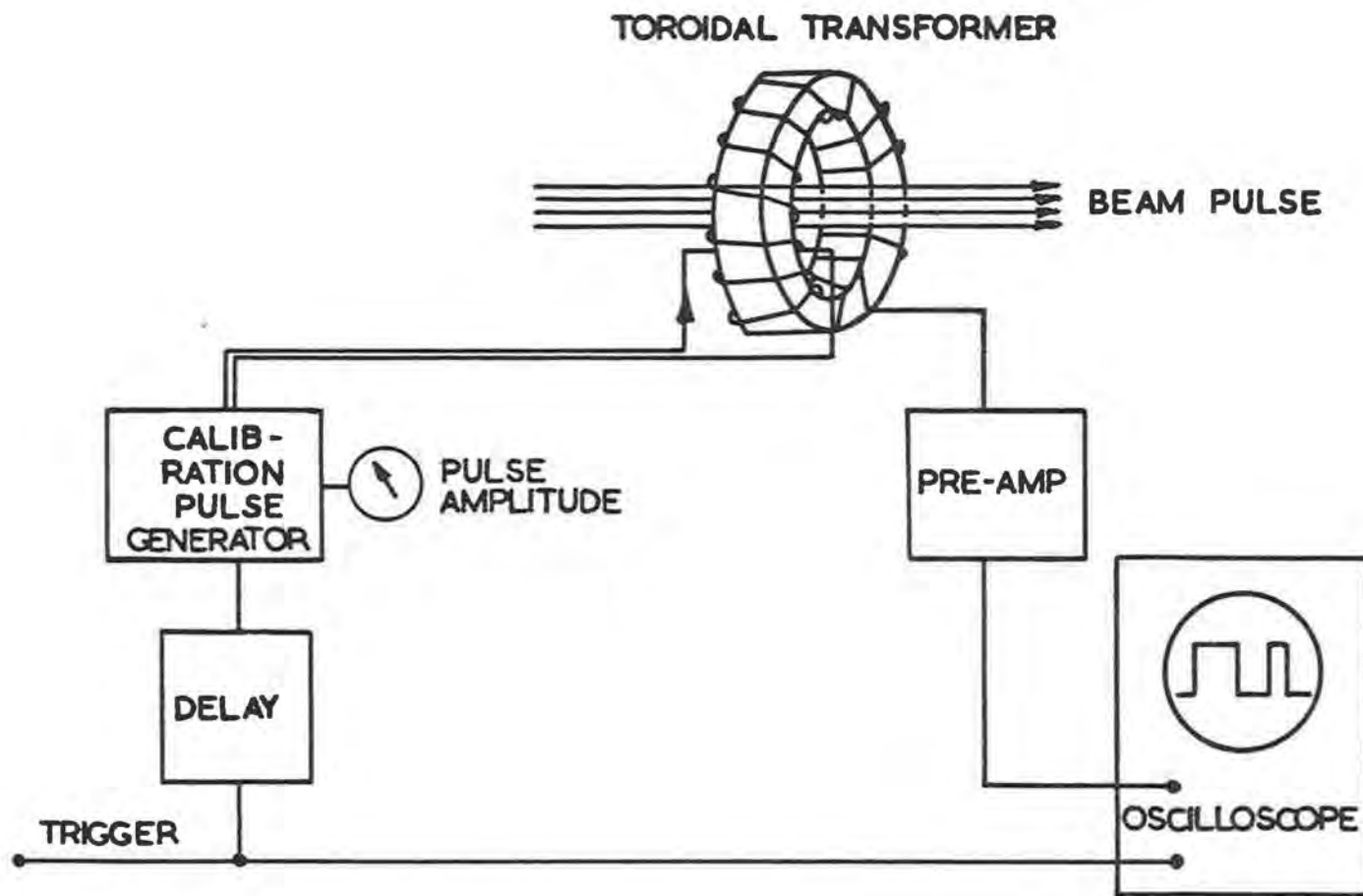


Fig. 3.6.1(i) Rudimentary beam monitoring system.

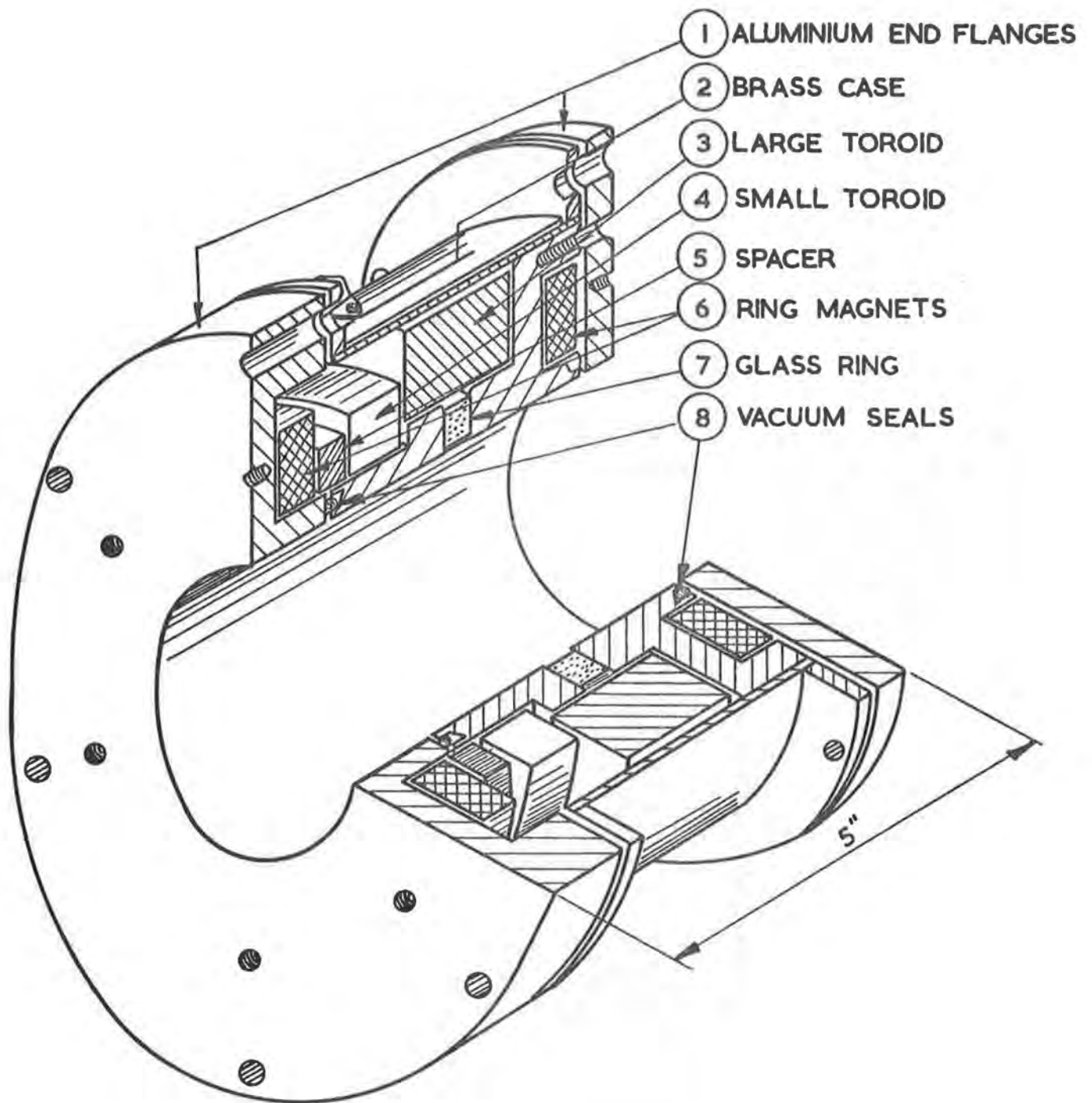


Fig. 3.6.1(ii) Screening mount for beam current transformers.

(d) Calibration Boxes (No. 1, 2 and 3)

These contain transistor circuits for delayed triggering and for the generation of the calibration pulse. The controls provided give -

Control of the calibration pulse currents; direct reading of the beam amplitude by a meter; variation of the calibration pulse time delay with respect to a standard trigger pulse input; control of the pulse length; 3-channel selection of the B.C.T.s; selection of the calibration pulse route; monitor outputs; and fault and warn indication using uniselector operation indicators.

The calibration pulse characteristics are -

Amplitude continuously variable (4 ranges)	10 μ A to 100 mA
Accuracy	$\pm 2\%$
Pulse length	100 μ s or 2.5 ms
Delay with respect to the input trigger	10 μ s to 10 ms.

The response of the complete system to a 2 ms rectangular beam pulse is limited by the amplifier output stage and the balance/unbalance transformer. The rise and decay times are less than 2 μ s and the pulse droop is not greater than 5%.

Operational Experience and Projected Future Development

The system has been developed steadily since it was first used some two years ago. Points of particular interest are:-

- (i) zener diode stabilisers in each head amplifier to eliminate inter-toroid coupling when using one central power supply,
- (ii) symmetrically disposed windings and external magnetic screens at the B.C.T.s to reduce the effect of external magnetic fields (50 c/s),
- (iii) gold-plated uniselector contacts for improved low level operation,
- (iv) magnetic screening of the balance/unbalance transformers.

To date, no trouble has been experienced from radiation damage to the head amplifiers and even with prolonged operation at full beam intensity, adequate life is anticipated. (Deterioration of the head amplifiers does not affect the accuracy of the measurement).

Measurements of beam current pulses with intensities less than 100 μ A can be taken on any of the B.C.T.s and intensities of less than 10 μ A can be monitored where magnetic screens have been fitted.

Modifications are in hand to improve the speed of the system. It will then be possible to monitor beam pulses of 300 ns with rise-times of the order of 100 ns. This accuracy is adequate for timing purposes.

3.6.2. Timing Facilities

A comprehensive fully transistorised timing system is proposed for the injector. This will allow maximum flexibility for experimental and commissioning purposes and apply minimum restriction to the main machine. The system has not yet been finalised but most of the basic units have been in use for some time.

The system uses pulses from the magnet field integrators, to provide timing information for 'acceleration cycles', and pulses derived from the main alternators, to enable parts of the injector to be run at multiples of the magnet pulse repetition frequency.

A description of the system is given in (18).

(a) Master Timer

The master timer, controls the gating of the pulses from the field integrators and from a counter chain locked to the magnet timer circuits. Provision is made for synchronised, single-shot operation of the magnet/injector (i.e. one magnet cycle synchronised with continuous pulsing of the injector) and for normal, unsynchronised, single shot. The master timer also contains a pulse generator for injector operation without the magnet.

(b) Delay Boxes

The delay boxes provide accurate, jitter-free, directly calibrated delays which are required for correct sequential operation of the injector equipment. Three independent delayed outputs are derived from each of four inputs. The delays introduced are directly proportional to the potential difference from the slider of a helipot, which is fed from a stabilised supply to earth. This approach was adopted to reduce to a minimum, the number of pulses interchanged between the injector control room and the main control room. The delays can be adjusted in the injector and main control rooms and by using a portable extension box in either control room.

The specification for the delay boxes is as follows:-

Input pulse - positive going, $20\text{ V} \pm 3\text{ V}$, rise time $< 1\ \mu\text{s}$, pulse length $5\text{-}50\ \mu\text{s}$, input impedance $10\ \text{k}\Omega \pm 5\%$, (or, with the remote input pulse monitor connected, $5\ \text{k}\Omega \pm 5\%$), minimum trigger level 10 V .

Output pulse - positive going, $20\text{ V} \pm 0.5\text{ V}$, rise time $< 1\ \mu\text{s}$, pulse length $10\ \mu\text{s} \pm 2\ \mu\text{s}$, output impedance $\approx 100\Omega$, decay time $5\ \mu\text{s} \pm 2\ \mu\text{s}$. This is the standard trigger pulse used throughout the injector timing circuits. Delay and jitter on the $10\text{-}100\ \mu\text{s}$ range and the $100\ \mu\text{s}\text{-}1\text{ ms}$ range is $\pm 0.1\ \mu\text{s}$; on the $1\text{ ms}\text{-}10\text{ ms}$ range it is $\pm 1\ \mu\text{s}$.

(c) Extraction Trigger Control

Using the standard trigger pulse, the extraction trigger control provides the following facilities:

(i) Square pulse of defined length, $20\ \mu\text{s}\text{-}2.5\text{ ms}$ (main extraction trigger),

- (ii) Square pulse of defined length, 20 μ s-200 μ s (pilot beam trigger),
- (iii) Selection of (i) and/or (ii) as required,
- (iv) Premature termination of the extraction pulse (beam 'axe')
- (v) Suppression of (i) (extraction 'lock-out')
- (d) Light Guide System

The light guide system is described in section 3.3.4.

Monitor channels to the Main Control Room

In addition to the monitoring and timing facilities already discussed, it is proposed to use a number of emitter follower units in the injector control room to provide low impedance circuits to the main control room. These units will have the following characteristics:-

There will be six channels (5 emitter followers and 1 direct link),

Input impedance \approx 100 k Ω for normal input and \approx 50 k Ω for fast input,

Output impedance - low (dependant upon input resistance).

Gain from the injector to the main-control room will be 0.5 (adjustable over a small range);

With a 2 ms pulse, the rise and decay times for normal input will be \approx 2 μ s, with fast input \approx 0.1 μ s;

Drop \gt 5%. The maximum input pulse amplitude will be \pm 40 V with separate plug-in boards for each polarity, maximum input d.c. level, \pm 350 V.

Connection to the main control room will be via a 100 Ω terminated cable.

3.6.3. Auxiliary equipment

Auxiliary equipment for the injection system is discussed in the relevant sections elsewhere in this report:

Injector vacuum system	. . .	Section 8.11
Injector control system	. . .	Section 9.1
Injector vacuum controls	. . .	Section 9.2.2
Injector auxiliary plant	. . .	Section 10.8

3.7. Beam Experiments

3.7.1. Emittance Definition in LEDES

A system of quadrupole triplets and defining apertures was set up in the LEDES with a view to defining the emittance (phase-space characteristics) of the beam entering the linac. The experiment confirmed the theoretical predictions of displacement acceptance but revealed a discrepancy as far as divergence is concerned. This will be investigated further.

3.7.2. Momentum Analysis

Momentum analysis of the 15 MeV beam has been carried out using one of the sector magnets which is used in the inflector system, in a temporary set up. The magnet is a 50°, 70 cm radius element, which, used with 1 mm wide slits, gives a resolution of about 40 keV.

A series of momentum spectra, taken at different field levels, is shown in Fig. 3.7.1(i). The graphs (a) to (f) may be compared with the spectrum computed for a 30° synchronous phase angle, shown in graph (g), and satisfactory agreement can be seen with the spectrum obtained at a 7.8 V monitor pulse height.

The way in which the momentum distribution should vary with field level can be deduced from Fig. 3.7.1(ii). This shows the computed energy-phase distribution of protons at the linac output and is for 30° synchronous phase angle, giving 2.65 linear phase oscillations. The effect of changing the linac field level is to change the number of linear phase oscillations and effectively to produce a rotation of the energy-phase curve. For example, for a integral number of half linear phase oscillations the momentum spectrum would have a strong central peak, while for an odd number of quarter phase oscillations it would have two prominent, widely spaced peaks separated by a plateau. These expectations are in broad agreement with the observed spectra. A similar set of spectra obtained for various linac field tilts show that the predominant effect of field tilting on the momentum distribution is also one of a change in the number of phase oscillations.

3.7.3. Emittance Measurements

A series of measurements of the emittance of the 15 MeV beam is being carried out in the HEDS. Information which relates the output emittance to the settings of the linac quadrupoles, is required before the tank focusing can be set correctly.

Because of limited aperture in the HEDS flight-tube, the normal method of measuring emittance with two movable slits is not feasible. A system has been worked out, see Fig. 3.7.2(i), using a steering magnet and a fixed central slit, to replace either or both of the movable slits. This system overcomes the aperture limitation sufficiently.

It can be shown that on the phase space diagram at the output end of the linac -

- (i) the lines corresponding to a constant value of 'd' (see Fig. 3.7.2(i)), have a slope of $1/l_1$ and cut the θ axis at $-dl_2/l_1l_3$
- (ii) the lines corresponding to a constant value of magnet current 'I', have a slope of $\frac{-1}{l_1+l_2}$ and cut the r axis at $-KI l_2$

(600 keV INJECTION ENERGY AND NOMINALLY FLAT FIELD)
 GRAPHS (a)-(f) EXPERIMENTAL : PARAMETER IS MONITOR VOLTAGE
 PROPORTIONAL TO LINAC FIELD LEVEL
 GRAPH (g) COMPUTED : CURRENT PER 50 keV INTERVAL FOR
 MOTION ON AXIS AT 30° SYNCHRONOUS PHASE ANGLE.

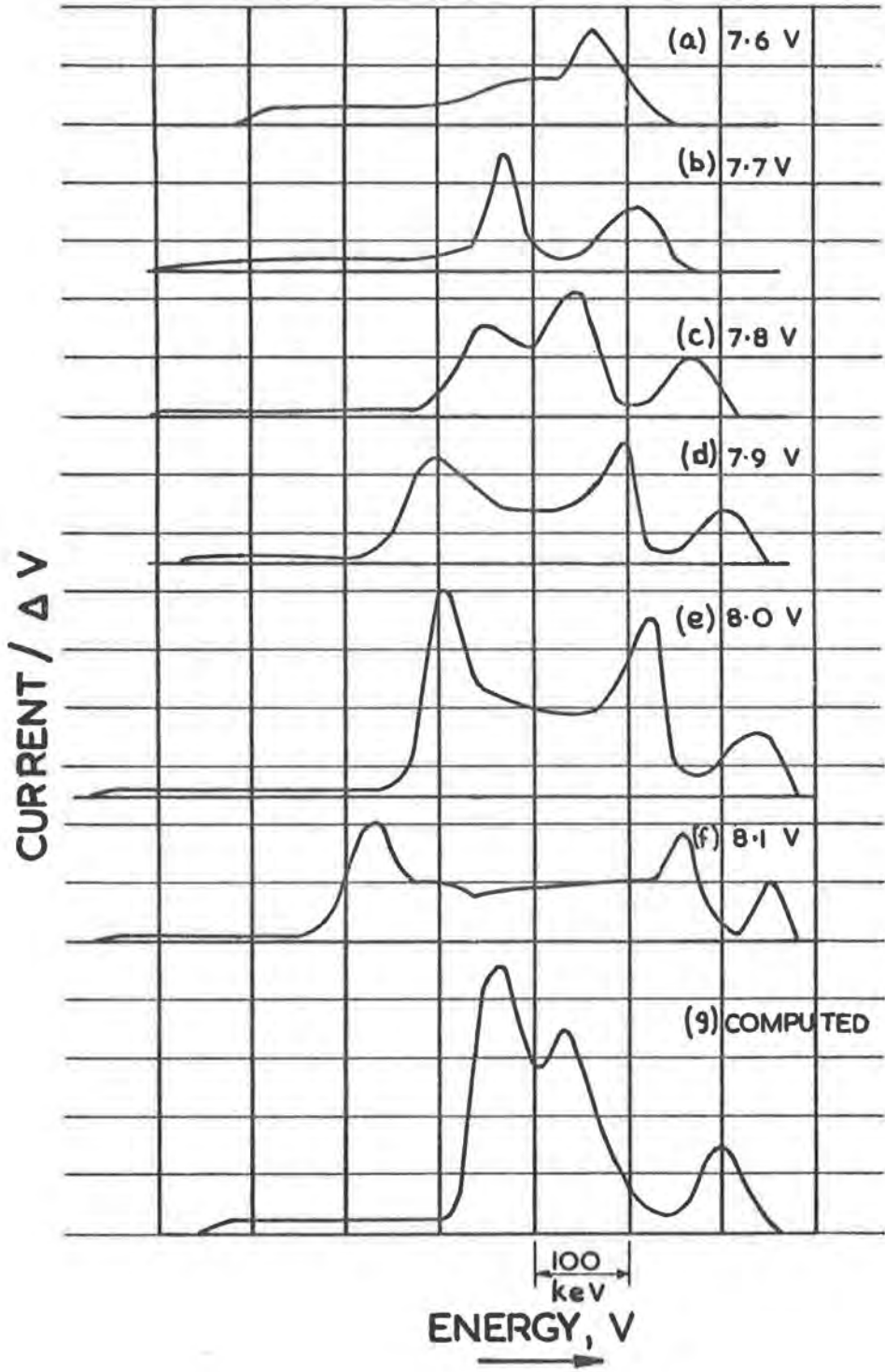


Fig. 3.7.1(1) 15 MeV Momentum Spectra at Various Linac Field Levels.

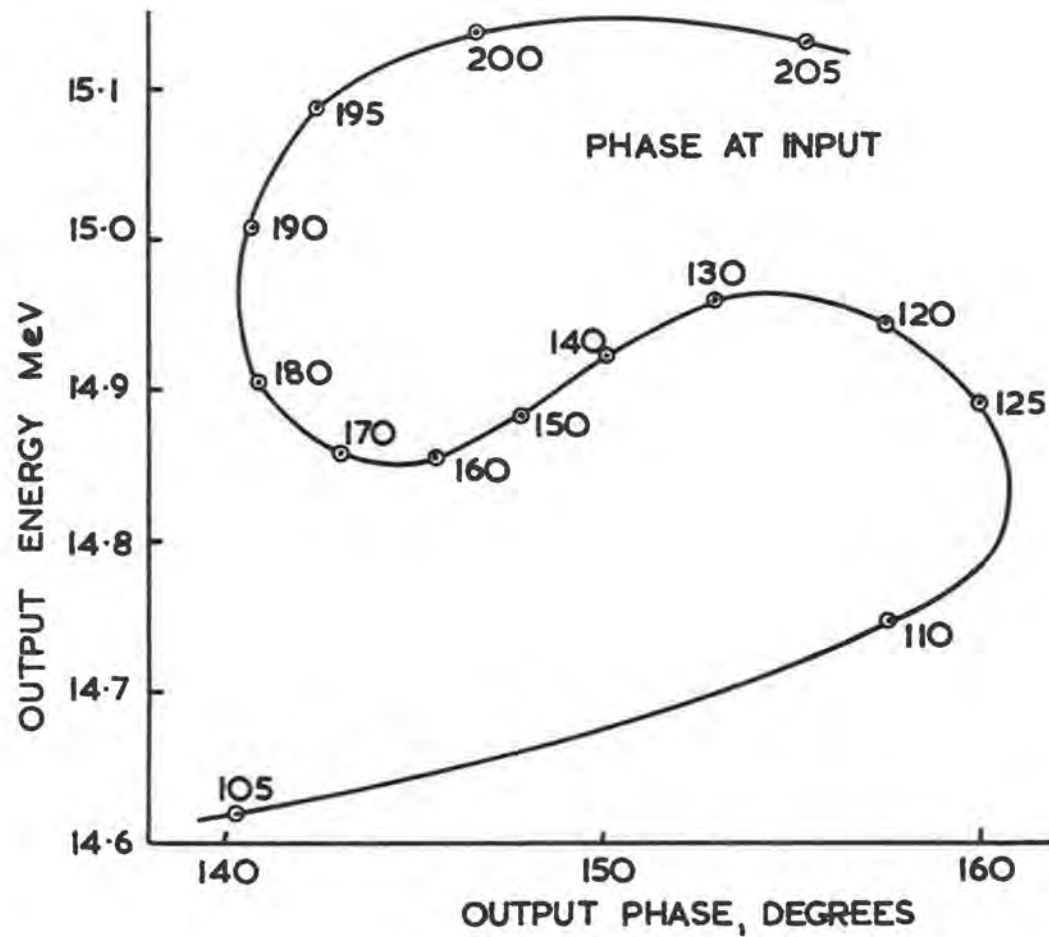


Fig. 3.7. 1(ii) Computed Proton Energy-Phase Distribution at the Linac Output.
 (For motion on the axis and a 30° synchronous phase angle).

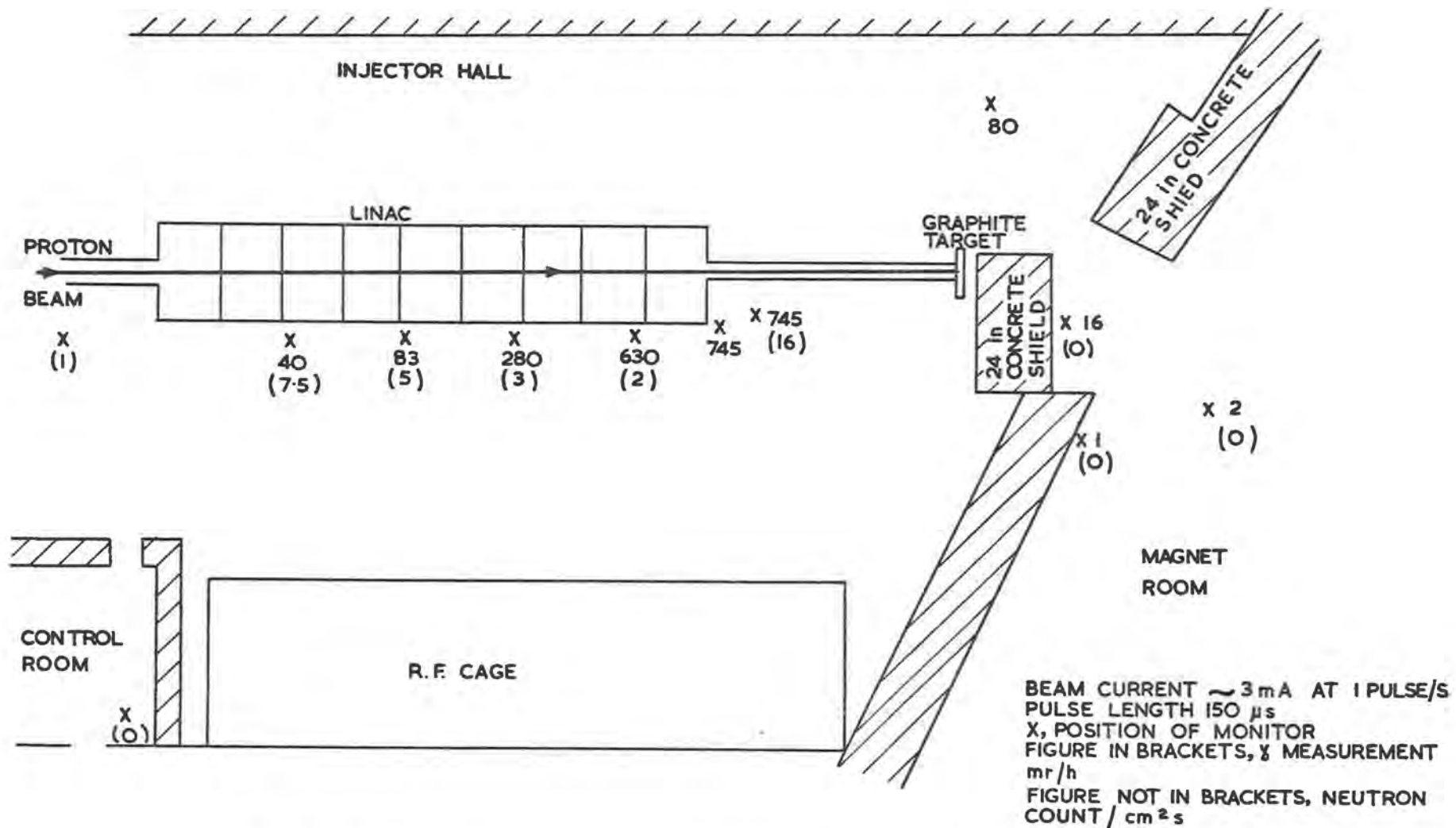
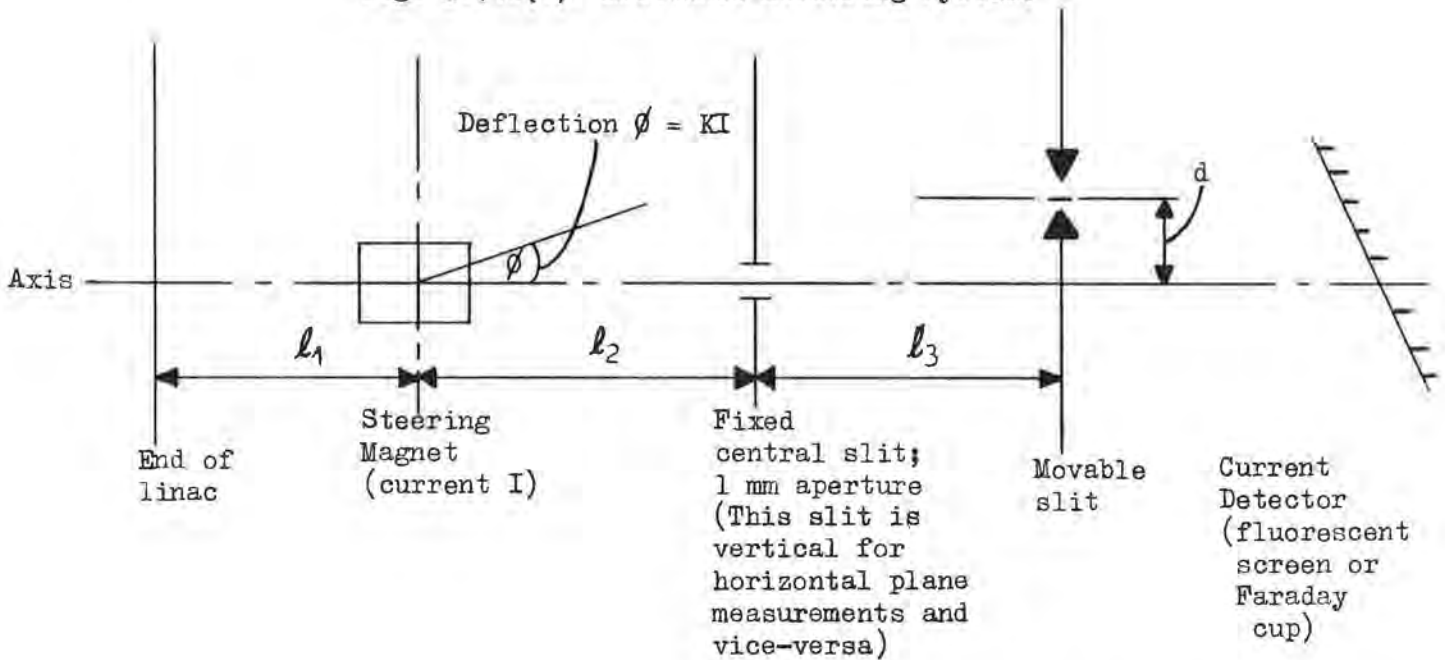


Fig. 3.7.3(i) Map of observed gamma and neutron levels (September 1962).

Fig. 3.7.2(i) Emittance Measuring System.



Charts have been prepared for both the horizontal and vertical planes on which the beam extinction settings of "d" and "I" can be plotted to give the linac output beam emittance diagram directly. Using the same equipment but a modified technique it is possible to plot current density profiles in the linac output phase space ellipse.

Further work remains to be done on the HEDS emittance measurements and on setting up the linac quadrupoles.

3.7.4. Radiation Survey

Fig. 3.7.3(i) is a map showing some observed gamma and neutron levels. The levels appear fairly reproducible, but the neutron flux, obtained from measurement of induced activity in Indium foils is subject to variations from run-to-run which are not at present properly understood. As far as possible, all surfaces in the HEDS, which are intentionally introduced so as to intercept the beam are of graphite, whose p-n production threshold is approximately 18 MeV. The drift tube bores from drift tube No.35 upwards are also lined with 1 mm thick graphite sleeves. Provision has been made to line the remaining drift tubes at a suitable opportunity.

At present levels of operation the integrated dose is nowhere excessive but when the injector is running at its design current and at full duty cycle, the neutron levels are expected to exceed tolerance in the vicinity of the 15 MeV beam.

REFERENCES FOR SECTION 3

1. T.R. Walsh. 'Provisional Selection of Some Injector Parameters' Internal Report HAG/INJ/7
2. R. Taylor. 'Calculation of Drift-Tube Dimensions in the Linac Injector for the 7 GeV Harwell Proton Synchrotron' A.E.R.E./R3012
3. R. Taylor. 'Acceptance of Axially and Radially Oscillating Particles in the Linac Injector for Nimrod' A.E.R.E./R3013
4. R. Taylor. 'Effects of Rotational Misalignments on the Radial Acceptance of the Linac Injector for Nimrod' A.E.R.E./R3096
5. E. Regenstreif. 'The CERN Proton Synchrotron. Chapter 5 Injection' CERN Report 60-26
6. CERN Internal Report PS/3396; MPS/Int. LIN 62-3
7. J.R. Pierce. 'Theory and Design of Electron Beams' D. Van Nostrand, New York
8. L.C.W. Hobbs et al. 'Plasma Physics' Vol.1, pp 130-134.
9. J.J. Wilkins. 'Design Notes on Resonators on Proton Linear Accelerators' A.E.R.E. GP/R1613
10. N.D. West. 'R.F. Model Measurements for the Injector Linac' Internal Report HAG/INJ/11.
11. J.T. Hyman. 'Design of Quadrupole Focusing Magnets' Internal Report HAG/INJ/9.
12. J.T. Hyman. 'Quadrupole Dimensions for the Synchrotron Injector Linac'. Internal Report HAG/INJ/12.
13. J.T. Hyman. 'Modified Design and Dimensions for the Injector Linac Quadrupoles' Internal Report HAG/INJ/14
14. R. Billinge. 'Beam Steering in the Nimrod Injector System' Internal Report HAG/INJ/16
15. J.T. Hyman. 'Some High Current Circuits Using Transistors' NIRL/R/17
16. R. Billinge. 'An Achromatic Inflector System for Nimrod' AERE/R3475
17. M. Bell. 'Injection into the 7 GeV Synchrotron' AERE/T/M155
18. J.T. Hyman. 'Injector Control Room Pulse Timing System' Internal Report HAG/INJ/24.

SECTION 4

MAGNET AND ASSOCIATED SYSTEMS

The Nimrod magnet is made up of eight sections (octants) separated by nominally field-free regions (straight sections). The magnet yoke of each octant contains 42 sectors. Early design information⁽¹⁾ and a description of the sectors⁽²⁾ are already available. Details of the foundations for the magnet ring are also published⁽³⁾.

4.1. Sector Testing

It can be shown that azimuthal variations of the guide field, B_z , lead to variations in the radial position of the proton closed orbit in the machine. This is equivalent to a loss of radial aperture; e.g. a first harmonic variation of B_z with amplitude $\frac{\Delta B_z}{B_z} = \frac{4}{10^4}$ leads to a loss of radial aperture of 1 inch.

Each magnet sector was therefore compared with a reference sector on receipt from the manufacturers to determine the following characteristics:-

- (i) Value of remanent field
- (ii) Relative values of field produced by current in the energising coils at values of field in the gap varying from 200 to 14,000 gauss
- (iii) Eddy current effects.

The electronic measuring equipment⁽⁴⁾, the model (see Fig. 4.1(i)) and its power supply have been described elsewhere⁽⁵⁾. The measurement programme took about sixteen months.

4.1.1. Results of Tests

Variations in the value of the remanent field and hence the value of gap field at low pulsed fields were the most noticeable. Fig. 4.1(ii) shows the value of the remanent field plotted against the order in which the sectors were manufactured. It is very noticeable that early sectors had a very much higher remanent field (up to 24 gauss) than later sectors. This was due to the fact that it was not possible to manufacture the whole quantity of steel in one batch and randomise completely. The steel which had been annealed early in the programme was the cause of the high remanence and was present in sectors up to about number 245.

The largest variation in relative field at low fields was directly due to variations in remanent field values. This is shown on Fig. 4.1(iii) which has a band containing the result of plotting relative fields at 200 gauss against remanent field. The width of the band was about 1.3%, or 2.6 gauss, compared with a remanent field band of 12 gauss. This graph also shows the interdependence of remanent field and low field permeability; viz, sectors with high remanent field have low permeability and hence relatively low pulsed field values at low fields.

There were differences in remanent fields measured for a given sector with the high and low dB/dt at low fields. In general the remanent fields of all sectors were lower with the higher dB/dt, and sectors with low remanent fields were depressed more at the higher dB/dt.

An attempt to measure eddy current effects was made using a saturating choke to vary dB/dt at 200 gauss. No variations in relative field outside the measurement accuracy were found for the two rates of rise.

The relative variation of gap field at 10 kilogauss is shown in Fig. 4.1(iv) and that for 14 kilogauss in Fig. 4.1(v). There was only slight correlation between gap field and sector weight (i.e. magnet cross-section or flux density) at 14 kilogauss. Polepieces on the test model with larger radial extent would have been an advantage in showing up high field permeability effects.

4.1.2. Distribution of Sectors Around Magnet

In order to prevent delay in placing sectors in correct positions on the monolith, allocation of sector positions as a result of the tests were made continuously as testing proceeded. End-of-octant sectors were chosen as those with good high field results and large weight since the end sectors were required to carry more fringe flux at high fields. Sectors were also required here with good mechanical shape i.e. constant width with radius along the gap. Eight sectors with similar properties at low fields were then allocated the same relative positions in each octant. Batches of eight sectors were then continuously allocated in such a way as to keep the total relative field in each octant and with equal distribution within a quarter of each octant. As described above the largest variation was at 300 gauss but a similar check on total field was kept at 600, 10,000 and 14,000 gauss. As an added insurance, at high fields the total weight per octant was equalised. The difference in remanent field for the different dB/dt values was also equalised.

The results of this exercise were gratifying. At 300, 10,000 and 14,000 gauss the average error per octant was adjusted to be lower than the accuracy of measurement (a few parts in 10^4). The total variation in octant weight was 12 hundredweight or about 0.1%; individual sectors varied by as much as 4 hundredweight.



Fig. 4.1(i) Magnet model IV used for sector comparison.

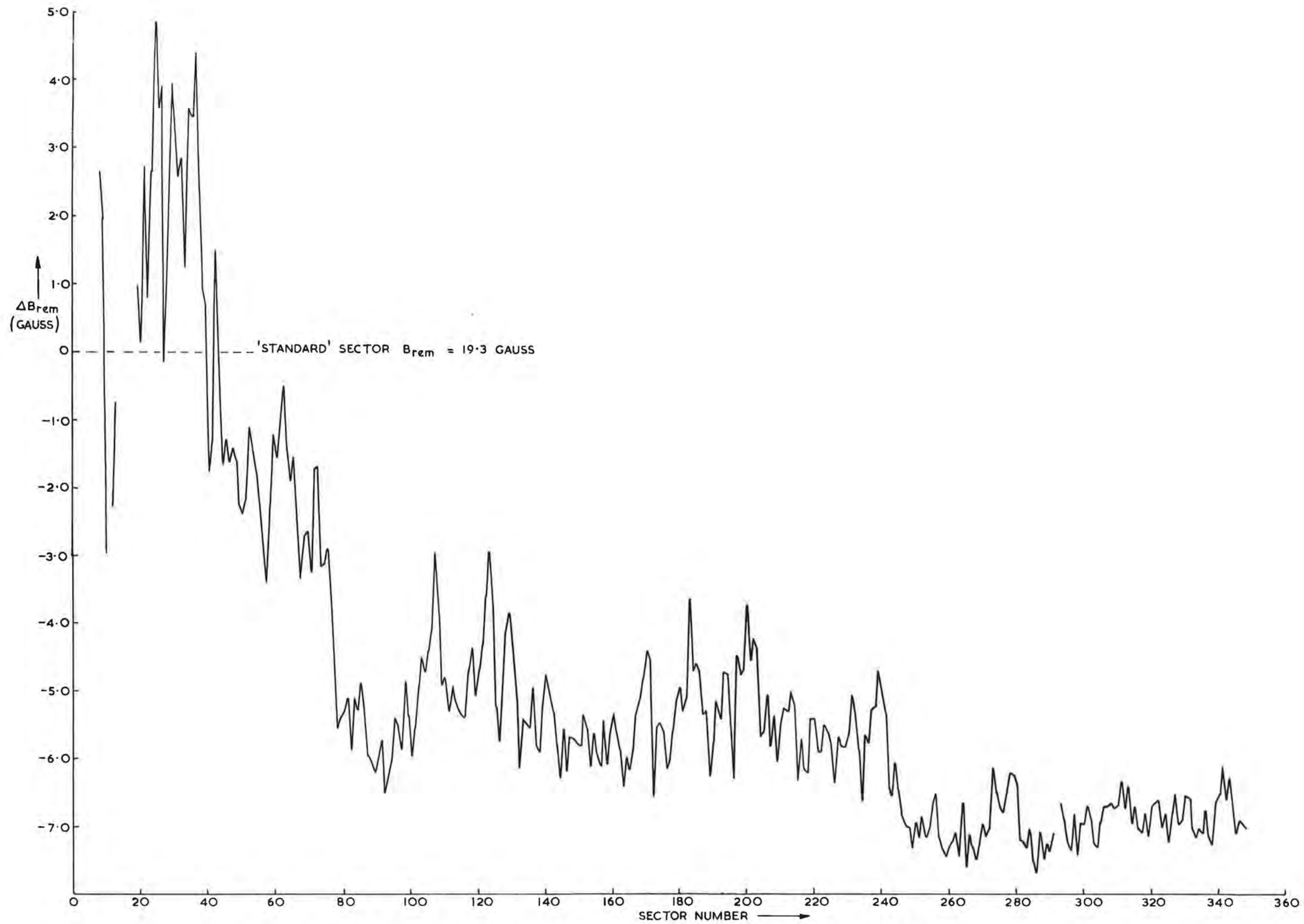


Fig. 4.1(ii) Variation of remanent field with order of production of sector.

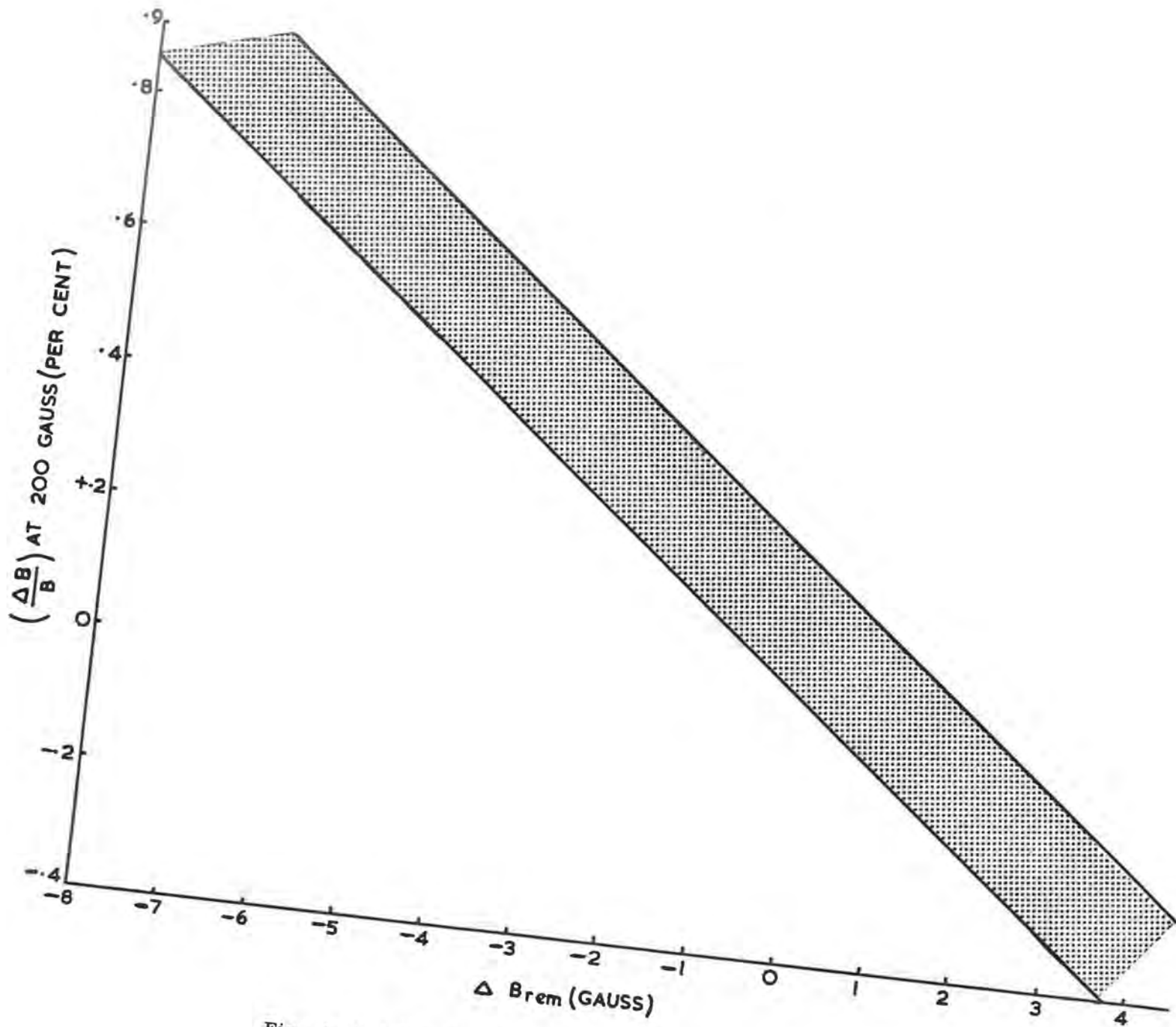


Fig. 4.1(iii) Variation of low field properties with remanent field.

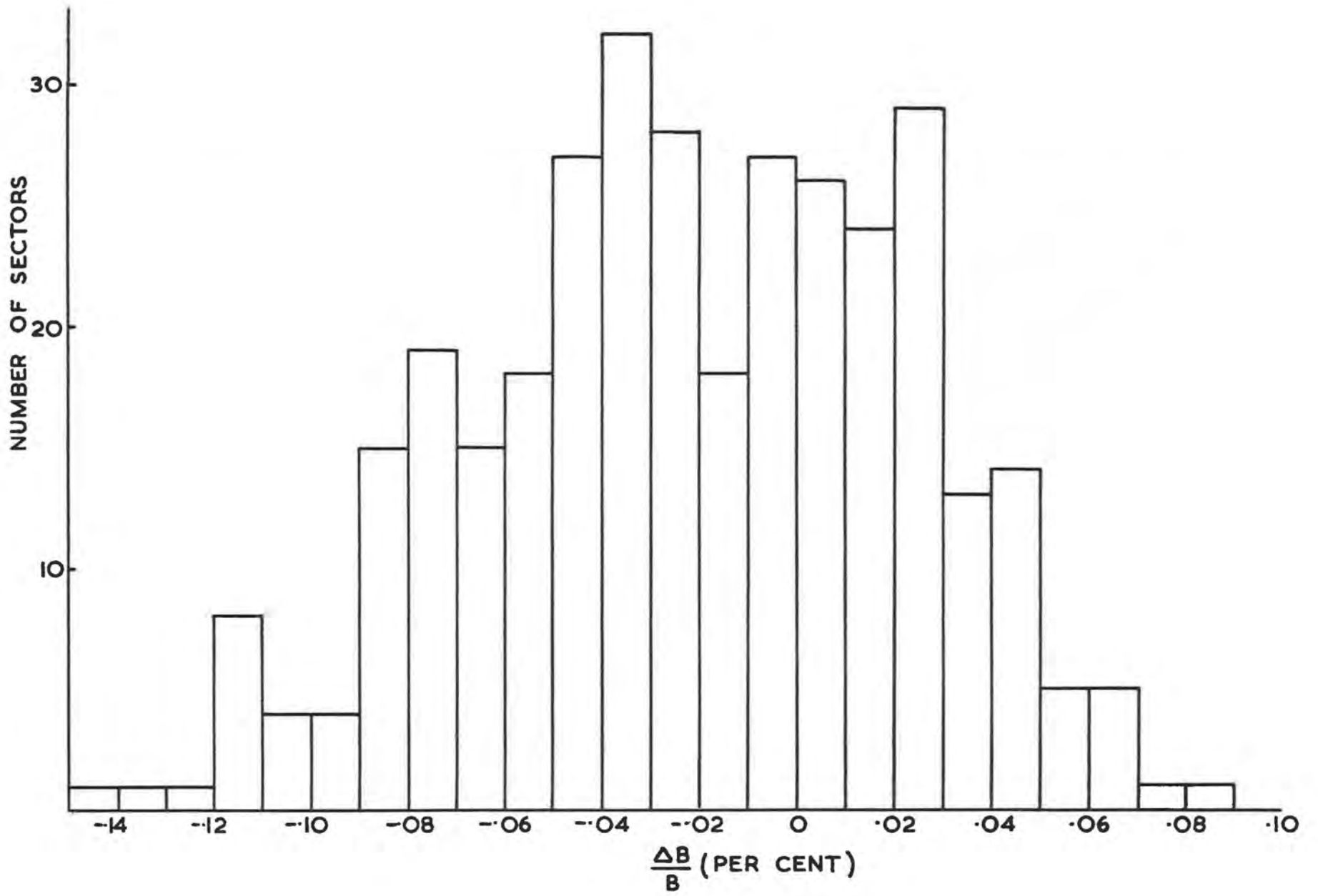


Fig. 4.1(iv) Variations in gap field at 10 kilogauss.

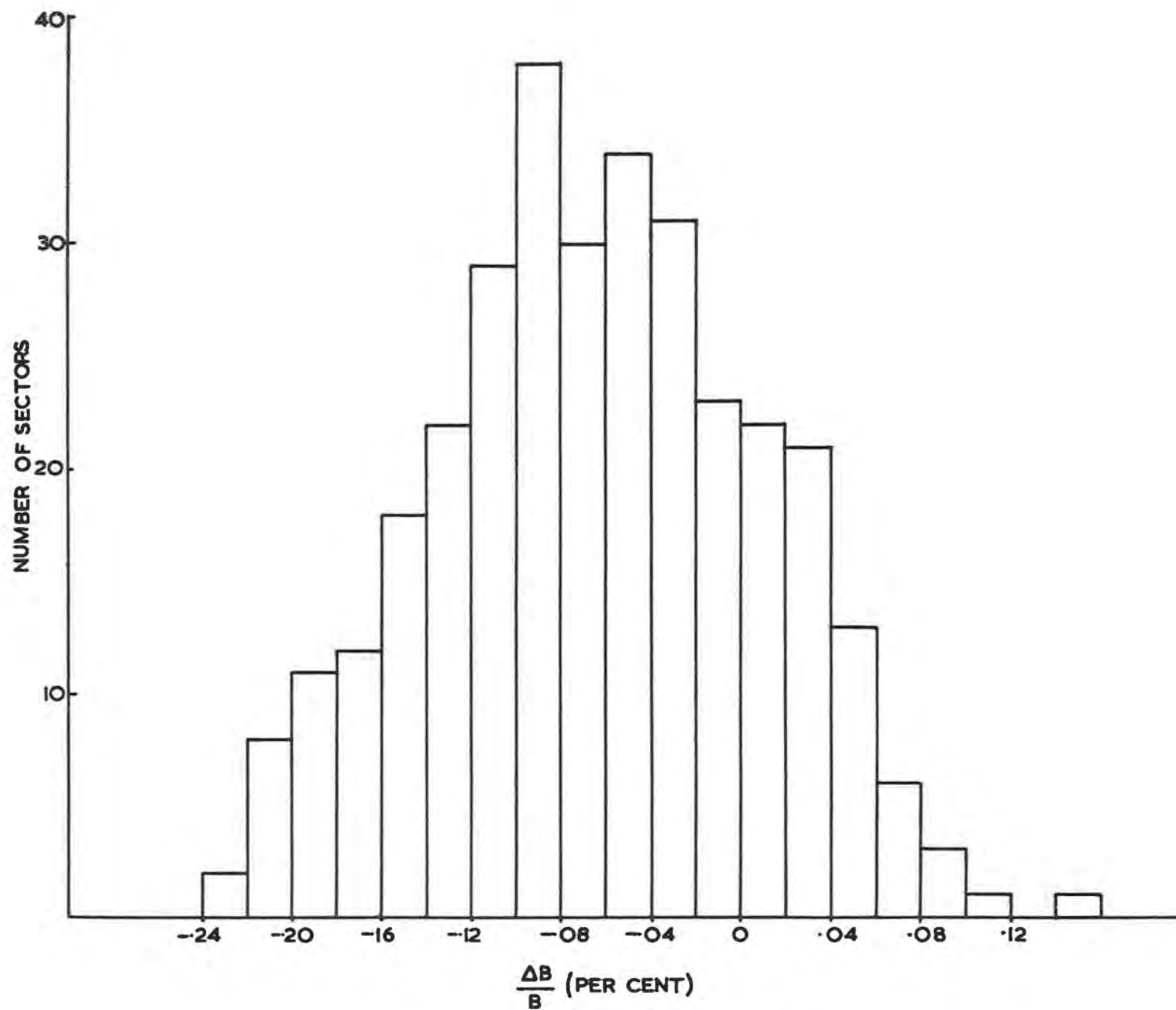


Fig. 4.1(v) Variations in gap field at 14 kilogauss.

4.2, Main Coils

During the early part of 1962 the installation of the longitudinal conductors, end conductors, and all the steel work connected with the octant and magnetic shielding was completed.

Clamping of the longitudinal conductors and end conductors is achieved by means of air bags pressurised to 25 lb/in². Three narrow bags stretch the length of the throat longitudinal conductors, and are placed between the upper and lower sets of conductors. These bags clamp the conductors against the lower and upper faces of the coil aperture. Two wide bags in front of the conductors press the conductors back into the throat of the magnet. A similar arrangement is used for the lip conductors.

The end conductors are held by air bags also. Three narrow bags clamp the conductors in a vertical direction, and one wide bag clamps them in a horizontal direction.

To allow for coil movement (and end conductors) due to temperature changes, e.g. when the coil cooling water drops below a pre-determined figure, hydraulic jacks used as stops could be operated to allow the end conductors to move inwards, after the vertical air bags had been evacuated.

A good deal of trouble was experienced in the operation of the jacks, oil leaks, sticking rams etc., and the jacks have now been replaced by solid paxolin packers, which can be released manually when required.

During the early stages of the pulsing various movements of the conductors were measured. The maximum amount of movement observed was at the ends of the upper lip conductors which at each pulse had an upward movement of the order of 18 thou.

4.3. Main Polepieces.

4.3.1. Design and Measurements

The main Nimrod polepieces are designed from the basic ideas detailed in (6). Briefly, saturable 'fins' are used at the radial edges of the polepieces in order to reduce the total flux to be carried by the magnet sectors at high gap fields. A design was chosen to save about 5% total flux at peak field. The aim was to obtain 36 in of useful field at injection and 14 in at peak field by using shims at both low and high fields.

For ease of construction of the poles, the shape of the laminations as used on small-scale poles was changed somewhat. The 'inner' lamination was made with the same profile as the 'outer' lamination except for the working profile (see Fig. 4.3(i)). To attain a pole with an effective fin corresponding to an 'f' of about 0.32 (f is the ratio of the amount of steel in a fin to the amount of steel if it were solid) holes were cut in both laminations. The holes were so arranged as to arrive at an effective pole at high field which was similar to the shape of the earlier 'inner' laminations. Since the flux in the fin when saturated has a direction corresponding to about 45° , matching of the saturation effects due to an f of 0.32 fin, requires an $f \sim 0.25$ in the crenellated region of the correction shims. (The n-values for an uncorrected pole are shown in Fig. 4.3(ii)). The inner lamination was .020 in thick 4% silicon steel; the outer was .030 in thick 1% silicon steel. The high field correction shims were designed with the aid of small-scale^{(7) (8)} and full-scale⁽⁵⁾ models. The basic method of correction is given in (6). If the height of the shim on the inner hidden lamination is d, the effective height of shim is $d(H/B_0)$, H being the field in the saturating steel and B_0 the flux density in the magnet gap. Simple shim theory is used to predict the corrections. In our case a match cannot be made (above about 10 kilogauss) between the correction due to the shims and the error in n as field varies. Three types of laminations with shims of different height are therefore used; the shallow recess corrects up to about 10 kilogauss, this lamination starts to saturate forming a crenellation with a different f value (~ 0.32) and gives a correction due to the shim on the medium recess lamination. This gives correction up to about 13 kilogauss. This lamination in turn begins to saturate giving a third f value with correction due to the shim on the deep recessed lamination. The corrections due to the three different f values are additive. The necessary f-values are obtained by adjusting the numbers of the different types of lamination. Correction of the base line of n is required at high fields; for this reason there is a superimposed slope on the medium and deep recessed laminations as described by the Saclay group⁽⁹⁾. A more detailed report on the design of the polepieces will be published later.

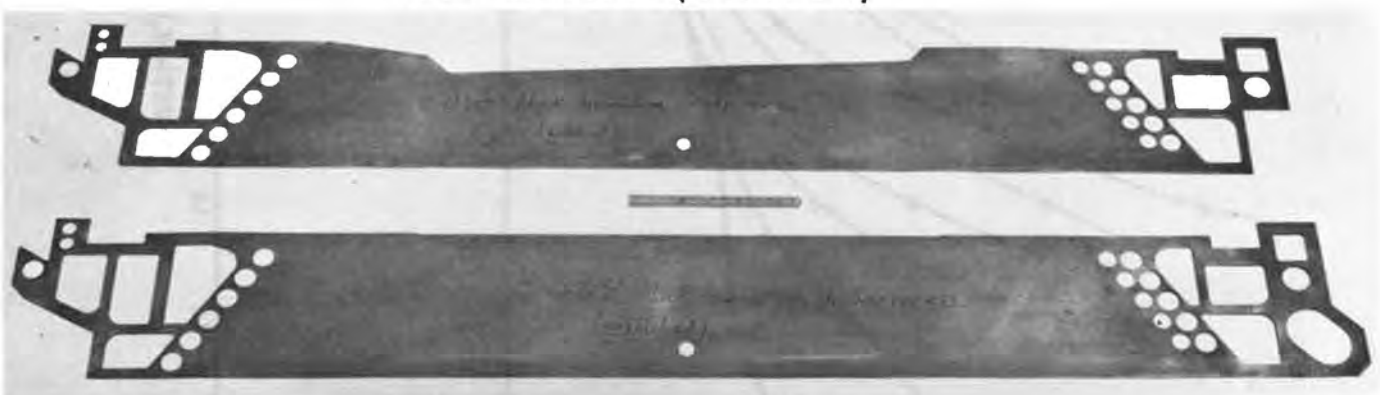
The design of the low field shims is based on (10). The field shapes at low field levels for the production poles when measured on Model V are shown in Fig. 4.3(iii). The high field shapes are given in Fig. 4.3(iv). It can be seen that the correction at the higher fields is not particularly good. This is thought to be due to differences in steel and incorrect allowance for packing factor on extrapolating from bolted up poles to bonded poles. For this reason and because of octant end effects discussed in section 4.4, Mark II poles were designed. These were made from laminations of the same profile but with different ratios of the various laminations (see Fig. 4.3(v)). The field shapes for these poles as measured on Model V are given in Fig. 4.3(vi),

0.020 IN. THICK LAMINATION
(NOTCHED)



0.030 IN. THICK LAMINATION
MEDIUM RECESS (UNNOTCHED)

0.030 IN. THICK LAMINATION
DEEP RECESS (NOTCHED)



0.030 IN. THICK LAMINATION
SHALLOW RECESS (UNNOTCHED)

Fig. 4.3(i) Polepiece laminations.

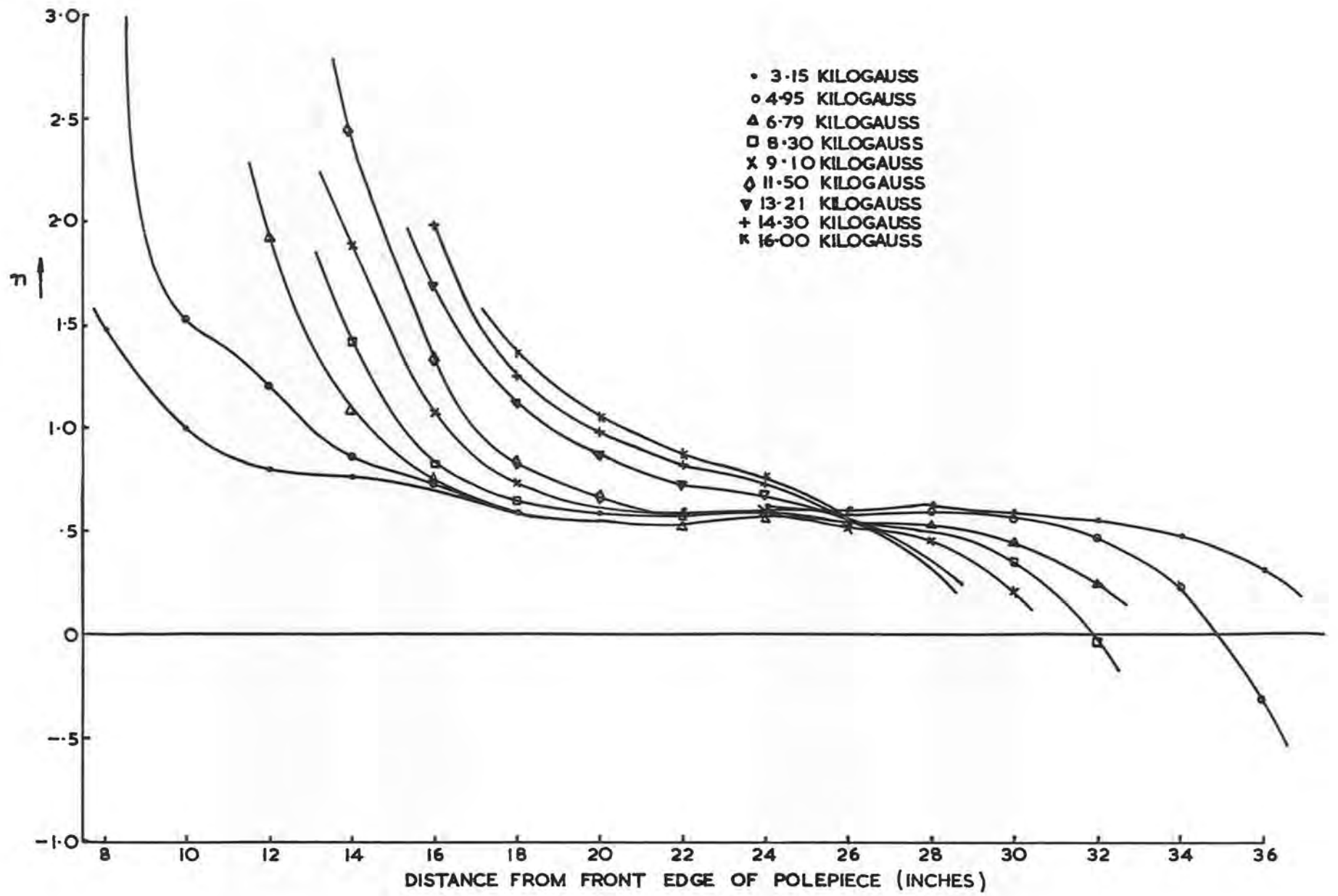


Fig. 4.3(ii) n values for uncorrected pole.

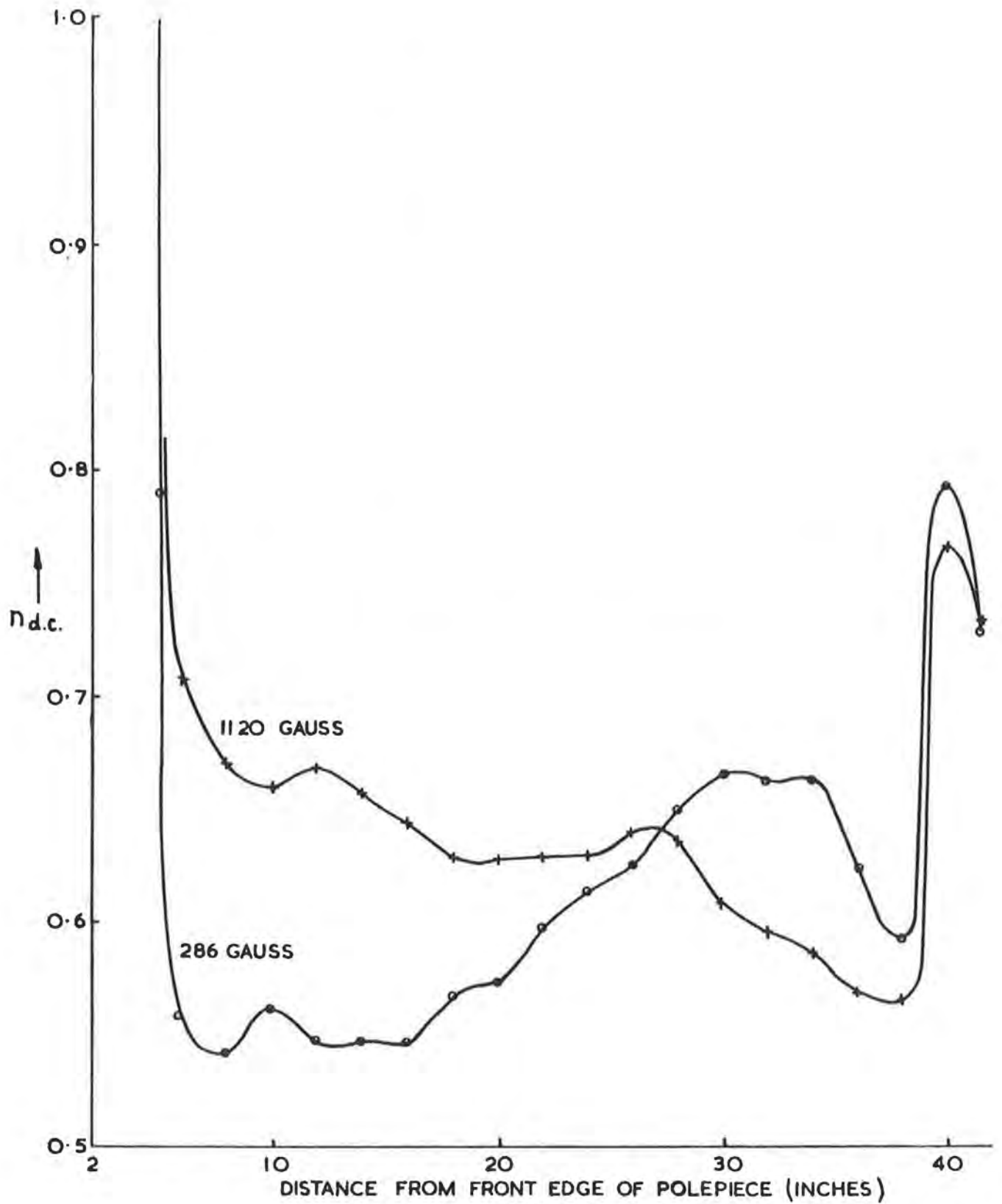


Fig. 4.3(iii) n values at low fields. Production poles on Model V.

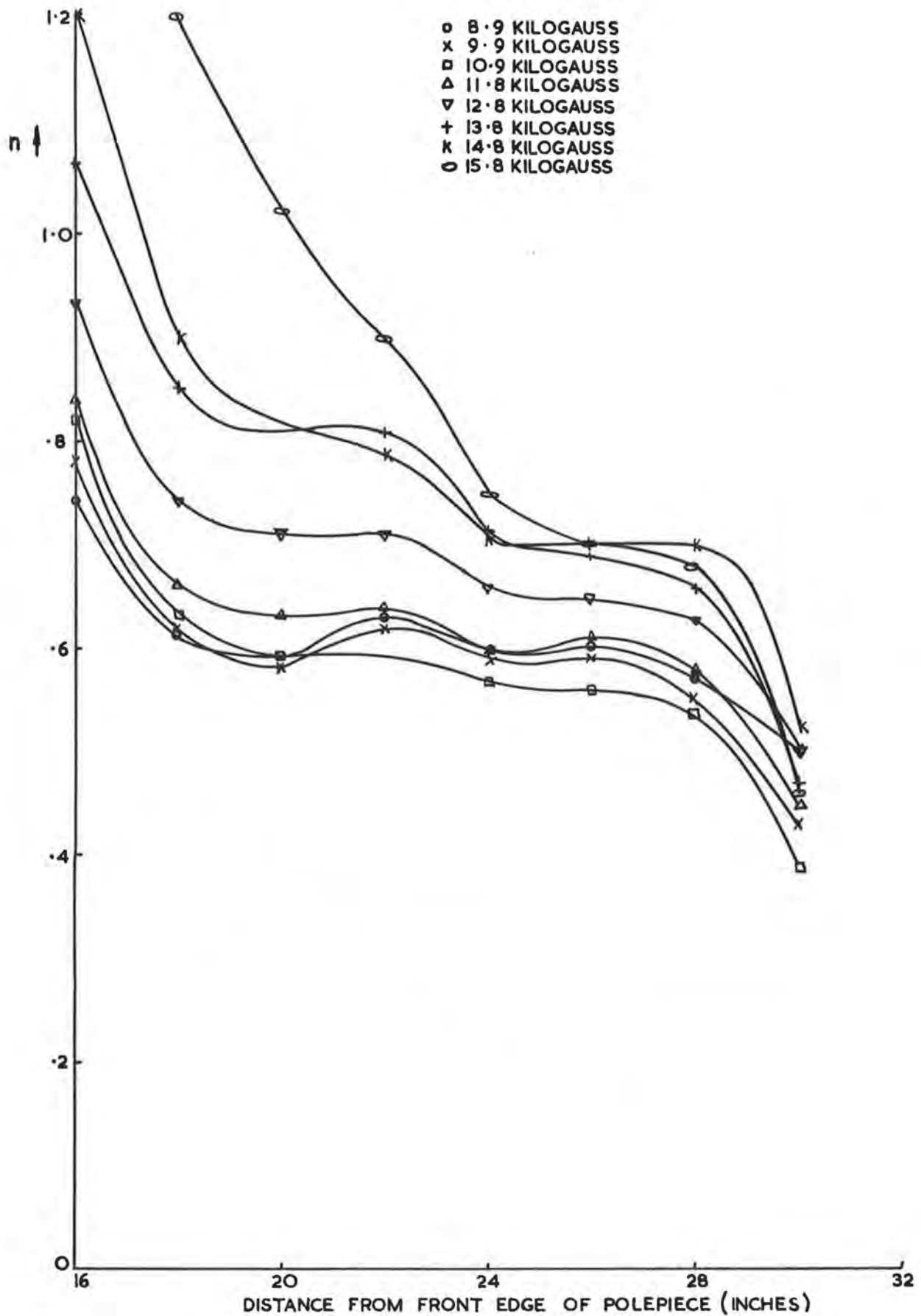


Fig. 4.3(iv) n values at high fields. Production poles on Model V.

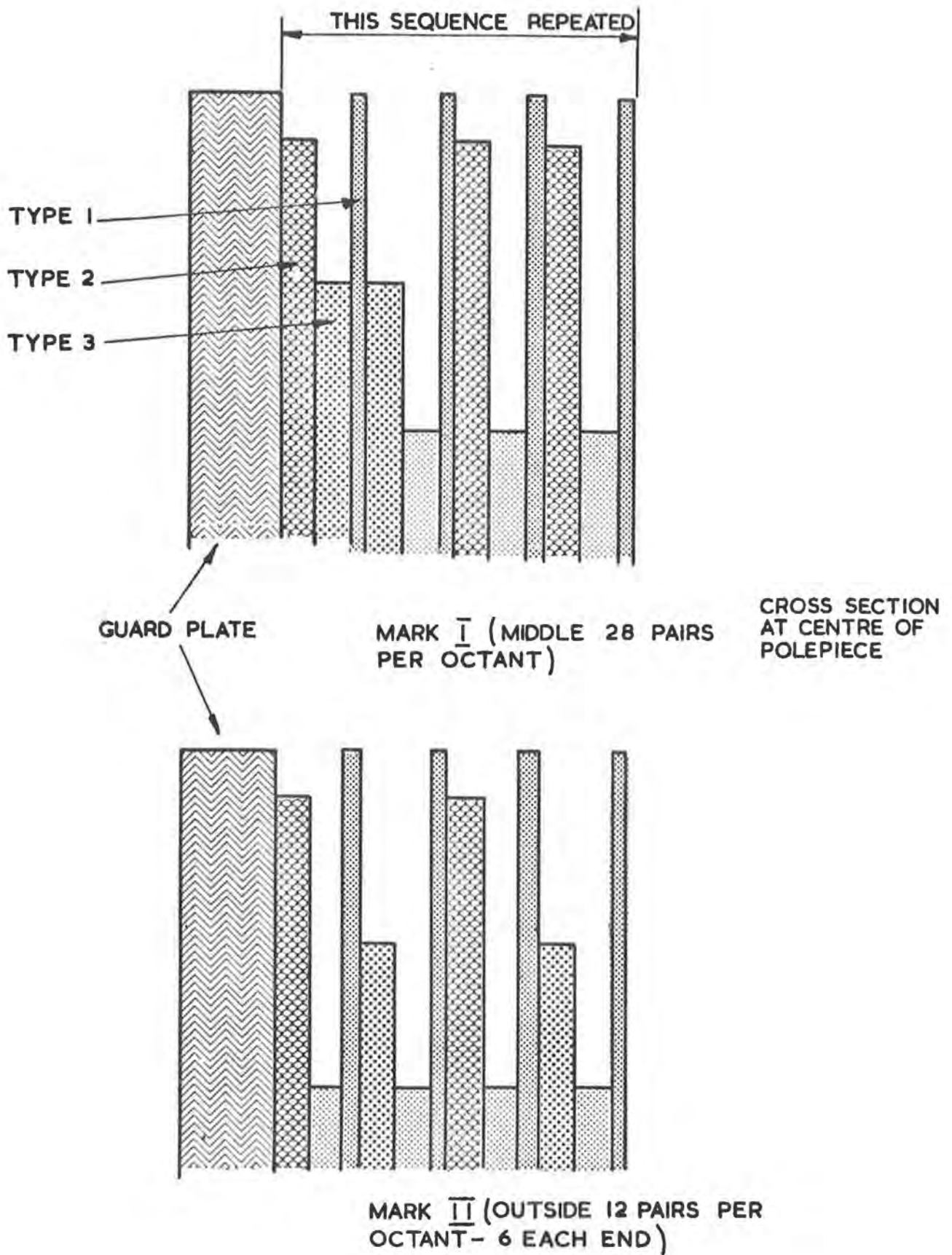


Fig. 4.3(v) Polepiece lamination arrangements.

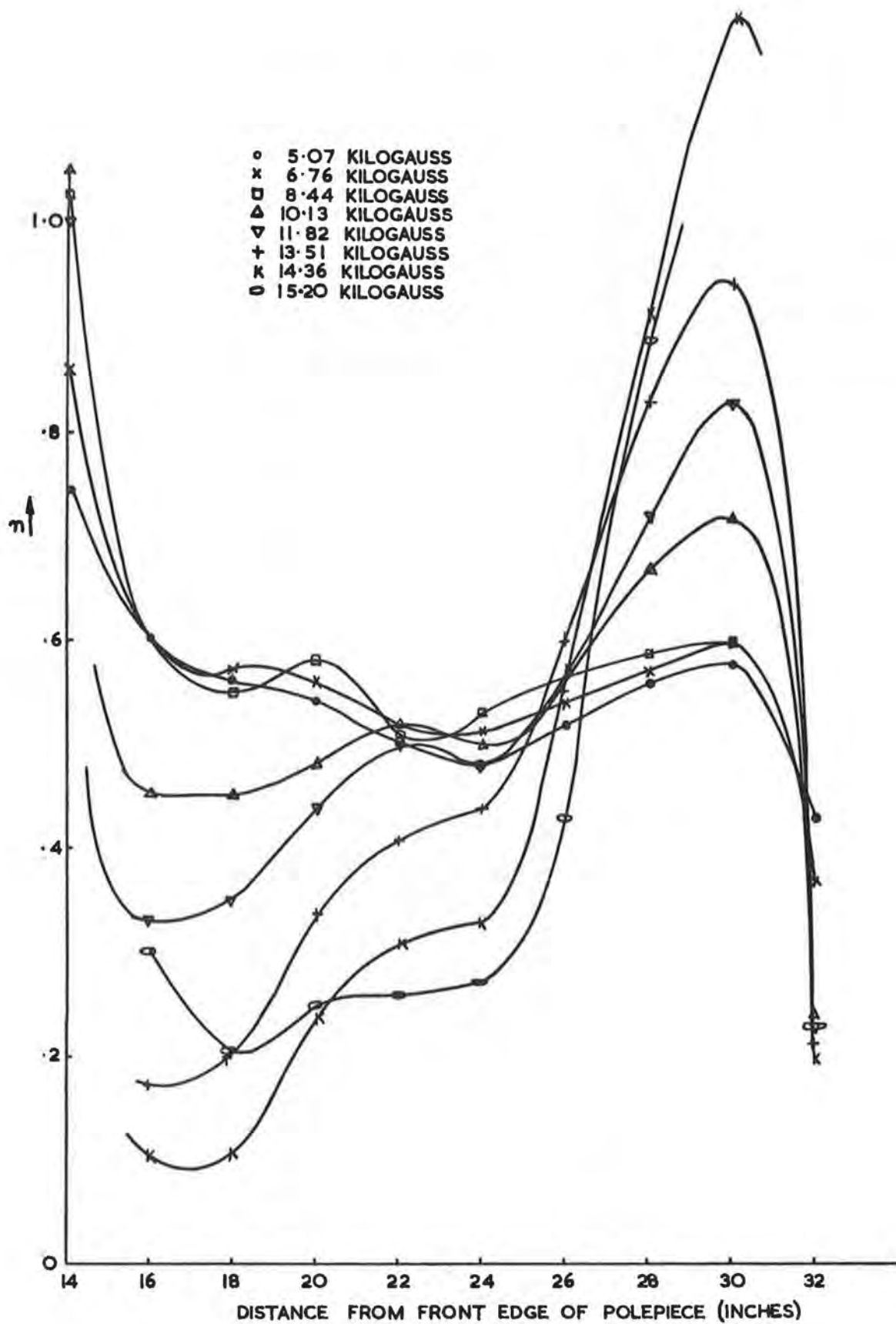


Fig. 4.3(vi) n values for Mark II polepieces on Model V.

The field shapes for the main poles measured during the Nimrod magnetic survey (see Section 4.6) are shown in Fig.4.3(vii), 4.3(viii) and 4.3(ix), these show that at low fields there is greater correction than on Model V. This is most probably due to the difference in energising coil configurations and the difference in the amount of magnetic materials around the coils in the two cases. At high fields, too, there are differences between Model V and the Nimrod magnet. These are probably due to end effects of Model V which is only 7 sectors long.

4.3.2. Manufacture

Each of the 336 magnet sectors is fitted with a pair of polepieces which are positioned between the inner and outer vacuum vessels and support the thin wall of the outer vessel against atmospheric pressure. Special polepieces are used on the end sectors of each octant to achieve the required magnetic field distribution in the straight sections. The assembled main polepiece is approximately 48 in long, 6 in deep and $13\frac{1}{2}$ in wide and is built up from approximately 450 laminations (0.020 in and 0.030 in thick) with a $\frac{1}{4}$ in thick guard or reinforcing plate on each side of the stack of laminations. It weighs about 800 lb. Each lamination is insulated from its neighbours, the insulation being a 0.002 in layer of epoxy resin adhesive, bonding the whole assembly solidly together. These glued joints resist the disruptive magnetic forces.

The guard plates are of a low silicon electrical quality steel identical to that used for the magnet sectors. The thin (0.020 in) laminations are a high quality transformer steel, about 3.5% silicon, with high permeability at low flux densities, whereas the thick (0.030 in) laminations are a low silicon steel with high permeability at high flux densities.

The polepieces are assembled with alternate thick and thin laminations in the ratio; 2 thick, 1 thin, 2 thick, 1 thin, etc. It was necessary to hold all the material in stock so that complete "shuffling" could take place prior to cutting to shape, to ensure a uniformity of magnetic properties in all polepieces which were produced in "matched" pairs. In addition, the laminations had to be cut and assembled in such a way that effects of taper and "crowning" of the rolled sheets were minimised and uniformity of thickness of assembled poles from start to finish of the production run were maintained.

The quarter million or so laminations had to be produced to very fine dimensional tolerances and variation of profile from lamination to lamination did not exceed 0.004 in. The laminations have a network of holes and slots arranged to achieve the required magnetic field. The general process of manufacture was to shear to overall size, pierce the holes, deburr, degrease, anneal, sort into pairs, blank profile, deburr, inspect, degrease and prepare the surface for adhesive. For the assembly, some very massive and rigid assembly jigs were designed and poles were assembled, prior to glueing, in a special clean conditions assembly room. A guard plate was first laid in the jig followed by a layer of adhesive, a lamination, a layer of adhesive, etc., all in a carefully controlled sequence, controlling weights as assembly progressed, until the complete stack was assembled. A slight modification to the assembly sequence was allowed over the last few laminations to permit the weight tolerance of $\pm 1\%$ to be achieved.

The whole assembly, complete in the jig, was then lowered into one of three specially designed curing ovens and subjected to a carefully controlled pressure to ensure dimensional correctness as the adhesive became fluid when subject to the

curing heat. The heating cycle was also very carefully controlled and consisted of approximately $3\frac{1}{2}$ hours to heat to 158°C , held at this temperature for $4\frac{1}{2}$ hours and then allowed to cool over a further $6/7$ hours.

After cooling, the assembled pole was carefully cleaned of surplus resin. A small amount of machining of a taper on the guard plates was completed on a milling machine and the pole was then subjected to an exhaustive range of insulation, dimensional and strength tests. When passed final inspection poles were packed, two pairs in a specially designed transport box, and transported to Nimrod.

The production of the poles, including the very extensive development period when manufacturing techniques were established and final profile shapes were worked out (from a very limited number of experimental poles) occupied a period of 24 months.

Liaison was necessary at all times with the manufacturers and an elaborate series of manufacturing specifications were produced to cover each stage of production in great detail.

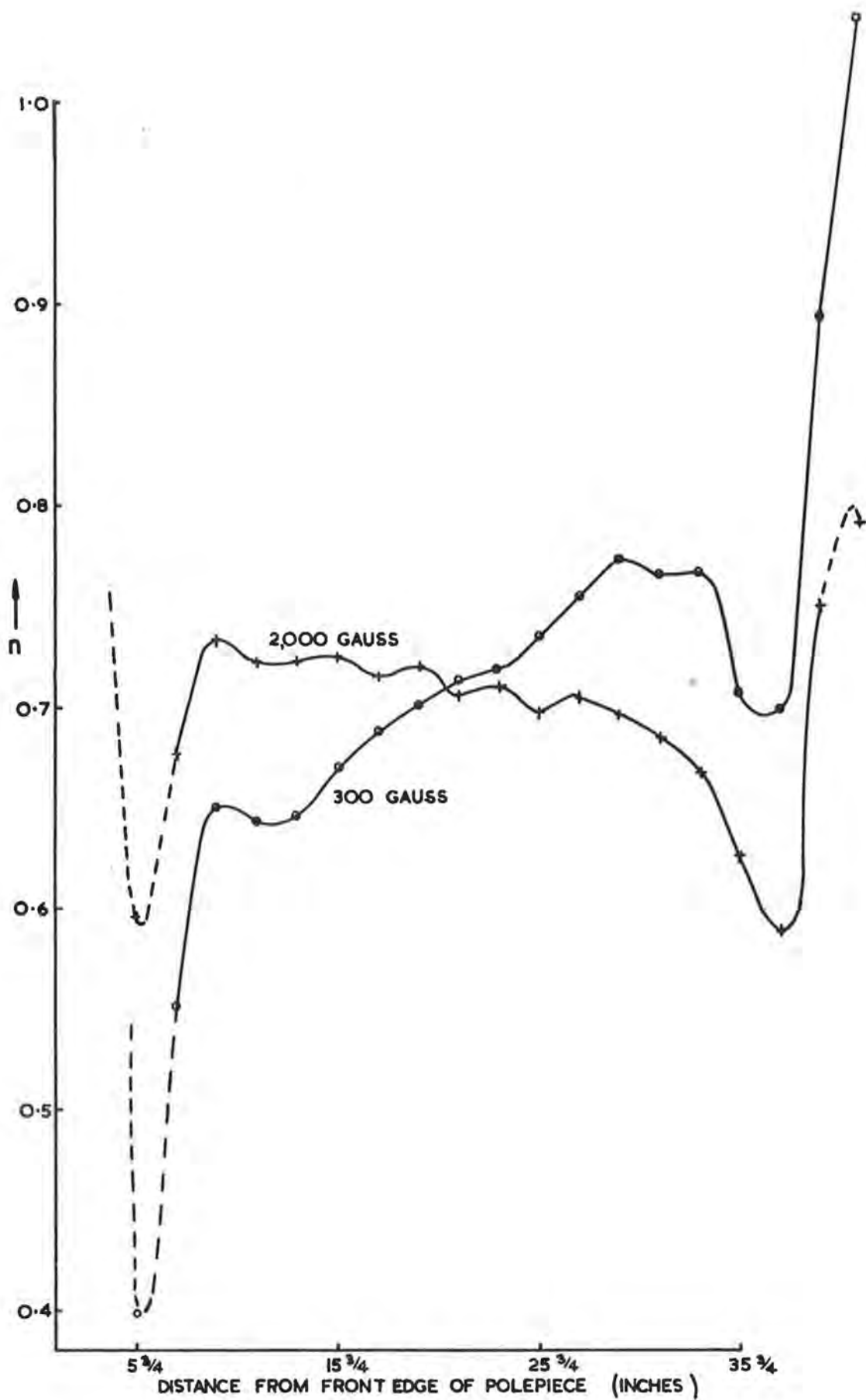


Fig. 4.3(vii) n values at low fields on Nimrod.

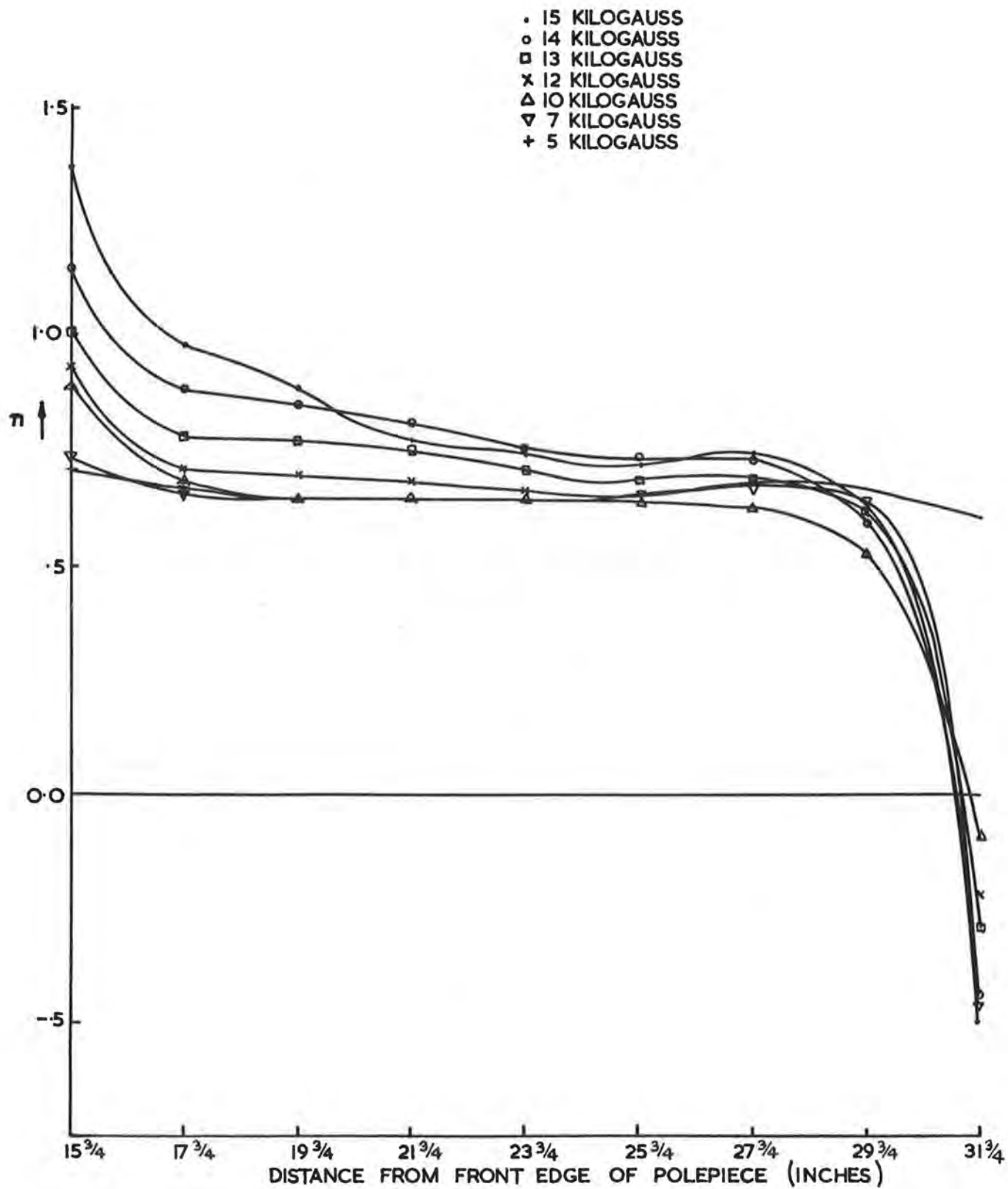


Fig. 4. 3(viii) n values for Mark I polepieces on Nimrod at high fields.

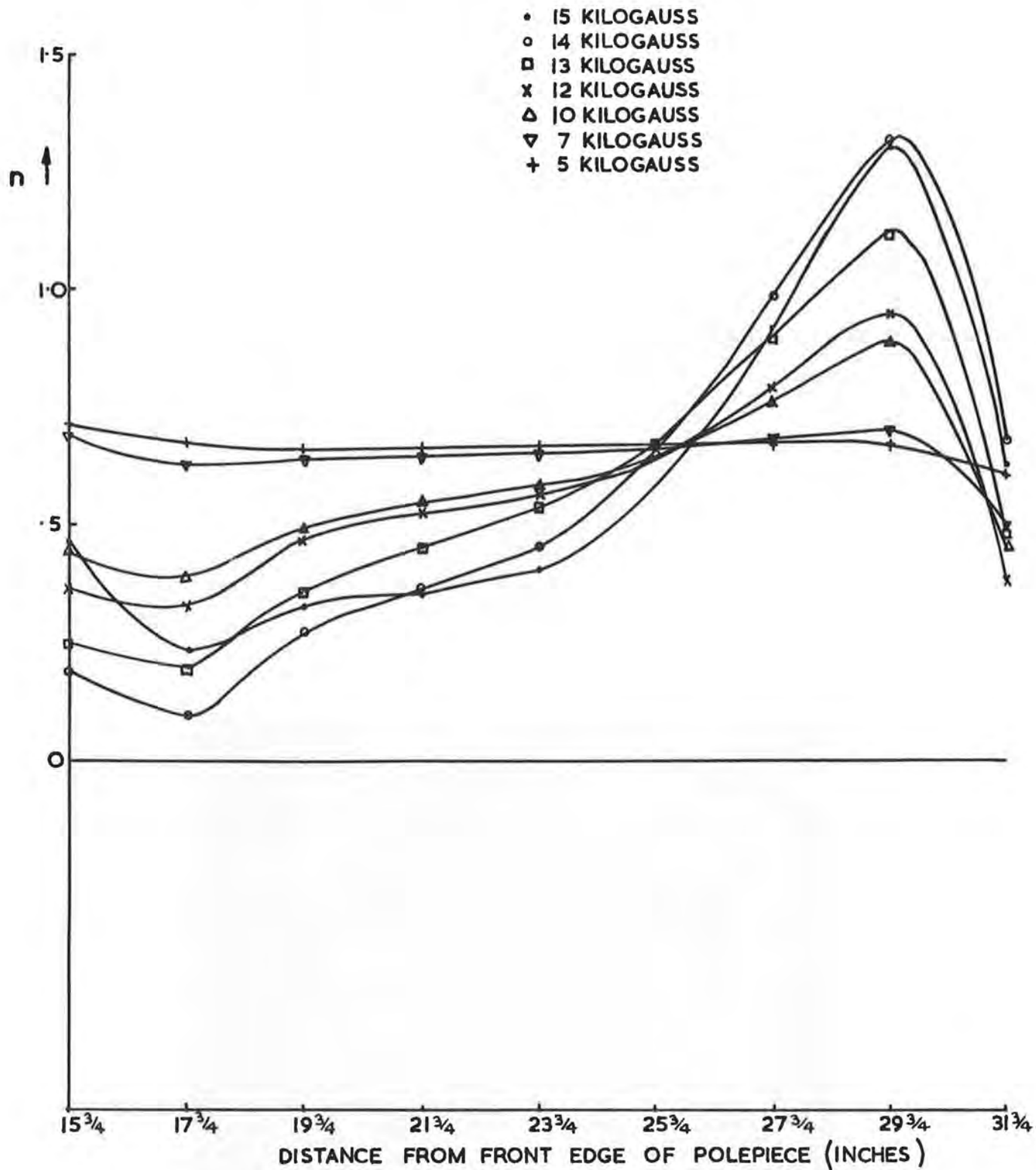


Fig. 4.3(ix) n values for Mark II polepieces on Nimrod at high fields.

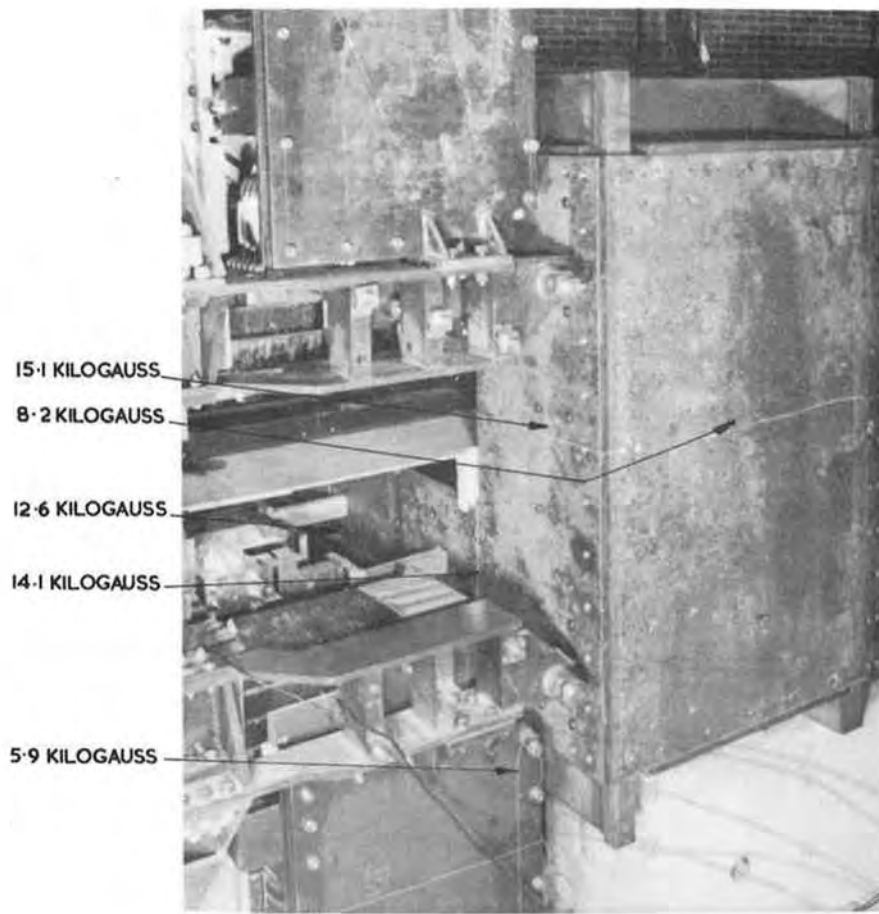


Fig. 4.4.1(i) Flux densities in straight section box.

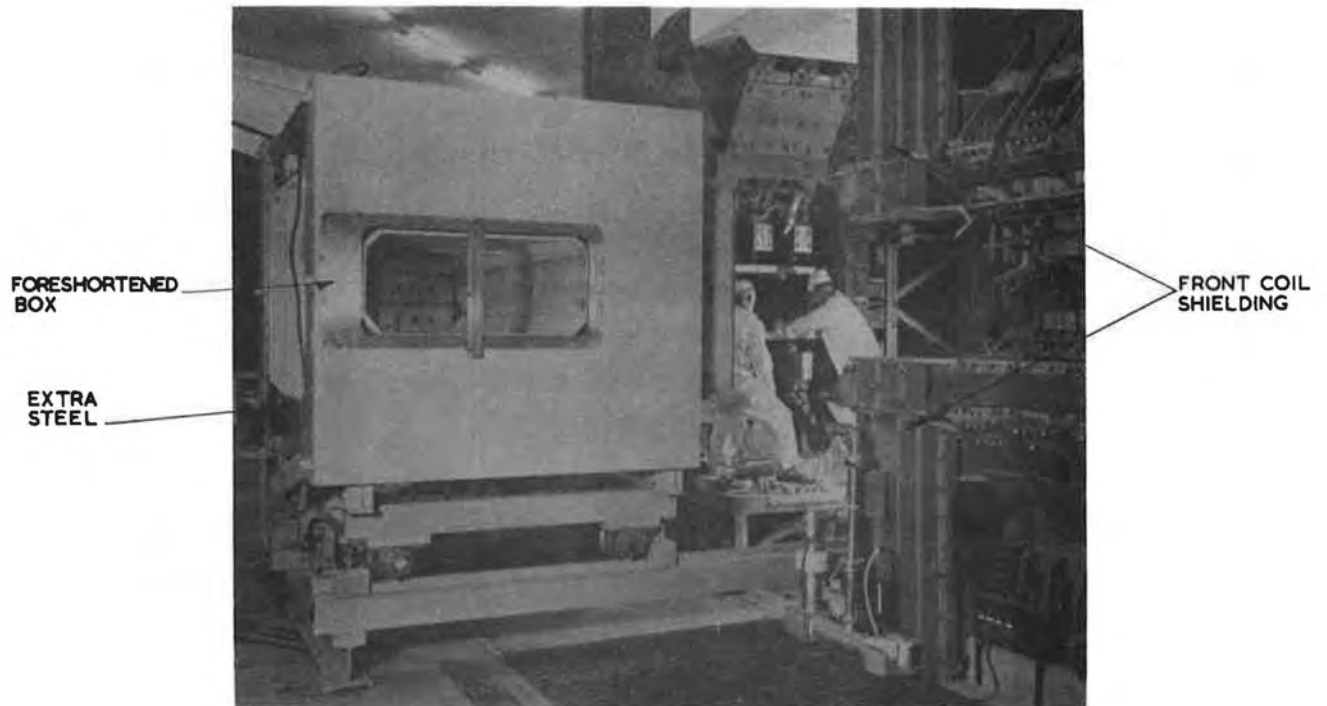


Fig. 4.4.1(ii) Straight section box and coil shielding.

4.4. Straight Sections

In the design of the straight sections and octant ends, the magnetic fields can no longer be taken to be two-dimensional. The design had to ensure:

- (i) That the field in the straight section would be reduced to such a value that it would not have too much effect on secondary beams scattered from a target near a straight section
- (ii) That the field from the magnet would not decrease the permeability of the ferrite in the r.f. accelerating cavity and that the ferrite would not distort the magnet field shape
- (iii) That the effective length of the octants would be as near to the theoretical length as possible at all field levels
- (iv) That the field shape at all field levels would be reasonably correct.

The three main components of the straight sections are straight section boxes, coil shielding and end pole-pieces. The following designs were established using Model III(8) and Model VI(11). Model VI had the same coil configuration as the main Nimrod magnet.

4.4.1. Straight Section Boxes

There was some distinction between the long (14 ft) and short (11 ft) straights. The design of the long straight boxes was dictated mainly by the requirements of the r.f. cavity; the inflector box was the main influence on the short straights. To provide good shielding of the straights mild steel boxes were chosen and the thickness of material required on the faces of the boxes was determined on Model III. Measurements of field gradients in the boxes showed that there was little difference in the field shape for the short and long straight cases. The flux densities measured on Model VI with a dummy r.f. cavity box with 2 in thick faces are shown in Fig. 4.4.1 (i). In order to get scattered particles from internal targets as near as possible to the forward direction, the outside edges of the working ends of some of the boxes were cut back, the steel being replaced as shown in Fig. 4.4.1 (ii).

4.4.2. Coil Shielding

The coil shielding is arranged to cut down the fringing flux from the main magnet coil and is shown in Figs. 4.4.1 (ii) and 4.4.2 (i). The flux densities as measured in Model VI are also shown on Fig. 4.4.2 (i).

4.4.3. End Polepieces

End polepieces were designed using Model III and Model VI. Measurements on Model III were made to ensure that the effective length of the octant would be approximately correct and that it would not vary with field level. (Provided that all octants are the same length, an error in effective length of a few inches is permissible). A pole which was tapered azimuthally was used; to obtain optimum conditions, a taper into the second polepiece would be required. The resultant shape of pole was used on Model VI. By suitably subtracting effects due to the poles on Model VI, the effects on field shape of the ends of an octant were predicted. These are shown in Table 4.4.3(I).

TABLE 4.4.3(I)

Effective error in average 'n' due to octant end effects

Field (kilogauss)	Distance from outside of pole (inches)				
	16	18	20	28	30
10	.08	.13	.11	-.04	-.13
12	.11	.17	.13	-.09	-.24
13	.15	.19	.13	-.11	-.37
14	.16	.19	.13	-.11	-.47

It can be seen that this gives an appreciable error in n in the operating region. Some correction could be achieved by crenellating the end polepiece. A sample was made from $\frac{1}{4}$ in thick laminations with crenellations as shown in Fig. 4.4.3(i) and measurements on Model III (see Table 4.4.3(II)) indicated that it was worthwhile using crenellations on the end polepiece.

TABLE 4.4.3(II)

Effective correction in average 'n' due to end polepiece crenellation

Field (kilogauss)	Distance from outside edge of polepiece (inches)					
	16	18	20	26	28	30
8	.04	.02	.01	0	0	-.01
10	.04	.02	.01	-.01	-.02	-.03
12	.05	.05	.03	-.03	-.06	-.07
13	.05	.06	.03	-.03	-.07	-.08
14	.08	.06	.04	-.03	-.07	-.10

4.4.4. Overall n-correction

By adding the effects predicted from 28 pairs of Mark I poles, 12 pairs of Mark II poles and the end effects, an overall average n-value for an octant was obtained (Fig. 4.4.4(i)). The values obtained during the survey are shown in Fig. 4.4.4(ii). The main difference in the predicted and measured values is at the inside of the good field region and is due to the greater correction of the Mark II poles mentioned in Section 4.3.

At low fields the effective n at the inside radius at the end of an octant was always high, even without inner shims on the end polepieces. This is because

0 KILOGAUSS
18.9 KILOGAUSS
10.3 KILOGAUSS
15.6 KILOGAUSS
3.1 KILOGAUSS

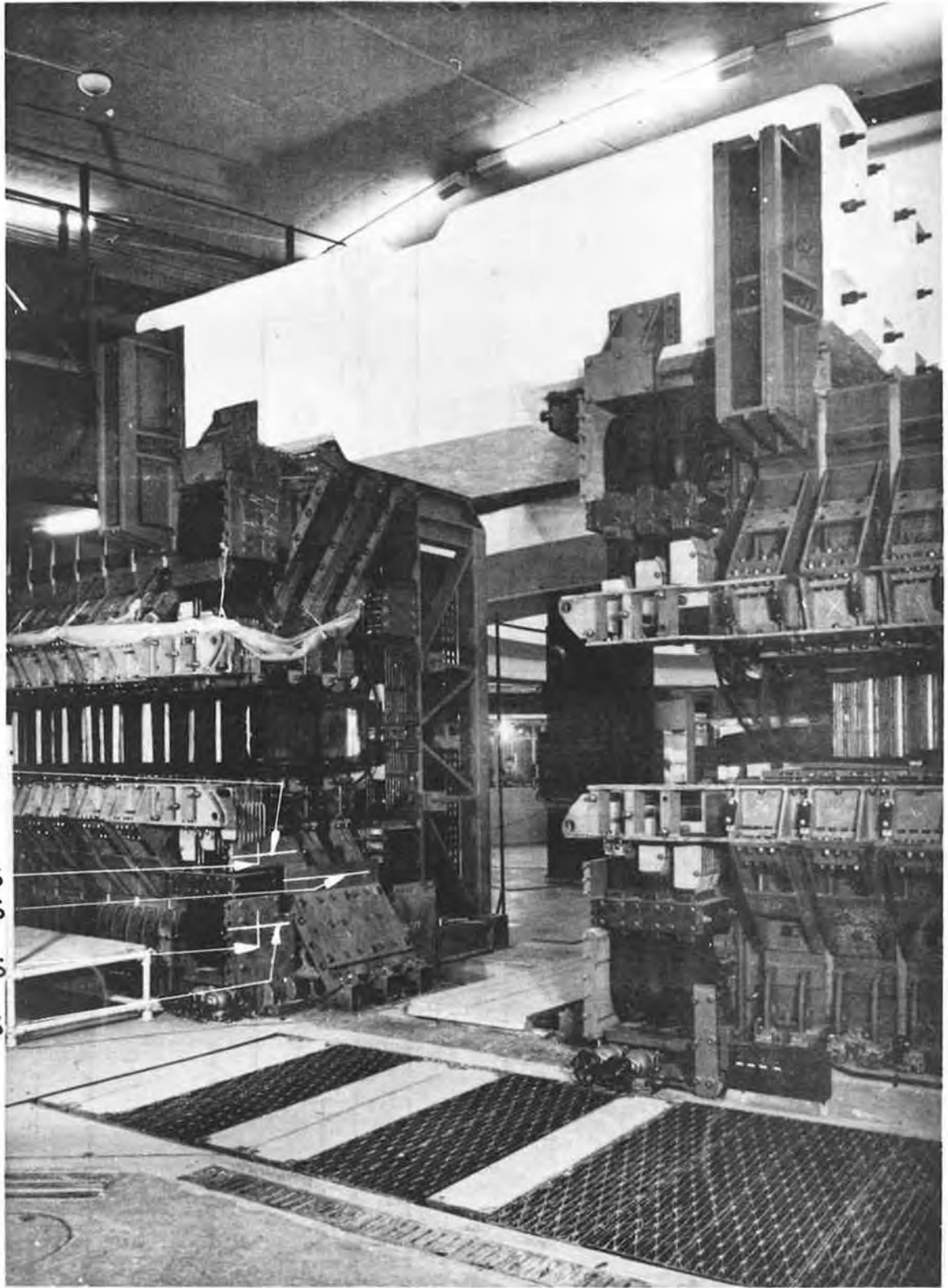


Fig. 4.4.2(i) Coil shielding.

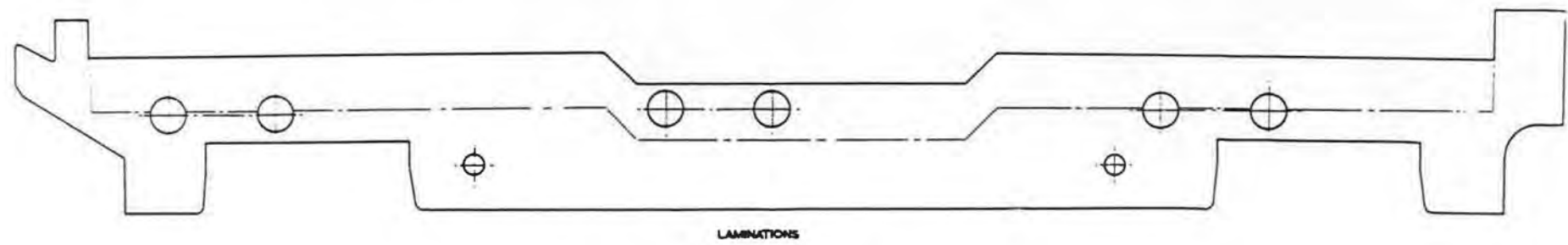
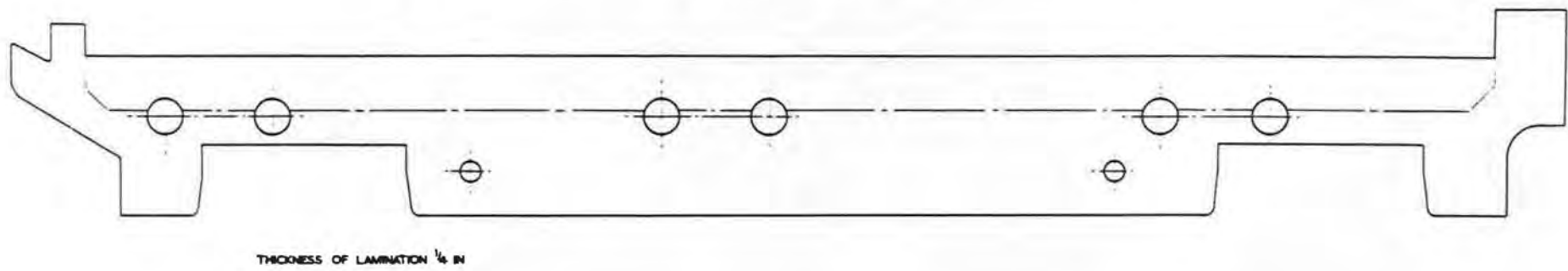
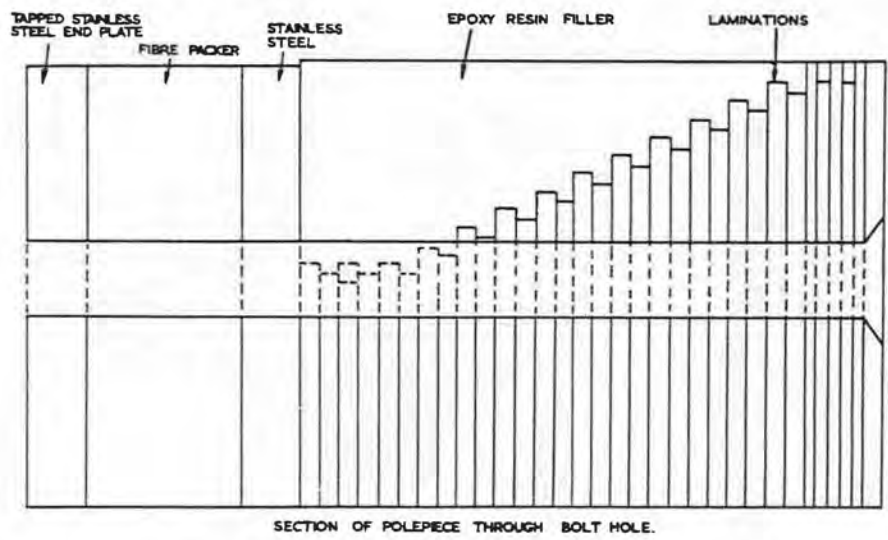


Fig. 4.4.3(i) End polepiece.

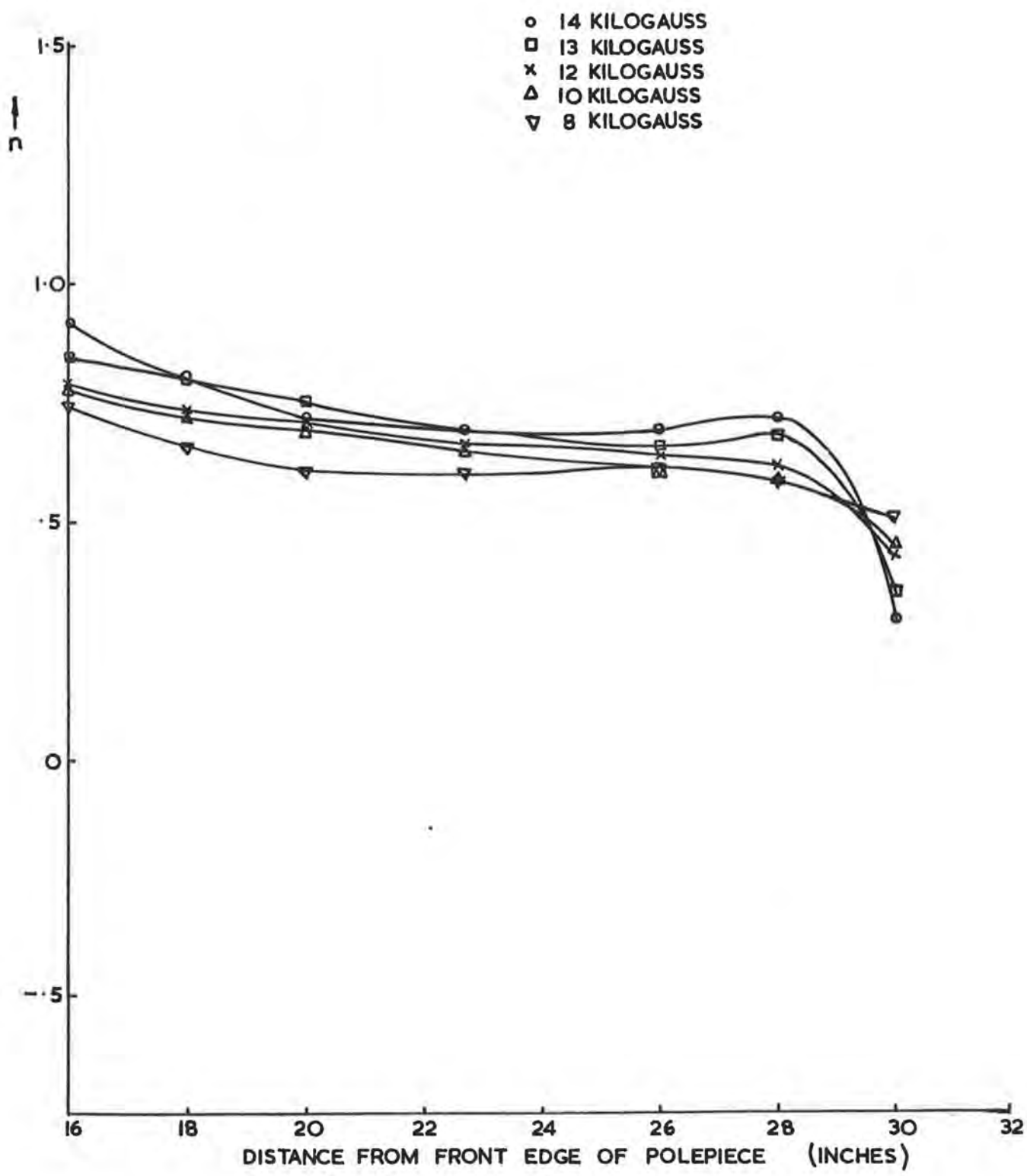


Fig. 4.4.4(i) Overall n; predicted.

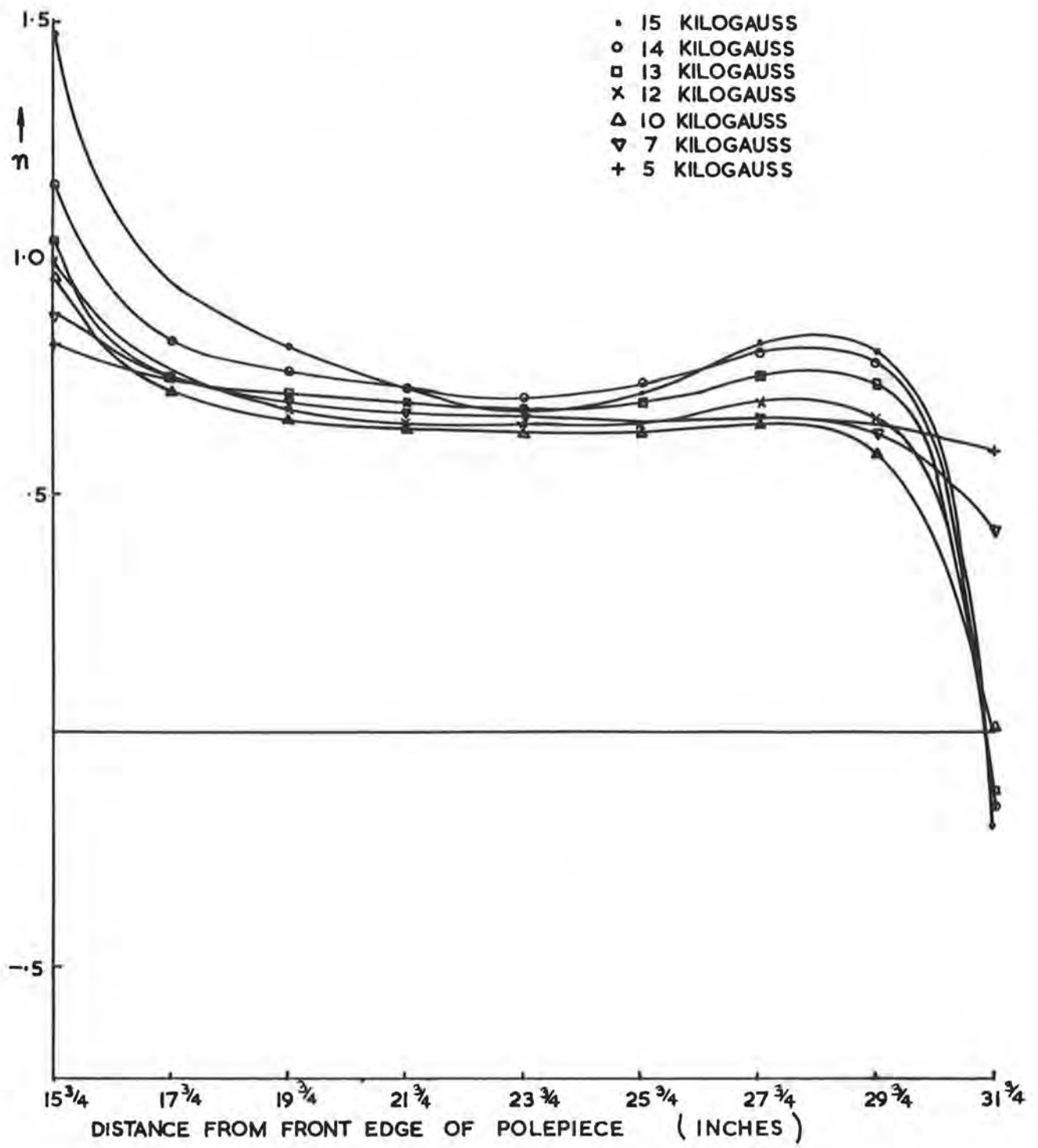


Fig. 4.4.4(ii) Overall n: measured on Nimrod.

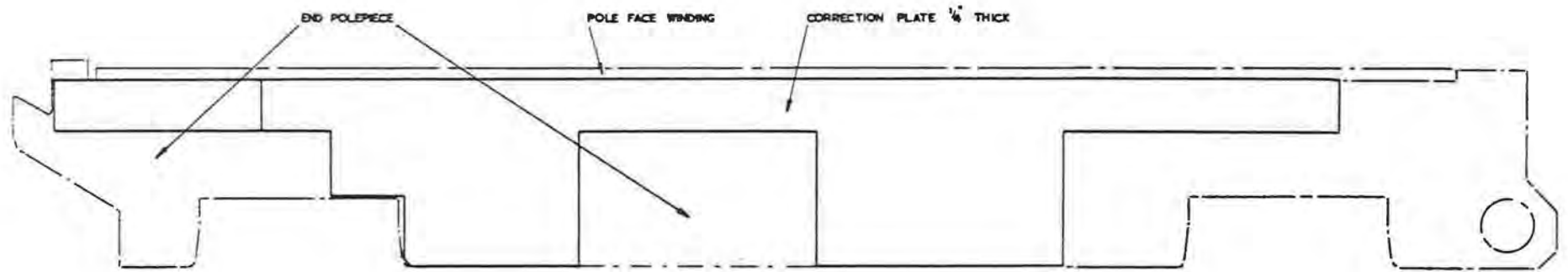


Fig. 4.4.4(iii) Correction plate on end polepiece.

the field at this position is influenced mainly by the presence of the gap coils. The outer shim was predicted from model measurements. Tapped holes were drilled in the end stainless steel plate of the end polepiece to enable correction plates to be affixed as dictated by the magnet survey. One $\frac{1}{4}$ in plate was found to be necessary, as shown in Fig. 4.4.4(iii) due to an overcorrection at the outside radius. These were fitted for the rest of the survey. There was still overcorrection of the inside radius; this is not so important since particles do not have useful closed orbits at this radius. The overall low field n-values are shown in Fig. 4.6.9(1).

Care was taken with the installation of straight sections to ensure, as nearly as possible, constant conditions around the magnet ring.

4.5. Mechanical Alignment of Sectors and Polepieces

4.5.1. Requirements

The mechanical alignment of sectors and polepieces had to meet the following tolerances:

- (i) The radial and azimuthal tilt of the polepieces must not exceed ± 0.001 in in 48 in and 13 in respectively
- (ii) The mean plane (defined by the mid point in height between the poles) must lie within a 0.040 in wide band around the whole 150 ft dia. circle, with limitations on the number of lobes and steps between adjacent octants and sectors
- (iii) All poles must be within 0.050 in of their correct radial position and the overall lengths of the octants must be correct to within 0.050 in with a limitation on changes between adjacent sectors.

4.5.2. Methods

The machine alignment was broken down into four stages:

- (i) Stage 1 involved installation and survey of 24 floor reference points defining the machine geometry. These 24 points formed a network of 8 triangles and 12 quadrilaterals. They have been surveyed 8 times in plan and 32 times in height and the height surveys are continuing.

The survey plan and equipment was designed to ensure that the position of any one of the 25 points was known accurately to within ± 0.005 in. From the survey measurements plan coordinates were computed, the difference between computed coordinates and nominal coordinates showing the error of each datum point. Height differences were also subject to a least squares computation, the results giving the height of each point in relation to the datum.

The surveys have shown that the plan position of any one point is known to within 0.008 in and its height to within 0.002 in at a confidence level of 95%

- (ii) Stage 2 consisted of setting datum screws and marks on the 336 magnets defining the features which were to be accurately aligned. Since the gap of the magnets which faced outwards was the only part machined and, for all practical purposes, there was no gap between sectors at the inner dia., it was necessary to define and reproduce datums at the rear and on top of the sectors which could be seen and measured from the octant centre. This operation became almost a production exercise with each sector having its datums set in relation to its characteristics in a measuring station.

- (iii) Stage 3 was the alignment of magnets in relation to the floor reference points. In each octant, six sectors, approximately equally spaced, were positioned by tape and theodolite using special purpose ancillaries. Heights and tilts were obtained using a surveyor's precise level. These principal sectors, when positioned, were used as references to "fair in" the remainder. For this a special large steel beam was used with a measuring station jig bored for each sector position.

Sector alignment was completed in four months and when complete the heights

of all 336 sectors lay between limiting planes 0.02 in apart. The instruments and methods used were capable of greater accuracy the larger part of the error being due to movements of the foundations.

(iv) Stage 4 was concerned with polepiece alignment and was a temporary installation without the vacuum vessel in place to allow the magnetic survey to be carried out.

All these stages were preparatory to the final task of aligning the polepieces inside the outer vacuum vessels within the limits stated above. This final installation took ten months (working 12 hours per day, seven days a week) and was completed at the end of January 1963. The reference marks on the front of the sectors were used as datums for polepiece positioning, a pair of poles was installed in each principal sector and the remaining pairs faired in. Heights and tilts were controlled optically, direct from the survey height datums. A considerable amount of special lifting, handling and alignment gear was designed for this operation, which was carried out under clean conditions.

4.5.3. Results

The alignment achieved is shown in Fig. 4.5.3(i). Table 4.5.3(I) relates these results to the original specification.

TABLE 4.5.3(I)

<u>Tilts.</u> Radial and asimuthal.	
Specified: ± 0.001 in	Achieved: 50% of all poles within ± .001 in
	80% " " " " ± .002 in
	95% " " " " ± .003 in
<u>Plan</u> Radial position.	
Specified: ± 0.05 in	Achieved: all sectors within ± 0.010 in
	all poles (in relation to sectors) within ± 0.005 in
	All sectors lay on their correct radius within ± 0.005 in
	and polepieces are correct to sectors within ± 0.003 in

4.5.4. Foundation Movement

The main reason for the poor results in height was foundation movement. For various reasons it was not possible to complete the earth mounding on the roof, which forms part of the biological shielding, until the polepiece installation programme was more than one third complete. The effect of the mounding has been to "bend" the monolith. It has been shown that the addition of 100 tons is the equivalent of 0.001 in deflection, not always however in the place most expected. "Spring back" when loads are removed appears to be very much less, perhaps less than a quarter of this figure.

Since the thermal co-efficient of the monolith is approx $7 \times 10^{-6}/^{\circ}\text{C}$ small

temperature gradients can cause dishing. Some dishing is also caused by the columns carrying the roof.

Temperature fluctuations of approximately 1°C are normal and probably account for the change in height of floor datums when they are measured monthly. These height measurements show a flutter of about ± 0.005 in in a random fashion month by month. Tilts also vary by about the same amount and it is unreasonable to expect the monolith to be more stable than this with the existing temperature controls.

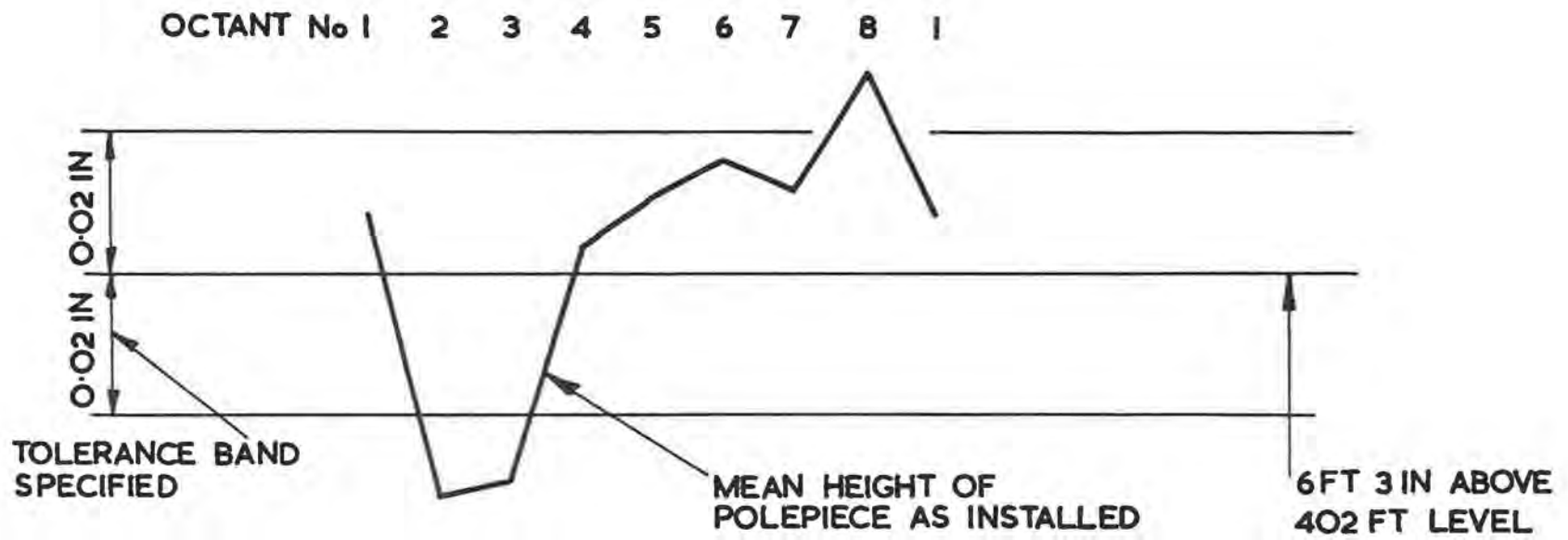


Fig. 4.5.3(i) Diagram of heights, showing alignment achieved.

4.6. Magnetic Survey

The survey of Nimrod magnet took place during the period April-August 1962. The measurements included

- (i) n-values and median plane height over the entire working area of the machine
- (ii) comparative measurements of flux density on the equilibrium orbit radius (R_0) to examine the symmetry of the machine
- (iii) measurements of the end-field at each gap between adjacent octants.

A detailed report (4) of the measuring equipment has been published.

4.6.1. Pulsed Field Measurements

The quantities mentioned above are functions of the instantaneous field level in the magnet gap and therefore, a continuous recording during the rising part of the field pulse was required. This recording had to be a two-channel one, whereby the magnet quantity of interest was recorded alongside an indication of the field level. Because the amount of data to be handled was large, it was decided to attempt to record it in the first instance in a form acceptable to a computer. A two-channel tape recorder was used, and the $\frac{1}{2}$ in tape produced was compatible with the IBM 7090 computer. The output from a search coil in a "standard position" on R_0 in the magnet was put on one channel, to give the field level and a search coil designed to be sensitive to the quantity of interest was connected to the other channel. The tape recorder sampled each search coil voltage alternately at a frequency of 10 kc/s. Each sample was digitized into a ten-bit number which was recorded in two write-cycles on the seven-tracks of the tape. The fourteen bits per reading thus available were used: ten for the digitised reading, one for a label to indicate the channel and the remaining three for parity-checking bits.

The tape recorder was not of the fast-stop-start variety, because the extra cost of such a device was not justified. In order to record a magnet pulse, the tape was run up to speed (100 in/s; run-up taking about 1 s) and then a pulse from the tape-speed circuits started the magnet pulse and also the record circuits. At the end of the magnet rise a pulse from the power supply timer stopped the recorder. A tape would hold about 90 such pulses.

Subsequently the tapes were fed to an IBM 7090 to process the information. The search coil voltages on both channels needed time-integration to arrive at quantities related to magnet flux rather than rate of change of flux. Because of the density in time of the samples (5 kc/s per channel) a sufficiently accurate integration could be achieved by simply forming a running total of the samples in the computer. Multiplication of this total by the appropriate constants gave the flux density on channel 1 and the quantity of interest on channel 2. In all cases, division of channel 2 by channel 1 (simultaneous values) gave a meaningful result. (For example; in n-measurements, channel 2 carried field gradient information $\partial B/\partial r$, so division gave $R_0/B \partial B/\partial r$, R_0 being included in the multiplying constants). Print-out was programmed at levels 300, 600, 900 and then every multiple of 1000 gauss up to peak field, which was about 15000 gauss.

The computer program was arranged to check the parity of the readings, rejecting any readings in error and registering a count of errors of various types. To eliminate drift of the zero-input reading of the recorder, use was made of the

interval between the initiating pulse and the magnet coming on, to establish a zero in the computer based on the actual recordings in the two channels. This zero was then used for the rest of that record and printed out at the end. Provision was made for setting up a four-figure identity which could be written automatically at the start of each record, before sampled voltages were recorded. The identity bits were written three times at the start of the record, which thus characterized a true record from any spurious bits which could be interpreted by the computer as a record. The sensitivities available were 40 mV up to 20 V in independent switched ranges on channels 1 and 2. The zero could be located either at the negative end of the voltage range, or half way, catering for unidirectional or bidirectional inputs.

4.6.2. Remanent Measurements

The remanent field in the magnet was about 8 gauss, an appreciable fraction of the injection field, 300 gauss, and therefore arrangements were necessary to survey the remanent field. In most cases this was done by moving a search coil in the field and integrating the resultant e.m.f. in an optical servo type fluxmeter, to give the flux change. The fluxmeter readings were recorded by a digital voltmeter, and both printed and punched on paper tape which was processed in a Ferranti Mercury computer. An exception to this method of measuring was the remanent median plane survey, where a fluxgate saturating strip magnetometer probe was used. For both the pulsed and steady field measurements, the search coils were located on paxolin trolleys and moved by compressed air cylinders. Rotation of the coils was achieved, when necessary, by use of paddle-type air-driven actuators. The search coils were formed on ground-marble formers and bonded with marble dust loaded resin.

4.6.3. n-measurements

The field index, n , was measured with an opposed coil-pair, sensitive to gradients, and not to uniform flux.

The n -values were taken at 2 in radial intervals and 3 sector (about 40 in) azimuthal intervals, all round the machine. The coil-pair was arranged to be 3 sectors long, so that all the machine area was covered. The n measurements were taken to an accuracy of about three decimal places.

4.6.4. Machine Symmetry Measurements

The flux-measuring search-coils used for these measurements were again 3-sectors long, and 2 in wide. In the pulsed field measurements a coil was placed in the standard position in the machine and connected in series opposition with an exactly similar coil which was carried round the machine. The computer program in this case was arranged to give percentage differences in flux density at the various machine locations, with an estimated accuracy correct to 0.001%.

The remanent comparison was made absolutely, to about 5 parts in 10^4 , using a search coil which was turned over in the field, indicating the resultant flux change on a servo-flux meter. The machine symmetry measurements were made only in the octants, and stopped $4\frac{1}{2}$ sectors short of the ends.

4.6.5. Effective Length

The pulsed effective length was measured by placing a long coil of accurately known width on the R_0 line at the end of the octants. This coil started at the point where machine symmetry measurements left off, i.e. $4\frac{1}{2}$ sectors from the octant end, and extended to the middle of the straight section. The coil was connected in series opposition to a flux coil in one of the standard machine positions and was of such a turns-area as to exactly oppose the long coil when the effective length of the end $4\frac{1}{2}$ sectors was equal to the geometric length.

For remanent measurements, a trolley carrying a search coil was arranged to follow the path occupied previously by the long coil described above. This search coil was indexed 2 in at a time and at each position the coil was rotated through 180° and the fluxmeter readings recorded. The recording (on punched tape) was used to integrate the remanent flux density at R_0 over the length of travel of the trolley.

4.6.6. Median Plane

In order to locate the median plane of a nearly uniform magnetic field, it is necessary to use a sensitive, direction-dependent, field-measuring device, which is capable of being orientated in the magnet gap with the position of its magnetic axis known very accurately. For instance, in Nimrod, with an n of 0.6, it can be shown that the curvature of the field lines in the gap is about 1000 in. To resolve a discrepancy of 0.1 in. between the geometric and magnetic median planes, therefore requires that the probe axis be angularly positioned better than 0.1 in 1,000, \approx 20 seconds. If the vertical component of the field is B_z , the 0.1 in displacement results in a change $10^{-4} B_z$ in the horizontal field; which the probe must be able to measure. Since remanent field is about 10 gauss, 10^{-3} gauss must be measurable.

Position measurements were made optically. A plane vertical mirror was mounted on the probe carrier so that altering the inclination of the probes tilted the mirror about a horizontal axis. By obtaining an auto-collimating effect in a telescope with a gauss eyepiece, when the cross wires and their reflected image were coincident, the mirror was perpendicular to the axis of the telescope. With the telescope previously levelled the mirror would be in a vertical plane and the probe carrier would have some definite orientation relative to the vertical. The telescope used was an automatically levelled instrument incorporating a suspended prism. This equipment proved stable, robust and quick to use. Resolution of 2 seconds could be achieved with ease.

Fluxgate magnetometer probes were used to measure the magnetic field. These were 6 mm in length and were sensitive to 10^{-5} gauss. For the pulsed measurements a 3-sector long coil with a turns-area of 200 m^2 was mounted with its axis horizontal. Alignment was carried out in a subsidiary magnet, whose field was fairly uniform and approximately vertical. In the remanent case the horizontal field component in the geometric median plane was recorded, one probe after another being displayed by means of a multiway switch. In the pulsed case, the computer print out was of radial field in the geometric median plane, expressed as a percentage of main vertical field.

To do straight section measurements of remanent median plane, an aluminium bridge was used to carry a row of probes through the straight section box. A levelling mirror was provided on each end. Examination of the pulsed median plane in the straight section boxes was not attempted.

4.6.7. Other Miscellaneous Measurements

By arranging a large board horizontally in the end of an octant and halfway into the associated straight section box, readings were taken of the field in the median plane. A 6 in reference grid was used for positioning, pulsed readings being taken on the tape recorder and remanent readings with an gaussmeter and probe. Using a similar technique a field plot was taken moving radially away from the magnet in 6 in steps. This was done at two azimuths, corresponding to the Mark I and Mark II polepieces.

4.6.8. Results of the Survey

The survey has shown that there are no errors in the magnetic field shape which are not capable of correction with the available poleface windings and their supplies.

4.6.9. n values

The value of n as a function of field and radius is of prime importance in determining how much of the magnet aperture is usable. The average value of n over the whole machine, including straight sections, for various field levels is shown in Fig. 4.6.9(i). The usable portion is increased by correcting windings; discussion of the variation of aperture with field will be deferred until the effects of the correction have been shown.

4.6.10. Machine Symmetry and Effective Lengths of Octant-ends

These results have been combined to obtain a comparison of the octant strengths. There is sufficient data to compare the octants only in pairs, since the initial part of the current waveform is not the same for all octants. Also it is difficult to buck out magnet ripple, which varies by 180° octant to octant, and correcting data is not available. The histograms of Fig. 4.6.10(i) show the relative levels of neighbouring octants at various fields. They are field levels in the hard-edged octant of the correct geometrical length($R_0 \pi/4$) calculated to give the same line-integral of vertical field as the actual octant, including its end-effects. The levels are expressed as a percentage of the reference field for each pair of octants. It can be seen that pairs of octants are similar to 0.1% (or better) in nearly all cases, and that the level relative to nominal field decreases by about 0.7% at high fields. This is due to the effective length of the end-field decreasing.

4.6.11. Median Plane Results

The median plane variations at 300 and 15000 gauss are shown in Fig. 4.6.11(i) and 4.6.11(ii). They have been averaged for each octant and expressed as the fraction Br/B_0 where Br is the radial field in the geometric median plane at any point and B_0 is the reference field. The signs have been chosen so that an upward displacement of the magnetic median plane is represented by a positive value of Br/B_0 . The general features do not change much with field level: there is a dip in the neighbourhood of octant 7 in the median plane, which otherwise is above the geometric median plane. The marked rise in Br on the outside edge of the magnet is similar to that found on the Cosmotron⁽¹²⁾. The general level of the magnetic median plane is about 0.1 in above the geometric median plane.

Some local distortions of the median plane were found. One large shift of

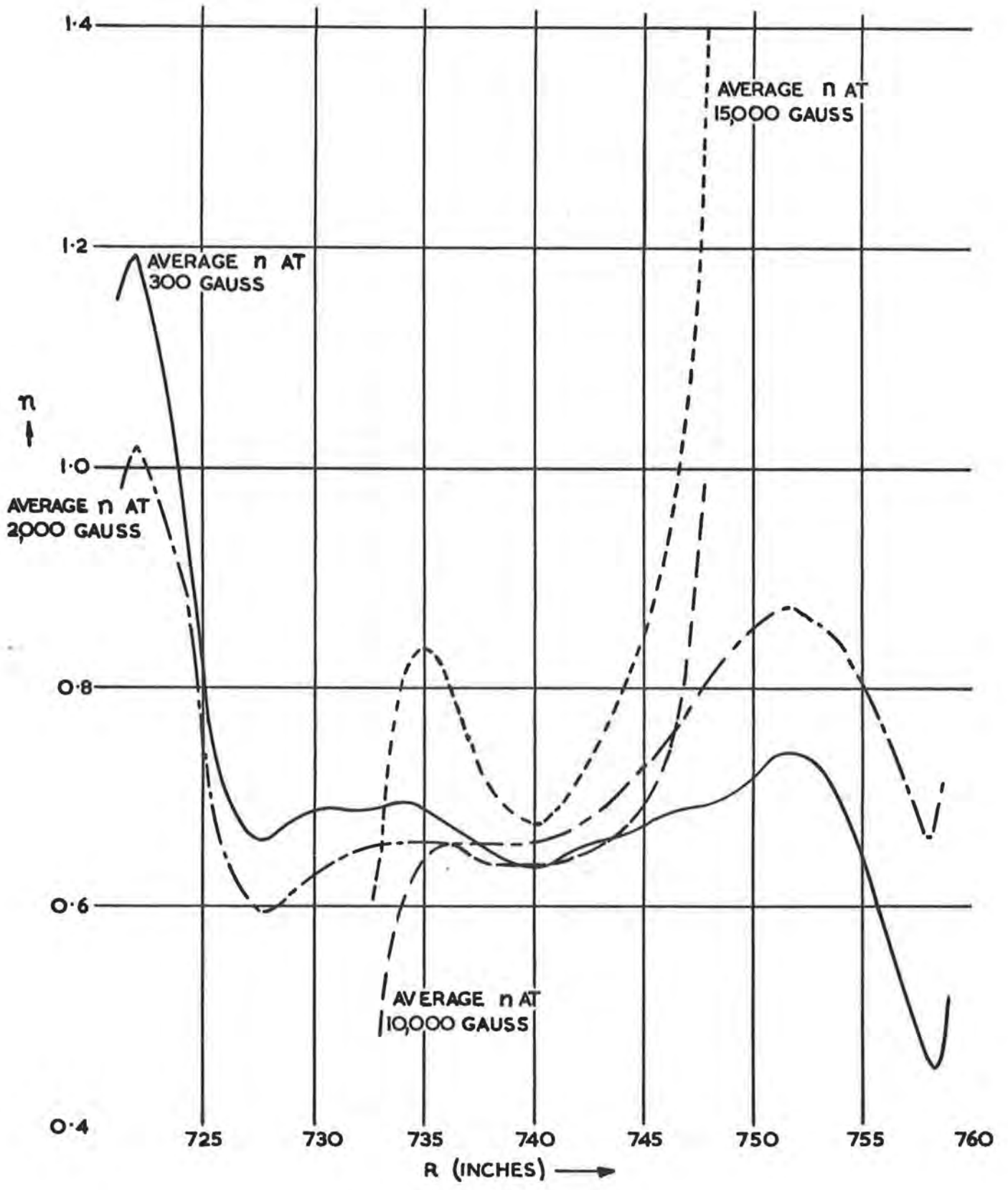
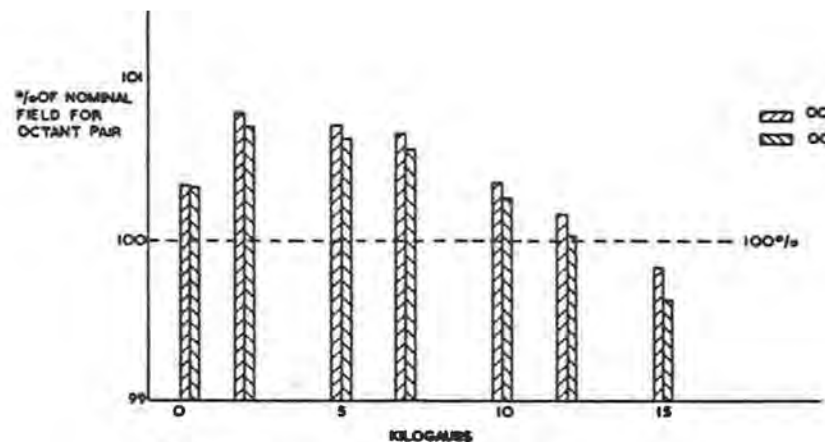
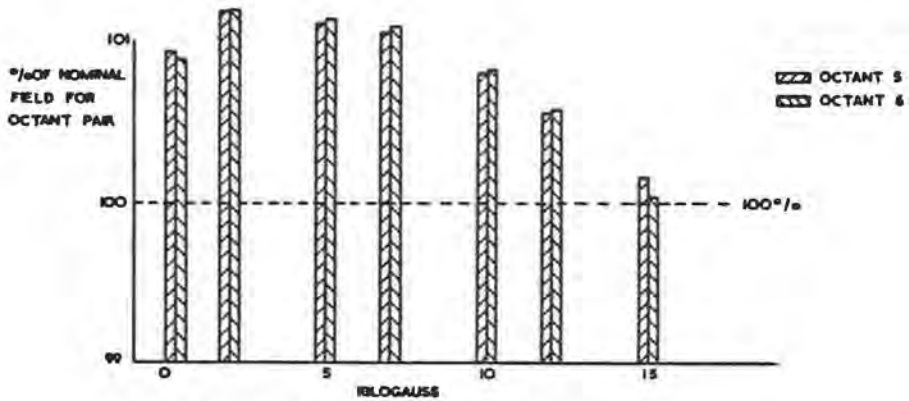


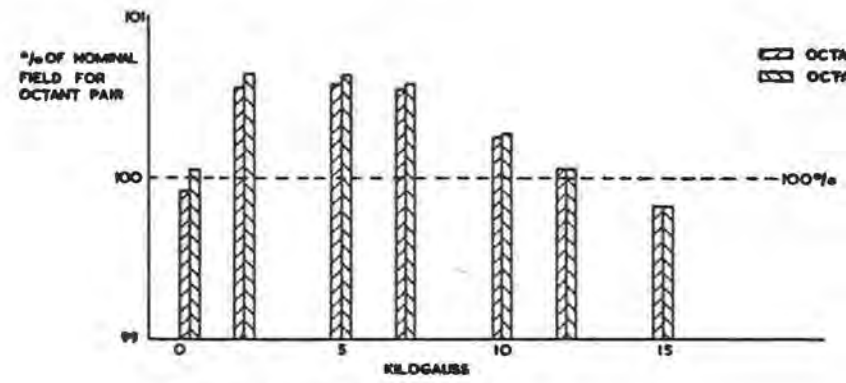
Fig. 4.6.9(i) Average n in Nimrod.



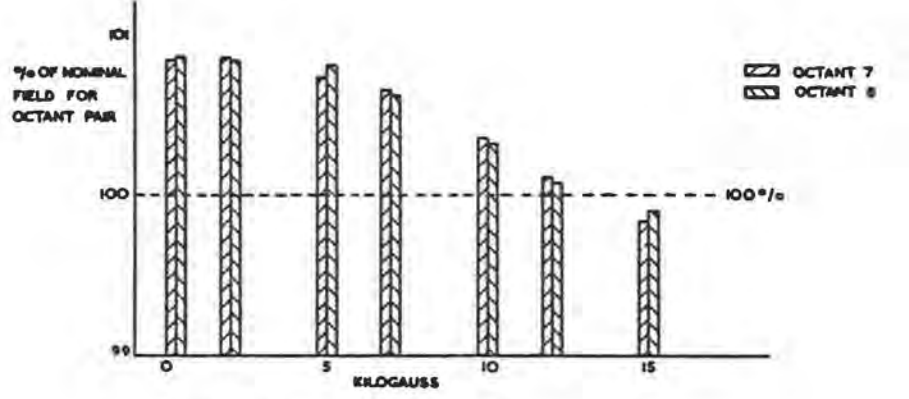
(a) OCTANTS 1 AND 2



(c) OCTANTS 5 AND 6



(b) OCTANTS 3 AND 4



(d) OCTANTS 7 AND 8

Fig. 4.6.10(i) Effective lengths of octants.

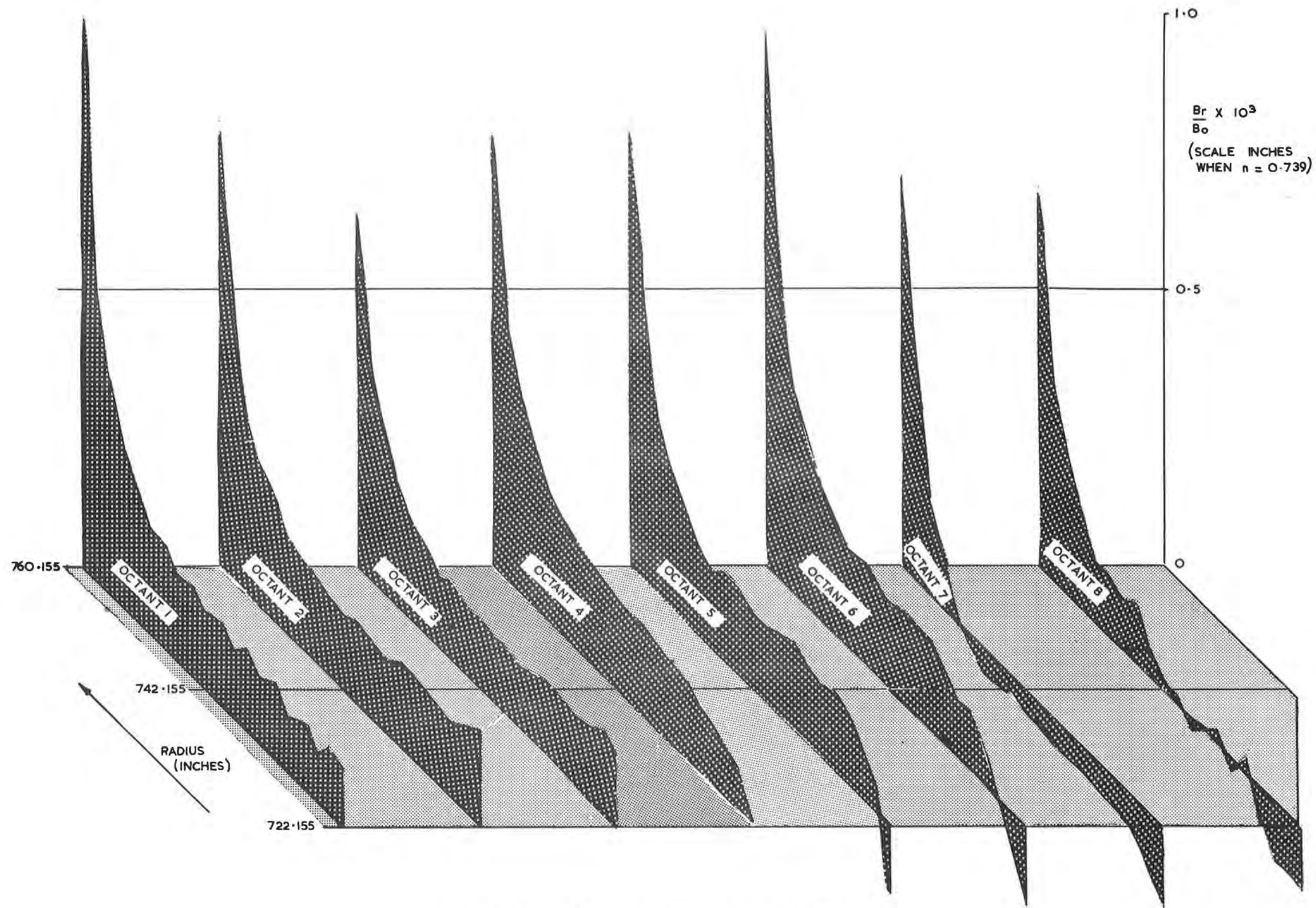


Fig. 4.6.11(i) Magnetic median surface at 300 gauss.

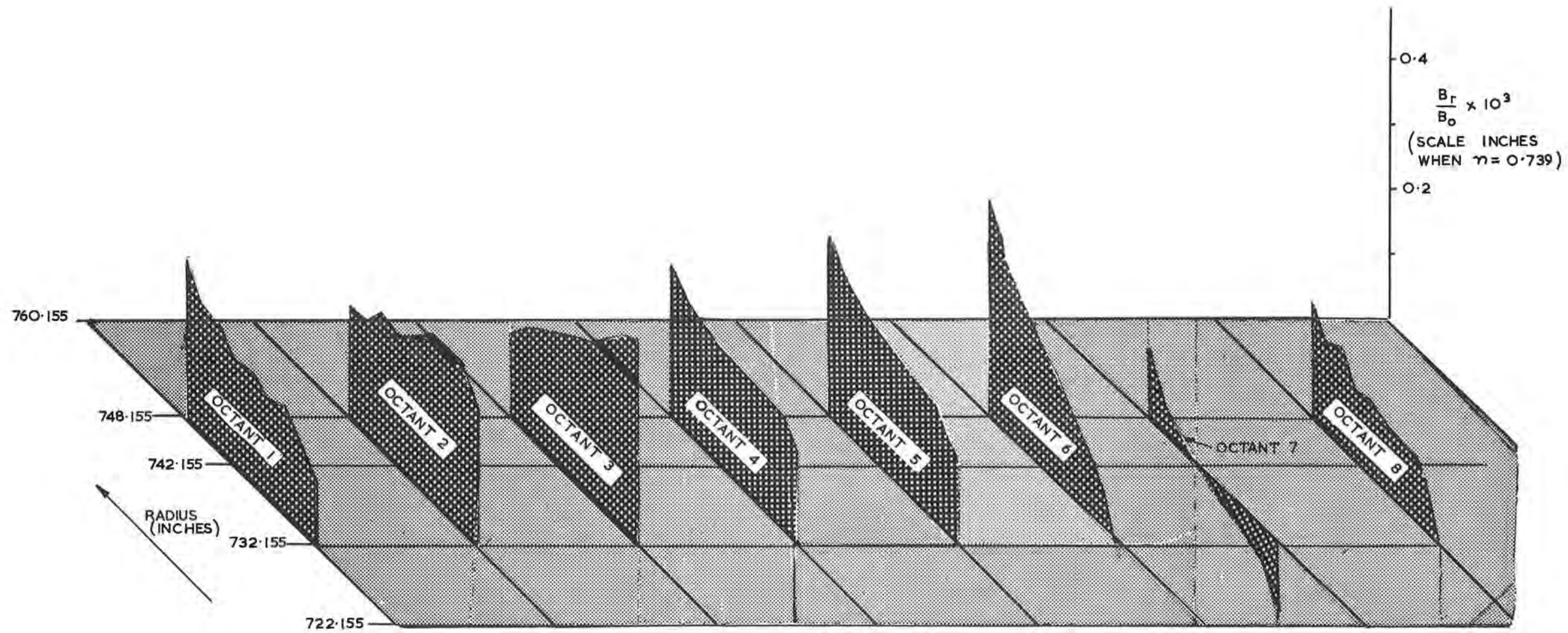


Fig. 4.6.11(ii) Magnetic median surface at 15,000 gauss.

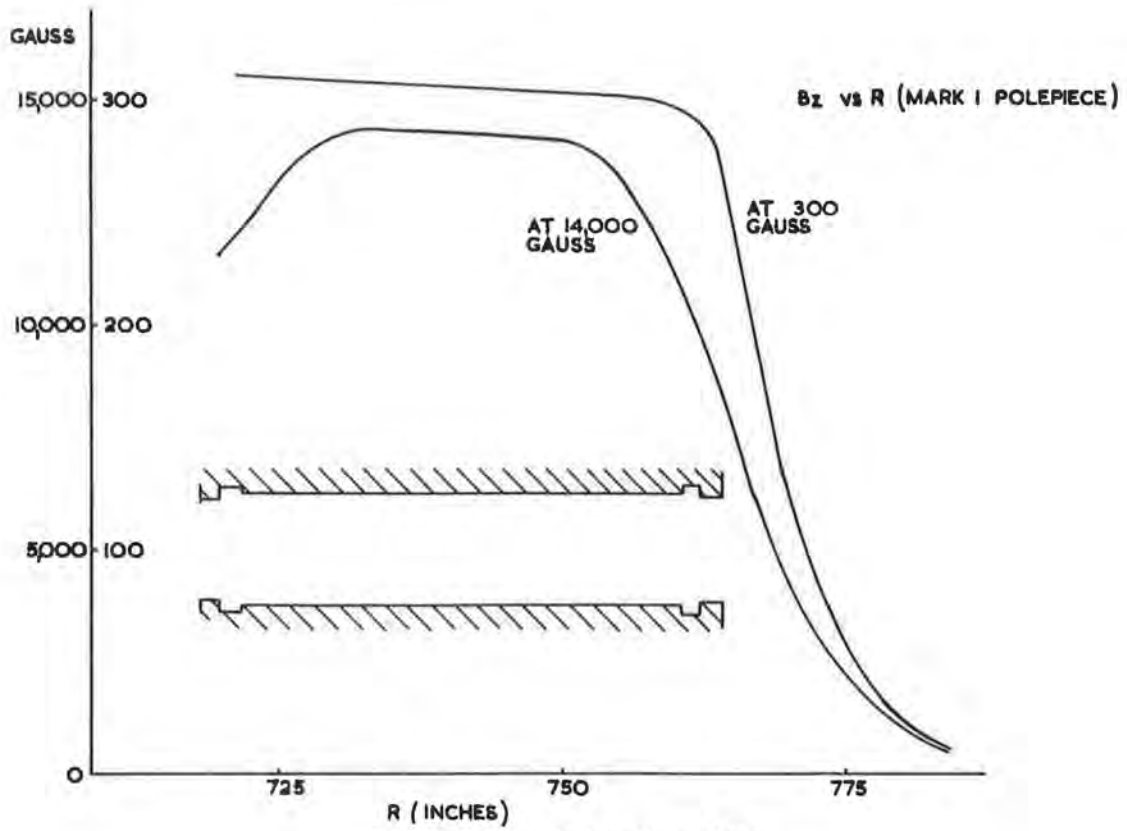


Fig. 4.6.12(i) Radial fringe field.

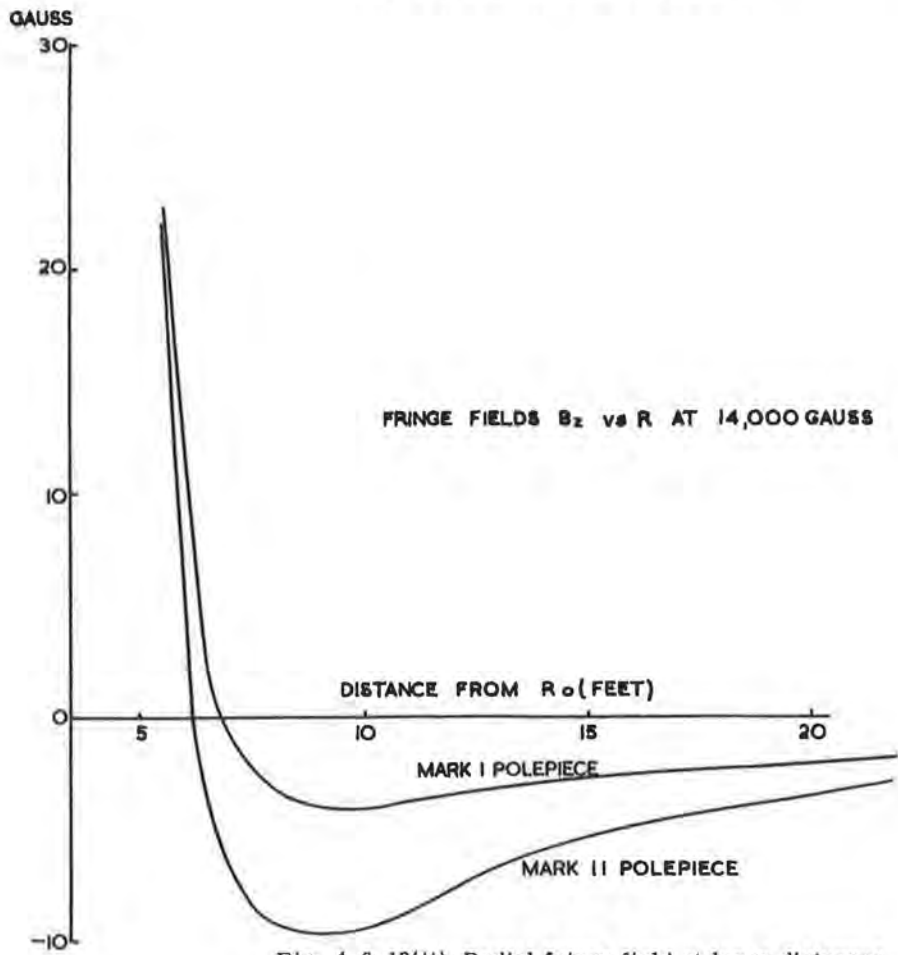


Fig. 4.6.12(ii) Radial fringe field at large distances.

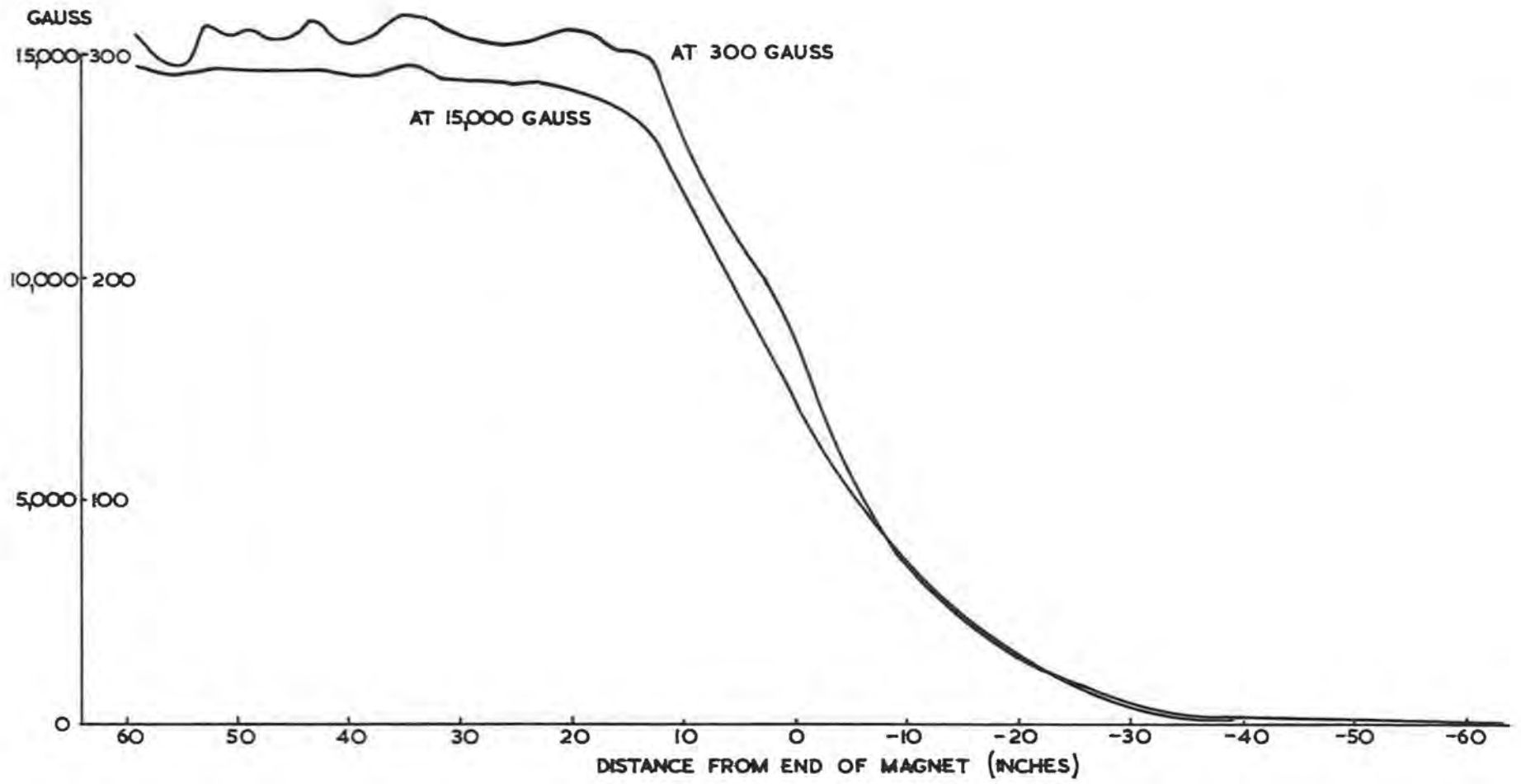


Fig. 4.6.12(iii) Fringe field into straight section.

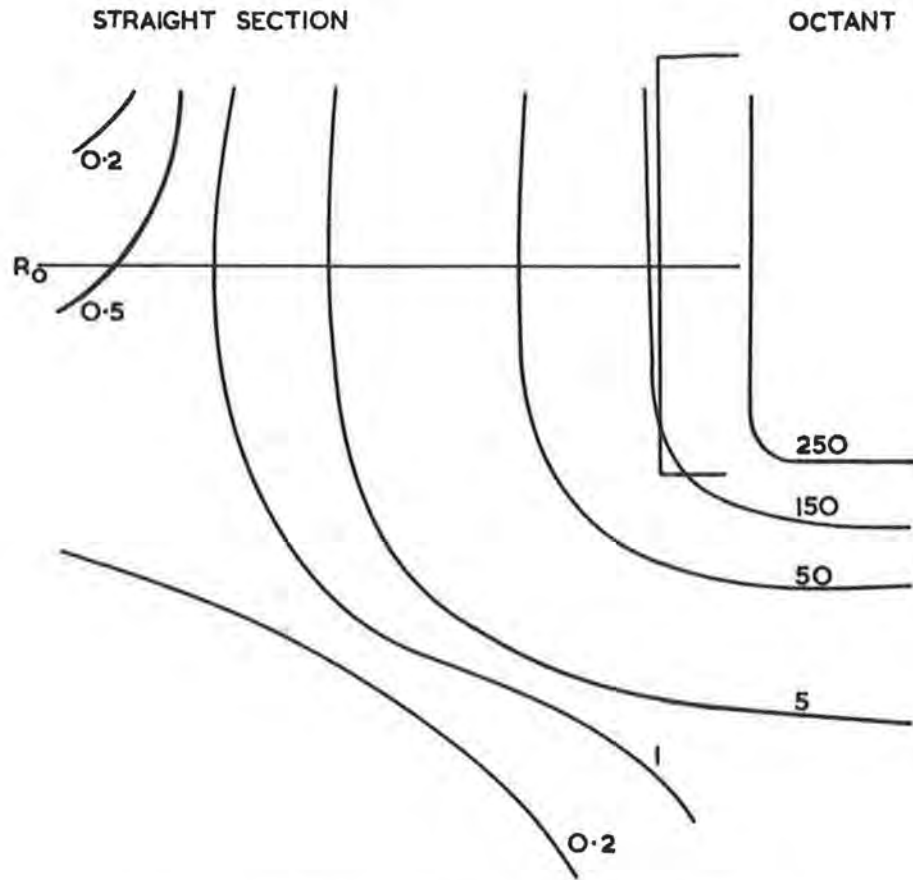


Fig. 4.6.12(iv) Field round end of octant at 300 gauss.

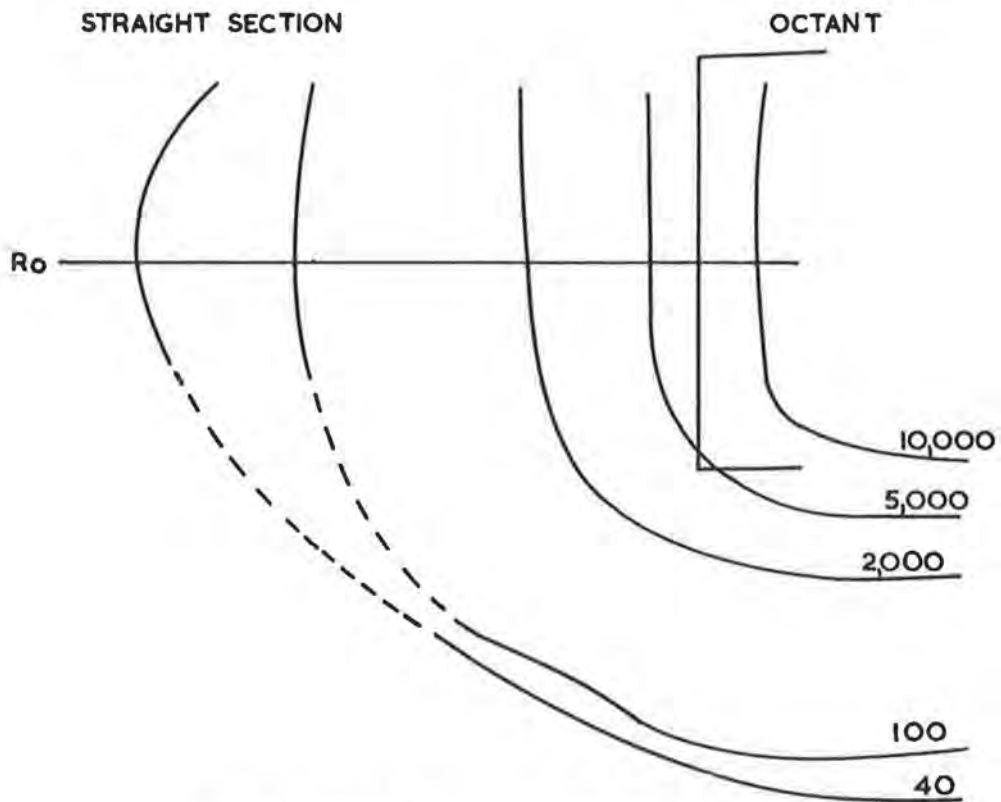


Fig. 4.6.12(v) Field round end of octant at 15,000 gauss.

about 3 in was found to be due to a temporary(1) mild steel jig about 1in x 7in x $\frac{1}{8}$ in which had been used during installation of the back return windings. Smaller shifts of about $\frac{1}{2}$ in. were found to be due to the use of silver steel instead of stainless steel for some 2 B.A. by $\frac{1}{2}$ in screws in some of the polepiece jacks. The extraneous objects have since been removed.

4.6.12. Miscellaneous Results

Figs.4.6.12(i) and 4.6.12(ii) represent the fall-off of field along a radius from the magnet, in the azimuth of Mark I and Mark II polepieces (over the range of Fig. 4.6.12(i) they are so similar that only Mark I is shown). The differences in fall-off are probably more due to the fact that Mark II polepieces are situated at the ends of the octants than due to differences between the polepieces.

Fig. 4.6.12(iii) shows the fall-off in field on R_0 at the end of an octant and in the straight section.

Mapping of the field in the region of an octant-end and straight section has been done at various field levels; for illustration Figs. 4.6.12(iv) and 4.6.12(v) show the maps at 300 and 15000 gauss respectively.

4.7. General Characteristics of the Magnet

4.7.1. Field Versus Current

The measured magnetic field and hence the proton energy of Nimrod for varying current is given in Table 4.7.1(I).

TABLE 4.7.1(I)

I (A)	B (kilogauss)	T (GeV)
2000	3.7	1.4
3000	5.6	2.4
4000	7.4	3.4
5000	9.3	4.4
6000	10.7	5.2
7000	12.1	5.9
8000	13.4	6.7
9150	14.6	7.3
10500	15.6	7.9
12000	(16.4) ⁺	(8.3) ⁺

+ estimated values

These are higher values of field than predicted in (1) due to the shaping of the poles (6) and the use of extra steel in crucial areas of the yoke (see Fig. 4.7.1(i)). These 'build-up plates' carry appreciable flux at high fields as shown by measurements on Model IV (Fig. 4.7.1(ii)). They also lead to a decrease in the remanent field in the magnet gap.

Calculations of rise times using predicted inductance or 'NA' figures have been confirmed in practice.

4.7.2. Eddy Current Effects

In addition to the normal depression of field due to eddy currents, (1), (7), (8) other eddy current effects become apparent when the control of flat-top slope was being investigated. The symptom was a very large transient depression ($\sim .25$ s) at the beginning of flat-top. Referring to Fig. 4.7.2(i), the curve XY gives the current expected from the impressed voltage on the magnet. The actual current obtained was on the path XZ. At high fields the size of the effect was much larger than the normal eddy current and hysteresis effect. Fig. 4.7.2(ii) shows the depression in current I_D as a function of rise time, i.e. peak current. Up to about 7,000 A the depression is constant at about 22 A and then rises sharply. The gap field in the magnet octant was depressed by an approximately constant amount as the rise time varied. Since a constant voltage is applied to the magnet and:-

$$V = NAdB/dt + RI \quad \dots \dots (i)$$

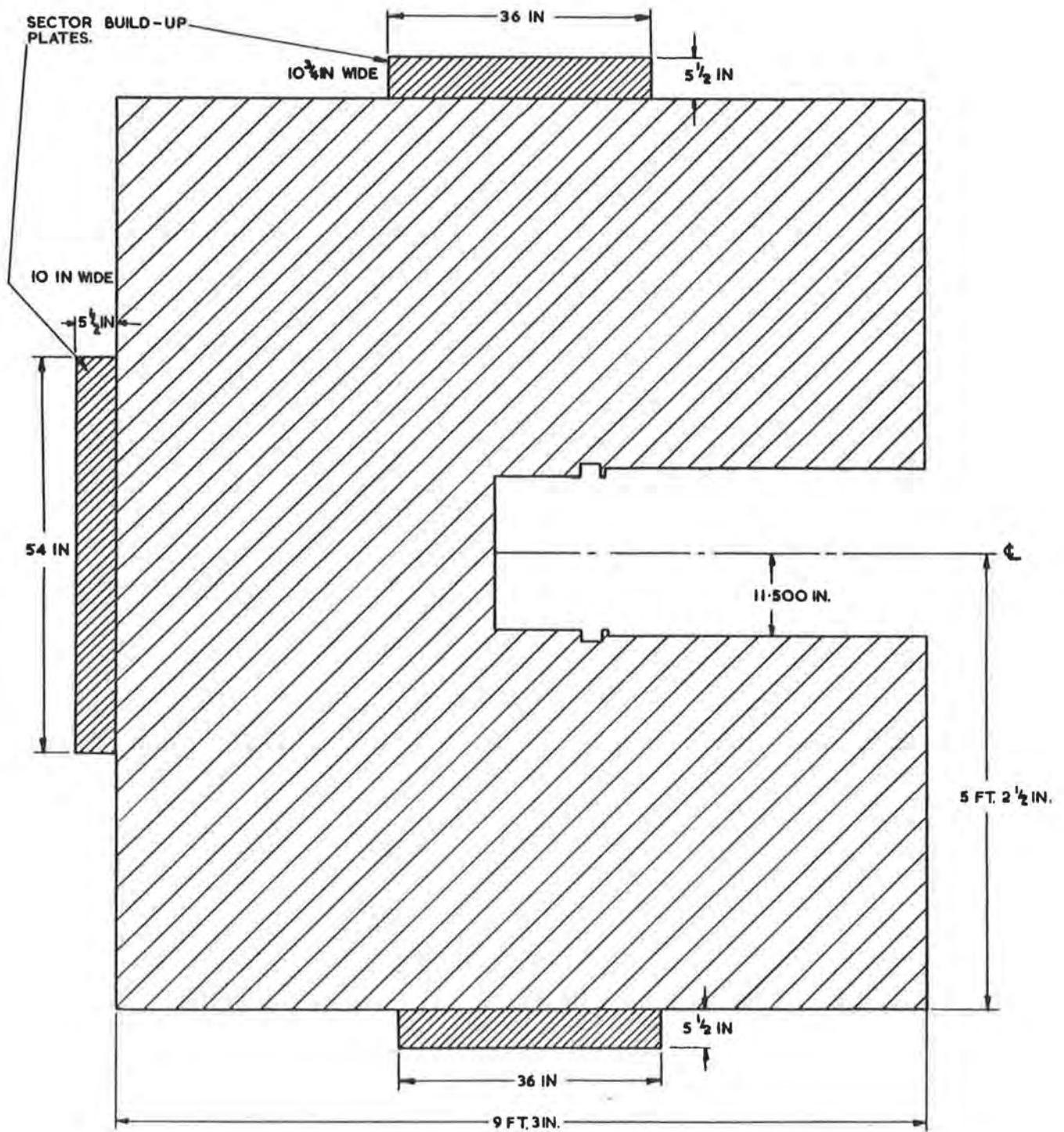


Fig. 4.7.1(i) Section build-up plates.

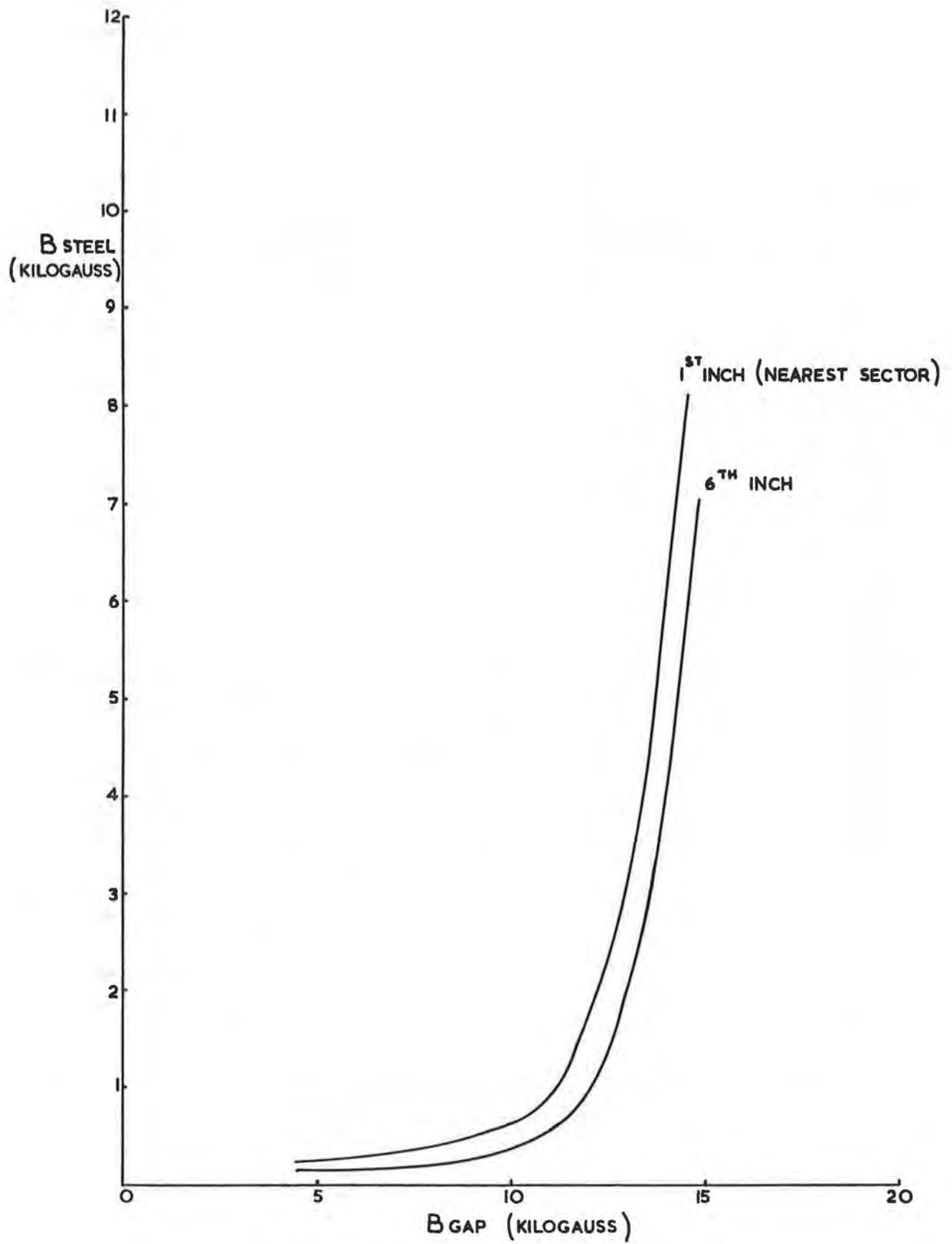


Fig. 4.7.1(ii) Flux density in build-up plates (Model IV)

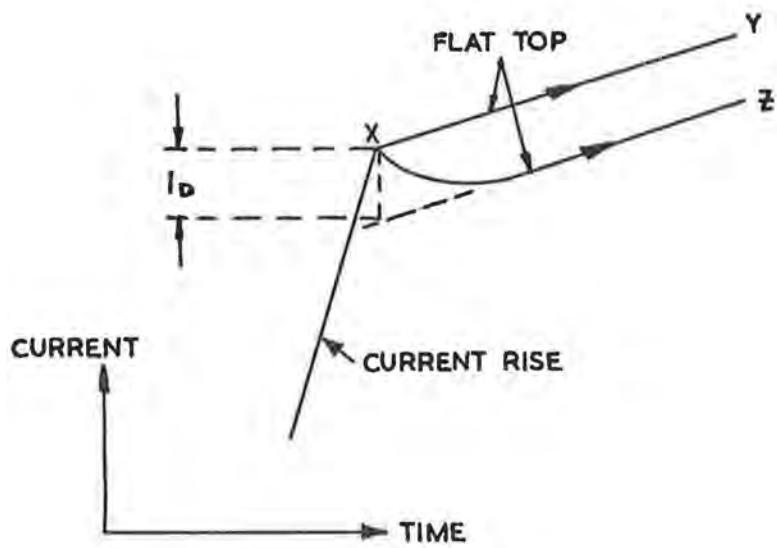


Fig. 4.7.2(i) Transient at flat-top.

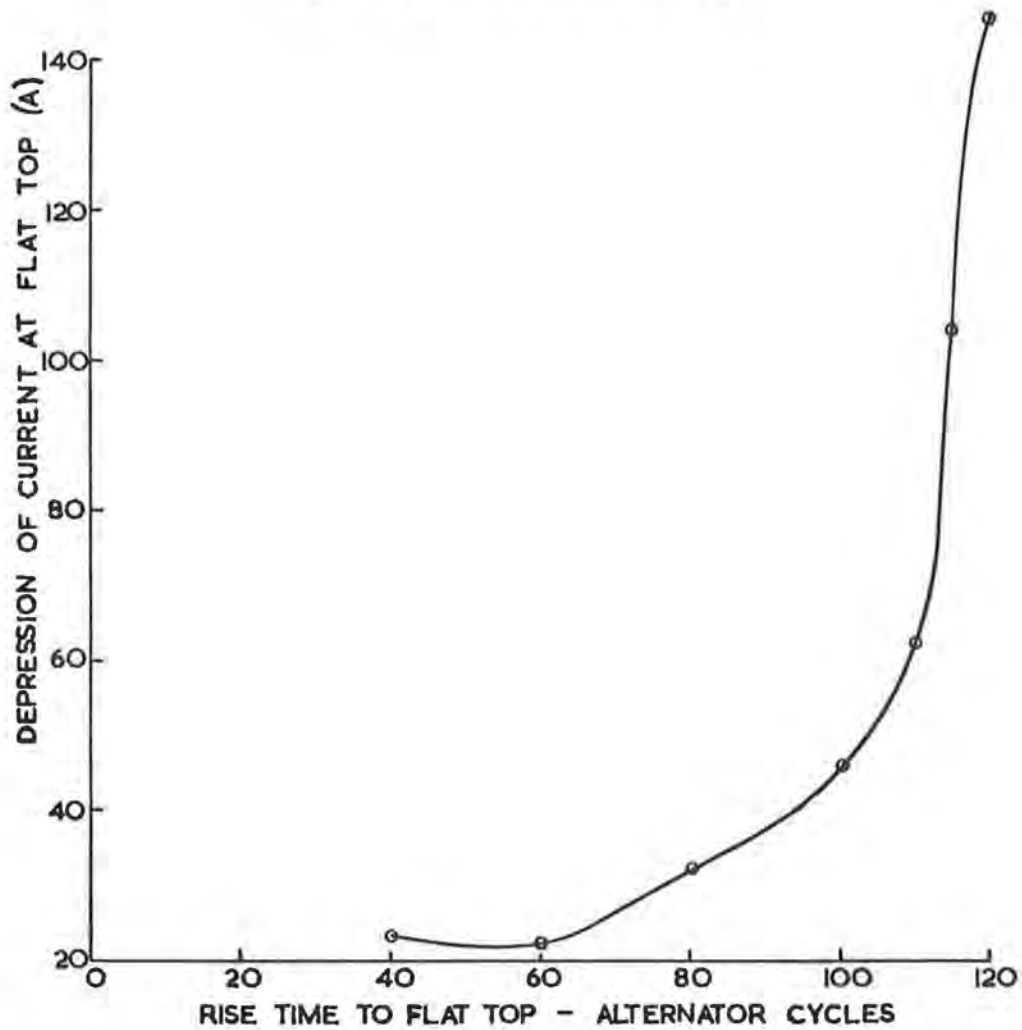


Fig. 4.7.2(ii) Depression of current at flat top with varying rise time.

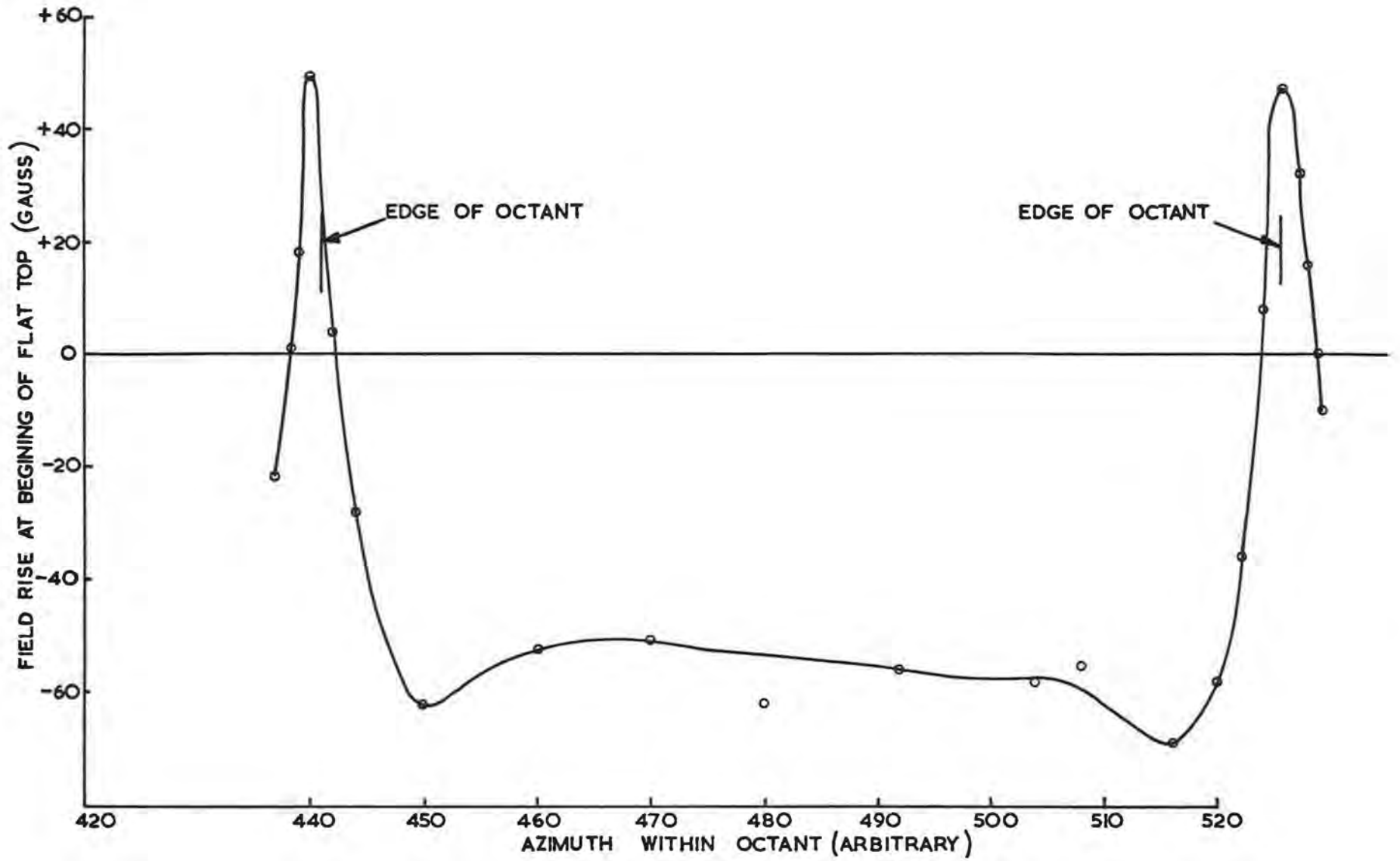


Fig. 4.7.2(iii) Variation of field within an octant at the beginning of flat-top.

there must be a redistribution of flux in the magnet.

Measurements of field depression azimuthally within an octant and straight section gave the result shown in Fig. 4.7.2(iii) showing a pronounced eddy current effect at the ends of octants at the transition from dB/dt on current rise to very small dB/dt on flat-top. This was the cause of the constant depression of field in the octant but did not explain the large depression in current at high peak currents. The eddy currents at the octant ends are due to fringe flux cutting the $\frac{1}{2}$ in end plates of the end sectors and also a $\frac{3}{4}$ in thick plate which was part of the coil shielding structure. This plate, which is thermally somewhat isolated, gets hot.

The high current effect was found to be due to the build up plates (Section 4.7.1). Measurements of the field just outside these showed a small value until the gap field reached about 10.5 kilogauss when there was a very rapid increase. This effect had also been found on Model IV; Fig. 4.7.1(ii) gives measurements of flux density in the build up plates versus gap field. Air gaps between the plates and the sector act as an impedance to flux until the sector starts to saturate, when there is a sudden increase of flux. Since the plates are laminated perpendicularly to the flux direction there are large eddy current effects. Again, from equation (1), since the total flux must remain at the correct value, as the eddy currents die away on going from current rise to flat-top, less current is required to maintain the flux and the current drops in the main magnet coils. Although the amount of eddy current power is quite considerable, no rise in temperature of the build up plates was detected.

Some correction for the depression in field will be required.

4.7.3. Transient Effects

The voltage from the power supply has a fast switch on rise time (~ 0.1 ms). The problem of transients in the magnet due to this voltage step has been discussed⁽¹³⁾. The ring in magnet voltage due to this transient is shown in Fig. 4.7.3(i) for two adjacent octants, forming a symmetrical quarter of the machine.

By differentiating equation 20 in (13) and since $V = NA(dB/dt)$ at low currents, the theoretical voltage transient is obtained. The theoretical and measured results for one octant are shown in Fig. 4.7.3(ii). The agreement is reasonable and confirms that the transient effects at the beginning of current rise, decay in a time short compared with the rise time to injection. The frequency of the oscillation is such that it will not be excited by the approximately 50 c/s voltage waveform used to produce the correct injection conditions.

4.7.4. Magnet Movements during pulsing

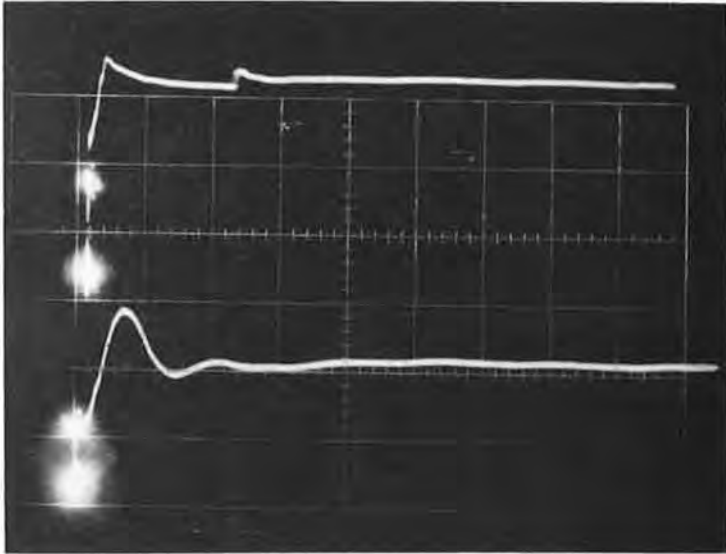
Movements of magnet components during pulsing have been measured at 10,700 A peak magnet current and are included in the Table 4.7.4(I).

TABLE 4.7.4(I)

Movements of magnet. (0.001 in).

Type of movement	Magnet component.	Sector Number.					
		42	41	40	39	38	37
<u>CIRCUMFERENTIAL MOVEMENT</u> (+VE INTO STRAIGHT SECTION)	SECTOR, TOP	+10	+8	+4	+1	+1	0
	P/P, UPPER (FRONT REAR)	+12	+8	+4	+3	+1	+1
		+7	+4	+3	+1	0	0
	SECTOR, BOTTOM	+10.5	+6.5	+4	+2	+1	+1
	P/P, LOWER	+10.5	+6.5	+4	+3	+2	+1
<u>RADIAL MOVEMENT</u> (+VE WHEN OUTWARDS DURING PULSE)	SECTOR, TOP	+3.5	+3	+3	+3	+2.5	+3
	P/P, UPPER	+3	+2.5	+2.5	+2	+1.5	+1
	SECTOR, BOTTOM	+1.5	+0.5	0	0	+0.5	+1
	P/P, LOWER	0	0	+1	0	+0.5	0
<u>CLOSURE OF THROAT</u> (UPPER POSITION: +VE DOWNWARDS) (LOWER POSITION: +VE UPWARDS)	SECTOR, TOP	+5	+10	+11	+11	+11	+11
	P/P, UPPER (FRONT REAR)	+7	+11	+12	+12	+11	+12
		+3	+4	+5	+7	+5	+5
	SECTOR, BOTTOM	0	0	0	0	0	0
	P/P, LOWER	0	0	0	0	0	0

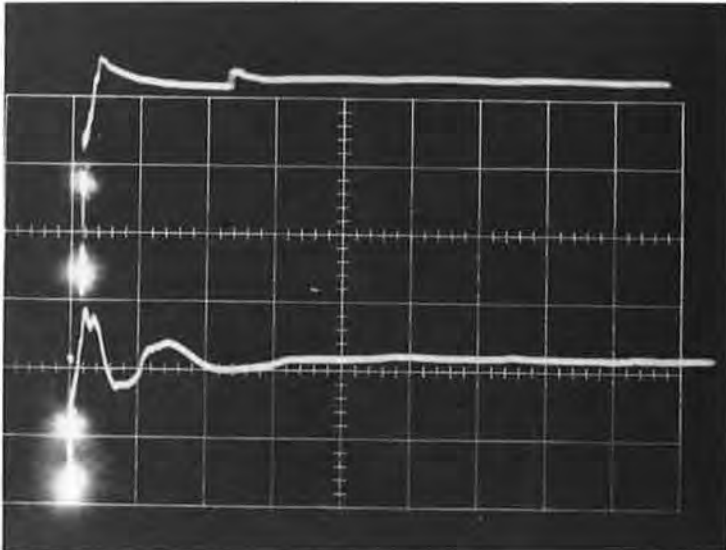
The movements recorded are all tolerable.



← VOLTAGE ACROSS
1/2 MAGNET

← VOLTAGE ACROSS
OCTANT 4

← 1 ms →



← VOLTAGE ACROSS
1/2 MAGNET

← VOLTAGE ACROSS
OCTANT 5

Fig. 4.7.3(i) Voltage transients at the beginning of current rise.

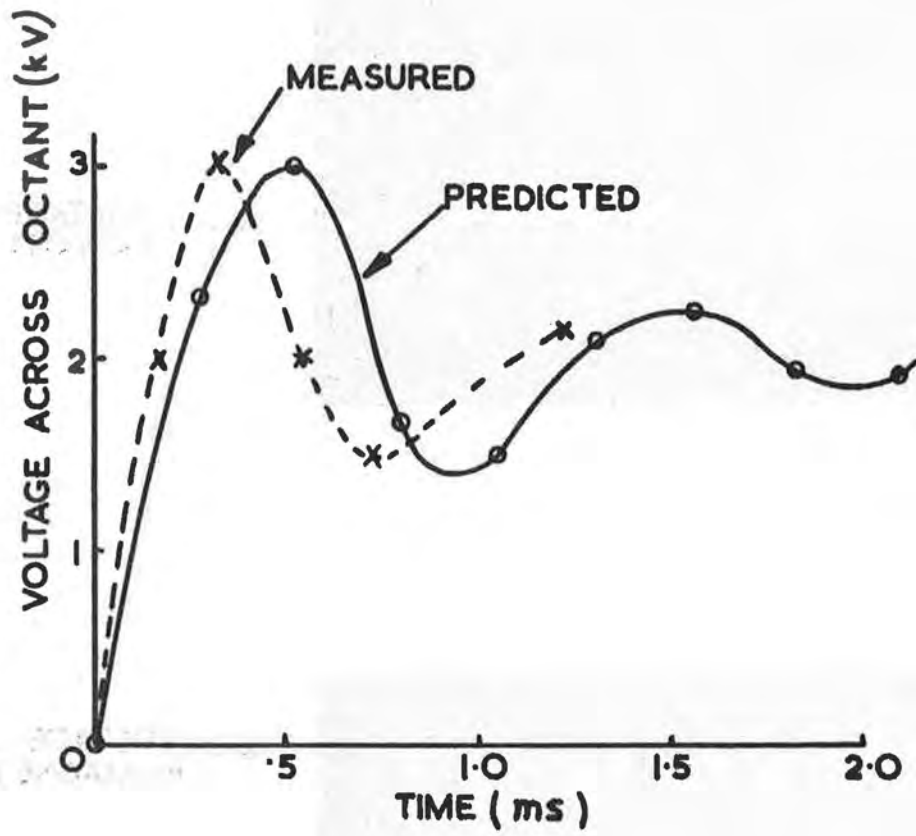


Fig. 4.7.3(ii) Measured and expected voltage transients.

4.8. Pole Face Windings

The dispositions of the windings with respect to the aperture are shown in Fig. 4.8(i) which also shows the function of each individual conductor. Return windings are situated in equal numbers on the inside and the outside of the aperture.

Consider a current +I to be passing through one pair of conductors (top and bottom): then the field gradient produced at the median plane is given by (see Fig. 4.8(ii)):-

$$\begin{aligned} \frac{dH}{dx} &= \frac{\pi^2}{10g^2} I \operatorname{sech}^2 \frac{\pi x}{2g} \quad \text{gauss/cm} \quad (I \text{ in A}) \\ &= 0.0129 I \operatorname{sech}^2 \frac{\pi x}{2g} \quad \text{gauss/in} \quad (g = 5\frac{1}{2}\text{-in}) \end{aligned}$$

This assumes an infinite permeability for the iron and neglects the gap between the windings and the poleface.

For a current sheet top and bottom,

$$\frac{dH}{dx} = \frac{2\pi I}{10g}$$

$$\text{or} \quad \frac{dH}{dx} = 0.09 I \text{ gauss/in} \quad (I \text{ in A/in})$$

Thus, at a field of 14,000 gauss, with $R_0 = 740$ in, 100 A/in produces a change in n of: $\Delta n = \sim 0.45$

For current sheets in the opposite direction, there is no change in n , but a net radial component is produced which alters the level of the median plane by an amount:

$$\Delta z = \frac{560 I}{B_0}$$

4.8.1. Overall Adjustment of n and the Median Plane

Once the field has exceeded about 2000 gauss it is essential to short out of the circuit those conductors in the current sheets which are not in the good field region. Because of the inhomogeneity of the field, large vertical forces would result on any winding carrying heavy current. In practice this means the removal from the circuit of the three conductors on the inside and the outside of the current sheet. This is achieved by switching as shown in Fig.4.8.1(ii), which is a more detailed description of the general circuit Fig.4.8.1(i). The octants are energized in pairs, so that the circuit of Fig. 4.8.1(i) is repeated for octants 2 & 3, 4 & 5, 6 & 7.

The 15 V, 5 A power units supply any current required during the injection period and up to a field level of about 1000 gauss. The current is then reduced quickly to zero, and switches A and C opened. The 60 kW supply is then brought into the

circuit by closing switches B and D. The e.m.f. induced in the windings is particularly troublesome because, although it has been minimised by juggling with return windings, during each acceleration pulse it reverses sign, as shown in Fig. 4.8.1(iii) and has a peak value of about 10 V per pair of octants.

Median plane adjustments are made with the 3.2 kW set, injecting oppositely directed current into the upper and lower layers. One set supplies the four pairs of octants in parallel.

4.8.2. Aperture at Injection

One 3.2 kW set will feed the whole magnet, the arrangement of connections being shown in Fig. 4.8.2(i). Considerations of available power and voltages induced in the windings by the rising field have led to a compromise arrangement whereby it will not be possible to make n quite as uniform across the aperture as was hoped. Four sets of windings are fed in parallel by the 3.2 kW set, these groups consisting of 2 and 25 Upper, 2 and 25 Lower, 4 and 23 Upper and Lower (in series), and 25 Upper and Lower. The currents are varied by means of rheostats in series with each group. To conserve current, 25 acts as the return conductor for 2, and 4 performs the same function for 23. These equal and opposite currents provide approximately the right correction to the field shape. Since conductor 25 lies at the outside of the aperture, the upper and lower windings have been placed in separate circuits so that the distortion in the median plane in this region may be corrected. The current arrangement is therefore as shown in Fig. 4.8.2(ii).

4.8.3. Aperture at High Fields

Because the current requirements for the windings at the inside and outside of the aperture are not the same, these windings have been placed in separate circuits (Fig. 4.8.3(i)). This arrangement has the disadvantage that the same current must be passed through four octants at a time but the indications are that this lack of fine control will not be much of a drawback, as the field shape at high fields is fairly similar from octant to octant.

4.8.4. B₀ Correction

Since it is not yet known what corrections have to be applied to B₀, no arrangements have been made apart from the provision of power supplies and four windings per octant.

4.8.5. Manufacture of Pole Face Windings

In each magnet octant there are two pole face windings, each continuous over the length of the octant; one is attached to the face of the upper set and one to the face of the lower set of pole pieces. The upper and lower pole face windings are housed in the interspace of the double walled vacuum vessel which is evacuated to a pressure of approximately 10⁻² torr. Demineralised cooling water is passed through all the conductors of the pole face windings at a temperature of approximately 18°C.

Each winding consists of 26 conductors and 2 coaxial cables moulded within a glass fibre epoxy resin laminate. The following materials are used:

- (i) Conductors - softened high conductivity tough pitch copper to BS.1037 with an electrical conductivity of not less than 98% I.E.C.

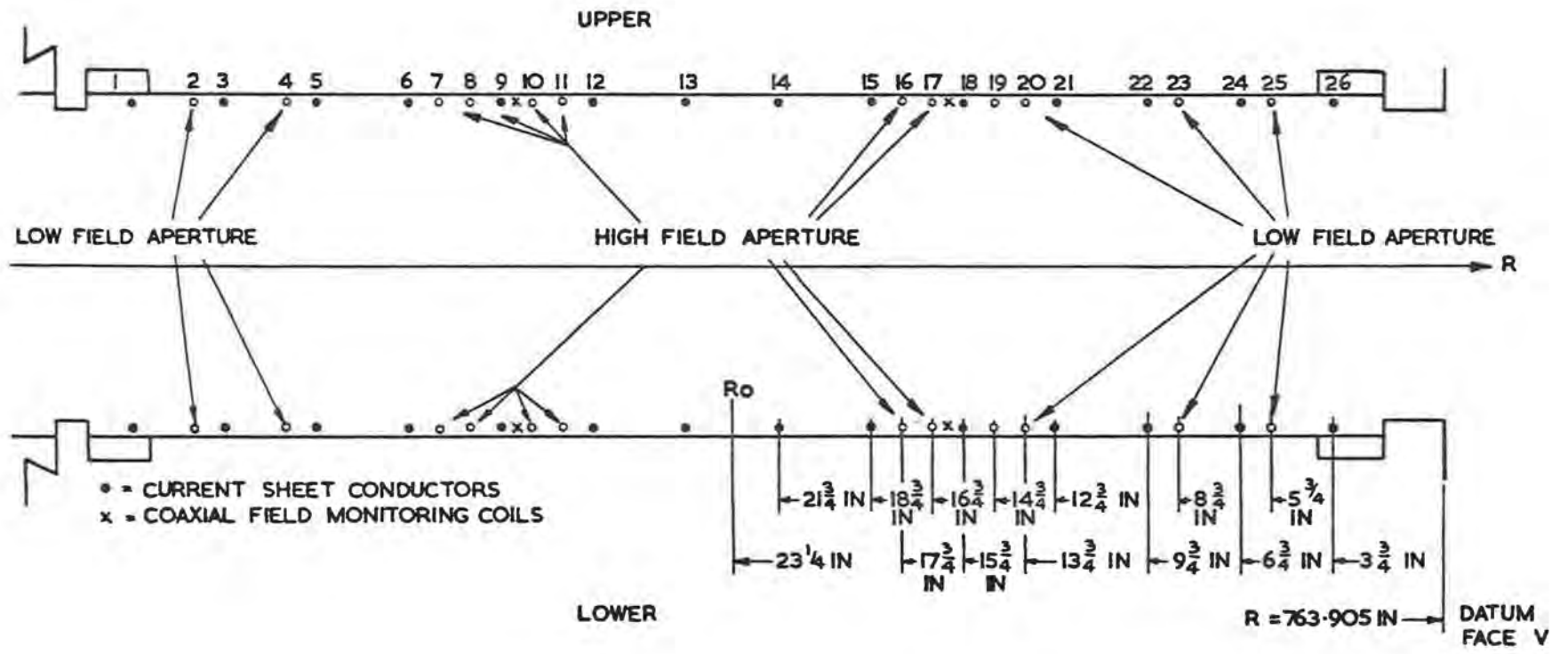


Fig. 4.8(i) Configuration of pole face windings.

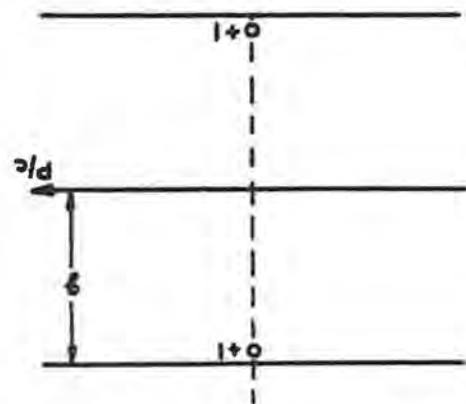


Fig. 4.8(ii) Diagram for winding calculation.

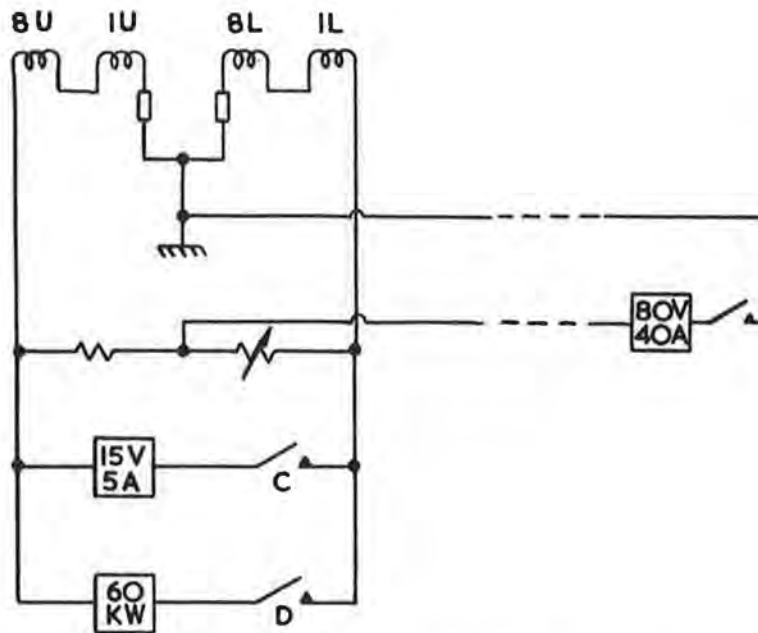


Fig. 4.8.1(i) Switching of conductors.

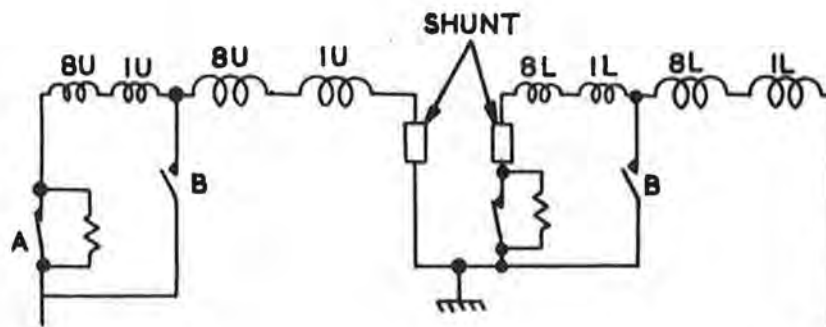


Fig. 4.8.1(ii) Switching of conductors (detailed)

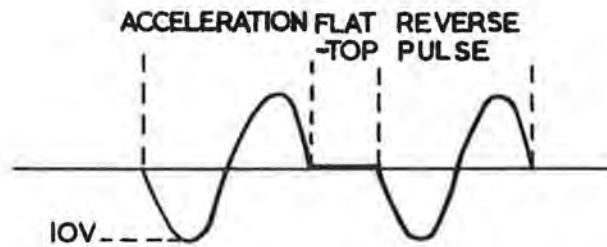


Fig. 4.8.1(iii) Voltage from n windings.

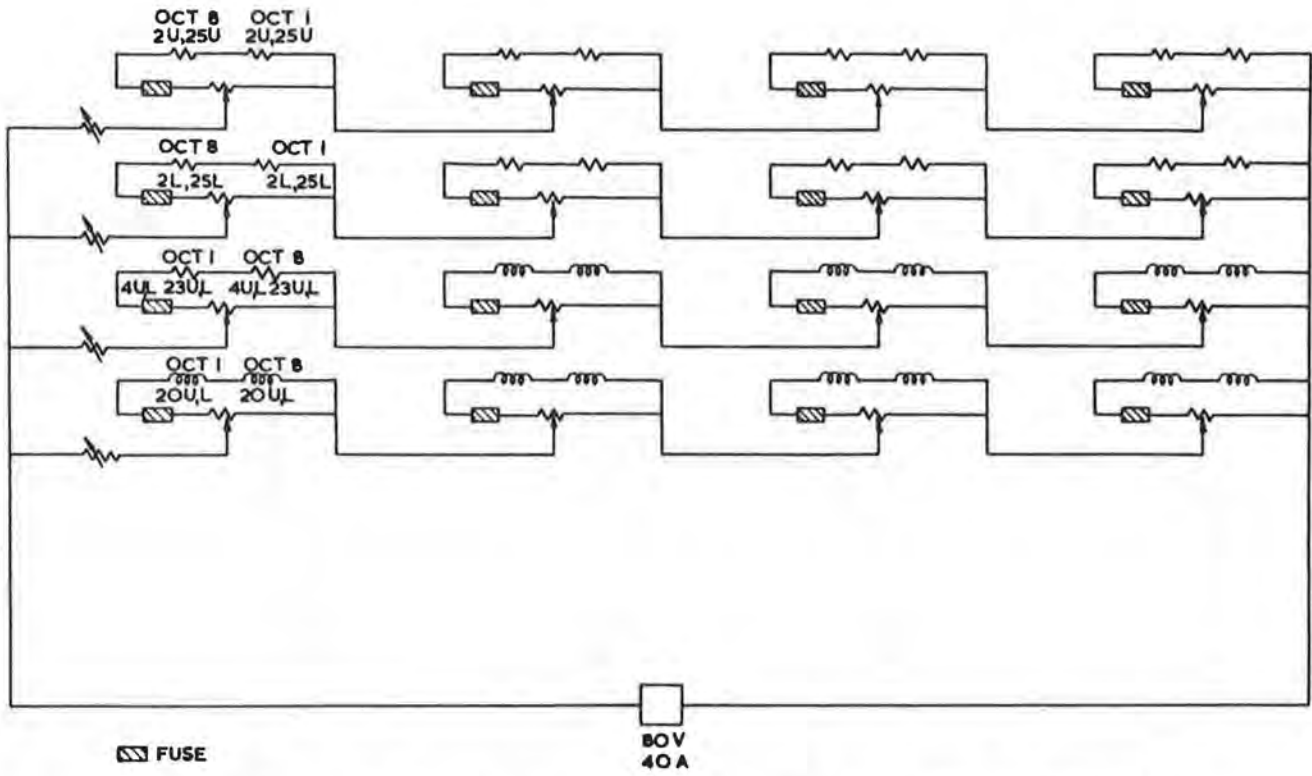


Fig. 4.8.2(i) Connections for aperture correction at injection.

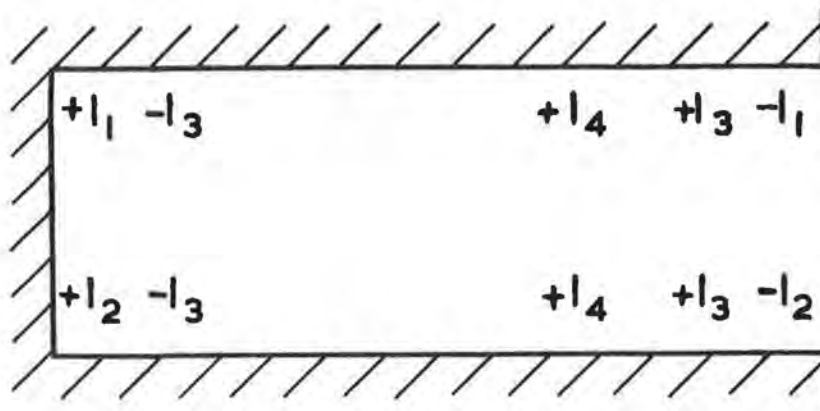


Fig. 4.8.2(ii) Current arrangement in windings.

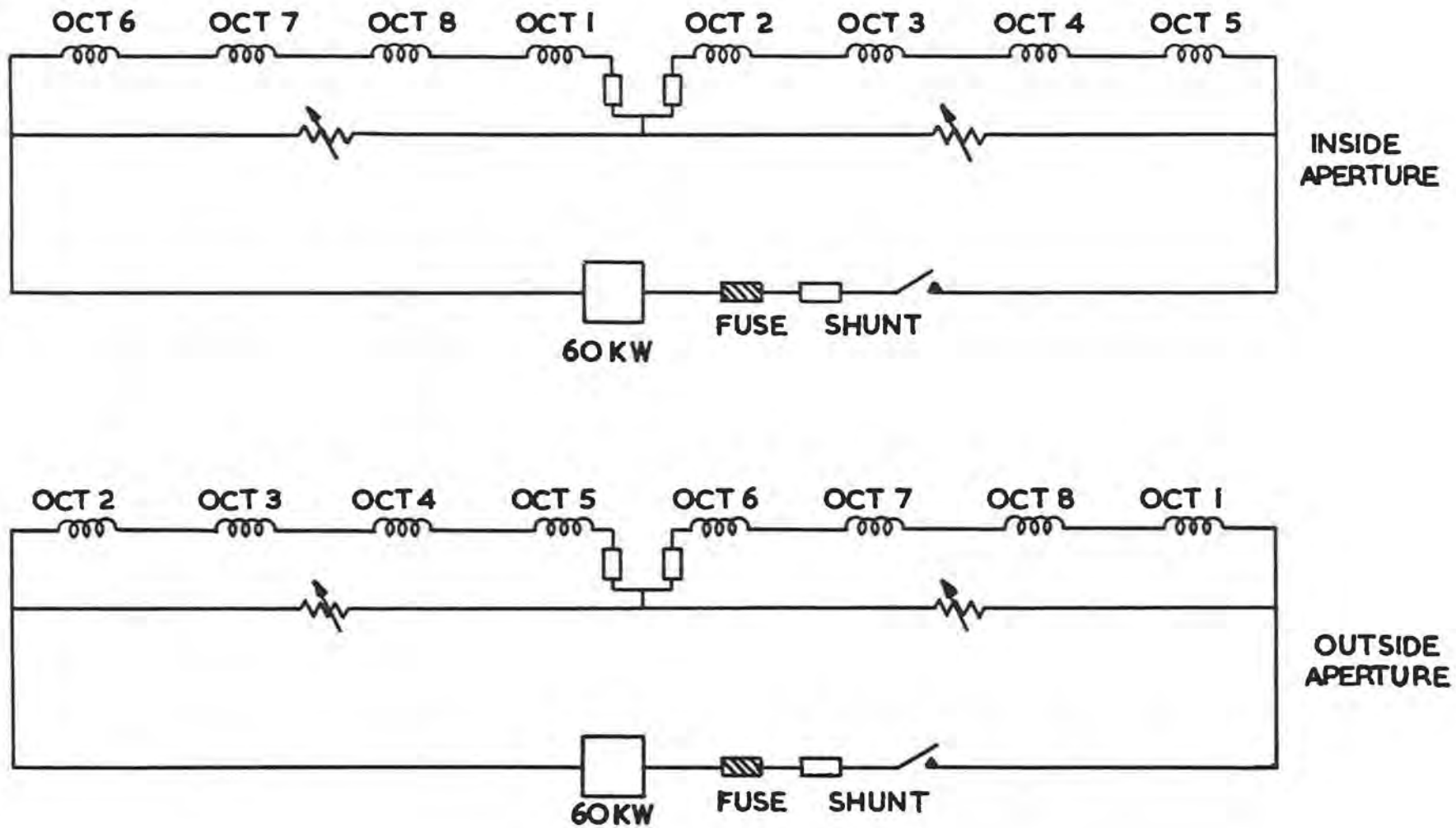


Fig. 4.8.3(i) Aperture correction at high fields.

and coated with polythene.

- (ii) Laminate - outer skins top and bottom, 0.006 in glass cloth.
Main core glass mat - pre-impregnated.
Resin system: Araldite MY 470 - 100 parts by weight
Methyl Nadic Anhydride - 80 parts by weight
Ciba 33/1266 - 3 parts by weight
(Cure temperature $100^{\circ}\text{C} \pm 10^{\circ}\text{C}$ for a minimum of 2 hours.)
- (iii) Conductor End Terminations - phosphor bronze, silver brazed to the ends of the windings, insulated with a polythene sleeve and wrapped with a pressure sensitive impact adhesive polythene tape.

The windings were carefully laid up on an approximately 50 ft long mild steel bed with the appropriate radius of curvature and cured on this bed. After the ends of the conductors had been shaped and vacuum tests performed, the windings were transported in pairs to the Laboratory.

4.9. Pole Face Winding Power Supplies

The power supplies are of three types:

- (i) 60 kW with a peak output of 400 V and 200 A.
- (ii) 3.2 kW at 80 V, 40 A.
- (iii) 15 V, 5 A.

4.9.1. Control Systems (General)

Each power supply has an associated control system which ensures that the currents through the pole-face windings are functions of the main field (B). The control systems are basically of the form shown in Fig. 4.9.1(i). The search coil is in the "good field" region of octants 5 and 6, and a voltage $V_1 = K_1 B$ is induced in it when the main winding is pulsed. This voltage V_1 is integrated, producing $V_2 = K_2 B$, and V_2 is operated on by a function generator to produce $V_3 = F(B)$. V_3 is fed into input 1 of a differential amplifier which is part of a closed control loop. The voltage (V_s) developed across the manganin shunt S, is fed into input 2 of the differential amplifier and the polarities of the inputs are arranged so that the output voltage from the differential amplifier is $G(V_3 - V_s)$, where G is the gain of the amplifier. The voltage $G(V_3 - V_s)$ is the control signal for the power supply and therefore the current through S is a function of B, to an accuracy dependent upon G.

4.9.2. Integrator Unit

A schematic diagram of the integrator is given in Fig. 4.9.2(i). Three integrators with different time constants are used, the amplifiers being Philbrick units. The feedback capacitors are shorted at the end of each pulse by a monostable multivibrator triggered from the end of the magnet current timing pulse. The integrator unit has been made and commissioned.

4.9.3. Function Generator

There are 13 function generators, one for each power supply. A schematic diagram is given in Fig. 4.9.3(i). The generator is a 10 point device which accepts a voltage proportional to the magnet field and converts to a voltage which is sufficiently finely controllable to be a specified function of the field. All 13 generators have been made and set up in the main control room.

4.9.4. 60 Kilowatt Supplies

The basis for these six units is a standard commercial 6-anode mercury arc rectifier set with transistorised grid control. This has a linear characteristic of output volts versus input control volts. The control and driver unit which is required for the supply is shown in Fig. 4.9.4(i).

All six sets have been delivered and are being installed. One set has been successfully operated under actual operating conditions with a full servo loop. Ripple at 300 c/s is reduced by a static choke-capacitor filter. At a current of about 150 A, 50 c/s ripple, which is inherently produced in the supply, is too great but modification of the grid control circuits should cure this.

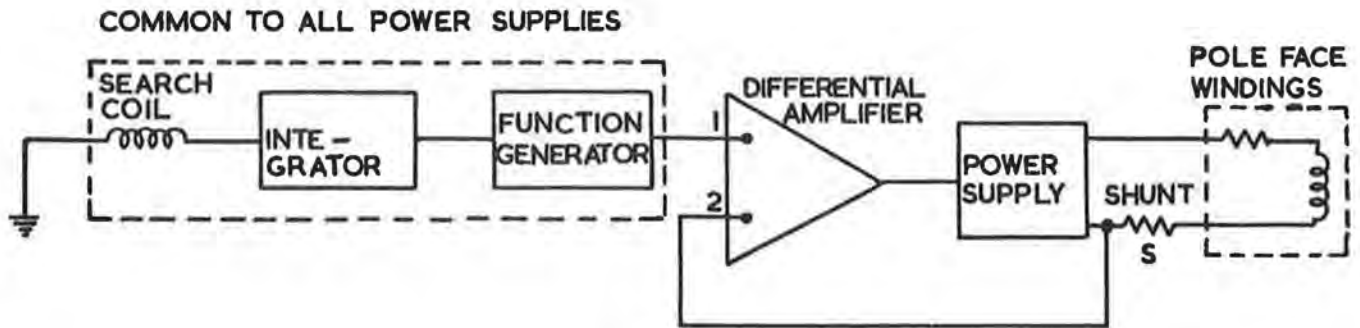


Fig. 4.9.1(i) Control system for pole face windings.

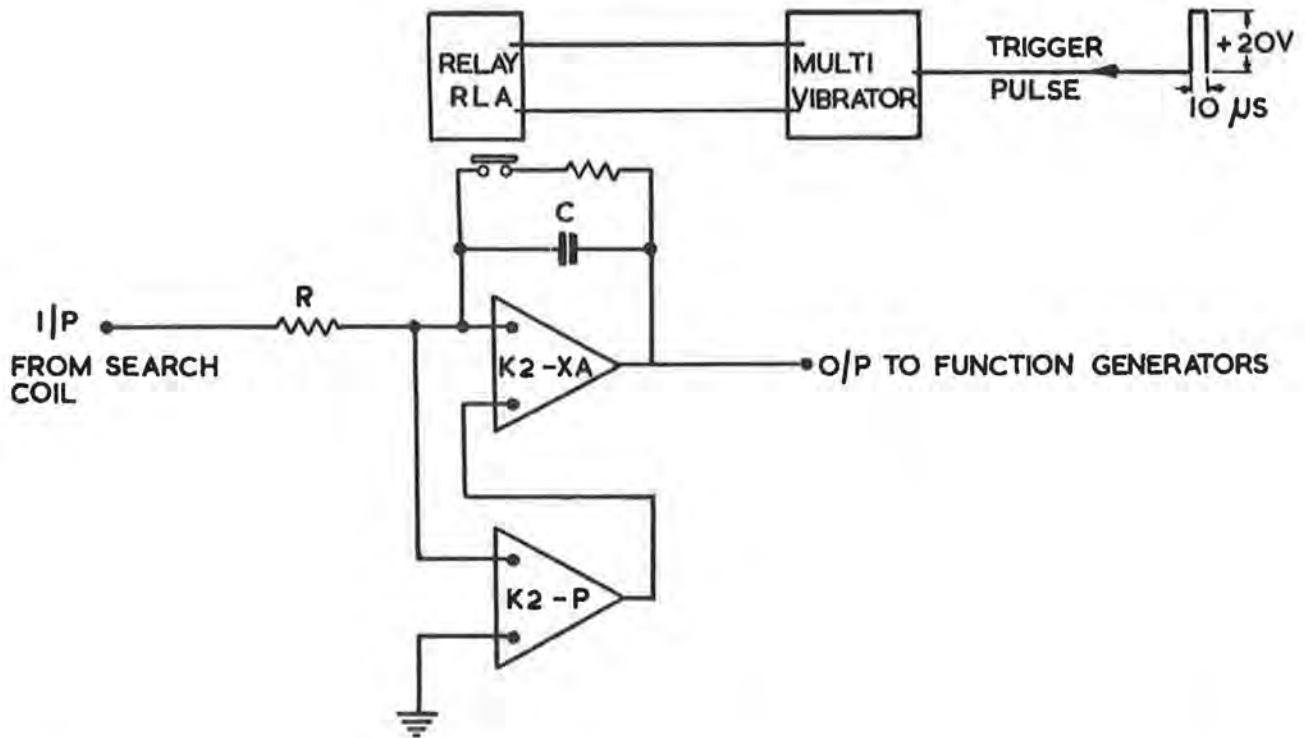


Fig. 4.9.2(i) Integrator.

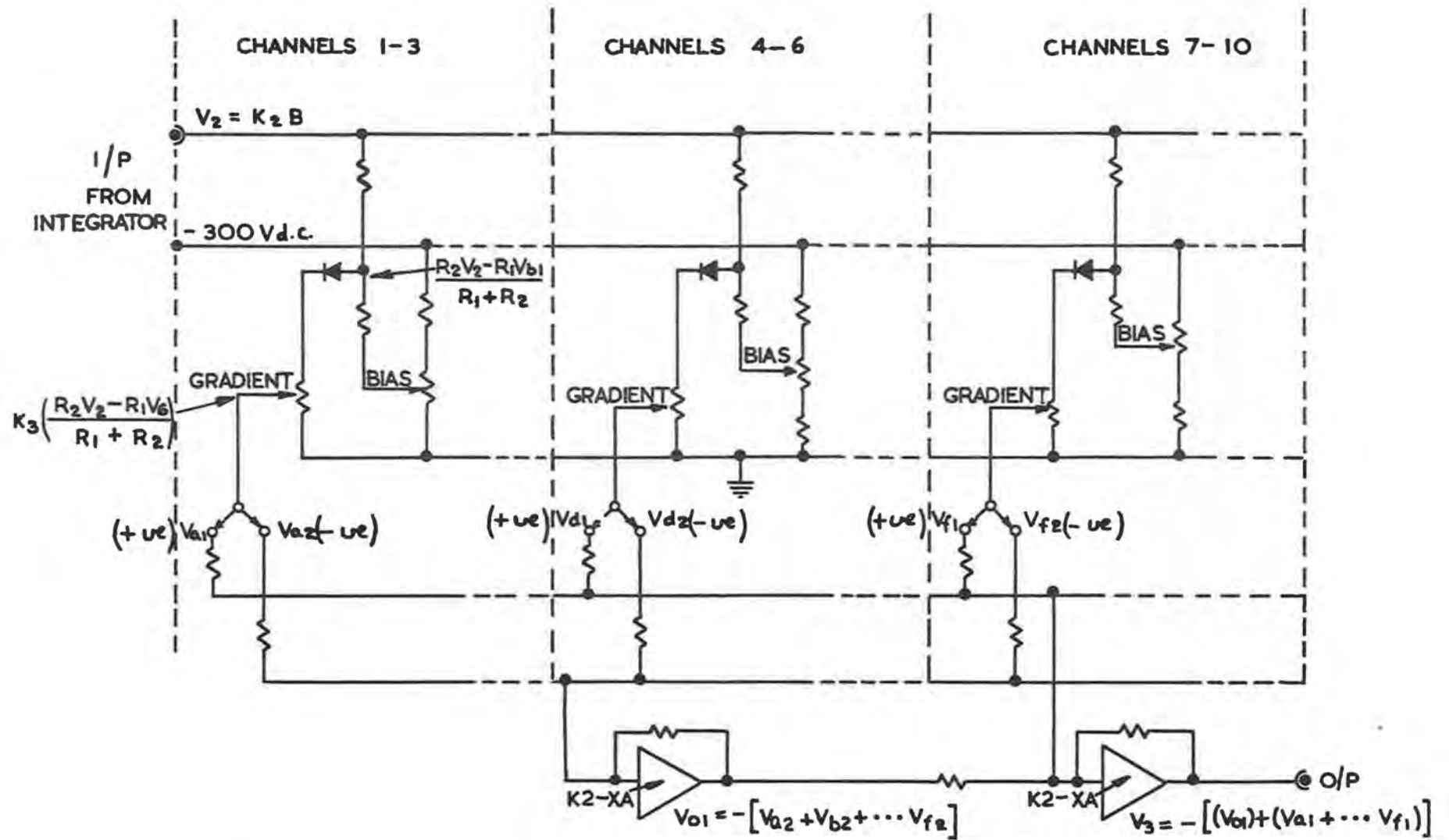


Fig. 4.9.3(i) Function generator.

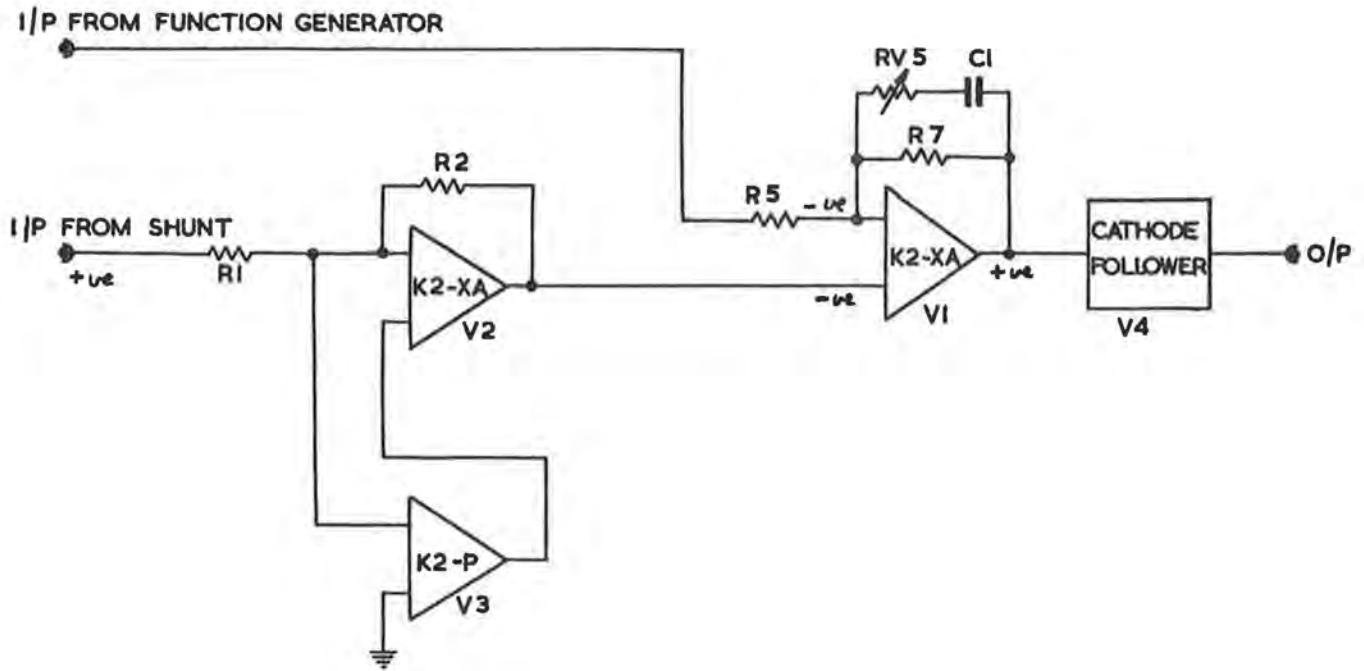


Fig. 4.9.4(i) 60 kW set controller and driver unit

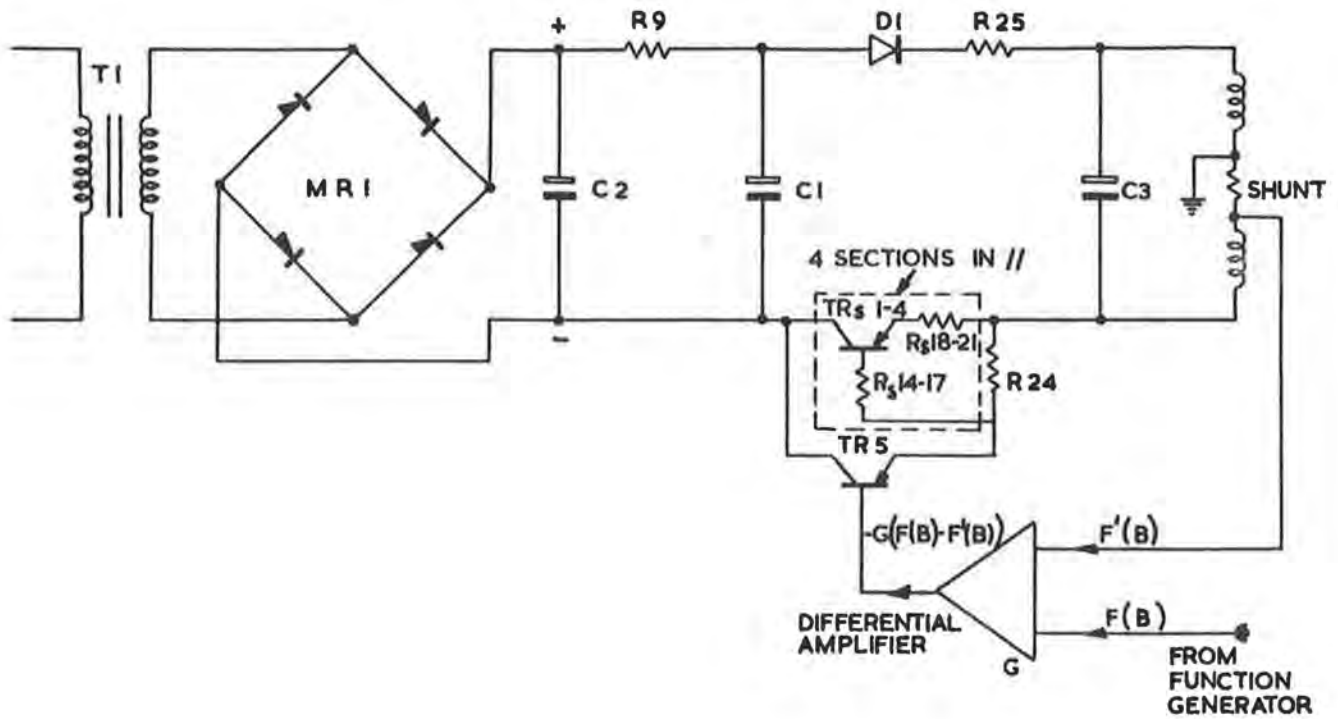


Fig. 4.9.6(i) 15 V, 5 A d.c. set.

4.9.5. 3.2 Kilowatt Supplies

The three sets have been designed commercially to outline specification. They each have their output current servo controlled by a demand input voltage from the function generator. Basically, the required variation of current is obtained by switching (using a varying mark to space ratio with controlled silicon rectifiers between positive and negative rails) and feeding through a filter network. The sets have been delivered and are being installed. Tests with a dummy load indicate that they work satisfactorily.

4.9.6. 15 Volt, 5 Amp Supply

A schematic diagram of the 15 V, 5 A, d.c. sets is given in Fig.4.9.6(i). Fundamentally these are ordinary bridge rectified, fixed output voltage, d.c. sets, with a series transistor which acts as an emitter follower to control the current through the load according to the demand signal F(B) from the function generator. The sets have been made and have all been tried out under actual working conditions, i.e. they have been used in a complete control loop to drive current through the pole face windings when the main winding was being pulsed. These tests showed that there is a large unbalanced e.m.f. of approximately 30 V peak to peak (including ripple) induced in the pole face windings when the main winding is pulsed at full current.

It is possible to arrange that the 15 V, 5 A, sets are aided by the induced e.m.f. during the part of the magnet cycle when they are in circuit. If, under fault conditions, they remain in circuit for a complete cycle, the induced e.m.f. reverses in sign, opposes the applied e.m.f. and can reverse the polarity of the voltage across the transistors. Diode D1 has therefore been added to guard against this and C₃ has been added to cut down the ripple voltage seen by the d.c. set. The L-C filter unit used previously showed a tendency to ring under conditions of fast current rise or decay and has been replaced by the present circuit of C₂, R_a, and C₁. In addition, an OC28 is now used as the driving stage (TR5) because of its ability to withstand reverse voltages. These modifications have now been completed and the sets are being installed. No other difficulties were encountered during testing and the modified sets are expected to operate satisfactorily, especially since the maximum current required is about 3 A.

4.10. Ripple Filter System

The power supply for the Nimrod magnet consists of two 24-phase grid controlled rectifier sets fed, via multi-phase transformers, from two tandem coupled motor-alternator-flywheel sets (see Section 5 of this report). The rectifier output has an inherent ripple voltage of approximately saw-tooth shape, of (nominally) 1200 c/s (the actual frequency varies over the period of a magnet pulse from 1123 c/s to 1164 c/s, dependant on the slip frequency of the slip-ring driving motors). The amplitude of this ripple varies during the course of a pulse. During flat-top it was found to have a maximum value of approximately 1200 V peak to peak (for each half of the power plant). This was observed during commissioning tests on the power plant and may ultimately be reduced. It was also observed that, during current decay, the ripple voltage rose to about 3000 V peak to peak. Additionally, the rectifier output contained a 100 c/s (nominal) component of about 175 V peak to peak amplitude. (This has since been reduced).

The effect of these ripple voltages on the operation of the proton synchrotron is particularly significant during flat-top⁽¹⁴⁾. Under this condition the ripple will modulate the spiral rate of the proton orbits, the degree of modulation being indicated by the ratio of E to V-IR, where E is the peak ripple voltage, V the mean voltage applied to the magnet during the flat top period, and IR is the ohmic drop in the magnet coil. For a flat-top duration of 0.5 s, V-IR has a value of about 50 V for the whole magnet, hence the ripple voltages referred to above will give a degree of modulation considerably greater than 100%; consequently, unless some form of ripple filter is employed, it will be impossible to spiral the beam smoothly onto a target. It is estimated that it will be necessary to reduce the ripple flux by a factor of 100 for satisfactory operation with a 0.5 s flat-top.

There are two ways of reducing the ripple flux in the magnet gap. The first method is to reduce the ripple voltage at the magnet terminals by developing a voltage, in phase opposition to that from the rectifiers, across an inductor placed in series with the rectifiers and magnets. The second method is to place an auxilliary winding around the magnet pole-pieces and use this to produce a flux acting so as to reduce the ripple flux in the useful region of the magnet gap. Both these systems will be employed on Nimrod to give the required reduction of ripple. The first system is referred to as the "primary ripple filter", the second system as the "secondary ripple filter".

4.10.1. Primary Ripple Filter

The system is shown schematically in Fig.4.10.1(i). It consists of two independent filters, one in each half of the magnet power supply. Each filter consists of a push-pull amplifier feeding into a transformer, the secondary of which is connected in series with the rectifier and magnet coils. The input to the amplifier is taken, via d.c. blocking capacitors, from across the ends of the magnet octants. The input voltage is thus the residual ripple E^1 and the amplifier output is GE^1 where G is the overall gain of amplifier and output transformer. Hence, if E denotes the ripple produced by the rectifiers, the resultant ripple is given by:-

$$E^1 = \frac{E}{1 + G}$$

A resistor is placed across the transformer secondary to damp out any

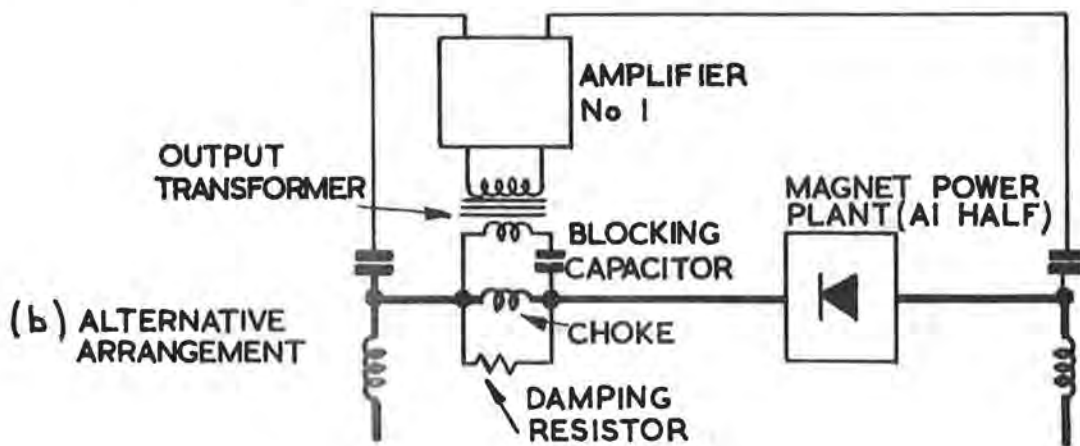
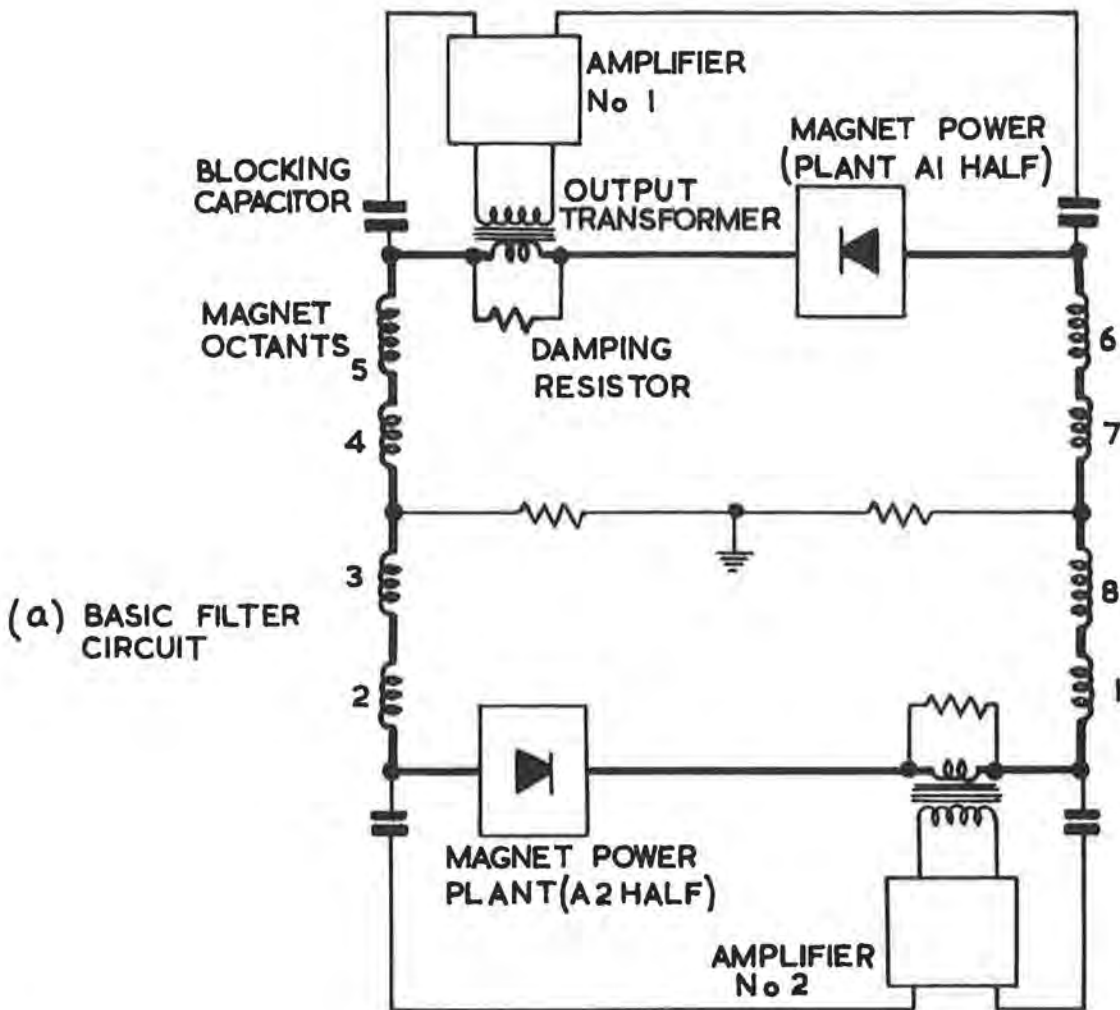


Fig. 4.10. 1(i) Magnet power supply and ripple filter circuits.

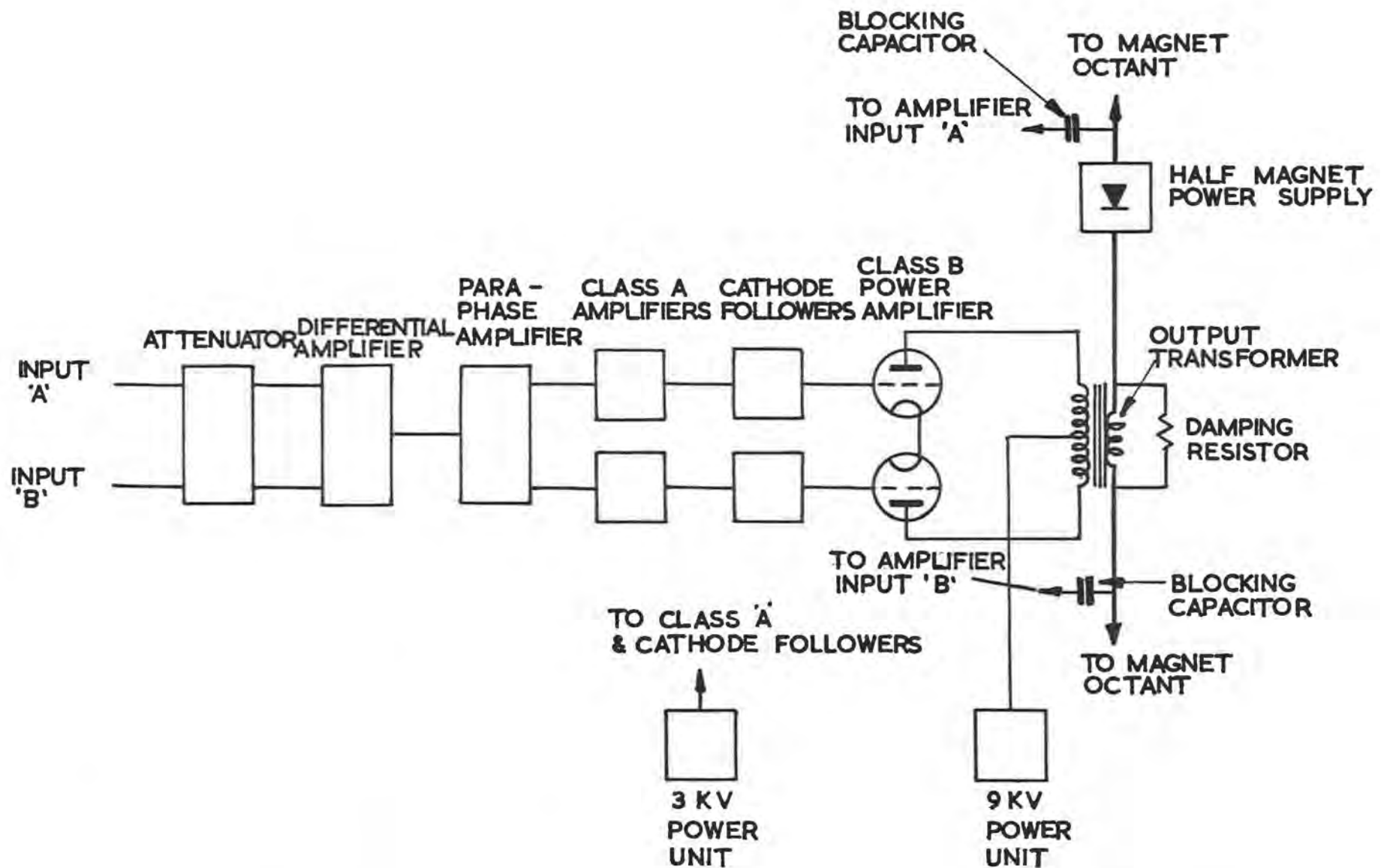


Fig. 4.10.1(ii) Schematic diagram of ripple filter amplifier.

resonances that may occur and to present the amplifier with a load that is reasonably constant with frequency.

Fig. 4.10.1(ii) shows one of the filters in greater detail. The earthing of the magnet system is such that the input to the amplifier is floating. The input is fed, via an attenuator, to a differential amplifier giving a single output proportional to the difference between the voltages appearing at its two input terminals. The output is then fed into a para-phase amplifier to give two equal anti-phase signals which are then further amplified by identical Class A amplifiers. The final drive to the output stages is through impedance matching cathode followers. The output stage consists of two water cooled power triodes operating under Class B push-pull conditions.

The major single item in the system is the output transformer. This has to carry the peak magnet current of 10,500 A in its secondary winding without saturation of the core. Under repetitive pulsing conditions the copper loss due to the magnet current is 100 kW necessitating the use of oil filled water cooled transformers. In view of the very large polarising current carried by the secondary winding, a large air gap and heavy conductors are required and no very great subtlety could be employed in the winding arrangement to minimise leakage reactances or winding capacitances to achieve a good high frequency response.

An alternative arrangement is shown in Fig.4.10.1(i)(b). Here the original output transformer is replaced by a choke, and an additional transformer is interposed between this and the amplifier. A blocking condenser between the choke and transformer prevents any polarising current flowing in the secondary and limits any a.c. voltages at pulse frequency, that may be impressed on the secondary terminals. This should allow considerable improvement in design with consequent improvement in band-width.

The difference in cost, weight and size of the transformer of Fig.4.10.1(i)(a) and choke of Fig.4.10.1(i)(b) did not appear to be significant and since the transformer could equally satisfactorily be used as a choke by the omission of the primary connections it was decided initially to proceed with the arrangement of Fig.4.10.1(i)(a).

The two amplifiers, which were built on the site, were installed in the annexe to the convertor house towards the end of 1961. The remainder of the equipment, which includes output transformers, amplifier power supplies and switchgear, was delivered and installed in the convertor house in the early part of 1962.

The magnet has been pulsed with the secondary of the output transformers connected and no undesirable effects on the operation of the power supply were observed. Tests were carried out on the individual amplifier units and their associated power supplies and the performance of these is within the required limits. Measurements of the frequency response of the output transformers were also carried out. These were rather poorer than had been hoped for due to the occurrence of resonances at frequencies of 10 kc/s and above.

The open loop performance and frequency response of the complete system was measured, the latter is shown in Fig.4.10.1(iii), and the system has been operated as a filter with the magnet pulsed. In the limited time available for this latter test it was only possible to reduce the ripple by a factor of three. A study of the frequency response characteristics indicate that improvements to a factor of four or five could be made.

An alternative system in which a fraction of the ripple voltage appearing across the rectifier is fed into the amplifier was also tried. This does not comprise a feed-back loop and hence no problem of stability arises. However, in this system, the amplifier gain and phase shift is very critical and the results were not very much better than with the original system. Again careful design of phase correcting networks would improve this; however it would not appear to be possible to compensate for the slight changes in gain and phase of the output transformer which occur during pulsing, owing to the change in polarising current in the secondary winding. Consequently it would not seem likely that a reduction factor of better than five could be obtained.

In order to achieve the required factor of ten or better it will be necessary to change to the arrangement shown in Fig.4.10.1(i)(b). A specification for a suitable transformer has been drawn up and enquiries regarding its manufacture are in hand.

A further problem arises due to the fact that the 100 c/s ripple component is greater than had been hoped for. The original scheme did not provide for any filtering of components below 1200 c/s although a sufficient margin was allowed in the rating of the amplifier for these to be handled. A difficulty arises here since, if the bandwidth of the system is extended down to 100 c/s, then it will also attempt to respond to the changes in magnet voltage which occur during pulsing. This would result in saturation of the amplifier. However, the 100 c/s component is sufficiently small to be neglected except during flat-top and it should be possible to overcome the difficulty by a switching arrangement whereby the low frequency cut-off is only extended during the flat-top period.

4.10.2. Secondary Ripple Filter

The secondary ripple filter is designed to reduce the ripple field in the magnet gap by a factor of 20. The principle of the ripple correction network to be used is shown in Fig.4.10.2(i). The search coil samples the field in the good field region of the magnet gap. An amplifier drives a current through the correction windings in such a way as to oppose the field producing the search coil voltage.

Suppose search coil and correction coil have a mutual inductance M . Then a current I in the correction coil will produce a voltage $V = j\omega MI$ in the search coil, thus the output voltage is shifted through 90° and increases with frequency. The resulting 6 dB/octave slope of the open loop response may be corrected by the introduction of a circuit with a sinusoidal response of the form $e_{out} \propto \frac{1}{j\omega} e_{in}$.

This may conveniently be done with an integrating circuit. The whole circuit is considered below.

(a) Design of the Ripple Chain

Suppose the unit consists of an integrator with time constant CR , an amplifier of gain G and a current amplifier of sensitivity S A/V. (see Fig.4.10.2(ii)).

To reduce ripple by a factor of 20:-

$$\frac{V_{out}}{V_{in}} = 19$$

$$\text{But } \frac{V_{out}}{V_{in}} = \frac{MGS}{CR}$$

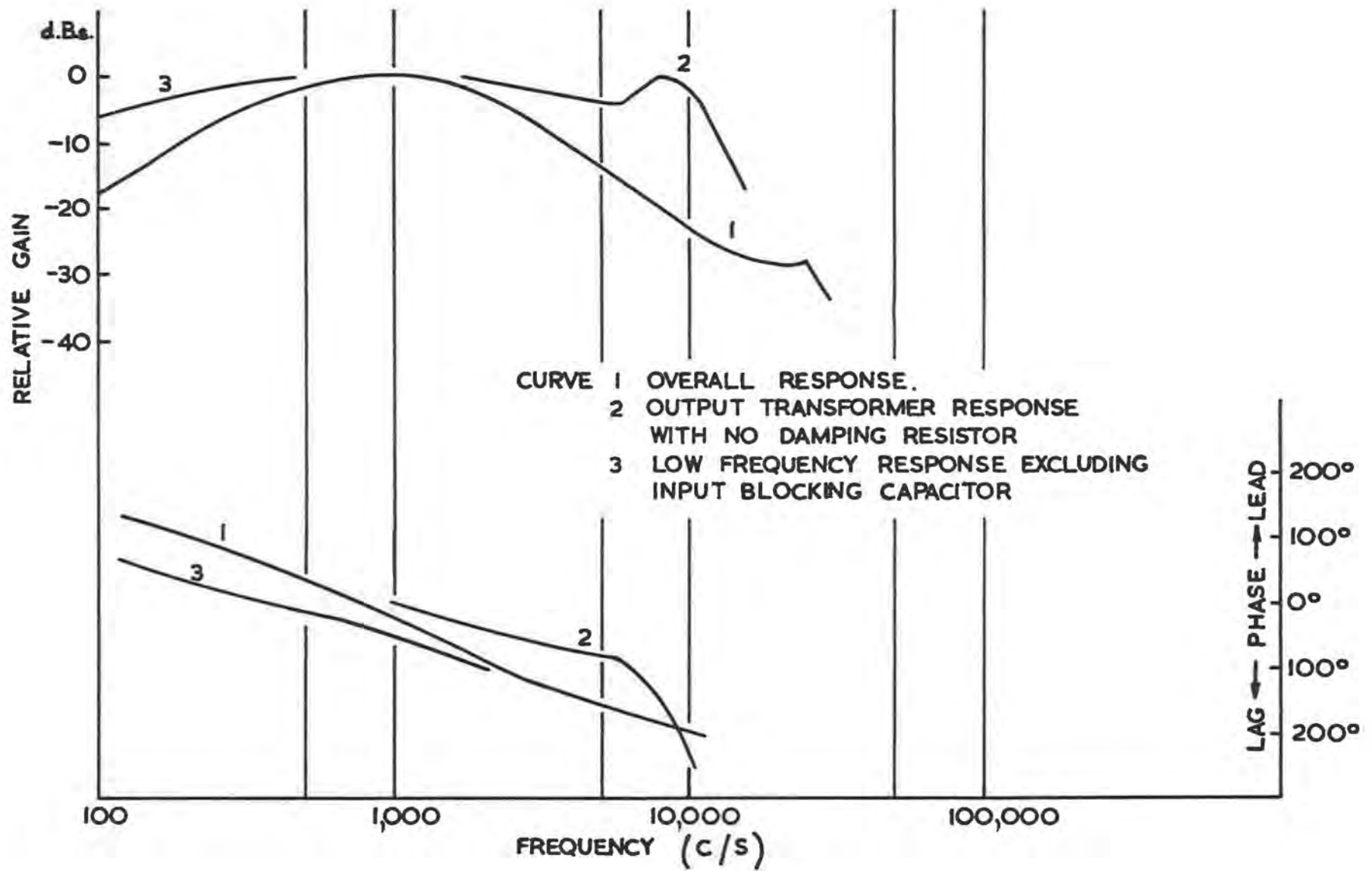


Fig. 4.10.1(iii) Ripple filter frequency response.

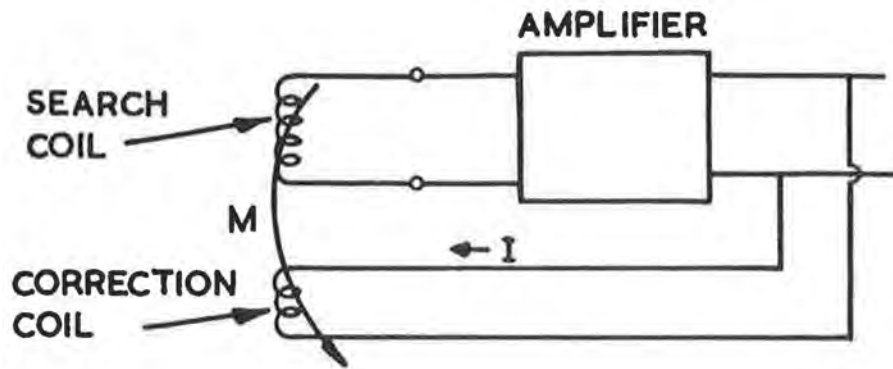


Fig. 4.10.2(i) Basic circuit of secondary ripple filter.

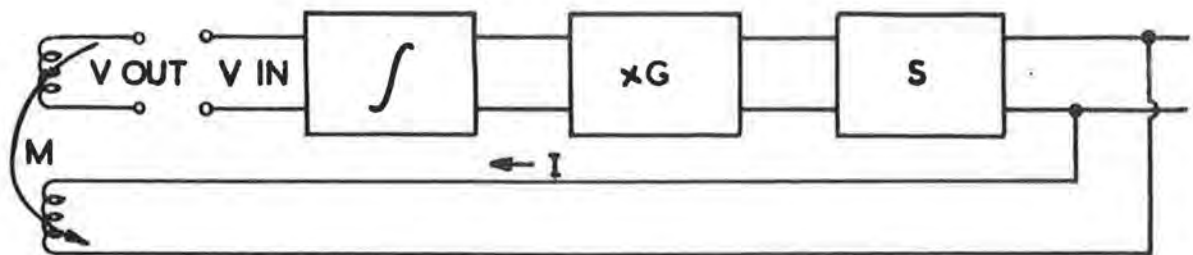


Fig. 4.10.2(ii) Ripple chain.

(b) Design Requirements

It is necessary:

- (i) to have sufficient current available to drive through the correction windings to buck the maximum ripple field produced at all frequencies.
- (ii) to eliminate the effect of the d.c. step produced in both correction and search windings.

(c) Mechanical Arrangement of Coils

The secondary ripple filter system will consist of four separate and independent amplifiers each one sampling the field in the gap of two octants and correcting the ripple on these two octants. The octants will be paired as follows: 1 and 2; 3 and 4; 5 and 6; 7 and 8. This gives a symmetrical arrangement azimuthally.

There are two conductors close to each of the top and bottom main lip coils, and two conductors with each of the top and bottom poleface winding return (see Fig.4.10.2(iii)). These may then be connected to form four correction loops per octant. The co-axial cable embedded in the poleface winding laminate will be used to provide the pick-up loop.

The method of interconnecting the conductors to form correction and search windings is shown in Fig.4.10.2(iv).

(d) Current Requirement

In order to calculate the current required in the correction windings to buck out the ripple field it is necessary to estimate the coupling (k) between the main and correction windings. (Fig.4.10.2(v)).

$$\begin{aligned} \text{At a frequency } f &= \frac{\omega}{2\pi} \\ M^2 &= K_1 K_2 L_1 L_2 \\ V_1 &= \omega L_1 I_1 - \omega M I_2 \\ V_2 &= \omega M I_1 - \omega L_2 I_2 \end{aligned}$$

Assume that the balance condition is:

$$N_1 I_1 = N_2 I_2$$

$$\text{Then, } V_1 = \omega \sqrt{L_1} - \frac{N_1}{N_2} \cdot M I_1 = \omega L_1 (1 - K_1) I_1$$

$$\text{and } V_2 = \omega \sqrt{L_2} - \frac{N_2}{N_1} \cdot M I_2 = -\omega L_2 (1 - K_2) I_2$$

Thus the impedances are reduced by factors: $(1 - K_1)$ and $(1 - K_2)$

When the secondary is open circuit,

$$V_1 = \omega L_1 I_1$$

$$V_2 = \omega M I_1$$

From this L_1 and M can be deduced. L_2 can be found similarly by considering the primary open circuit. K_1 and K_2 can then be deduced.

Since the Nimrod magnet was not available, coils were wound on magnet Model V to simulate correction windings, and values of L_1 and L_2 and M (and hence K_1 and K_2) were obtained by experiment, at frequencies from 25 c/s to 120 kc/s. From these results and the physical parameters of Nimrod it is possible to estimate the current required to buck the expected ripple field.

These parameters are shown in Table 4.10.2(I).

TABLE 4.10.2(I)

Number of:-	Nimrod (one octant)	Magnet Model V
Polepieces (main coil)	42	8 (effectively)
Polepieces (correction coil)	42	4
Main coil turns	42	160
Correction coil turns	4	20

Considering inductance as being proportional to area and (turns)² it follows that:-

$$L_p = 0.724 L_M$$

$$L_B = 0.84 L_C$$

where L_p is the inductance of Nimrod main coil (over 2 octants)

L_B is the inductance of Nimrod correction coil (over 2 octants)

L_M is the inductance of Model V main coil

L_C is the inductance of Model V correction coil

The ripple potential for each half of the power supply applied to Nimrod magnet before any form of ripple correction may be 600 V peak to peak (at 1135 c/s).

If the primary ripple filter reduces this to $1/10$ the ripple potential becomes 60 V peak to peak across 2 quadrants or 30 V peak to peak across 2 octants.

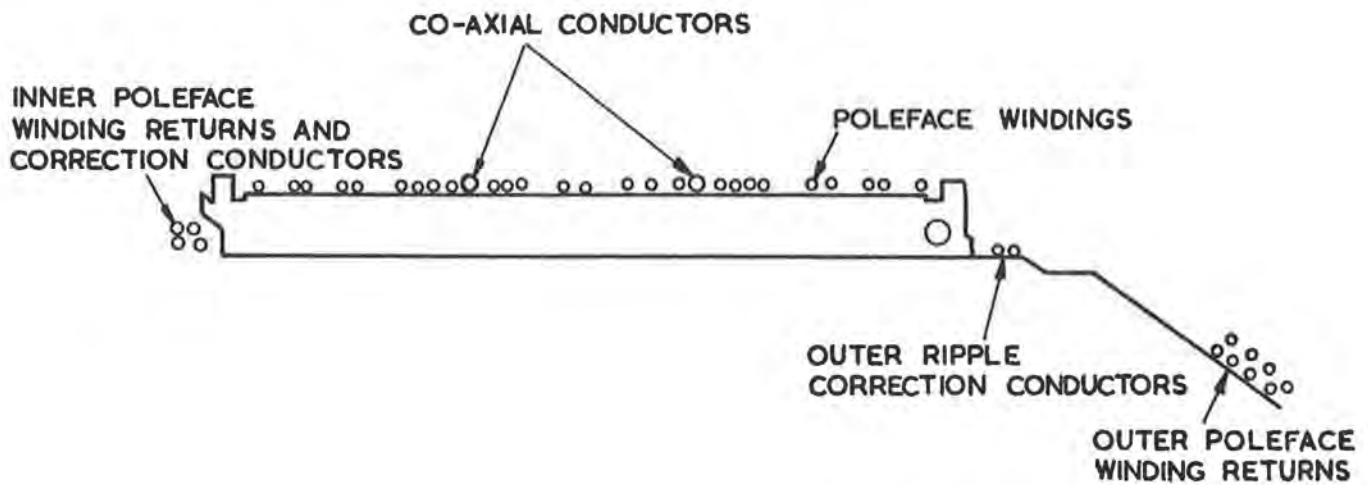


Fig. 4.10.2(iii) Mechanical arrangement of ripple coils.

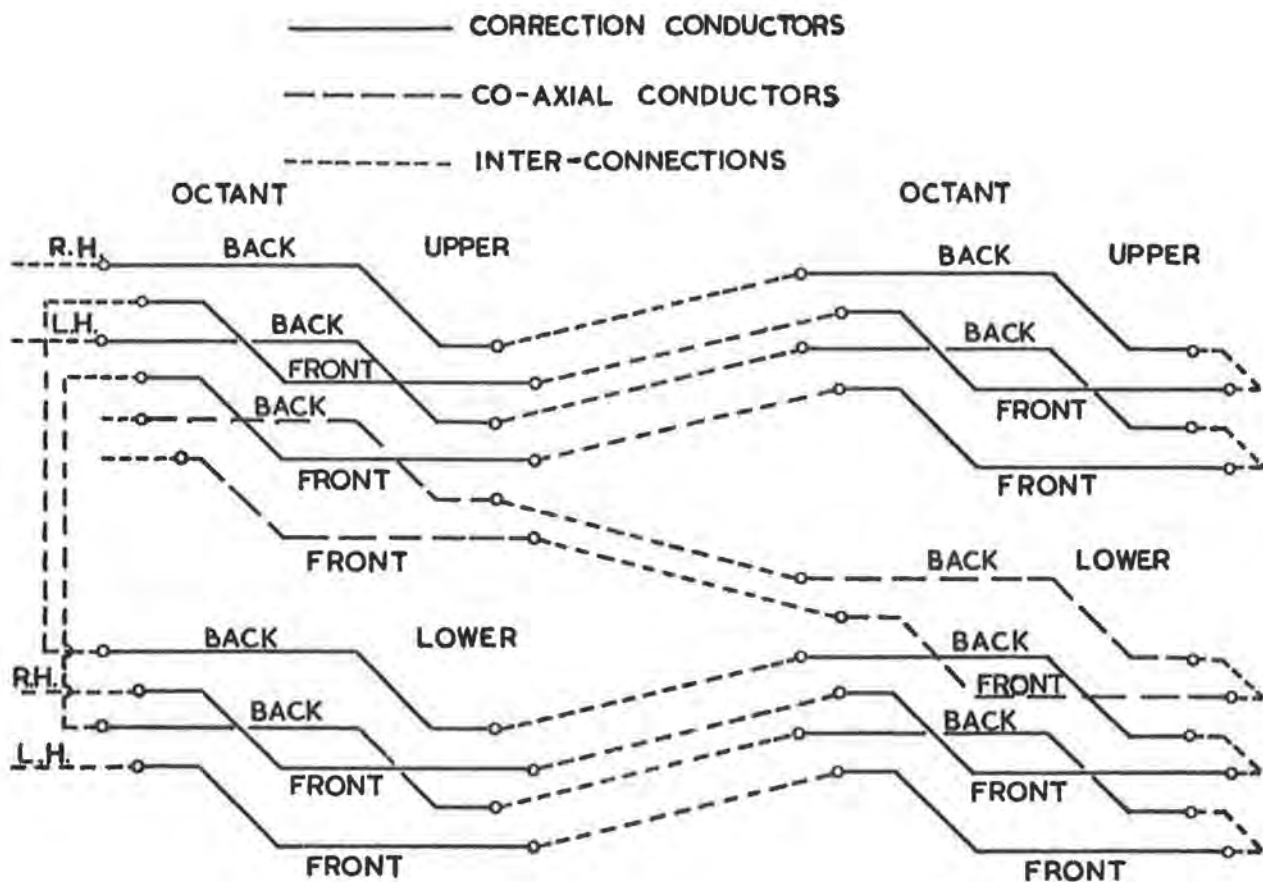


Fig. 4.10.2(iv) Interconnection of ripple windings.

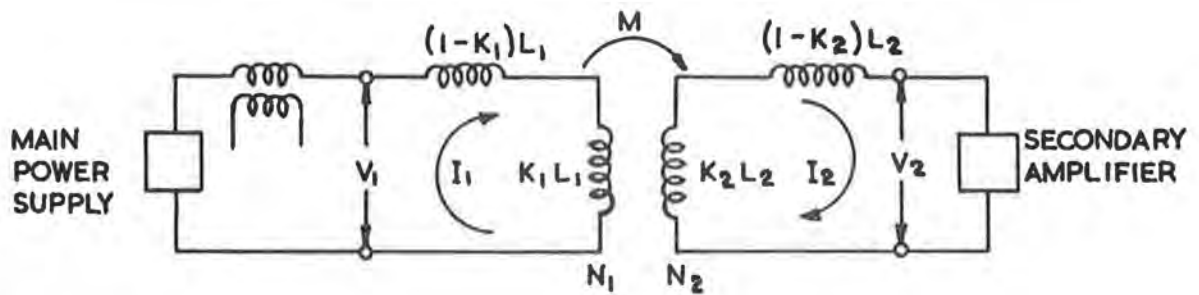


Fig. 4.10.2(v) Basic circuit for secondary ripple filter.

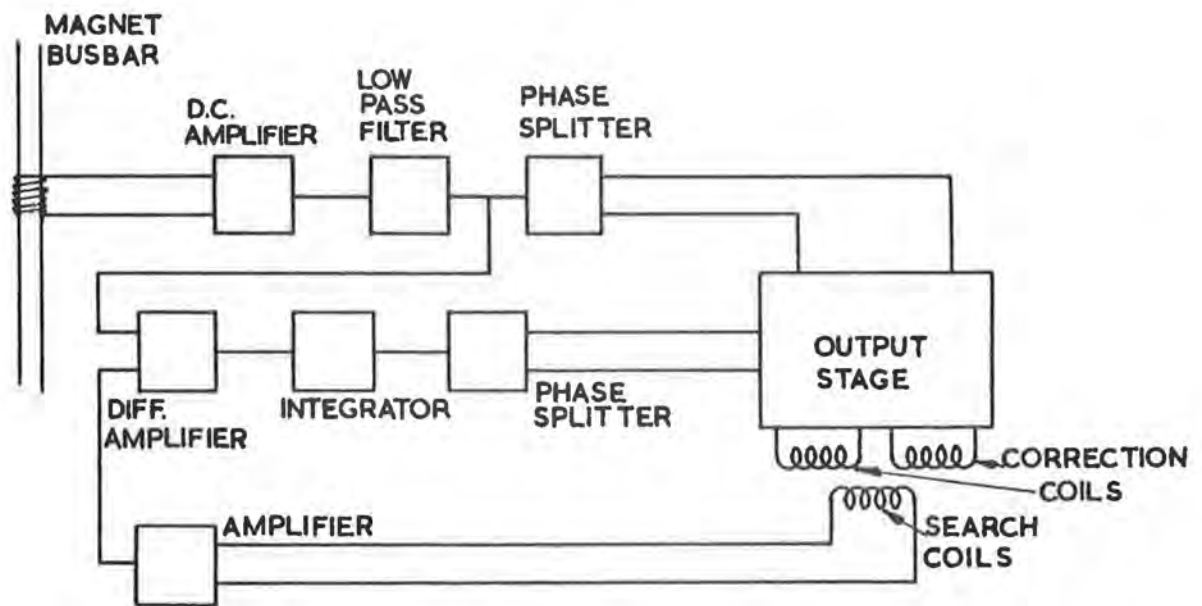


Fig. 4.10.2(vi) General circuit for secondary ripple filter.

Since: $V_1 = \omega L_1 (1 - K_1) I_1$

or $V_p = \omega L_p (1 - K_1) I_p$

and also: $L_p = 0.724 L_M$

and $N_p I_p = N_B I_B$

N_p is the number of turns on Nimrod main coil

I_p is the current in Nimrod main coil

N_B is the number of turns on Nimrod correction coil

I_B is the current in Nimrod correction coil

Hence: $I_B = 450 \text{ mA}$ is obtained at 1135 c/s

Also since $V_B = \omega L_B (1 - K_2) I_B$

$V_B = 2 \text{ volts}$ is obtained at 1135 c/s

(e) Back E.M.F.'s.

An estimate of the size of the voltage V induced in one turn per octant of the correction windings due to the current rise and decay may be obtained from:

$$V = \frac{\text{No. of correction turns}}{\text{No. of main coil turns}} \times \text{Voltage across one octant } (V_o)$$

$$= \frac{1}{42} V_o$$

This gives 50 V compared with the measured value on Nimrod of 42 V.

(f) General Circuit

The projected system is shown in block form in Fig.4.10.2(vi).

The output stage is a current source capable of driving the necessary current through the correction coils.

Elimination of the effects of the d.c. step, produced in the correction coils by current rise and decay in the main coils, takes place in the output stage. A step voltage substantially the same as that produced in the correction winding must be generated and fed to the output stage and the diagram indicates one way of producing this.

The ripple field is sampled by the search coil and the signal fed through suitable integrating and amplifying stages (the d.c. step removed) and then to the output stage which drives an appropriate bucking current through the correction coils.

(g) Tests on Magnet Model V

Prototypes of the output stage and the servo system have been constructed and measurements carried out on magnet Model V to check the values of current required to buck the ripple field. The ripple field was produced by using an external amplifier. The system operated on a closed servo loop and reduction factors of 17 were obtained for various frequencies of ripple at amplitudes within the designed range.

(h) Tests on the Nimrod Magnet

Using the primary ripple filter as an external source, ripple was fed to the Nimrod magnet and measurements were made to check the calculations of the bucking currents required at various frequencies. At 1000 c/s, 0.420 A were required to buck 30 V of ripple compared with a computed value of 0.5 A. The discrepancy is probably due to the differences between Model V and the Nimrod magnet resulting from the very different lengths, and variation in positions of the coils.

The frequency response of the output stage was investigated using the Nimrod correction coils and the search coils. Further investigations will be required.

(i) Frequencies below 1200 c/s.

Detailed measurements of the ripple on the Nimrod power supplies have shown that considerable ripple is present at frequencies very much lower than those anticipated. Since the current required for bucking is approximately inversely proportional to frequency, it will probably be necessary to redesign the output stage to cope with the extra current requirements.

4.11. Peaking Strips

The peaking strip and associated equipment determines the starting point for the primary frequency generator by giving out a trigger pulse when the field in the magnet gap passes through a pre-set value; it is needed because the starting point of the field in the magnet is variable due to the remanent field.

The principle of the device depends on the fact that only a small field change is required to alter the flux in mu-metal from saturation in one direction to saturation in the other direction. Since this reversal occurs at around zero field, it can be used as a null detector indicating when the magnet field becomes equal to a reference field applied to it in the opposite direction.

The layout is shown in Fig. 4.11(i). The bias solenoid produces a field along its axis in the opposite direction to the magnet field in which it is placed. A small piece of mu-metal wire is supported at the centre and when the rising magnet field equals the solenoid field a flux change occurs in the wire which generates a pulse in the pick-up coil wound on it. The signal to start the primary frequency generator is derived from this pulse.

The bias solenoid has 20,000 turns of 30 s.w.g. enamelled copper wire producing a field of 120 gauss with about 47 mA. The mu-metal wire is $2\frac{1}{2}$ in long by 4 thou. in diameter and the pick-up coil has 3,000 turns of 50 s.w.g. enamelled copper wire. In a field changing at the rate of 10 kG/s the pulse shown in Fig.4.11(ii) is produced.

An overall long term stability in field of 1 part in 10,000 was required. The system is made up of a number of components each of which contributes to the total variation and it is necessary to attempt to reduce each contribution to 1 part in 100,000. The two main parts are the bias current source and the pulse circuitry.

4.11.1. Bias Current Source

Fig.4.11.1(i) shows the basic circuit used to provide a stable current for the bias solenoid. Factors causing variation were:

(a) Series Resistor R

This was made of manganin which has a temperature coefficient of about 1 part in 100,000 per °C. The ambient temperature variation catered for was 18-32°C and it was mounted in an aluminium block thermostatically controlled to 1°C with a contact thermometer.

(b) Reference Potential, e_R

The circuit is shown in Fig.4.11.1(ii). Leading from a stabilised -300V line, two extra stages of stabilisation are provided by zener diodes. The final pair (X3 and X4) have a temperature coefficient of less than 1 part in 100,000 per °C and are also mounted in the thermostatically controlled block.

(c) Noise and Hum

The reference potential is about 10 V so that any noise generated in the

summing resistors should be kept down to $100 \mu V$. Any current flowing through the bias solenoid but not through R, or through R but not through the bias solenoid as a result of stray capacitance causes error. At the minimum bias current of the range (30 mA) the noise current needs to be not more than $0.3 \mu A$ a.c. peak to peak. Mains wiring can feed about $2 \mu A$ a.c. to earth into any unscreened conductors via the stray capacitance so that screening of every part of the solenoid circuit is necessary.

(d) Voltages Induced by the Magnet Field

A voltage proportional to the magnet supply voltage is induced in the bias solenoid. This has a d.c. and an a.c. component, the latter having a fundamental component of about 1200 c/s. At these frequencies the capacitance of the cable connecting the solenoid to the stabiliser and the capacitance of the solenoid itself, bypass the stabiliser. The solenoid is in fact self-resonant at around 8 kc/s but fortunately at 1 kc/s it is sufficiently off the resonance. The effect of the cable capacitance is reduced by backing off the voltage in the solenoid with an identical one placed next to it connected in series opposition.

4.11.2. Pulse Circuitry

A change of 0.6 gauss is needed to drive the mu-metal from saturation to saturation so it is not accurate enough just to use the output pulse without further treatment. Amplitude selection off one edge of the pulse was rejected because the height is proportional to rate of change of magnet field. The pulse is integrated to give an output proportional to flux density in the mu-metal which is directly related to the magnet field. A stable trigger circuit is operated when it reaches a pre-set level.

4.11.3. Mechanical Construction

The magnetic properties of mu-metal are destroyed by any permanent physical deformation and the wire is very thin so the pick-up coil is wound on a thin walled glass capillary tube (o.d. 23 thou.) and the wire threaded down afterwards. The coil is insulated and screened with 1 thou. copper foil and 1 thou. Micalex. The connections are then brought out in a tail of 34 s.w.g. enamelled copper wire and the final o.d. is approximately 130 thou. For protection this rather delicate assembly is cast in a cold setting Araldite to an o.d. of 0.145 in.

The bias solenoid design is limited by power dissipation since heat can be removed only by radiation. For a multi-layer solenoid the dissipation is determined by its dimensions, the field and the specific resistance of copper and is reduced by making the ratio of inner radius to outer radius as small as possible. This has led to using the solenoid without any former at all. The wire is wound onto a former which is removed after the wire has been set in Araldite. The dimensions are shown in Fig.4.11(i). The power is reduced further by placing the peaking strip assembly in the fringe field of the magnet where it operates at half the gap field.

The assembly is situated in the high vacuum region and consequently is covered with metal to reduce outgassing. This is done by electroplating with copper. Unfortunately a continuous metal surface like this constitutes an unpleasant shorted turn which would modify the field locally in an unpredictable way so it is necessary to break up the surface. All the metal has to be earthed to stop it charging up. Both these objects are achieved by etching vertical lines, using

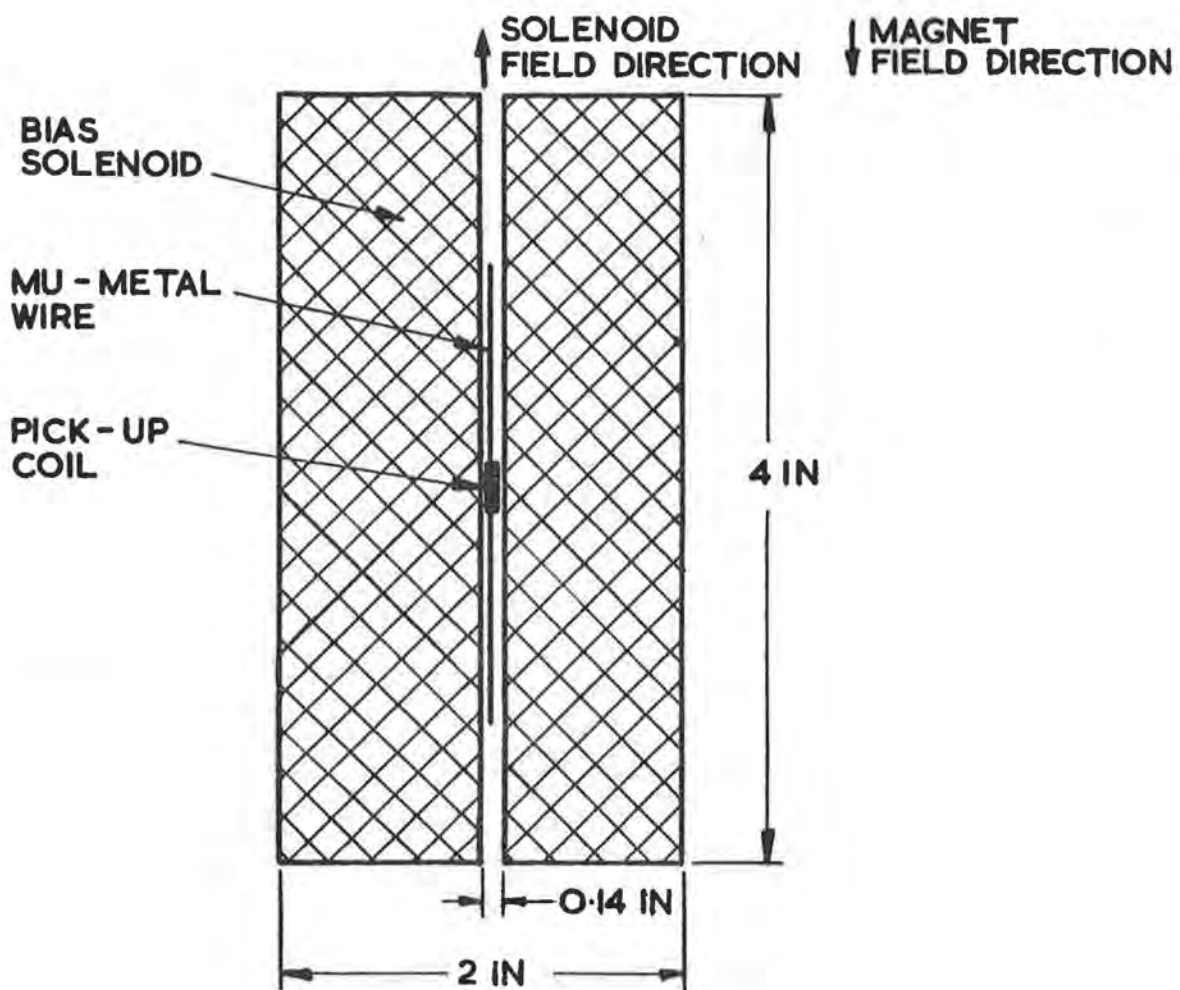


Fig. 4.11(i) Layout of peaking strip.

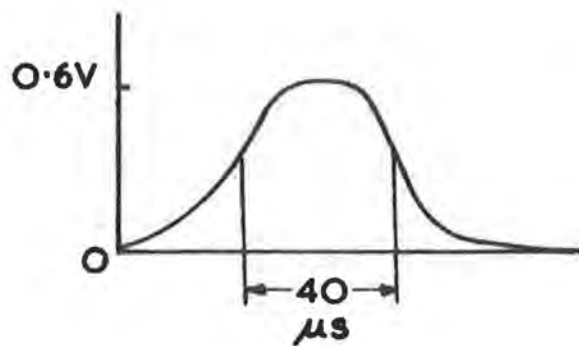


Fig. 4.11(ii) Pulse from peaking strip.

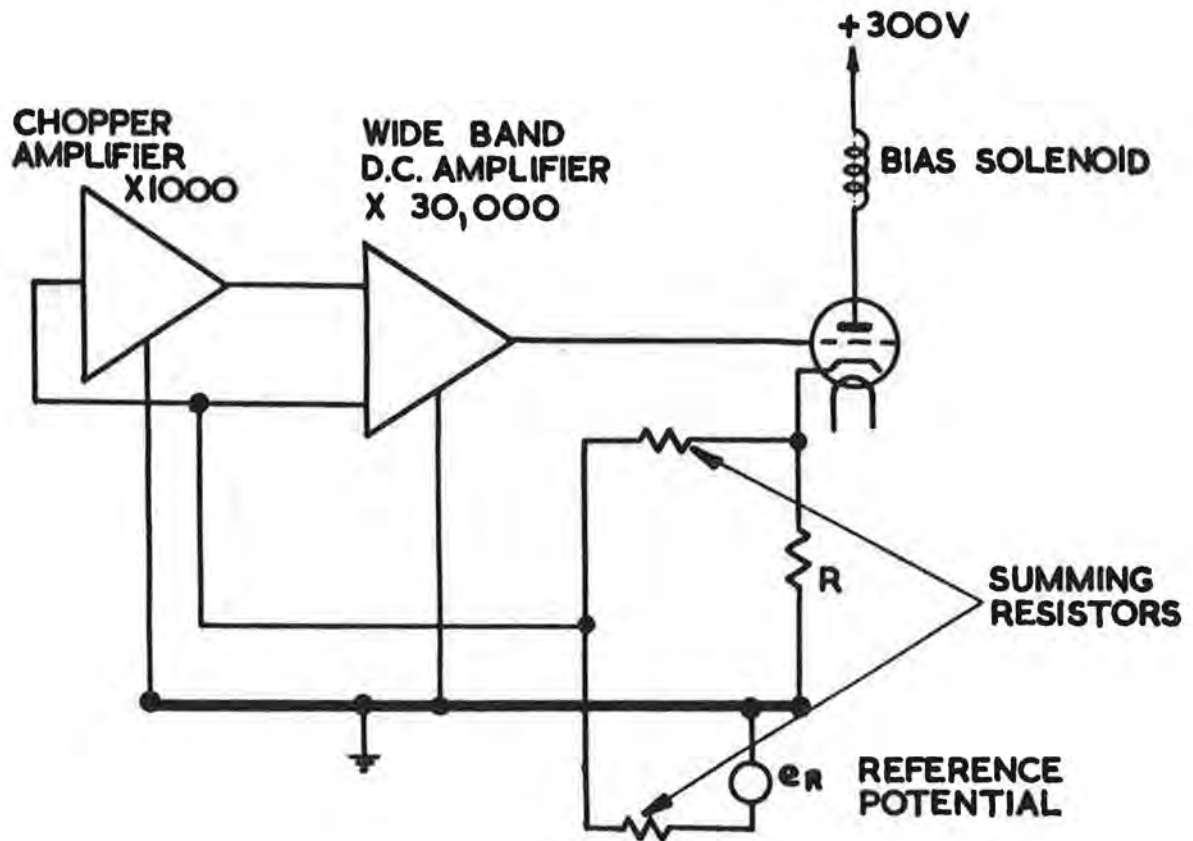


Fig. 4.11.1(i) Basic circuit of current stabiliser for peaking strip

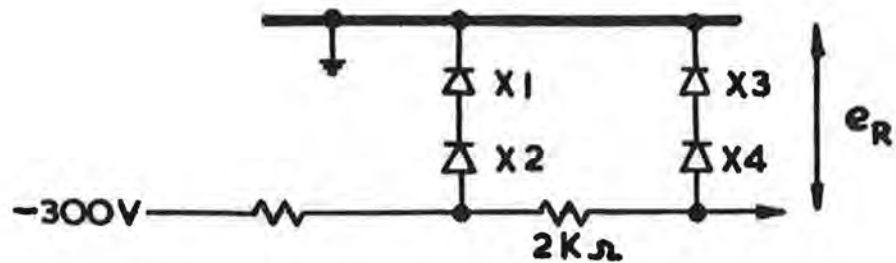
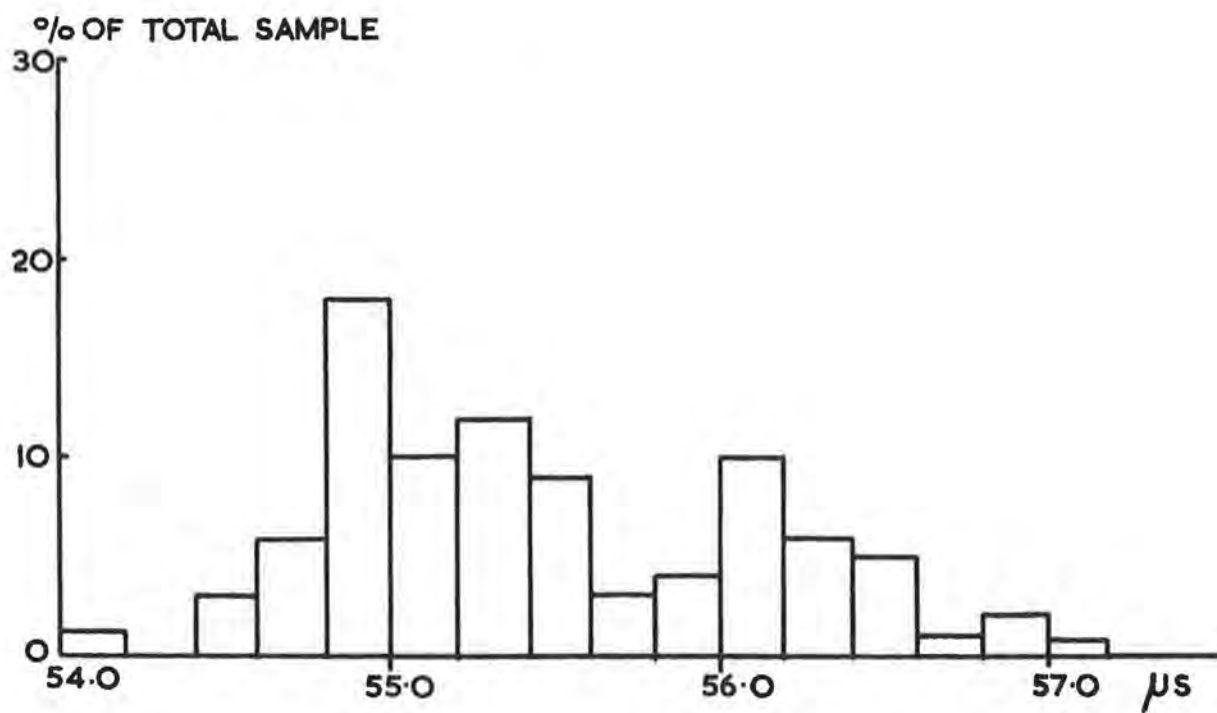
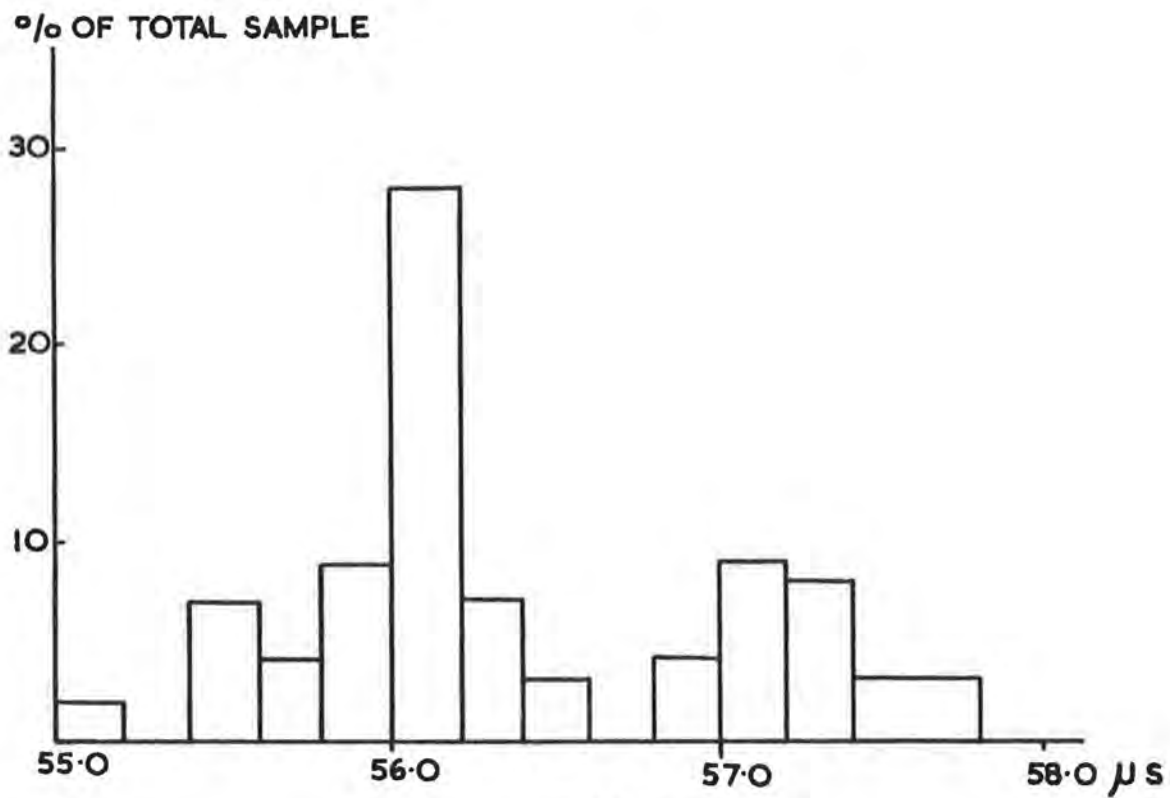


Fig. 4.11.1(ii) Reference potential supply



HISTOGRAM (a)



HISTOGRAM (b)

Fig. 4.11.4(i) Time between two peaking strip pulses.

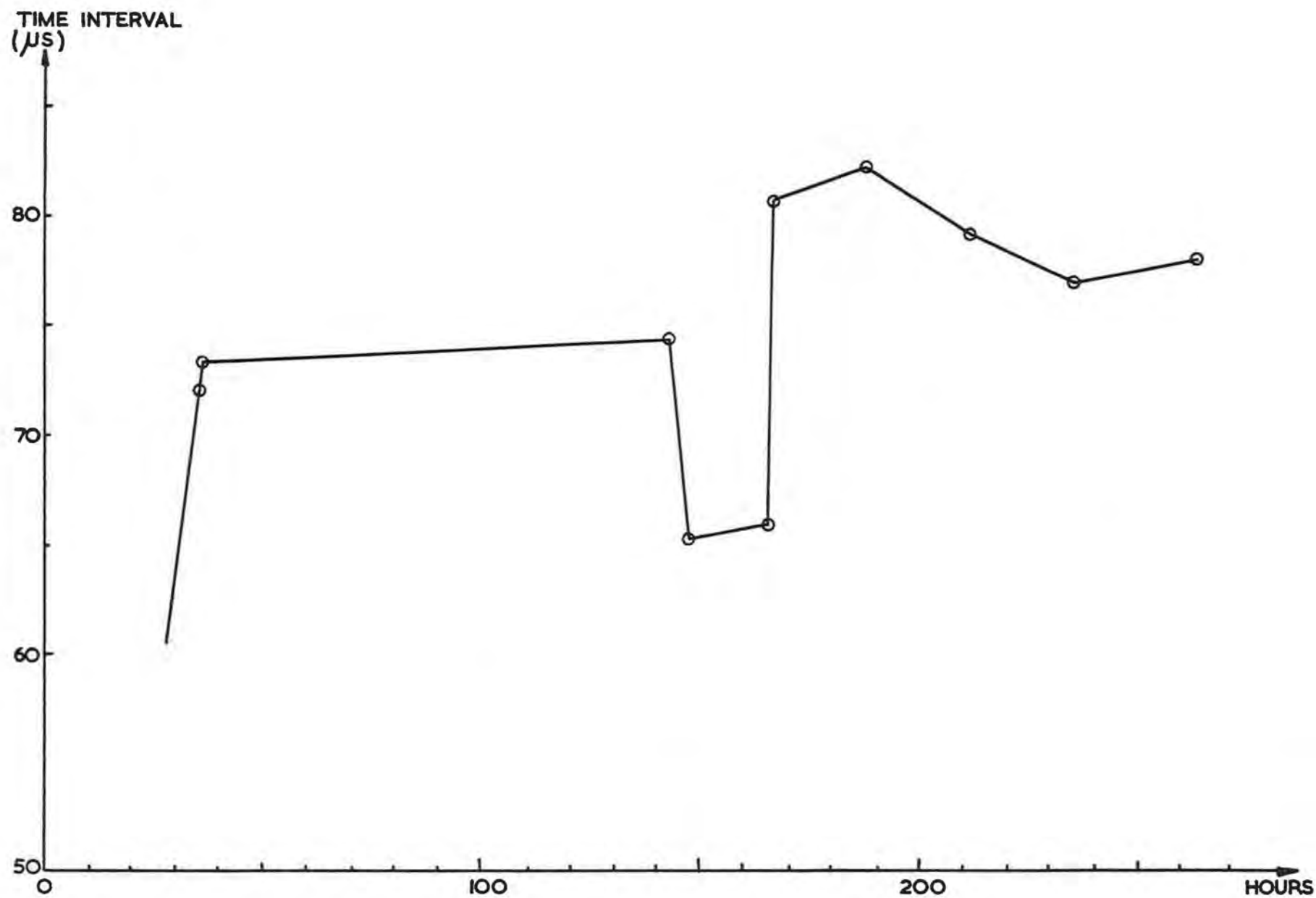


Fig. 4.11.4(ii) Long term drift of peaking strip.

ferric-chloride, joined at the top but not at the bottom.

4.11.4. Progress

It is not easy to prove that one has achieved a stability of 0.01%. Fig.4.11.4(i) shows two histograms of the time intervals between two identical devices. Each histogram is the result of 100 consecutive readings taken over a period of 2 min 20 s. Histogram (b) was taken 7 min after (a) during which the median shifted by $0.6 \mu\text{s}$. Under the conditions of these measurements 0.01% of the peaking strip operating field, 0.024 gauss, was $1.2 \mu\text{s}$; the required tolerance is $\pm 0.01\%$, and two strips were being compared with each other so that readings lying within a band of $4.8 \mu\text{s}$. are acceptable. As can be seen the short term jitter is well within tolerance, being about ± 0.010 gauss per strip. The double peaked structure is probably due to the disturbing factor being roughly sinusoidal with time (the results were taken at regular intervals). Fig.4.11.4(ii) shows the results of some long term measurements, which are less satisfactory. The sudden changes may be accounted for by the fact that commissioning work was being carried out on the power supply at the time and the operating conditions of the magnet were not steady.

As a result of these and other measurements the final design of the equipment has been fixed and at the time of writing one bias current stabiliser unit has been completed with three others still under construction. The pulse amplifier and discriminator unit is being drawn up prior to manufacture.

REFERENCES FOR SECTION 4.

1. J.J. Wilkins and A.J. Egginton. A.E.R.E. GP/R 2181. 1957.
2. P. Bowles. Nuclear Engineering. April 1959.
3. G.W. Dixon and A.G. Entwistle. Nuclear Engineering. April 1959.
4. D.A. Gray et al. NIRL/R/4, 1963.
5. A.J. Holt and J.D. Milne. A.E.R.E. R 3312, 1960.
6. J.J. Wilkins and D.A. Gray. NIRL/R/33, 1963.
7. D.A. Gray, A.H. Spurway and J.J. Wilkins. A.E.R.E. A/R 2626.
8. D.A. Gray, A.H. Spurway and J.J. Wilkins. A.E.R.E. A/R 2845.
9. G. Bronca et al. L'onde Electrique No.387. 463, June 1959.
10. J.J. Wilkins and A.H. Spurway. NIRL/R/6, 1962.
11. A.J. Holt and J.D. Milne. NIRL/R/3, 1961.
12. J.P. Blewett et al. R.S.I. 24, 773, Sept. 1953.
13. P.F. Smith. A.E.R.E. A/R 2849, 1959.
14. J.J. Wilkins. A.E.R.E. R. 1860, 1959.

SECTION 5

MAGNET POWER SUPPLY

5.1. Introduction

The Nimrod magnet power supply plant comprises two 60 MW motor-alternator-flywheel sets which power the magnet via a mercury arc convertor installation of similar rating supplied from the alternators through phase splitting transformers giving 24 phase operation.

This report covers the period up to 31st December, 1962 and does not refer to details of design. These design aspects, with indications of the historical reasons for adopting the final design chosen are given in the following three papers published in Proc. I.E.E., Vol. 110, No. 3, March 1963.

Paper 1 General	}	All three papers have the main title:- 'Magnet Power Supply for the 7 GeV Proton Synchrotron Nimrod'.
Paper 2 Rotating machines		
Paper 3 Mercury arc convertors		

The main power circuit is shown in Fig. 5.1(i).

The first 60 MVA motor-alternator-flywheel set was commissioned for open circuit running conditions during the last two months of 1961 and it was then used to carry out preliminary 'on load' commissioning using each half of the convertor installation in turn, with four of the magnet octants as load, during the first quarter of 1962. From April 1962 until the end of August 1962 one motor-alternator-flywheel set and one half of the convertor plant was used to pulse the magnet (four octants at any one time) in order that the magnetic survey could be carried out.

The second alternator was delivered at the beginning of September 1962. Installation was completed in about six weeks and the second motor alternator flywheel set ran up to speed for the first time on 21st October, 1962.

After further commissioning, and also re-alignment of the first motor-alternator-flywheel set to the recently installed second set, the final fitted bolts and bushes were installed in the flywheel to flywheel coupling and on 21st November, 1962 the complete rotary plant on its common 100 ft long solidly connected shaft system ran up to speed for the first time. On load testing and final commissioning could not be carried out immediately since the magnet was not available. Detailed final commissioning of power supplies was planned for January 1963 using four magnet octants and February 1963 using the whole of the magnet. This period will be covered in the second part of this report.

However, early experience on the plant has shown that when the plant is operating at its full thermal rating, pulse repetition rates will be at least 10% higher than those quoted in the design stages.

The following general operational information may be of interest:

Total running hours from October 1961-31st December, 1962	..	1,600
Total pulsing hours	700
Pulsing hours at standard pulse and/or standard pulse +15%	460

Running hours during magnetic survey period	750
Pulsing hours during magnetic survey period	400
(300 of these hours at standard pulse + 15%)		
Approximate number of pulses during magnetic survey	..	132,000
Approximate number of pulses October 1961-31st December,		
	1962 ..	557,657

During the period September-December 1962 the power plant erection programme had to be phased so that two separate one week duration pulsing periods were available for 'magnet shakedown' purposes. During these 'shakedown' periods the opportunity was also taken to carry out such work as the determination of a variety of maximum repetition rates and ripple content of the magnet voltage. Stress values experienced on the outer vacuum vessel were also measured for the Design Group.

The two shakedown periods were 7th October-12 October, 1962 and 25th November-30th November, 1962. During these two periods the number of magnet pulses produced was about 132,000 and the period 7th October-12th October proved to be the most intensive period of pulsing to have been carried out so far. The statistics applicable to this period are as follows:

Total running hours	69½
Total pulsing hours	58 (50½ of these at standard pulse + 15%)
Total number of pulses	..	74,785 (72,270 of these at standard pulse + 15%)

Power Supplies personnel have been responsible for the operation of the plant and have also worked as a team with the staff of the power supply plant contractors during installation and subsequent early commissioning.

In the following report items of interest relative to the rotary plant and the convertor plant have been mentioned. An effort has been made to avoid repetition of the subject matter contained in the three I.E.E. papers referred to on the previous page. Nevertheless for the sake of completeness a little overlapping has occurred.

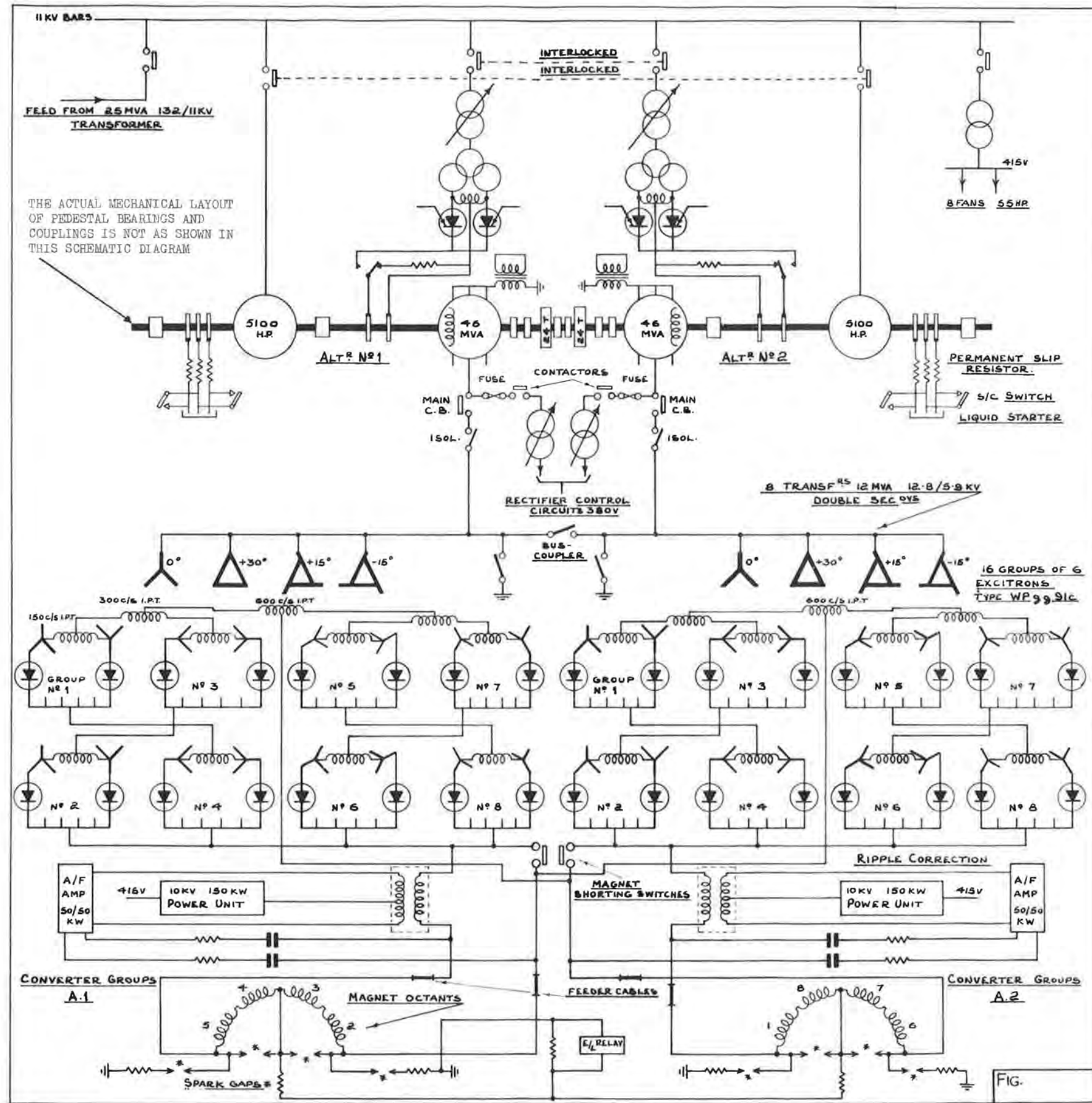


Fig. 5.1(i) Nimrod Power Plant Schematic Diagram.

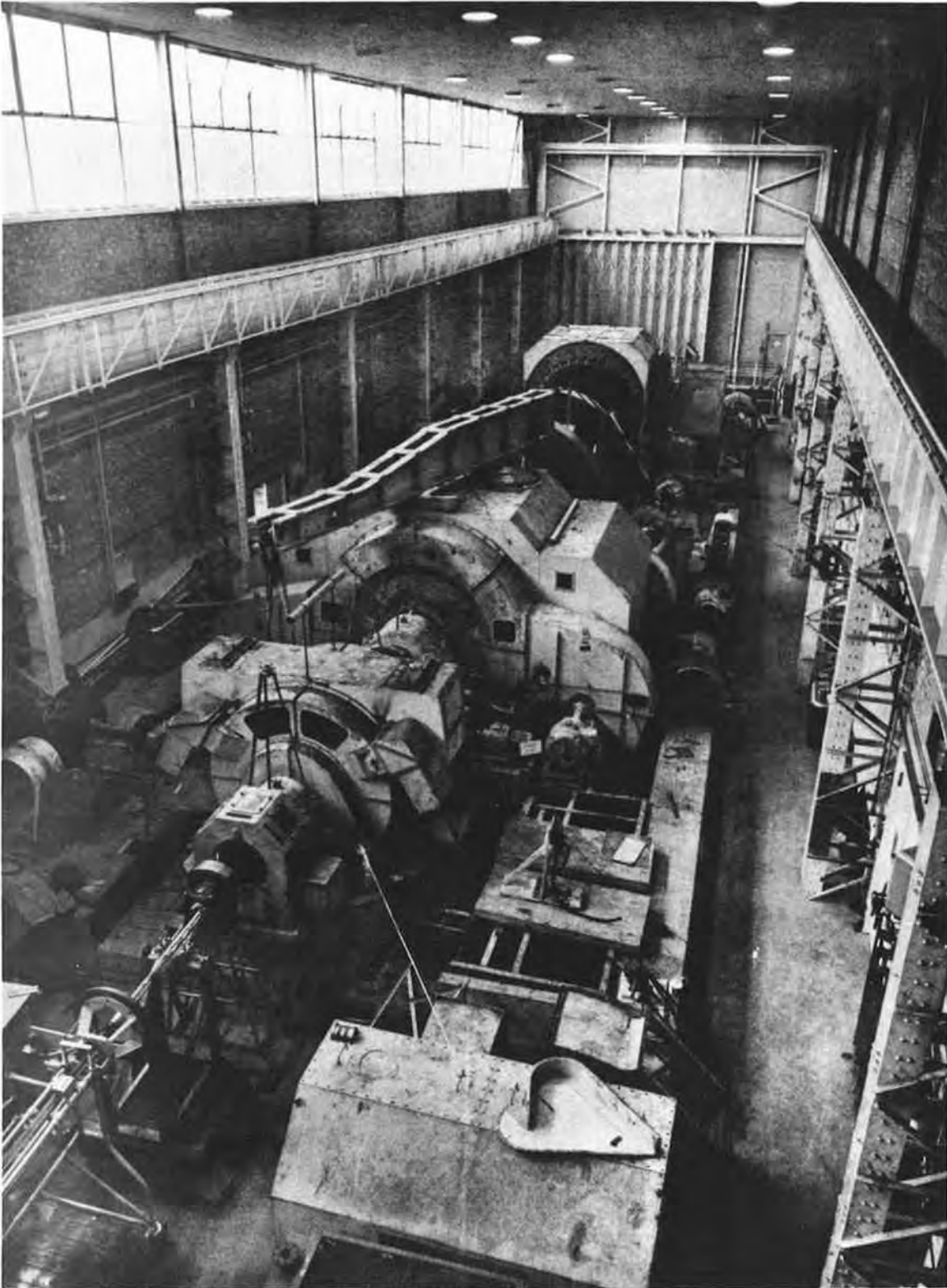


Fig. 5.1 (ii) View of Motor-Alternator-Flywheel Set during final stages of Erection. (Some of the ultrasonic equipment used for checks on the rotor forgings can be seen in the left foreground)

5.2. Rotating Plant

By 31st December, 1962 the whole of the rotating plant and its associated auxiliaries were installed and commissioned, although No. 2 motor-alternator set had only been operated under open circuit conditions.

5.2.1. Brief Note on Commissioning Work Outstanding after 31st December, 1962

There remained, however, a considerable volume of outstanding work to be completed during the first half of 1963. This will be detailed in the second part of this report but for completeness, a brief mention of a few outstanding items still to be carried out is given below:

- (i) Final balancing of the twin motor-alternator-flywheel set.
- (ii) Re-alignment of the set.
- (iii) The grouting in of the complete set.
- (iv) Determination of the behaviour of No. 2 alternator A.V.R. system.
- (v) Shaft torsional oscillation frequencies with differing plant arrangements (e.g., one motor-alternator set with two flywheels) to be determined.
- (vi) Investigation into the behaviour of the complete set feeding the whole of the convertor plant and a complete magnet (eight octants will not be available until February 1963).
- (vii) Extensive flaw monitoring of the plant forgings from the bore by specially developed ultrasonic test equipment.
- (viii) Installation of an emergency lubrication system for the set.
- (ix) Examination of one of the alternator rotors (the original No. 2 rotor). This rotor had not been accepted on an ex-works basis, but had been virtually on loan to allow the magnet survey to be carried out.

5.2.2. The Foundation Block and its Behaviour

Since the rotating plant is rapidly changing from generating to motoring modes of operation with resultant torque reversals, it was decided to mount this plant on a reinforced and post-stressed concrete block. The rotary plant and its foundation block weigh about 1,600 tons and this weight is supported on eighty spring units and twelve viscous damper units. A simplified sketch of the foundation block is shown in Fig. 5.2.2(i).

Distribution of mass and stiffness in the block ensured that the range of natural frequencies of the foundation block is about 21-24 c/s, i.e. well above the frequency of the highest set running speed which is about 16.5 c/s.

The natural frequencies of the spring system are within the range 3 c/s to 4.5 c/s, i.e. well below frequencies associated with machine running speeds but sufficiently above the 2 c/s frequency applicable to the highest pulse repetition rate.

Post tensioning of the foundation block in the longitudinal direction (installed to give a compressive stress of 200 lb/in² in the concrete) was adopted

as an insurance against the possibility of development of transverse cracks in the suspended block since such cracks would tend to lower the block natural frequency and bring it near to machine running frequencies.

The dampers serve to limit block movement during short circuit conditions and they also limit any effects of resonance while the machine is being run up or shut down.

Foundation settlement measurement equipment is installed on the block. Twelve measuring devices known as slave units are installed on the block (five along each side and one at each end). Their respective positions with respect to a master unit mounted at one end of the block can be determined to an accuracy of better than ± 0.001 in.

Having obtained a set of readings it is necessary to apply a suitable method of analysis to these to eliminate:-

- (i) the effect of compression of the supporting springs due to particular loading conditions and
- (ii) tilting of the whole block due to non-uniform loading conditions.

Having eliminated these effects it is possible to see just how much the block profile changes.

Effect of Block Profile Changes on Alignment

Any change in the block profile obviously means an alignment change since the machine bearing pedestals are mounted along the centre line of the foundation block.

Fig. 5.2.2(ii) shows that in as little as twenty-four hours of operation at full thermal loading the block profile can develop an increased 'hogging' characteristic of as much as 0.06 in peak to peak along its entire length. It is expected that this hogging effect can develop to a figure of 0.2 in from the original cold profile condition at which plant alignment takes place.

Reference again to Fig. 5.2.2(ii) shows that over the central 30 ft section of the block where six very critically aligned large bearing pedestals are located, although the two curves show a total peak change of 0.025 in, the relative variation between pedestals over this range is only 0.006 in.

Nevertheless it has proved necessary to misalign the machines when cold in order to achieve improved running conditions. Fig. 5.2.2(iii) shows the results achieved on No.1 motor to alternator coupling on the first occasion that this was attempted. Final alignment is always checked by strain gauge methods. When No. 1 motor to alternator coupling was first made off, the misalignment stress measured at 90° intervals as the coupling was rotated was recorded (Column A in the table). After the machine had been running, a set of readings was taken with the machine hot (Column B in the table). This shows an increase in stress of more than 1000 lb/in^2 . As a result of these observations the drive motor was re-aligned to the alternator during a convenient shut down period but care was taken to ensure that in aligning the two couplings angularly, a gap of 0.002 in was introduced at the bottom. The corresponding strain gauge figures immediately after doing this are recorded in Column C. Note the appreciable tensile stress

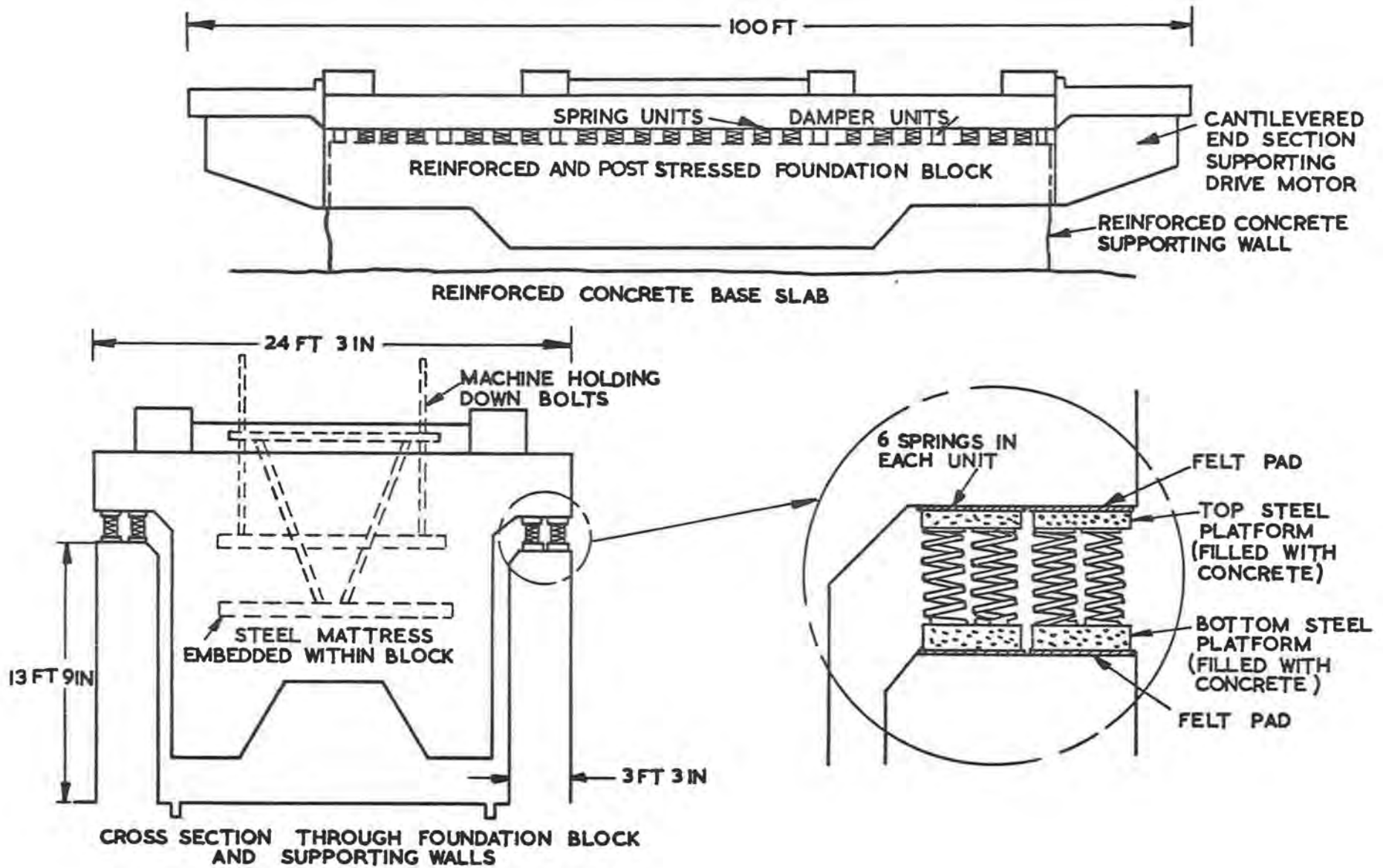
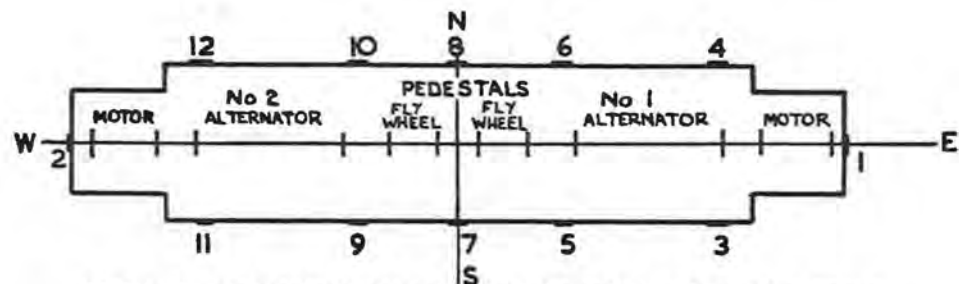


Fig. 5.2.2 (i) Simplified Sketch of Rotating Plant Foundation Arrangement



FOUNDATION BLOCK SHOWING POSITIONS OF SLAVE UNIT AND PEDESTAL BEARINGS SCALE 1IN = 20 FT

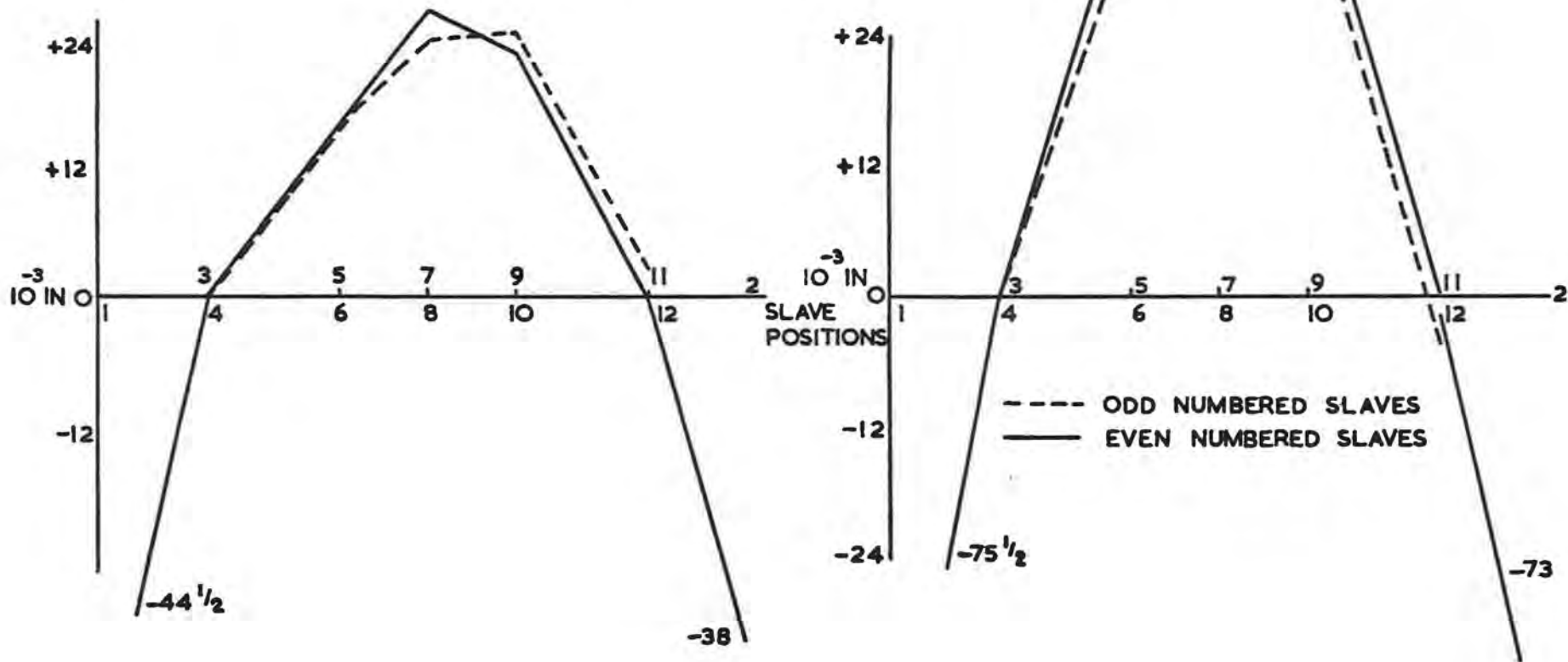


Fig. 5.2.2 (ii) Typical Foundation Block Profile Change in 24 Hours

No 1 MOTOR TO ALTERNATOR COUPLING

COUPLING ROTATION	STRESS (LB/IN ²)			
	COLUMN A (MACHINE COLD)	COLUMN B (MACHINE HOT)	COLUMN C (MACHINE COLD)	COLUMN D (MACHINE HOT)
TOP	0	0	0	0
BOTTOM	-7.5	-1035	+390	-15
SOUTH	+22	-375	+240	-15
NORTH	-15	-480	+45	+7.5

- INDICATES COMPRESSIVE STRESS
+ INDICATES TENSILE STRESS

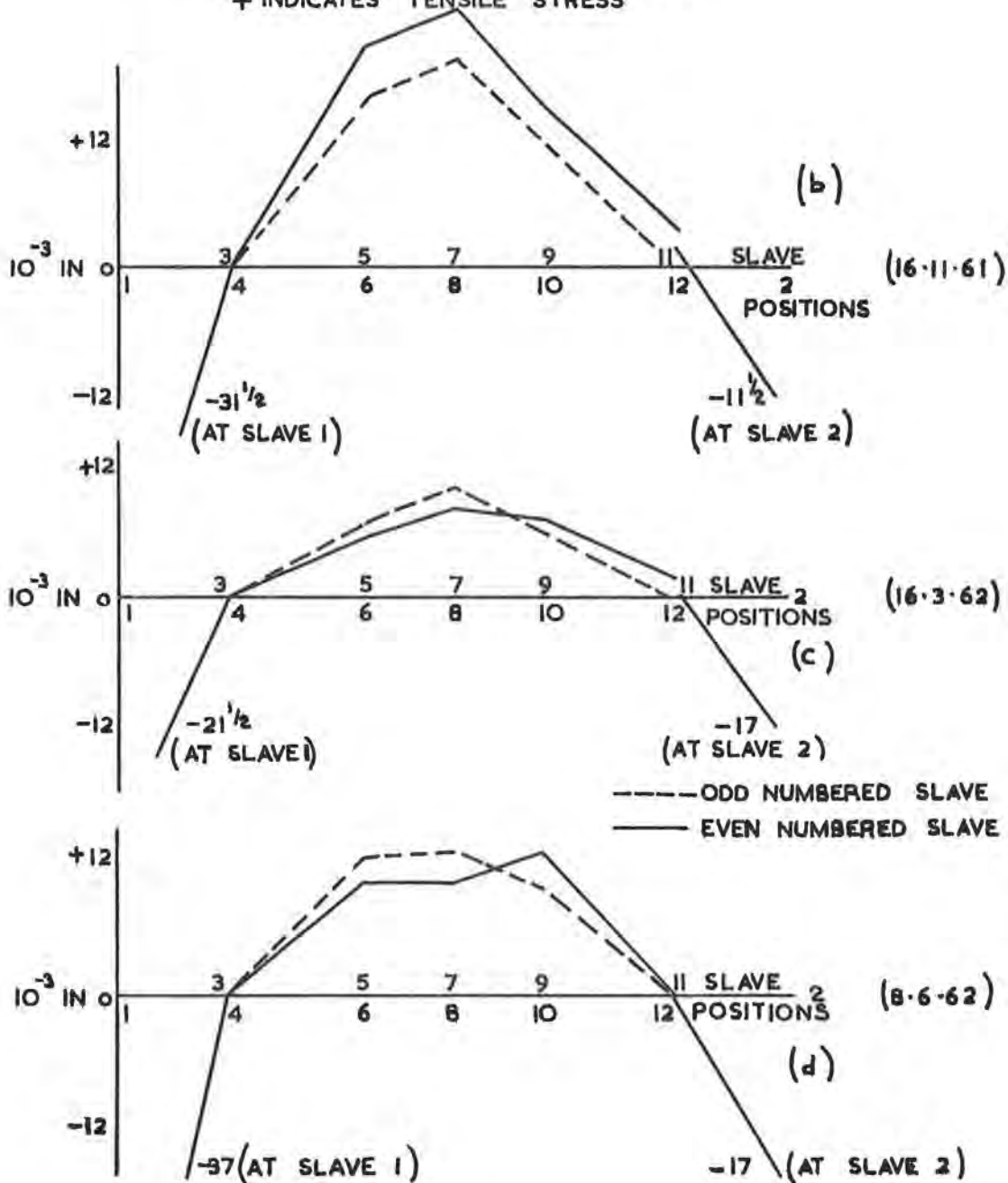


Fig. 5.2.2 (iii) Effect of Deliberate Misalignment between Motor and Alternator

introduced at the bottom of the coupling, and the appreciable degree of deliberate misalignment compared with Column A figures. Column D shows the result of an alignment check at the motor to alternator coupling with the machine hot, the indication being that the movement of the foundation block towards an increasingly hogging profile (see graphs (c) & (d) in Fig. 5.2.2(iii), had cancelled out the bending stress initially deliberately introduced to give negligible misalignment stresses with the machine hot (a reduction from 1035 lb/in² down to 15 lb/in²). The corresponding foundation block profiles corresponding to the readings tabulated at B, C & D are shown in graphs (b), (c) and (d) respectively.

5.2.3. Bearing Pedestal Vibration Levels

No. 1 motor drive and bearing pedestal developed about 0.003 in peak to peak vibration before the re-alignment to which reference has just been made. This was reduced after re-alignment to 0.001 in and so far it has proved practicable to keep vibration levels down at all bearing pedestals to less than 0.001 in peak to peak.

5.2.4. Machine Bearings

Bearing temperatures are indicated in the power supplies control room and the white metal temperature does not normally exceed 65°C. During commissioning and early running one bearing has been changed because of blistering of the white metal. The bonding of the white metal to the shell has been checked ultrasonically on all bearings. Differential pressure switches across orifice plates in the oil supply pipes to the bearings, operate to trip the set if the rate of oil flow to any bearing falls too much.

5.2.5. Shaft Eccentricity Levels

Eccentricity of the shaft system is measured in the immediate vicinity of each alternator bearing pedestal and these four eccentricity values are fed to a four channel recorder. Levels of eccentricity are normally of the order of 0.001 in peak value although, on occasions, levels approaching 0.003 in have been recorded.

5.2.6. Shaft Torsional Stress Monitoring System

On each alternator a pair of phonic wheels each having 540 teeth are mounted on the alternator shaft at positions as indicated in Fig. 5.2.6(i). These phonic wheels, in conjunction with magnetic pick ups, give, by phase comparison of the output from the pick ups, a direct measure of shaft twist. The output from the pick ups is fed to a transistorised phase meter which in turn operates transistorised alarm and/or trip relays whenever the appropriate level of torsional stress is reached.

At present the alarm and trip settings are as follows:-

Alarm Setting (1.5 per unit torque) = 0.0784° mech. = 42.6° elec.

Trip Setting (3.0 per unit torque) = 0.1569° mech. = 85.2° elec.

This equipment has operated quite satisfactorily during the commissioning and early operational stages, but the phonic wheels are to be replaced with wheels having teeth even more accurately machined in order to reduce the noise level further.

Fig. 5.2.6(i) shows not only the location of the phonic wheels but illustrates generally the monitoring of the shaft system. Fig. 5.2.6(ii) shows the behaviour of the shaft system at Stations A & B (see position 4 in Fig. 5.2.6(i)) monitored by the strain gauges installed at these locations. The flat top timer has incorporated in it a 1000 c/s crystal controlled oscillator, so that flat top times can be adjusted to be an odd number of half cycles of shaft torsional frequency to prevent possible build up of excessive shaft torsional stress.

5.2.7. Starting and Pre-heating of the Set

The complete set is equipped with four oil jacking pumps so that oil at 1000 lb/in² is introduced at the bottom of each bearing so that the shafts are lifted on a film of oil to ease starting conditions and to help avoid possible bearing damage. The selected main oil flood pump, capable of delivering 325 gal/min at a discharge pressure of 50 lb/in² has to be started before switching on the jacking oil system. After starting up the main flood pump and the jacking pumps the barring gear can be engaged to rotate the set at $1\frac{2}{3}$ rev/min.

The main lubrication oil tank is fitted with 30 kW of heating. In addition about 30 kW of heating is installed in each alternator stator frame. The lubricating oil is raised to a temperature of 40°C so that as the set is barring, the shaft temperature can be lifted to a minimum of 30°C before arduous pulsing commences. Stator heating can be used to assist in this process.

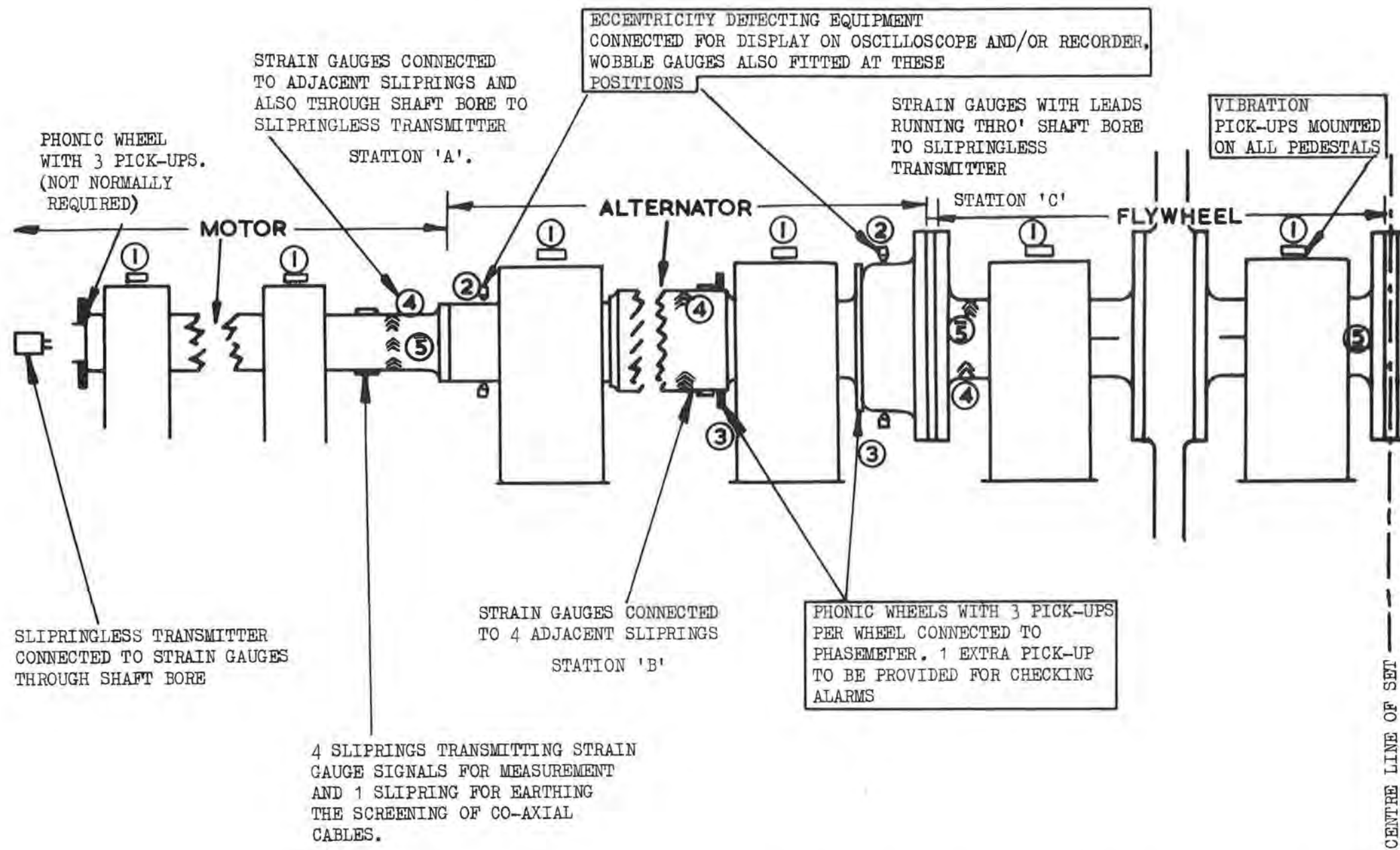
(a) Reason for Pre-heating

This pre-heating is carried out to ensure maximum security of the shaft system by ensuring that the transition temperature of the steel is reached or exceeded before appreciable pulsing stresses are set up. It seemed advisable to do this, particularly since extensive investigation on the Bevatron power supply had shown that it was prudent to pre-heat the Bevatron flywheel shafts to a point at which Charpy-Izod tests indicated satisfactory energy absorption levels. (2).

(b) Transition Temperatures of Chrome Molybdenum and Low Nickel Vanadium Steels

It is true to say that varying opinions are held on the subject of brittle fracture and machine failures. Nevertheless large rotors have burst and such failures have caused attention to be directed to the brittle behaviour of alloy steel forgings. It was found that if the notch toughness of the steel is evaluated over a range of temperatures by means of the Charpy-Izod impact test it becomes evident that the energy required to fracture test specimens decreases rapidly with decreasing temperature. This can be readily seen from the curves shown in Fig. 5.2.7(i) which are applicable to the steels used in Nimrod power plant forgings. If a line is drawn at, say, 15 ft lb and if the mean of the spread of results is taken for the two steels, it can be seen that the temperature corresponding to 15 ft lb fracture energy is about 20°C for the low nickel vanadium (LNV) steel and -2°C for the chrome molybdenum steel. Above these temperatures the steels will behave in an increasingly ductile way and below these temperatures in an increasingly brittle way. The temperature at which a steel specimen absorbs 15 ft lb of energy during fracture is called the transition temperature.

Again sudden failures due to extremely rapid crack propagation, will only occur if there is a sufficiently severe stress concentrator to act as a point of



- ① VIBRATION PICK UPS ON EVERY PEDESTAL (PERMANENT EQUIPMENT)
- ② SHAFT ECCENTRICITY DETECTION POINTS (PERMANENT EQUIPMENT)
- ③ TORSIONAL STRESS MONITORING (PERMANENT EQUIPMENT)
- ④ STRAIN GAUGES USED FOR COMMISSIONING TESTS (TEMPORARY)
- ⑤ LINEAR STRAIN GAUGES USED FOR MACHINE ALIGNMENT CHECKS (SEMI-PERMANENT)

Fig. 5.2.6(i) Monitoring of the Shaft System.

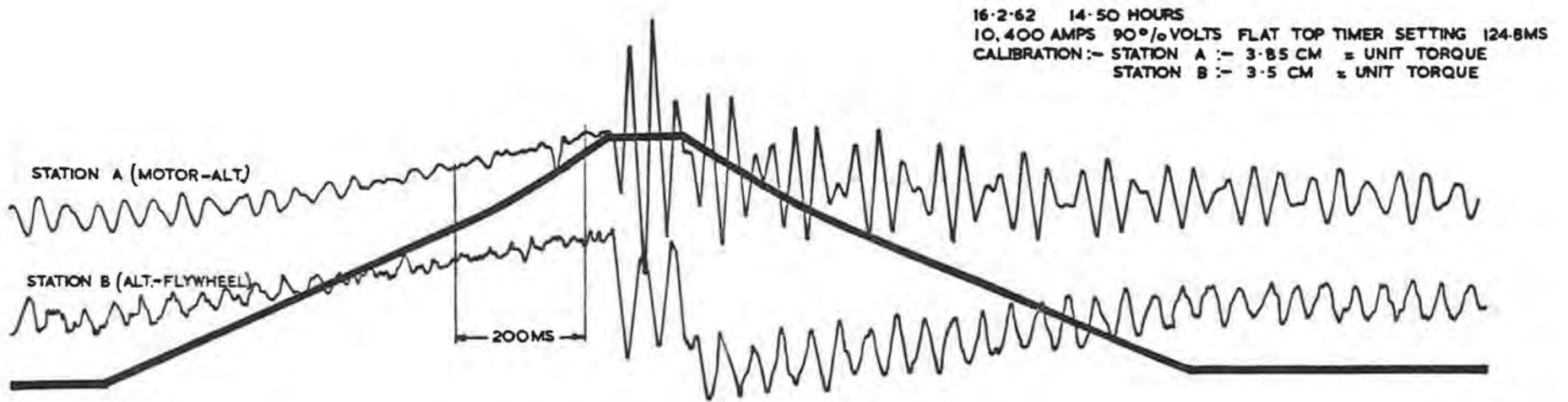


Fig. 5 - 2.6 (ii) Behaviour of the Shaft System

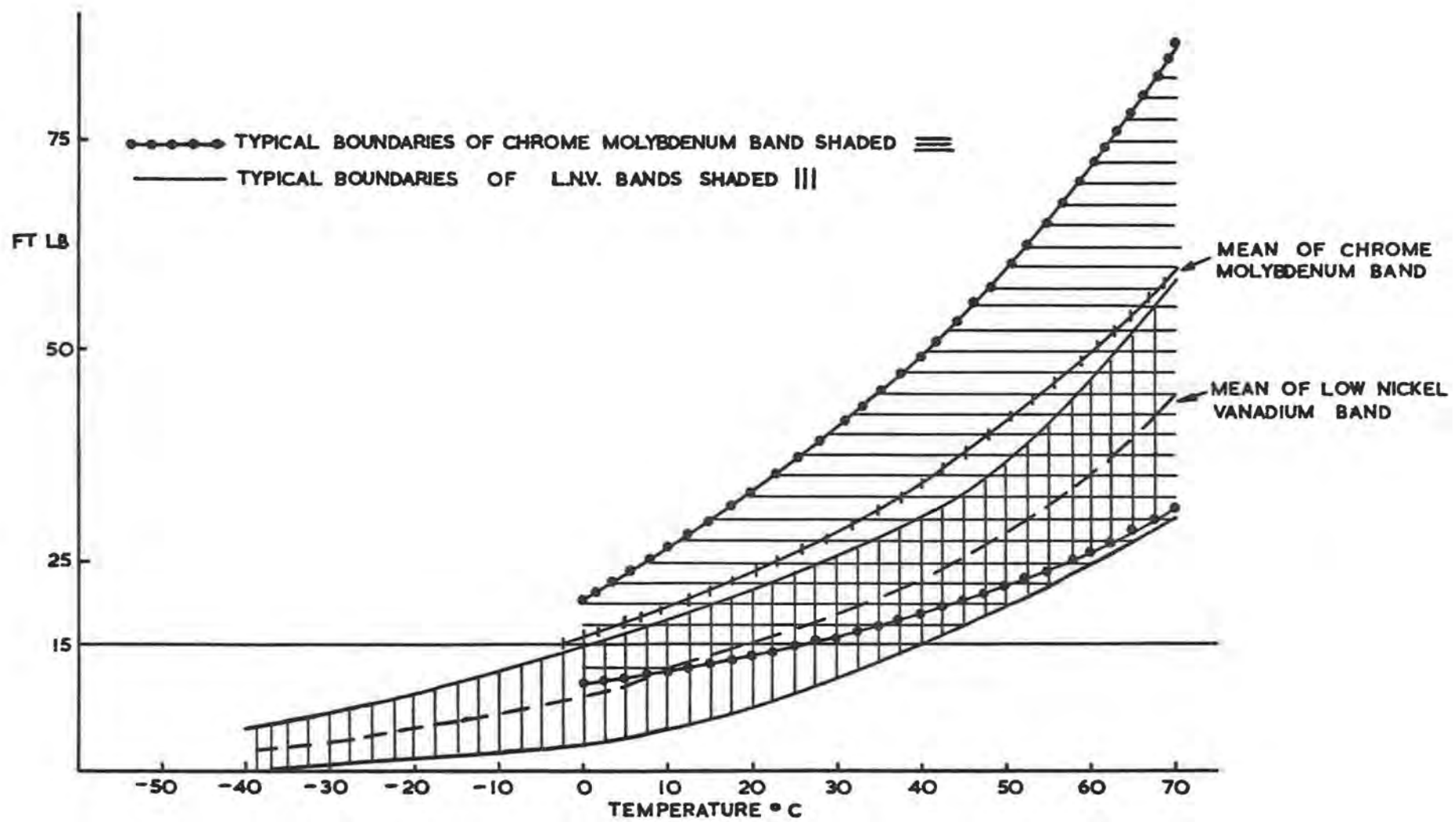


Fig. 5.2.7 (i) Charpy - Izod Tests on Forging Steels

origin. However it is not practicable, even in very high quality forgings, to be certain that no flaws whatever are present. Where failures have occurred, most have taken place when the steel temperature has been below the transition temperature.

One of the difficulties in the determination of the transition temperature is the wide spread of results obtained from specimens taken from various parts of the same forging. Fig. 5.2.7(i) shows the spread of results for the alternator LNV rotor forgings and the chrome molybdenum motor forgings. The flywheel half shafts are also made from chrome molybdenum steel. It can be seen from Fig. 5.2.7(i) that in our case, from a transition temperature viewpoint, the alternator forgings are more of a problem than the motor or flywheel shafts. If the mean curve of the LNV spread of results is taken, a figure of 15 ft lb is not achieved until a temperature of 20°C is reached. It seems prudent therefore to pre-heat to at least 30°C.

In practice this temperature is achieved by alternator and lubricating oil heating as far as is practicable, followed by a pulsing programme specifically suited to mercury arc convertor ageing requirements. Since this mercury arc convertor ageing programme is carried out with long flat top times (typically 8 s) at a magnet current of 5 kA and only 30% of peak voltage, the shaft torque levels are low so that this duty can be carried out not only to effect the necessary convertor plant ageing, but also to assist in raising machine and shaft temperatures. This does mean, however, that the power supplies and the magnet load have to be available for 2 hours before normal pulsing is required. At the end of the pulsing programme 20 min are required to bring the set to rest with the brakes fully on after which the set is barred for a further hour or so, so that the rotors cool down evenly and possibilities of shaft bending are avoided. Power supplies plant has therefore to be operational for approximately 3½ hours in excess of the pulsing period required.

5.2.8. Lubrication Oil System

A certain amount of difficulty has been experienced with air entrainment in the oil system with resultant difficulties of pump priming. This could be particularly serious in the event of a pump failure or a site electrical failure since the stand by pump which should automatically cut in, could fail to build up pressure. A temporary continuous bleed system was installed to greatly reduce the likelihood of failure. In 1963 modifications will be carried out to the existing pipework and in addition to this an emergency gravity fed system will be installed. The head of oil available may not be sufficient to prevent some bearing wipe but should be sufficient to avoid serious damage to the journal and bearing system.

5.2.9. Routine Intrascope Inspections

The alternator poles are 115 in long. The laminations are clamped between 5 in thick steel end plates and the poles are keyed to the rotor body as shown in Fig. 5.2.9(i). During the early life of the set intrascope inspections were carried out at locations X and Y (Fig. 5.2.9(i)) in order to ascertain whether changes were occurring in this region. It was possible to ascertain, for example, whether any gaps between laminations (or between laminations and end plates) had changed, whether there appeared to be any significant key movement, etc. All changes observed have been recorded and the changes noted so far do not give cause for undue concern.

5.2.10. Flywheels

Tests have been carried out to determine the temperature rise of the flywheel when either the eddy current braking system or the mechanical band braking system is applied. The rise in rim temperature is somewhat similar in the two cases and temperatures of up to 140°C at the rim are reached. The running temperature of the flywheel is normally not less than about 60°C , thus the temperature rise does not exceed 80°C . It is important that this rise should not be significantly exceeded otherwise the compressive stress in the rim approaches the yield point of the steel very closely. For this reason eddy current braking and mechanical braking cannot be used simultaneously for a more rapid shut down. Furthermore one mechanical brake or one eddy current brake must not be used to stop the complete twin set.

An ultrasonic survey has been carried out on both flywheels and it was found that in the case of No. 1 flywheel there were 132 significant defect echoes distributed in about a 270° arc of the flywheel disc whereas No. 2 flywheel had only about 28 flaws distributed within about a 90° arc. It would appear that No. 1 flywheel disc is peppered with slag inclusions. It is reasonable that the two flywheel discs should not give similar results when ultrasonically scanned, since they were separately made and not from the same melt.

The flywheels will be ultrasonically scanned at intervals to try to ensure that no significant change occurs in the known flaw patterns. It must be emphasised that these remarks apply only to the flywheel discs which are made from quite an ordinary steel having a minimum yield point of 20 ton/in^2 .

The chemical composition is:-

Carbon	0.28/0.34%	Silicon	0.1/0.3%
Manganese	0.8/1.1%	Sulphur and Phosphorous	0.05%

The half shafts are made from a chrome molybdenum steel having a minimum yield point of 40 ton/in^2 . The chemical composition is:-

Carbon	0.25-0.35%	Chromium	2.5-3.5%
Silicon	0.1-0.35%	Molybdenum	0.3-0.7%
Manganese	0.65% max.	Sulphur	0.05% max.
Nickel	0.4% max.	Phosphorous	0.05% max.

These half shafts will also be scanned ultrasonically at bearing journal locations during the final commissioning stages in 1963 (see section 5.2.13 on ultrasonics).

5.2.11 Alternator Automatic Voltage Regulation System

Fig.5.2.11(i) shows a block schematic of this system. The basic reference voltage is generated by reference neons fed from a stabilised supply. The output of the reference circuit is fed to a potential divider chain so that any selected value in the range 20% to 100% can be obtained to within a fraction of 1%. The transient voltage characteristic of the alternator is curved and if the excitation is controlled to follow a similarly shaped characteristic, the A.V.R. duty is less arduous and therefore more accurate than would be the case if the excitation followed a linear characteristic. This shaped characteristic is

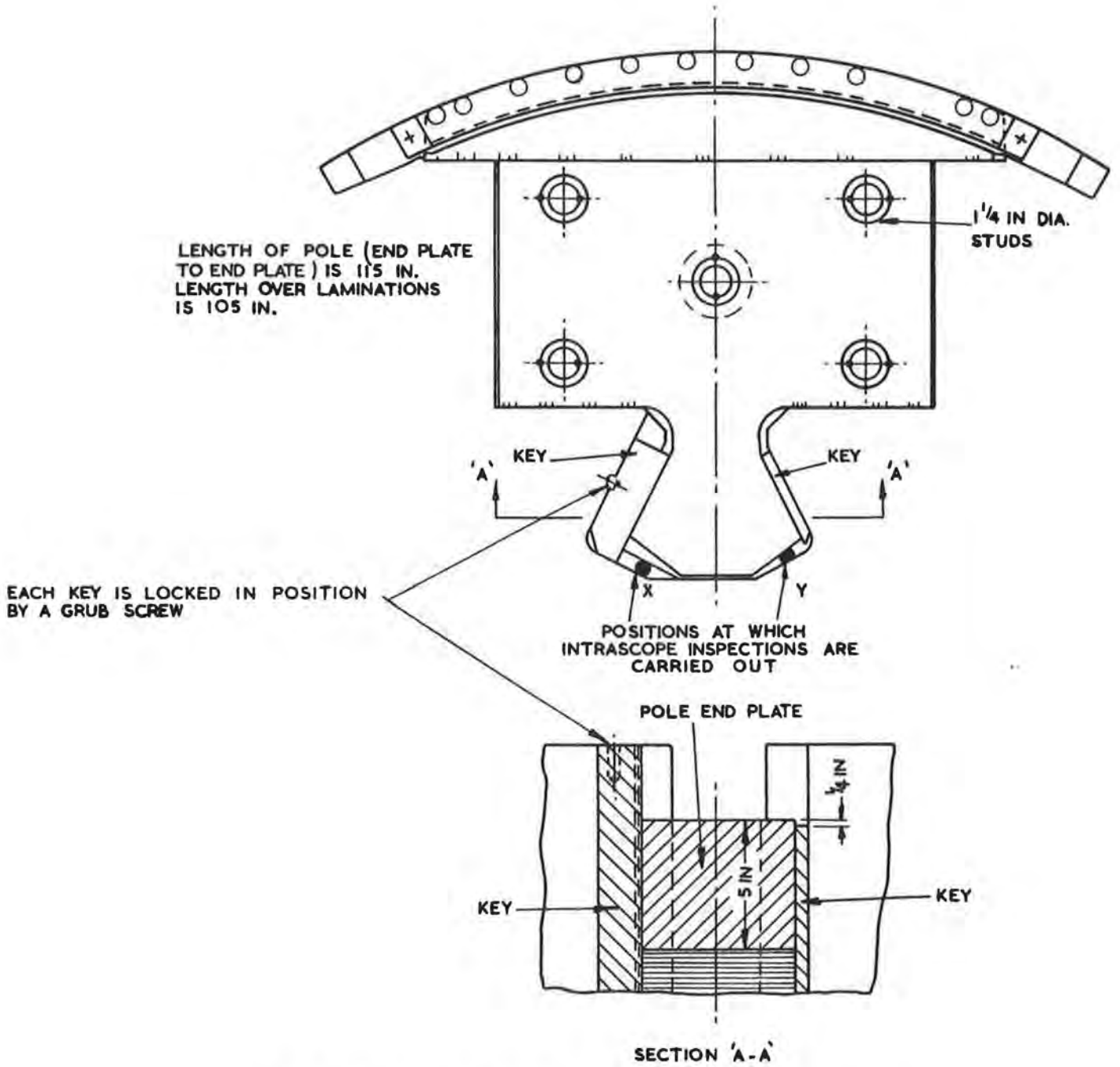


Fig. 5 - 2.9 (i) Pole/Rotor Dovetail Assembly

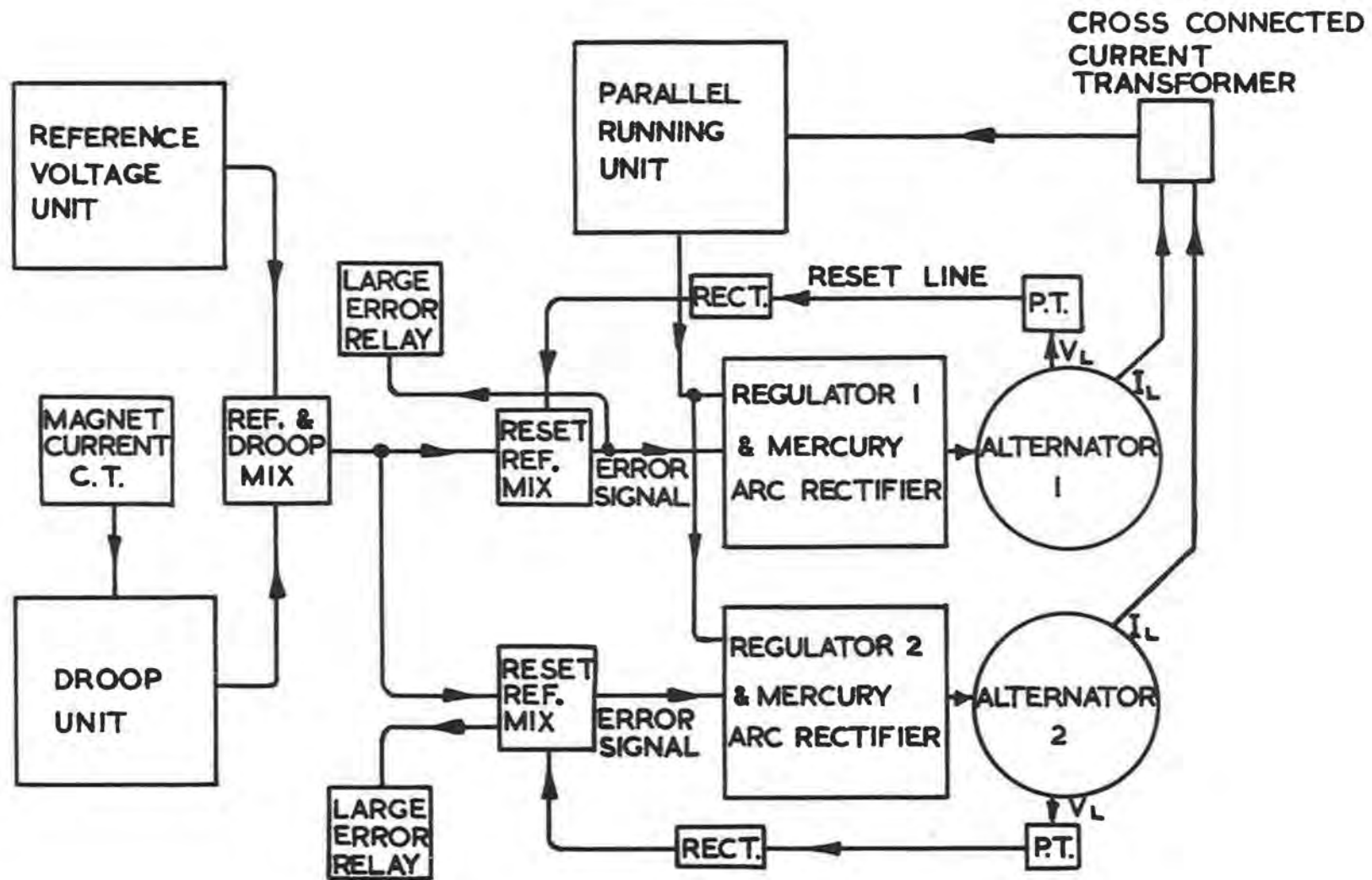


Fig. 5.2.11 (i) Block Schematic Diagram of A. V. R. System

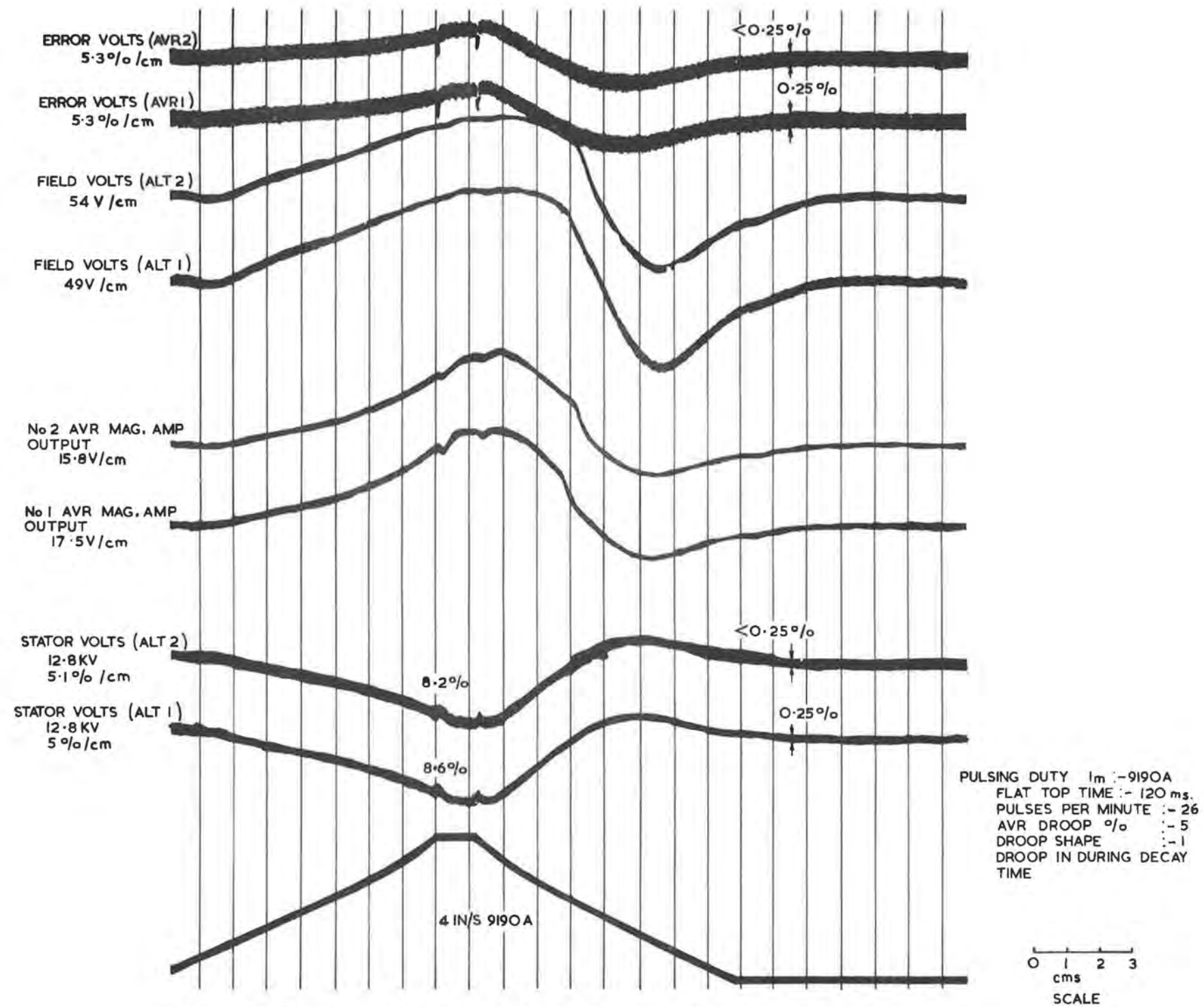


Fig. 5.2.11(ii) Aspects of A. V. R. Performance (Beginning of 12 hour run).

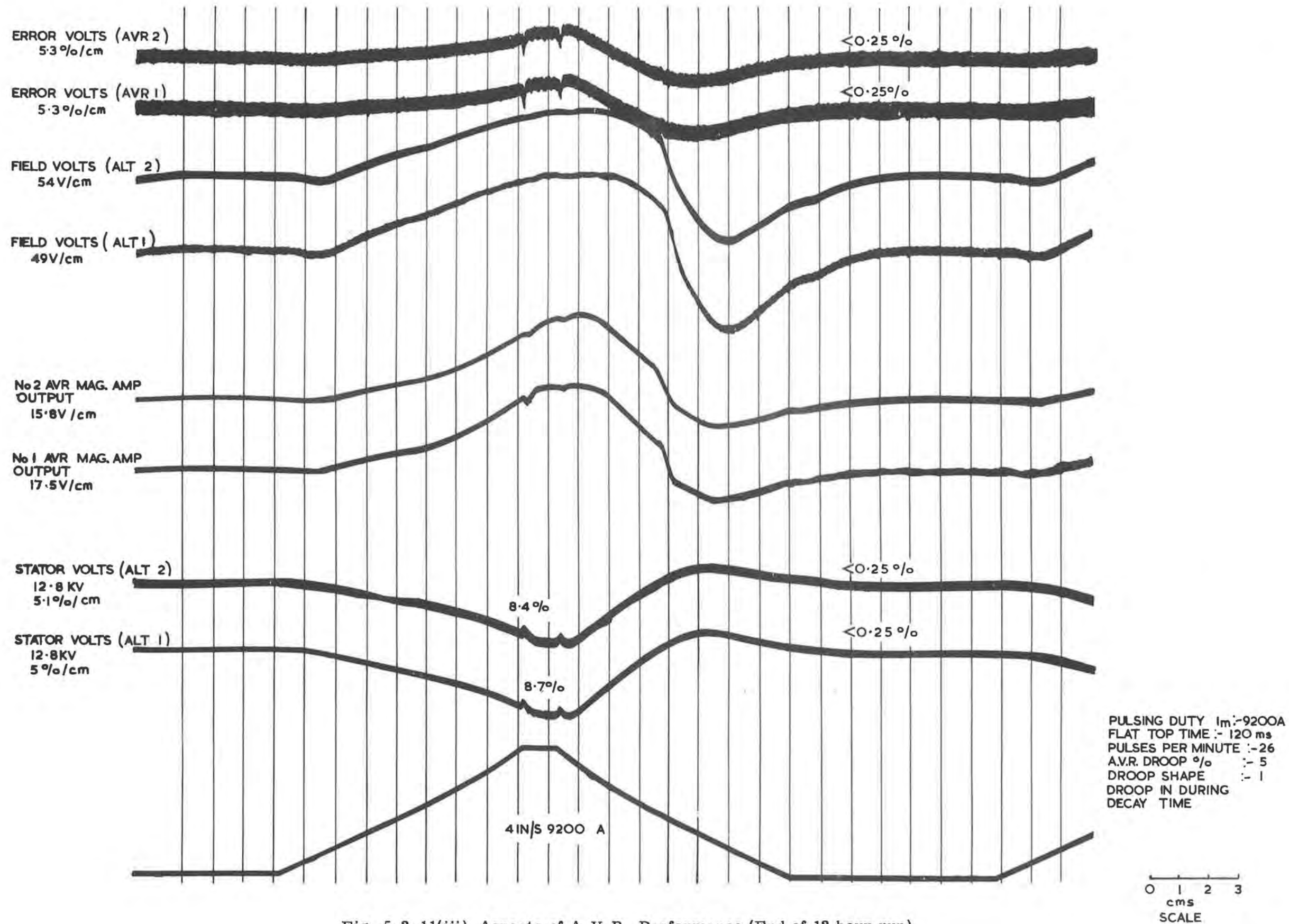


Fig. 5.2.11(iii) Aspects of A. V. R. Performance (End of 12 hour run).

achieved by the use of the droop unit which provides a controlling voltage (which is a non-linear function of the magnet current) to modify the reference voltage.

The alternator voltage transformer (12.8 kV/180 V) output is rectified, to produce a voltage proportional to the average of the three line voltages, and fed back to be compared with the combined outputs of the reference and droop circuits. The resultant error is applied to the regulator magnetic amplifier, which in turn controls the grid control unit supplying the grid impulses to the mercury arc excitation rectifiers.

Should the alternators ever run in parallel, a circulating current will flow between them if their excitations are unequal so a pair of cross connected current transformers are used to measure this current. Their outputs are fed to a phase sensitive rectifying circuit to produce a direct voltage proportional to the circulating current and of polarity dependent on the phase of the current. The voltage so produced is fed in opposing senses to each regulator amplifier to correct the excitation of the alternators.

An essential requirement of A.V.R. performance is that pulse to pulse repeatability must be maintained and one of the closest tolerances specified was that the alternator voltage should have recovered to within $\pm 0.25\%$ of 12.8 kV within 0.2 s of the end of the decay period.

Figs. 5.2.11(ii) and 5.2.11(iii) show traces of (a) error volts AVR1 and AVR2, (b) magnetic amplifier outputs AVR1 and AVR2, (c) field volts alternator 1 and alternator 2, (d) stator volts alternator 1 and alternator 2 under standard pulse conditions both at the beginning and end of a twelve hour pulsing period. The close similarity of the stator voltage traces may be noted; similarly, error volts have remained virtually the same over this period. On both alternator voltage traces, the voltage has recovered to within $\pm 0.25\%$ of 12.8 kV within 0.2 s of the end of the decay period.

5.2.12. Brief notes on General Routine Commissioning

In this report certain items which it is hoped will be of general interest have been mentioned. Much time was inevitably spent in the period under review in carrying out routine work associated with plant of this nature. The following list is by no means complete but serves as an example of such work:-

- (i) Primary and/or secondary injection testing of all plant protection.
- (ii) Checking the extensive sequence interlocking system on the plant - also the complete alarm and tripping system.
Fig. 5.2.12(i) lists the main protective devices on the plant together with the switches, etc., with which they are associated.
- (iii) Electrical pressure testing of plant and cables.
- (iv) Phasing out of transformers.
- (v) Setting up and adjusting switchgear and ensuring that closing and tripping performances are in accordance with those laid down in B.S.S.
- (vi) Commissioning tests on all auxiliaries: e.g., motors, cyclic resistors, liquid controllers, batteries, oil purifiers, etc.
- (vii) Checking excitation and ignition circuits of the excitation rectifiers, grid-anode phasing, etc.

- (viii) Dry out runs on alternators and static dry out procedures on the motors.
- (ix) Pressure testing of oil and water circuits and the calibration of orifice plates in these circuits.

5.2.13. Ultrasonic Scanning of the Rotary Plant

Reference has been made in sections 5.2.4 and 5.2.10 to flaw detection by ultrasonic methods on the flywheel discs, and the checking of the bonding between the white metal and the steel shell of machine bearings. Conventional ultrasonic test equipment is, of course, freely available to carry out such examinations and also examinations from the exterior surface of bearing journal locations. It was by this means that the East generator shaft of the Bevatron magnet power supply was found to have serious flaw patterns in the vicinity of a bearing journal. Flaws were also found on the West generator shaft but these were not so serious. However in a Bevatron Engineering Note (3) a comment is made that in the case of the East generator shaft the ultrasonic observations were sufficient to reject the shaft on current inspection standards for installation in new equipment. Ultrasonic survey programmes were set up on a three shift basis for both machines.

In the case of the Nimrod machines, the locations at which ultrasonic examination can be carried out is limited to the bearing journal positions. In the case of the alternators this amounts to about 13% of the shaft length.

However, the Nimrod motor-alternator-flywheel set has central boreholes throughout the shaft system. In the 14 ft 6 in long motor rotor forging the borehole is $2\frac{3}{4}$ in dia., in the 25 ft long alternator rotor forging it is $4\frac{1}{2}$ in dia. and in the 4 ft 6 in long flywheel half shaft it is also $4\frac{1}{2}$ in dia.

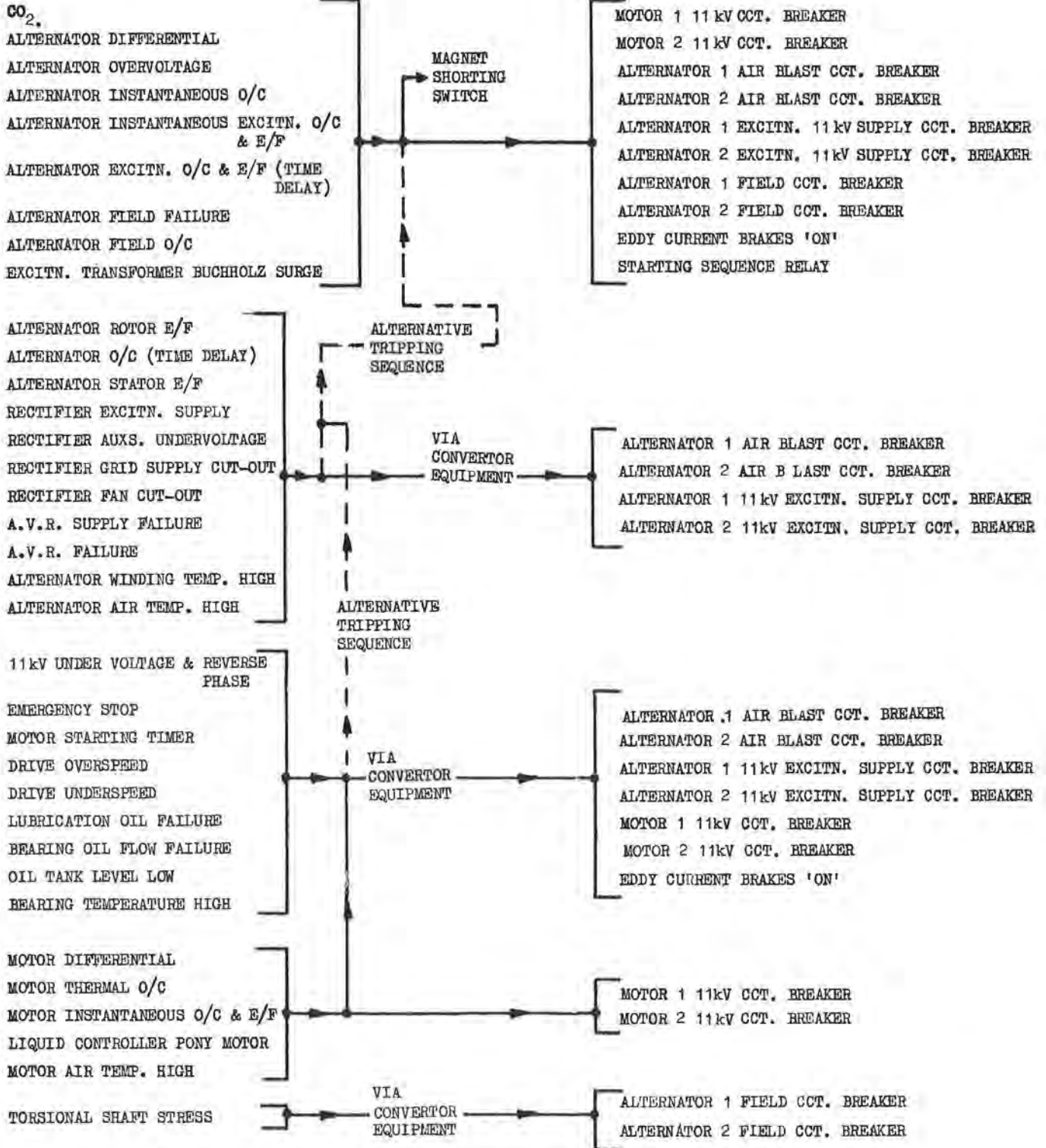
Since ultrasonic techniques have been accepted for many years as a means of evaluating the soundness of parts of rotary plant (e.g., end bells of turbo-alternator rotors) and in view of the American experience, it appeared prudent for ultrasonic inspection to be carried out on Nimrod. The practicability of scanning from the bore was considered. This had the obvious advantages that no machine dismantling need take place and very much more of the forgings could be examined.

There was no commercially available equipment to carry out this work and various firms were approached to see whether a reasonable development contract could be arranged to investigate this problem. There were obvious difficulties to be overcome some of which are now mentioned:-

- (i) The ultrasonic probe head would be out of the sight of the operator and up to 45 ft away from him, yet acoustic coupling conditions between the probe and the bore surface had to be constant throughout a survey. Furthermore the probe head had to pass through the $2\frac{3}{4}$ in dia. motor rotor bore before entering the $4\frac{1}{2}$ in dia. bores.
- (ii) Time of inspection had to be as short as possible. In this connection it is interesting to note that to examine the alternator rotor forging alone for bore surface flaws, and also flaws from the bore surface radially into the forging up to a distance of 10.5 in from the bore (to the base of the pole dovetails), requires results to be obtained at about 60,000 probe locations.

PROTECTION

ITEMS OPERATED



THE ALTERNATIVE TRIPPING SEQUENCES, SHOWN - - - - OCCUR ONLY IN THE EVENT OF A FAILURE IN THE MAIN LINE TRIPPING SEQUENCE, SHOWN ————

Fig. 5.2.12 (i) Rotating Plant Protection (Simplified)

- (iii) This means that it was necessary to devise, in effect, a continuous survey system which incorporates automatic trace recording and alarm features.
- (iv) The probe system had to be capable of being set up to achieve high repeatability accuracy in radial and longitudinal locations in order to achieve direct comparison with previous scanning results.
- (v) It had to be possible to set up the equipment within half a day so that use could be made of short shut down periods of say, two days duration.
- (vi) Results had to be capable of relatively easy interpretation.
- (vii) This in turn meant that the probe system had to give results which were accurate and comparable with previous results irrespective of the forging temperature, which can vary at least over the range 20°C-70°C.
- (viii) Another difficulty is caused by the fact that there is increasing signal attenuation as greater steel thicknesses are penetrated; thus the amplitude of the flaw trace is not constant for a given flaw size over the range of interest. However this problem can be overcome by suitable swept gain amplifier design to increase sensitivity with increasing range.

A development contract was placed in April 1960. It soon became apparent that a standard barium titanate/perspex probe could not meet the specified conditions but by August 1960 a much more satisfactory "free oil column" probe had been produced. This was basically an immersion technique using oil.

By March 1961 a prototype had been produced which permitted the probe head to pass through the $2\frac{3}{4}$ in dia. motor rotor bore into the alternator and flywheel bores. Early field trials had also been carried out direct into the alternator rotor bore at the alternator manufacturer's works. To keep the probe at a constant temperature irrespective of rotor steel temperature, the couplant oil system was designed to have a suitable flow, combined with a couplant oil heating system arranged to give very close temperature control. A couplant oil then had to be found which would have suitably stable characteristics at the operating temperature required.

This project was commenced sufficiently early in the manufacturing stages of the rotating plant to make it possible to enlist the aid of the manufacturer in arranging for certain holes in various parts of the rotor forging to be flat bottomed. These, of course, give a vastly different signal response when scanned ultrasonically and acted as 'navigation' marks, which was particularly helpful in the early development trials. The bore surface finishes were also improved to a 15 μ in finish. It would appear that a 50 μ in finish would have been adequate. By this time it had also been decided not to scan the motor from the bore since this complicated probe head design even more. Extra complication was not justifiable since half the length of the motor bore has a $2\frac{3}{4}$ in dia. insulated liner in it as part of this particular type of motor construction. Ultrasonic scanning in this region is therefore not possible in any case.

As the work progressed it became apparent in the first half of 1962 that it would be helpful to attempt to improve the probe design further. The oil columns incorporated in the probe design attenuated longitudinal ultrasonic waves only to a small degree, thus considerable reverberation signals existed which tended to mask the useful flaw signals. The oil column probe was finally

replaced by a Nylatron G.S. column probe incorporating suitable couplant oil channels. This proved to be a major improvement and early results showed that interpretation of the results obtained was very much simpler.

The final probes which will be supplied are as follows:-

- (i) A circumferential surface wave probe. The range of detection to be over a 90° arc of the bore surface. The sensitivity to be such that a V scratch 0.25 in in length, having an included angle of $3-5^\circ$ and a depth of 0.005 in, will be clearly and unmistakably indicated. Frequency 2.5 Mc/s.
- (ii) A longitudinal surface wave probe. Minimum range of detection to be 3.5 in ahead of the probe. Sensitivity as defined in (i) above. Frequency 2.5 Mc/s.
- (iii) A longitudinal wave (V.L.O.) probe. The sensitivity requirement to be such that the probe is capable of detecting $\frac{1}{8}$ in dia. flat bottomed holes drilled radially over a range from 0.1 in below the bore surface to 10.5 in from the bore surface. Frequency 2.5 Mc/s.
- (iv) Suitable standard type probes for scanning the four 11 in dia. journals and the eight 20 in dia. shaft journals from the exterior.

The development phase of this contract was virtually completed by December 1962. The commissioning of the final equipment and the initial and very detailed ultrasonic surveys of the rotary plant will take place during the first half of 1963 and will be described in the second part of this report. Before then a paper will be published on this project.

This introduction has been given at some length since no information is at present available elsewhere on the general background and considerations which led to the development of this special equipment. As far as is known this is the first time that such a comprehensive equipment has ever been produced for monitoring forgings in service from a central bore hole.

5.3. Converter Plant

In this section some of the more interesting problems which arose during the commissioning of the converter plant are discussed. As an introduction, a general description is given of the main power circuit of the converters and the essential control items. As already mentioned in section 5.1 a more detailed description, together with early design considerations, will be found in the three papers published in the proceedings of the I.E.E. (1).

5.3.1. General Description of Power Circuit

The basic circuit is shown in Fig.5.1(i). It will be seen that the converter installation is in two identical parts and that each half is made up of eight groups of converters. Each group itself comprises six single anode converters, and these are of the water cooled, continuously evacuated, excitron type.

For each half of the plant there are four main rectifier transformers having a primary rating of 11.93 MVA and supplied at 12.8 kV from the alternators via an air blast circuit breaker. Each transformer has two secondary windings connected double star with an interphase transformer, the no load secondary voltage being 3,400 V phase to neutral. The primary windings of the transformers are connected star, delta, extended delta + 15° and extended delta - 15° respectively, and this has been arranged so that each half of the converter plant operates as a 24 phase installation. The secondary windings of the transformer having the star connected primary, are associated with converter groups 1 and 2; the delta connected transformer with groups 3 and 4 and so on. The groups are connected in a series parallel arrangement shown in Fig.5.1(i) and the manner in which they operate to give a 24 phase output, and the function of the interphase transformers, will be explained by reference to Figs.5.3.1(ii), 5.3.1(iii), 5.3.1(iv).

The magnet current pulse is such that it demands three distinct modes of operation of the converter plant.

- (i) A period of approximately 0.7 s during which time all converters are operating as free firing rectifiers and current is increasing in the magnet. The actual time of current rise is variable depending on the value of magnet field required.
- (ii) A short period which is adjustable in 1 ms increments during which time the magnet current is held approximately constant.
This condition is obtained by arranging that only one group of converters in each series pair operates as a rectifier, whilst the second group functions as an inverter. The degree of inversion is such that there is just sufficient forward voltage as a resultant output across the series pair to overcome the resistive drop in the load and its connections.
- (iii) A period of time similar in magnitude to the current rise time (i) during which the magnet current decays to zero.
During this time all converters function as invertors to transfer the energy stored in the magnet to the power supply system.

A typical magnet current pulse waveform is given in Fig. 5.3.1(v) while Fig.5.3.1(ii) shows the build up of the d.c. voltage waveform across one series pair of converter groups. It has been assumed that the angle of overlap for the condition considered is $37\frac{1}{2}^{\circ}$ and that the safety angle during inversion is $22\frac{1}{2}^{\circ}$.

Curve 1 shows the anode voltage of one star group of say convertor group No.1; curve 2 shows an anode voltage associated with the other star of the same transformer secondary. Because of the action of the 150 c/s interphase transformer, each anode conducts for 1/3rd of a cycle and the d.c. current is shared equally between the two star windings. Since anodes associated with each star group are conducting simultaneously, the effective d.c. voltage due to the convertor group is the mean of curves 1 and 2 and is drawn as curve 3. The voltage across the 150 c/s interphase transformer will be the difference between curves 1 and 2.

Curve 4 is similar in waveform to curve 3 but is displaced in phase by 30° to represent the d.c. voltage of the series convertor group, say group 4.

When changing into flat top condition the d.c. voltage waveform of group 1 convertors moves into the negative inverter region as shown by curve 3 whilst curve 4 remains in the positive rectifier region until the end of flat top.

The nett d.c. voltage across the series pair of convertors is the algebraic sum of the voltages due to the individual groups and is indicated by the heavy full line on the Fig. 5.3.1(ii).

The nett d.c. voltage due to series convertor groups 3 and 2 will be similar in waveform to that due to groups 1 and 4 already considered, but since group 3 is 30° out of phase with group 1, then switching into flat top cannot occur at the same instant. On Fig. 5.3.1(iii) the waveforms for groups 1-4 and 3-2 are shown dotted and the effect of the 300 c/s interphase transformer is that the nett d.c. voltage output across the four groups is the average of the two curves, and is shown by the full heavy line. The voltage across the 300 c/s interphase transformer is the difference between the two dotted curves, and it can be seen that during full rectification and full inversion this should be zero.

Convertor groups 5, 6, 7 and 8 are all phase displaced by 15° relative to groups 1, 2, 3 and 4 already discussed, and perform in precisely the same manner.

It follows that the output voltage waveform of these two parts of the plant will be similar in shape but displaced in phase by 15° . This is shown on the dotted curves of Fig. 5.3.1(iv) and the effect of the 600 c/s interphase transformer is that the nett d.c. voltage output from each half of the convertor installation is as shown by the full heavy line. The voltage across the 600 c/s interphase transformer is the difference between the two dotted curves as indicated.

5.3.2. Commissioning Experience

No attempt will be made here to cover all the commissioning tests which have been carried out. Many of these were of a routine nature of limited general interest, and a complete record is available in the form of test schedules which were completed as the various tests were carried out. It is considered preferable to describe some of the more interesting aspects of the plant, and tests which were carried out to establish the plant performance.

(a) Main Rectifier Transformers

One of the tests carried out on the main transformers was a pressure test at 30 kV d.c. During this test one of the transformers broke down at approximately 12 kV d.c. and it was necessary to remove the transformer from its tank to find



Fig. 5.3.1 (i) View of Converter House showing the rectifier gallery with control gear underneath. The two primary ripple filter chokes can be seen in the centre of the picture and to the right the Brentford regulating transformers.

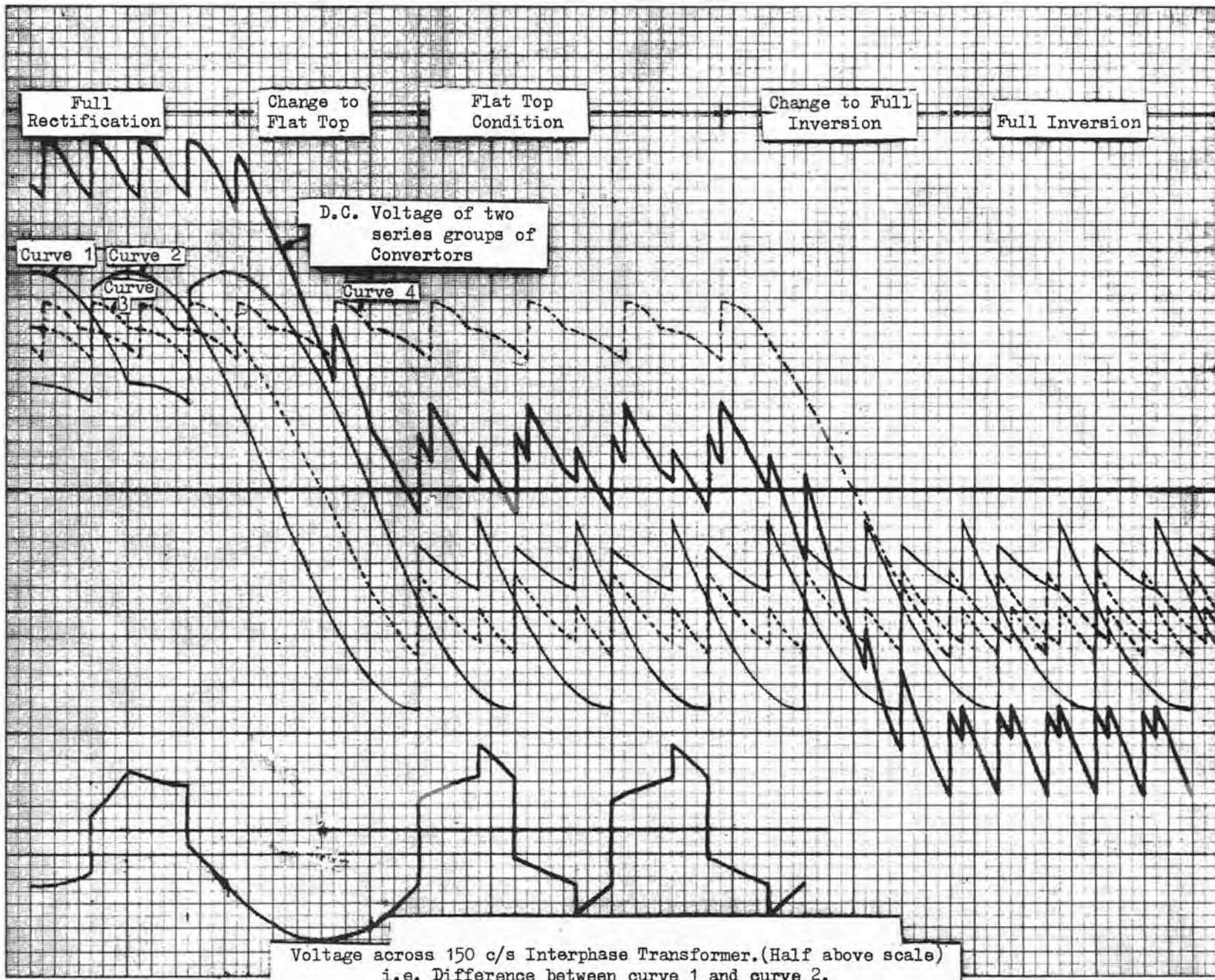


Fig. 5.3.1 (ii) Analysis of D.C. Output Voltage Waveform and Interphase Transformer Waveforms (Part 1)

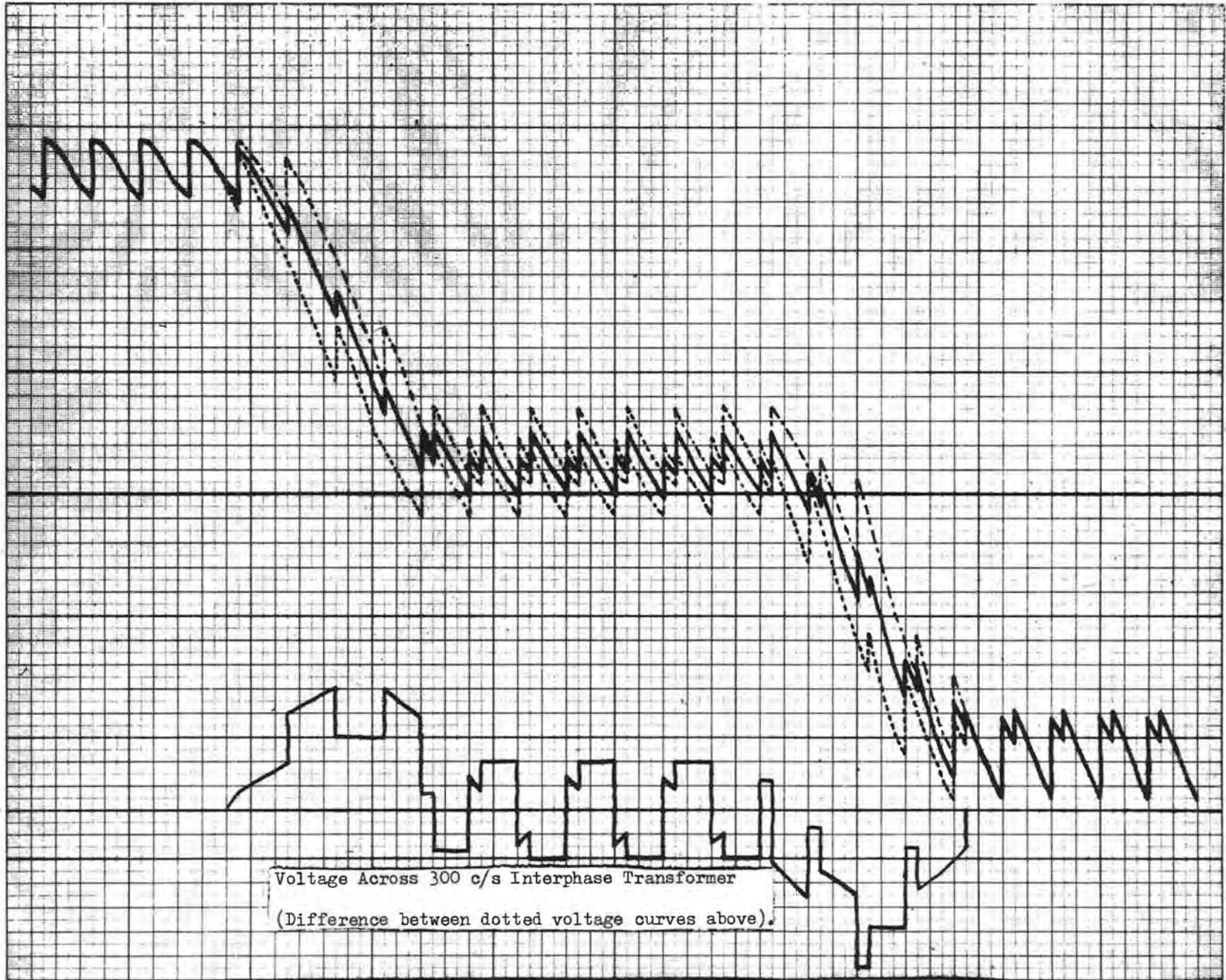


Fig. 5.3.1 (iii) Analysis of D. C. Output Voltage Waveform and Interphase Transformer Waveforms (Part II)

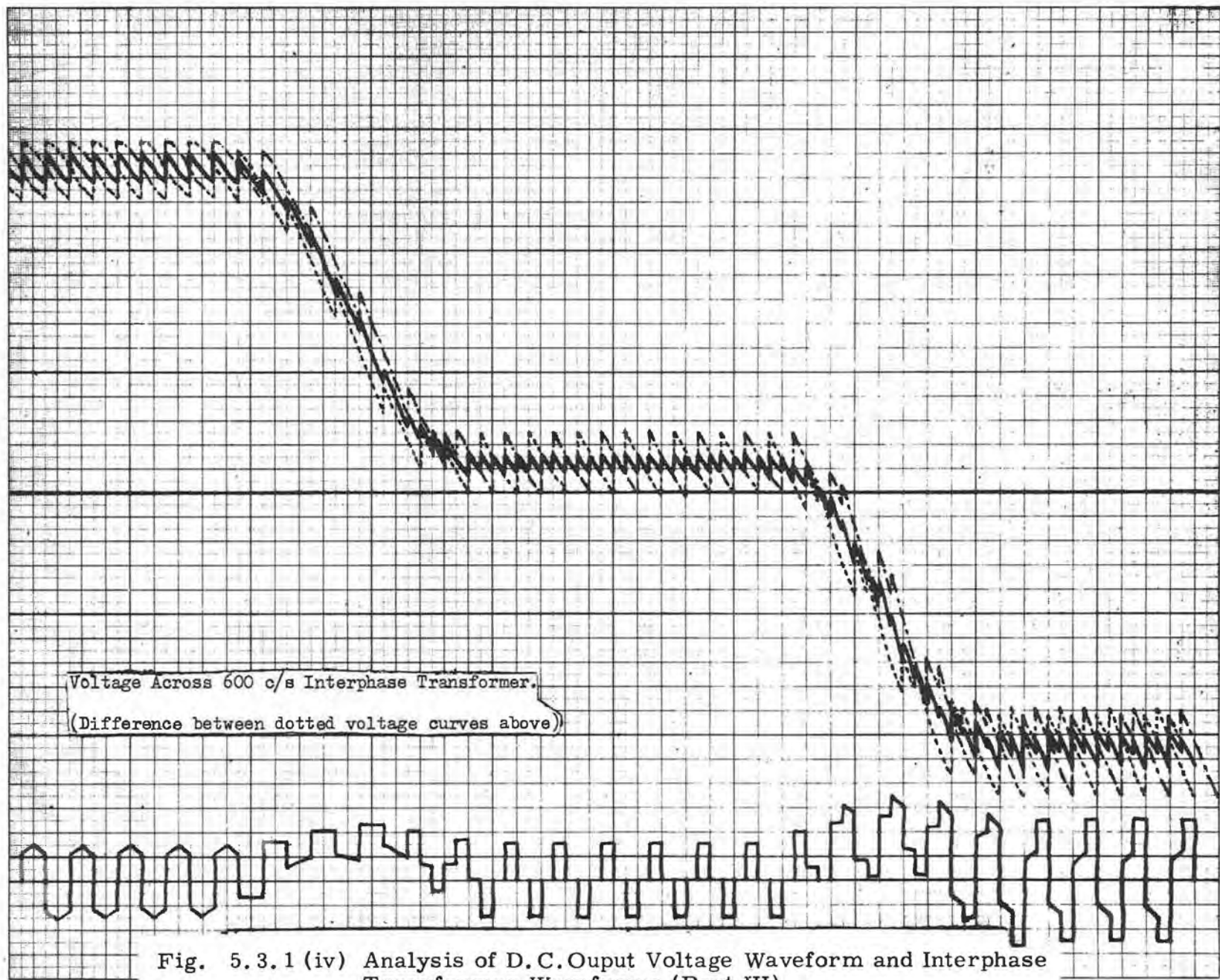


Fig. 5.3.1 (iv) Analysis of D.C. Output Voltage Waveform and Interphase Transformer Waveforms (Part III)

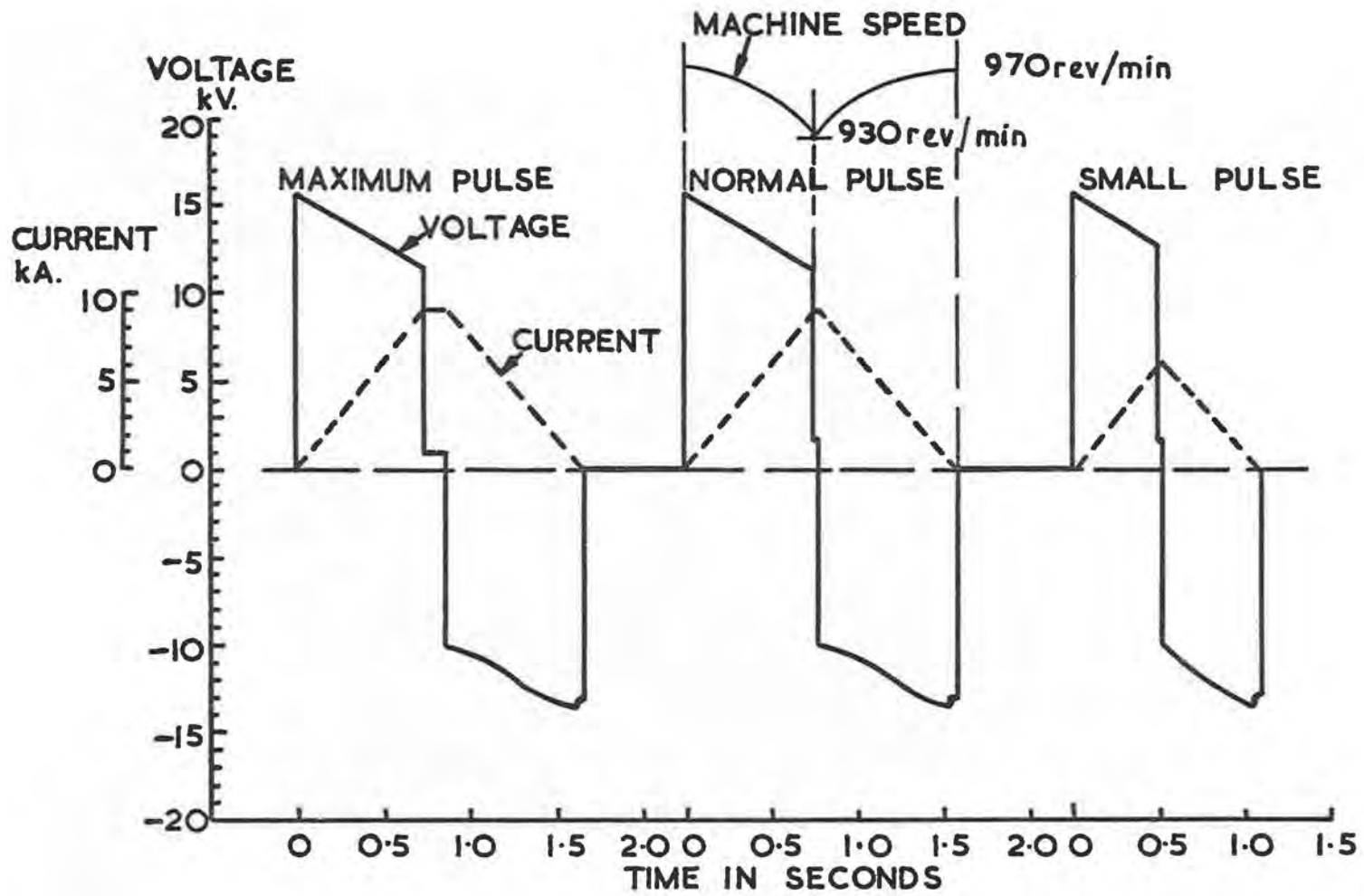


Fig. 5.3.1 (v) Pulse Shapes from the Magnet Power Plant

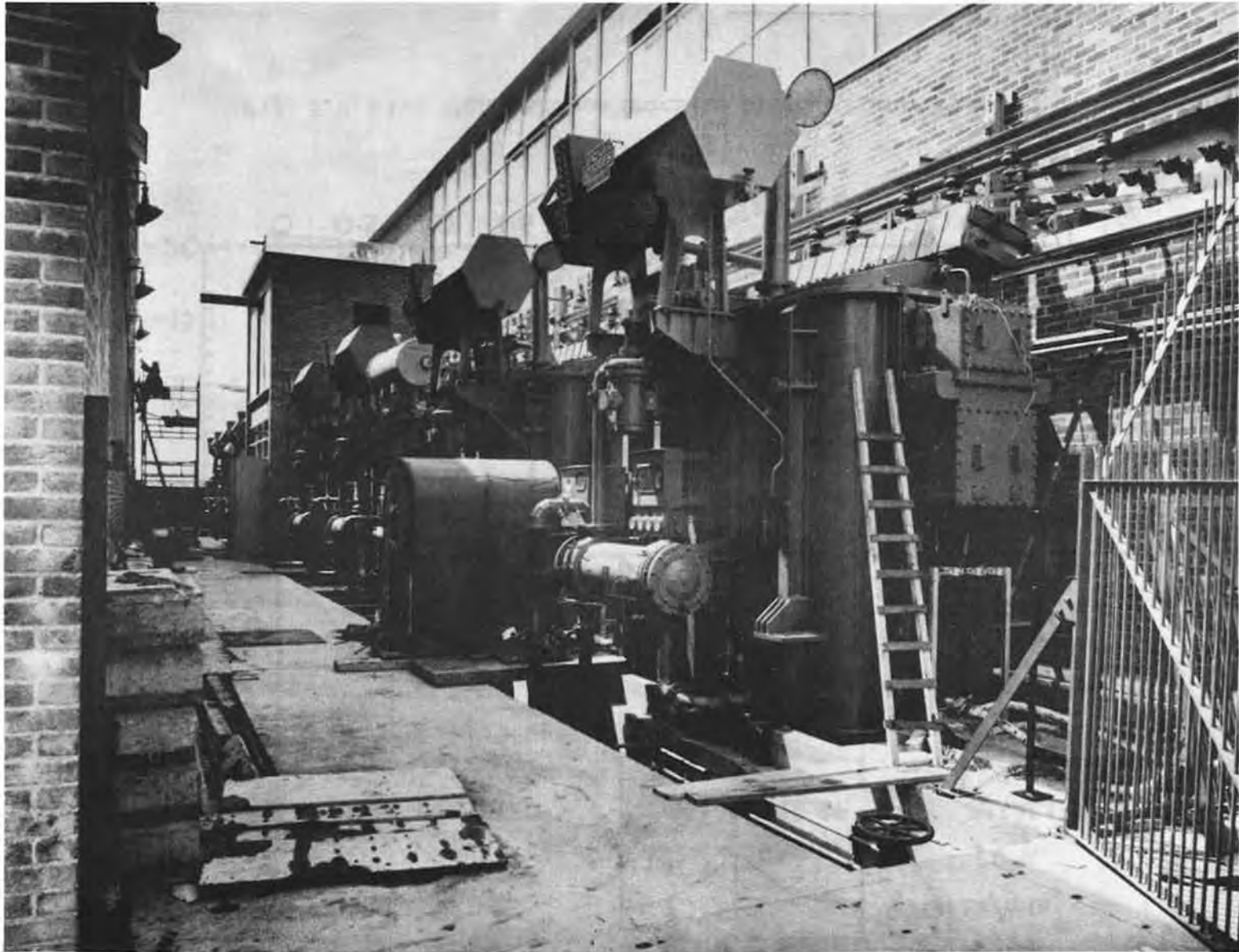


Fig. 5.3.1 (vi) View of Transformer Yard
(The building in the centre of the yard, with open doors,
contains the air blast switchgear).

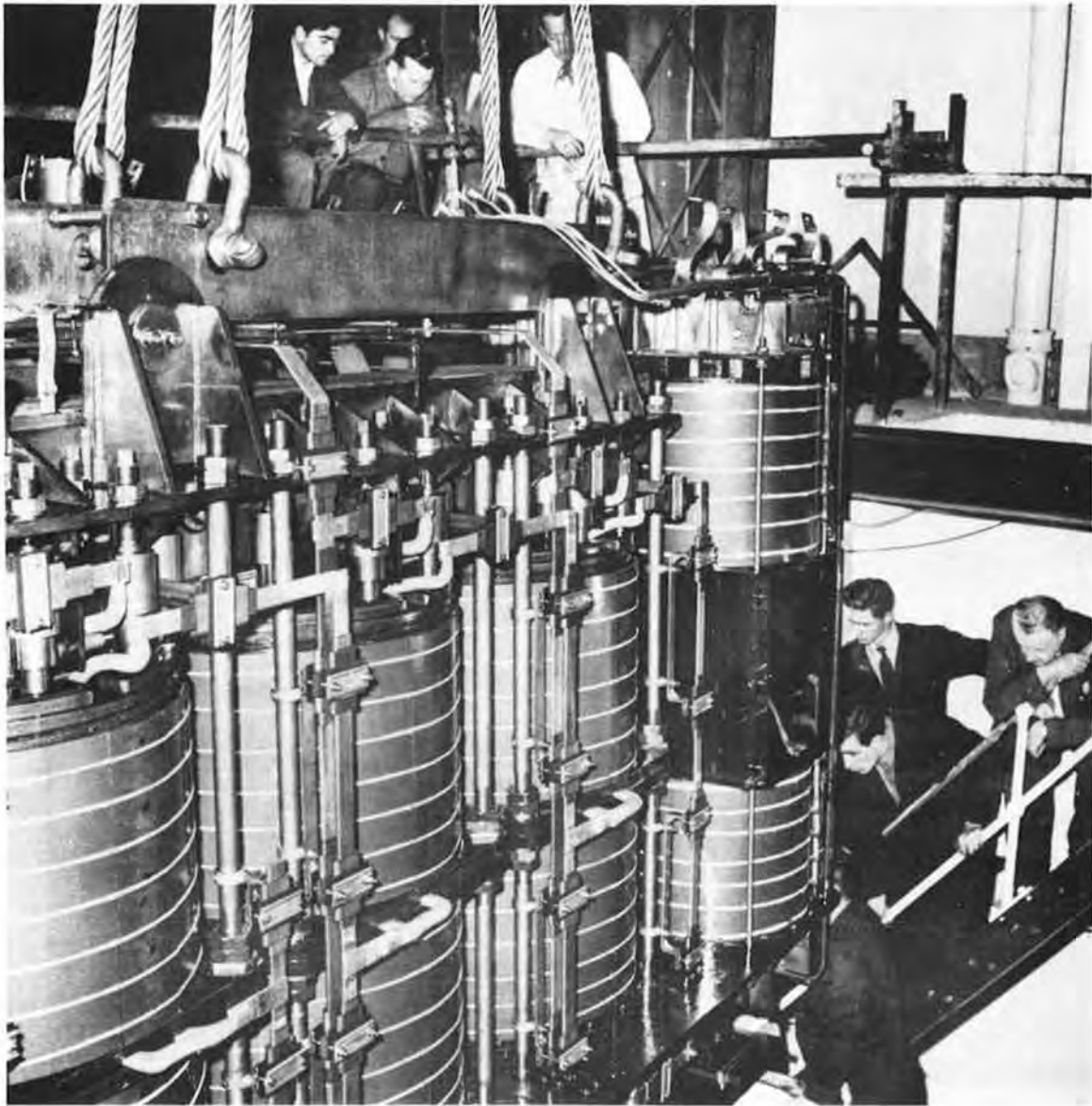


Fig. 5.3.2 (i) General View of Rectifier Transformer Removed from its Tank

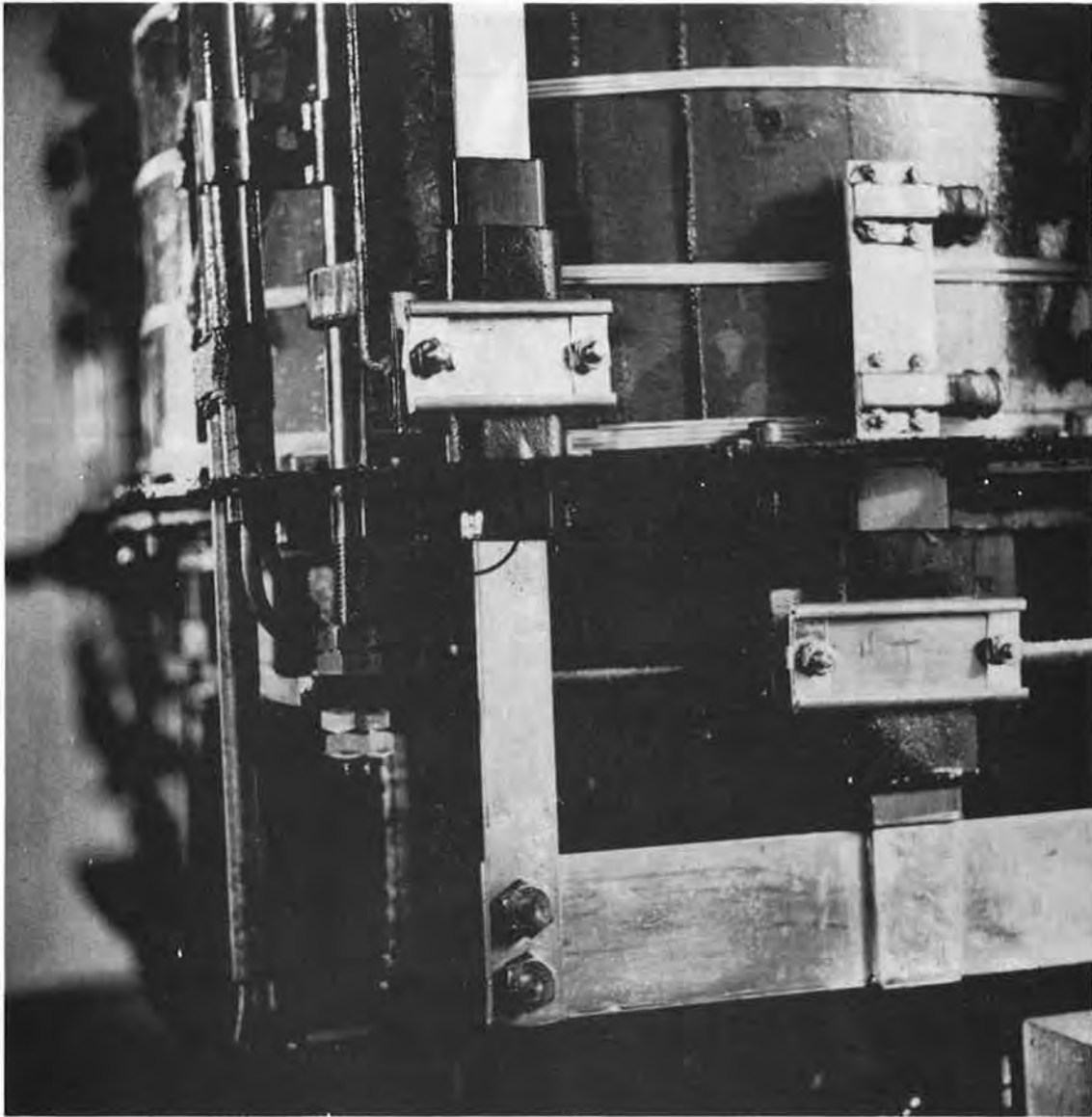


Fig. 5.3.2 (ii) View of Rectifier Transformer Neutral Connection Showing Damaged Insulation

the cause of the trouble. It was found that at one point there had been insufficient clearance between a neutral connection and a web on the side of the tank. It was concluded also that the method of locating the transformers in their tanks was not positive, and that movement had occurred in transit.

Photographs are included of the transformer being removed from its tank, and a close up of the neutral connection showing the damaged insulation where chafing had occurred, resulting in breakdown on pressure test (Figs. 5.3.2(i) and 5.3.2(ii)).

As a result of these findings it was necessary to examine each of the eight transformers and to modify the method of locating the transformers in their tanks. Fortunately it was possible to do this by draining down the oil and working through inspection covers in the sides of the tanks.

(b) Convertor Load Sharing

By far the largest part of the commissioning time has been spent in carrying out adjustments to the plant to obtain reasonable load sharing between the paralleled convertor units. The causes of poor load sharing have in general been due to one of the following:-

- (i) Current compensation influence on grid phasing.
- (ii) Incorrect operation of the interphase transformers.
- (iii) Unsymmetrical capacity to earth of the d.c. connections to the magnet.
- (iv) Faults in the grid impulse generating circuits.

The last item is of little general interest and will not be dealt with further. The first three items will be treated under their separate headings.

(i) Current Compensation Influence on Grid Phasing

In order that the synchrotron as a whole may operate at its maximum repetition rate, it is necessary that at the end of the flat top period the magnet current is reduced to zero as quickly as possible. This is done by so phasing the convertor grid impulses that the anodes can only conduct during the time when their voltages are negative relative to the transformer neutral. Thus the convertors are operating as invertors. This is possible due to the high inductance of the magnet, which produces a back e.m.f. to force the current through the convertors from anode to cathode, against the direction of the applied anode voltage.

It is desirable to operate with the maximum degree of inversion possible, and this involves continually altering the phasing of the convertor grid impulses as a function of load current. Fig. 5.3.2(iii) explains the reason for this. At (a) is shown one of the double star main transformer connections and the anode voltage waveforms produced by this transformer are shown at (b) and (c) with the convertors operating as invertors. At (b) anode 1 is shown commutating to anode 2 at an angle δ before the anode voltage waveforms cross each other. Commutation can only occur from one anode to another which is more positive and therefore would be impossible if the grid impulse of anode 2 were retarded beyond the cross over point. In fact commutation must be complete well before this cross over point to allow sufficient time for de-ionisation of the space surrounding the extinguished anode which would otherwise re-ignite. The minimum time in which

commutation must be completed before the cross over point, is called the safety angle and is shown as the angle δ on Fig. 5.3.2(iii). This diagram has been drawn neglecting commutation time, i.e. angle of overlap μ which is shown in (c). Since we must maintain the safety angle δ after commutation, it is necessary that the grid impulses must be advanced by an angle μ giving $\beta = \delta + \mu$. The overlap angle is a function of load current and commutating voltage and Fig. 5.3.2(iv) shows the amount of grid advance applicable for given currents at the various operating voltages. This control is known as 'current compensation'.

The circuit which initiates the generation of convertor grid impulses relies on an a.c. waveform of alternator frequency being cut by a d.c. voltage. By varying the level of the d.c. voltage input, the point at which this cuts the a.c. waveform and hence the phase position of the grid impulses, is changed. Each group of convertors has its own current compensation control, which is obtained by connecting in series with the d.c. input to the grid control units a component which is a function of d.c. current fed via d.c. current transformers (see Fig. 5.3.2(v)). The original scheme was such that the d.c. current for each group supplied its own current compensation control. This scheme was unstable and various forms of cross connection were tried to provide some current compounding control to give even load sharing between the convertor paths. The scheme finally adopted is shown in Fig. 5.3.2(vi) which indicates, for example, that the d.c. current in group 1 influences the grid phasing of groups 3 and 7, whilst the currents in groups 3 and 7 also influence the grid phasing of group 1. Current compensation is only effective during inversion and does not influence impulse phasing during rectification. During flat top the cross compounding of groups 1, 3, 5 and 7 will be operative to assist load sharing and during current decay groups 4, 2, 8 and 6 will behave similarly.

It will be clear that the primary function of the current compensation control is to provide an adequate safety angle. The current sharing feature is a secondary aspect and is not a closed loop control in the normal sense, in that there is no controlling influence operating directly as a function of current unbalance. Load sharing will only be correct if the current compensation controls are precisely set up and any differences in the settings between one convertor group and another will in fact enforce current unbalance.

(ii) Incorrect Operation of Interphase Transformers

The function of the interphase transformers (I.P.T's) has been explained in section 5.3.1. It will have been seen that the largest voltage/time areas across the I.P.T's, and hence the maximum flux conditions, occur when switching from rectification to inversion or from inversion into rectification. The latter condition applies at the end of an injection platform which is produced at the beginning of the current pulse at approximately 170 A. The injection platform is produced in the same way as flat top is produced at peak current. At the end of the platform period the odd numbered groups of convertors are switched from inverter to rectifier duty to continue the current rise period. Fig. 5.3.2(vii) shows the I.P.T. waveform obtained on a programme with injection platform and a very small peak d.c. current. It is included to show the voltage/time areas to which the I.P.T's are subjected when changing from rectification to inversion and vice-versa.

The control of convertor switching from rectification to inversion and vice-versa is from a master timing unit which is set up to provide the required periods for current rise, injection platform, flat top and repetition rate. The timer

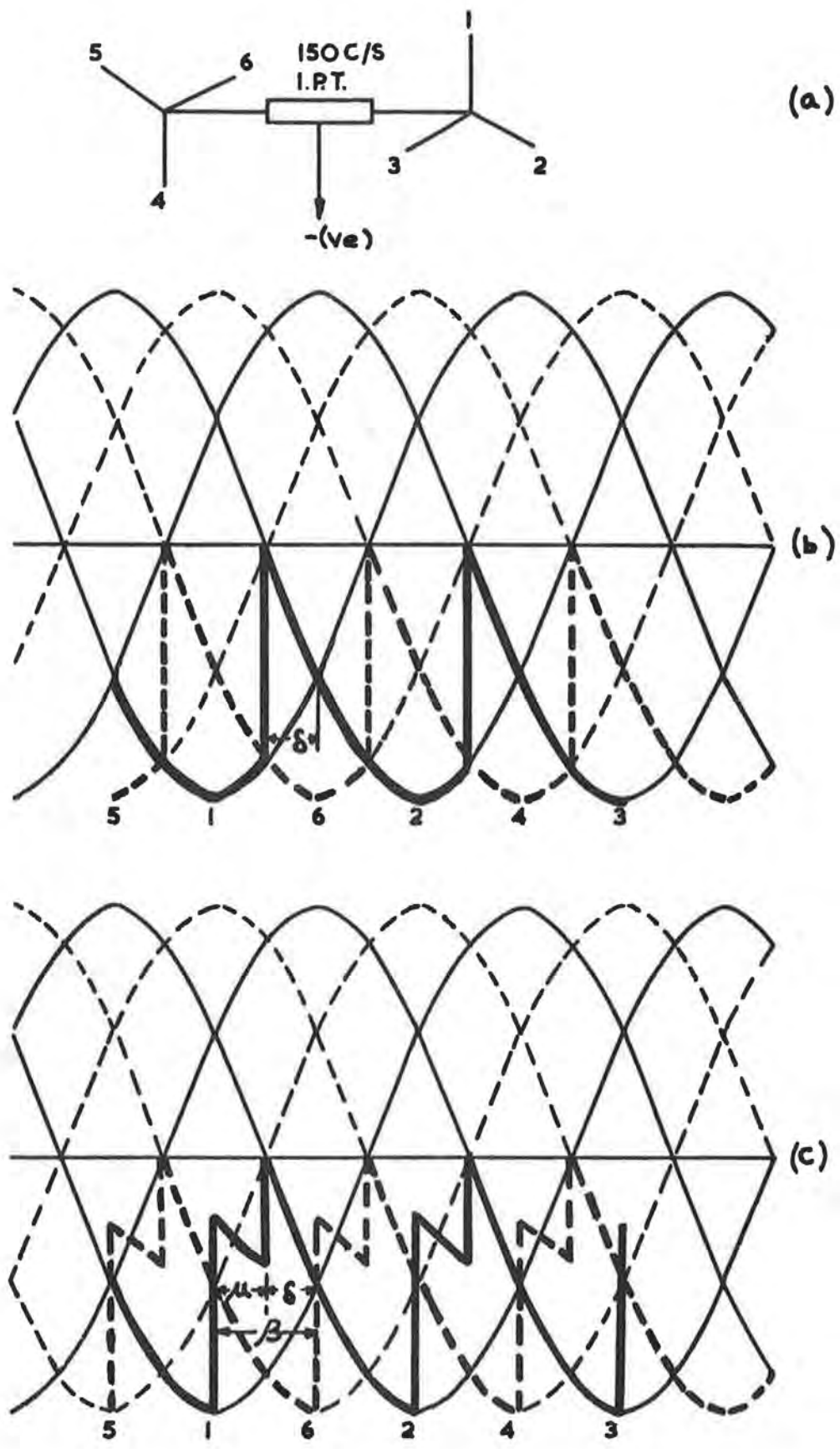


Fig. 5.3.2 (iii) Effect of Current Compensation Control on Inverter Operation

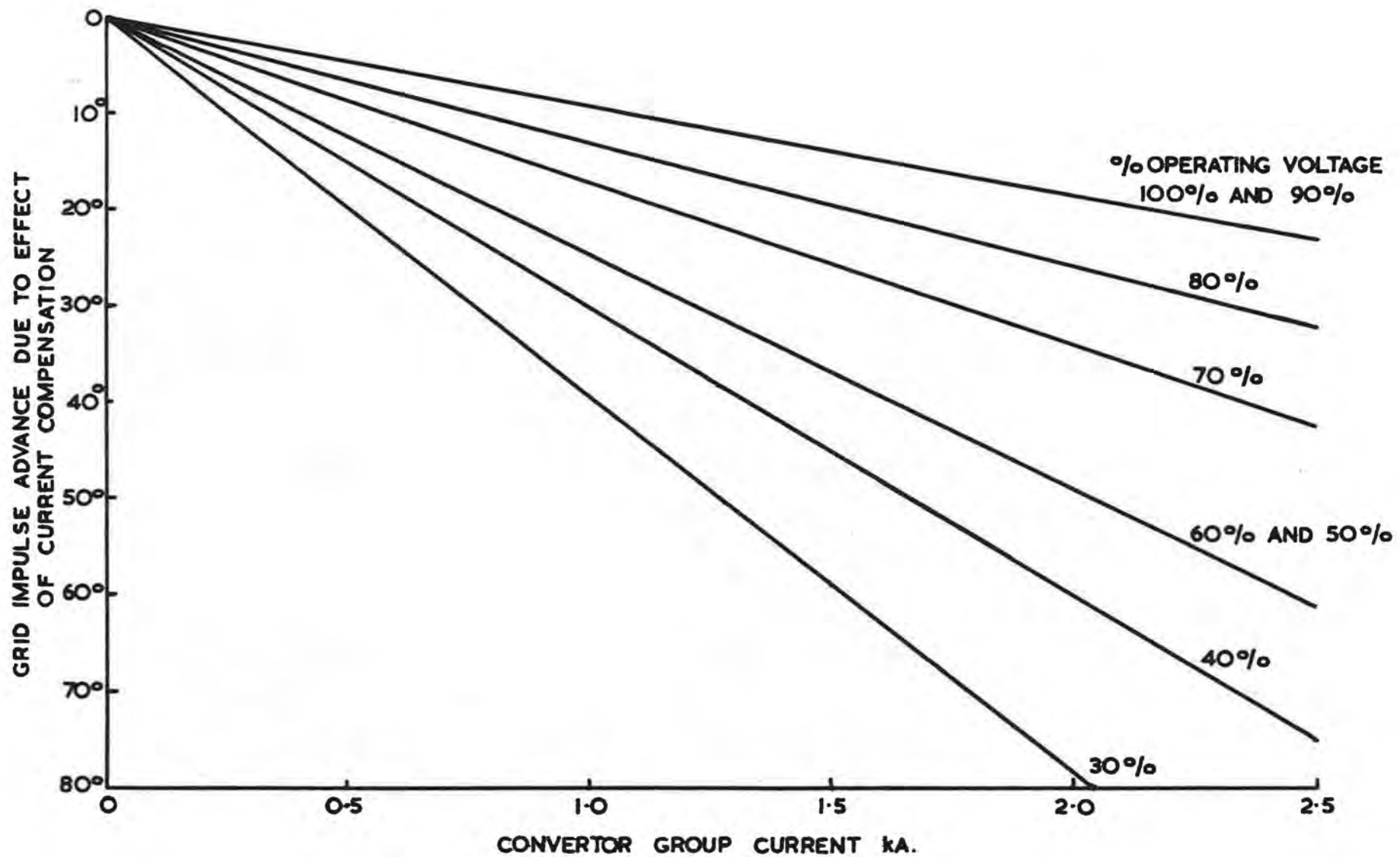


Fig. 5.3.2 (iv) Degree of Phase Advance due to Current Compensation

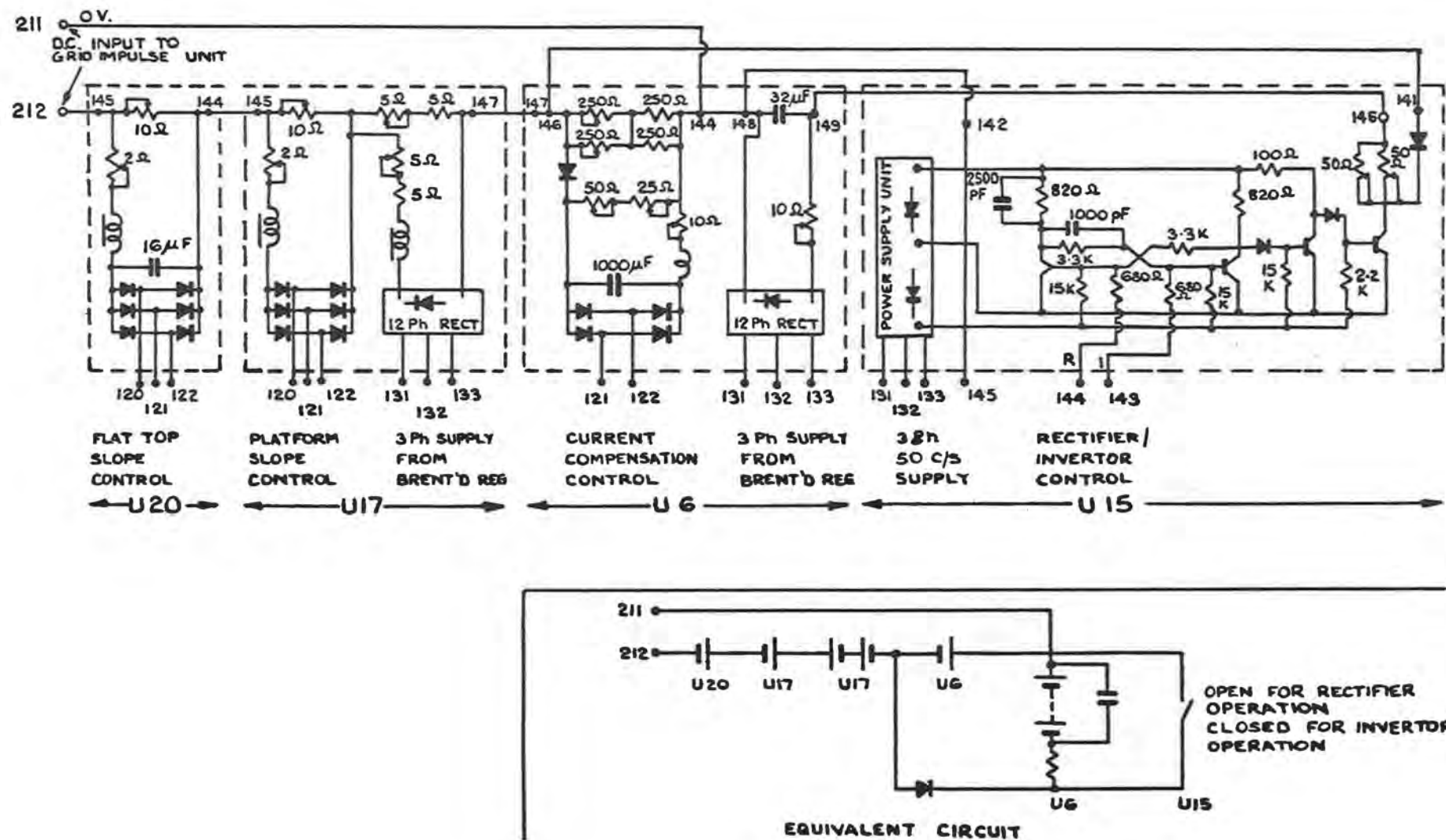


Fig. 5.3.2 (v) Circuit Diagram Showing Components Contributing to the D.C. Input Voltage of Grid Control Units

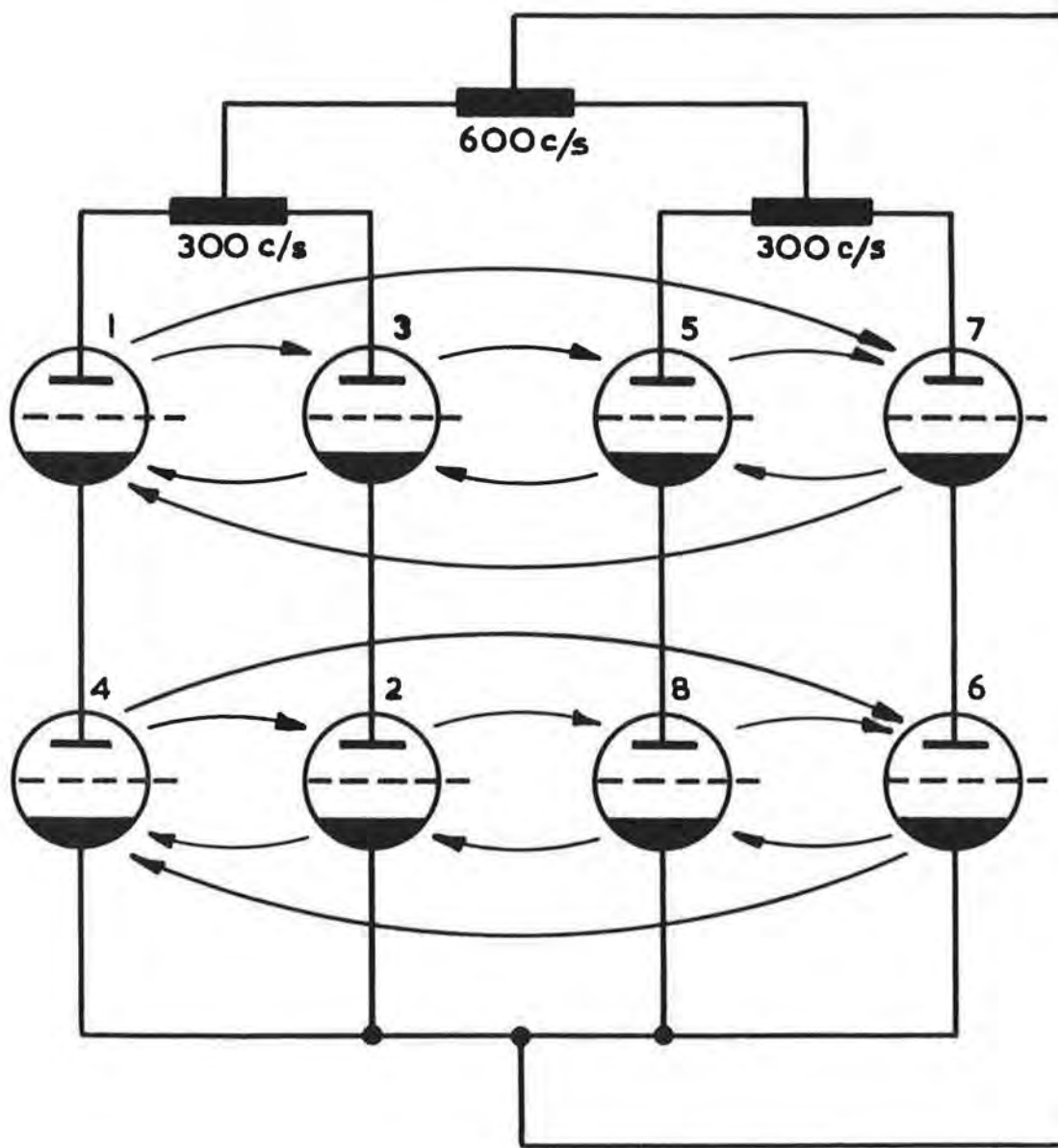


Fig. 5.3.2 (vi) Cross Connection of Current Compensation Control Circuits

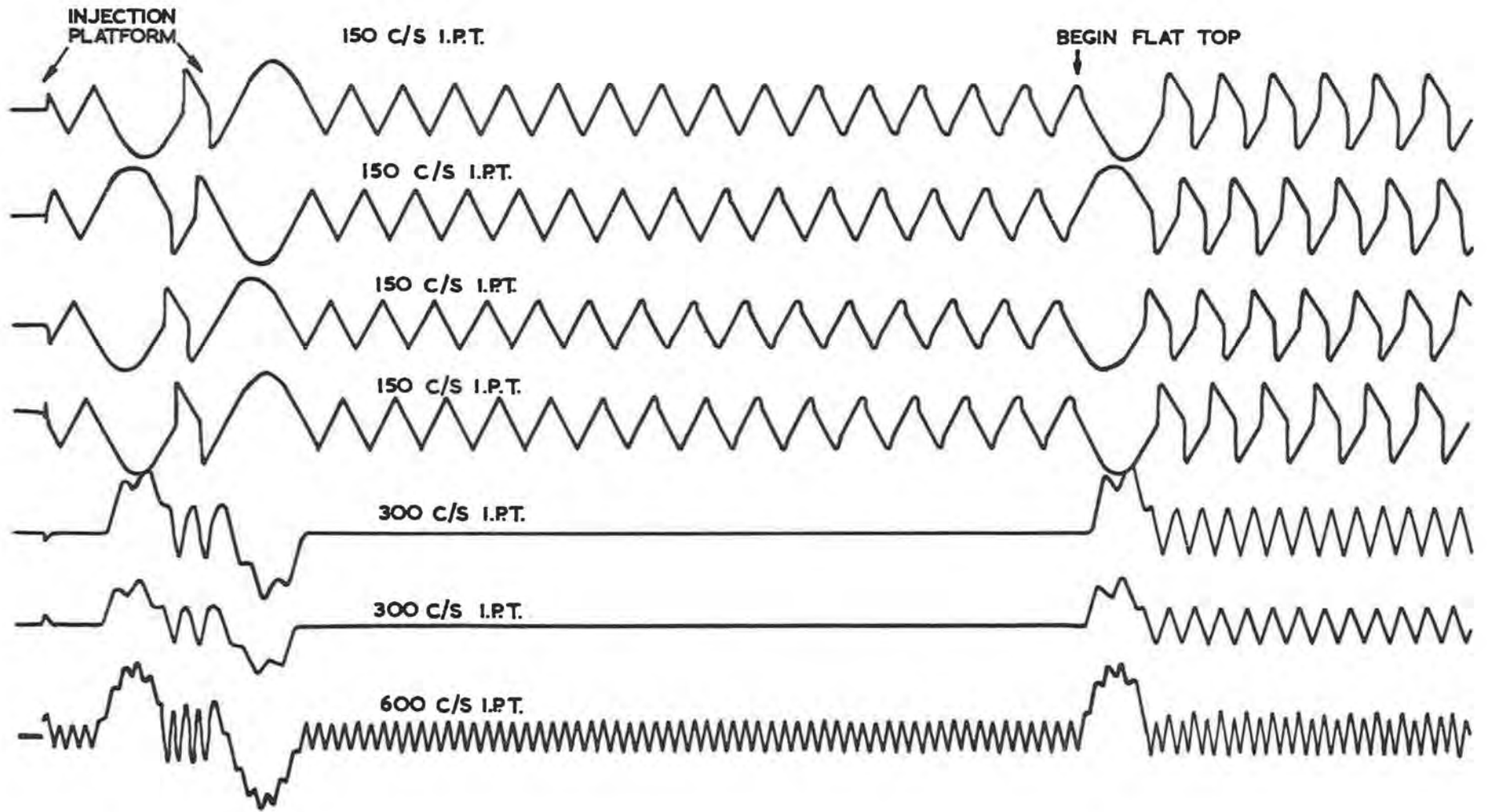


Fig. 5.3.2 (vii) Interphase Transformer Waveforms with Premagnetisation

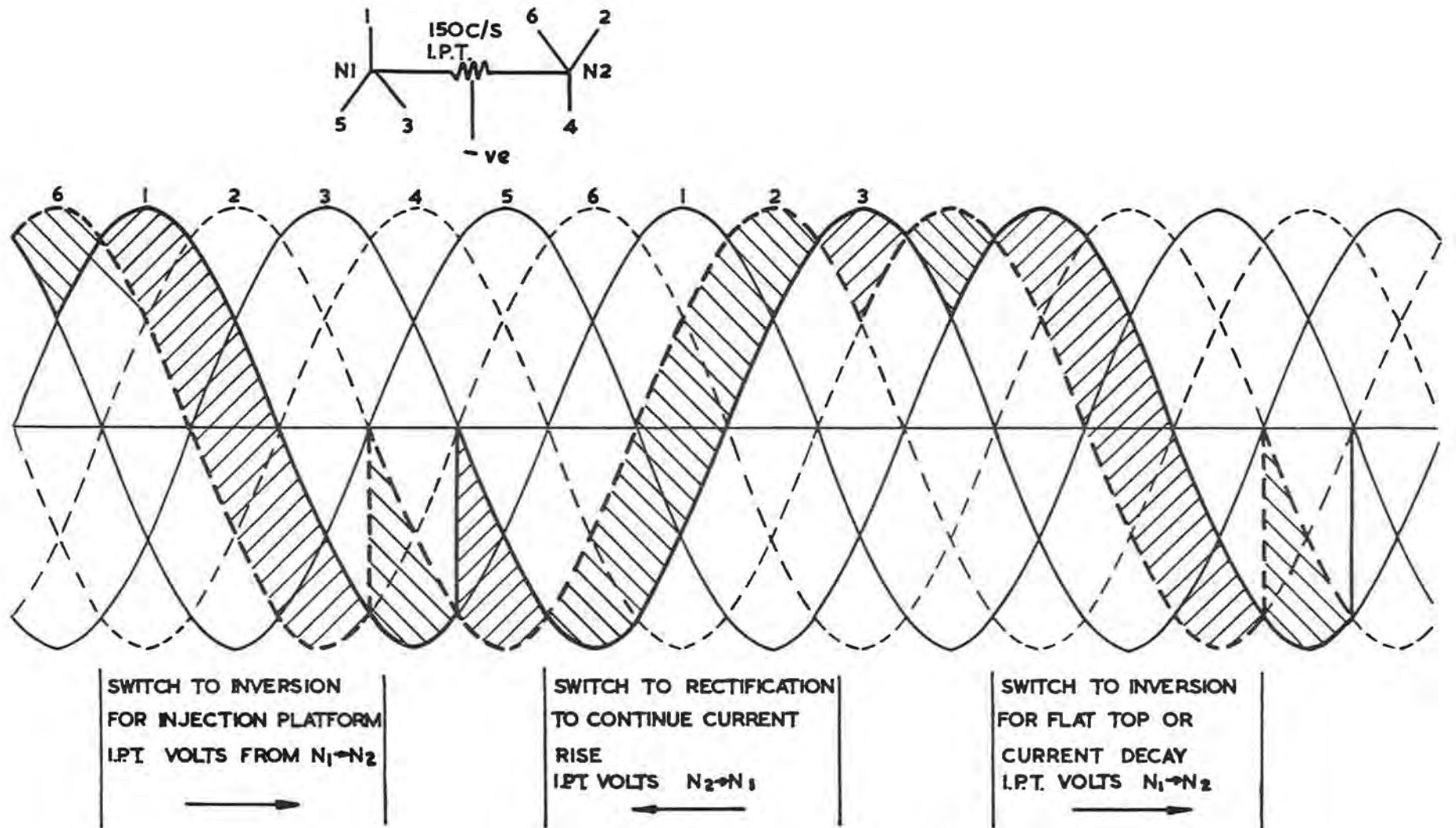


Fig. 5.3.2 (viii) Polarity of 150c/s I. P. T. Voltage Waveforms

output pulses operate via impulse amplifiers and transformers, and multivibrator switches to change the d.c. input level to the grid control units as explained above. This alters the phase position of the grid impulses and gives the required operating mode, i.e. rectification or inversion. The design of the timer is such that the large voltage/time areas to which the I.P.T's are subjected occur in opposite directions each time the converter operating mode is changed. Fig. 5.3.2(viii) indicates how this occurs for the 150 c/s I.P.T. and the same applies for the 300 c/s I.P.T. This can be seen by reference to Fig. 5.3.2(vii). In the case of the 600 c/s I.P.T. the same condition applies for injection platform, but the flux change at the beginning and the end of flat top are in the same direction and it is not possible to avoid this.

Early operating experience showed that the design of the interphase transformers was such that precise setting up of the grid circuits and current compensation circuits was essential if I.P.T. saturation at the end of flat top was to be avoided, particularly so in the case of the 300 c/s I.P.T's. Fig. 5.3.2(ix) has been drawn to show the effect of current compensation errors on the 300 c/s I.P.T's during flat top. At (c) is shown the I.P.T. waveform when current compensation settings are precise. At (b) the case is shown where there is a 3° error in current compensation and at (a) a 7½° error is shown. At (c) it is clear that alternate positive and negative voltage/time areas are equal whilst at (a) and (b) this is not so and the d.c. component of flux will quickly cause saturation.

Test results confirmed that the dimensions of the I.P.T's were such that they would not function properly without pre-magnetisation of the core. If the plant commenced operation with the I.P.T. cores fluxed at remanance level, saturation would occur on the first large voltage/time area to which they are subjected at the beginning of injection platform. Fig. 5.3.2(x) is included to show this effect and can be compared with Fig. 5.3.2(vii) which was taken under identical conditions but with pre-magnetisation. Pre-magnetisation is obtained by passing a pulse of d.c. current through the I.P.T. windings from an external source immediately before the commencement of each magnet current pulse. The idealised fluctuation of flux in the core of the I.P.T's is shown in Fig. 5.3.2(xi) which indicates the reversals of flux in the 300 c/s I.P.T. In practice the flux does not remain at the pre-magnetising level as indicated but tends always to move towards the remanance level. This is particularly so when the I.P.T's are subjected to an alternating flux change which, due to the hysteresis characteristic of the material, produces a de-magnetising effect. The 300 c/s I.P.T's have proved particularly troublesome in that they tend to saturate at the end of flat top and the probable reasons for this are:-

- (i) Physical dimensions of the I.P.T's are inadequate.
- (ii) The effect of pre-magnetisation has reduced considerably before the end of flat top time and the core flux has reduced to remanance value, accelerated by the de-magnetising effect of the 300 c/s alternating flux during flat top, which can be seen in Fig. 5.3.2(vii).
- (iii) Load unbalance during flat top due to inaccuracies in current compensation control (see Fig. 5.3.2(ix)).

If the I.P.T's saturate when subjected to the large voltage/time area at the end of flat top, all the load current is transferred from one series group of invertors to the group in parallel with it, which results in inverter arc through

and a shut down of the plant.

The problem has been overcome by deliberately causing an out of balance of current to exist in the series groups of convertors on each side of the 300 c/s interphase transformers. This produces a d.c. flux in the I.P.T. core in the opposite direction to that to which it is subjected at the end of flat top. This effect has been obtained by introducing small phase shifts in the convertor grid circuits.

(iii) Unsymmetrical Capacity to Earth of the D.C. Connections to the Magnet

During the commissioning stages it was not always possible to use the eight magnet octants as a load and various connections were made to octants as available, in groups of four. Some connections were such that the lengths of cable were dissimilar from the positive and negative terminals of the power plant, and it was observed that under this condition load sharing between the convertor groups was poor. This was due to the unbalanced capacity condition which existed with different cable lengths. Experiments were carried out to simulate the condition under symmetrical cabling arrangements and it was found that although up to 20 μF could be connected between the positive connection and earth with no ill effect on load sharing, a 1.16 μF capacitor connected from the negative terminal to earth could make the plant inoperative.

Investigation showed that on the odd numbered groups of convertors a small step appeared on the leading edge of the grid impulses (see Fig. 5.3.2(xii)) when the 1.16 μF capacitor was connected from the negative terminal of the plant to earth. This step caused premature firing of the anodes and bad load sharing between groups. It was noted that this effect only occurred during full inversion (i.e. magnet current decay period) and that the grid voltage step corresponded with a disturbance in the d.c. input to the grid control units.

The cause of this trouble is not yet clearly understood but it was cured by connecting a 1 μF capacitor across the terminals of the grid control units.

(c) Power Supply Harmonics

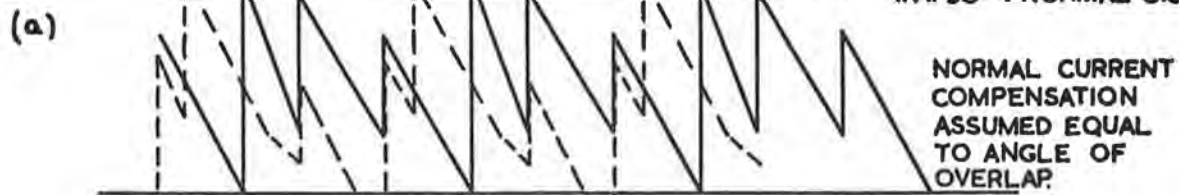
The harmonic voltages present in the power supply d.c. output were measured. To do this, an amplifier with tuned negative feed-back was constructed and the results for the case of 10,500 A peak magnet current having a 844 ms flat top with no slope control are given below (Table 5.3.2(I)). All voltages are peak to peak. The harmonics are expressed relative to the fundamental frequency of the alternators, the actual frequency depending on the pulse dimensions and repetition rate. The values given are those at the power supply terminals and take no account of the ripple filter equipment which has not yet been commissioned.

TABLE 5.3.2(I). HARMONIC VOLTAGES

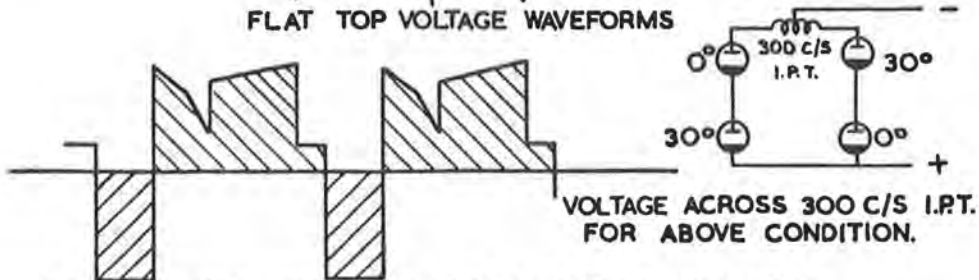
Harmonic	1st (Fundamental)	2nd	3rd	6th	12th	24th	48th	72nd
A1 Power Supply	25	65	30	50	60	250	130	85
A2 Power Supply	30	60	30	50	60	250	125	100

THE VOLTAGE WAVEFORMS BELOW ASSUME AN ANGLE OF OVERLAP OF $37\frac{1}{2}^\circ$ FOR RECTIFIERS & INVERTORS. SAFETY ANGLE OF $22\frac{1}{2}^\circ$ ASSUMED FOR INVERTORS.

— RECT. 30°
 INV. $0^\circ + 7\frac{1}{2}^\circ$ EXTRA C.C.
 - - - RECT. 0°
 INV. $30^\circ +$ NORMAL C.C.



FLAT TOP VOLTAGE WAVEFORMS



I.E. DIFFERENCE BETWEEN FLAT TOP VOLTAGE WAVEFORMS

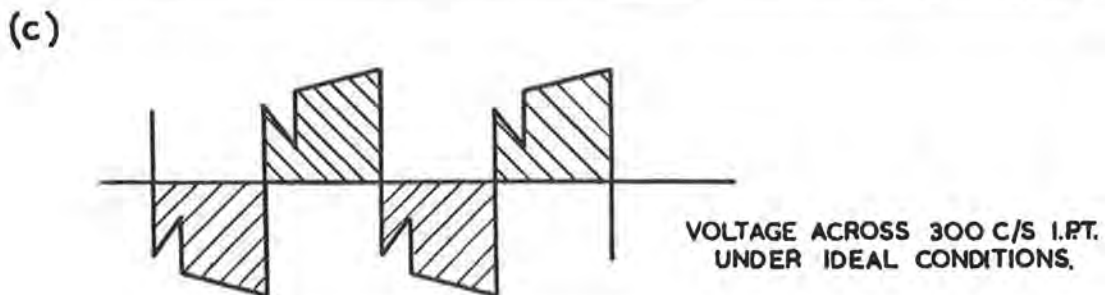
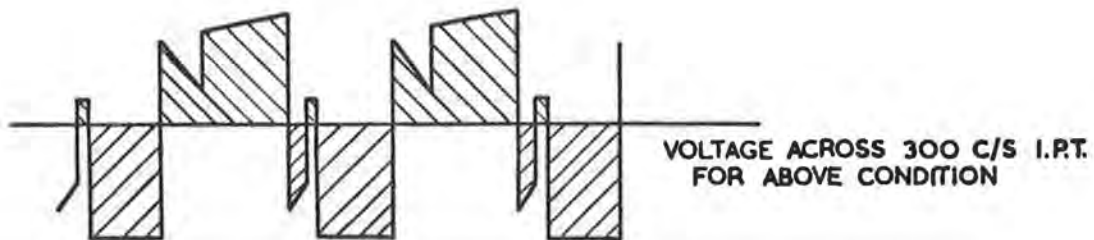
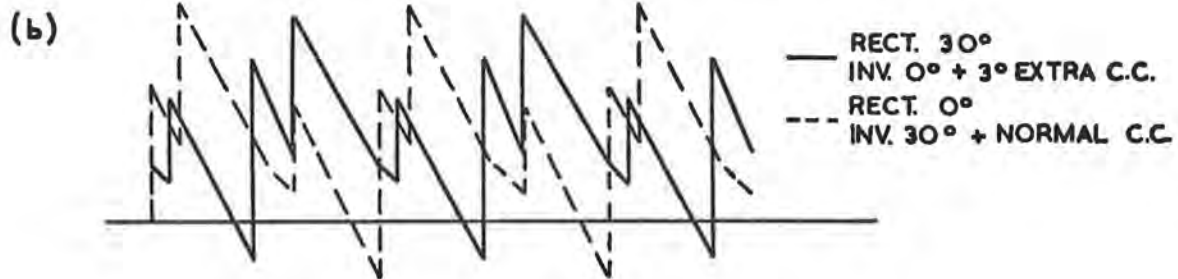


Fig. 5.3.2 (ix) 300c/s I. P. T. Waveforms Showing Effect of Incorrect Grid Phasing

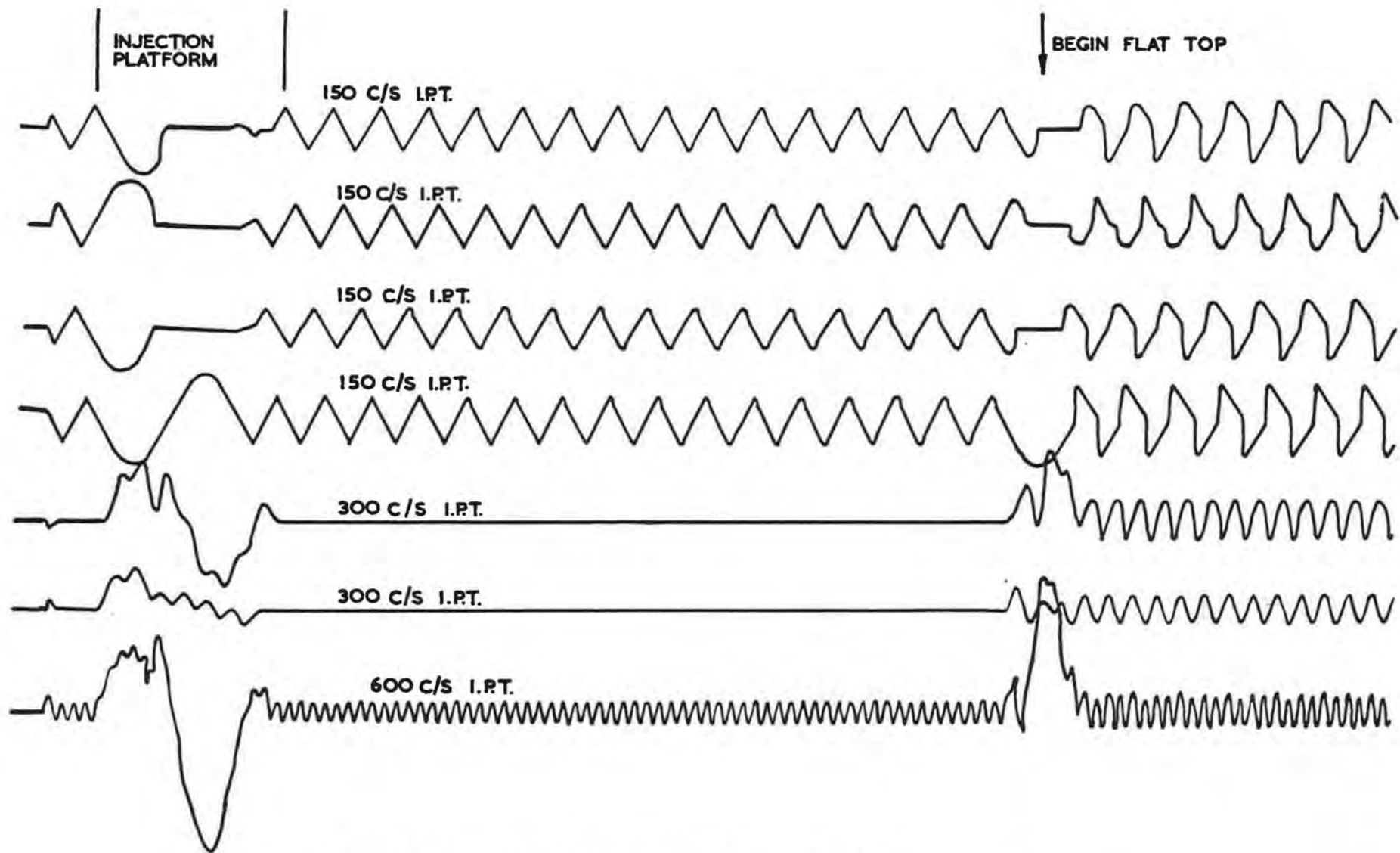


Fig. 5.3.2 (x) Interphase Transformer Waveforms with no Premagnetisation

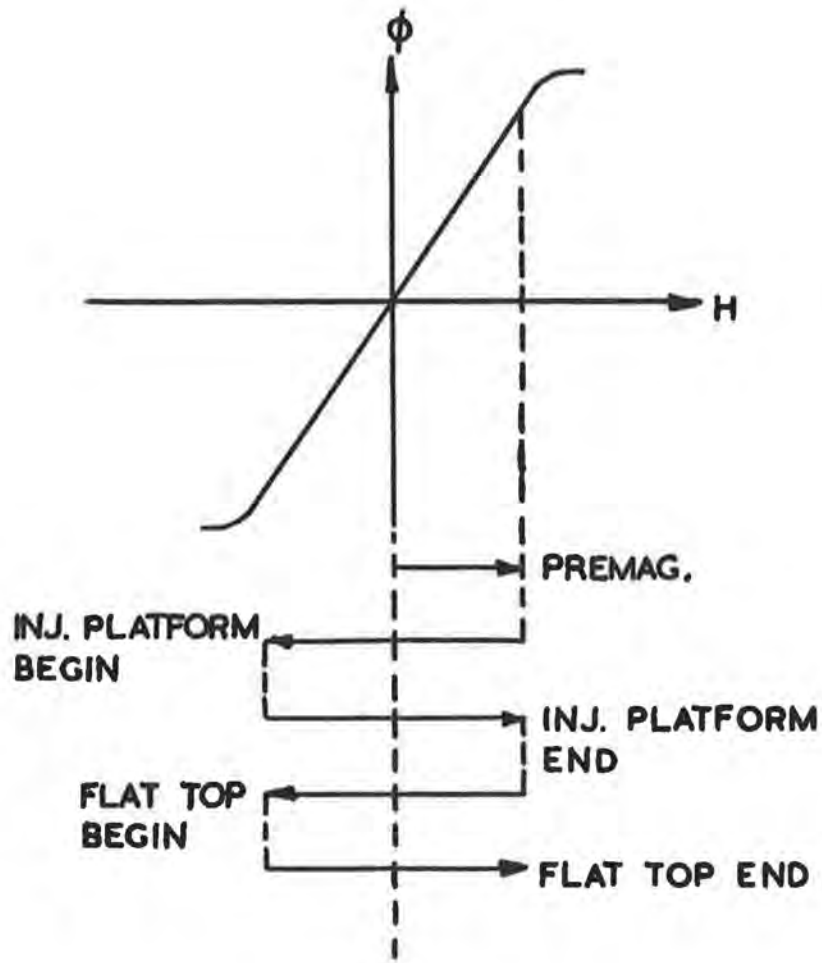


Fig. 5.3.2 (xi) 300 c/s I. P. T. Flux Changes.

GROUP A2-7

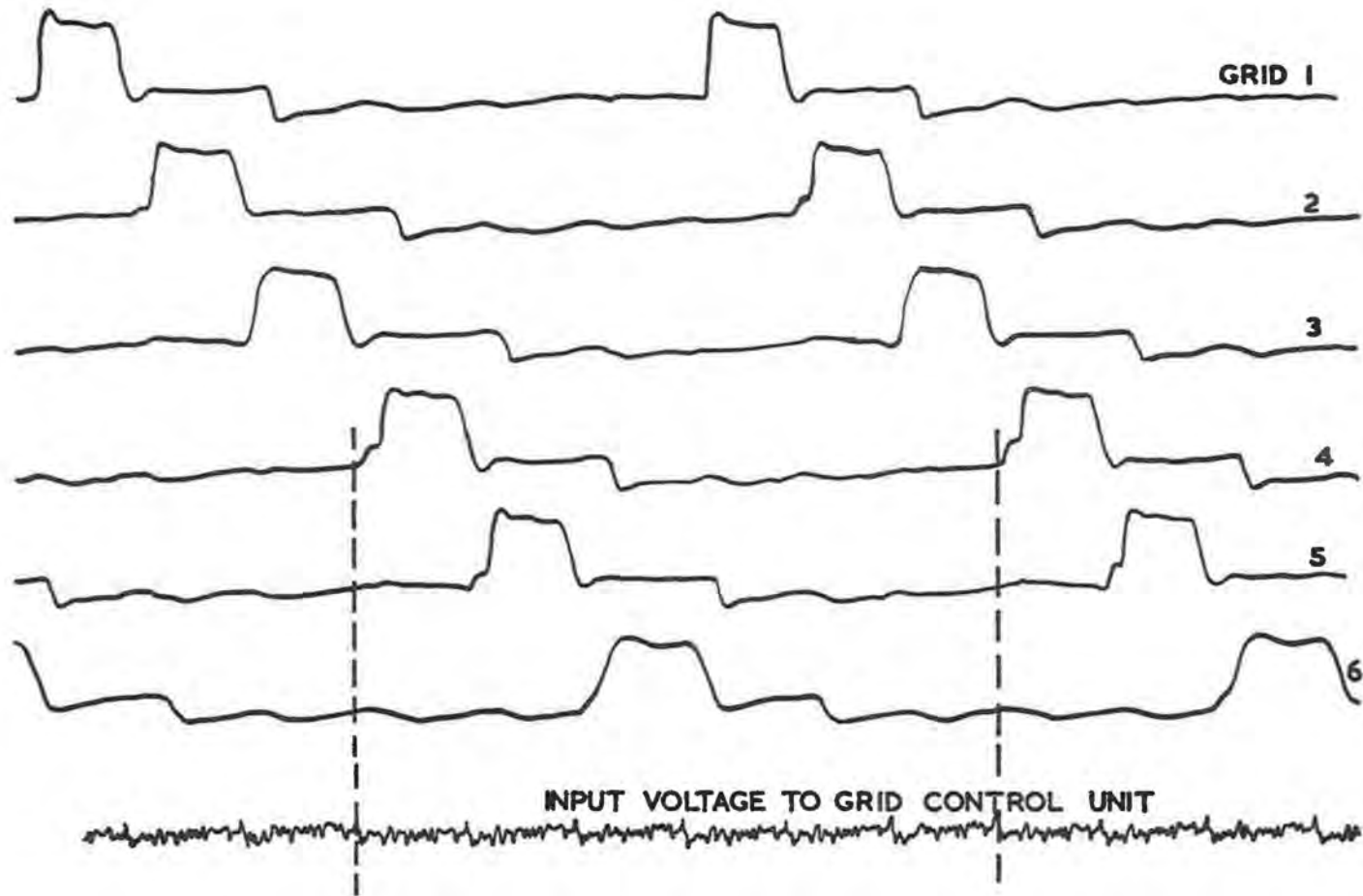


Fig. 5.3.2 (xii) Step on Grid Impulses with Capacitor Connected to Power Supply Negative Terminal

The second harmonic (approximately 100 c/s) was reduced to the value of 65 V peak to peak from a value of approximately 230 V peak to peak. Tests carried out to investigate the cause of the large 2nd harmonic, showed that this was due to a presence of this harmonic in the d.c. input voltage of the grid control units. It was found that this was being generated in the current compensation circuit (see Fig.5.3.2(v)) due to the action of the d.c. current transformers supplying this circuit. By connecting a 1,000 μ F capacitor across the circuit the reduction in ripple in the power supply output voltage was obtained. It is felt that inherent inaccuracies of approximately 2% between the impulses of the grid control units largely account for the remaining low frequency harmonics.

(d) Flat Top Slope Control

To enable experiments to be carried out in the beam path of the synchrotron, it is necessary to control the rate of change of the flux during flat top to move the beam radially inwards, or outwards, on to targets. This involves being able to control the slope of magnet current during flat top, and is achieved by a preset variable component in the input voltage to the grid impulse generating units associated with the odd numbered groups of invertors. See Fig. 5.3.2(v). By this means the degree of inversion of these groups is controlled, so that the nett d.c. voltage applied to the magnet is either just sufficient to overcome the circuit IR drop (true flat top), or is more negative or more positive than this value to give negative or positive flat top slopes as required.

A similar control to that explained above is included to control the slope of the injection platform, so as to obtain the precise magnet field level required for injection of protons into the synchrotron.

The flat top slopes possible for 100%, 90% and 80% voltage operation are given in Table 5.3.2(II).

(e) Protection Circuits

For the sake of completeness a summary of the main protection devices on the convertor plant is given, although the detailed commissioning tests carried out on these devices will not be included.

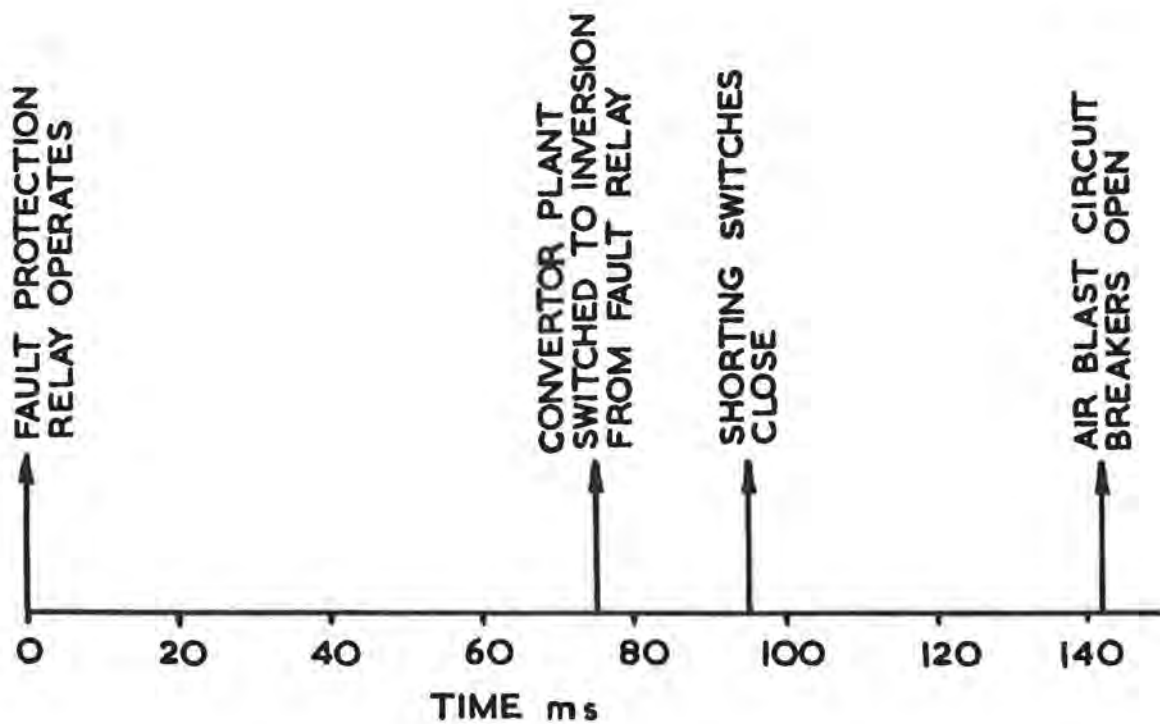
The primary protection on the plant, which operates in the event of a serious fault or overload, comprises two air blast circuit breakers which isolate the convertor plant from the source of a.c. power, and two air operated high speed magnet shorting switches. These items and their position in the power circuit are indicated in Fig.5.1(i). In addition, in the event of a fault, all the convertor groups are switched to full inversion. The order of operation of the primary protection is as follows:-

- (i) All convertors switched to full inversion.
- (ii) Magnet short circuiting switches close.
- (iii) Air blast circuit breakers open.

The times between the inception of a fault and operation of the protection have been measured from an oscillograph and are as indicated on Fig. 5.3.2(xiii).

TABLE 5.3.2(II) MAGNET CURRENT FLAT TOP SLOPES

Alternator Voltage	Magnet Current At Start of Flat Top	Slope Control Regulator Setting	Slope (amps/second)
100%	10,000 A	0	-650
"	"	20	0
"	"	45	+610
"	9,180 A	0	-500
"	"	25	0
"	"	45	+680
"	7,500 A	0	-330
"	"	20	0
"	"	30	+200
"	"	40	+400
"	5,000 A	0	-110
"	"	13	0
"	"	20	+110
"	"	25	+140
"	"	30	+225
"	3,000 A	0	-70
"	"	3	0
"	"	10	+70
"	"	15	+140
"	"	17	+170
"	"	20	+200
90%	9,700 A	0	-820
"	"	37	0
"	"	50	+280
"	9,100 A	0	-800
"	"	20	-140
"	"	37	0
"	7,500 A	0	-440
"	"	32	0
"	"	50	+210
"	5,000 A	0	-240
"	"	20	0
"	"	35	+150
"	"	40	+180
"	3,000 A	0	-90
"	"	10	0
"	"	20	+90
"	"	25	+120
80%	9,150 A	0	0
"	"	20	+380
"	"	25	+530
"	7,300 A	0	-90
"	"	8	0
"	"	30	+380
"	5,100 A	0	-80
"	"	5	0
"	"	30	+225
"	3,000 A	0	-45
"	"	15	+70
"	"	20	+125



Note: It is important that the convertors are switched into inversion before the shorting switches close. Switch into inversion normally takes place via an electronic circuit within a few milliseconds of a protective relay operating. But in the event of failure of this circuit, back up protection is provided via an impulse choke connected across the shorting switch operating coils. The oscillogram from which the times indicated above were taken was a case where switching into inversion was from the back up circuit to prove that this was satisfactory.

Fig. 5. J. 2. (xiii) Sequence of Operation of Primary Protection

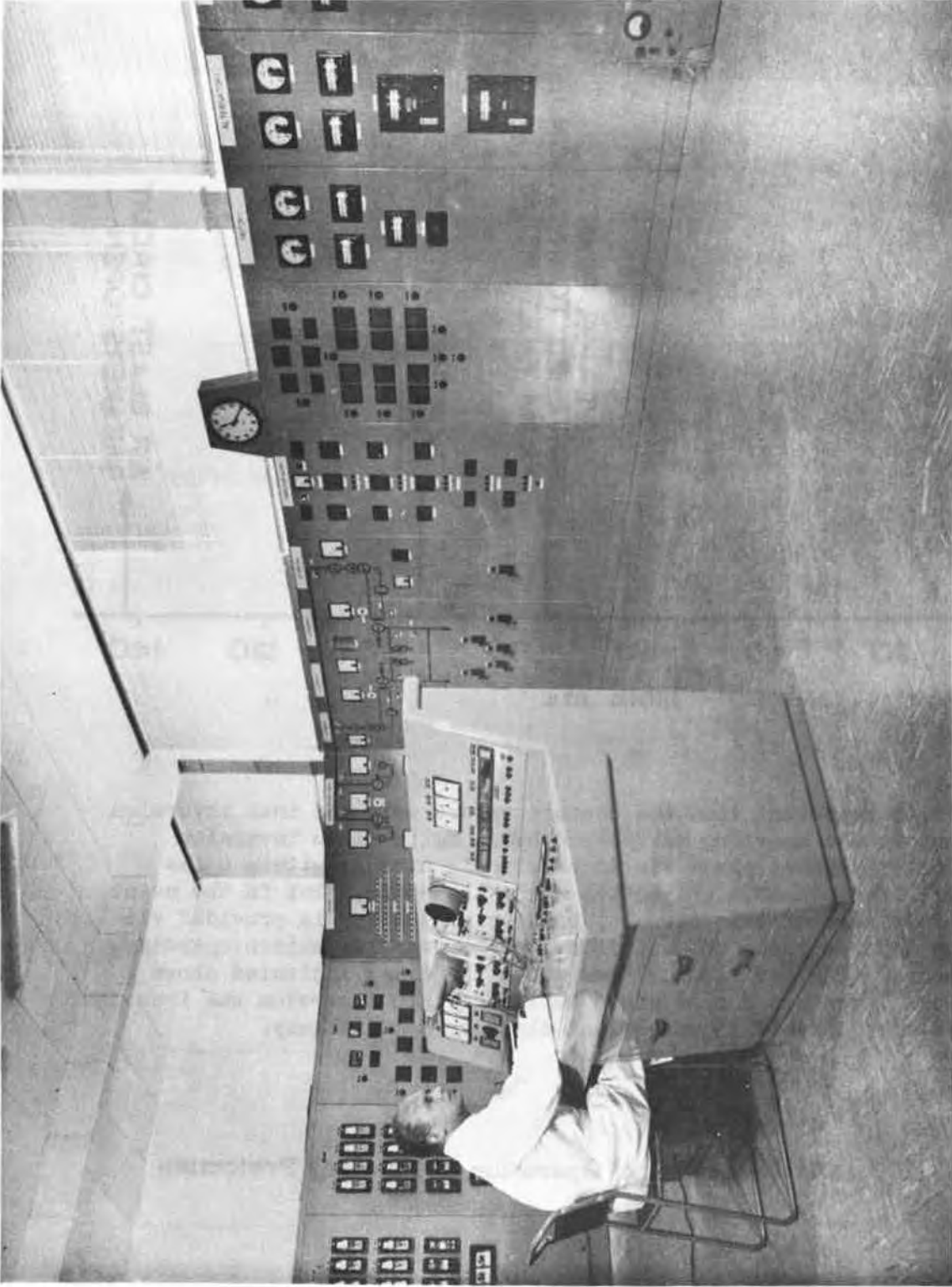


Fig. 5.3.3 (i) Power Supply Control Room

The main protection devices are:-

(i) Back Fire Protection:

In the event of reversal of current a biased off impulse choke in each anode connection provides an impulse which operates a multivibrator to operate the primary protection.

(ii) Arc Through Protection:

A transformer connected from cathode to neutral of each convertor group responds to the large voltage swing in the event of an arc through of any anode of the group. The secondary voltage is connected to a half wave rectifier and the output is applied to a multivibrator circuit, to operate the primary protection. Half wave rectification of the transformer voltage makes the circuit direction sensitive, and it only responds to an arc through from inversion to rectification - not from rectification to inversion. This is a modification incorporated during commissioning. The protection is automatically suppressed below approximately 1000 A and is switched in at this level of magnet current by an impulse choke in the main d.c. busbar. This suppression is required to prevent operation when changing from inversion to rectification at the end of the injection platform. The original arc through protection circuit was not direction sensitive and each time the master timer sent out an impulse to switch the plant to inversion a second impulse was required to operate an electronic circuit to suppress the arc through protection circuit. By modifying the circuit to make it direction sensitive it was possible to delete the protection suppression feature and to simplify the overall circuit.

(iii) D.C. Overcurrent Protection:

The output from d.c. current transformers in each of the series groups of convertors is fed to a biased off multivibrator circuit which can be adjusted to operate at different input levels. There is one multivibrator circuit for each half of the plant and the circuit is so arranged that an overload in any series group will cause the protection to operate.

(iv) Transformer Protection:

A conventional relay in the primary supply to each transformer gives protection against short circuit and overload faults. There is an element in each phase of the supply with time delay and instantaneous settings.

(v) Magnet Overvoltage:

Spark gaps are connected across magnet octants and to earth as indicated in Fig. 5.1(i). In the event of a gap breakdown the fault current causes an output pulse from bi-directional impulse chokes to operate a multivibrator circuit, which in turn operates the primary protection.

(vi) Magnet Earth Leakage:

In the event of an earth fault, a conventional relay operates the primary protection (see Fig. 5.1(i)).

5.3.3. Further Work

Although the initial commissioning tests on the convertor plant had been completed by the end of 1962 there remained a considerable amount of work to be done. Some of the more interesting work then outstanding is summarised here:-

(a) Reduction of Backfire Rate

The backfire rate on the plant was excessive and unacceptable. It was thought that the cause of the backfires was known and further tests were to be carried out by the manufacturers to overcome this trouble. It was considered preferable to delay issuing further details until investigations were completed. The extent of this problem was not fully appreciated until early 1963 after prolonged pulsing periods became available.

(b) Platform and Flat Top Slope Controls

At that time the controls for flat top slope and injection platform slope were to some extent interdependent. Work was proceeding to separate these two controls.

(c) Grid Control Units

The grid control units are standard items of equipment as used on normal industrial installations. For this particular plant extremely precise grid units are desirable, as will be appreciated from what has already been said relative to the problems of load sharing during flat top, saturation of interphase transformers, and low frequency ripple in the d.c. output voltage. Further work was programmed to improve the accuracy of the grid units.

The existing grid control units were not satisfactory from the point of view of access to component parts. Also it was very desirable that the grid control circuits generally should be at earth potential to allow adjustments and checks to be made during plant operation. The possibility of modifying the grid control arrangements to enable this improvement to be incorporated was under consideration.

(d) Modification to Flat Top Voltage Characteristic

It had been found that at the commencement of flat top a re-distribution of the magnet flux takes place which reduces the flux level over the effective part of the magnet octants. This problem is dealt with in more detail in section 4.7.2. Thus at the start of flat top the magnet flux drops to a lower level, and consideration is being given to a modification to the grid control circuits of the convertor plant to produce a d.c. voltage transient to counteract this effect.

REFERENCES FOR SECTION 5

1. Magnet Power Supply for the 7 GeV Proton Synchrotron 'Nimrod':
 - Part 1 General
 - Part 2 Rotating Machines
 - Part 3 Mercury Arc Convertors } Proceedings I.E.E.
Vol 110, No. 3, March 1963.
2. Bevatron Engineering Note No. 7302-04 M39 dated 25th March, 1959.
"Notch Brittleness Tests on Generator Shafts".
3. Bevatron Engineering Note No. 7302-04 M38 dated 3rd March, 1959.
"Review of Generator Shaft Ultrasonic Survey Results".
4. "Application of the Griffith-Irwin Theory of Crack Propagation to the
Bursting Behaviour of Discs including Analytical and Experimental
Studies" by D. H. Winne and B. M. Wundt.
Pages 1643-1658, Transactions of A.S.M.E., Paper No. 57-A249,
Oct. 1957.

SECTION 6

R. F. SYSTEM

6.1. Introduction to the Synchrotron R.F. System

6.1.1. The energy necessary to raise the accepted protons from 15 MeV to 7 GeV will be provided by an accelerating voltage in a r.f. cavity mounted in a straight section. Protons will obtain an average increase in energy of 6 keV on each traversal of the cavity. The orbital frequency of the proton beam increases from 355 kc/s at injection to 2.02 Mc/s at an energy of 7 GeV. The r.f. frequency is four times the orbital frequency (harmonic number = 4) and a fraction of the injected protons will be trapped into four phase stable regions or bunches, each proton describing a synchrotron oscillation about the stable phase angle of the accelerating voltage. The harmonic number of 4 is a compromise figure involving the radial synchrotron oscillation amplitudes and the effect of the total energy spread in the oscillations on the trapping efficiency. Initially, the betatron and synchrotron oscillations of some of the protons will occupy the entire vacuum chamber. Although these oscillations will reduce in amplitude as acceleration proceeds, it is important that the mean radial position is held near the centre of the vacuum chamber (R_0), or at whatever controlled deviation may be required.

6.1.2. During acceleration the magnet guide field rises from 290 gauss to 14 kilogauss and the frequency of the r.f. voltage from 1.41 Mc/s to 8.1 Mc/s. To maintain the correct radial position the frequency must follow accurately a given function of the magnetic field. Because successful acceleration depends on limited coherent phase motion, it will also be necessary to control the phase of the beam relative to the phase of the accelerating voltage.

6.1.3. A simplified block diagram of the planned system is given in Fig 6.1(i). The system will have four main sections:-

- (i) The high power r.f. equipment, providing the accelerating voltage.
- (ii) The low power r.f. equipment, or primary frequency generator (P.F.G.), providing an accurate and controllable frequency source for the high power r.f. system.
- (iii) The beam control system, providing a means of comparing the radial position and phase of the proton bunches with suitable reference values and of correcting any deviations via the P.F.G.
- (iv) The beam diagnostic system, giving the dimensions, positions and movement of the beam in the vacuum chamber at all times from injection to full energy.

6.1.4. A considerable amount of work has proceeded both on the beam control and diagnostic systems but, for clarity and the presentation of a coherent story, it has been found convenient to defer the account of this work to the second part of this report where a description of the use of the systems during commissioning can be included. This account concentrates on the details of the low and high power r.f. systems and the accelerating cavity.

6.1.5. The high power r.f. equipment is situated in straight section 8 in the magnet ring (Fig. 6.3.9). A pair of transmitter triodes supply r.f. power to the accelerating cavity (Figs. 6.3.1(i) and (ii)). The cavity is loaded with ferrite to allow tuning

over the required frequency range. Power losses in the ferrite have a peak value of 42 kW and the load due to the proton beam rises to 1.6 kW per 10^{12} protons at 7 GeV. Two series gaps in the cavity each develop 6 kV peak r.f. voltage and at the normal magnet field rise rate of 20 kilogauss/s, the synchronous phase angle is 150° .

6.1.6. The power triodes are driven from a drive chain with an input of about 2 V r.m.s. at an impedance of 100Ω derived from the P.F.G. The cavity is tuned to the accelerating frequency by means of a bias winding around the ferrite carrying up to 900 A peak from a special bias power supply. There are two alternative bias supply systems available; one (thermionic) was developed during the early design stages, the second (using high power transistors) was developed later and will normally be used in the system since it has considerably greater frequency response. The amplitude of the accelerating voltage at the cavity gaps is controlled by means of an automatic level control (A.L.C.) loop by which the accelerating voltage is maintained equal to a voltage analogue of the rate of rise of the magnetic guide field (\dot{B}), thus keeping the synchronous phase angle constant.

6.1.7. The low power r.f. (P.F.G.) is situated in the Nimrod main control room. It supplies a low level c.w. signal of accurately controlled frequency to the drive chain. Coarse control is arranged as follows:

- (a) The magnet field rise rate (\dot{B}) is measured by a pick-up loop in the magnet field.
- (b) The pick-up loop output is integrated (giving a voltage analogue to B) and used to control the bias current on the ferrite core of a r. f. oscillator coil. The relationship between the oscillator frequency and the bias current is arranged to be very close to the law relating orbital frequency and guide field.

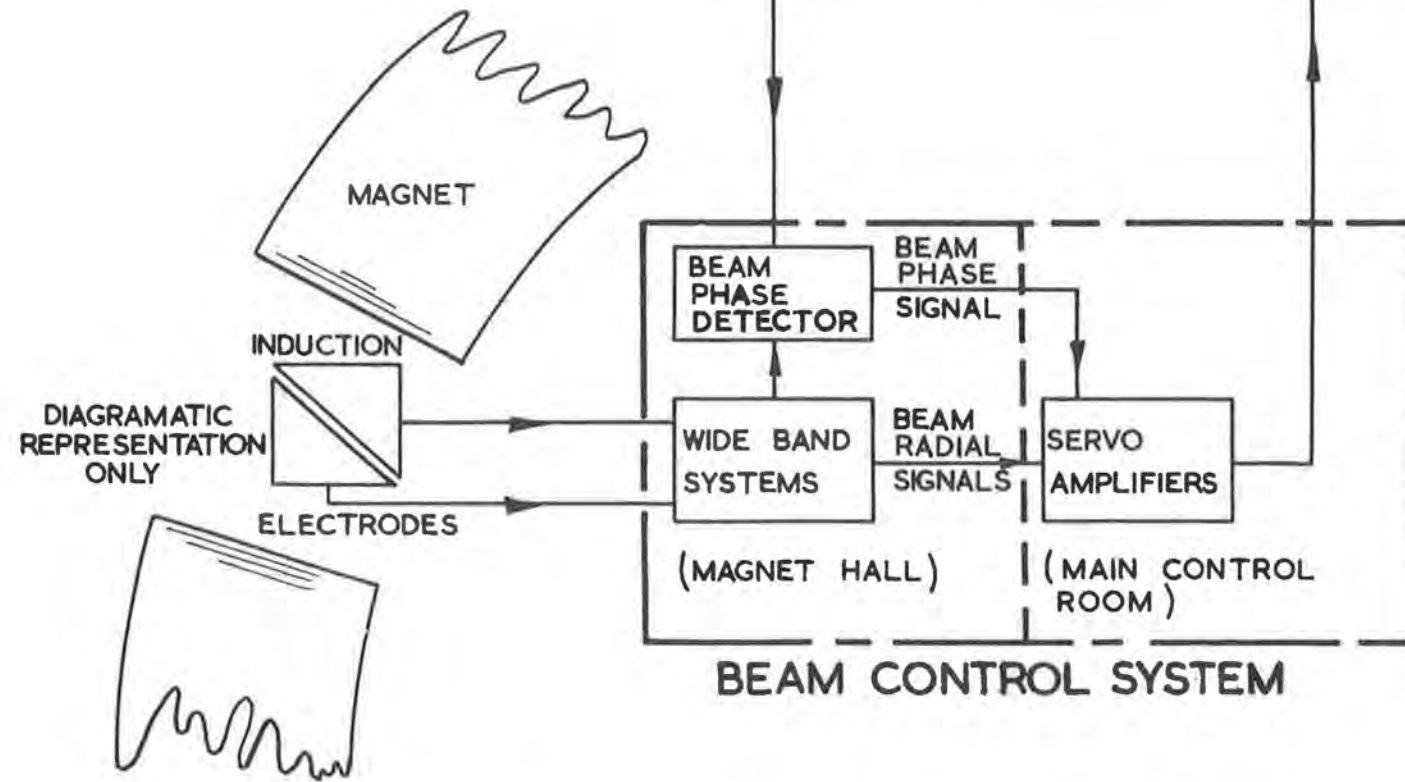
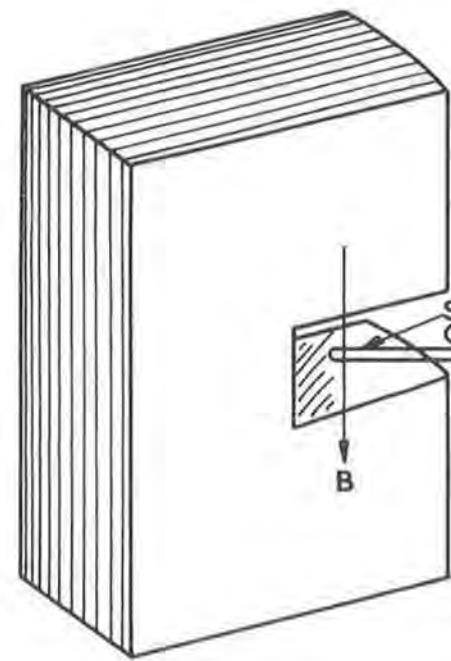
Fine control is obtained by regulating the voltage across two variable capacity diodes in parallel with the oscillator tuned circuit. The oscillator output is fed through an amplifier and gate to the drive chain. The P.F.G. has a voltage function generator, the curve corrector, which can correct the oscillator frequency through several hundred kilocycles at fixed intervals of magnet field. Thus the frequency law and the radial position of the beam can be set to close limits. The frequency at injection is accurate to ± 300 c/s.

6.1.8. The P.F.G. is also a source of timing pulses for many other machine functions. The B and \dot{B} signals generate these pulses which are thus related directly to the magnet field and hence to the proton energy in the machine. Time delayed pulses are also available for injector timing signals and for functions such as target programmes during magnet 'flat top'. The \dot{B} signal is also available for controlling the cavity voltage via the A.L.C. loop of the drive chain.

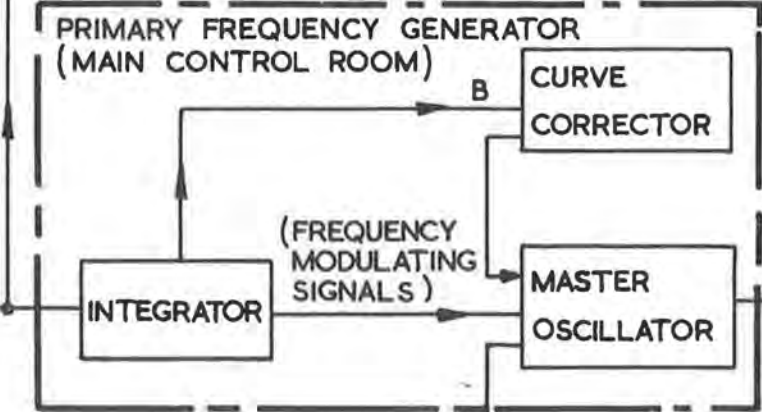
6.1.9. Besides providing open loop control of the accelerator frequency, via the curve corrector, the P.F.G. will also be an essential part of the beam control system. The radial and vertical position of the beam will be measured by means of induction electrodes through which the protons circulate. The radial electrodes will be slit diagonally (Fig 6.5.2(ii)) so that the voltages induced on the two halves will be equal when the beam is at R_0 . The sum of the two voltages will be a measure of beam intensity and their difference divided by their sum will give the radial position. The radial signal will be compared with a reference voltage, the error signal being fed (via a low pass network) to the variable capacity diodes in the P.F.G.

6.1.10. Phase Control will also be via the P.F.G. A beam phase detector will compare the phase of a signal induced on an induction electrode with the phase of the r.f. cavity voltage.

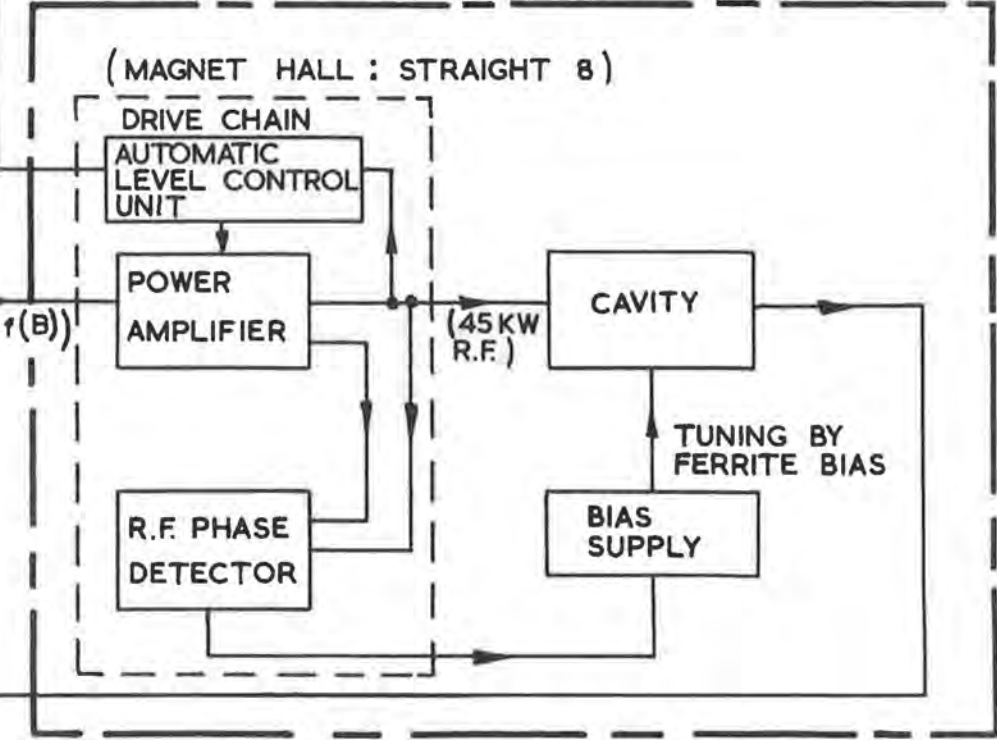
DIAGRAMATIC REPRESENTATION OF MAGNET AND SEARCH COIL (IN PRACTICE THIS COIL EXTENDS OVER WHOLE MAGNET RING)



LOW POWER R.F. SYSTEM



HIGH POWER R.F. SYSTEM



FOR POWER AMPLIFIER, CAVITY AND BIAS SUPPLY
(MAGNET HALL : CAVERN 8 B)

COOLING SYSTEM

BEAM CONTROL SYSTEM

Figure 6.1(i) Simplified block diagram showing the principle of the planned r.f. accelerating system.

6.1.11. The two control loops will be gated independently. The radial loop should ensure consistent operation of the r.f. system without recourse to much adjustment of frequency via the curve corrector. The phase loop should damp coherent synchrotron oscillations induced by magnet ripple, and r.f. voltage and frequency errors.

6.1.12. Signals proportional to the magnitude, radial position, vertical position and phase of the beam are essential in tracing faults and adjusting many of the machine parameters. They will be used in combination with signals from diagnostic probes which will take the form of targets made of metal (for charge collection) or plastic scintillator. The induction electrode signals obtained with chopped injected beams will be particularly useful for the measurement of radial betatron oscillations during injection and vertical oscillations, if they exist. The diagnostic probes will be positioned at ten points around the machine (see part 2 of the Nimrod report). They will be accurately located by means of remotely controlled position servos. They will be useful for emittance and energy spectrum measurements on the injected beam and for closed orbit studies. For more direct observation of the beam, it is planned to use transparent grids made of fine wire coated with fluorescent material. These grids can be swung diagonally across the vacuum chamber behind windows in each octant. They will be controlled remotely and will be viewed through the windows by a closed circuit television system which will display all the grids simultaneously on a split field tube.

6.1.13. Assessment of changes in machine parameters may involve the simultaneous measurement of a number of quantities such as beam intensity, radial position, magnet field or accelerating voltage and frequency. The usual methods of oscilloscope measurement are inadequate in many instances for these requirements. A data recording system is therefore being developed which can handle six channels of voltage analogue information, each at a rate of 1000 readings/s. Read out will be either by means of punched paper tape which can be fed into a teleprinter or direct to an on-line computer.

6.2. Low Power R.F. System

6.2.1. Introduction

The purpose of the low power r.f. system (N.B. the "heart" of the system is often referred to as the primary frequency generator or P.F.G.) is to produce a r.f. voltage whose frequency is related to the guide field of the magnet as shown in Fig. 6.2.1(i).

The required performance can be considered under four headings:-

- (a) Frequency stability at injection,
- (b) Frequency tracking,
- (c) Frequency stability at full energy and
- (d) Frequency deviation noise.

The development took place in three stages: first, a system using thermionic valve circuitry throughout; second, a system using valves in the r.f. and d.c. amplifier circuits and transistors in the ancillary control circuits, and finally, using transistor circuitry throughout. Comparing the first and last systems, the volume has decreased from five racks of equipment to two, and the power consumption from over 1 kW to less than 90 W. Each stage of development improved the performance. The "perfect" switch action of transistors and the general lower impedance level resulted in circuits that were more stable and less sensitive to outside interference.

6.2.2. Description of System

A schematic diagram of the system is shown in Fig. 6.2.2(i).

A voltage proportional to the rate of rise of the magnet field is produced by a pick up loop in the magnet gap and this is integrated to produce a voltage proportional to the magnet guide field. The integrator is controlled by signals derived from the magnet power supply and from a peaking strip which determines the constant of integration.

The oscillator is a permeability tuned Colpitts oscillator, with a frequency range of 1.4 to 8 Mc/s, obtained by varying the incremental permeability of the ferrite inductance using a polarizing current of 4 A maximum. The output voltage of the integrator (30 V maximum) is converted into a current (4 A maximum) by means of the voltage to current converter.

The tracking law of frequency against magnetic field is chiefly derived from the design of the oscillator tank circuit and small deviations are corrected by means of an arbitrary function generator controlled by the magnet field. When the synchrotron is finally operational it is probable that this function generator will be replaced by a voltage derived from measurements of the radial beam position.

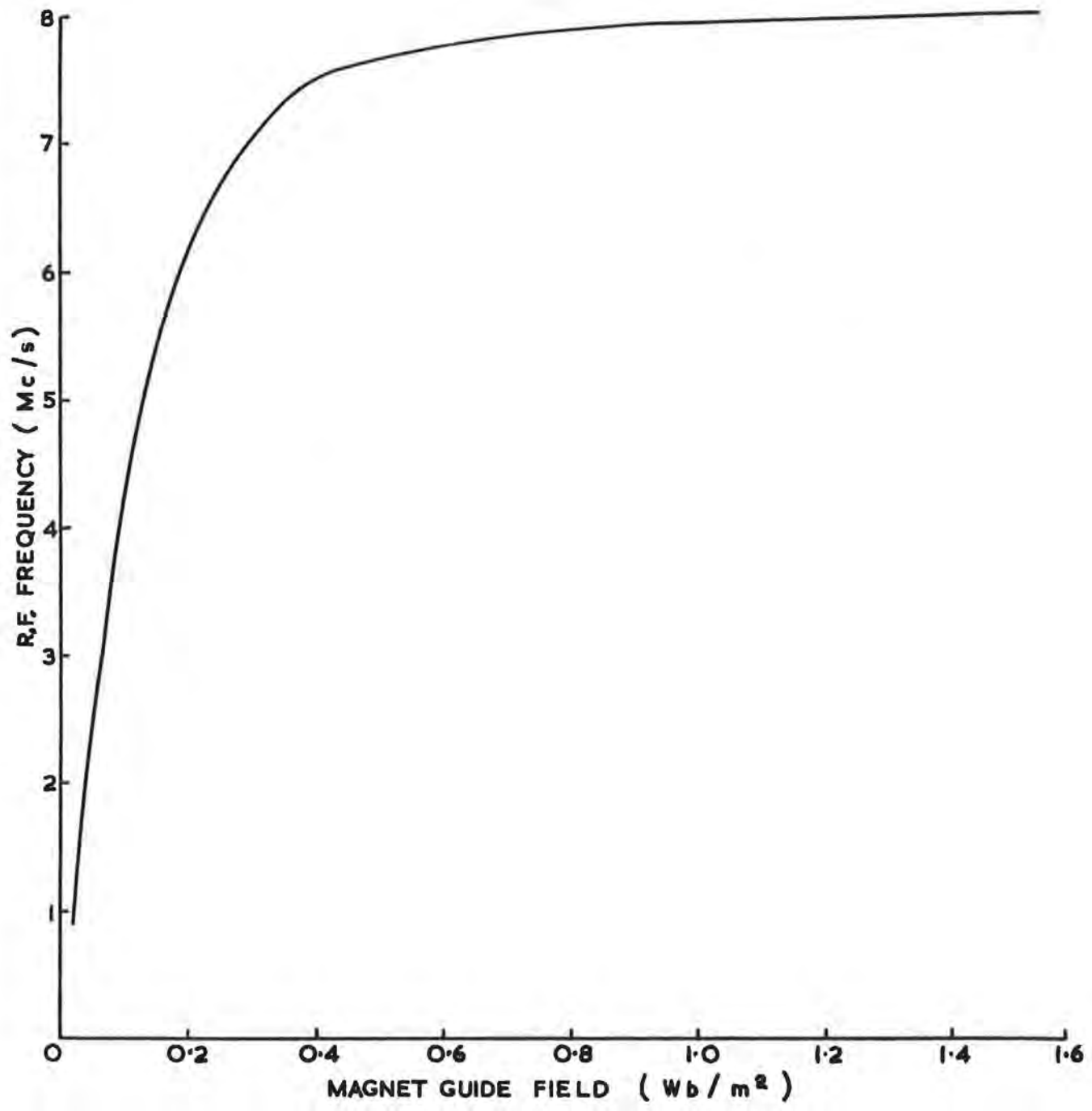


Fig. 6.2.1(i) Relationship of r.f. frequency to magnet guide field.

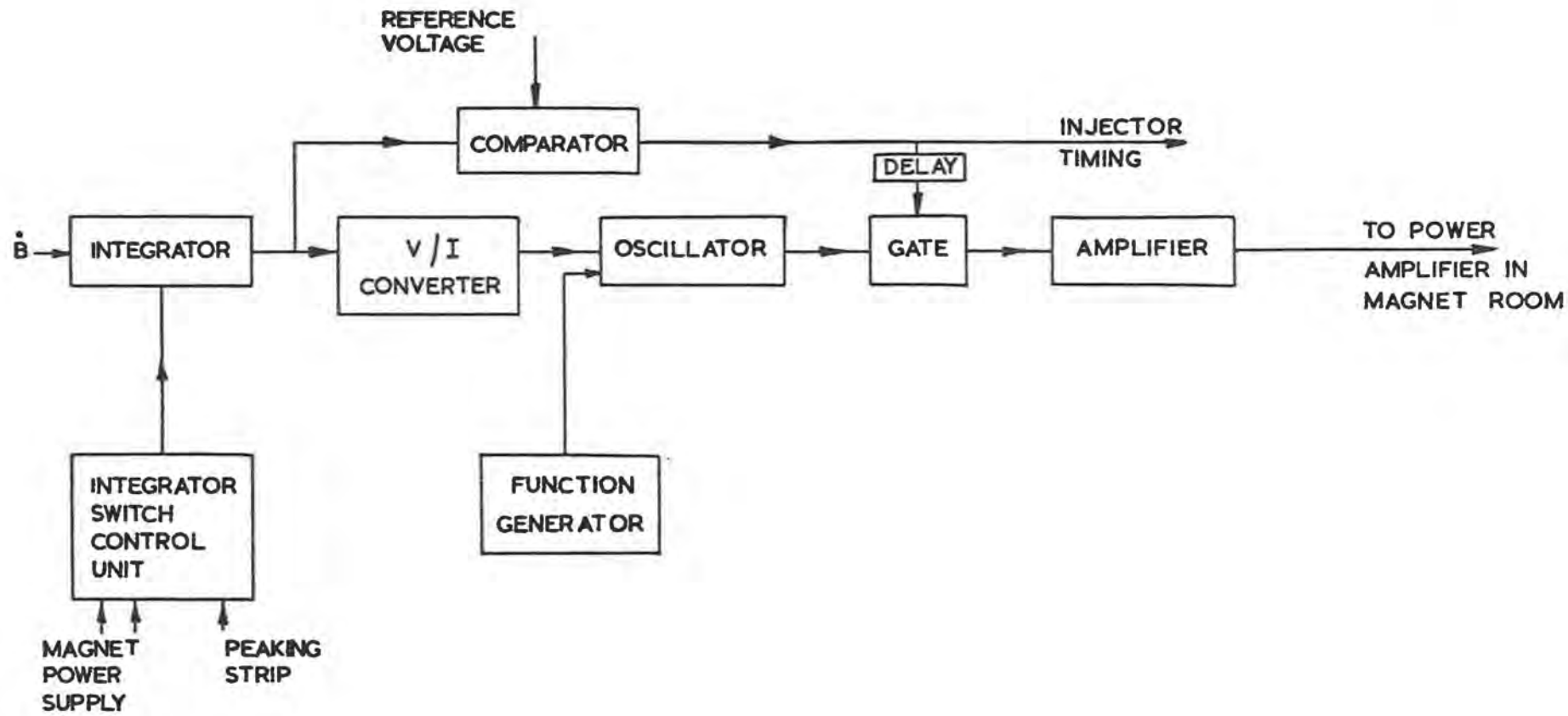


Fig. 6.2.2(i) Schematic diagram of low power r.f. system.

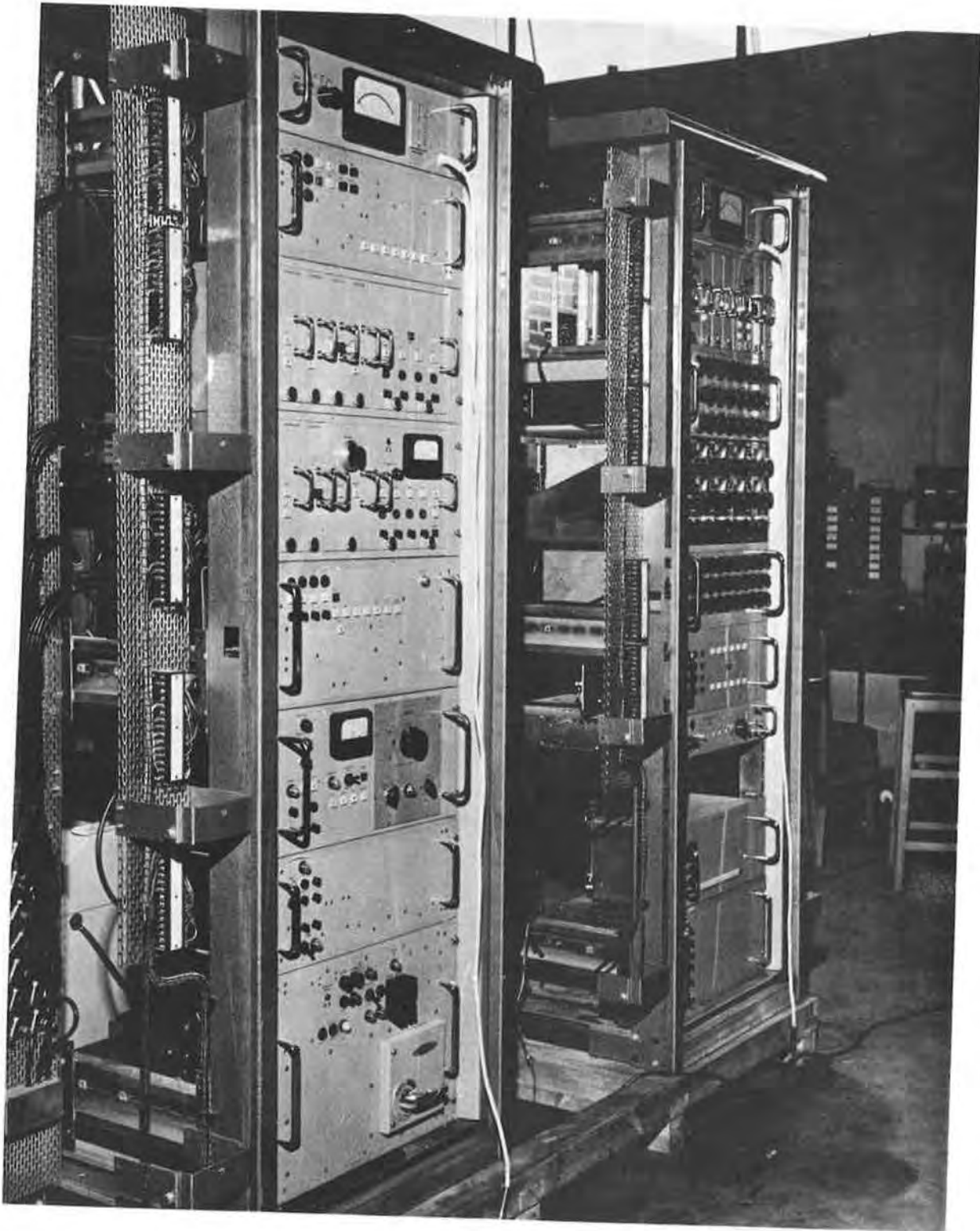


Fig. 6.2.3(i) Front view of low power r.f. units.

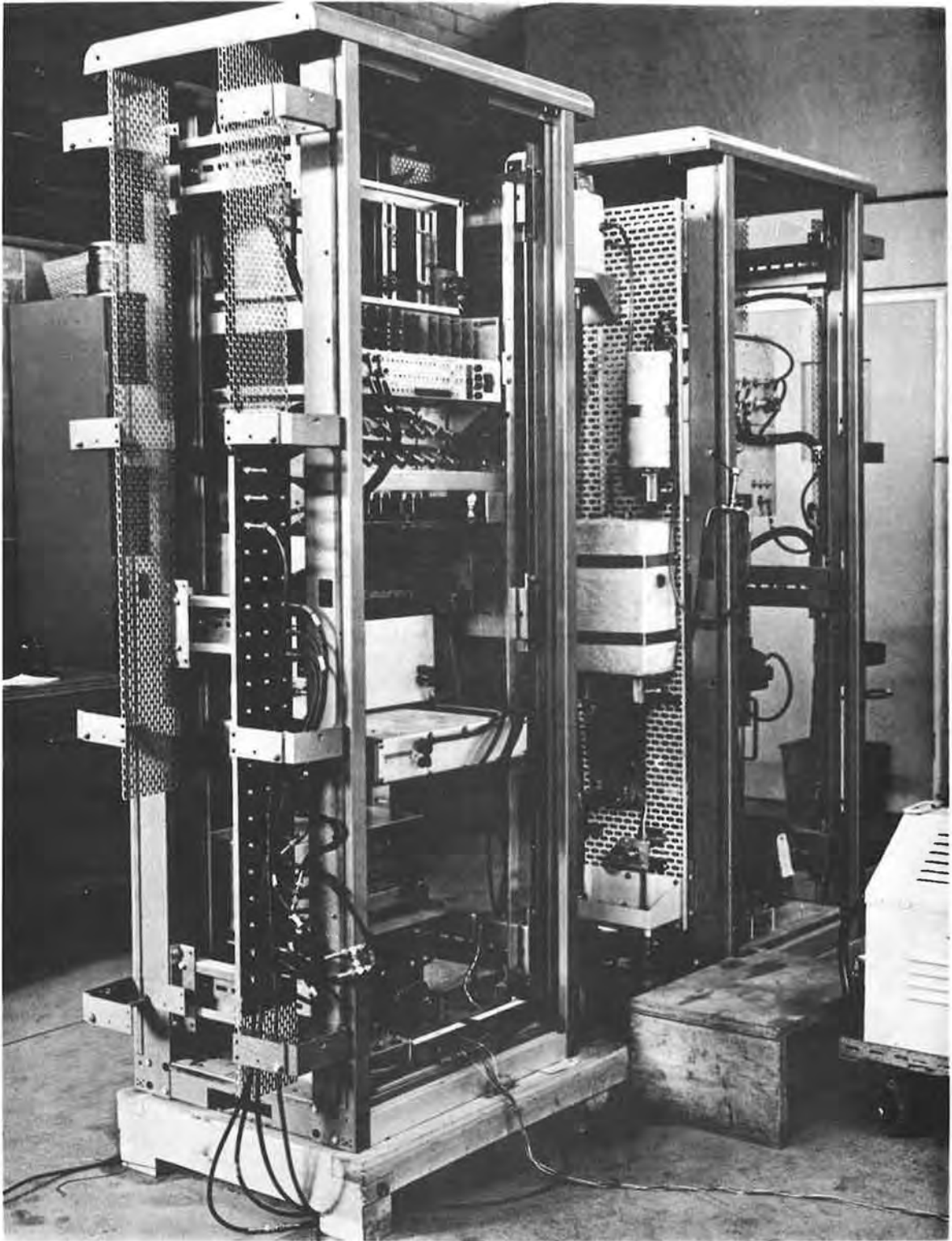


Fig. 6.2.3(ii) Rear view of low power r.f. units.

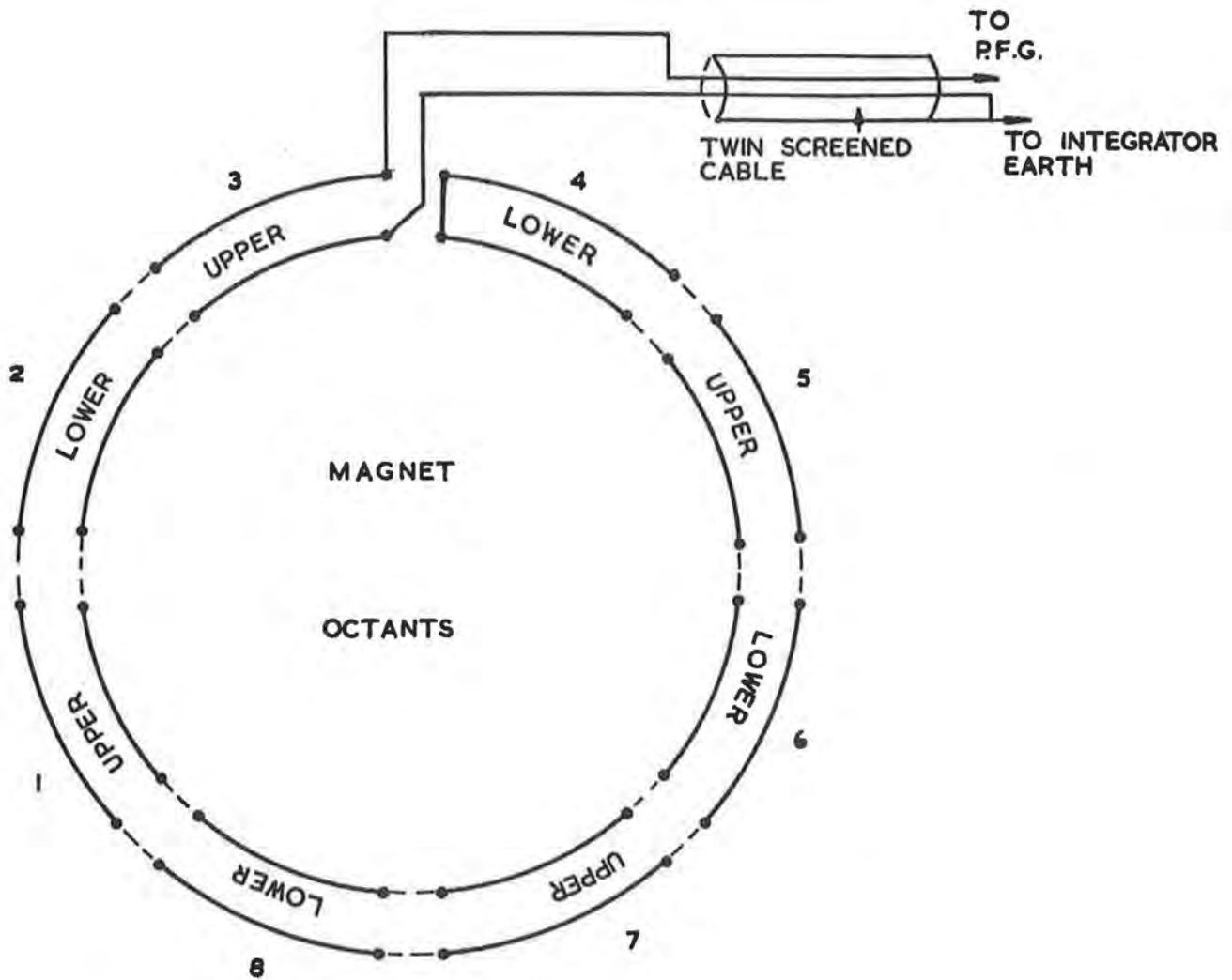


Fig. 6.2.3(iii) Schematic layout of pick up loop.

The peaking strip signal is obtained when the magnet field is approximately 160 gauss and the accelerating voltage has to be switched on at approximately 280 gauss. This delay is introduced by feeding the integrator output into a comparator, which produces an output pulse when the input voltage is equal to a reference voltage. This comparator could also be used for triggering the injector by an appropriate choice of reference voltage and a further delay introduced between this signal and the gate opening signal.

6.2.3. Component Circuits

Figs. 6.2.3(i) and 6.2.3(ii) show the general constructional methods used for the units. Emphasis has been placed on "in situ" accessibility rather than on compactness.

(a) Pick up loop.

The pick up loop, Fig. 6.2.3(iii) encloses approximately the central third of the magnet aperture, radially. There is one section in each octant, with windings alternately in the upper and lower pole face to measure the average field seen by the protons. The eight sections are connected in series to give the correct level for optimising drift in the integrator.

(b) Integrator unit

This unit, Fig. 6.2.3(iv), is designed around a d.c. amplifier with the addition of an output stage (shown inside dotted lines) to increase the output voltage swing from ± 6 V to ± 30 V. The second amplifier in the unit is used for monitoring.

The voltage from the pick-up loop enters the unit by a screened twin feeder. One side of the loop is taken to the signal earth of the d.c. amplifier, which acts as the earth reference of the pick-up loop; the live side of the loop is fed to a potential divider, which is used to adjust the scale factor of the integrator.

The amplifier summing resistor is split into two parts, the centre of which is connected to an electronic switch to control the application of the pick-up voltage. The integrating condenser is a plastic foil type. As the current in the magnet coils falls, this condenser is discharged by RL and the contact on RL1. For test purposes the pick-up voltage can be simulated by a fixed voltage derived from the Zener diodes MR1 and MR2.

(c) Integrator switch control unit

The unit, Fig. 6.2.3(v), controls the integrator on receipt of three input pulses, P_1 , P_2 and P_3 . These are derived at the following times: P_1 - just before the magnet field starts to rise; P_2 - at a precise value of magnet field (approximately 160 gauss) just before the field corresponding to injection; P_3 - after acceleration, at the end of the magnet flat top. Pulses P_1 and P_3 are supplied by the magnet power supply control system and P_2 from a peaking strip.

There are two parts to the unit, the first, J1 to J4 controlling the relays RL1 (situated in the integrator unit) and RLC (situated in the V/I converter unit); the second, J5 to J8 controlling the clamp MR7-10, which is applied to the junction of the summing resistors in the integrator unit.

J2 and J3 form a conventional bistable circuit, the windings of the above relays forming the collector loads of J2 and J3. The circuit is set and reset by J1 and J4. A positive pulse P₃ applied to J4 closes the relay contact RL1-1 which discharges the integrating capacitor; it also operates the relay contacts RLC-1 to change from the forward to the reverse bias condition of the ferrite core of the oscillator tank inductance. A positive pulse P₁ applied to J1 reverses the action, allowing the integrator to operate and changing the reverse bias back to forward bias (via the V/I converter).

J6 and J7 form a complementary bistable circuit set and reset by J5 and J8. A positive pulse P₃ applied to the primary winding T₃ results in the transistors J6 and J7 being cut off. Current flows from the positive supply rail via R27 and R25 through the bridge MR7-10 and then via R16 and R15 to the negative supply rail. This results in the output point SK16 being clamped to earth. The potentiometer RV1 is adjusted to eliminate mismatch between the diodes.

A positive pulse P₂ applied to J5 causes the transistors J6 and J7 to saturate and reverse biases the bridge diodes and so unclamps the output point, allowing the voltage from the pick-up winding to be applied to the integrator.

(d) V/I converter

The output from the integrator approximates to a sawtooth with 28 V corresponding to 14 kilogauss. The frequency modulation characteristic of the oscillator is such that this has to be converted into a sawtooth of current, with 4 A corresponding to 14 kilogauss.

The unit (Fig. 6.2.3(vi)) is designed round the same d.c. amplifier as used in the integrator. The high voltage output stage is, in this case, followed by an emitter follower J5 driving a pair of transistors J6, J7 connected in parallel. Resistors R31-40 are used to improve load sharing between the transistors. The load, which is the polarizing winding on the oscillator tank inductance, is shown in dotted lines. The current through the load is monitored by the 4 Ω resistor (also shown dotted) and the voltage across this is fed back to produce a stable, linear transfer characteristic.

To compensate for a slight non linearity in the initial frequency modulation law of the oscillator, the transfer characteristic of this unit is modified by the diodes MR1 and MR2 and their associated components.

The reverse bias potentiometer is set for approximately 30 mA of reverse current in the polarizing winding of the oscillator tank inductance to cancel the polarized memory left by the 4 A forward saturation current of the ferrite, which would increase with successive cycles. The forward bias control is set so that the r.f. "start" frequency is correct at injection magnet field.

(e) Oscillator and gated amplifier

The oscillator unit (Fig. 6.2.3(vii)) contains the oscillator transistor J1 and most of the frequency determining elements, all mounted in a brass cylinder through which oil is circulated at a constant temperature. The oscillator circuit is a common collector Colpitts circuit with inductors L3 and L4 (in parallel) and capacitors C6 and C7 as the principle components. L3 and L4 are each wound on a separate ferrite toroid with a common polarizing winding L5. The two r.f. windings are connected so that no r.f. voltage is induced in the polarizing winding. The final frequency and the shape of the frequency modulation characteristic at the knee are determined by the inductance L6 and variable capacitor VC1.

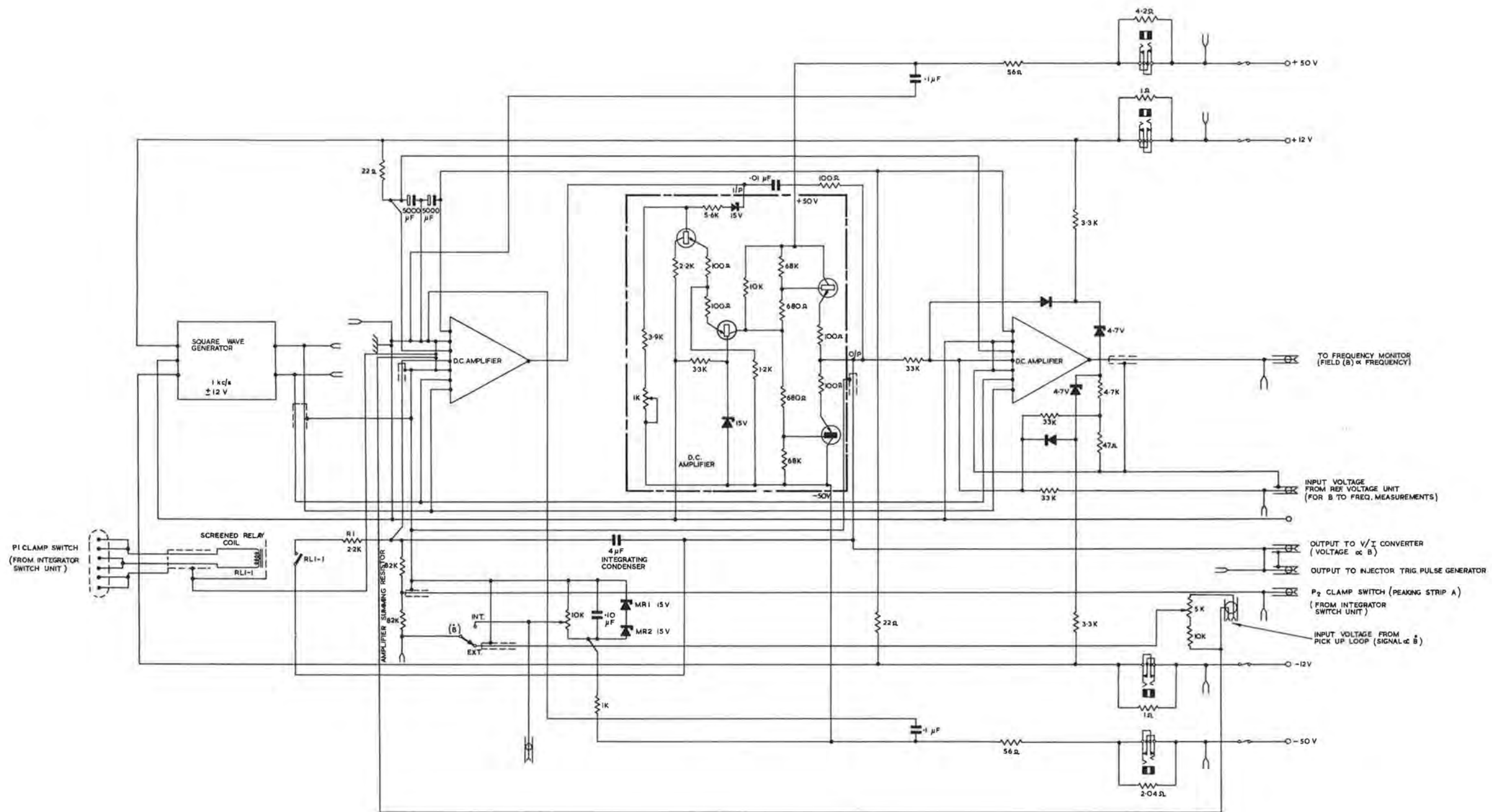


Fig. 6.2.3(iv) Circuit diagram of integrator.

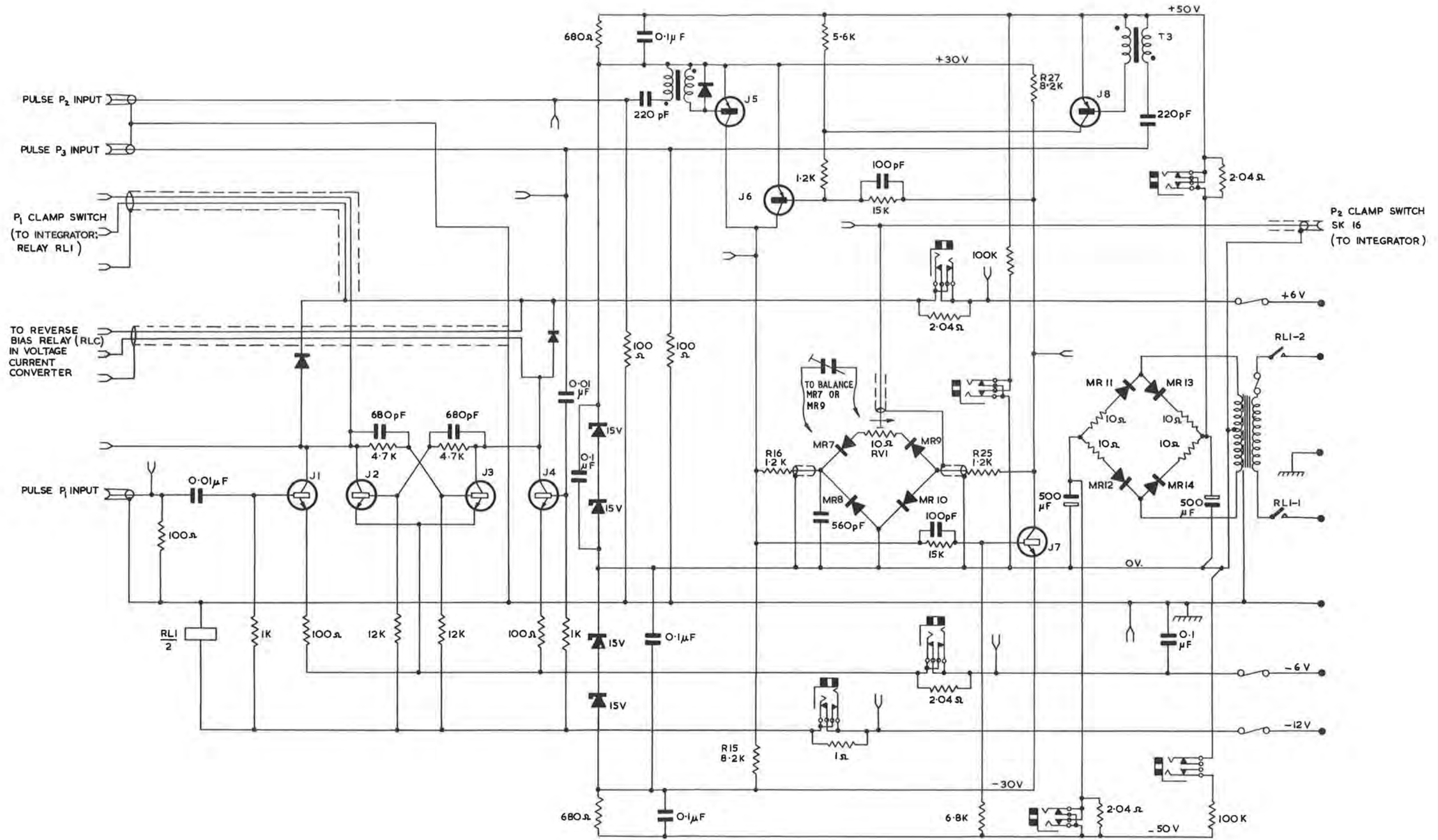


Fig. 6.2.3(v) Circuit diagram of integrator switch control unit.

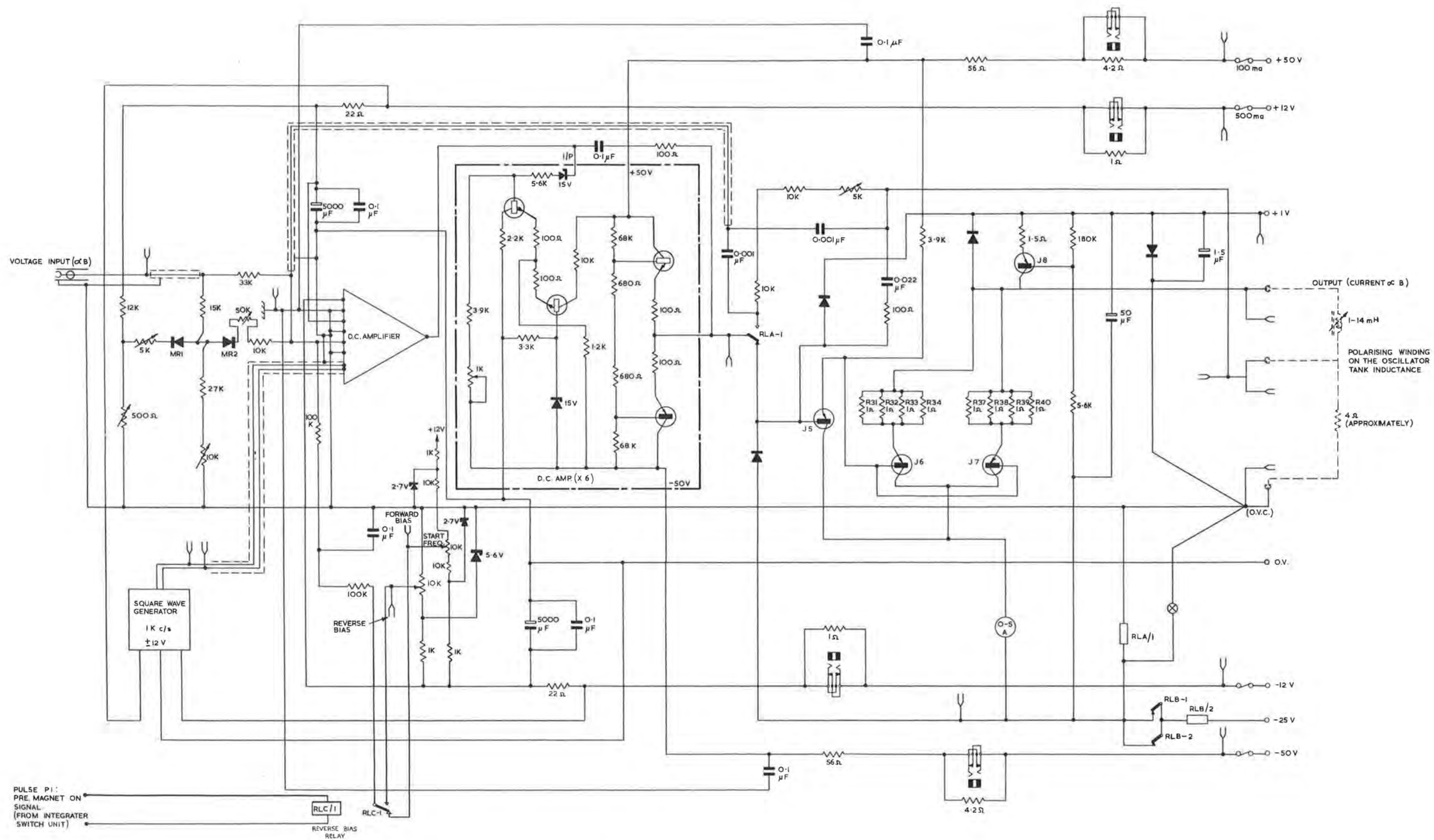


Fig. 6.2.3(vi) Circuit diagram of V/I converter.

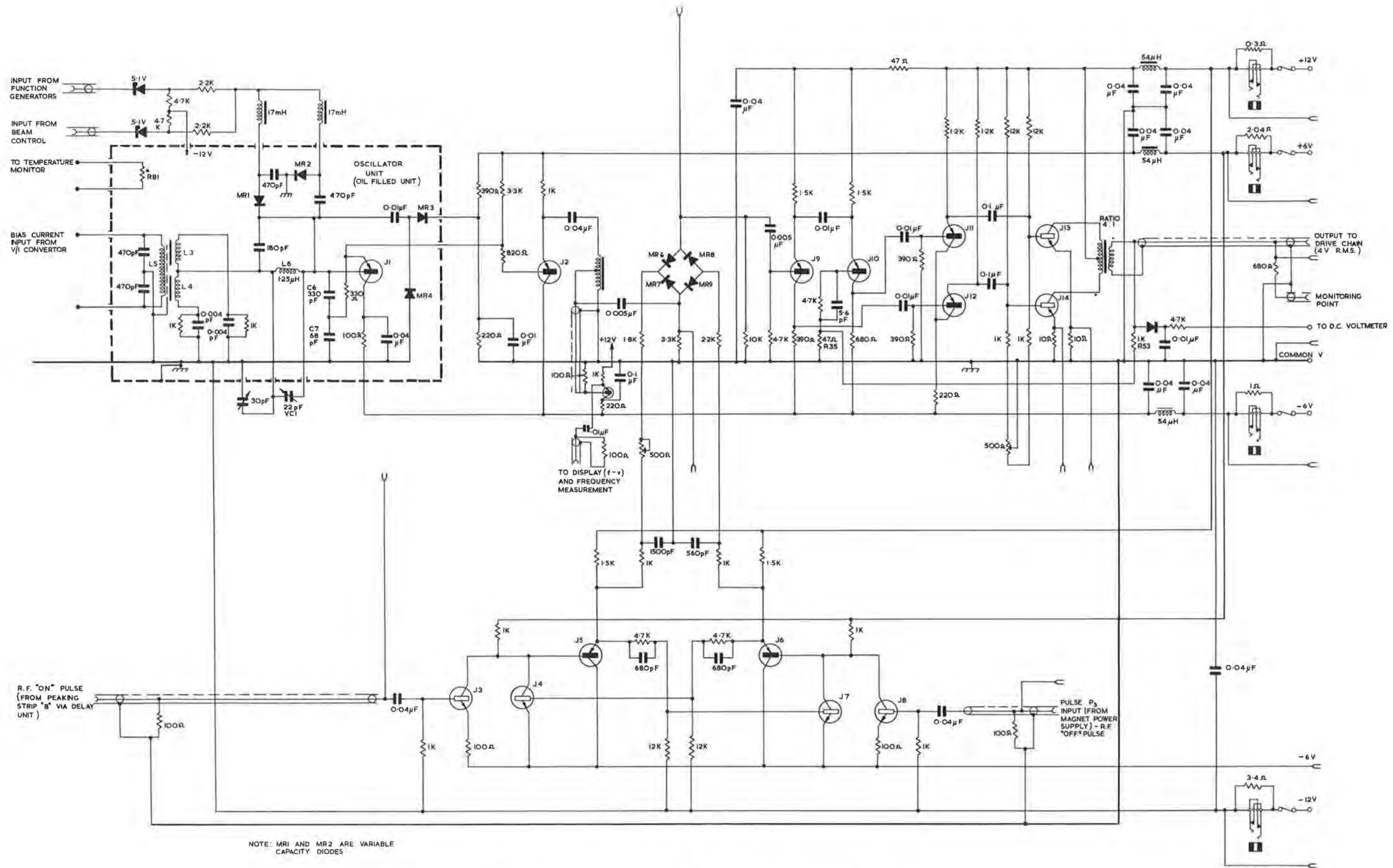


Fig. 6.2.3(vii) Circuit diagram of oscillator and gated amplifier.

Corrections to the frequency modulation characteristic are obtained by means of a voltage applied to the variable capacity diodes MR1 and MR2. The amplitude of the oscillator output is limited by the diodes MR3 and MR4. The oscillator is connected to the diode gate MR6 - 9 by the isolating emitter follower J2. The output from the gate is amplified and phase split by the emitter coupled amplifier J9 and J10 and applied to the output push pull pair J13 and J14 via emitter followers J11 and J12. The gain, stability and frequency response are improved by feedback via R53 and R35 to the base of J10.

The gate is controlled by the bistable circuit using transistors J3 to J8.

(f) Comparator

The comparator circuit is shown in Fig. 6.2.3(viii). The output from the integrator has a scale factor of 28 V representing 14 kilogauss. The delay to be introduced is approximately 100 gauss represented by 0.2 V. The integrator voltage is first amplified by a factor of 10 and then compared with a reference of 2 V derived from Zener diode MR6 and its associated potential divider.

The difference is amplified by the second d.c. amplifier which, having no feedback, produces a rapid transition from negative to positive saturation as the amplified integrator voltage passes through the reference voltage. The output is further sharpened by the complementary trigger circuit J1 and J2, and triggers the output blocking oscillator J3.

The performance of the comparator (also known as the injector trigger pulse generator) is described in detail elsewhere (5).

(g) Function generator (Curve corrector)

The function generator is discussed in general terms:

If a clock pulse train feeds an eight stage binary counter which (in turn) feeds a digital to analogue converter, then the first 256 pulses produce a staircase waveform with 256 steps at the output of the digital to analogue converter. After these 256 pulses, the counter is automatically changed from an "up" counter to a "down" counter, causing the output of the digital to analogue converter to decrease, again in 256 steps, to zero. The counter is then changed back to an "up" counter and the cycle repeated.

The resultant output waveform is marked (a) in Fig. 6.2.3(ix) where the steps are smoothed out. By taking outputs from both sides of the binary stages the interleaved waveform shown dotted is produced. The outputs during the periods T_1 , T_2 , T_3 etc. can each be independently adjusted to any value between $\pm A$ and therefore a function with the waveform marked (b) in Fig. 6.2.3(ix), can be generated.

The advantage of this method of generating a function by a series of triangles rather than linear sloping segments, is that any one of the function points can be adjusted without having to alter any of the adjacent points.

The above description, indicates an operation which will produce an output as a function of time. It can be converted to a function of magnetic field, B, by replacing the clock train by a train of pulses, each pulse corresponding to an equal increment of B. This pulse train is obtained from B by using a digital integrator with an output pulse for every increment of 0.4 gauss.

With this system, each segment of the function generator corresponding to 256 clock pulses is 102.4 gauss and the 20 segments in the generator correspond to 2.05 kilogauss. This does not cover a sufficient fraction of the 14 kilogauss increase in magnetic field but the fine steps of 100 gauss are needed at the start.

These limitations are overcome by feeding the magnet ΔB train into two binary dividers B_1 and B_2 , (Fig. 6.2.3(x)). The original input and the outputs from the two dividers are fed to gates G_1 , G_2 and G_3 , with a common output which is used as the new input train from the magnet.

Control waveforms are applied to the gates, such that G_1 is opened for say the first 6 segments, G_2 is opened for say the second 6 segments and G_3 is opened for the remaining segments. Under these conditions the interval for the first 6 segments will be 100 gauss, for the second 6 segments will be 200 gauss and for the last 7 will be 400 gauss.

6.2.4. Performance of System

Most attention is given to considerations of cycle to cycle jitter as this is much more troublesome than a gradual regular drift, which can be offset by an operator if the time between these adjustments is of the order of hours. A figure of 10% instability in beam current is regarded as an acceptable level.

Most of the measurements quoted have been taken under dynamic conditions corresponding to a standard machine pulse.

(a) Frequency stability at injection

At injection, when the aperture is "full" of particles, any frequency deviations will cause a loss of beam. It is uncertain at present, how the particles will be distributed in terms of betatron oscillation amplitude but a pessimistic assumption indicates that a 10% loss of particles will be produced by a frequency error of 0.05%. With a starting frequency of 1.43 Mc/s the tolerance is 715 c/s.

Since the "zero" of the system is determined by the peaking strip, errors in the peaking strip signal will be reflected as frequency errors. Assuming random errors equally distributed between the peaking strip and the low power r.f. system, the stabilities required are 0.1 gauss for the peaking strip and 500 c/s for the r.f. The frequency jitter corresponding to injection has been measured using simulated input signals and has a standard deviation of 360 c/s. This total has contributions from several sources and an attempt has been made to split the error into its various components.

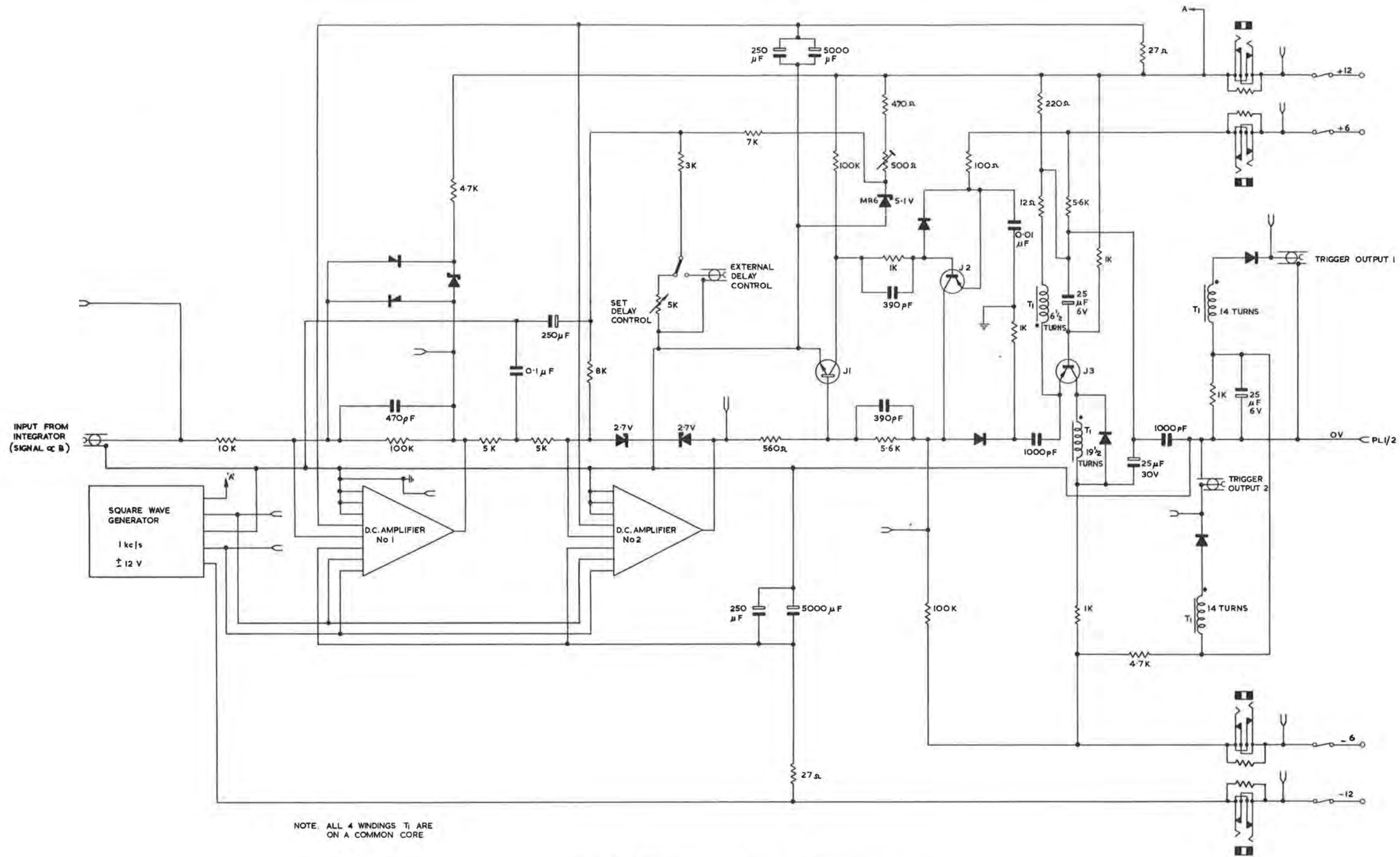


Fig. 6.2.3(viii) Circuit diagram of comparator.

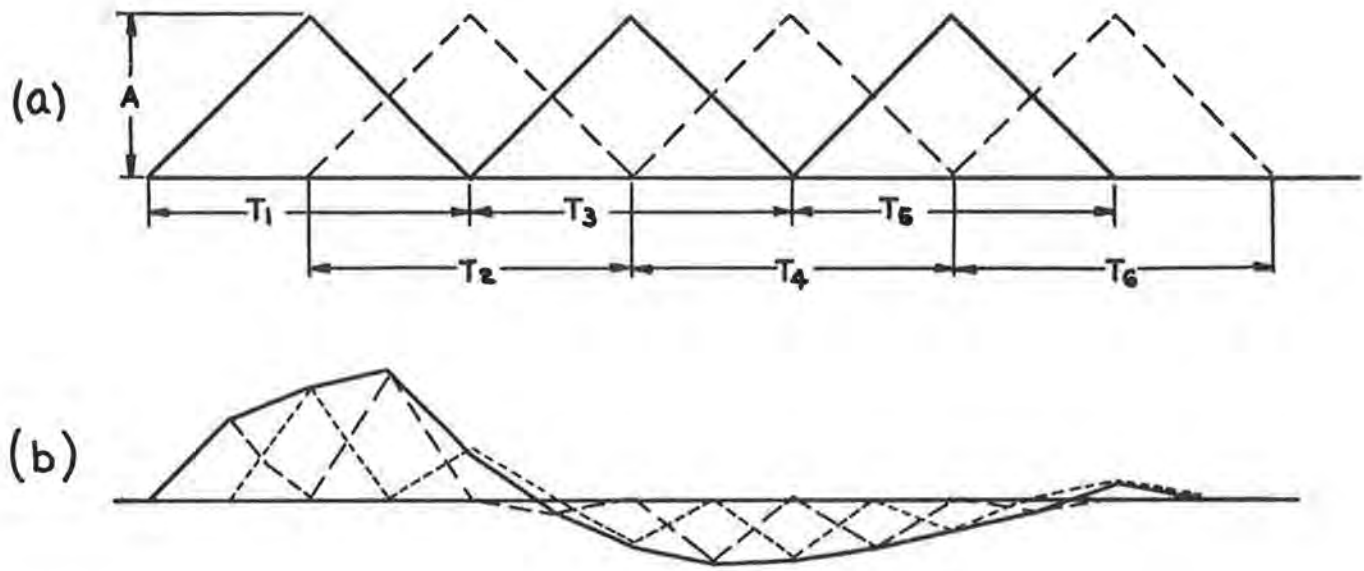


Fig. 6.2.3(ix) Waveforms at output of converter.

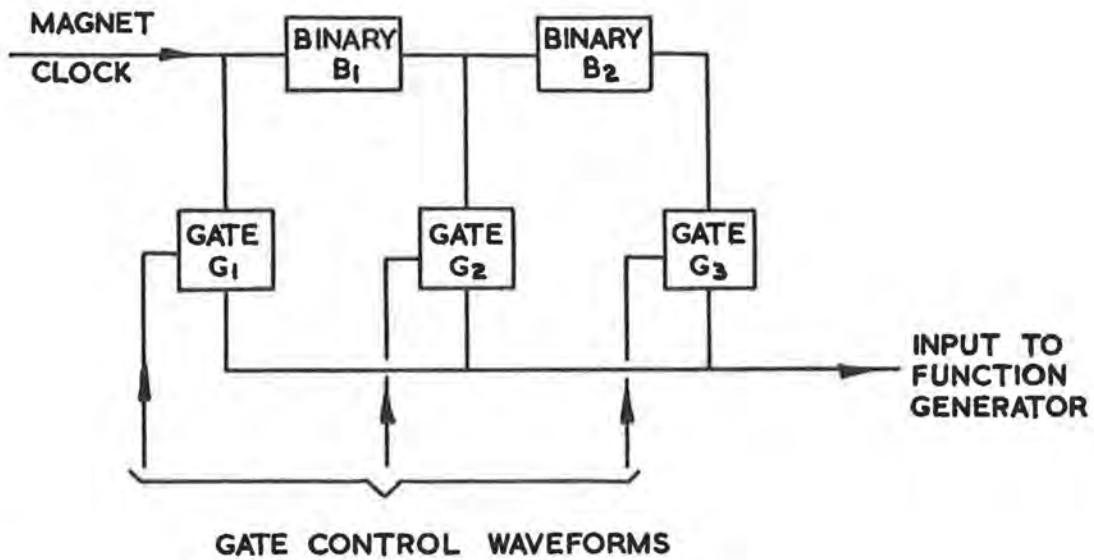


Fig. 6.2.3(x) Block diagram of gate and scaling unit.

The integrator has a jitter equivalent to 30 milligauss, corresponding to 150 c/s in oscillator frequency; the jitter in the voltage to current converter is $8 \mu\text{A}$, corresponding to 80 c/s; the amplitude of the f.m. noise in the oscillator is 10 c/s, and the measuring error is 60 c/s.

The sum of these components, assuming they combine in a random manner is 180 c/s which is not in good agreement with the measured value. Since the total jitter figure is well below the assumed limit, this anomaly has not been investigated but could well be due to the difference in environment between the measurements taken on the individual units and those taken on the combined system.

(b) Frequency tracking

As the magnetic field rises after injection, the betatron oscillation amplitude becomes less and small frequency errors can be tolerated without further loss of beam. Taking this into account along with the decrease in effective aperture, the permissible frequency error is shown in Fig. 6.2.4(i). Above an arbitrary field level, say 6 kilo gauss, it can be assumed that further restrictions due to target or extraction requirements will be imposed and the frequency tolerance should follow the curve shown dotted in Fig. 6.2.4(i).

The possible variables are shown in Fig. 6.2.4(ii) where the frequency determining tank circuit of the oscillator is shown in some detail. The oscillator is essentially a Colpitts circuit which is frequency modulated by varying the inductive element. The main variable inductor consists of two ferrite toroids each with a r.f. winding, surrounded by a common polarizing winding. The connections are such that no r.f. voltage is induced in the polarising winding. (This arrangement has been used on other large proton synchrotrons.)

Without the shaping circuit shown in Fig. 6.2.4(ii) the oscillator frequency varies with bias as shown in Fig. 6.2.4(iii)-(a) between 1 and 12 Mc/s. The first part of the curve is very non-linear and is not used (it is traversed while the magnetic field rises from 200 to 300 gauss). By suitable choice of fixed bias on the inductor, the frequency at injection field can be chosen to correspond to the frequency of the particles. Also, by choosing a scale factor relating bias current to the magnetic field, the early part of the curve can be made to fit the required frequency law closely.

By suitable choice of a fixed "shaper" inductance the frequency law can be made to saturate at a frequency corresponding to the near relativistic frequency of rotation of the particles (Fig. 6.2.4(iii)-(b)). This enables the frequency at high energies to be determined by a fixed inductor with a correspondingly high frequency stability which can be adjusted relatively independently of the settings made for injection.

The fixed inductance is further shunted by a small capacitor so that the resonant frequency of the two is slightly above the asymptotic frequency. The combination may therefore be used to adjust the degree of 'squareness' of the knee of the frequency curve as shown in Fig. 6.2.4(iii)-(c). Curve 1 corresponds to the case where the self resonant frequency of the combination is closer to the asymptotic frequency than it is for curve 2. The range of adjustment covers the

theoretical curve so that the components can be set to give an optimum fit. There is a slight disadvantage in that the adjustment of final frequency and degree of squareness are not independent.

The adjustments available on the oscillator can then be summarised as follows:-

(i) an arbitrary choice of the constant of integration to give the correct starting frequency

(ii) choice of the scale factor relating biasing current to magnetic guide field to give optimum tracking over the first phase of acceleration

(iii) adjustment of the final frequency

(iv) adjustment of the squareness of the knee

The optimum adjustment of these controls gives a curve with a tracking error indicated by the points marked in Fig. 6.2.4(i). It can be seen that over the first part of the cycle the points lie inside the curve corresponding to no loss. The maximum deviation from the correct curve is 4% and this is compensated for by the function generator. This applies a correcting signal to the voltage sensitive capacitor, shown in Fig. 6.2.4(ii) as the variable capacitor shunting the tank circuit of the oscillator.

The maximum correction that the function generator (or curve corrector) can apply is 5% and its stability is 0.5% of full scale so the final adjustment should be well inside the curve of Fig. 6.2.4(i).

(c) Final frequency

At the end of acceleration, factors in addition to retention of the beam apply. For example, if the final frequency has a jitter of 0.05% this corresponds to 1 cm in equilibrium radius and would have no effect on beam intensity. However, with a long output pulse, say 500 ms, it would result in a jitter in the timing of the output pulse of the order of 50 ms.

The oscillator circuit is such that the final frequency is determined by "fixed" components which should give high stability. Measurements have confirmed a cycle to cycle jitter in final frequency which corresponds to less than 1 mm of equilibrium orbit radius.

(d) Frequency modulation noise

The phase motion of the particles is a lightly damped oscillatory motion which is excited by frequency and phase modulations of the accelerating voltage. Though the phase oscillation frequency varies over the range 2 to 5 kc/s during the acceleration period, the forcing function is wide band noise which contains components at this frequency at all times. The phase motion is therefore continually excited during the acceleration period.

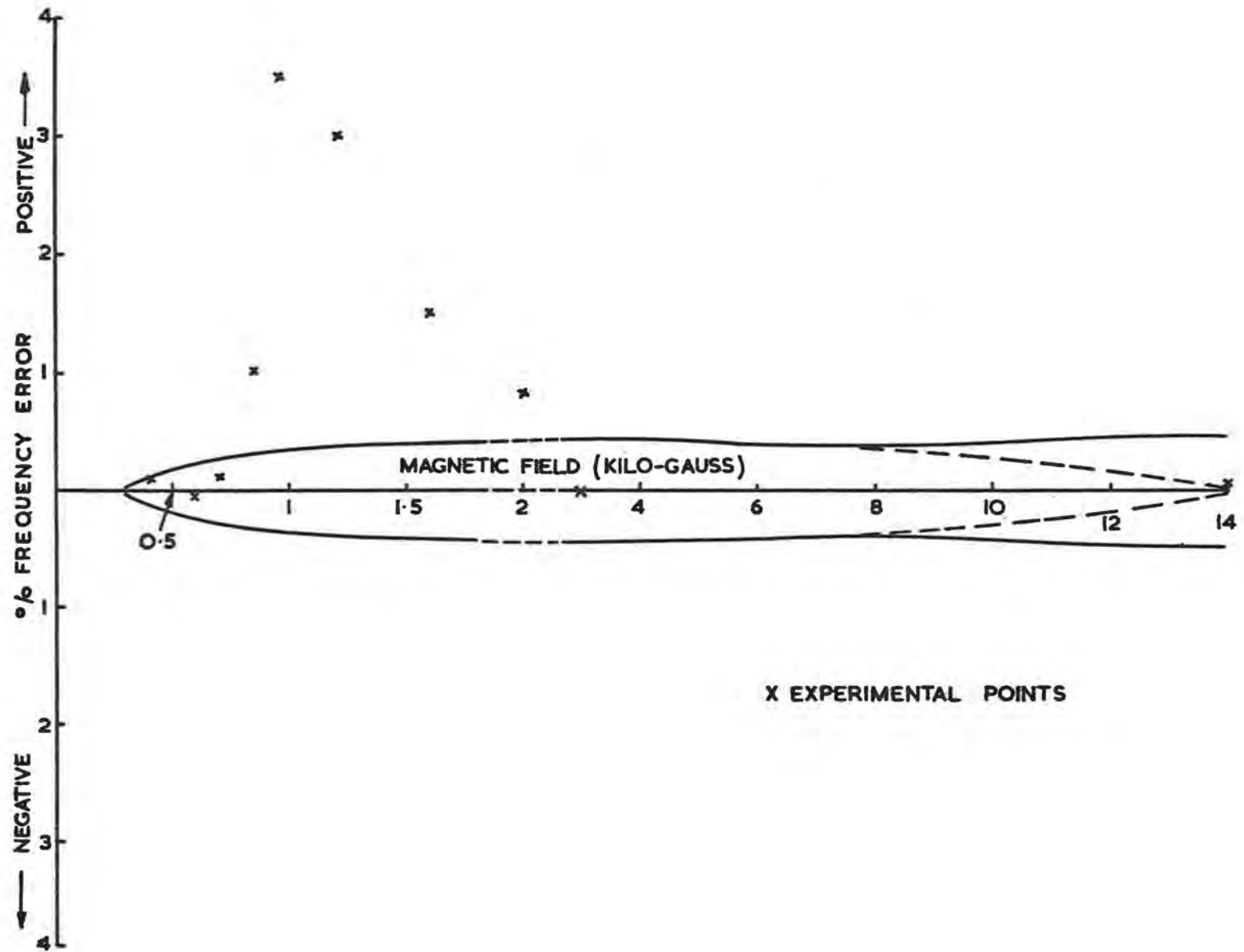


Fig. 6.2.4(i) Permissible frequency error during current rise.

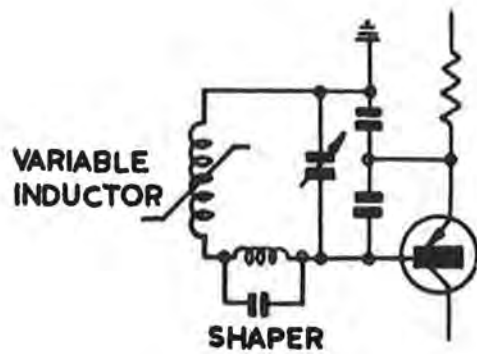
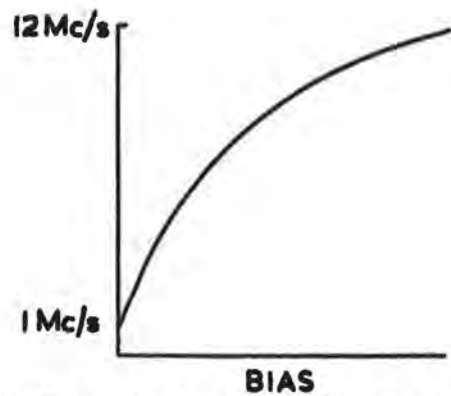
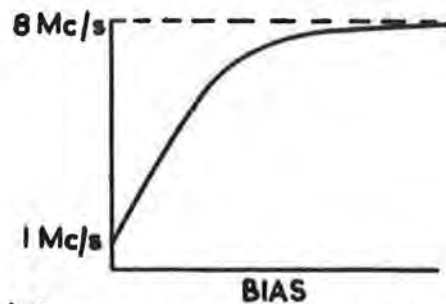


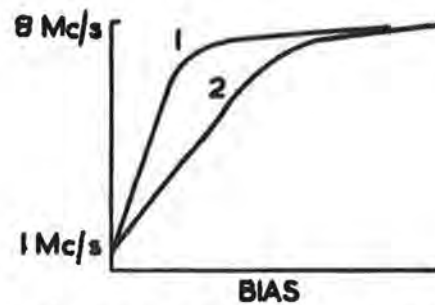
Fig. 6.2.4(ii) Frequency determining tank circuit of oscillator.



(a) WITHOUT THE SHAPING CIRCUIT



(b) FIXED SHAPER INDUCTANCE



(c) WITH CONDENSER SHUNT

Fig. 6.2.4(iii) Frequency variation with bias.

The noise consists of two components; the inherent noise of the oscillator and the current noise in the amplifying chain providing the bias current. The latter component becomes less important as the slope of the frequency/bias current curve becomes small after the first part of the accelerating cycle.

The r.m.s. noise in the oscillator is 10 c/s and the r.m.s. noise current in the bias chain is 2.5 μ A. This latter figure differs from the 8 μ A used in section 6.2.4(a) which includes a large "flicker" component, whereas the 2.5 μ A only includes components in the frequency range 1-10 kc/s.

Making an approximate allowance for the relative proportions in which these two components are combined the expected build up of phase oscillation amplitude is 0.4 radians. The resulting loss of particles depends on the detailed way in which the particles are distributed in the phase stable region but is expected to be between 10% and 25%.

6.3. High Power R.F. System

6.3.1. Introduction

The high power r.f. equipment comprises the r.f. cavity, the power amplifier, and the bias supply. A block diagram is shown in Fig. 6.3.1(i) and a cut away view of the cavity in Fig. 6.3.1(ii). The single two-gap accelerating cavity is energised from the power amplifier and automatically tuned by the bias supply. The bias supply is controlled by a phase detector sensing the load susceptance. There is also a closed loop amplitude control associated with the power amplifier, acting directly from the gap voltage.

The r.f. frequency programme and also a level control programme are fed to the power amplifier from the primary frequency generator (see section 6.2). The required frequency rises from 1.423 Mc/s to 8.012 Mc/s in 0.75 s; this is repeated every 2 s. The required energy gain per turn averages 6 keV, being proportional to \dot{B} . Special voltage programmes may be required at injection and extraction; the system is required to function over a 10:1 range of amplitude at injection. The normal r.f. stable-phase angle is 150° .

The r.f. frequency is the fourth harmonic of the proton orbital frequency. This harmonic number was chosen as the best compromise between the reduction of synchrotron oscillation amplitude and the deterioration of ferrite properties with increasing frequency.

6.3.2. Accelerating Cavity (Figs. 6.3.2(i), 6.3.2(ii))

(a) Basic description

Initially a critical comparison was made between the loaded cavity type structure and the "Bevatron-type" drift-tube structure. It showed the cavity structure was obviously the more efficient (1). This is mainly due to the large beam aperture in Nimrod coupled with the relatively short straight section which would make a low impedance circuit inevitable with the drift-tube arrangement, leading to a necessity for a high peak voltage and hence a high power requirement.

A third alternative, consisting of a cavity incorporating a variable capacitor, was also considered and rejected because of awkward mechanical problems which would introduce jitter and noise. The power requirement would again be high because the ferrite would be less heavily biased (and therefore more lossy) at high frequencies and the capacitance at low frequencies would be higher, leading to a lower impedance.

The loaded cavity consists of two highly re-entrant E_{010} resonators side by side. They are loaded symmetrically by a total of four ferrite cores to provide a large variable inductance. The capacitance is not varied. The two accelerating gaps are paralleled and connected to the output of the push-pull amplifier. The ferrite is biased by a d.c. winding which links the two cavities in opposite senses, to buck out r.f. voltages. The d.c. winding is distributed round the cores and being inside the cavity, it also acts as the main r.f. winding (its turns are paralleled by capacitors for this purpose) and the cavity walls can be

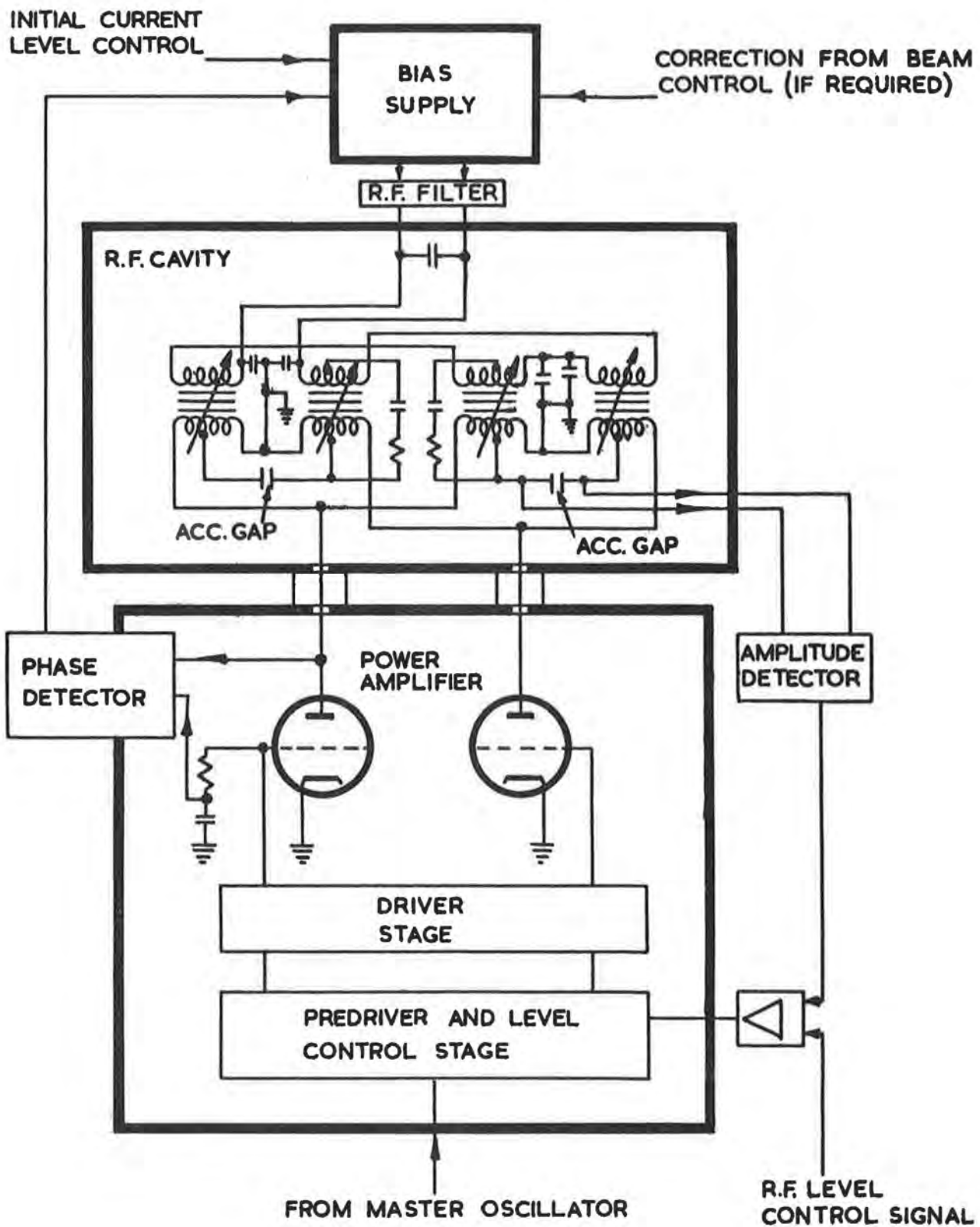


Fig. 6.3.1(i) Block diagram of high power r.f. system.

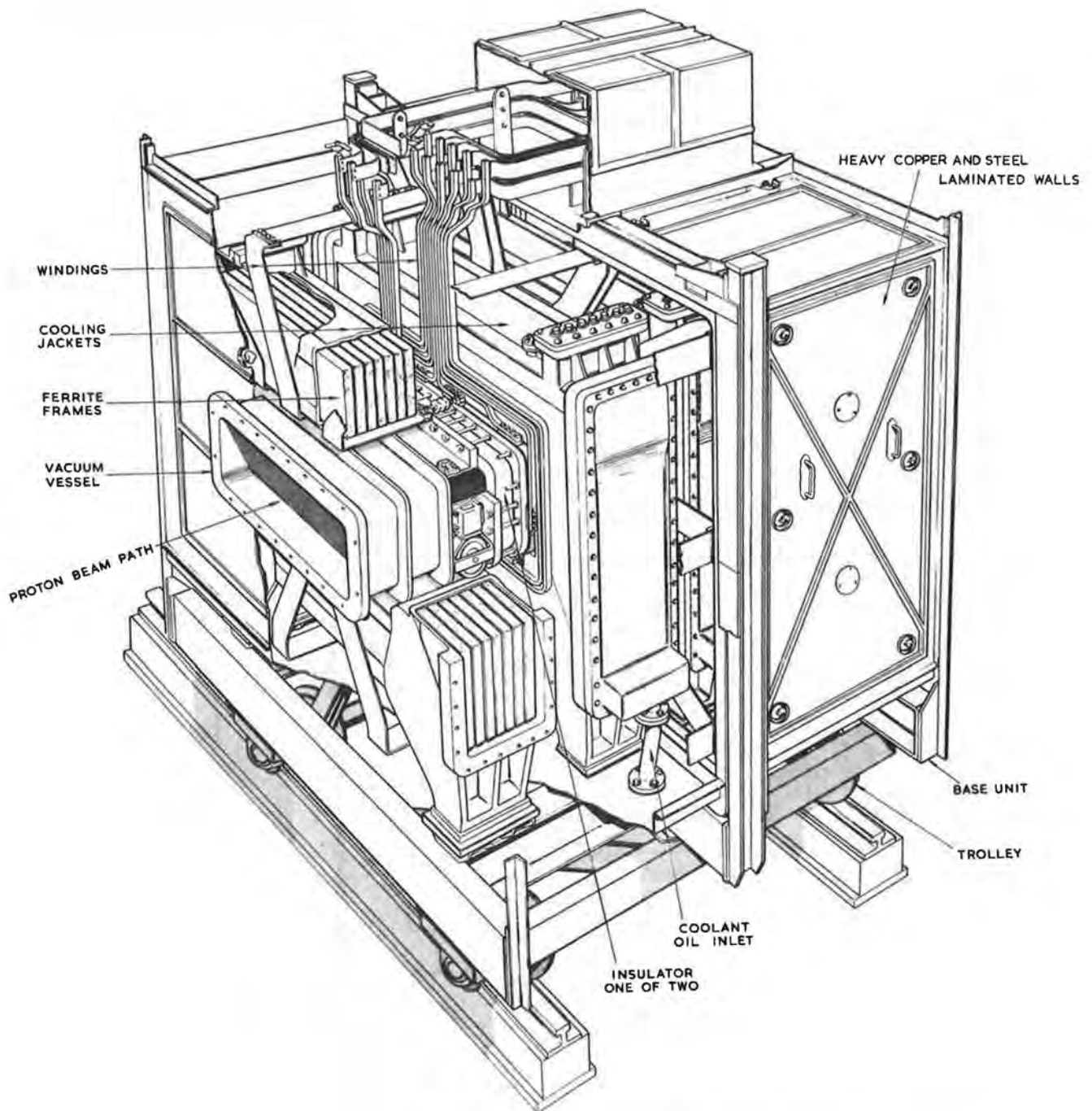


Fig. 6.3.1(ii) Cutaway view of the r.f. cavity.

N.B. This drawing shows the original design for the cavity. Later modifications included new side covers, removal of tuning capacitors and addition of separate r.f. windings (see para. 6.3.2).

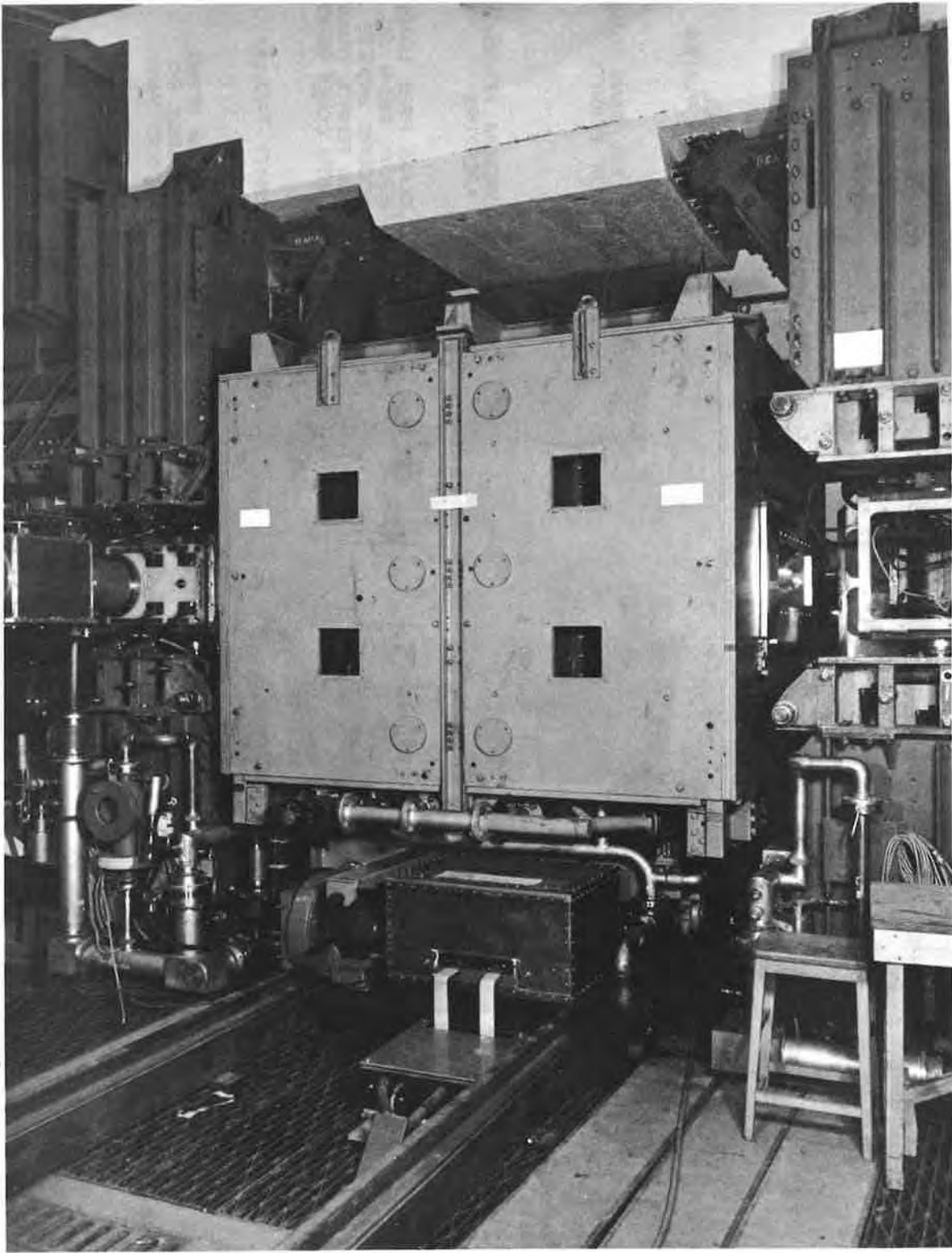


Fig. 6.3.2(i) View of the accelerating cavity in position in straight section 8.

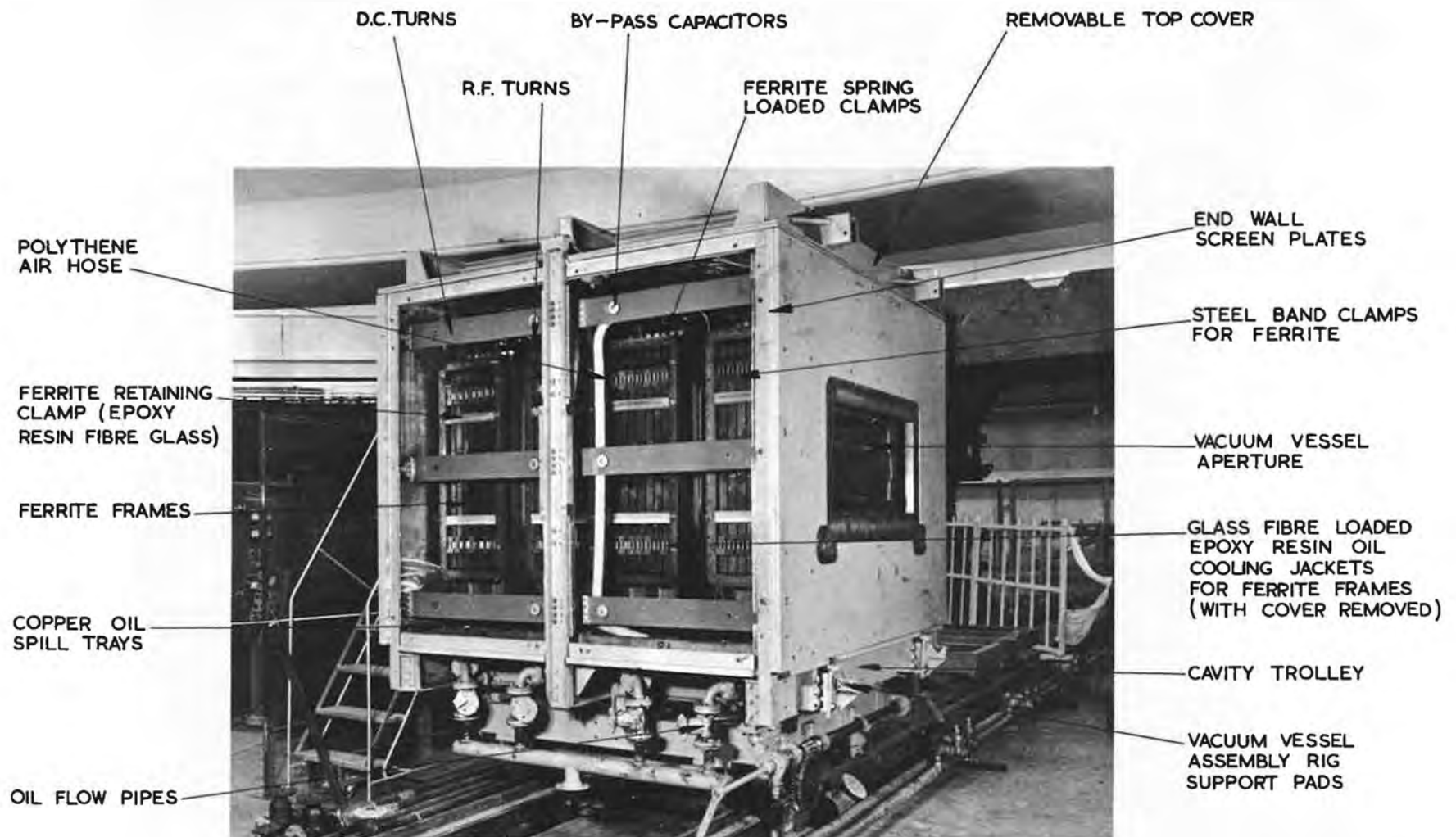


Fig. 6.3.2(ii) View of the accelerating cavity.

considered to perform the function of a screen. The central dividing wall between the cavities is not present, as it performs no useful electrical function.

(b) Vacuum vessel

The vacuum vessel is a rectangular cross section stainless steel tube with two insulating gaps, across which the accelerating voltage is developed. When the cavity is moved out of its position in the magnet ring for servicing, the vacuum vessel can be rolled on wheels out of the cavity (in the beam direction) for inspection of the insulators and seals. The wheels run in locating grooves on the epoxy resin boxes enclosing the ferrite. Large spring fingers make electrical connections to the end walls of the cavity. Various materials were considered for the insulators including glass, fibre-glass and epoxy resin, alumina and other ceramics, polythene and P.T.F.E. The principal requirements of the material are that it shall have:-

(i) a combination of low dielectric loss and high thermal conductivity, i.e. $(\epsilon \tan \delta) / K$ must be as small as possible;

(ii) low vapour pressure and gaseous permeability;

(iii) reasonable mechanical strength, freedom from plastic flow and a high radiation resistance;

(iv) suitable properties to allow manufacture to the shape shown in Fig. 6.3.2(iii).

The results of the investigations were as follows:-

(i) Glass fibre and epoxy resin

The choice of an epoxy resin was abandoned since experiment showed that the temperature rise of at least 90°C. would lead to a very high vapour pressure and that a fairly extensive air blowing system would be required.

(ii) P.T.F.E.

This material would have a temperature rise during operation of approximately 22°C. which, together with a surface temperature of 20°C., might just be satisfactory from a vacuum point of view, although the vacuum seal could have proved difficult due to plastic flow of the P.T.F.E. A number of manufacturers were asked to produce an insulator of this material but they declined, due to difficulties in making a suitable mould. P.T.F.E. also has poor radiation resistance.

(iii) Alumina ceramic

Several types of ceramics satisfied the principle requirements, although the gaseous permeability could have proved troublesome in some cases. Again manufacture proved difficult, mainly due to the break up of the formed item during firing.

(iv) Glass

A special telescopic glass slab, having good vacuum and r.f. qualities and high radiation resistance, was manufactured. Insulators were cut from this slab and proved satisfactory when tested under the operating conditions expected in the r.f. cavity. The cost of this type is, however, rather high.

(v) Polythene

Polythene insulators have been adopted and are in use but glass ones are available as an alternative. The polythene insulators have proved satisfactory under operating conditions although the effect of radiation is not yet known.

Insulator tests

All insulators were subjected to vacuum and high voltage tests on a test rig in which the insulator was secured between two stainless steel vessels by 32 tie bars. One of the vessels was fitted with a diffusion pump provided with a refrigerated baffle. Both the cavity vacuum vessel and the insulator test rig vacuum vessels have special metal stops fitted, equally spaced, around the inner faces to prevent excessive strain on the insulators when under vacuum. With both polythene and glass insulators a vacuum of 5×10^{-7} torr was achieved after about 48 h pumping.

High voltage tests were carried out using a portable r.f. transmitter with an output power sufficient to produce approximately 8 kV across the insulator. During these tests the vacuum vessels were carefully insulated and screened by a copper box.

The test rig was eventually modified so that it can be attached to the cavity vacuum vessel when the cavity is withdrawn from the magnet ring to its test position in the centre of the magnet hall. Under these conditions the normal cavity power amplifier is available to provide a source of r.f. voltage, since it remains attached to the cavity.

Tie Bars

The original specification for the 32 tie bars securing each insulator between the flanges of the cavity vacuum vessel called for a material having a low dielectric constant and a low power factor to avoid overheating when placed in a r.f. field. Ceramic and epoxy resin glass fibre types were tested, the latter proving the better both for mechanical strength and r.f. properties. The breaking strain of each tie bar is 5 ton.

Each end of a tie bar is provided with a split collar and a special nut which is tightened only by means of a torsion spanner while the collar is held in place by a tool provided. Abrasion and scoring of the tie bar ends by the split collars has been overcome by binding the ends with a single turn of 0.002 in. aluminium alloy strip before assembly.

The bars have a relatively large surface area to cross section ratio and do not overheat but a little air is blown over them as a safety precaution.

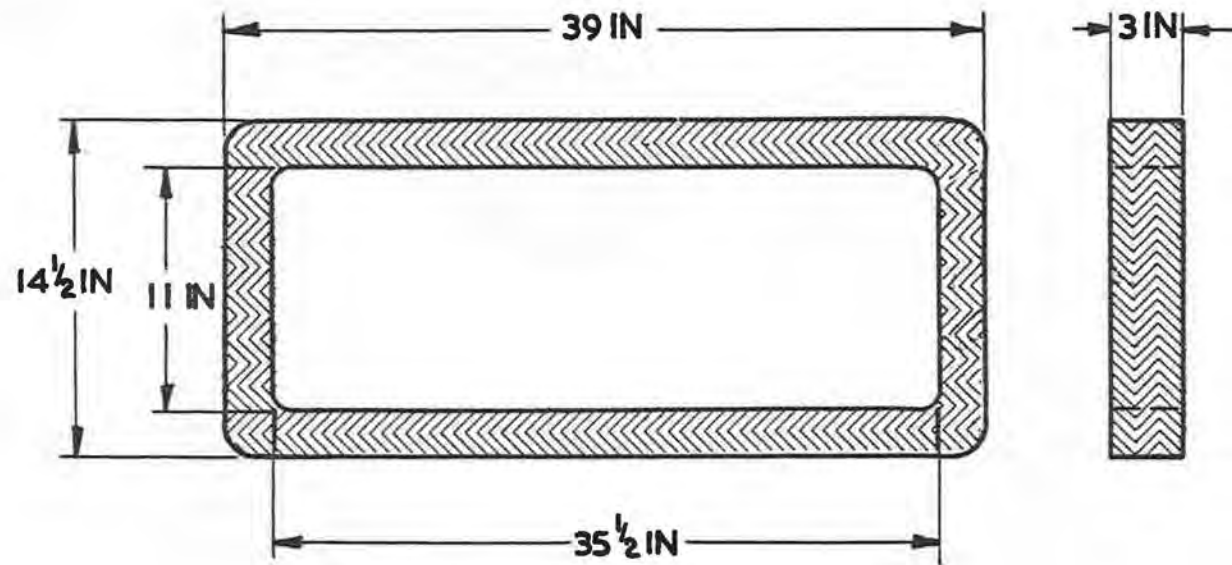


Fig. 6.3.2(iii) Shape of vacuum vessel insulators.

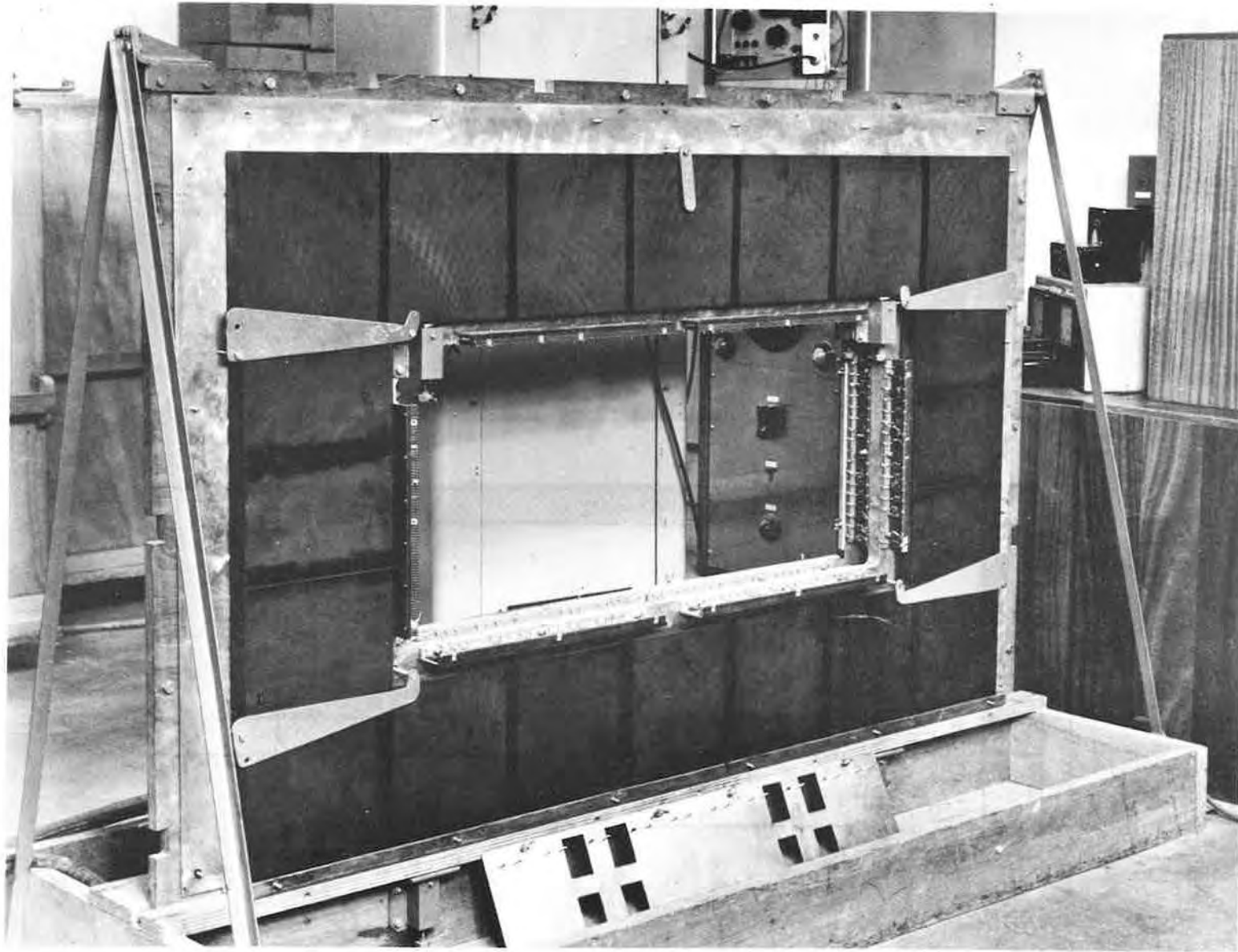


Fig. 6.3.2(iv) View of a ferrite core 'window frame'.

(c) Ferrite

A careful investigation was made of all available materials. A full account of this investigation has been reported elsewhere (2). The requirement was for the best compromise for the product μQ over the frequency range and the ampere turns required to pull the resonant frequency from 1.4 to 8.0 Mc/s. (μ = permeability of ferrite; Q = loaded Q of complete cavity with ferrite filling). It was also necessary for the manufacturer to be capable of manufacturing large blocks to the required mechanical and electrical tolerances. The material finally chosen was a special Philips material similar to Mullard B₁, but with a slightly lower permeability and correspondingly higher Q . At 1.4 Mc/s unbiased: $\mu = 600$ and $Q = 10$ at 60 gauss peak flux density. When biased to 8.0 Mc/s: $Q = 40$ and the bias field is 12 AT/cm. The ferrite is made in "window frames" 4 cm thick (Fig. 6.3.2(iv)). The long limbs are each made of seven blocks (25 cm by 23 cm) and the short limbs of three narrower blocks. The four limbs of a window frame are loaded individually into the cavity and are held together by gravity and by spring loaded clamps on the top surface.

A problem arose over the joining together of the blocks to form limbs. Originally all the limbs were made by glueing the blocks together with cold-setting Araldite. However, during assembly into the cavity some of the long limbs broke in the centre, and it was found after an extensive investigation by the manufacturers that the strength of the cold-setting Araldite bond decreased with time, reaching zero after a period of 4 or 5 weeks, due to water vapour from the air reaching the bond through the porous ferrite. A technique was developed for glueing the limbs using a hot setting Araldite, which also loses some strength during the first few weeks after glueing but levels off at a value which is still very high. However, in the meantime a method had been found to hold the long limbs together using stainless steel clamps. These clamps were sufficiently small to fit in the cavity without affecting the oil flow around the ferrite, and they included an insulating portion to avoid the possibility of induced currents in the clamps. The short limbs rely on gravity to assist the strength of the original Araldite bond.

There are 28 frames in the cavity (7 in each core), with a total weight of nearly 6 ton. The amount of r.f. power absorbed by the ferrite varies with frequency but has a peak value of about 42 kW at 4.5 Mc/s. The four ferrite cores are enclosed in individual fibre-glass loaded epoxy resin jackets filled with transformer oil, which is cooled by circulation through a heat exchanger, the inlet temperature being maintained at 58°F (14.5°C).

(d) Bias Winding

The ferrite requires a total bias field of approximately 7,000 AT. If this were provided by a single winding carrying 7,000 A the peak voltage required to obtain the desired rate of rise of current would be approximately 5 V. The cavity was designed and built in such a manner that the actual cavity walls could be used as a single turn winding of this type, but it was decided that the most convenient impedance at which to work would be provided by a 10-turn winding requiring a peak current not exceeding 800 A and a peak voltage of 50 V and this was the arrangement finally used. The path followed by any one turn of the winding is shown in Fig. 6.3.2(v). The input is underneath the centre of the cavity and the 10 turns are distributed circumferentially around the ferrite. The input is bypassed with a 0.01 μ F capacitor, and is connected through the r.f. filter

to prevent even small r.f. currents getting to the sensitive operational amplifiers in the bias supply. There is a considerable problem in avoiding subsidiary resonances in the bias winding system. These, in general, are due to the air-cored stray inductances and capacitances between sections of winding and the adjacent cavity wall. The bias winding is the main conductor for r.f. currents, and to ensure a uniform current distribution the windings are paralleled for r.f. by $0.01 \mu\text{F}$ capacitors.

In addition, each winding is decoupled to the cavity wall. Originally each was decoupled in at least two places and also bypassed to the actual flange of the accelerating gap. This combination led to the existence of a host of absorption resonances in the 1 to 8 Mc/s band, giving a low input impedance at some frequencies and high voltages at certain decoupling capacitors. It was found that owing to the complex arrangement of the bias winding turns within the cavity, it was impossible to eliminate all resonances within the 1 to 8 Mc/s band from the cavity.

After removing all except one decoupling capacitor on each turn, and bypassing only one of the turns to the gap flange, most of the resonances disappeared. However, to eliminate one severe "double-humping" condition associated with the central part of the vacuum vessel, it was necessary to bypass the winding to the gap flange on the inner side only of each gap. This latter bypass capacitor circuit was found to carry a very large current at one frequency and to prevent the capacitor being destroyed in the event of the cavity being energised continuously at this frequency, a 2Ω , 200 W damping resistor was inserted.

Lesser resonances were found to overheat some of the other decoupling capacitors at certain frequencies and eventually a simple filter arrangement was used between each turn and the wall, consisting of a $0.01 \mu\text{F}$ capacitor in series with a parallel combination of a $0.01 \mu\text{F}$ capacitor and a 6Ω , 20 W resistor.

(e) R.F. winding

The accelerating gaps in the cavity are connected in parallel by the bias winding and the original intention was to connect the power amplifier directly to the centre point of this parallel connection. This, however, presented a rather low impedance to the power amplifier and it was decided to increase the input impedance of the cavity by making the cavity a two-turn to one-turn, step-down auto-transformer. To accomplish this, each input lead from the amplifier goes once round the appropriate ferrite core before being attached to the flange at the accelerating gap. The configuration of the windings is shown in Fig. 6.3.2.(v) while a theoretical equivalent circuit for the cavity and the bias and r.f. windings is given in Fig. 6.3.2(vi).

The arrangement introduces two new factors; the leakage inductance of the transformer and the stray turn-to-turn capacitance. The effect of the stray capacitance is to lower the resonant frequency of the cavity and all the lumped tuning capacitance which was originally incorporated had to be removed. This was also necessary because the output capacity of the power amplifier is seen by the cavity through the 4:1 impedance transformation. The effect of the leakage inductance is to reduce the voltage at the gaps and also to cause a series resonance to appear when the leakage inductance resonates with the gap capacitance. This resonance tends to occur between 10 and 20 Mc/s and it was decided to push it above 16 Mc/s, i.e. above the second harmonic of the maximum operating frequency. A low inductance winding is required to do this and in the final

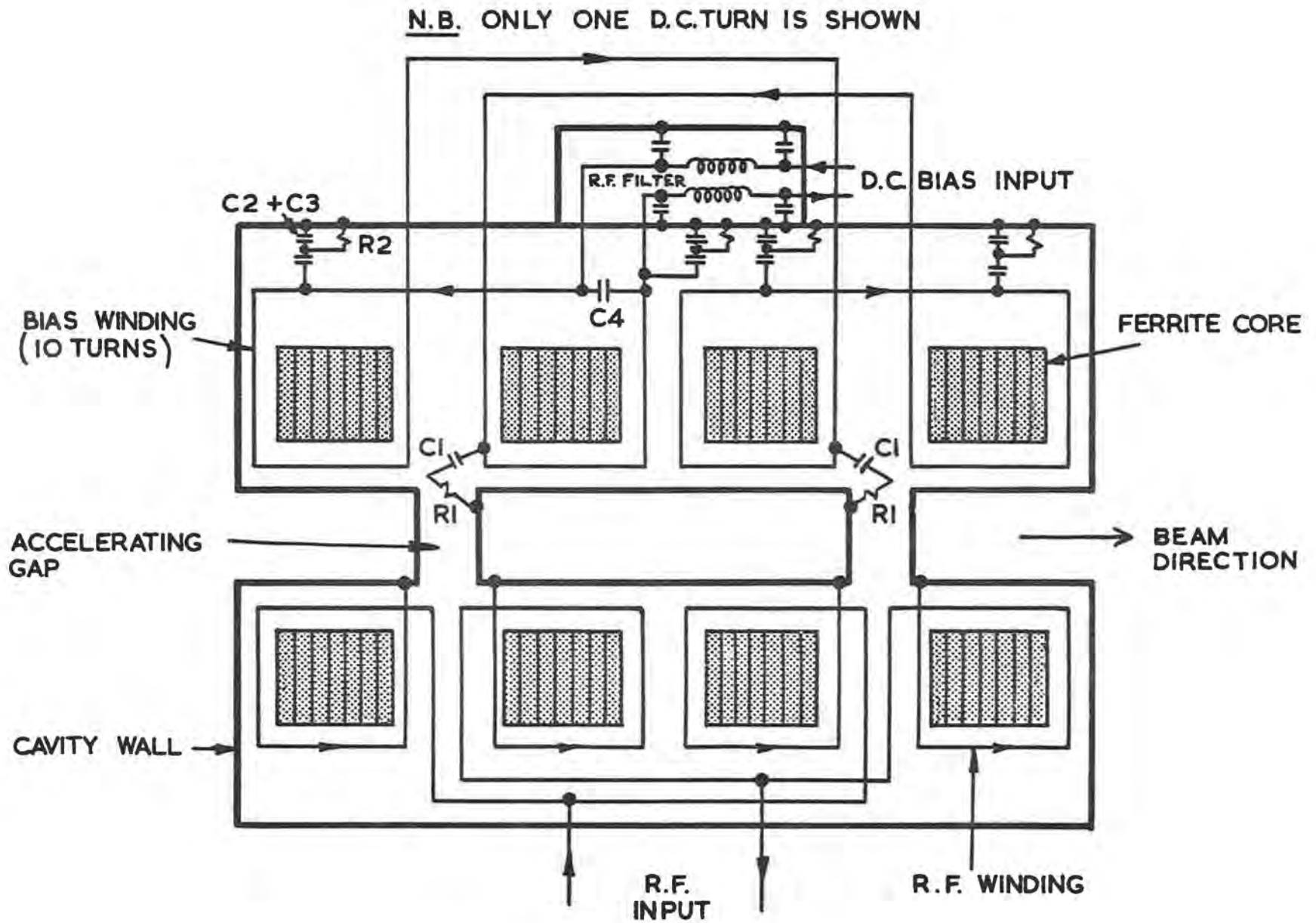
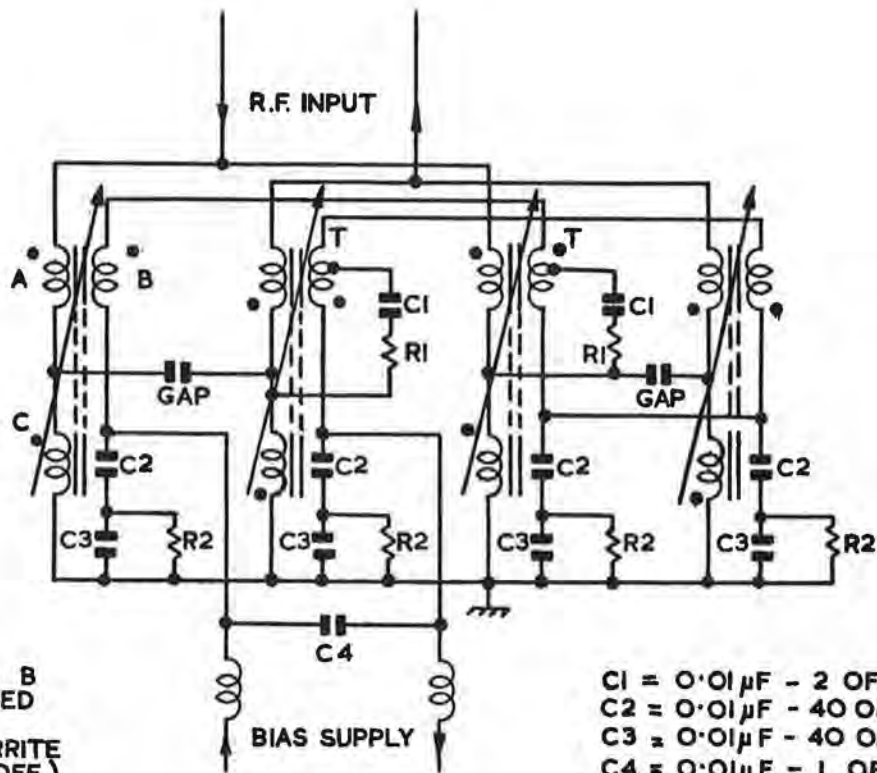


Fig. 6.3.2(v) The winding configuration of the accelerating cavity.



WINDINGS A AND B
WOUND EQUISPACED
AND INTERLACED
ROUND EACH FERRITE
CORE FRAME (4 OFF)

C1 = 0.01 μ F - 2 OFF
 C2 = 0.01 μ F - 40 OFF
 C3 = 0.01 μ F - 40 OFF
 C4 = 0.01 μ F - 1 OFF
 * C5 = 0.01 μ F - 40 OFF (NOT SHOWN)
 R1 = 2 ohm 200 watt - 2 OFF
 R2 = 6 ohm 20 watt - 40 OFF
 (* SEE NOTE 6)

Windings

- A = 5 parallel r. f. turns (\approx 1 turn)
- B = 10 turn bias winding; all turns paralleled for r. f. by capacitors (\approx 1 r. f. turn).
- C = Cavity walls (\approx 1 r. f. turn)

Notes

1. The r. f. turns form a 2 : 1 transformer
2. Each bias turn is effectively in parallel with the r. f. coupling circuit.
3. The gaps are fed in parallel with r. f. power (at 6 kV); they are seen in series by the proton beam ($= 12$ kV for $\phi_g = 30^\circ$).
4. Polarity:- The bias winding links the two halves of the cavity in opposite senses to buck out r. f. voltages.
5. T = Equalising tap circuit to damp out secondary resonances.
6. C5, coupling capacitors (0.01 μ f, 40 off) which parallel the 10 bias turns for r. f. are not shown in this diagram.

Fig. 6.3.2(vi) Cavity equivalent circuit diagram.

arrangement, each input busbar from the amplifier goes towards the accelerating gap, then splits into five parallel turns distributed around the cavity. These link the ferrite once and connect by knife switches to the gap flange.

The power amplifier is situated as close to the cavity as possible and the connection is made by large diameter conductors to reduce the stray inductance. To shorten connections to the minimum the tee junction between accelerating gaps is inside the cavity.

The r.f. winding was not incorporated in the original design of the cavity and as the length of the cavity is severely limited by the dimensions of the magnet straight section the space available for the r.f. winding is rather limited. Originally, considerable difficulty was experienced with arcs between the r.f. turns themselves and to the bias winding. These always involved surface tracking across the fibre-glass oil jackets around the ferrite.

Tests on samples showed that the fibre-glass material was highly resistant to surface tracking at 1 to 8 Mc/s, with or without red anti-tracking paint. However, quite small traces of dirt (or more particularly moisture) lead to tracking at quite low voltages. Since the jackets could not be kept clean, air insulation had to be used. Ceramic stand-off insulators were glued to the jackets to support the r.f. turns, with a clearance of $\frac{3}{8}$ in to the fibre-glass. This solved the arcing problem completely.

(f) Cavity screening

The cavity must be magnetically screened, to ensure an approximately field free region which will minimise any effect of the main magnet field on the ferrite. Consequently all walls of the cavity, which is roughly a 7 ft. cube, are made of copper and steel laminations. The top, bottom and side walls are made up from two $\frac{1}{2}$ in. plates, the outer one being steel while the inner one is copper clad steel ($\frac{7}{16}$ in. steel and $\frac{1}{16}$ in. copper). The end walls consist of two $\frac{1}{2}$ in. steel plates, together with an inner $\frac{1}{2}$ in. copper clad steel plate. The laminations are separated by paper insulation and all clamping bolts are insulated. Every joint in the cavity is bridged by internal spring fingers. The total weight of the shielded cavity containing the ferrite is of the order of 20 ton.

Despite the magnetic shielding there is an appreciable effect on the ferrite. It is at a maximum when the ferrite is fully biased, owing to the non linear variation of permeability with flux. The effect is two-fold: first, the required bias current for 8 Mc/s is slightly increased (to values still within the capability of the bias supply), second, the effect is asymmetrical so that the power amplifier sees an unbalanced load (the unbalanced currents are also within the capability of the amplifier and its stability is not affected).

6.3.3. High Power R.F. Amplifier Development

(a) Specification

The amplifier has to accept a signal of about 2 V r.m.s. amplitude at 100 Ω impedance from the Primary Frequency Generator and to deliver the necessary voltage and power to the accelerating cavity. The design for the amplifier is

based on the specification in (3). Important features are displayed in the following figures:-

Fig. 6.3.3(i) shows the peak voltage required plotted against frequency; it is about 6 kV over the band. Fig. 6.3.3(ii) shows the impedance presented to the amplifier plotted against frequency. Each valve of the output stage has an anode load which falls to 250Ω . Fig. 6.3.3(iii) shows the power loss which is almost entirely absorbed in the ferrite cores; the skin loss and beam loading effects are negligible by comparison. The graphs in the last two figures were based on estimates from a sample ferrite testing programme. Fig. 6.3.3(iv) shows the assumed equivalent circuit for the cavities. It was decided at an early stage that to assess the behaviour of the cavities, the amplifier must be capable of operating with a c.w. output. In considering the valve line-up therefore, no account is taken of the 3:1 duty factor in the actual machine cycle.

From Fig. 6.3.3(i) and (ii) allowing a safety margin, the most stringent peak conditions for each output valve of the amplifier are:-

Required anode swing	= 3.5 kV
Load impedance	= 250Ω
Fundamental component of anode current	= 14 A (peak)

Considering only triodes: for a reasonable angle of anode current flow, the peak space current to meet the above condition could be 35 A which demands a high peak usable cathode current. A low anode efficiency and high peak grid current would follow and would require a high input driving voltage. There is the further problem of the input capacitance of these large valves, since a wideband untuned stage would be needed to drive the output stage of the amplifier. If a conventional push-pull amplifier is correctly cross-neutralised the input capacitance = $2(C_{ga} + C_{gf}) + \text{strays}$ (say 200 pF total). There is, therefore, a large reactive current demand from the driver at 8 Mc/s.

Further examination of the likely load impedance leads to the decision to incorporate a 4:1 impedance transformation ratio into the cavities by carrying the input leads once round the ferrite cores before connecting them to the accelerating gaps. Each valve then runs under the following conditions:-

Required anode swing	= 7 kV
Load impedance	= 1000Ω
Line current	= 7 A (peak)

At this stage an analysis was carried out as described in (4). The analysis covered a wide range of possible valves and a large number of possible operating conditions. The final choice was the English Electric Co. Type BW 161 with the following specifications:- $V_a \text{ max} = 12 \text{ kV}$; Anode dissipation = 30 kW; Peak usable cathode current = 45 A; $G_m = 23 \text{ mA/V}$; $\mu = 45$; $C_{ga} = 36 \text{ pF}$; $C_{gf} = 57 \text{ pF}$. The basic circuit arrangement used is shown in Fig. 6.3.3(v). To prove the power output capability of this circuit it was tested using a dummy load as shown in Fig. 6.3.3(vi). This load had impedance v. frequency and Q factor v. frequency characteristics similar to those of the cavity.

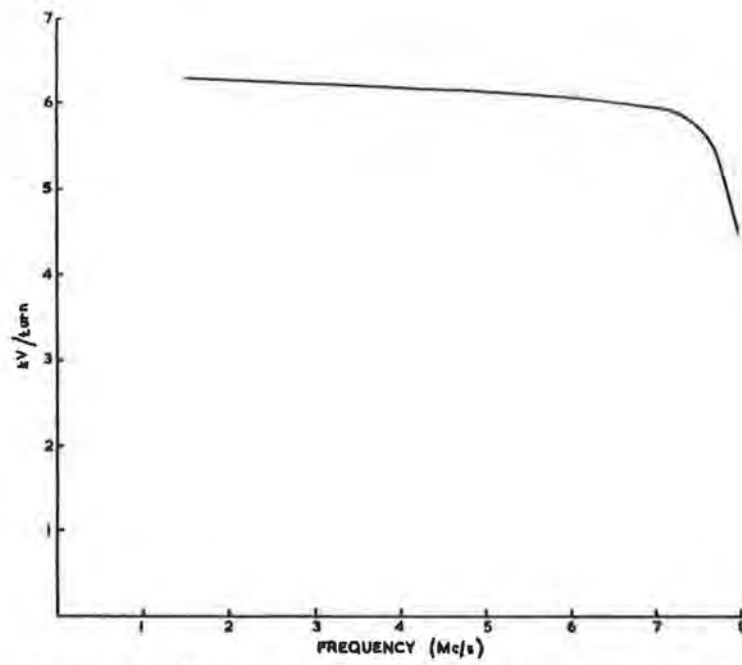


Fig. 6.3.3(i) Required accelerating voltage v. frequency.

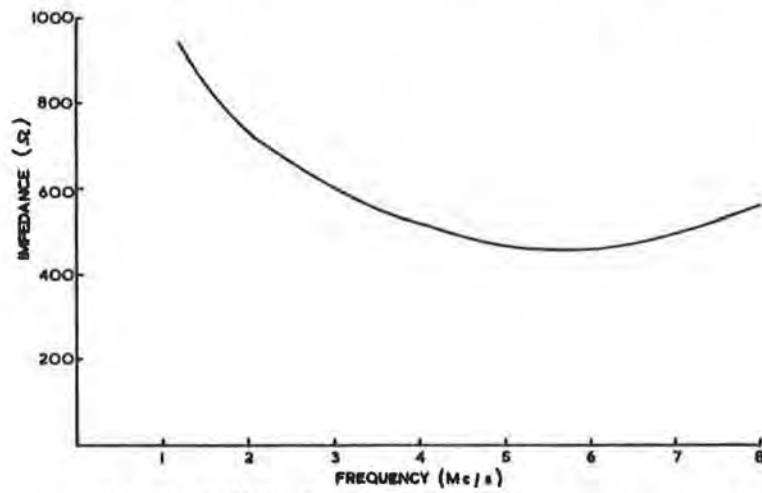


Fig. 6.3.3(ii) Cavity load impedance v. frequency.

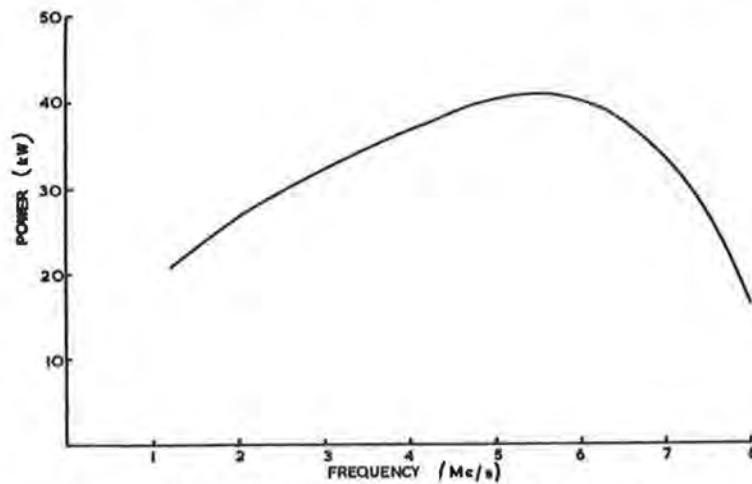


Fig. 6.3.3(iii) Power loss v. frequency.

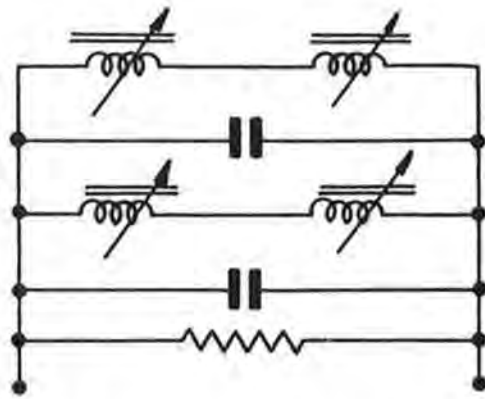


Fig. 6.3.3(iv) Equivalent circuit of the cavities.

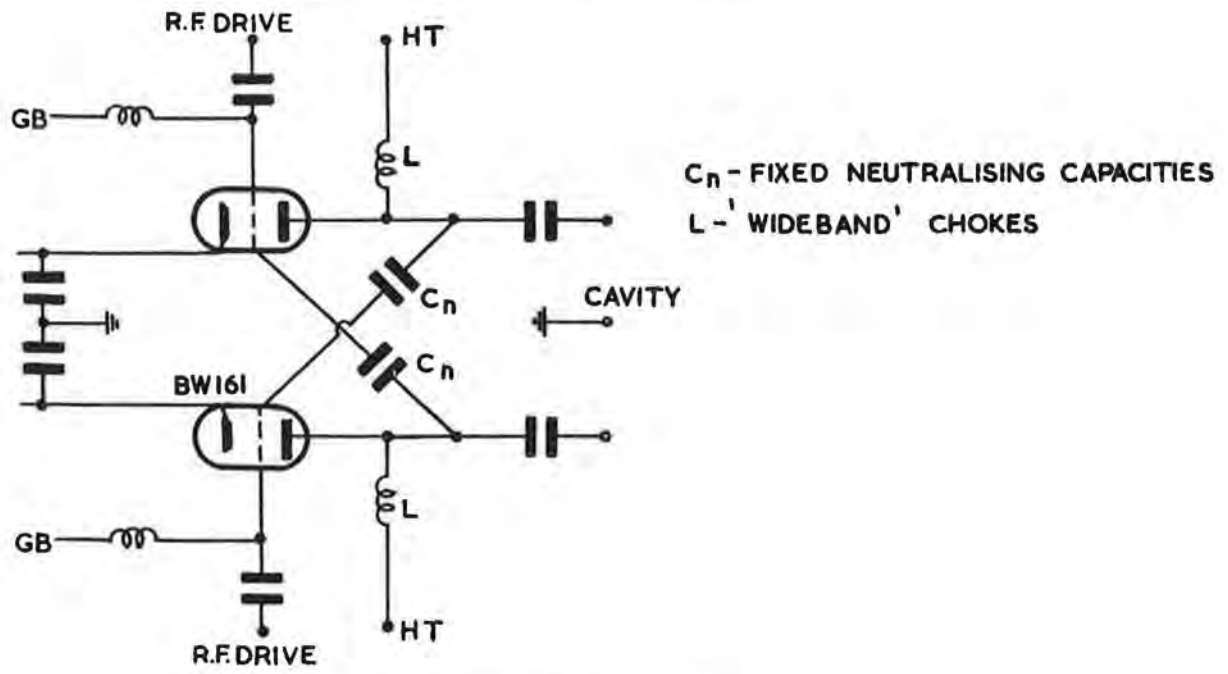


Fig. 6.3.3(v) Basic circuit of the output stage.

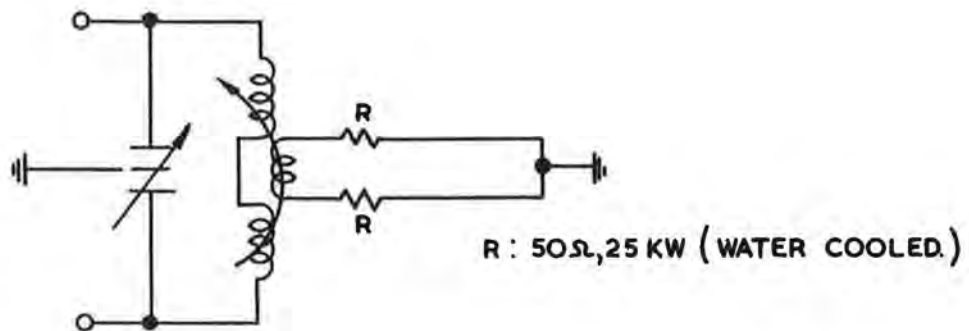


Fig. 6.3.3(vi) Dummy load for tests on amplifier output stage.

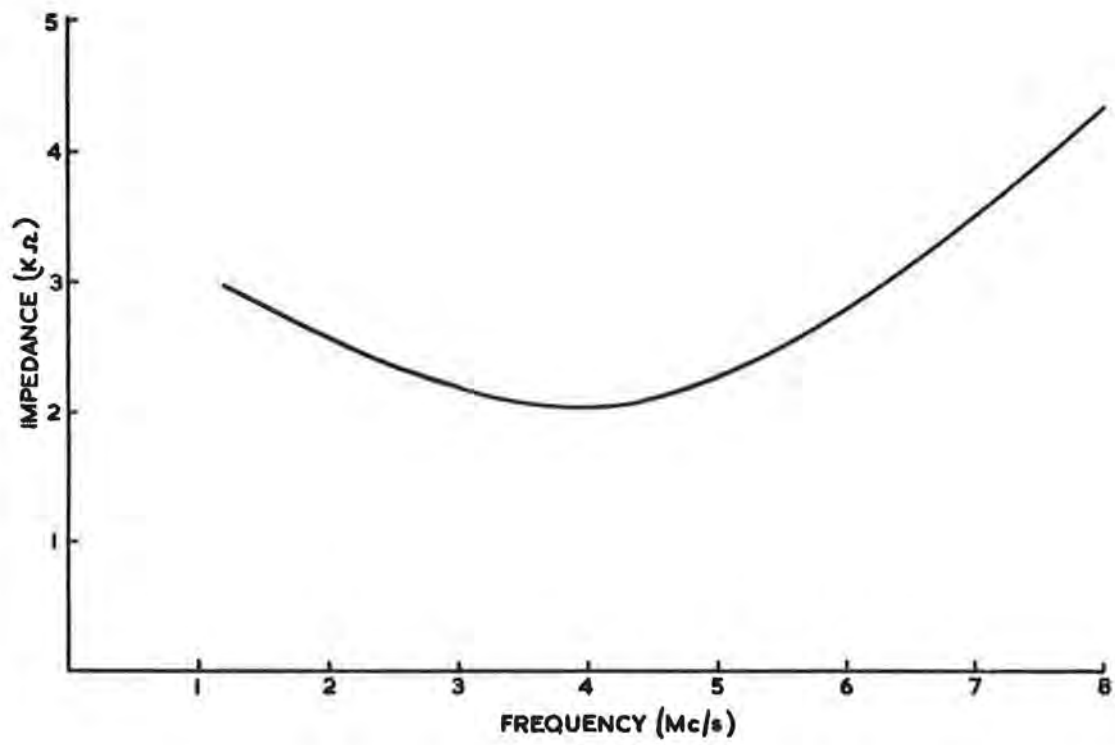


Fig. 6.3.3(vii) Actual load impedance v. frequency.

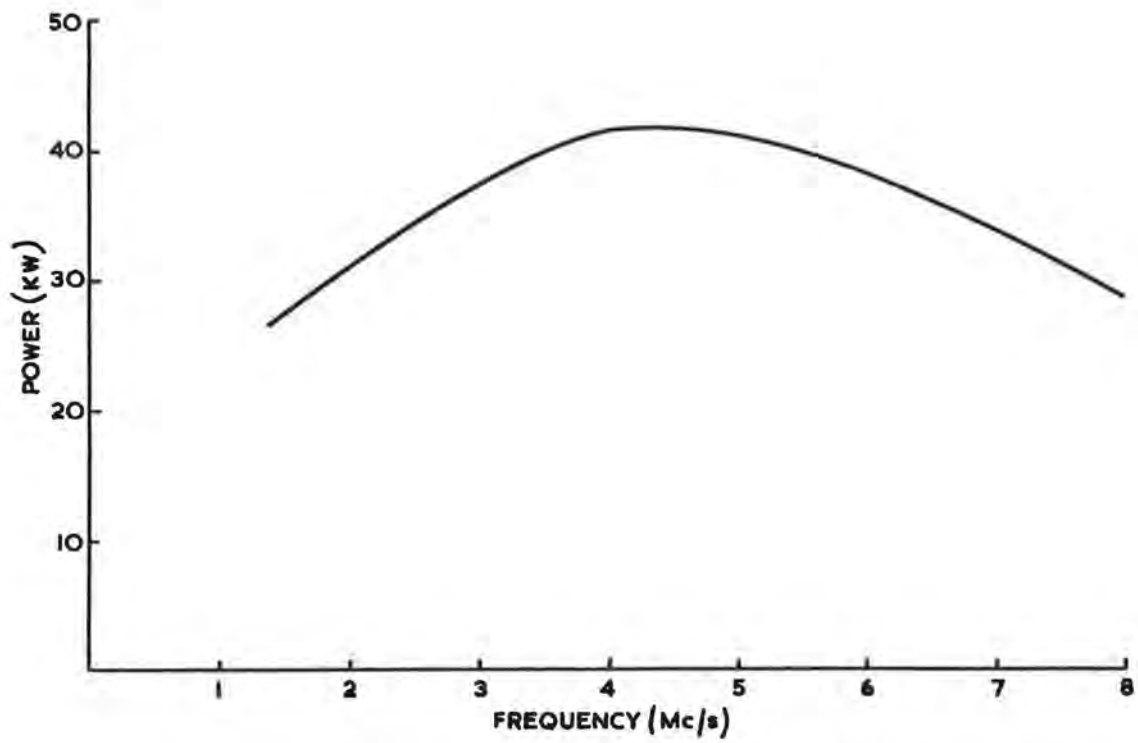


Fig. 6.3.3(viii) Actual power loss v. frequency.

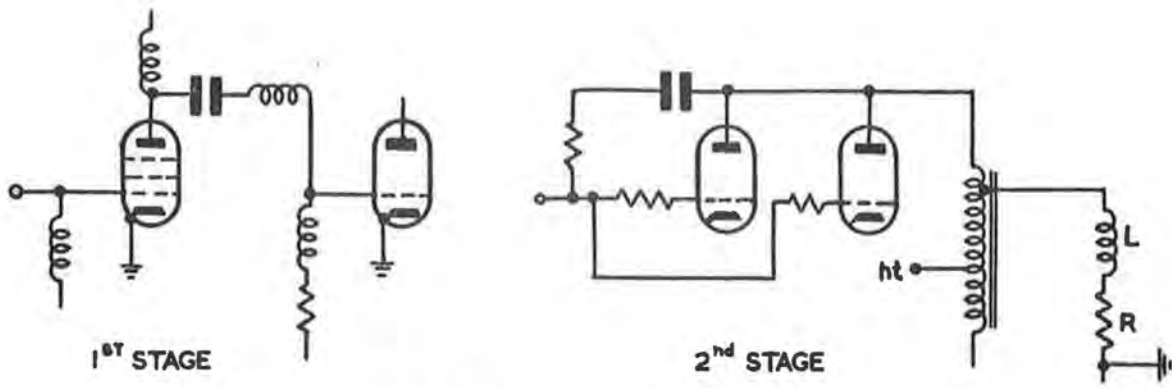


Fig. 6.3.3(ix) Pentode stage circuits.

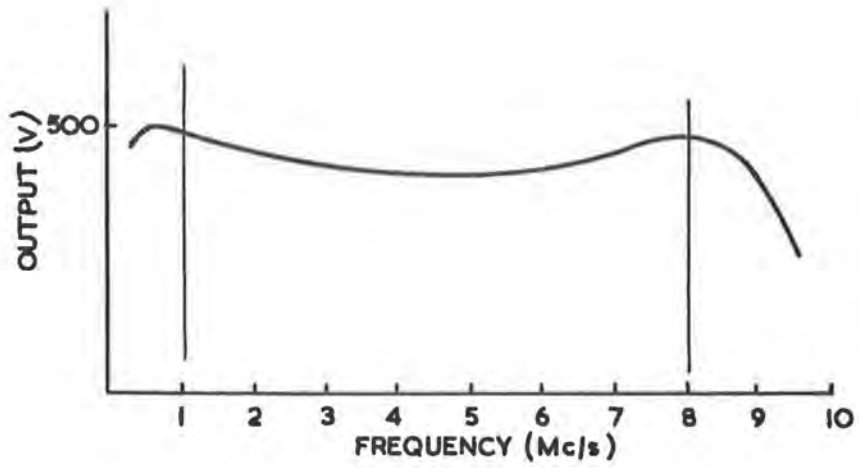


Fig. 6.3.3(x) Response of QY5/3000A (tetrode) driver stage.

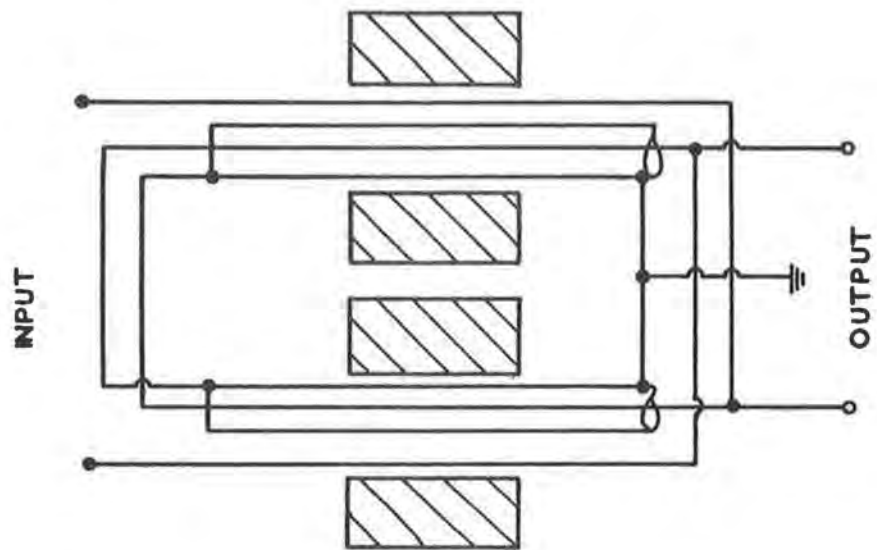


Fig. 6.3.3(xiv) Winding arrangement on the driver output transformer.

During the development of the cavity and the incorporation of the integral r.f. transformer the characteristics became more accurately understood and the graphs in Fig. 6.3.3(vii) and (viii) give the actual conditions seen by the amplifier.

To meet the load conditions applicable at a frequency of 4.5 Mc/s, the output valves work under the following approximate conditions:- $V_b = 10$ kV, $E_a \text{ min} = 3$ kV, $V_c = -140$ V, $E_g \text{ max.} = +300$ V, $E_g \text{ drive} = 440$ V, $P_{\text{out}} = 23$ kW, $P_{\text{in}} \approx 50$ kW, $P_a \text{ diss.} = 27$ kW, $\theta_p = 180^\circ$, $P_{\text{grid diss.}} = 200$ W, $I_m \approx 18$ A. There is considerable grid current. If $I_g \text{ total} = 3$ A, then $I_g \text{ fundamental} \approx 1.3$ A and the impedance seen by the driver at this frequency is about 300Ω shunted by $-120j\Omega$. Both the grid current and reactive current components of the driver load vary considerably over the band.

(b) Experimental driver

The only designs considered for the driver had wideband untuned stages throughout. For power amplification, two types of valves were used: The first was an output pentode (EL 34) rated for 25 W anode dissipation and intended for audio reproduction. It has $C_{\text{out}} = 8.4$ pF and $g_m = 11$ mA/V. A pair in push-pull were used to drive four in parallel push-pull. The anode loads of the first pair were given high frequency compensation by shunt peaking as shown in Fig. 6.3.3(ix). The anode load of the second stage was an autotransformer feeding an inductance peaked resistive load which was designed to swamp the input impedance of the succeeding stage. The resistance value was 300Ω . The output transformer used two tape wound coil stacks side-by-side on a small toroidal ferrite core and the stage delivered a 70 V peak signal to the succeeding stage with a flat response over the band. Feedback was used to improve linearity and to maintain a good sinusoidal waveform in the output; the second of the two stages ran under Class A conditions. The basic circuit configuration of this stage is also shown in Fig. 6.3.3(ix).

The next stage used the second type of valve (QY5/3000A) in push-pull and Class A. The valve is a high power forced-air cooled tetrode rated for anode dissipation of 3 kW and primarily intended for use in VHF television transmitters. It had the desirable qualities of $C_{\text{out}} = 8.4$ pF and $g_m = 19$ mA/V with C_{in} no more than 23.5 pF. This stage ran with quiescent anode currents of 1 A at $V_b = 2$ kV and $E_c = 0$ V. The anode load was again a wideband ferrite cored autotransformer feeding a resistive load of 300Ω , and the stage delivered a 200 V peak signal with flat response over the band, and faithful reproduction of the input waveform. Up to this point the core sizes and wire lengths involved in the wideband transformers had not brought any unwanted resonances within the band or caused lack of end coupling. The design of the output coupling transformer for the final driver stage did, however, involve these, and other factors.

The aim was to provide a signal of 600 V peak over the band into the load already defined as the input impedance of the amplifier output stage. This was achieved by using four of the tetrodes in parallel push-pull, Class B condition, with grid current. The valves parallel very readily at these frequencies and three on each side have been used very satisfactorily. Screen and control grid stoppers were used but not anode stoppers.

To keep the flux swing in the output transformer core to a reasonable level the core was necessarily large and the leakage inductance and winding capacitances were high. The toroidal core size was 150 mm OD, 50 mm ID, 40 mm thick and carried a total of 32 turns of wire. The leakage inductance of this transformer was arranged to resonate with the input capacitance of the final amplifier BW 161 tubes and for a level input over the band the driver output stage produced a response curve as shown in Fig. 6.3.3(x). It shows a characteristic peak below the bottom frequency of the band due to shunt winding resonance, then a slight droop and a flattened peak just above 8 Mc/s. The flattening was achieved by resistors placing 350 Ω across the transformer primaries and has the effect of maintaining the screen currents of the tetrodes at an acceptable level throughout the band.

Complete circuit diagrams for the prototype transmitter are given in Figs. 6.3.3(xi), 6.3.3(xii) and 6.3.3(xiii). This driver and output stage was used successfully through all the early testing of the cavity, the automatic gap voltage control and the automatic cavity tuning system.

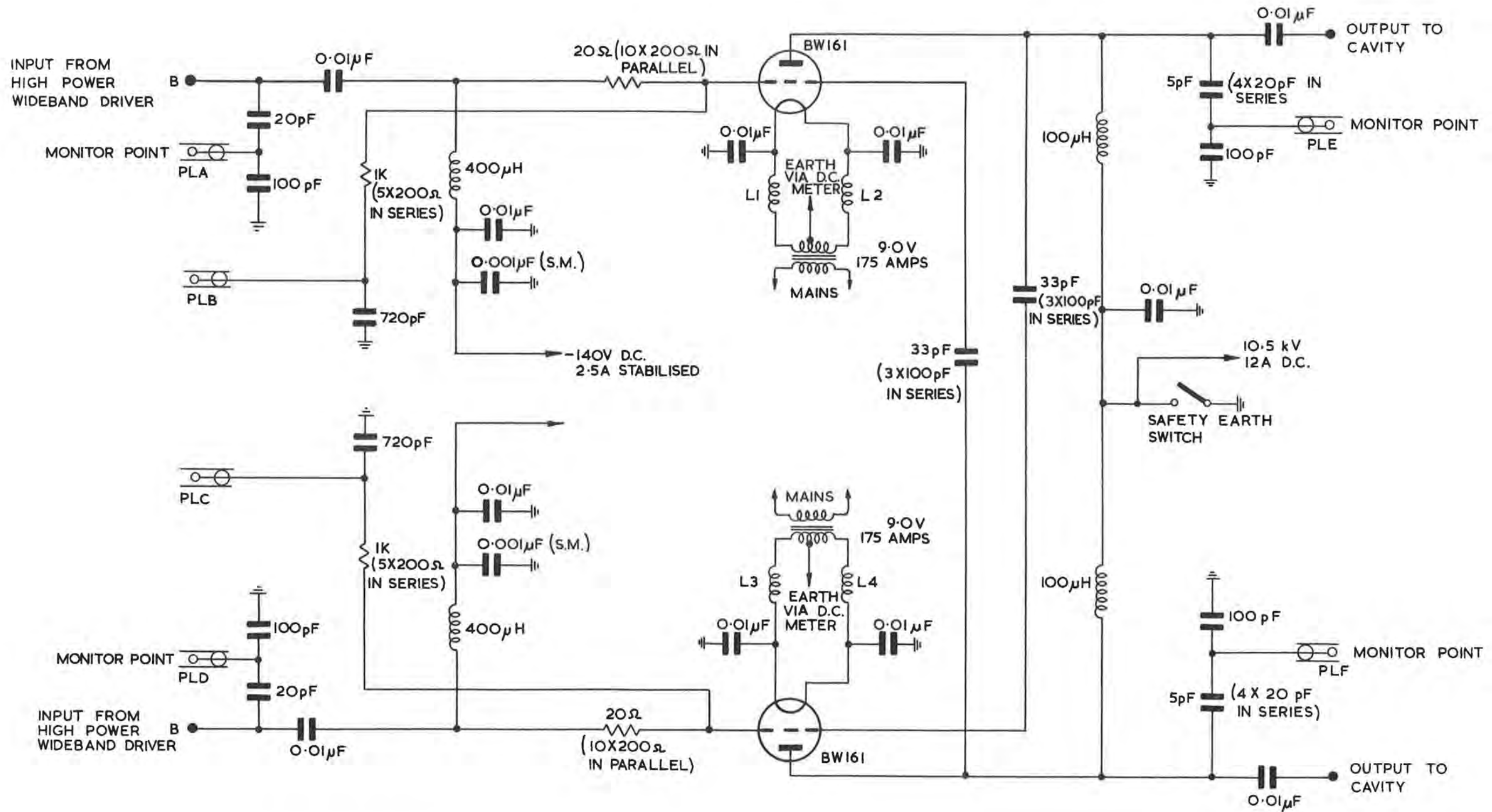
(c) Wide band transformer development

Further work was carried out on the driver output transformer and a large number of winding and core configurations were tried. The following design considerations were incorporated in the transformer. It would couple the anodes of six of the tetrodes connected in parallel push-pull to the grids of the BW 161 valves and give a flat response over the range 1.4 Mc/s to 8 Mc/s. The use of transformer coupling enables a leakage inductance to be selected which will separate the output and input capacitances of the stages to be coupled to form a π network at the upper frequencies. In this way it is possible to achieve a flat response characteristic over the band and to introduce a transformation ratio to accommodate the difference between the two capacitances. At an upper frequency limit of 10 Mc/s the reactance of the 200 pF looking into each BW 161 is 80 Ω . The load resistors from each grid to ground were therefore fixed at 75 Ω .

The total anode capacitance of each side to ground is 100 pF, the reactance at 10 Mc/s being 160 Ω . Together with strays, this gives an anode-anode impedance of 300 Ω . The impedance ratio required for the transformer is therefore 300:150 Ω ; a turns ratio $\sqrt{2}$:1. The nearest possible figure with the low number of turns required is 1.5:1.

The transformer must handle a peak drive voltage to each BW 161 of 500 V. The total r.m.s. drive power is therefore 3300 W. The transformer losses must be kept low because of heating and for efficiency. It was manufactured on a core consisting of eight ferrite toroids each having OD = 3 in, ID = 1 in and axial length 1.57 in. These were arranged in binocular form with concentric and strip windings to give limited impedance matching through the windings.

The transformer design met the specification and could be overloaded to deliver 1000 V from each output terminal to ground at 6.3 Mc/s. The basic winding arrangement is shown in Fig. 6.3.3(xiv).



L1 - L4 ARE V.H.F. CHOKES.

Fig. 6.3.3(xiii) Prototype transmitter - Final stage power amplifier.

6.3.4. Final Amplifier Design

(a) Output stage

Early in 1960 it was necessary to consider production of a fully engineered version of the experimental transmitter capable of unattended operation from a remote station.

The choice of valve for the output stage was the BW 161.

The valves operate in conditions which utilise their characteristics to produce a transition from Class A to Class C as the drive signal is increased. Initial grid bias sets the quiescent anode currents at approximately 2 A each. These currents rise as the drive signal is increased but, due to the operating transition mentioned, are no more than 5 A when they are delivering the required maximum output power. The output stage is arranged as a wideband amplifier with aperiodic grid circuits and loosely coupled anode circuits, and the valves are cross-neutralised by variable vacuum capacitors. The basic circuit arrangement remained the same as that used for the experimental transmitter.

Neutralising the cold amplifier is achieved using a portable oscillator and detectors made for the purpose. A filter network is incorporated in the neutralising connection to prevent a self-oscillatory condition at the frequency at which the input of the cavity load shows a series resonance (about 18 Mc/s).

(b) Driver stage

At the higher frequency end of the band, the anode swing required from the BW 161's is increasing and under these conditions the reactive component of drive current is comparable with the peak electron grid current which has almost triangular waveform. A driver of the cathode follower type having low impedance, good regulation and the necessary bandwidth for the harmonic content was therefore considered. Various designs had previously been considered working in Class A with large standing valve currents. The driver circuit finally evolved is a combined push-pull phase-splitter/cathode follower. Type TY6/5000 W triodes having a high slope characteristic and consequently low cathode impedance are used. They operate with zero bias under quiescent conditions and with grid resistors returned to chassis. When driven, a transition from Class A to Class B operation takes place as increasing grid current develops grid bias.

At high input signal levels with the valves in Class B the driver produces only positive-going half cycle outputs from each cathode. Thus in any half cycle one cathode follower valve and one power amplifier are cut off. But the power amplifier tube is cut off by its steady d.c. bias voltage under a condition in which, due to push-pull coupling in the anode circuit, the anode potential is rising and this leads to an inefficient anode condition. The driver valves are therefore used additionally as phase splitters. Outputs are taken from resistance loaded anodes to the opposite grids by capacitors and the negative-going signals are used to swing the opposite valve into a true cut-off condition.

Under conditions of low signal input, this stage will operate in Class A to produce full waveform outputs in antiphase. D.C. returns to both grids and cathodes of this stage are made by a r.f. choke. The basic circuit is shown in Fig. 6.3.4(i).

(c) Low-power driver stage

To provide the required output of about 500 V peak from the cathode-follower phase-splitter stage an input of about 900 V peak is needed. To give this, the sub-driver has four radiation-cooled tetrodes (QY4/250) in parallel push-pull working in Class AB.

The interstage coupling has two elements: a shunt-fed transformer and a frequency compensating filter network. The transformer has very tightly coupled windings to transfer signals in push-pull to the input of the succeeding stage. The filter network can be described as having one and a half sections of a low pass, constant K filter with a mid-series termination which allows the input capacitance of the succeeding stage to be used as the mid-shunt capacitance. The stage is conventionally equipped with stopper resistances.

This sub-driver is itself driven by a cathode follower which has two radiation cooled triodes (Type TY3/250) in Class A push-pull. The output impedance of the stage matches the control grid requirement of the sub-driver amplifier. The r.f. input to the stage is fed via a full section, constant K filter network. The amplifier chain is completed by the five cascaded stages of the pre-amplifier.

The low-level r.f. excitation signal is fed into the first R.C. coupled single pentode stage together with the automatic level control signal which is applied to the high slope suppressor grid. Then follows a second R.C. coupled single pentode as a buffer amplifier. The next stage is a push-pull voltage amplifier, also used to provide unbalanced to balanced signal conversion, followed by an amplifier operated as a long-tailed pair and finally a Class A push-pull stage using two valves type QV06/20. These last two stages are also R.C. coupled but with some inductive compensation so as to utilise their high gain qualities.

The output of the tetrode (QV06/20) is about 180 V peak at an impedance level which matches the requirement of the cathode follower (TY3/250). Fig. 6.3.4(ii) shows the completed amplifier cubicle in position.

(d) Beam loading

The original r.f. specification included a maximum accelerated beam of 2×10^{12} protons per pulse. The power absorbed by the beam from the r.f. amplifier is proportional to frequency, and at 8 Mc/s is 1.6 kW for each 10^{12} p.p.p. From the actual performance of the amplifier at all frequencies, it is estimated that 5×10^{12} p.p.p. could be accelerated. The first limiting point is at 4.5 Mc/s where probably it would be dangerous to increase the phase angle.

6.3.5. Automatic Level Control of Gap Voltage

(a) Introduction

During the operating cycle, the amplitude of the accelerating voltage at the cavity gaps has to be controlled by a d.c. signal fed to the r.f. amplifier from an external source. This signal is derived from the same pick-up coil (placed in

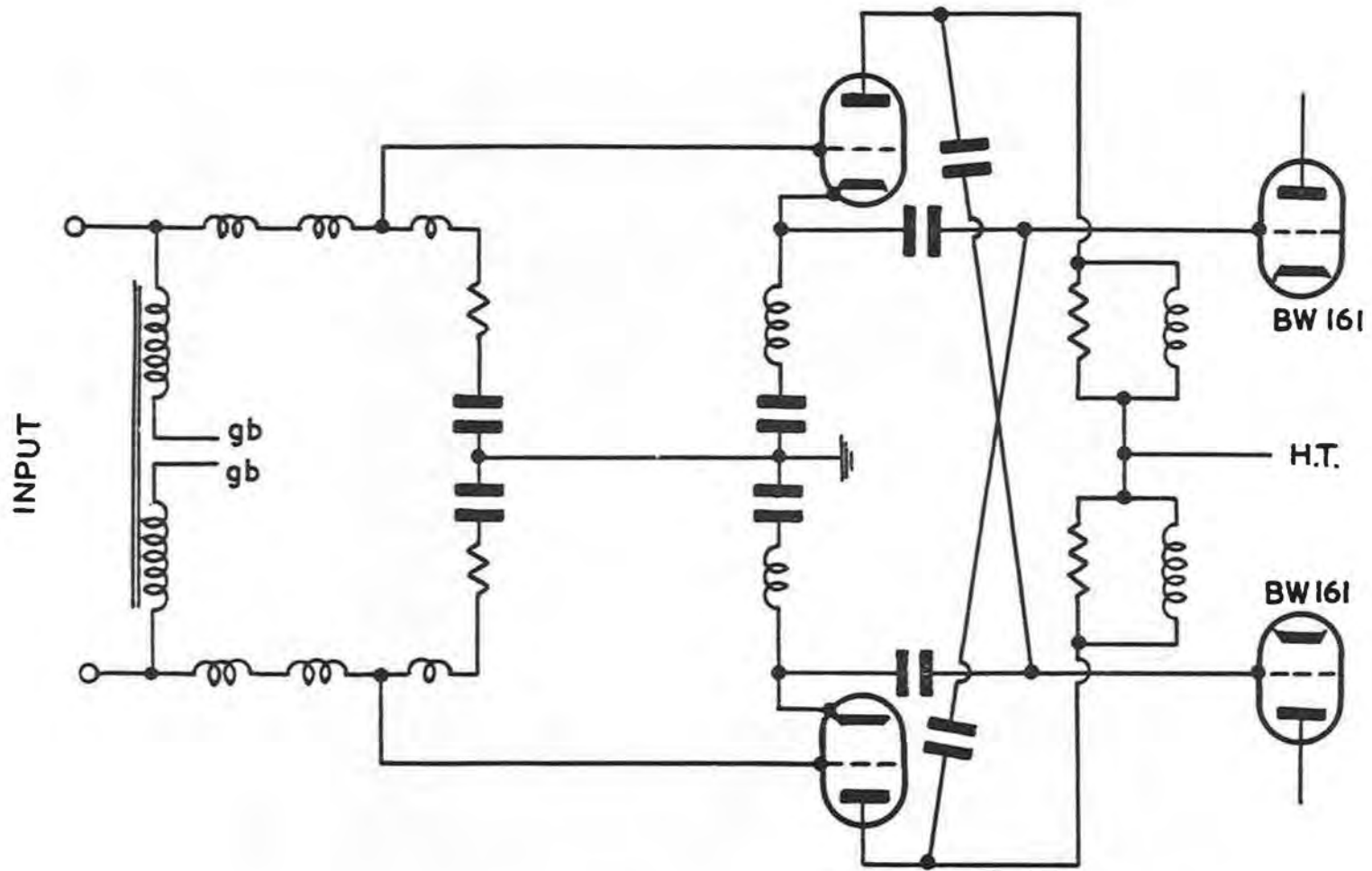


Fig. 6.3.4(i) Phase splitter/cathode follower driver circuit.

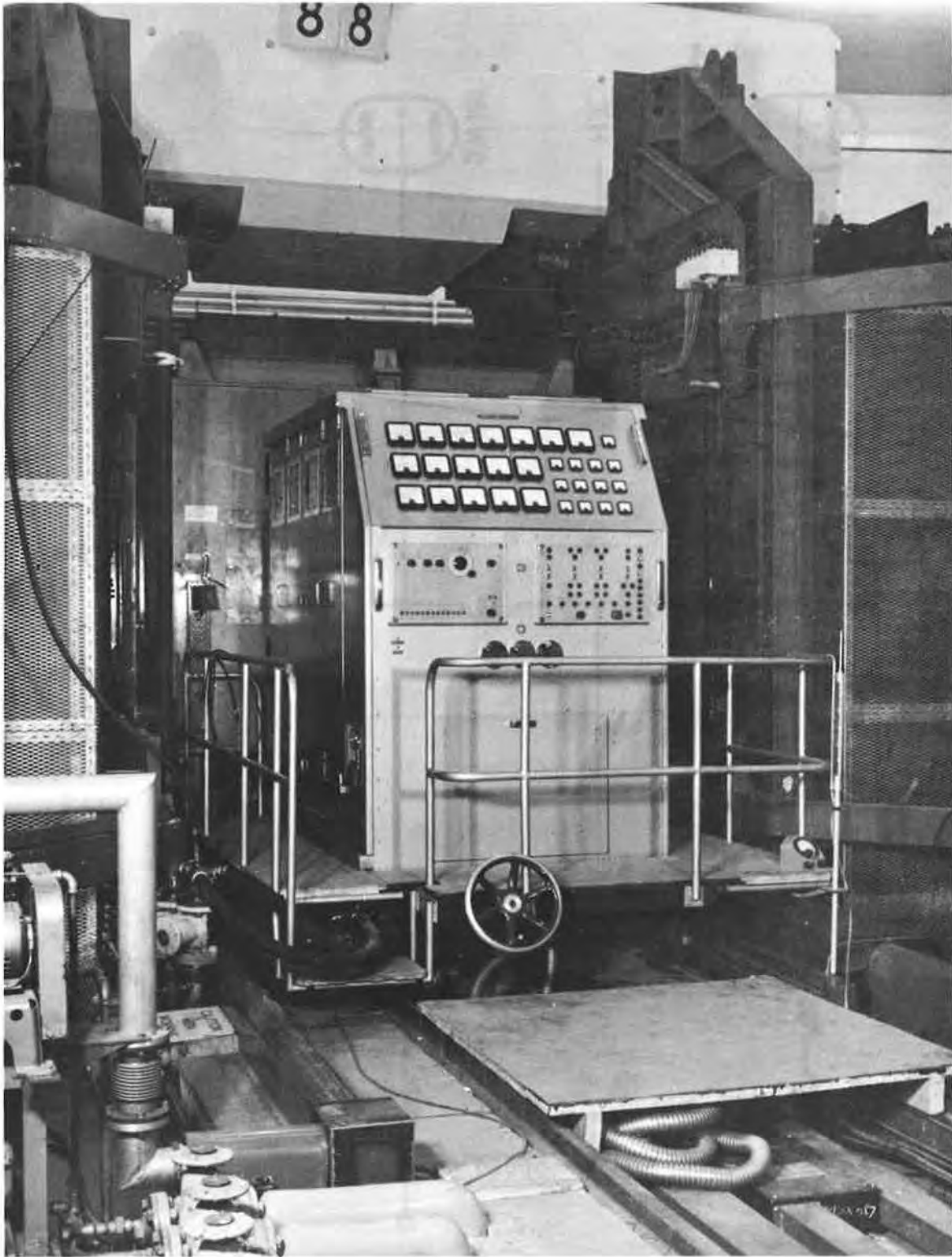


Fig. 6.3.4(ii) View of final amplifier cubicle in position.

the main magnet field) as that feeding the B signal to the P.F.G. and it is fed via a shaper to an emitter follower in the main control room. A control labelled "Synchronous Phase" feeds a pre-set proportion of this signal from the emitter follower to the r.f. amplifier. The cavity gap voltage must be proportional to this signal over a range extending down to at least one sixth of the full accelerating voltage.

A further requirement is that internally generated disturbances to the gap voltage such as those arising from ripple on H.T. supplies to the r.f. amplifier must be reduced to an acceptable level. These requirements are met in the closed loop circuit shown in Fig. 6.3.5(i).

A two-valve circuit is connected at the front end of the r.f. amplifier chain. The r.f. drive signal from the primary frequency generator is fed to the control grid of the first valve. The voltage on the suppressor grid is used to control the output from this stage. The gap voltage is reduced by a factor of 120 in a capacitance divider and rectified in a peak detector; this envelope is applied to the summing junction of a d.c. amplifier-cathode follower combination. At the summing junction it is compared with the programme voltage from the magnet field coil and the difference is amplified and fed to the suppressor grid of the automatic level control stage valve as a correction signal.

(b) Circuit details and performance

The amplitude sensing, capacitance potential divider is connected to the gap flanges of the drift-tube assembly and the output is fed through the cavity wall at a convenient point adjacent to the power amplifier. The cable from the divider must thread the ferrite core once on its way to the cavity wall and is necessarily rather long. Care is taken to damp any cable resonances which appear at low harmonics of any frequency within the band.

The detector uses germanium diodes in a simple voltage doubler circuit and is placed at the divider output terminal on the cavity itself. The output from the detector is fed via a 4.7 k Ω resistor to the summing junction of a d.c. amplifier which is followed by a cathode follower. A feedback resistor of value 56 k Ω is connected from output to input of this combination and across this resistor are connected Zener diodes and the series R-C combination shown in Fig. 6.3.5(i).

The series R-C combination serves to prevent the closed loop being self oscillatory in the frequency range in which its gain-phase shift characteristics would otherwise make it so. The combination is chosen not to have too adverse an effect on the transient response of the loop, which could be important under the following condition: if a signal exists on the gap voltage control terminal before the r.f. signal from the primary frequency generator is gated on, the suppressor grid of the first valve will be at approximately zero volts when the full r.f. signal is applied to its control grid. Full gap volts will appear in the cavity and these volts must be brought under automatic control in a time which is short compared with phase oscillation period. In the arrangement described this time is about 40 μ s. The Zener diodes limit the voltage of the suppressor grid of the valve to the required range (and no more), the diode current being provided by the cathode follower.

In the normal mode of operation of the system the gap voltage control signal will be gated at a time which eliminates the over-shoot of gap voltage.

The gain of this d.c. amplifier network in the low audio frequency range is seen to be approximately 12. The gain at these frequencies, between the suppressor grid of the first valve and the output of the detector, is approximately 13, and therefore the internally generated ripple voltages at these frequencies are reduced by a factor of about 150.

6.3.6. Phase Detector

(a) Principle

The basic principle is that of the conventional overlap phase detector, depending upon the production of rectangular current pulses, whose width depends upon the overlap between the positive half cycles of two input sine waves. These variable width pulses are then integrated to give a demodulated output. The two inputs are obtained, one from the grid of the final power amplifier valve via a 90° phase lag network (reference signal), and the other from the anode of the final valve via a 200:1 capacitive potential divider. Coincidence is measured using a 6BN6 gated beam valve so that when the power amplifier valve anode voltage is 180° out of phase with its grid, the grids of the 6BN6 are in quadrature, placing the phase detector at the centre of its range. If the valve anode is other than 180° out of phase with respect to the grid, then the 6BN6 grids will overlap to a greater or less extent.

Development of the phase detector has taken place in the three stages.

(b) First circuit

The final r.f. power amplifier stage is in push-pull and advantage was taken of this to employ two 6BN6's with paralleled outputs connected, as shown in Fig. 6.3.6(i)-(a), thus deriving two current pulses per r.f. cycle instead of one. This doubled the sensitivity.

Performance was satisfactory provided the r.f. amplifier operated at full gap voltage throughout the frequency band. However, the cavity is required to operate at a much lower gap voltage at injection, and choosing a figure of 1 kV from 1.4 Mc/s to 2.0 Mc/s, there is insufficient input at this level to the 6BN6's (particularly from the power amplifier grids). It was necessary to provide gain at the lower r.f. frequencies between the phase detector inputs and the 6BN6's. This was achieved by replacing the cathode followers with cathode coupled limiters (Fig. 6.3.6(i)-(b)).

(c) Second circuit

Identical limiters were used, the simplified circuit being given in Fig. 6.3.6(ii). The advantages of this circuit are:

(i) At high input levels, it functions as a symmetrical clipper and thus assists the 6BN6 in amplitude limiting;

(ii) At low levels, it functions as an amplifier, consisting of a cathode follower driving a grounded grid stage, so that the input impedance is high and the amplifier is stable without neutralising;

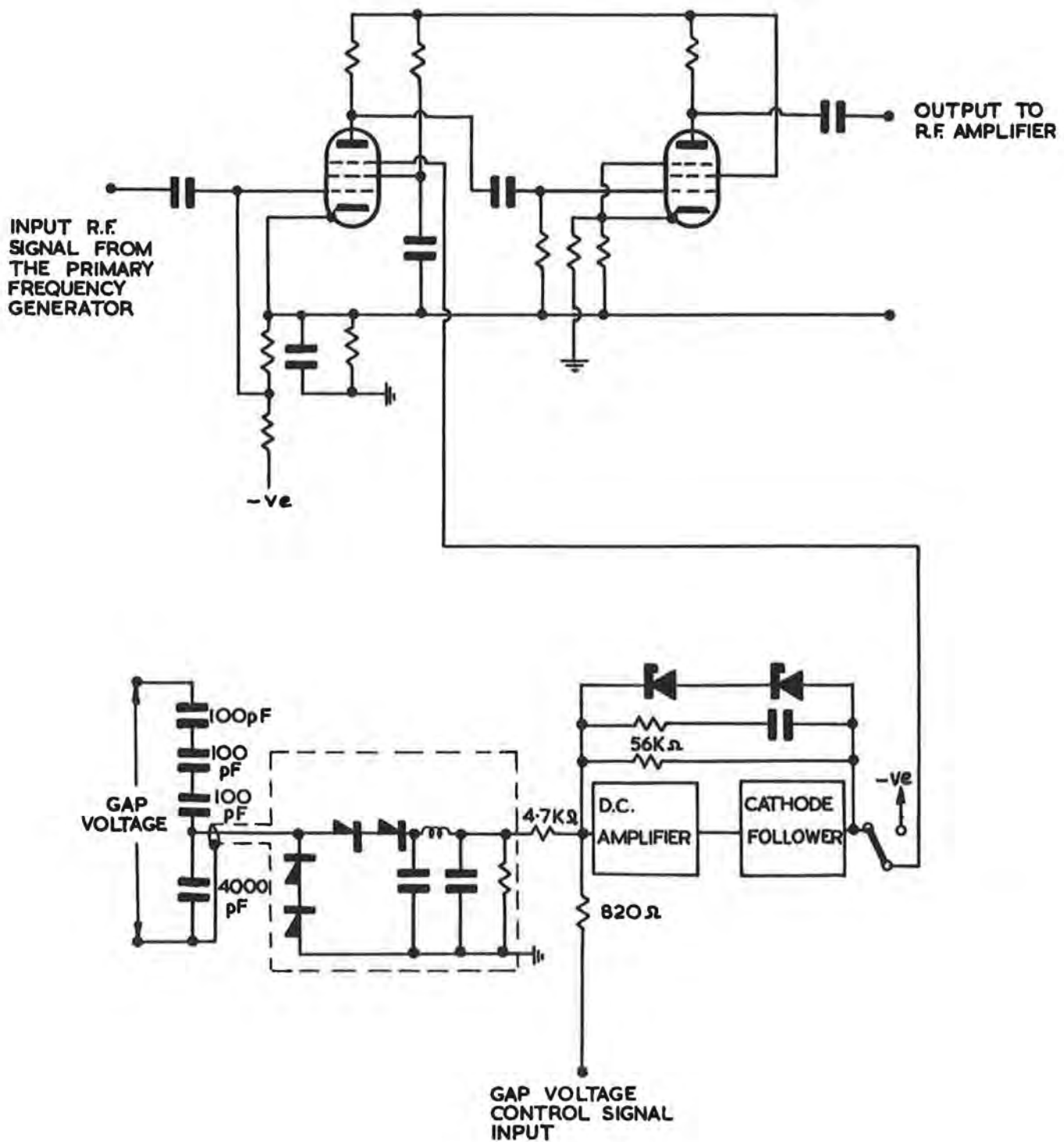


Fig. 6.3.5(i) Circuit for the automatic level control of gap voltage.

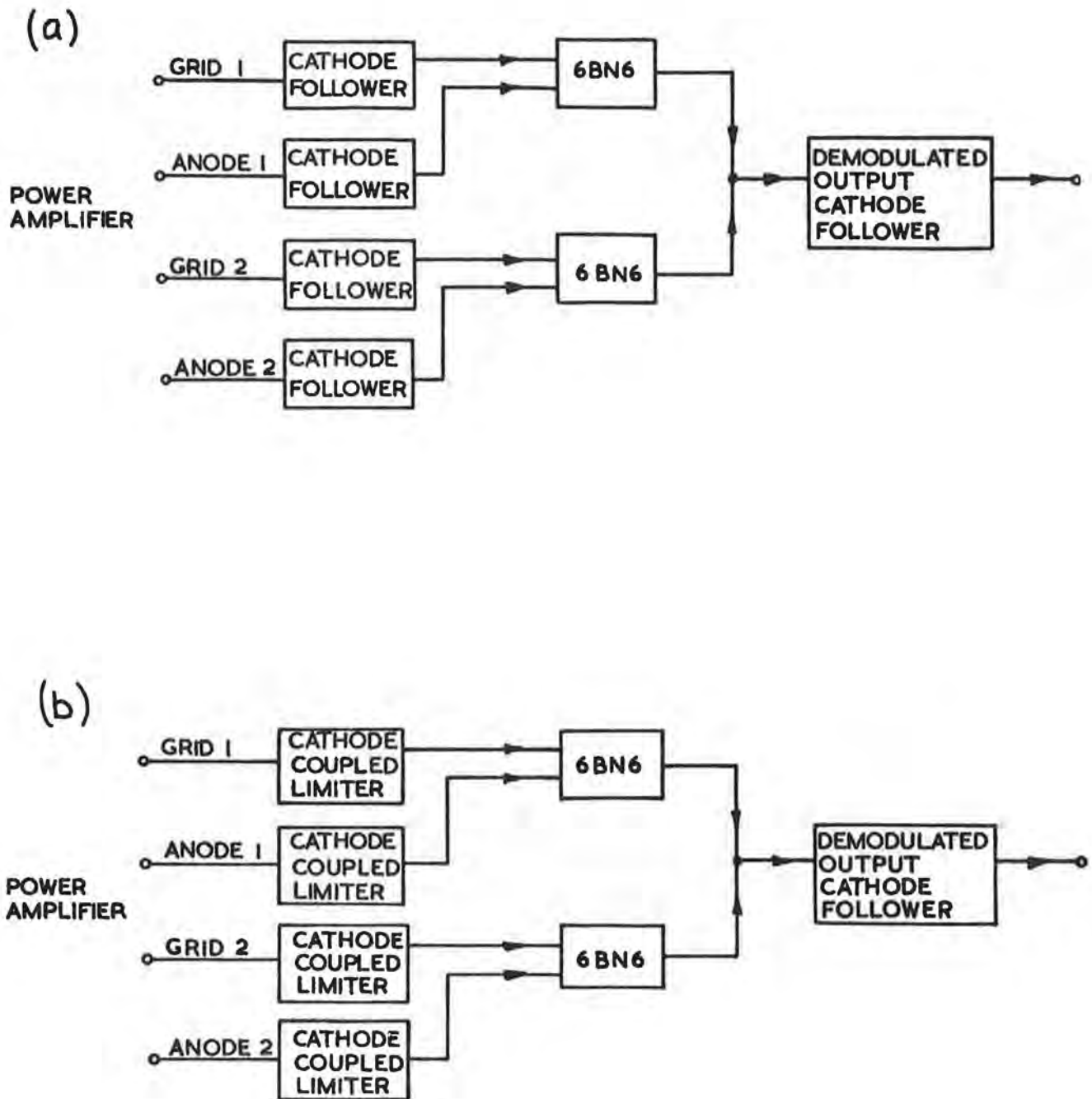


Fig. 6.3.6(i) Block diagrams of the first phase detector circuits.

(iii) Limiting is achieved by anode current cut-off on both half cycles of r.f. input (V1a then V1b) and, ideally, no grid current flows.

The gain of the limiters in the region 1-2 Mc/s is about 4.5 (there is some variation as the 6BN6's draw slight grid current which varies with input amplitude).

With this modification the detector functioned at a much lower gap voltage, particularly at the lower r.f. frequencies. However, variation in the level of the gap voltage caused the set zero to change since the current pulses at the anodes of the 6BN6's are not perfect square waves. The larger the input signal to the phase detector, the better the limiting and the faster the rise time, so that after integration the mean level increases. The difficulty has been largely overcome in the final version by using a differential system.

(d) Final circuit

Comparison of Fig. 6.3.6(iii) with Fig. 6.3.6(i)-(b) will show that the final version consists essentially of two phase detectors V5/V6 and V7/V8 with the difference that the inputs to V7/V8 are crossed over (e.g. V8 6BN6 functions with the power amplifier anode 1 and grid 2). This means that the outputs of V5/V6 and V7/V8 are in push-pull and are converted to single ended output via the differential amplifier. Variations in the rise times of the current pulses produce a common mode signal at the output of V5/V6, V7/V8, and this is rejected by the differential amplifier.

From 3 kV to maximum peak gap voltage, the performance is satisfactory over the whole r.f. band with a sensitivity of 0.55 V/degree. At 1.4 Mc/s to 2 Mc/s the detector functions normally down to 600 V peak gap voltage, but at higher frequencies anything lower than 3 kV results in a much lower sensitivity and a reduced maximum available output. Maximum output swing is $\pm 25^\circ$, which is sufficient to cover the initial transient phase error in the servo loop.

With the cathode-coupled limiters each feeding two 6BN6's, capacitive loading puts the linear bandwidth of the former at around 8 Mc/s. At the higher frequencies there is, therefore, considerable phase shift through the limiters, but this is balanced on all four inputs and the overall error is small. The practical circuit layout is symmetrical so that stray capacities are equal on all four limiters.

(e) Phase lag network

The 90° phase lag network from the grids of the power amplifier is a simple R-C filter comprising a series 1 k Ω resistor and a parallel 1200 pF capacitor. These values put 1.4 Mc/s at approximately ten times the filter cut-off frequency, giving a phase lag of 85° . One disadvantage of this network is the fall in output with increased frequency at the rate of 6 db/octave, but it does have the advantage that harmonics are attenuated, (2nd harmonic - 6db, 3rd harmonic - 9.5db). Second harmonic distortion of the type encountered in the grid waveform, after transmission through the network, would result in a waveform which is

symmetrical about the time axis, and has zero crossing points which are not displaced so that the phase detector functions correctly. The exaggerated waveforms shown in Fig. 6.3.6(iv) illustrate this point (the waveform (b) has been amplified x 10 for comparison).

Transmission time through such a network is not constant for all frequencies. The power amplifier grid waveform is however, fairly sinusoidal and there is no problem from the distortion point of view.

(f) Physical arrangement

The phase detector unit is mounted in the r.f. amplifier cubicle, and connected to the anode potential dividers and the grid lag networks with coaxial cables of length 5 ft and 7 ft respectively. At the sending end of these cables, resistors of value equal to the cable Z_0 (100Ω) have been inserted in series. On the assumption that the cables are lossless and terminated in an open circuit (a good approximation as the phase detector input impedance is high), it can be shown that the magnitude of the ratio of source voltage to received voltage at the detector is unity and independent of the line length. This reduces voltage variations that would occur due to transformation on the cables. Furthermore, viewed from the phase detector, the cables are approximately matched instead of presenting a high-Q circuit at the $\frac{\lambda}{4}$ resonant frequency of 24-30 Mc/s. The phase relationship between the source and the detector input now depends on line length as in a matched line ($\phi = \tan^{-1} \beta l$). The 2 ft difference in grid and anode leads contribute a maximum error of 5 degrees as the r.f. frequency changes but this is compensated for elsewhere.

(g) Semiconductor phase detector

Earlier in the development programme a transistorized phase detector was designed operating on the same principle of overlapping square waves. This showed promise when tested on the bench but difficulties arose in adapting the unit to the r.f. amplifier. The maximum input to the detector (determined by transistor base-emitter ratings) was around $+0.5$ V, and it was necessary to employ diode limiters on all inputs (Fig. 6.3.6(v)).

In this circuit the clipping and squaring of the waveform was performed at the outset before reaching the phase detector proper. Unsymmetrical clipping displaced the zero crossing points and the detector did not function correctly. Symmetrical clipping was difficult to achieve, due to variations in the detector input impedance as the input transistors were switched. There were also hole storage effects in the diodes. It was difficult to balance phase shifts through the diode limiters, as the input levels from the power amplifier varied over such a wide range.

Development was not pursued as the thermionic detector showed more promise, but it is not thought that a semiconductor phase detector is impossible, especially with improvements in modern transistors and diodes. Considerable work on the problem would be required, however, and the question of adequate cooling in the power amplifier cubicle would require special attention. Alternatively, to avoid damage by radiation, the phase detector would have to be located remotely, and long, matched cables would have to be used.

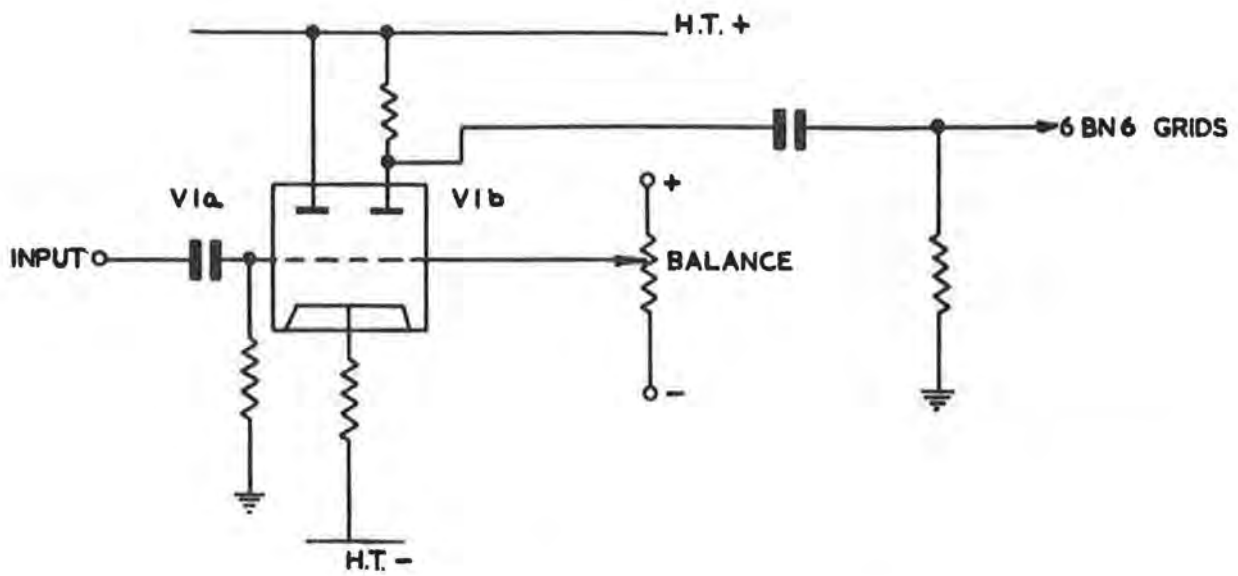


Fig. 6. 3. 6(ii) Second phase detector circuit.

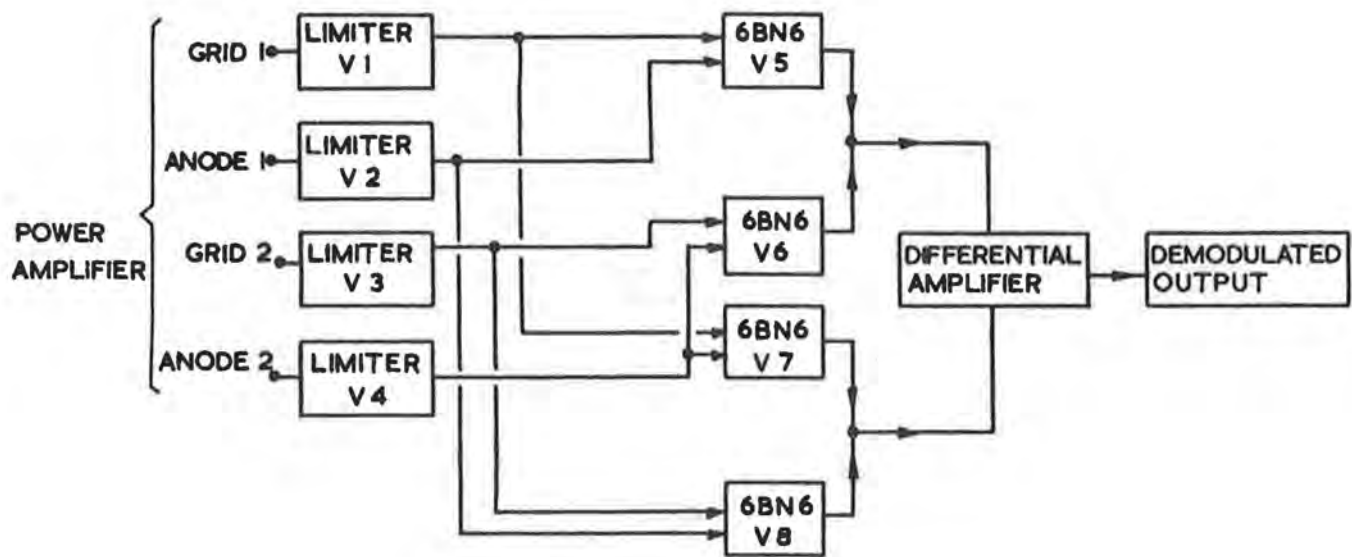


Fig. 6. 3. 6(iii) Block diagram of final phase detector circuit.

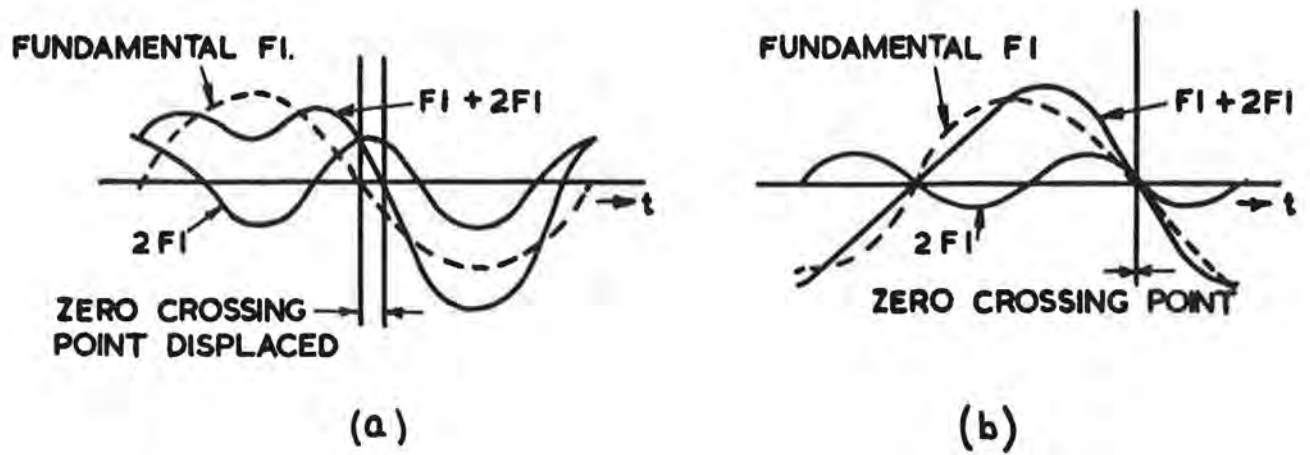


Fig. 6.3.6(iv) Waveforms transmitted through the phase lag network.

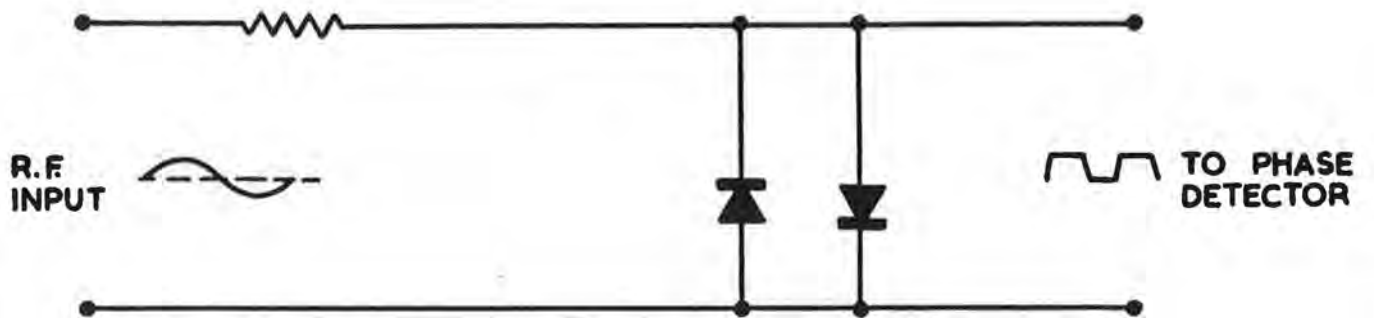


Fig. 6.3.6(v) Diode limiters on the semiconductor phase detector input.

6.3.7 Mark I (Thermionic) Bias Supply

(a) Basic circuit

The control circuit of this supply is essentially the same as that used with the Bevatron. Fig. 6.3.7(i). Each phase of the input three-phase transformer, T1, has its secondary connected in series with each corresponding primary of the load transformer, T2. The delta arrangement of T1 secondaries and T2 primaries feeds the selenium rectifier MR1, on which there is a variable load made up of the two control valves LV1 and LV2. Variation of the current through LV1 and LV2 effectively controls the voltage applied to the T2 primary. The secondary voltage of T2 is rectified by the germanium rectifier MR2 to provide the load current up to a maximum of 800 A. Ideally, with the control valves biased to cut-off, the output would be zero, but the inverse resistance of the selenium rectifier draws current and the output of the germanium rectifier has a standing current of some 10 to 15 A. This is backed off as described later.

(b) Ripple

The utilisation of a three-phase supply ensures that the ripple current in the output is small and is approximately 4% of the d.c. load current, though this percentage varies throughout the current range as the cavity inductance changes. Reduction of this ripple with a conventional smoothing circuit is not possible, for this would increase the bias supply time constant, but with the application of voltage feedback the current ripple has been reduced to less than 0.3% over the whole range. With the bias supply in the phase detector and cavity tuning loop, the phase modulation due to bias current ripple is never more than 1° peak in the r.f. frequency range 1.4 Mc/s to 2.0 Mc/s, and negligible over the remainder of the band.

(c) Voltage feedback

In designing the voltage feedback circuit, measurement of the transfer function from the control valve grids to the output was complicated by the presence of the large 300 c/s ripple component, which was far greater in amplitude than the measured signal frequency. The Resolved Component Indicator with its ability to discriminate, was used successfully for the lower frequencies, while, for the higher frequencies, a Wave Analyser gave the amplitude plot and phase was estimated from this. The small signal d.c. gain varied with current level from -23 db to -36.5 db with a response flat to approximately 5 kc/s. To improve the high frequency response, a transformer was connected with the primary in series with the control valves anode circuit and the secondary in series with the output of the germanium rectifier. The turns ratio of this transformer is 200:1, which is the same as the germanium rectifier transformer T2, thus maintaining ampere-turns balance and extending the frequency response smoothly up to some 50 kc/s. Above this frequency the cavity bias winding no longer presents a simple inductance to the bias supply but enters a series of resonance and anti-resonance points, due (it is thought) to the distributed decoupling capacitors from the bias winding to the cavity skin forming, in effect, an artificial transmission line. The performance of the fast transformer is such that it will pass to the load all signal frequencies

above about 20 c/s, while signal frequencies below 20 c/s to d.c. reach the load via T2 and the germanium rectifier. As a result of the load inductance a rapid decrease of cavity current can demand a negative voltage swing, although the current will remain unidirectional. Without the fast transformer in circuit this is not possible as the germanium rectifier acts as a clamp to earth for negative potentials. The available negative swing however is limited, particularly at low current levels, where the control valves are biased towards cut-off.

The preamplifier preceding the control valves is a conventional d.c. amplifier consisting of two long tailed pairs and an output cathode follower. Overall voltage feedback is taken from the output of the cathode follower back to the first long tailed pair. The small signal d.c. gain is in the range +30 to +34 db, with a 3 db bandwidth at approximately 50 c/s. The response has been carefully tailored by networks in the feedback path to give a gradual fall of gain with a maximum phase shift of 60° in the region of 500 c/s and less at higher frequencies. Initially the peak in the closed loop response of this unit occurred close to 100 kc/s placing a high impedance in the grid circuit of the control valves at this frequency. With a 100 kc/s resonance in the anode circuit there was sufficient feedback for these valves to oscillate. The peak has now been reduced and moved to beyond 250 kc/s and the system is stable.

With the addition of a high gain operational d.c. amplifier, the voltage feedback loop is arranged as in Fig. 6.3.7(ii).

The d.c. gain of the d.c. amplifier is 60 dB with a bandwidth of 150 c/s and determines the d.c. drift of cavity voltage. This amplifier is a chopper stabilised type with a low drift figure. With the closed loop gain set at $\times 9$, the long term drift in bias current is about 0.05 A, assuming a resistance of about 20 m Ω for cavity winding and leads. It is possible therefore, to set the initial cavity bias sufficiently accurately for the cavity to be less than one degree off tune at the commencement of the acceleration cycle (≈ 1.4 Mc/s). The backing off supply shown in Fig. 6.3.7(ii) enables the cavity current to be zero despite the standing current mentioned in 6.3.7(a). The standing current will equal the backing off supply current, whilst the voltage feedback maintains zero volts across the load for zero signal input. Adjustment of R now provides a means of setting the standing current to a value higher than the previous minimum and still maintaining zero current in the cavity. This is useful, as the control valves will now function with a higher initial bias and a reasonable quiescent current, so that the voltage feedback is fully operational. Drifts in the backing off currents are not important as they are automatically compensated for by the feedback loop.

The bandwidth of the supply with voltage feedback as above is 3 db down at 20 kc/s.

(d) Automatic cavity tuning

Fig. 6.3.7(iii) shows in simplified form the arrangement of the bias supply in the automatic cavity tuning loop. The auxiliary amplifier raises the d.c. loop gain by +17 db and is tailored to stabilise the control loop consistent with the best frequency response. The auxiliary amplifier response can be approximated as shown in Fig. 6.3.7(iv). The complete closed loop frequency response varies with the bias current and is plotted against r.f. frequency in Fig. 6.3.7(v).

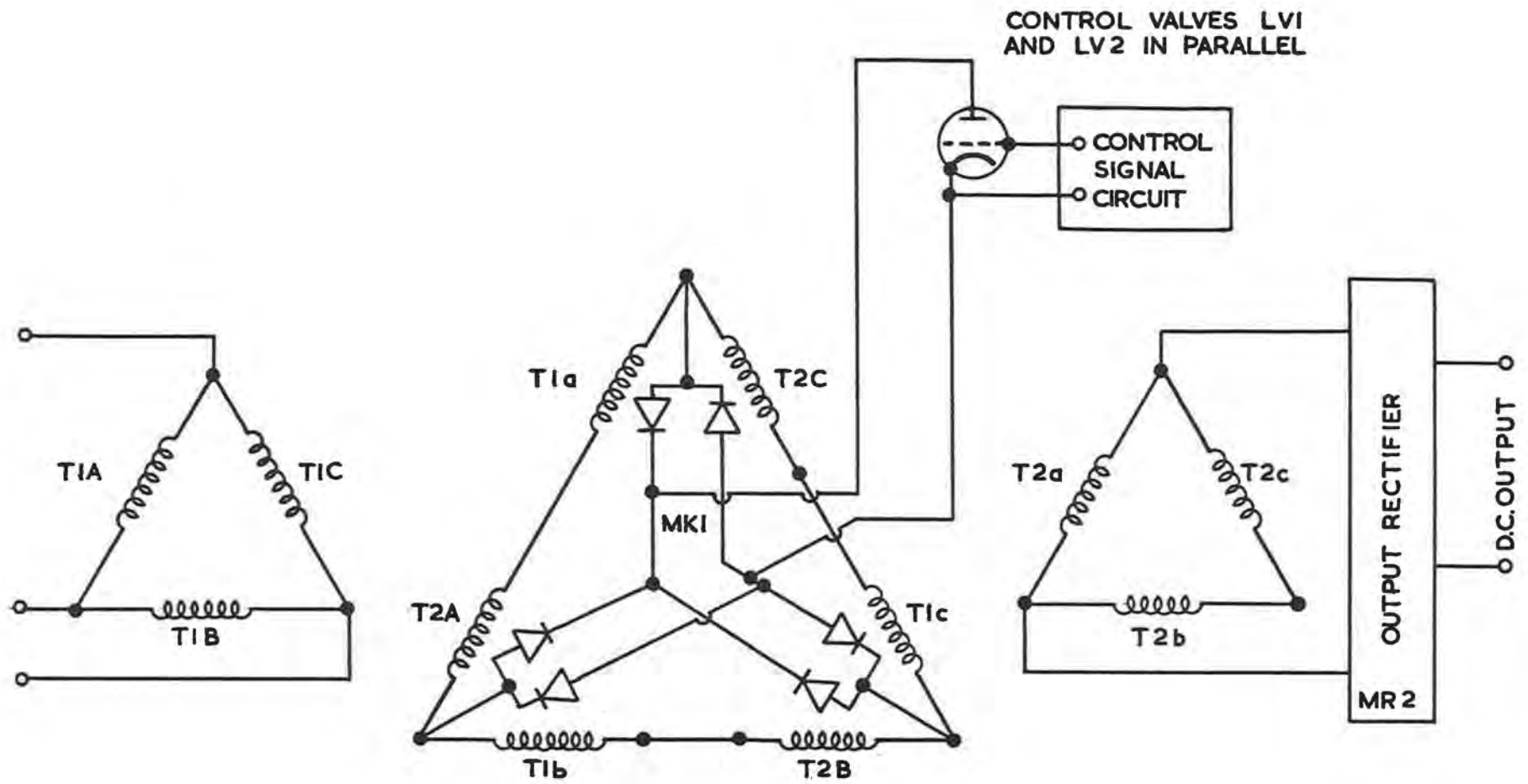


Fig. 6.3.7(i) Mark 1 thermionic bias supply circuit.

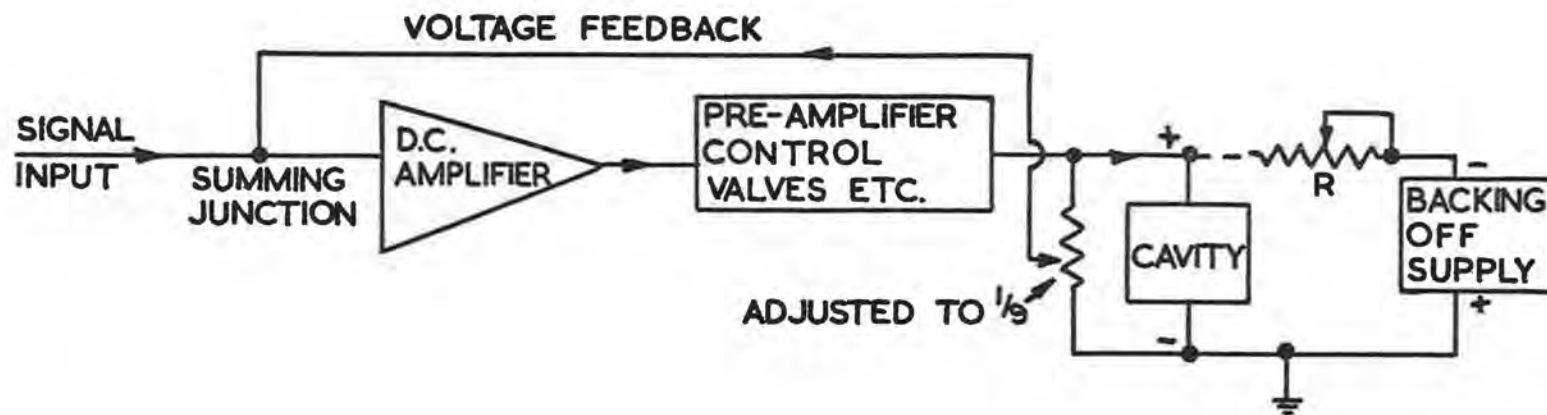


Fig. 6.3.7(ii) Arrangement of voltage feedback loop.

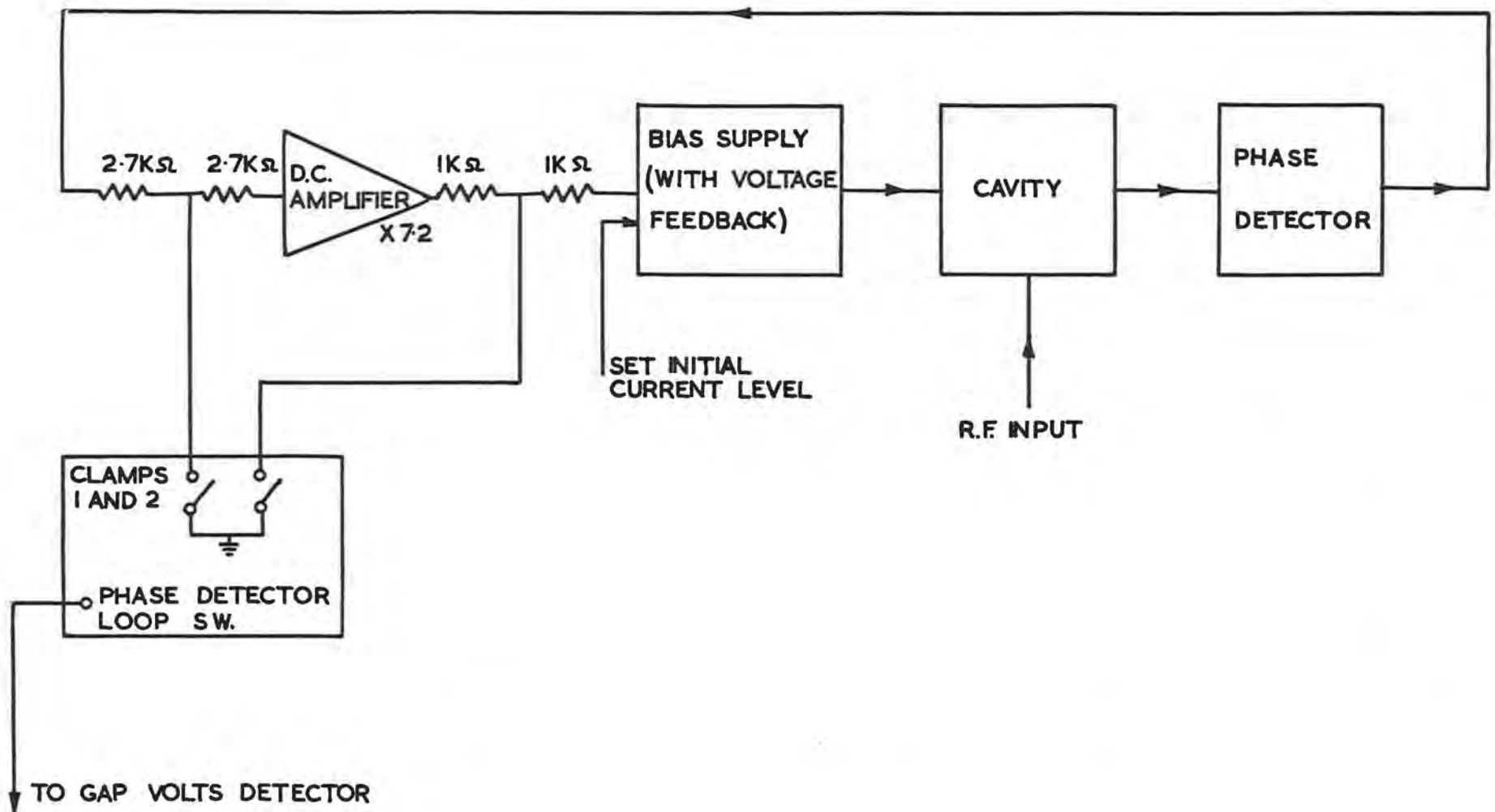


Fig. 6.3.7(iii) Arrangement of the bias supply in the automatic cavity tuning loop.

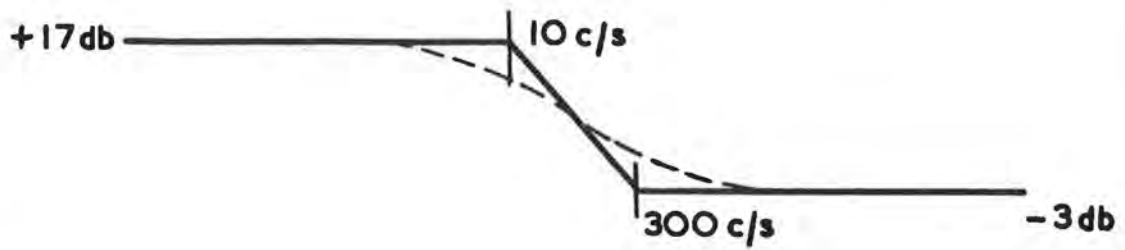


Fig. 6.3.7(iv) Auxiliary amplifier response.

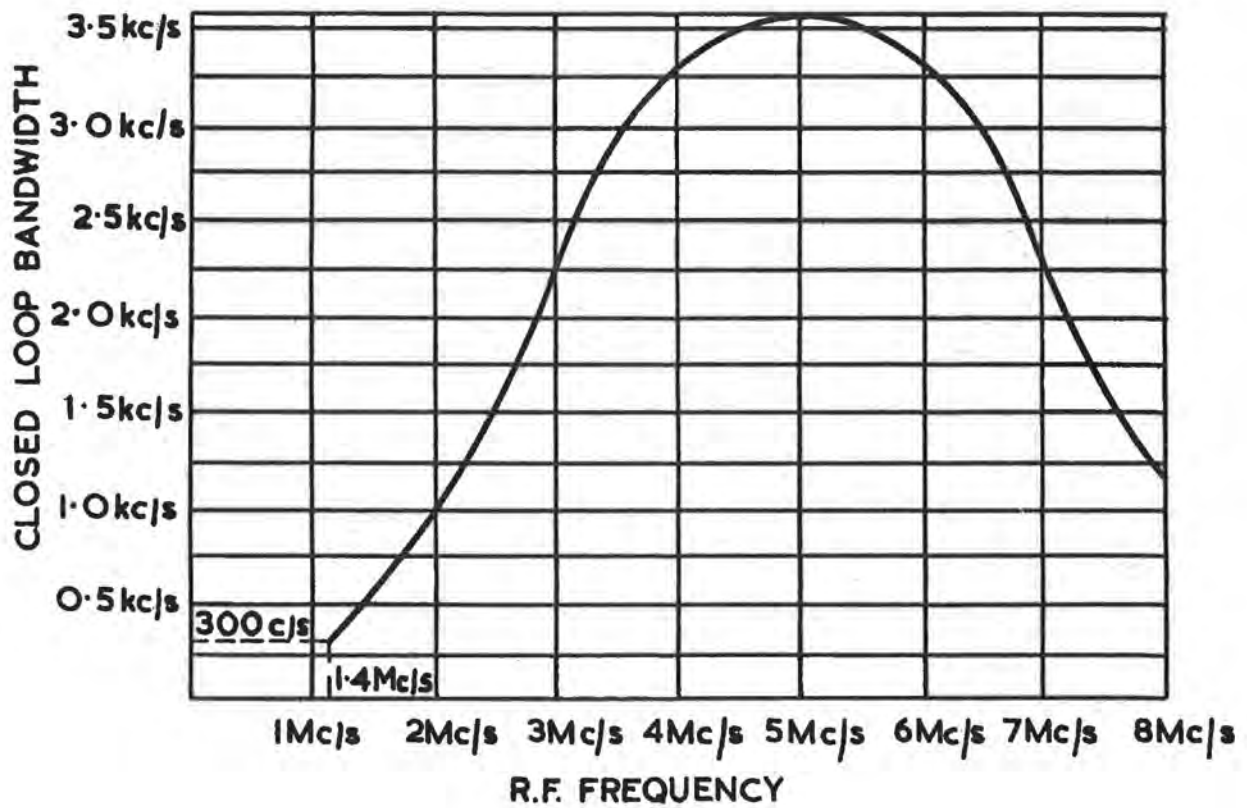


Fig. 6.3.7(v) Plot of closed loop response against frequency.

At the commencement of acceleration (≈ 1.4 Mc/s) the control loop frequency response is 300 c/s with an open loop d.c. gain of approximately 3000, these figures primarily determining the initial transient phase error which takes the form shown in Fig. 6.3.7(vi). After the transient, the phase error is negligible being less than 2° over the band (disregarding inaccuracies in the phase detector). In designing the servo loop, small signal measurements indicated the possibility of bandwidths greater than those achieved, but these were unobtainable in practice because of oscillation (at 1 kc/s) under large signal conditions, initiated by overloading at the higher signal frequencies.

Referring again to Fig. 6.3.7(iii), the inputs to the auxiliary amplifier and bias supply are clamped to earth in the absence of r.f. volts on the cavity gap. This ensures that the control loop is only closed when the cavity is on tune, and therefore, the error signal is within normal working limits. Under certain open loop conditions the output of the phase detector may be quite large and the use of two clamps following one another ensures that no residual input reaches the bias supply (this would modify the set initial current level). In preference to two clamps in series on the input to the bias supply, one is used on the input to the auxiliary amplifier to prevent saturation of this amplifier under open loop conditions, since recovery would then have a long time constant.

(e) General remarks

(i) Efforts to increase the complete control loop frequency response at the 1.4 Mc/s point (to reduce the transient error) are restricted by the variation in cavity time constant as the current increases. The time constant is progressively reduced as the current increases, the change being in the ratio of 32:1 over the band, which makes stabilization difficult. The application of current feedback to the bias supply would reduce the time constant but not necessarily the ratio. A further difficulty in achieving stability over the band is a change in the open loop gain of 14.5 db with variation in bias current. This is plotted against r.f. frequency (without auxiliary amplifier) in Fig. 6.3.7(vii).

The fall in gain of some 9 db between 2 Mc/s and 1.4 Mc/s (the graph of bias current against frequency has an inflection at this point) is unfortunate, as the highest d.c. gain is needed here.

(ii) Given normal conditions in the cavity, no great difficulty was experienced with r.f. interference in the bias supply. The d.c. amplifiers (particularly the voltage feedback amplifier with its high d.c. gain of $\times 1000$) required the most attention, and it was necessary to prevent r.f. loop currents flowing through the signal earths. This has been achieved by grounding the signal earths to the chassis via capacitors, and increasing the impedance of the signal earth connections with r.f. chokes. Direct grounding of the signal earths, which is desirable from the r.f. point of view, was not possible due to difficulties with low frequency loop currents. To facilitate the isolation and reduction of earth loop currents, all co-axial leads have been terminated on insulated material, with provision for grounding or inserting resistance in the screens as required. It was noticeable that some differences in earth potentials (for example between the r.f. driver chain and bias supply) were only apparent when the magnet was pulsing.

(iii) Due to hole storage effects in the germanium rectifiers there are large voltage spikes on the bias supply output at 300 c/s repetition frequency. These spikes have a ringing frequency of approximately 100 kc/s and damp out in about 5 to 10 cycles. Spikes of approximately 1-2 degrees of phase modulation are also visible on the output of the phase detector. The practice of employing hole storage capacitors across the T2 secondary has not been employed, as it is preferable to retain the high ringing frequency of short duration.

(iv) The voltage needed across the bias winding is dependent chiefly on dI/dt rather than I , and it is not therefore possible to protect the supply against current overload by limiting the voltage in any way. Current limiting must be achieved by monitoring the actual bias current, and originally the voltage drop across a resistor in series with the cavity was used for this purpose. However, the current required has increased to a level (800 A) where load resistance has to be reduced to a minimum, and this monitoring resistance has had to be dispensed with. An alternative solution is being sought.

(v) Referring to the transfer function of control valve grids to the output, there is considerable attenuation at 300 c/s and higher frequencies, which implies a large 300 c/s ripple component on the grids of these valves. At mean grid levels of approximately -10 V the superimposed component of ripple is just swinging into grid current. Any increase of mean level over -10 V, limits the voltage feedback loop gain and the ripple component is no longer "bucked out". Similarly with the higher signal frequencies, the limit is set by the onset of grid current and is the overloading referred to in 6.3.7(d). Once overloading does occur, the onset of distortion is sudden and drastic as a consequence of the voltage feedback.

The transfer function also shows that at the higher current levels the d.c. gain from control grids to output is approximately $\times 0.06$. At a given output current, a small change in load resistance will demand a change in grid voltage 17 times that of the output voltage. For example, assume the current is 800 A, then a 2 m Ω increase in load resistance will require 1.6 V rise at the output, and this in turn requires an increment at the control grids of $1.6 \times 17 = 27$ V. The Mark I supply is therefore very dependent on keeping load resistance to a minimum at these high current levels.

(vi) The present transient phase error is considered satisfactory but if it should prove unacceptable in the future, there is the possibility of programming the bias supply over the first 2 ms or so of the frequency sweep. This could be achieved by injecting a suitable waveform into the summing junction of d.c. amplifier No. 2.

6.3.8. Mark II (Transistorised) Bias Supply

(a) Purpose

The Mk II bias supply was developed to provide a more flexible means of automatically tuning the r.f. cavity with a better overall performance.

It was designed:-

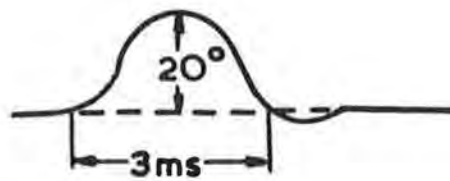


Fig. 6.3.7(vi) Initial transient phase error.

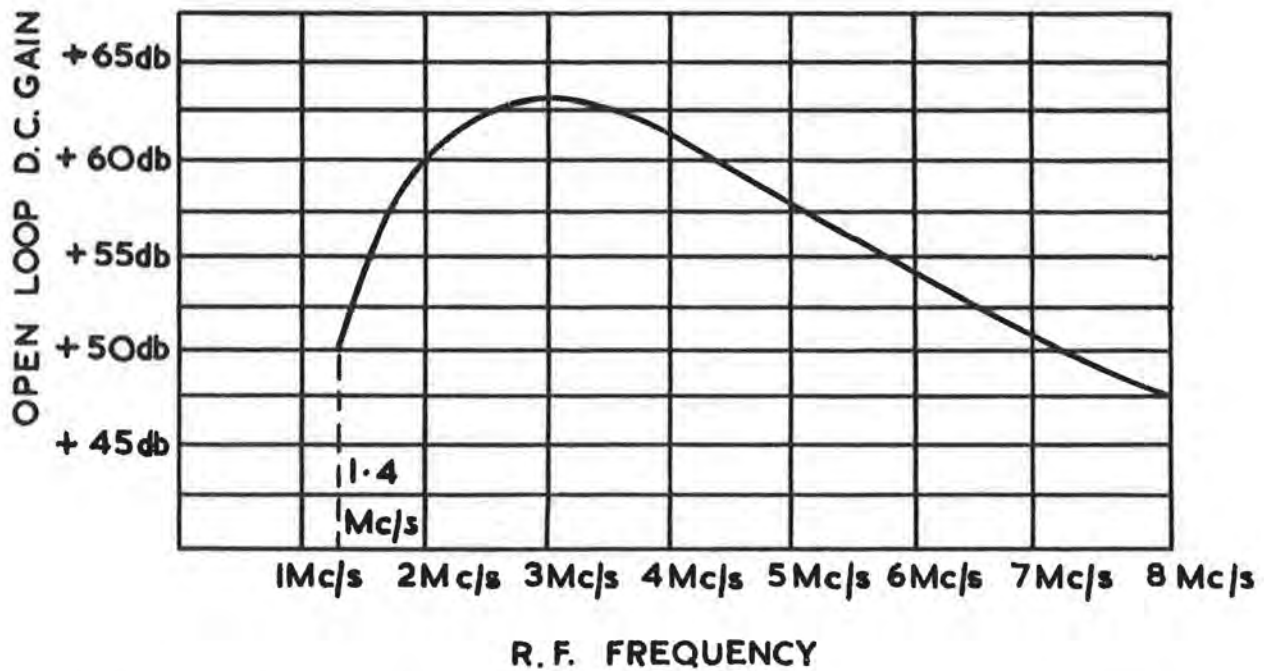


Fig. 6.3.7(vii) Plot of open loop d. c. gain against r. f. frequency

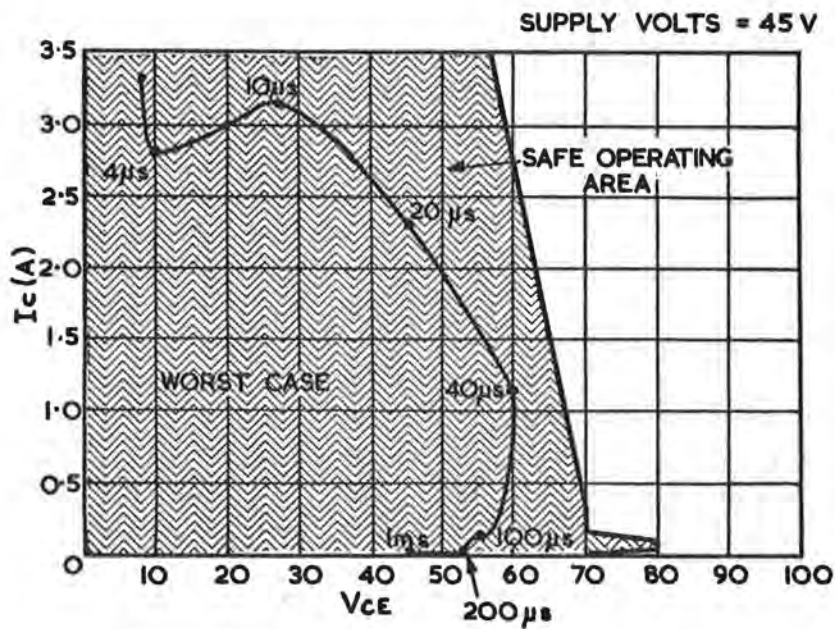


Fig. 6.3.8(i) Transistor voltage-current locus at turn off.

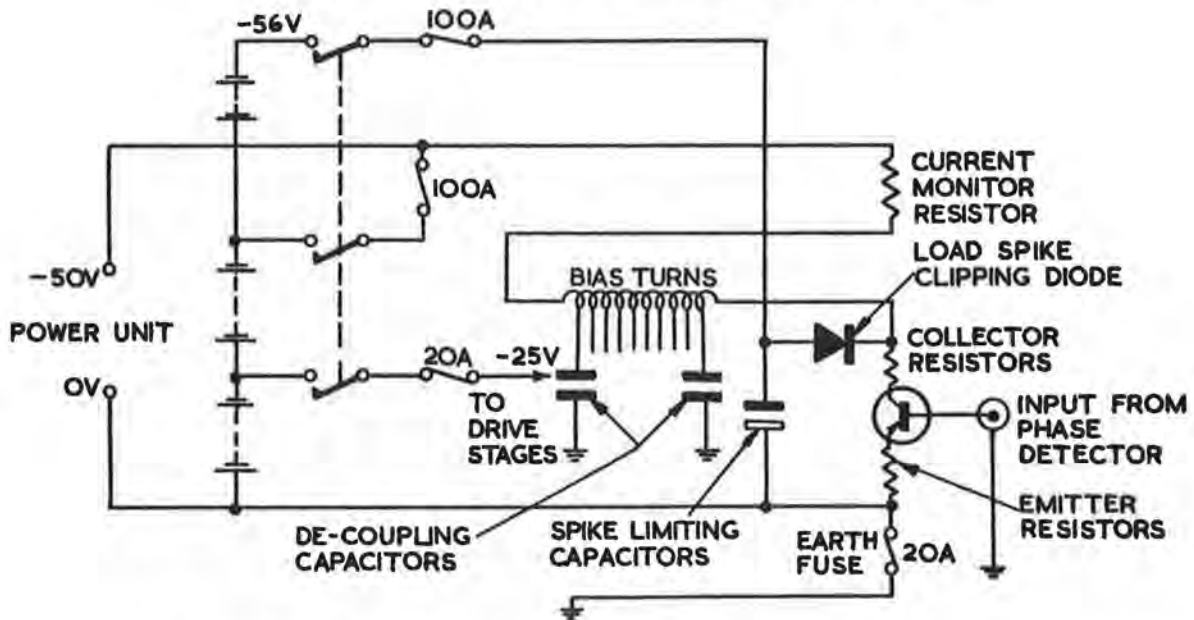


Fig. 6.3.8(ii) Arrangement of control unit, power unit and load.

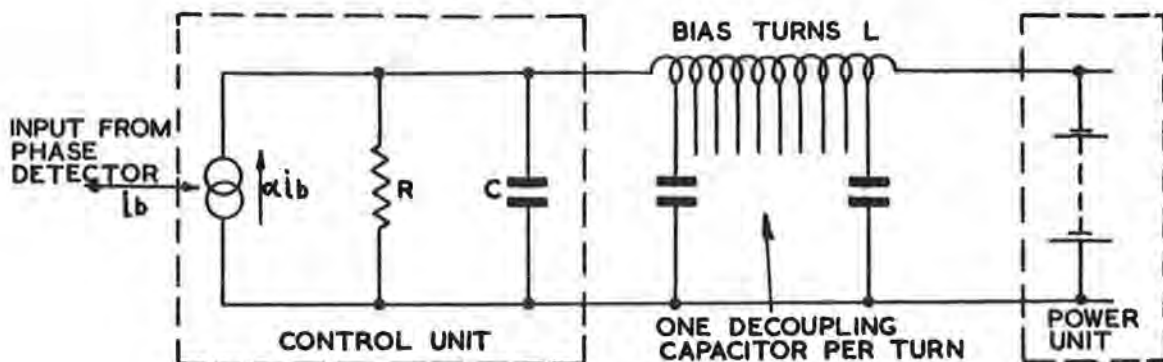


Fig. 6.3.8(iii) Simplified equivalent circuit of phase loop.

(i) to provide accurate phase control of the cavity r.f. voltage over the frequency sweep period,

(ii) to permit phase modulation of the cavity r.f. in the 2 to 5 kc/s (i.e. the synchrotron oscillation) band,

(iii) to deliver if required an increased current to the bias turns in the r.f. cavity.

The supply comprises a direct current power unit capable of delivering up to 900 A at 50 V via a control unit to the bias turns.

(b) Control unit

The control unit dissipates most of the output from the power unit. It consists of a parallel array of 192 power transistors divided into 8 distinct blocks, each operating with emitter and collector load resistors. There are subsidiary circuits, including drive stages, fault protection and fault readout circuits associated with each block. Under conditions of maximum power the emitter load resistors, collector load resistors, and power transistors dissipate 11, 18 and 10 kW respectively. Several cooling systems are employed in the control unit to remove the dissipated power: the emitter and collector resistors are mounted in ducts through which air is forced by a radial flow blower to an air-water heat exchanger; the transistors are mounted on water cooled heat sinks through which chilled demineralised water continuously circulates; and a smaller axial-flow fan ensures air flow through the main body of the unit to remove power dissipated in the drive stages.

A comprehensive system of interlocks ensures that all cooling systems are operative before the load is switched on. If a transistor breakdown occurs in any block, this is detected, the block is isolated and the position of the faulty transistor indicated. The control unit may then be used with 7 blocks operative and can carry up to two faulty blocks. If a fault occurs it is necessary that:-

(i) all transistors in the block containing the faulty transistor should be protected by bottoming,

(ii) the position of the failed transistor should be displayed so it can be quickly removed and replaced,

(iii) the faulty block should be disconnected automatically so that operation can be resumed without a complete shutdown.

(c) Choice of transistors

The important transistor ratings are:-

(i) Maximum collector emitter voltage (V_{CE} max.) (i.e. with base and emitter shorted). This was compared with a careful assessment of the collector voltage under all transient conditions. Since the load is inductive, the most severe conditions occur at turn off on full load, especially when turn off time

is rapid ($100 \mu\text{s}$ or less). Charts of maximum reliability area, available from the transistor manufacturers, are most useful in assessing the operating conditions. Fig. 6.3.8(i) shows the voltage-current locus for a single power transistor during the first millisecond of turn off from full load.

(ii) Maximum power and junction temperature. To ensure good reliability the junction temperature in the output transistors is kept low. The transistor finally chosen is rated at 150 W and 100°C . The actual maximum power per transistor under fixed frequency conditions is 70 W, a requirement to be met occasionally during tests. Under these conditions the junction temperature does not exceed 60°C .

(iii) Cutoff frequency in common emitter circuits. This was specified at 10 kc/s or above to meet the phase modulation requirement.

(d) Power units

The possibility of power transistor breakdown, due to mains surges, rectification spikes and the stored energy associated with the inductive load, placed a special requirement on the power supply. The margin between E_{Δ} (the nominal output voltage at 50 V d.c.) and $V_{ce} \text{ max.}$ (80 V) requires good smoothing to reduce rectification spikes and ripple to a tolerable level. The energy stored in the bias turns at full load is about 60 J, this must be safely absorbed by the power supply also. The following possibilities, all employing 3 phase transformer/rectifier sets as the basic system, were considered:

(i) Output regulation by means of series transducers in the primary side was rejected because it was felt it offered insufficient protection.

(ii) Regulation by means of silicon controlled rectifiers (S.C.R's) was also rejected for the same reason.

(iii) Series regulation by motor-driven Brentford regulator - fast transients being absorbed by a heavy duty lead acid battery floated across the output. This was chosen as the most simple and reliable arrangement providing continuous protection, although it is somewhat bulky.

(iv) As (iii) but with a nickel cadmium battery of compact sintered block construction - heavy current access to the battery taking place via S.C.R's only when surges occur and when the load energy is delivered at the completion of each sweep.

This was rejected because of its greater complexity though it is considered it would work effectively and be more compact than (iii).

A skeleton circuit showing the arrangement of power unit, control unit and transistors is shown in Fig. 6.3.8(ii). The capacitors are high current heavy duty electrolytics for reducing very fast spikes at the transistor collectors (where these are of order tens of microseconds, battery inductance becomes a considerable factor). It is important that they and the spike clipping rectifiers be placed as close as possible to the control unit terminals.

(e) Battery fuses and earth fuse

For safety reasons the battery is fitted with isolator and fuses. Standard H.R.C. fuses at 100 A were chosen to compromise between low resistance and low fusing current.

A low current fuse provided between +50 V and earth, which is essential for safety reasons, developed unwanted feedback voltages in series with the input signal path. It was necessary to separate signal and earth return paths to avoid unstable modes in the phase and current feedback loops.

(f) Phase and current feedback loops

The control of phase or current are alternatives determined by the conditions required at the start of the frequency sweep. At the end of injection, a few hundred microseconds may elapse before the full voltage is applied to the r.f. cavity. During this interval, the current control loop is designed to maintain bias current at the right value, rising at the correct rate to ensure that phase errors are minimised in the cavity and r.f. drive chain. At the instant full volts are applied to the cavity, the bias loop is automatically switched to phase control and remains so until the completion of the sweep. The current reference may be derived from an independent source or from the integrated B signal derived from the magnet.

Because the bandwidth requirement of the current loop is not stringent, stabilisation is not difficult. The phase loop presents a more serious problem. The basic open loop transfer function of the phase loop is of the form:

$$\frac{1}{LC S^2 + \frac{L}{R} S + 1} \times \frac{1}{S + 2 \pi f_a}$$

with an equivalent circuit as shown in Fig. 6.3.8(iii).

	<u>No Load</u>	<u>Full Load</u>
L = bias turns inductance	5 mH.	0.13 mH
C = combined depletion layer capacitance of the power transistors	1.42 μ F	7.2 μ F
R = total parallel output resistance of the power transistors	12.5 Ω	1.46 Ω
f_a = cutoff frequency of the power transistors	100 kc/s	25 kc/s

The three principle elements form an overdamped LCR circuit:

		<u>No Load</u>	<u>Full Load</u>
Natural frequency f_n	$= \frac{1}{2\pi\sqrt{LC}} =$	1.9 kc/s	5.3 kc/s
Damping factor D	$= \frac{1}{2R}\sqrt{\frac{L}{C}} =$	2.4	1.5

The variation of f_n from no load to full load is not great because as the bias turns inductance falls with increasing load current, the capacitance associated with the transistors increases. Also the resistive component of the output impedance falls, so that D does not vary greatly. The actual situation is altered by the presence of 0.1 μ F r.f. decoupling capacitors between the bias turns and earth. Their effect is to make the bias winding look like a transmission line with a large propagation constant. The open loop phase-frequency responses show phase lags in excess of those associated with the simple circuit of Fig. 6.3.8(iii).

In order to provide the bandwidth necessary for beam control purposes, series stabilisation was chosen to compensate for the considerable lags in the bias turns. The limitations on such methods arise from noise and other unwanted signals in the error signal path. By keeping ripple and other forms of interference low in the bias loop, closed loop bandwidths of order 10 to 15 kc/s have been obtained.

The equipment was fully tested under pulsed and swept frequency r.f. conditions.

6.3.9 General Arrangement of High Power R.F. System

(a) Layout of equipment in magnet room

In the normal working position the cavity is located in straight section 8 and the power amplifier immediately adjacent to it on the inside of the magnet ring (Fig. 6.3.9). The cavity and amplifier are both mounted on wheels and run on radial rails on the floor of the magnet room. To examine the cavity, it can be detached from the amplifier and rolled towards the outside of the ring; for r.f. test purposes, both amplifier and cavity can be withdrawn towards the centre of the ring. All electrical connections to the cavity and amplifier are made by flying leads to junction boxes on the floor and these junction boxes are paralleled to extension boxes near the centre of the ring for use when the cavity and amplifier are in the test position. The level control and phase detector circuits and their power supplies are situated inside the amplifier cubicle.

The thermionic bias supply sits on the magnet room floor a little way from the straight section. The transistor bias supply, because of its sensitivity to radiation damage, is located in a cellar below the ring close to the r.f. straight section. It is hoped that the transistor bias supply will have the better performance and be normally used, but the thermionic bias supply is being retained for some time as a spare and the connections can easily be interchanged.

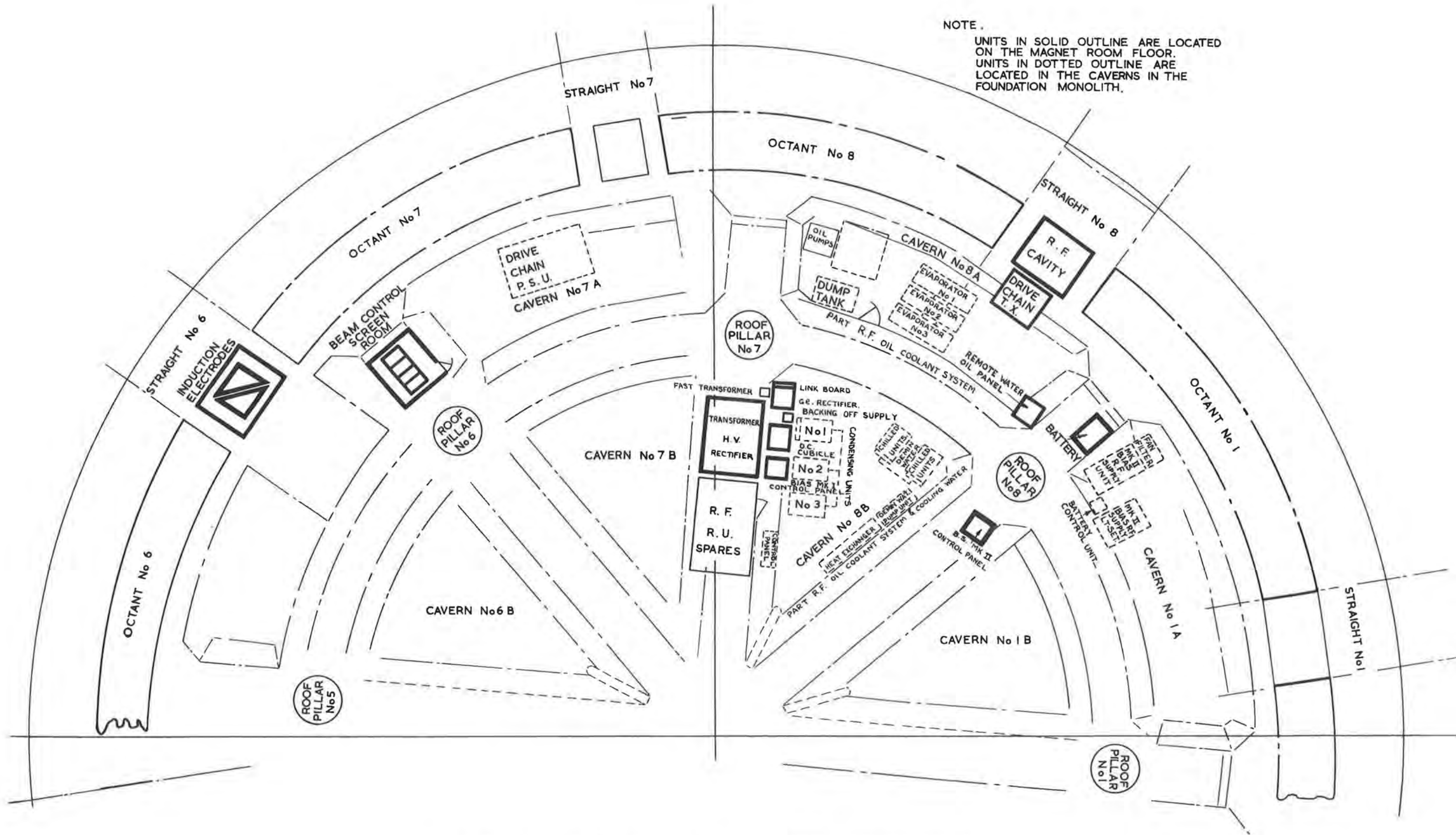


Fig. 6.3.9 Layout of high power r.f. equipment in the magnet room.

Also in an adjacent cellar are the water cooling plant for the r.f. drive chain and bias supplies, the oil chilling plant for the cavity, and the d.c. power supplies to the power amplifier.

The whole of the r.f. system including water and oil plant can be operated from the magnet room floor.

(b) Main control room

The high power r.f. equipment is controlled from two 6 ft racks in the main control room. One rack holds the remote indication and controls for the power amplifier, and remote indication and control of the oil chilling unit. In the adjacent rack is an oscilloscope and a patch panel for monitoring of all relevant waveforms. Also in this rack are panels for metering indication and control of both bias supplies. A further panel provides adjustment of the nominal stable phase angle by altering the gain of an amplifier which feeds the B signal from the primary frequency generator to the power amplifier for control of cavity voltage amplitude.

Also brought to these racks are an indication of the correct functioning of the primary frequency generator and some monitor points from that equipment. Indication and control of the cooling water is incorporated in the overall water controls panel for the machine.

REFERENCES FOR SECTION 6

1. D. J. Thompson. Notes on a drift tube cavity for a proton synchrotron. Internal report HAG/RF/1.
2. D. J. Thompson. Ferrite for the accelerating cavity of Nimrod; its electrical properties and their measurement. NIRL/R/5.
3. P. D. Dunn, S. M. Third and D. J. Thompson. The electrical characteristics of the r.f. accelerating cavity for the 7 GeV proton synchrotron. Internal report HAG/RF/8.
4. F. E. Terman. Calculation of Class C power amplifier performance. Radio Engineers' Handbook, Section 5, page 444.
5. L. J. C. Appleby, R. C. Hazell, R. Kur and P. Wilde. The performance of an injection trigger pulse generator. NIRL/M/22.

SECTION 7

EXTRACTION SYSTEMS AND INTERNAL TARGETS

7.1. Slow Extraction System

7.1.1. Principles of Operation

(a) Review

The aim of the proton extraction system is to produce an external beam which contains an appreciable fraction of the accelerated protons and which can be focused with quadrupole lenses to a small image at a target. Small images are particularly necessary when using electrostatic separators in the secondary particle beam.

The basis of the system is that used on the Cosmotron (1,2). A target of a light material is used and the beam is moved towards the target to strike the "lip" (3) - a thin piece of the target standing proud of the main body. This lip reduces the amplitude of the radial betatron oscillations, reduces the energy spread of protons entering the target and also ensures that they traverse the whole target. The energy loss produced by ionization in the target causes the proton to take a new path, oscillating now about a mean orbit which is at a smaller radius than the target. Approximately at the innermost part of their oscillating path, the protons pass through the aperture of a magnet whose field deflects them outwards again. The deflection given is sufficiently large for the protons to travel right across the aperture of the machine and emerge as an extracted beam.

In emerging from the main magnet the protons have to pass through the fringe field which is defocusing in the radial direction and causes the beam to diverge. In the "Cosmotron" this divergence is counteracted by "extraction shims" attached to the outside of the magnet which reshape the fringe field in the region of the beam.

Preliminary calculations revealed that on Nimrod such a system would result in a beam which was too large to be accommodated by standard quadrupoles (mainly because of the larger machine radius) and also that it would be difficult to ensure good enough beam optics in the fringe region (even using special lenses) to allow the beam to be focused to a reasonable spot in the horizontal direction.

The first modification investigated consisted of incorporating a field gradient which was radially focusing in the deflecting magnet. (This was independently suggested by Gan'zhin (4)). This improved the beam considerably but not as much as was desirable. The beam at the magnet M (see Fig. 7.1.1(i) is spread out due to the variation of energy loss in the target (5) and is diverging due to the scattering of the protons in the Coloumb fields of the nuclei in the target (6) (the target is imaged at the extractor magnet). Hence while a focusing magnet can improve the situation with regard to the first effect it is unable to affect the second. A compromise by placing the magnet at a different position is not significantly better than the placing shown in Fig. 7.1.1(i).

(b) The Nimrod System

In the system designed for Nimrod (6) an additional element, a radially

focusing quadrupole, is introduced between the target and the magnet and by suitably adjusting its strength the system can be made achromatic, i.e. the effect of differences in energy of the protons after leaving the target is eliminated by the time they reach the magnet (presuming, of course, that the energy losses will allow them to pass through the available apertures of the elements). The target is not now imaged at the magnet, rather the scattered protons are diverging, and the gradient of the magnet is adjusted to produce a focus in the region of the fringe field (Fig. 7.1.1(ii)). Calculations indicate that the beam should have a small diameter in the fringe field, expanding again to a few centimetres outside the machine where it can be refocused by quadrupoles.

As described so far the distances between the target and the quadrupole and between the quadrupole and the magnet would be equal but, because the path from the magnet to the fringe field is in the magnet, further momentum resolution takes place. This can be allowed for by increasing the target-quadrupole distance and by reducing the field in the quadrupole, which leaves the beam not quite corrected at the magnet but achromatic again at the exit.

The vertical motion has so far been ignored. It is not possible to control this independently within the scope of the scheme outlined, but it is found that the motion is contained within reasonable vertical apertures in the magnets and since the fringe field is focusing for vertical motion, the beam is small enough to go into the external quadrupoles. The approximate shape of the vertical profile is indicated in Fig. 7.1.1(ii).

7.1.2. Practical Considerations

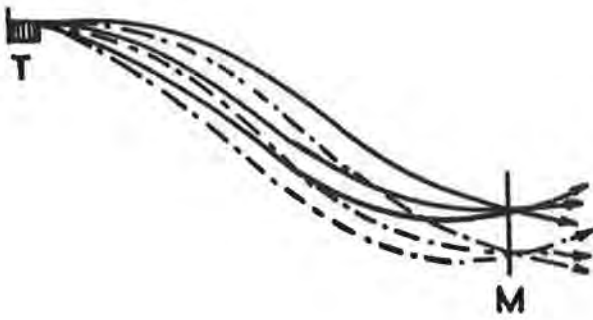
In order that the extraction system should work in the manner described it is necessary that the properties of the machine magnetic field be reasonably uniform in the region where the protons are travelling from target to magnet and this implies that the magnets are within the radial range of what is known as the "good field region", although they are, of course, located in straight sections. At high fields, after acceleration, the circulating beam will have shrunk to a narrow radial width within the "good field region" but the whole of the aperture is used at injection and consequently the extraction system magnets must be "plunged". The magnets are withdrawn at the start of the acceleration cycle and rapidly pushed into position for extraction. The target must also be moved in a similar manner but it is small and is raised up from the bottom of the vacuum vessel.

7.1.3. Apparatus

The target consists of a 3.25 cm long beryllium block which is erected to beam height by one of the Mark 1 target mechanisms described elsewhere in this report. (section 7.4.).

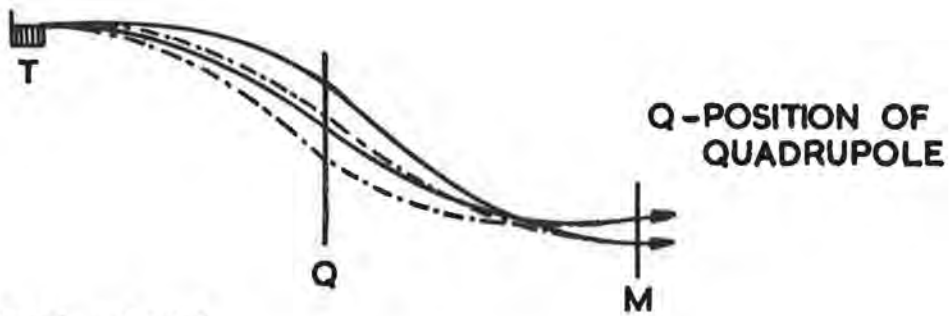
The quadrupole must be placed very near the circulating beam and yet must have a usable aperture only a few centimetres away since on the average the energy loss in the target causes the protons to change their orbit by only a few centimetres. A conventional quadrupole is not satisfactory in this respect and a current sheet quadrupole (7, 8) is used.

The extraction magnet which will be installed initially is of conventional C-shaped design and has a usable radial field of 9 cm. The ratio of the gradient to the magnet strength is fixed by the angle of the pole pieces. It would be

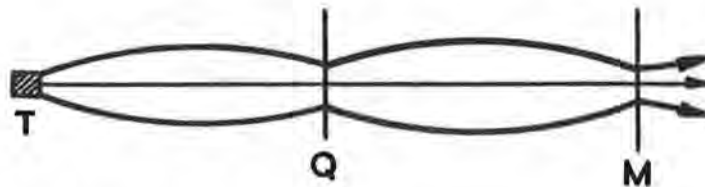


T - Target. M - Position of Magnet
 The chain linked lines represent the paths of protons which have lost energy in the target compared with other protons following the solid lines

Fig. 7. 1. 1 (i) Piccioni System



(a) RADIAL PATHS



(b) VERTICAL PATHS

Nimrod extraction system.

Fig. 7. 1. 1 (ii) Paths of Protons, NIMROD extraction system.

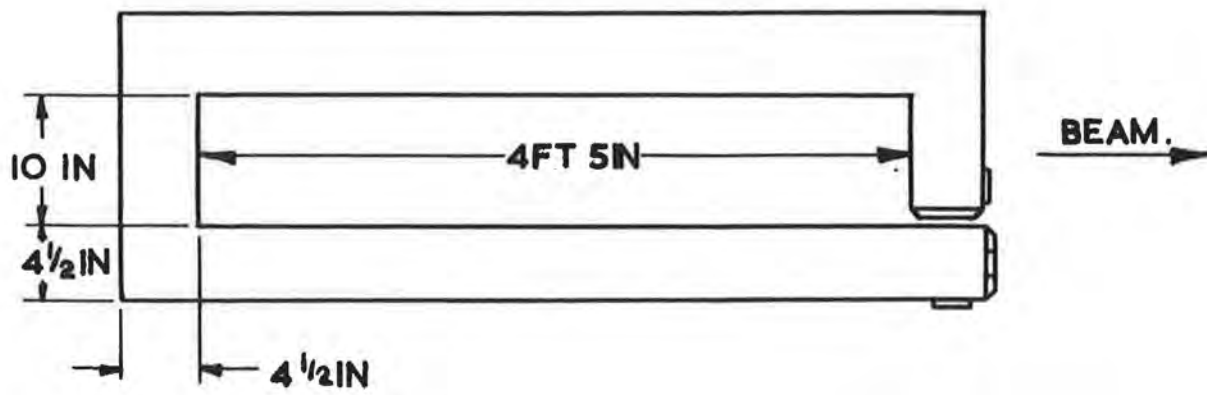
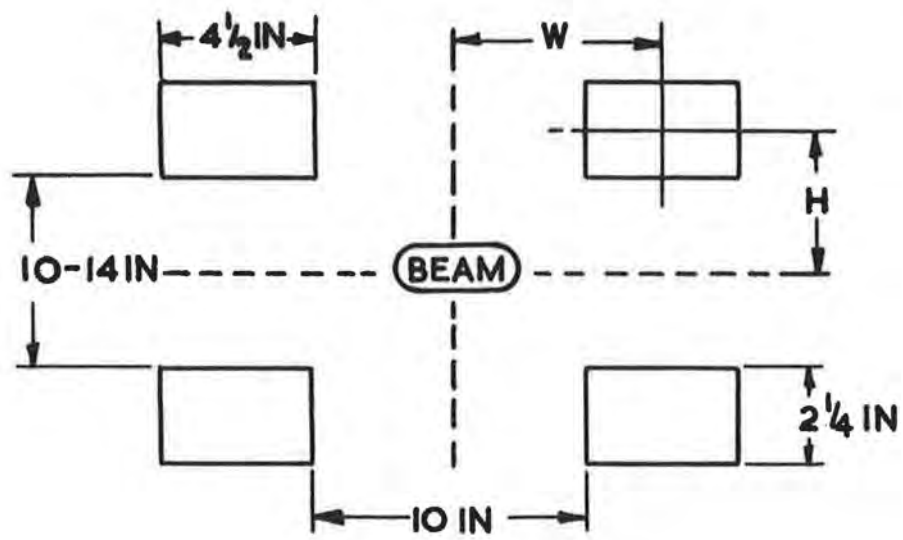


Fig. 7.2.1 (i) Fast Kicker Coil

desirable to have a slightly larger aperture and also to have an adjustable gradient; in order to produce this a magnet of a "window frame" C-style which has gradient correction coils, was designed. This more complicated magnet is being manufactured and should be available for installation in 1964.

7.1.4. Emergent Beam

The characteristics of the emergent beam have been computed. It should have a phase area of approximately 5×10^{-5} metre radians in the horizontal plane and 1×10^{-4} metre radians vertically. The spot sizes which can be achieved depend on the quadrupole system used externally and should be of the order of 0.5 cm by 0.5 cm.

It is expected that with the extraction system in its final form, about 50% of the circulating beam will be available externally.

7.2. Kicker for Fast Beam Extraction

7.2.1. Principle of Operation

In addition to the slow extraction system described in section 7.1, fast extraction (about 50 μ s) is required. A kicker coil is used to distort the closed orbit so that protons hit a target and are moved into the same channel as in the slow extraction case.

The radial motion of the proton beam is given by:-

$$\begin{vmatrix} y \\ \dot{y} \end{vmatrix} = \begin{vmatrix} \cos 0.71\phi & \frac{\sin 0.71\phi}{0.71} \\ -0.71 \sin 0.71\phi & \cos 0.71\phi \end{vmatrix} \begin{vmatrix} y_0 \\ \dot{y}_0 \end{vmatrix}$$

where ϕ is the angle of rotation of the protons past the kicker coil and the factor 0.71 is Q_r for Nimrod with an n of 0.6.

For a closed orbit: $\phi = 360^\circ$, $y = y_0$ and $\dot{y} = \dot{y}_0 - \delta$.

If the change in divergence is δ cm per radian the equation of the perturbed orbit is:-

$$y = \frac{\delta}{1.12} \cos 0.71 (\phi - 180^\circ) \text{ cm}$$

The factor 1.12 comes from $\sqrt{\frac{R_m}{R_0}}$ where R_0 = radius of curvature of the magnet octants

$$R_m = R_0 + \frac{L}{2\pi}$$

L = total length of straight sections.

At the coil ($\phi = 0$) the perturbation is -0.55δ cm, while at the Piccioni target ($\phi = 122^\circ$) it is 0.67δ cm (= Y), where:

$$\delta = \frac{\int B dl \text{ (through coil)}}{B_0 \text{ (in machine)}} \text{ cm}$$

For the coil to be effective, the beam must be deflected through at least half its width at the Piccioni target, i.e. $Y = \frac{1}{2} \text{ width} = 0.67 \frac{\int B dl}{B_0} \text{ cm}$

$$\therefore \int B dl = \frac{B_0 \times \frac{1}{2} \text{ width}}{0.67} \text{ gauss cm}$$

TABLE 7.2.1(I)

Beam Energy T (GeV)	B_0 (gauss)	Beam $\frac{1}{2}$ width (cm)	Required $\int B dl$ (gauss cm)
8	15,800	7.2	170,000
7	14,000	7.6	158,000
6	12,200	8.0	146,000
5	10,400	8.5	132,000
4	8,600	9.3	119,000
3	6,800	10.2	104,000
2	5,000	11.7	87,300
1	3,000	14.7	65,800

Theoretical values of $\int Bdl$ can be calculated from the field produced by four parallel wires, with a current I flowing through them. The horizontal distance between the wires is $2W$ and the vertical distance between them $2H$.

Then at the centre of the four wire array there is a vertical field only, as the horizontal components of field cancel out.

$$\begin{aligned} \text{The field per unit length of the coils is } B &= \frac{I}{10} \left(\frac{2}{\sqrt{W^2 + H^2}} \right) \left(\frac{4W}{\sqrt{W^2 + H^2}} \right) \\ &= \frac{4}{5} \cdot I \left(\frac{W}{W^2 + H^2} \right) \end{aligned}$$

$$\text{For coils } S \text{ cm long:- } \int Bdl = \frac{4}{5} SI \left(\frac{W}{W^2 + H^2} \right)$$

In practice the coils are two loops of copper-tube, of cross-section $4\frac{1}{2}$ in x $2\frac{1}{4}$ in and of overall length 5 ft 2 in and width 1 ft 7 in. The vertical distance between the centres of the loops is variable between $12\frac{1}{2}$ in and $16\frac{1}{2}$ in (see Fig. 7.2.1(i)). The current I through the coils is produced by discharging a condenser bank through the coils.

Theoretically all the stored energy in the condensers is transferred into magnetic field energy in the inductive coils:-

$$\frac{1}{2}CV^2 = \frac{1}{2}LI^2.$$

So :-

$$\begin{aligned} I &= V\sqrt{\frac{C}{L}} \\ \therefore \int Bdl &= \frac{4}{5} S \cdot \left(\frac{W}{H^2 + W^2} \right) V\sqrt{\frac{C}{L}} \end{aligned}$$

This is a theoretical maximum field which takes no account of ohmic resistance power losses in the coil and leads, and inductive losses in the leads. Also the coils are not parallel wires but rectangular cross-section copper loops.

The coils are placed in straight section 1 of Nimrod and are connected in series electrically, with one coil above the beam and one below it.

Not only can the distance between the coils be varied as described above but the radial position of the coils is also adjustable.

7.2.2. Powering circuits

The coils are powered by discharging a capacity of $500 \mu F$ (charged to a voltage which is variable up to 12 kV maximum) through ignitrons in series with them. The oscillation voltage across the coils is clamped by using more ignitrons and damping resistors (see Fig. 7.2.2(i)).

The capacitor bank consists of 50 capacitors each of which is $10 \mu F$; they are rated at 12 kV and 50% voltage reversal is allowed. The capacitors are connected in groups of 5 in parallel and with the low voltage terminals of all the 50 capacitors connected together. Each group of 5 capacitors is discharged by one ignitron (see Fig. 7.2.2(i)) and the cathodes of the ignitrons are all connected in parallel to one end of the kicker coils. The other end of the coils

is connected to the common low voltage terminal of the capacitor bank. The damping resistors and ignitrons are connected to the ends of the coil by suitable leads. The 10 damping resistors are each made from a length of resistance wire and are connected together at the low voltage end of the coil leads. The other ends of the resistors are connected separately to the anodes of the damping ignitrons. The cathodes of these ignitrons are also connected in parallel and are connected to the cathodes of the firing ignitrons.

Both sets of 10 ignitrons are fired at the same time causing an almost sinusoidal rise in magnetic field in the coils but the damping ignitrons only start conducting when the voltage across the coils reverses. Hence the magnetic field shape is sinusoidal up to the maximum and then it decays in an almost exponential manner.

The charging unit is arranged to charge a capacity of 500 μF to 12 kV (to an accuracy of 1%) in 2 seconds and to smaller voltages in correspondingly shorter times. The charging of the condensers is initiated by a standard timing pulse at the end of the "flat top" of the Nimrod magnet field. The discharge trigger is a similar pulse at, for example, the beginning of "flat top". This trigger pulse can be delayed by up to 120 ms and after amplification it is used to fire a thyatron which in turn fires two ignitrons. One of these fires the ten main firing ignitrons and the other fires the damping ignitrons. The delay circuit and amplifier are similar monostable multivibrators. The hydrogen thyatron (CV 372) discharges a capacity of 0.5 μF (charged to 3 kV) through two pulse transformers which trigger the two firing ignitrons. Each of these ignitrons discharges a capacity of 10 μF (charged to 6 kV) through the ignitors of 10 of the main ignitrons.

7.2.3. Model Measurements

Some work on a full scale model fast kicker coil has been done using a 250 μF condenser bank. The model coils are now being used as a dummy load for testing the apparatus in the magnet room. On the model the magnetic field was measured for different voltages (up to 12 kV maximum) on the condenser bank. The field in the centre of the coils and also across a horizontal plane through the centre of the coils was measured. A longer search coil than the kicker coil was used so as to measure the integrated field. The field was found to increase according to theory but its decay was not as smooth as the theory indicated. The maximum field for each voltage was not as high as predicted but the theory does not take into account the resistance of the circuit or the inductance of the leads.

According to theory, with a 250 μF capacity charged to 6 kV and a coil and lead inductance of 3.37 μH :-

$$I = V\sqrt{\frac{C}{L}} = 6 \times 10^3 \sqrt{\frac{250}{3.37}} = 5.2 \times 10^4 \text{ A}$$

With $W = 9.125 \text{ in}$, $H = 7.0 \text{ in}$ and $S = 60 \text{ in}$:-

$$\begin{aligned} \int B dl &= \frac{4I}{5} \left(\frac{SW}{W^2 + H^2} \right) \\ &= \frac{4}{5} \left(\frac{5.2 \times 10^4 \times 60 \times 8.125}{7^2 + 8.125^2} \right) \\ &= 17.5 \times 10^4 \text{ gauss cm} \end{aligned}$$

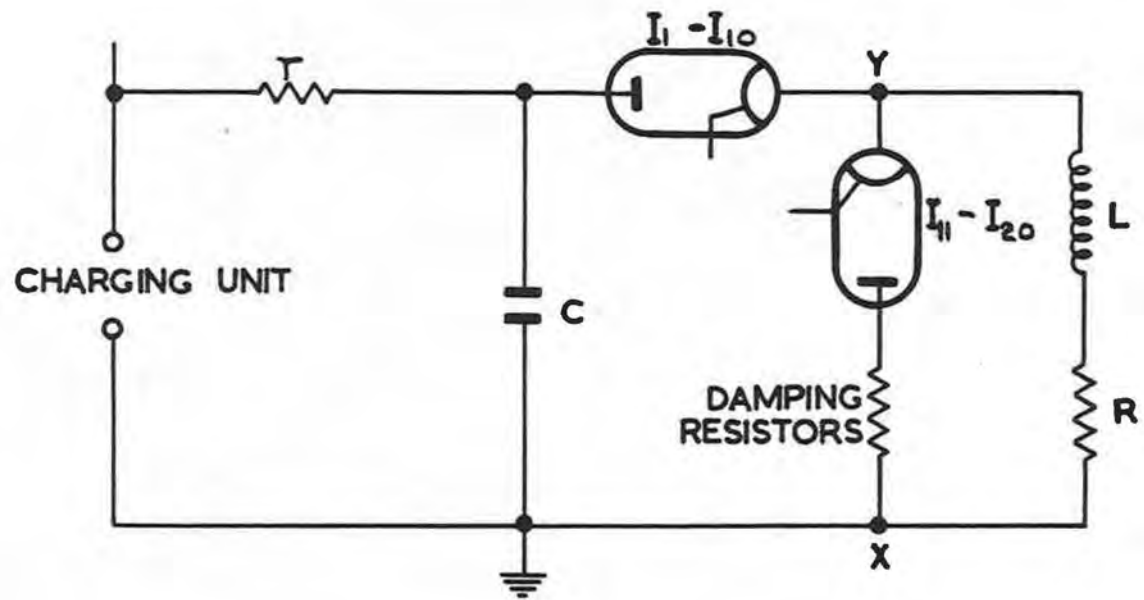


Fig. 7.2.2 (i) Basic Fast Kicker Circuit

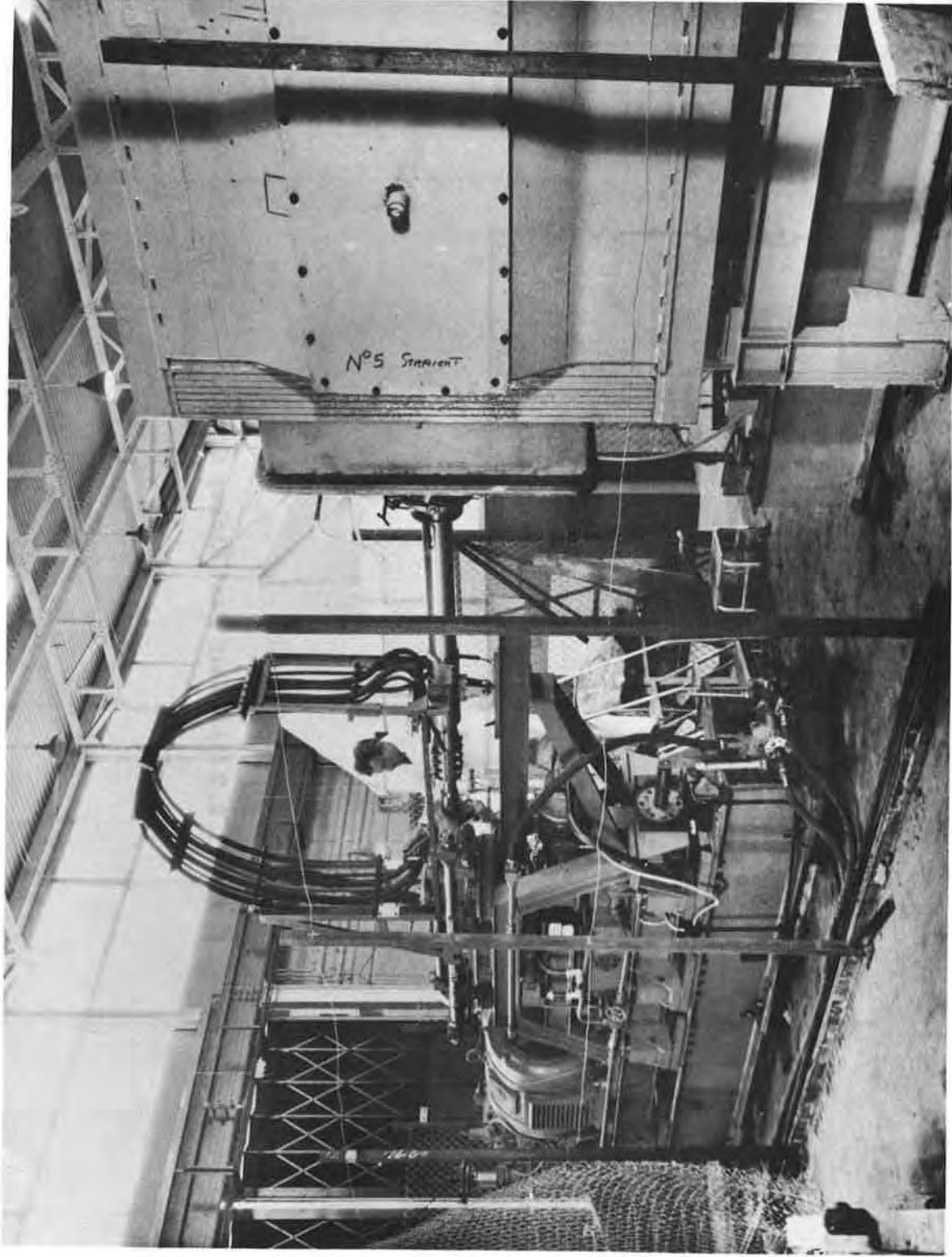


Fig. 7.3 (i) Plunging Mechanism

The measured maximum field under these conditions was 10.5×10^4 gauss cm, so the efficiency of the system is about 60%

7.2.4. Present status

The charging unit, the capacitor bank and the ignitron rack have been installed and preliminary discharge tests have been made.

7.3. Plunging Mechanisms for the Extractor Magnets

7.3.1. Description of System

The plunging mechanisms provide the motive power for moving the extraction and quadrupole focusing magnets into operating position each accelerating cycle of the machine; together with a small target, these form the Piccioni system for extracting the proton beam from Nimrod.

Two separate operations are performed by the plunging mechanism: one is a fixed stroke of 20 in, to a given displacement-time pattern, for plunging the magnet into the beam region and the other provides adjustment for the terminal position of the 20 in stroke.

The plunging action is obtained from a hydraulically operated ram driven by two variable-delivery pumps whose output is controlled by small electro-hydraulic servo-valves. These and all the electric driving motors, auxiliary pumps and hydraulic circuit (including a tank to provide the necessary oil capacity for the hydraulic system) are assembled on a steel structure (see Fig. 7.3(i)): The assembly is held down on to a fixed steel bed with pre-loaded clamps, the fixed bed being bolted down to the main concrete monolith supporting the Nimrod magnet.

The servo-valves are fed by error signals from a digital control system. A position pick-off delivers a pulse signal for every 0.01 in movement of the magnet ram. These pulses are passed to a binary counter which is compared many times during a stroke with a series of numbers carried in a store or programme. This programme consists of a plug-in unit containing a 50 x 56 diode matrix so arranged as to represent the desired magnet displacement-time characteristic in numerical form. Variations in stroke time of about 4:1 can be obtained by adjusting the running speed of a master oscillator which sets the time scale for the counter and programme comparisons.

The error between counter and programme at each sampling point is converted to an analogue signal which is amplified and fed to the servo-valves. Various safety devices and interlocks are built into the control system to cater for such contingencies as excess error, pick-off failure etc.

Adjustment to the terminal position of the 20 in stroke is obtained by unloading the clamps and slowly moving the steel structure along the fixed bed using hydraulically operated rams for both operations. Interlocks ensure that adjustments cannot be made whilst the magnet is being plunged.

The magnet and carriage move on three rails sited in the straight section box; the two outer rails support the weight and the centre rail guides the magnet along its required path. Columns from ground level pass through the base of the straight section box to support the rails, bellows being provided between the columns and the box to ensure vacuum tightness and to prevent any loads and vibration from the moving magnet being transmitted to the box.

A hollow steel shaft connects the magnet to the operating ram of the mechanism. A friction coupling is interposed between the shaft and the ram to permit a small free endwise movement of the shaft relative to the ram in the event of the ram becoming uncontrollable near the end of the stroke. The shaft passes through a

self-aligning seal assembly to complete the vacuum tight straight section box. The seals comprise three groups of P T F E chevron rings with two evacuated chambers and one oil filled.

Rigid copper tubes in the bore of the shaft carry the power and water circuits, which are routed from the reciprocating shaft to a fixed point on the top of the mechanism by flexible leads attached to a spring steel arch.

TABLE 7.3(I)

<u>Design Data</u>	Extractor Magnet	Quadrupole Magnet
Moving Mass	1 ton	0.2 ton
Minimum time for plunging stroke	200 ms \pm 20 ms	
Rest time	50 ms to single shot	
Minimum time for withdrawal stroke	200 ms \pm 20 ms	
Minimum cycle time	500 ms	
Stroke length and terminal position tolerance	20 in \pm $\frac{1}{32}$ in	
Datum adjustment per stroke	\pm 5 in	
Maximum acceleration and deceleration	\approx 5 g	

TABLE 7.3(II)

<u>Mechanism Data</u>	Extractor Magnet	Quadrupole Magnet
Operating pressure	3500 lb/in ²	
Maximum oil throughout	150 gal/min	
Piston Dia.	3 $\frac{1}{2}$ in	
Maximum piston speed	16 ft/s	
Main electric motor	120 hp	

7.3.2. Present Status

Two mechanisms, with one main pump each, have been delivered to the site and initially these will be capable of plunging the magnets in 0.7 s. One mechanism together with a one ton mass, connecting shaft, straight section box and vacuum seal box for the shaft has been assembled in a test bay.

Short term, manually controlled, tests were followed by sinusoidal cycling of the ram. Response tests for the complete variable delivery pump, ram and servo-control loops are now being carried out.

7.4. Target Mechanisms

The target mechanisms are required to bring a target weighing up to $1\frac{1}{2}$ lb into position beside the circulating beam in about 0.2 s or less.

The Type I mechanisms, which will be in use initially, consist of a frame 1 in high which spans from the inner to outer radius of the vacuum vessel. This carries a shaft which can be rotated through 90° from outside the vacuum vessel by hydraulic apparatus. If the target is short, it is carried on a fixed arm and is raised from the floor of the vessel to median plane height by the rotating shaft. Longer targets are mounted on an arm provided with pulleys and stainless steel belts which keep the target in the same orientation so that it undergoes only a translation on being raised. Vibrations of the target are of the order of 1 thou in significant directions under most operating conditions.

A mechanism providing remote adjustment of target radius and azimuth is nearly designed and should be available for use by the end of 1963.

REFERENCES FOR SECTION 7

1. O. Piccioni et al. Rev. Sci. Inst. 26, 232, (1955).
2. B.T. Wright. Rev. Sci. Inst. 25, 429, (1954).
3. E. McMillan. Rev. Sci. Inst. 22, 117, (1951).
4. M.A. Gan'zhin. Inst. & Exp. Tech. 4, 529, (1959).
5. B. Rossi. "High Energy Particles". Prentice Hall, New York, (1952).
6. R.G.T. Bennett and J.W. Burren. J. Nucl. Energy, Pt. C. 3, 14, (1961).
7. L.N. Hand and W.K.H. Panofsky. Bull. Am. Phys. Soc. Ser. II. 3, 421, (1958).
8. L.N. Hand and W.K.H. Panofsky. Rev. Sci. Inst. 30, 927, (1959).

SECTION 8

VACUUM SYSTEM

8.1. Introduction

The design of the Nimrod vacuum system presented problems peculiar to accelerators. The vacuum vessel had to meet special environmental requirements and it had to allow a sufficiently low pressure to be achieved to keep the loss of particles, due to scattering by residual gas molecules, down to an acceptable level. The particles travel a distance of about 100,000 miles within the vacuum vessel while being accelerated to the full energy of the machine and this distance is far in excess of the mean free path, even in ultra high vacuum conditions (mean free path at 10^{-9} torr is about 30 miles), so that collision between the accelerating particles and residual gas molecules is inevitable. The scattering effect is greatest at injection and it has been shown(1) that to keep the particle loss below 10%, a pressure of not more than 10^{-6} torr is required. This pressure is readily achieved in small laboratory apparatus but presented problems on equipment of the size and complexity of the Nimrod vacuum system.

The vacuum vessel was designed with the following requirements in mind:-

- (i) It must take up as little of the magnet aperture as possible. The horizontal walls of the vessel must be as thin as possible since, with a known vertical aperture required for the beam, the gap between the polepieces is decided by the vessel thickness.
- (ii) The material used in the construction of the vessel must be non-magnetic and sufficiently non-conducting to avoid influencing the magnetic field by eddy-current effects.
- (iii) Since a high level of radiation is inevitable, the vessel must be made from materials which would remain structurally sound after exposure to a radiation dose of at least 10^9 rads. (2),(3).
- (iv) It should be possible to remove and replace vessels easily.
- (v) The interior of the vacuum vessel should be readily accessible for experimental devices and it must be possible to extract beams past the outer edge of the vessels.
- (vi) To avoid charge build-up affecting the beam, it must not be possible for electrostatic charge to accumulate on the surface of the vessel.
- (vii) The vacuum properties must allow the operating pressure to be achieved with a reasonable pumping speed in a reasonable time and these properties must not be readily degraded by irradiation.
- (viii) Manufacturing feasibility, must obviously be taken into account bearing in mind the vessel dimensions, (approximately 7 ft by 1 ft in cross section in the form of a torus with a mean diameter of 155 ft).

8.2. Vacuum Vessel Design

8.2.1. Choice of Material

The search for the most suitable material for the construction of the vacuum vessels proceeded in parallel with the study of the mechanical design. Several materials, such as glass, ceramics and stainless steel, possess excellent vacuum properties but their use is prohibited by one or more of the above requirements. The material which most nearly fulfilled all the requirements was considered to be one of the glass fibre reinforced resins and many varieties of laminate were evaluated for vacuum properties and irradiation resistance. The types of resin included phenolics, polyesters, melamine formaldehydes, silicones and epoxies. Other properties such as shrinkage on curing were weighed against ease of manufacture and epoxy resin was finally chosen.(4)

Although this material was not ideal in every respect it had the advantage that the vacuum vessel could be constructed by a matched metal moulding process to the required engineering tolerances, while retaining acceptable vacuum properties and irradiation resistance. The reinforcing glass cloth was, in general, a 0.006 in plain weave cloth with a general purpose silane finish but a heavier fabric was used as a coring material on the thicker header vessels.

The resin system finally chosen consisted of a bisphenol 'A' diglycidylether cured with methyl 'Nadic' anhydride. This formulation is stable at room temperatures for periods of 12 to 15 weeks and even when suitably catalysed with a tertiary aromatic amine, considerable stability is retained at room temperature while a reasonable cure takes place at higher temperatures. The catalyst chosen (5) was a proprietary material known as 33/1266 (an aromatic amine salt) and this gave the best cure consistent with the longest stability at room temperature to allow the vessels to be handled for long periods during fabrication.

A satisfactory laminate may be obtained with this formulation after a cure time of 2 hours at 150 C. It was found that irradiation resistance and mechanical strength were only slightly affected by varying the catalyst. The considerations which dictated the final choice of material have been recorded in greater detail elsewhere (6) (7) (8).

Laboratory tests indicated that an ultimate flexural bending stress of 100,000 lb/in² was possible while under production conditions ultimate stresses of 40,000 to 50,000 lb/in² would be achieved for large panels and joints.

8.2.2. Choice of Design

Many designs were considered (9) in one or other of the following categories:

(i) Using the magnet as the walls of the vessel.

With this type of construction the pole pieces are inside the vacuum region and the problem arose of finding an adhesive for the laminations in the pole pieces compatible with high vacuum. The scheme was rejected because of the possibility of long pump down times to reach the required operating pressure.

(ii) Using self supporting vessels.

These could be manufactured from:-

(a) Insulating materials - a moulded ceramic section joined by rubber gaskets was considered but because of the large magnet aperture the construction was beyond the

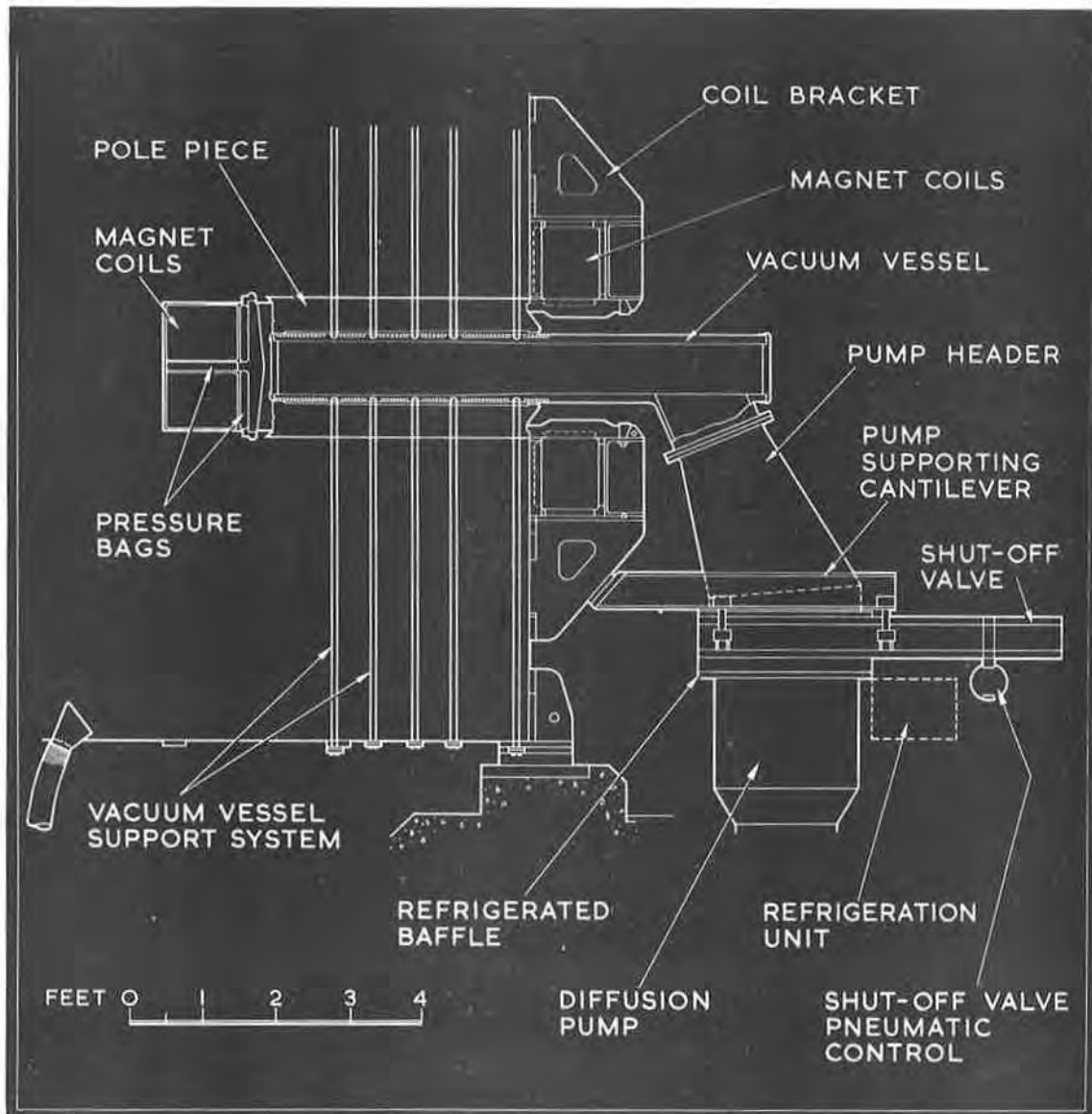


Fig. 8.2.2(i) Design of externally supported vessel.

capabilities of the ceramic ware manufacturers (in 1958) and was eliminated.

(b) Metal laminations bonded together with insulating materials - tests carried out with adhesives which had suitable vacuum properties showed that existing knowledge of this type of construction was not adequate. (A satisfactory vessel of this type might have been developed in time.) The difference in the thermal and mechanical properties of the metal and the bonding materials made the structure susceptible to mechanical failures, to short circuiting between adjacent metal laminations and to gaseous leaks.

(c) Discontinuous metal reinforcement moulded in an insulating material - this was rejected because of the amount of space which would be taken up in the magnet aperture.

(d) Metal framework clad with an insulating material - this was also rejected because it consumed several inches of magnet aperture.

(iii) Using externally supported vessels.

The design of an externally supported vessel which permitted the use of a thinner walled vessel seemed very promising and a prototype vessel 6 ft long was manufactured. This design (Fig. 8.2.2(i)) was a single wall construction of epoxy glass fibre resin laminate, externally supported by ties to the magnet sectors. The main difficulty in structural design was the high stress concentration at the point where the supporting tie secured to the inserts in the laminate. Another uncertainty was the effect of the stainless steel inserts in the laminate (to which the ties were secured) on the magnetic field. The 6 ft prototype vessel was manufactured from a laminate chosen for its vacuum and mechanical properties and its radiation resistance. The pole face windings were secured to the outer skin of the vessel and it was intended to coat the inner surface of the vessel with a metallic film which would serve to conduct away static charge and to screen 99% of the epoxy resin surface from the vacuum. The vessel extended beyond the poles of the magnet forming a duct which enabled the vessel to be pumped from below. This left the periphery of the machine free for beam extraction. The loss of magnet aperture due to the pole face windings and the vessel was less than 2 in.

This design was eventually rejected as it was considered that the expected life under irradiation would be inadequate (10),(11).

(iv) Using a double walled vessel.

A double walled vacuum vessel manufactured from thin stainless steel sheet was rejected because of the excessive heat which would be generated by eddy currents. A complete design study considered using epoxy glass fibre laminate, moulded into a double walled type of construction using thin sections of laminate. The inner vessel, which is subjected to a high level of radiation, which will in time degrade the mechanical properties of the material, was surrounded by an outer vessel. This outer vessel could be evacuated so that the inner vessel was stressed to a minimum, allowing the inner vessel to be much thinner and to have a longer life. The gain in aperture and the elimination of external ties were the main advantage of this scheme. Its disadvantages were its complexity and the close dimensional tolerances which were required.

This design was selected and manufactured in epoxy resin glass fibre. It was not an ideal solution but the one which best met most of the requirements.

8.2.3. Design Details

The vacuum chamber consists of eight curved sections approximately 54 ft long which correspond to the magnet octants. Each section comprises an outer, inner and header vessel joined together at a common radius (Fig. 8.2.3(i)). The header vessel provides a means for attaching the vacuum pumps, while leaving the outer periphery of the machine clear for beam extraction.

8.2.4. Outer Vessel

The internal working pressure is required to be below 1 torr.

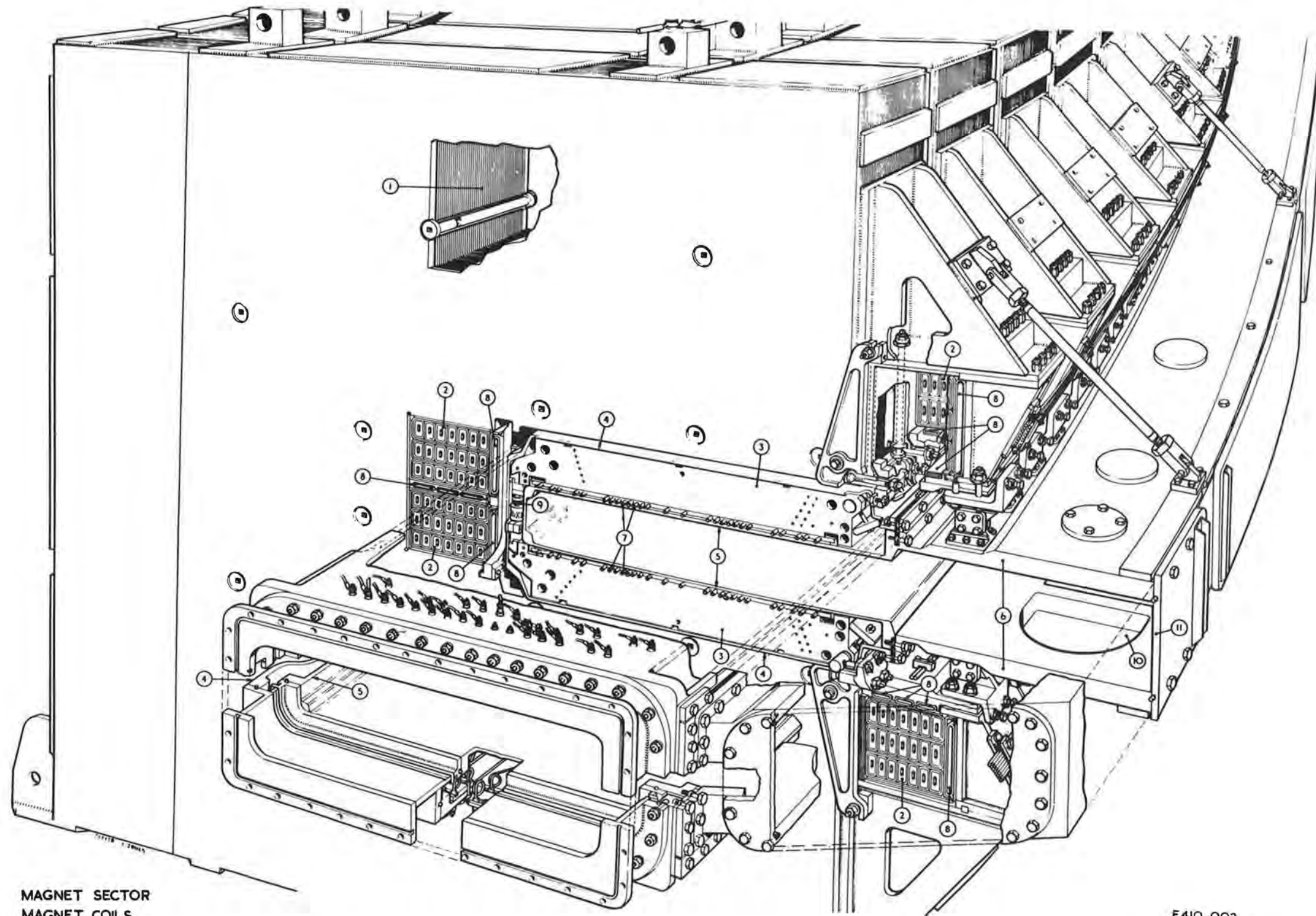
The outer vessel is nominally $\frac{1}{8}$ in thick on the horizontal surfaces. The back is $\frac{3}{16}$ in thick and the flanges, at the edge of the pole pieces, are $\frac{1}{4}$ in thick. The vessel is supported between the pole pieces and the magnet sector on the horizontal surfaces and by the pole piece jack shims on the back face. It is stiffened sufficiently in this way to withstand atmospheric pressure. The external front flange is supported from the front of the pole piece by a shim formed by a resin filled bag, which is cured in situ, and by shims from the header vessel flange. 24 in at the end of each vessel extends beyond the magnet octant and is thickened up to 1 in and supported on sliding faces by bolster pads and a rigid beam. Since the end sectors and pole pieces move at each magnet pulse, the whole of the vessel in this area is supported on rubbing surfaces; the horizontal faces are supported by the underside of the pole pieces and by the bolster plates. To prevent trapping the outer vessel between the end pole piece and the magnet face when the magnet is pulsing, the end pole piece (see Fig. 8.2.4(i)) is stood off the magnet sector by four pillars which pass through holes in the outer vessel. These holes are sealed by a special triplicate seal which allows movement of the pole piece and the sector relative to the vacuum vessel.

The general stress level throughout the vessel due to atmospheric pressure is less than 2000 lb/in² but additional stresses are introduced in the re-entrant corner (See Fig. 8.2.5(i)) during installation, since the vessel tolerances are adjusted to allow clearance for insertion of the vessel in the throat of the magnet. The theoretical maximum clearance is 0.036 in top and bottom. When the pole pieces are drawn up hard this clearance is eliminated by distortion of the vessel and stresses of approximately 5000 lb/in² were indicated. When the outer vessel is clamped in position by the pole pieces an additional stress between 2,000 and 6,500 lb/in² may be introduced because of the different heights between adjacent magnet sectors. Pole piece retaining studs pass through the front vertical faces and the front horizontal surfaces. The horizontal studs are sealed with 'O' ring seals (Fig. 8.2.4(ii)) and the vertical pole piece bolts are sealed by a special external seal. The pole face windings are individually brought through the outer vessel and sealed at the end of each octant (Fig. 8.2.4(iii)).

8.2.5. Inner Vessel

The internal working pressure is required to be below 10^{-6} torr.

The crowned inner high vacuum vessel has a thickness of $\frac{1}{4}$ in except at the flanges and inner corners. The vessel is an interference fit between the pole face windings. This is achieved by crowning the vessel so that contact is maintained with the pole face windings under the vessel's own weight and 1 torr of external pressure. The tolerances are such that with the smallest vessel placed in the largest aperture there is a minimum interference of approximately $\frac{1}{4}$ in while the maximum interference is



- ① MAGNET SECTOR
- ② MAGNET COILS
- ③ POLE TIPS
- ④ OUTER VACUUM CHAMBER (LOW VACUUM)
- ⑤ INNER VACUUM CHAMBER (HIGH VACUUM)
- ⑥ HEADER CHAMBER (HIGH VACUUM)
- ⑦ POLE FACE WINDINGS
- ⑧ PRESSURE PADS
- ⑨ POLE TIP JACK
- ⑩ MAIN PUMPING PORT
- ⑪ BEAM EXIT WINDOW

E410-002

Fig. 8.2.3(i) Isometric cross section of an octant.

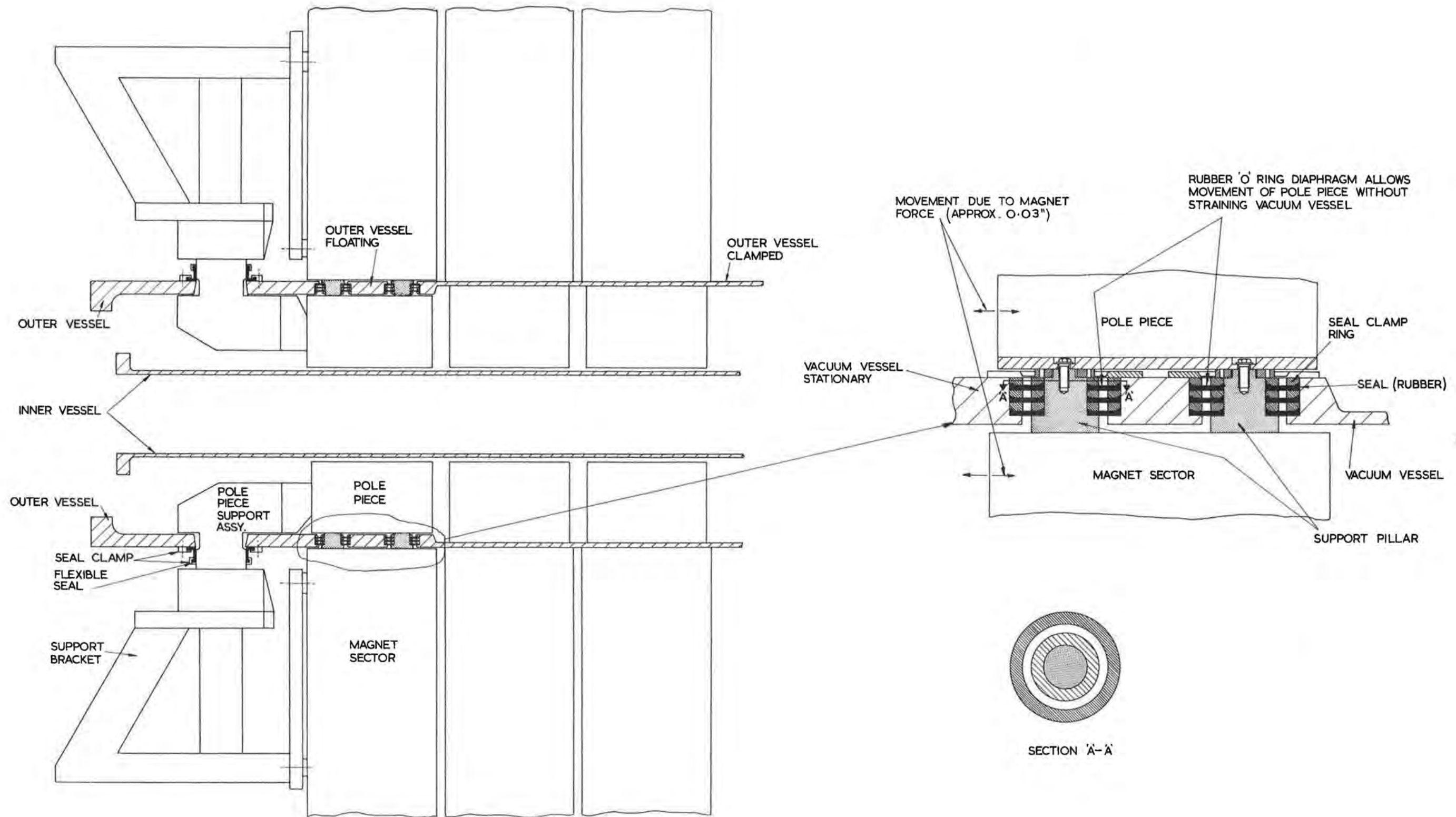


Fig. 8.2.4(i) End pole piece assembly.

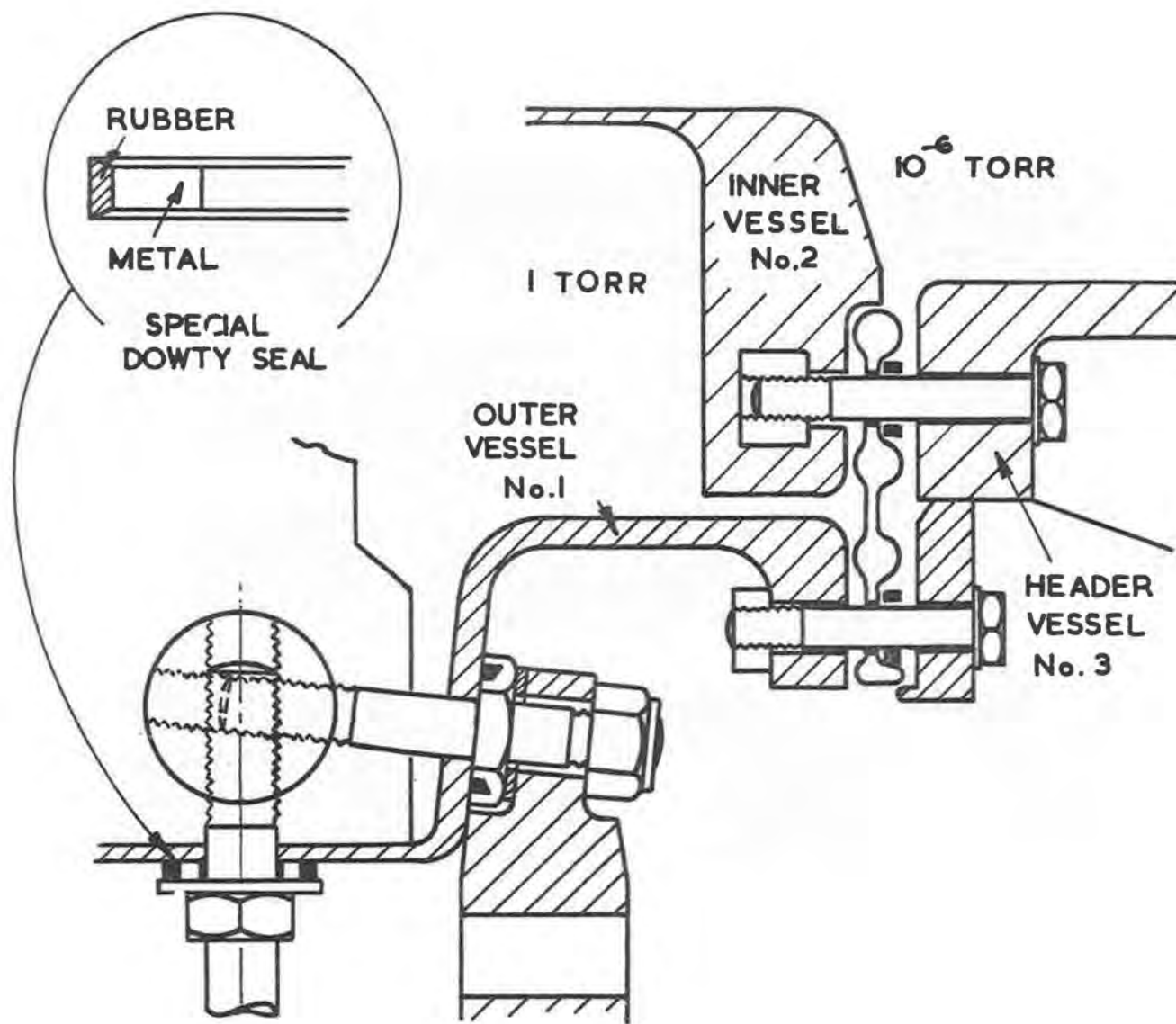


Fig. 8.2.4(ii) Vacuum vessel sealing arrangement.

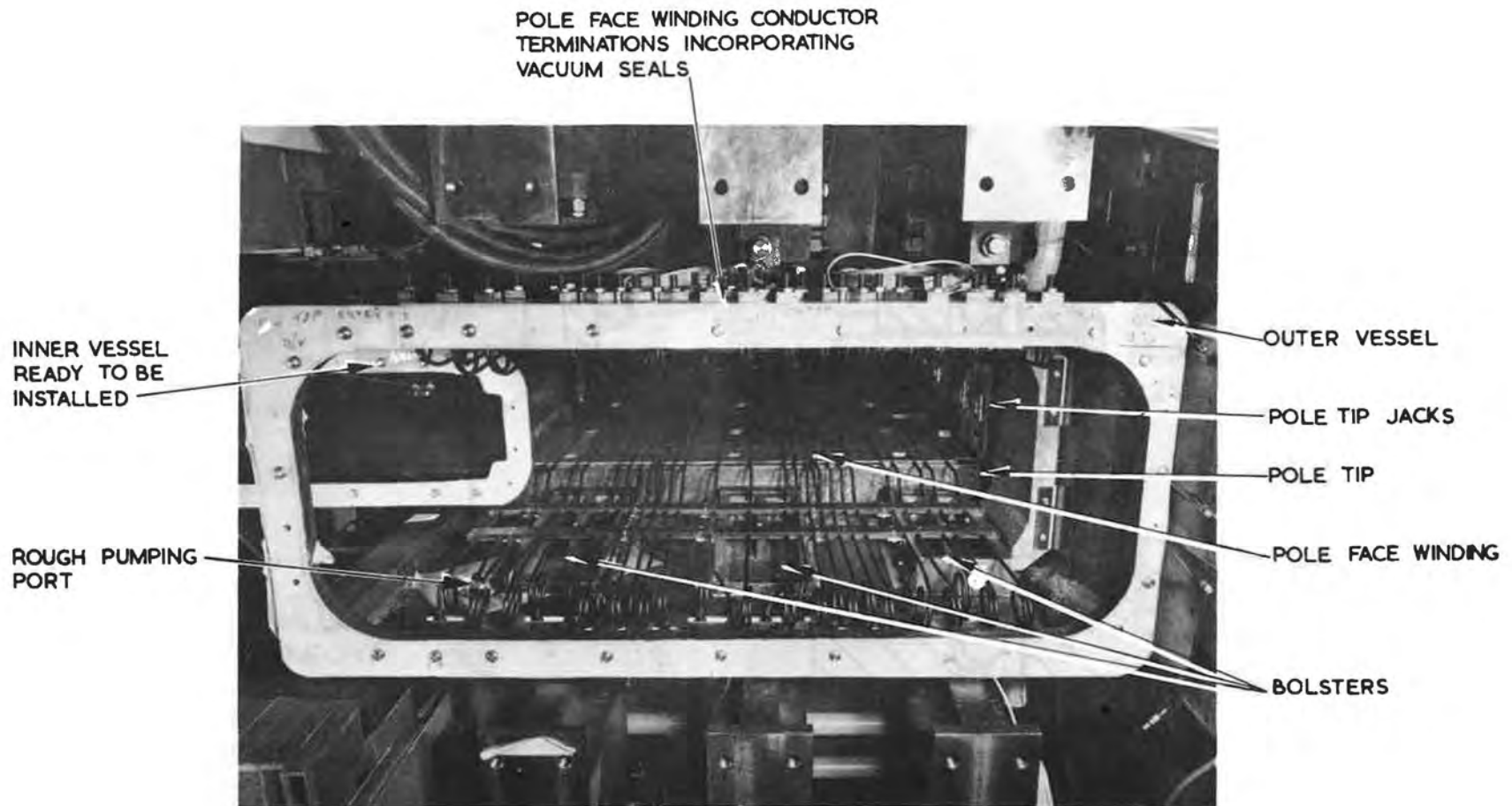


Fig. 8.2.4(iii) Pole face windings

of the order of $\frac{3}{8}$ in. The crowning shape consists of flat sides with a 10 in wide flat top (Fig. 8.2.5(i)).

One of the main features of the design of the double walled chamber is that if the outer vessel is pumped to approximately the same pressure as the inner vessel, there are negligible stresses on the inner vessel. The resin for the inner vessel could therefore be selected chiefly for its vacuum and radiation resistance properties and also, the degradation of mechanical properties by irradiation are not as serious as they would be if the chamber were highly stressed. Stresses introduced during installation were approximately 2000 lb/in².

A large pressure difference between the inner and outer vessels would cause catastrophic failure of the inner vessel and the pumping systems for each vessel need to be interlocked. In the event of failure of the interlocking devices, a bursting disc collapses and equalises the pressure in the two vessels (section 8.10.4).

At the ends of the vessels the crowning is tapered off to meet the rigid end flanges. Tapped inserts are secured to the back wall of the inner vessel for the future fixing of targets, etc. To conduct away the electrostatic charge, which would accumulate on the surface, and to minimise the resin area exposed to the vacuum (hence reducing the effect of the outgassing of the resin), the inside surfaces are lined with stainless steel foil 0.002 in thick and 4 in wide. The foil is bonded to the epoxy laminate, with small gaps between adjacent strips, and covers 99% of the laminate surface.

After the flange is manufactured, it is drilled and serrated metal inserts are bonded in position with an epoxy adhesive. The minimum pull out load for these inserts is required to be 3 tons.

8.2.6. Header Vessel

The internal working pressure is required to be below 10^{-6} torr.

The header vessel completes the vacuum enclosure at the outer circumferential edge of the inner vessel and varies in thickness from $\frac{1}{2}$ in to 2 in epoxy laminate. The vessel is supported from swinging brackets which give freedom in a tangential direction to allow the vessel to expand (Fig. 8.2.3(i)). The supports for the vessel are loaded by full atmospheric pressure acting on the whole surface of the vessel. The vacuum loads on the horizontal faces are taken by posts around the outer periphery of the vessel and by the swing bracket supports. Vacuum loads on the outer vertical face are transmitted through the horizontal faces of the vessel and taken at the swing brackets. At the outer periphery, the top and bottom horizontal surfaces are prevented from closing together by posts approximately 22 in apart. The compression load on each post is approximately 4000 lb. Five pumping ports are provided on the underside of each header vessel; each port is bridged in two places by integral struts to prevent radial collapse of the vessel. The struts are reinforced by a short, stainless steel, upper pump header with deep webs, which correspond to the integral struts in the header vessel to which they are clamped.

The maximum stress in the vessel is approximately 5000 lb/in².

The outlet windows on the header vessel are aluminium $\frac{7}{8}$ in thick and are stressed at 3500 lb/in². They are secured back to anchor bars which are in turn secured to the top and bottom faces of the vessel.

The header vessel (for the same reasons as the inner vessel) is lined with stainless steel foil. Inside the vessel, inserts have been bonded in suitable positions for fixing experimental equipment. 6 in diameter holes fitted with cover plates are positioned at intervals in the top and bottom faces to give access for instrumentation and experimental equipment.

A flexible sealing diaphragm (section 8.9), manufactured from PVC nitrile, is secured to the inner vessel and seals the inner and header vessels. At the same time it marries to and seals the outer vessel. The flexibility of this seal accomodates small inaccuracies in manufacture of the curved vessel flanges.

8.2.7. Polythene Closing Plate

At a later date in the construction of the machine, polythene closing plates were designed to replace the header vessels for half of the octants where provision for beam extraction was not necessary. This achieved a considerable saving in cost and speeded the construction programme. The use of polythene as a structural material required special consideration of the working stress levels because of the creep characteristics of polythene. It was specially selected for good vacuum properties and adequate radiation resistance. Low density polythene was used since, at the time of manufacture, no manufacturer was prepared to attempt to make the plates in high density polythene. The polythene plate is 54 ft long $1\frac{1}{4}$ in thick and is made from pieces, each approximately 5 ft long, welded together.

The atmospheric load carried by the polythene plate is taken by a system of tie rods as shown in Fig. 8.2.7(i). Each tie rod is secured to the polythene via a bracket and four inserts. The load applied to each insert is 245 lb while the actual pull out strength is 2100 lb. In the region of the pumping ports, seal clamp rings are used around the pump header tubes to seal the hole and support the polythene. The maximum stress in the polythene due to bending is approximately 220 lb/in².

Special attention was needed during installation to achieve uniform load distribution. Creep of the plate which causes the inserts to be displaced is minimised by the low stress levels used in the design; nevertheless, creep at the centre of the plate (without allowing for stiffening which will take place in time due to irradiation) is about 0.07 in/year.

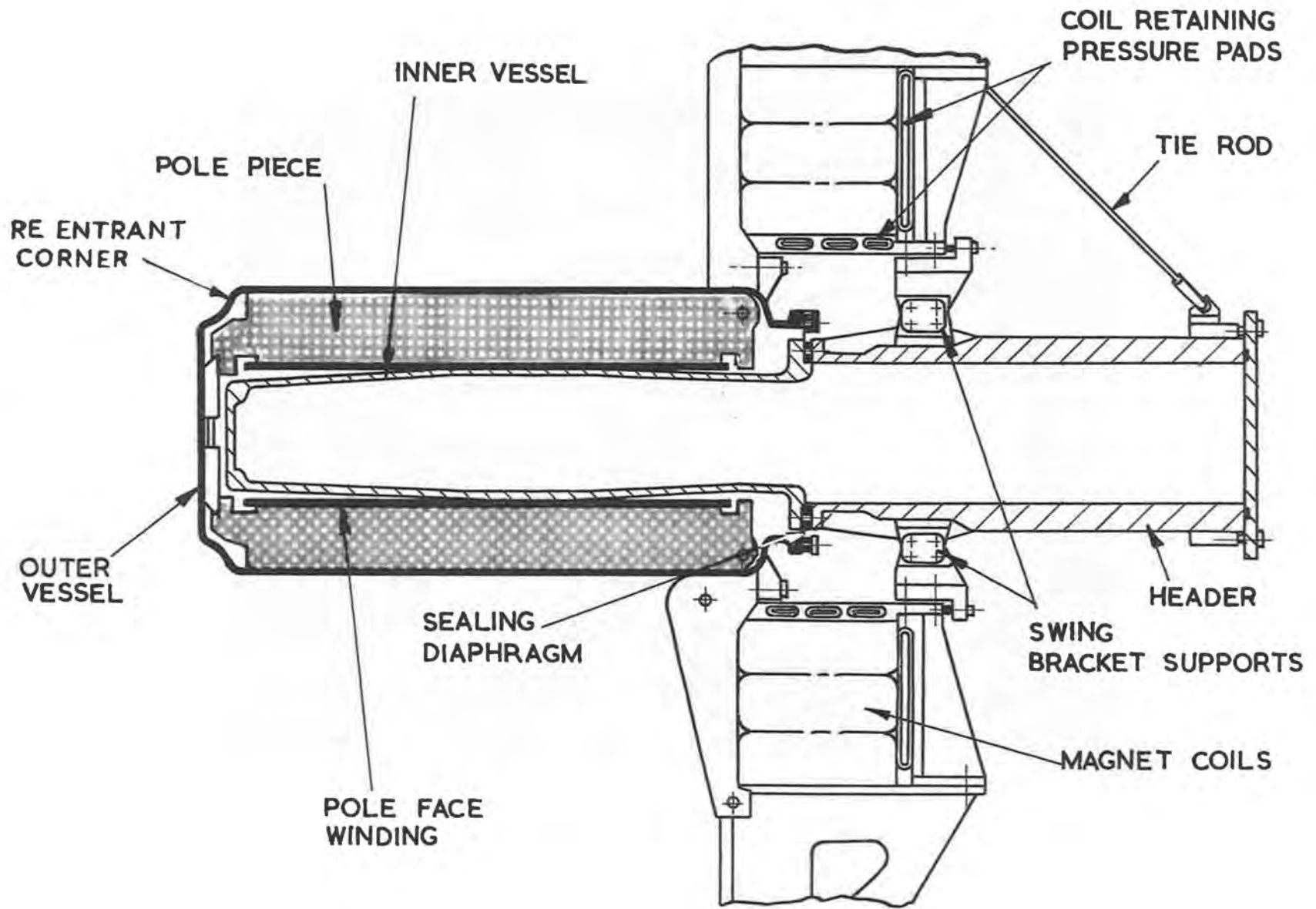


Fig. 8.2.5(i) Inner vessel crowning and header supports

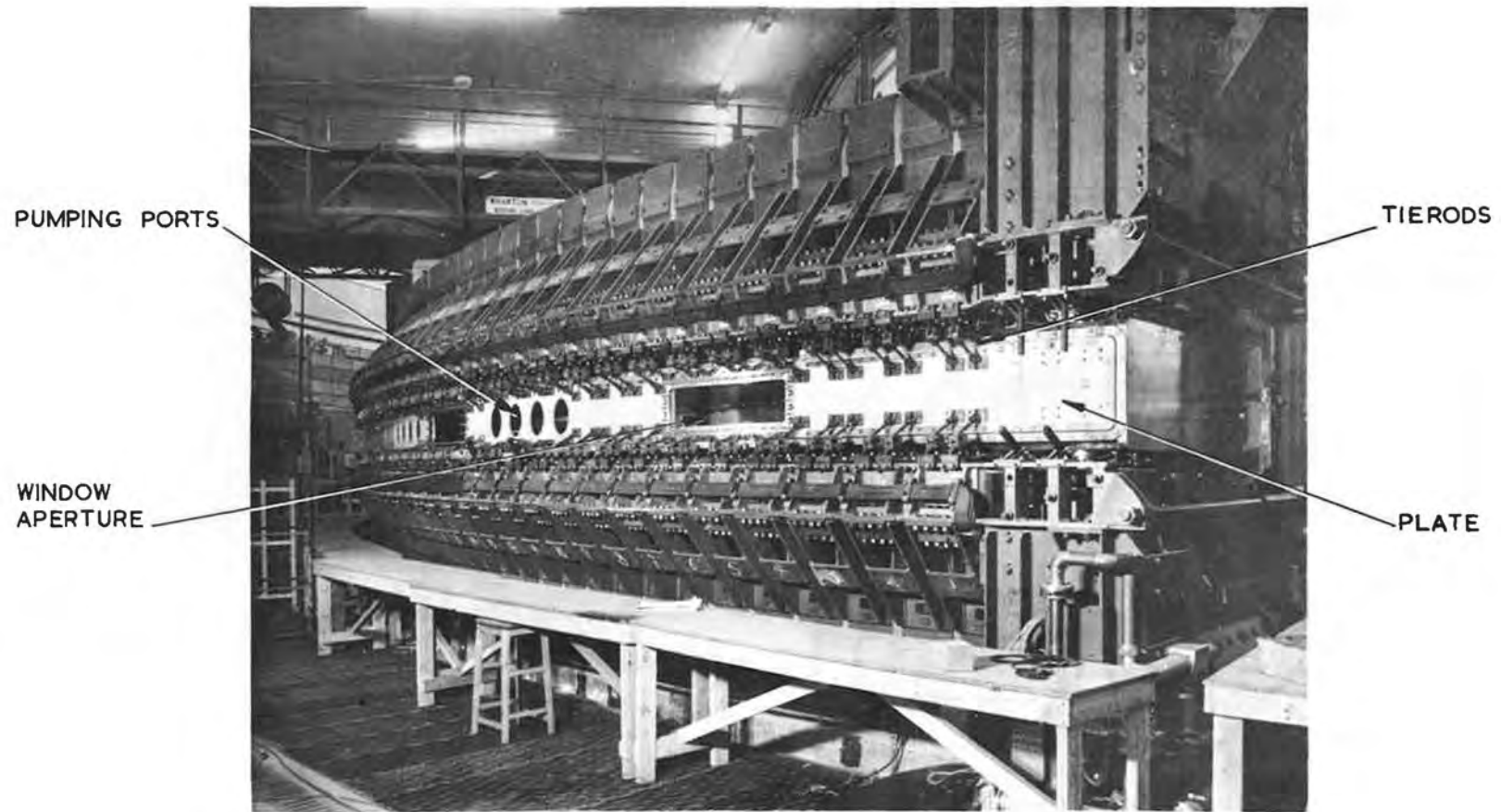


Fig. 8.2.7(i) Closure plate tie rods.

8.3. Vessel Manufacture

8.3.1. Summary of Method Used

The following paragraphs summarise the method used and the difficulties encountered in the manufacture of the vacuum vessels. The problems are more fully described in reference 12.

For reasons of convenience and economics each vessel was fabricated from a number of pieces, which were basically units of one third of the length of a vessel side (Fig. 8.3.1(i)). Each third of a side was produced by laying up glass cloth and resin on a curved die bed approximately 20 ft long and 5 ft wide. The individual dies were about 14 in wide and were fitted with control of heating and/or cooling. A limited length of the die bed could be covered by punches with similar heating and/or cooling facilities. These punches were moved in steps along the bed as manufacture of the laminate proceeded (Fig. 8.3.1(ii)).

The glass cloth was pre-impregnated with resin and allowed to soak for 24 hours. Lengths were then cut and laid along the die bed, alternate layers being placed diagonally to give more uniform strength to the finished laminate (Fig. 8.3.1(iii)). Additional resin was added during the process and, every few layers, the laminate was rolled to force out air bubbles trapped between the cloths and to consolidate the lay up. Pre-fabricated, semi-cured (or 'B' stage) packs, specially shaped to form the main vacuum flange and dorsal shoulder were positioned on the outer and inner circumferences of the die bed and retained by the boundary layers of glass cloth (Fig. 8.3.1(iv)). For an outer vessel further cloths were added to the laminate at one end of the die bed to increase the thickness to 1 in, the remainder of the area consisting of 20 layers of 0.006 in cloth. Punches were then positioned and a portion of the lay up cured by heating. To facilitate subsequent processes, whenever the edge of a laminate was to be joined to another component by splicing, that edge of the punch and die was cooled so that the resin was not cured and could in fact be washed out of the protruding cloths by solvents. This allowed the fabricated sections to be stored indefinitely.

The next third of a side was manufactured similarly but with the thickened portion at the opposite end of the die bed. A complete vessel side (Fig. 8.3.1(v)) was then formed by laying these two opposite handed sections on extensions to the die bed. The protruding cloths from the ends were re-impregnated with resin and interleaved with new cloths laid on the die bed to form the centre section of the side and this portion cured by the same step by step movement of punches and by temperature cycling as before.

After two such sides had been produced they were spliced together on a special rig where the dorsal wall and the two end flanges were formed. Each side was clamped vertically against the rig with the larger circumference nearest the floor. The protruding cloth ends at the smaller circumference were then re-impregnated with resin and spliced across the width of the rig, (Fig. 8.3.1(vi)) beginning at the centre, with additional cloths to form a laminate 30 layers or 3/16 in thick. Special tools were then positioned to press the laminate to shape and raise the temperature to cure it. At the ends, other tools, in the form of a "picture frame", were positioned so that the re-impregnated cloth ends from the two sides could be formed with additional 0.017 in thick cloths into a flange 2 in thick. The vessel was then moved to a loft plate for inspection and the many machined and drilled holes were provided in the walls and flanges using accurately positioned jigs.

Finally, all surfaces which were required to form a vacuum sealing surface, such as the vessel flanges, rough pumping ports, pole face winding and pole piece fixing bolt holes, were prepared. All of these areas had to be smooth and free from scratches or other blemishes. The surfaces were dressed by hand or by portable sanding machine, as appropriate, to smooth the surface to the correct profile, and then coated with an epoxy varnish and rubbed down by hand with 'wet and dry' Garnet paper.

Inner vessels were produced in a similar manner on a different die bed. These vessels were smaller in cross section and the walls were $\frac{1}{4}$ in thick. The covering of stainless steel foil on the high vacuum surface of the vessel was laid on top of the resin and glass cloth before the punches were lowered to press and cure the laminate.

Header vessels required a slightly different approach since they were mainly 2 in thick. To maintain the strength of the laminate while shortening the lay up time, only the outer layers on each side were wholly of 0.006 in cloth, the bulk of the laminate consisting of 0.017 in cloths, interspersed with 0.006 in cloths every seven layers to reduce resin drainage to the bottom of the laminate.

The inner flange rail on the moulding bed was fixed but the outer flange rail was sectioned and components made interchangeable to allow the contour to be varied for each third of a side. The differing thicknesses of laminate necessitated an assembly of metal shoes and plates to form the correct contour. The shoes were fixed to loading arms stretched between inner and outer flange rails.

After lay up, the whole moulding bed was moved on a wheeled trolley into a gas-fired oven for the curing schedule. The technique of splicing components to form sides and then vessels, was similar in principle for the header vessels to that for the other vessels. Selected sides were machined to provide the apertures for the pumping ports on the completed vessels.

8.3.2. Production Problems

(a) Outer vessels

(i) Release

The release of the epoxy resin laminates from the moulding tools presented the manufacturer with a difficult problem. Many types of release agent were used to coat the forming tools but without obtaining a completely successful release. Ultimately a glass cloth based on PTFE release agent 'Tygaflor' was used to cover each tool and proved highly successful.

(ii) Appearance of voids

The thermostatically controlled heating for both punches and dies caused bowing of the tools by setting up severe temperature gradients through them. This produced vacuum voids on or near the surface of the laminate. The fault was eliminated by reducing the rating of the electrical heating, so that less power was applied more often to the tools to maintain the required temperature.

(iii) Regions of undercure

It was noticed on some laminates, particularly along the edges of each die sector, that mouldings were receiving an inadequate degree of cure. By re-arranging

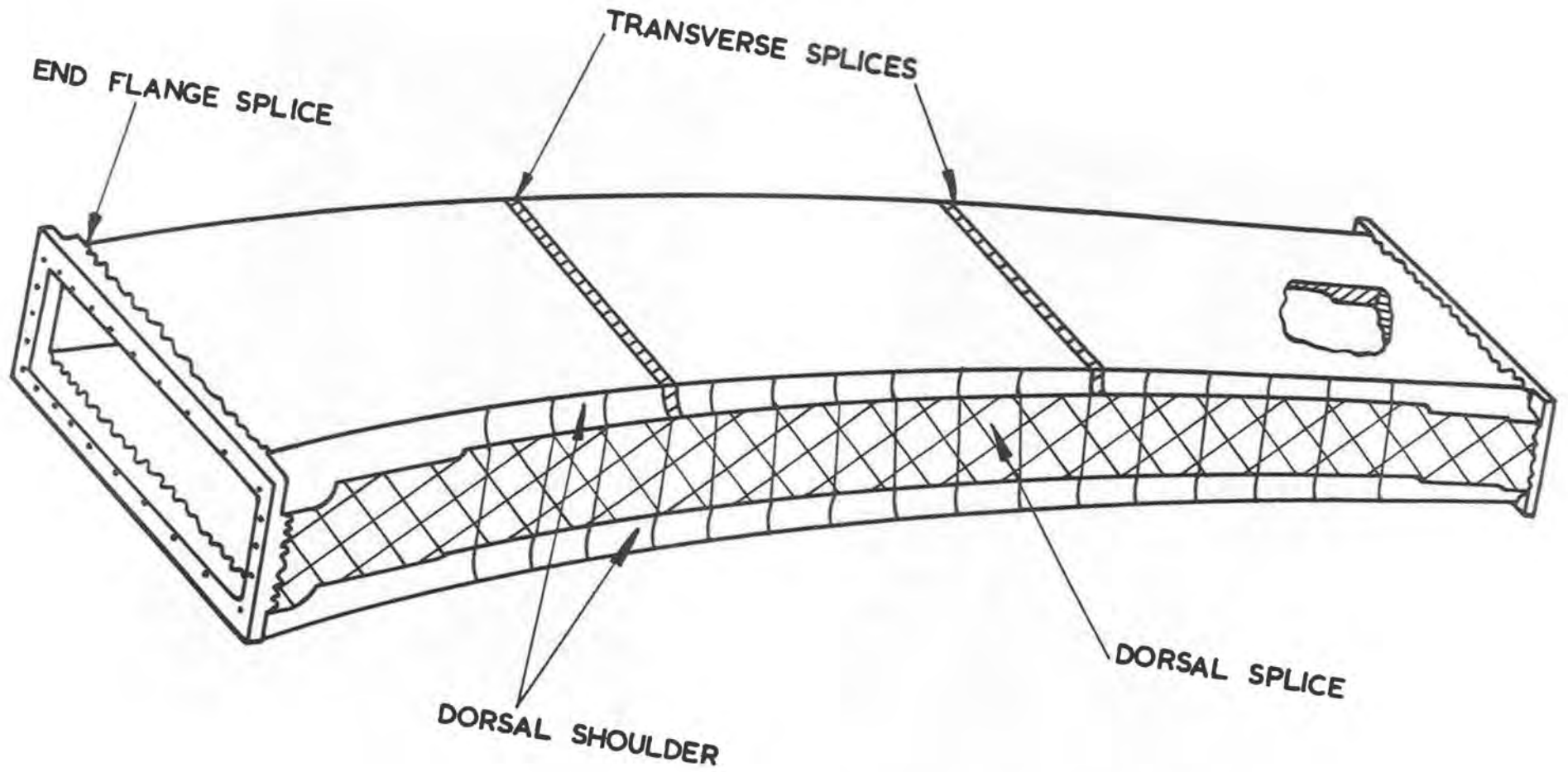


Fig. 8.3.1(i) Outer vessel splices.

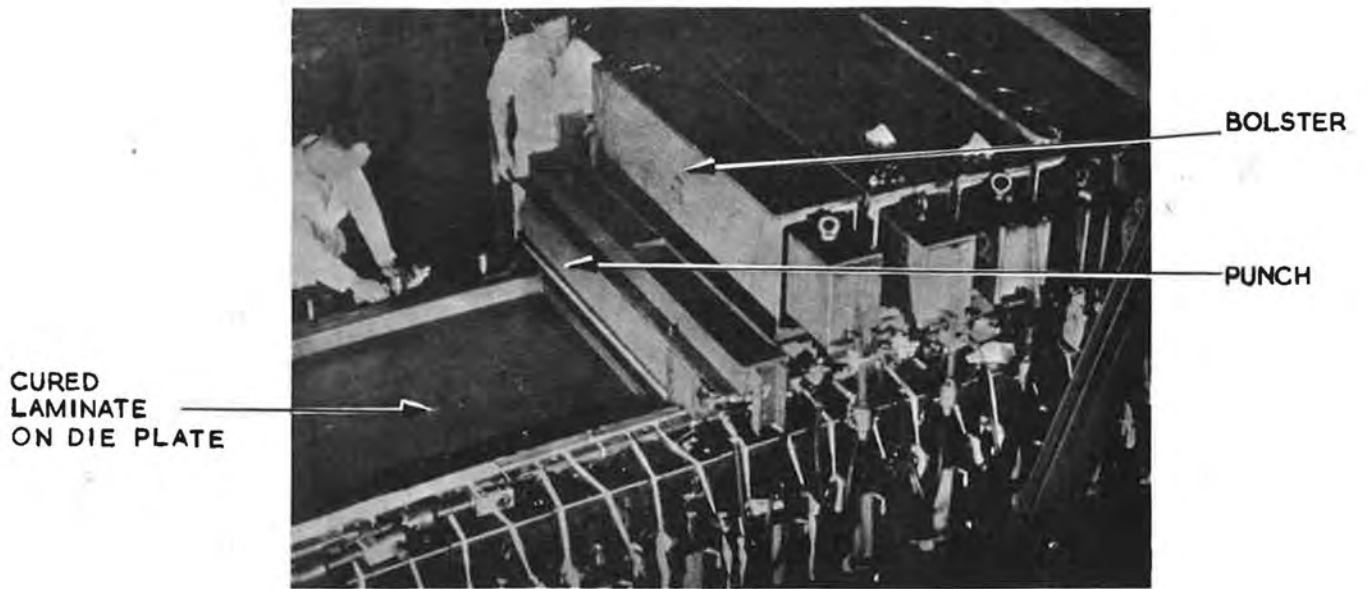


Fig. 8.3.1(ii) Curing a section of an outer vessel on a die bed.

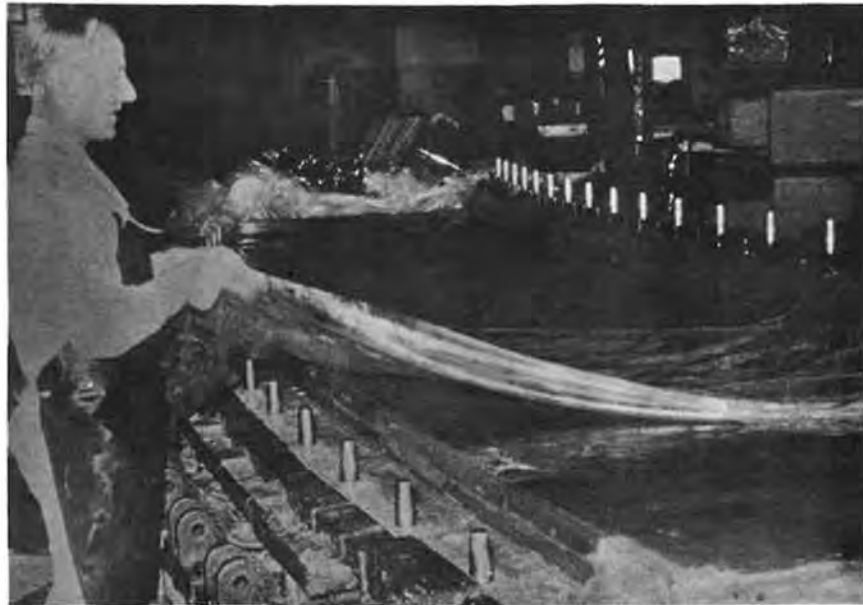


Fig. 8.3.1(iii) Laying impregnated cloth on a die bed.

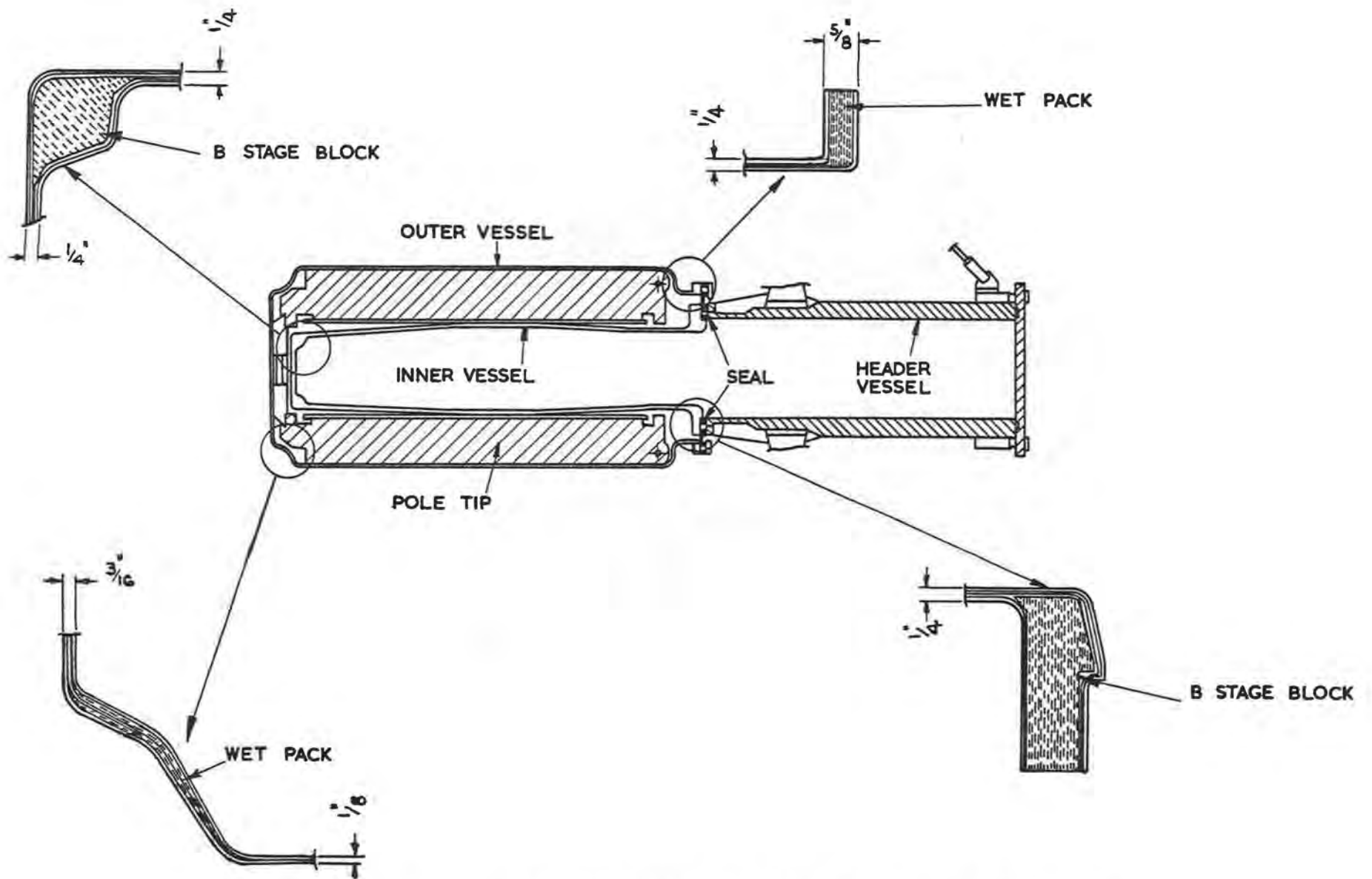


Fig. 8.3.1(iv) Cross section of Vessel and Flanges showing "B" stage Blocks and "Wet Packs".

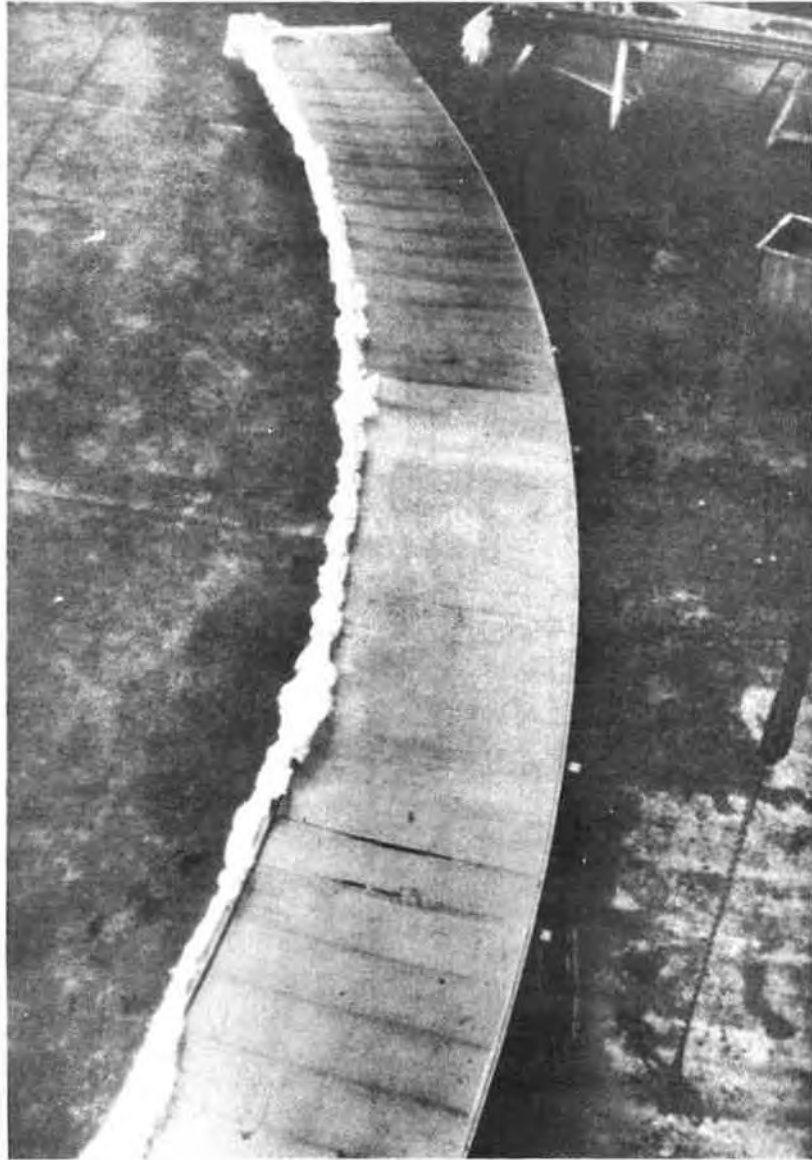


Fig. 8.3.1(v) View of a vessel side.

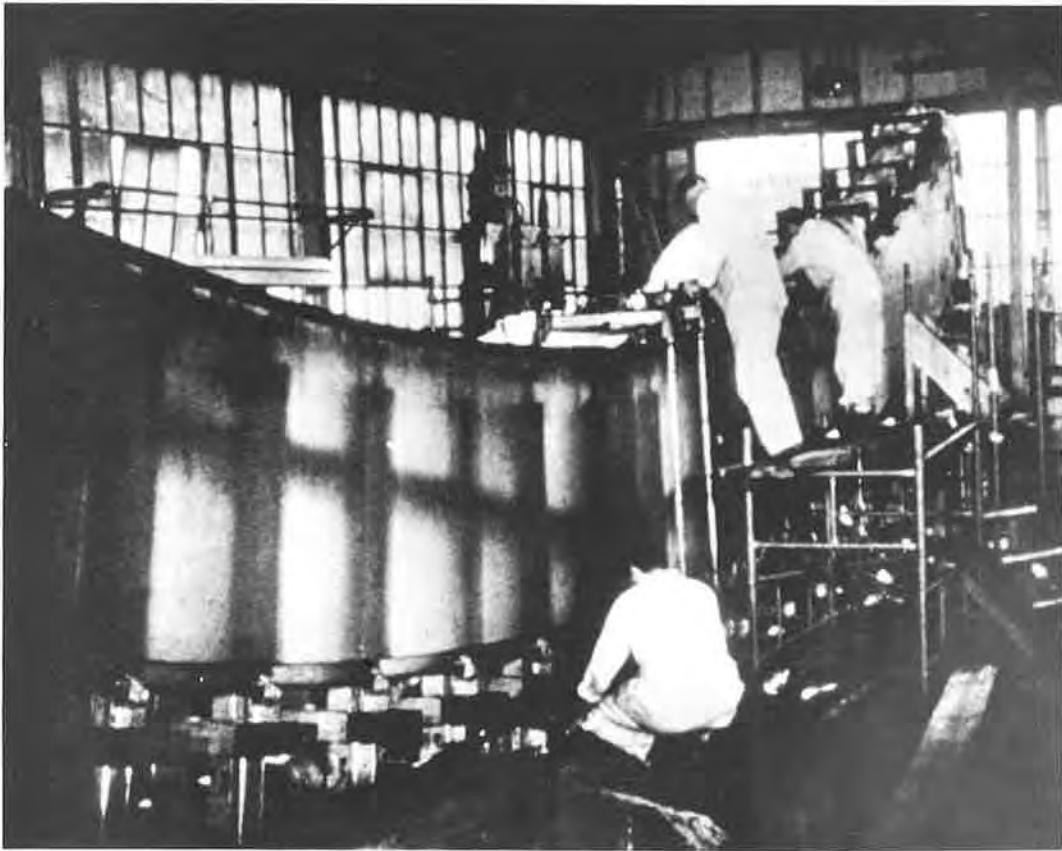


Fig. 8.3.1(vi) Dorsal splicing in progress

the heater network in the punches and dies, more heat was supplied to these areas with a satisfactory result.

(iv) Whitening in the dorsal region of tool intersection

This was caused by a relative movement of adjacent tools during the latter part of the curing cycle. This caused glass cloth and resin to be crushed and the effect was visible as a whitened strip on the laminate. To reduce the fault, shims were used on the top and bottom of all laminate inter-sector lines and, on completing the cure, the punches were lifted $\frac{1}{8}$ in and their temperature maintained for a further two hours. In this way the shearing action on the laminate, caused when the punches and dies were allowed to cool in the loaded position, was substantially reduced and crushing of the laminate minimised.

(v) Void and resin richness on the vacuum flanges

This was caused by the difficulty of positioning a pack of 65 layers of cloth. The layers were cut from bulk supplies of cloth which gave a frayed edge and caused resin rich areas during lay-up. The fault was rectified by using $1\frac{1}{4}$ in cloth tape with selvages which, as well as reducing resin richness at the edge of the pack, allowed the layers of overlapping cloth from the main laminate to be cut and formed more accurately.

(vi) Dorsal pack location

Considerable difficulty was found in maintaining the position of this pack during lay up, which led to resin drainage from the bottom of the wall. It was overcome by securing tapes to the pack and tying the loose ends of the tape to the moulding bed and ensuring that positioning of overlapping cloths was carried out as quickly as possible.

(vii) End flanges

Because of the length of time taken to shape the profile of the end flange before the cure could be attempted, resin drainage gave areas of resin richness and cavitation. It was overcome in two ways - first by increasing the bulk factor of the flange and compressing it to its final size, (this consolidated the cloths and expelled air) and second, by adjusting the accelerator content of the resin mix to ensure a shorter gel-time. Care was taken to control the rate of heating such that, during the subsequent cure, the resin mix did not turn liquid before solidifying. With practice, the time scales for the formation of the end flange was reduced and, with the introduction of thixotropic resin, the accelerator content could be reduced to regain the longer pot-life of the resin mix.

(b) Inner vessels

Many problems overcome during the production of the outer vessels also applied to the inner vessels.

(i) Application of stainless steel foil

Some work was done on this problem by I.C.I. Ltd. (13)

Two faults, which had not previously been resolved, soon became apparent. First, the inadequacy of the bond between the stainless steel foil and the laminate

and second, the ripple on individual strips of foil after lay-up. It was possible to increase the bond strength by ensuring that an acid primer was used on the appropriate surface of the stainless steel, before it became the inner surface layer of the third side and was subsequently cured with the side. The ripple fault was rectified by slightly tensioning the strips of stainless steel once they were located on the laminate. Lowering of the punches prior to the cure was also expected to increase the tension in the foil. Care was taken during this process to ensure that the ends of the foil strip retained their positions.

(ii) Laminate quality

The dorsal splice had many faults which, because of the pressure of the production programme, remained unsolved. However, it was found that removing three layers of cloth from the dorsal wall and replacing them by three fresh cloths, provided a leak free laminate.

(c) Header vessels

(i) Poor definition between cured and wet end material

When a third of a side was produced, the protruding cloths from the ends and outer circumference of the side were found to be either cured and quite rigid, or uncured, with a region of undercure or uncure extending into the laminate. This fault was eliminated by ensuring that the wet ends were adequately cooled during the cure cycle of the laminate.

(ii) Steps on the top surface of the laminate

This fault was caused by the floating action of the plates laid on the top of the laminate. During cure, the change in relative position between adjacent plates caused steps to form on the laminate. A modified system of loading was devised and the plates were no longer allowed to float but were clamped in position. The surface finish of the laminate was not as good but a nearly step-free laminate was produced.

(iii) Dorsal splicing and end flanges

Great difficulty was experienced in wetting the 2 in bulk of cloths before splicing occurred. The only way this problem could be resolved was to repair these areas after the laminate had been cured. Some extensive repairs were necessary and a dielectric heater was used to obtain uniform heating throughout the repair.

8.4. Inspection at the Manufacturers' Works.

8.4.1. Introduction

Inspection of the vacuum vessels was carried out by two teams - the manufacturer's own staff (who carried out the bulk of the dimensional checks and the process control during manufacture) and a resident U.K.A.E.A. team supplied by the Inspection and Progress Group, Risley.

The overall inspection task was a formidable one because of the vast number of checks which had to be carried out and the extreme stringency on dimensional accuracy and quality of material required. In addition, all the checks had to be recorded and the records kept in such a manner that analysis of the checks would show any wrong trends.

The supervisory staffs were involved in all aspects of manufacture and their assistance was used on manufacturing processes such as the resetting of the arcs of tools to counter-act cooling and arc shrinkage on the finished laminate.

8.4.2. Flexibility in Inspection

A part of a vessel was not automatically rejected because of any one error. Tolerances were specified so that, if all were held, the vessel would be acceptable dimensionally even if the errors were cumulative. Because of the large sizes involved, the tightness of the tolerances and the unique method of manufacture with relatively unconventional materials, it was necessary to train the supervisors to recognise which dimensions were interdependant. Only three factors were essential:

- (a) The vessels should fit the machine and their mating parts,
- (b) They should be made of the correct materials,
- (c) They should have the required vacuum and strength properties.

8.4.3. Process Control

In the majority of engineering jobs, process control is left in the hands of the supervisory staff. After the initial production of several sections of laminate, which were faulty for a variety of different reasons, it became obvious that two steps should be taken. First, sporadic errors due to the measurements being taken by different people had to be eliminated by the introduction of a process control team, and second, an examination of the actual processes had to be implemented.

The method of process control was to:-

- (i) Set up a group of process controllers as members of the inspection team,
- (ii) Establish a chart enumerating each individual step in the process,
- (iii) Stop any step being taken before the process controller had stamped the chart, that he was satisfied with the previous step. Initially, each step was also checked and stamped off by the U.K.A.E.A. inspector as well as the manufacturers process controller. This improved the quality of the laminates but slowed the production rate. Eventually, after about one quarter of the final production of each

type of vessel was complete, a satisfactory balance was found between rigidity of control and rate of production.

8.4.4. Quality Control

Quality control is described more fully in reference 14.

Basically it comprised the following stages:-

(i) Inspection staff obtained samples of all batches of raw material before it was supplied by the manufacturers. The samples were sent to the Rutherford Laboratory for chemical and physical tests after being made up into laminate and cured.

(ii) All raw materials, on delivery at the factory, were held in a special store and the date of delivery was noted. Only materials drawn from this store were used in making vessels.

(iii) Each mix was checked by inspection staff and before it was released a gel-time test was performed. A sample of the mix was sent to the Rutherford Laboratory for an independent cross check.

(iv) As lay-up and cure proceeded, a sample laminate was laid up and cured from the main laminate mix. The resulting sample was sent to the Rutherford Laboratory for physical tests.

8.4.5. Production Tool Inspection

This inspection involved three separate stages:-

(i) Initial inspection for faults, flaws, and dimensional accuracy. (Sufficient inaccuracy was found to justify this inspection).

(ii) Erection inspection for correctness of assembly and dimensional accuracy of setting up.

(iii) Subsequent checks during production.

The inner and outer vessel side moulding beds were stout steel structures built about 3 ft high and approximately 20 ft by 5 ft in plan view. The top surface of the structure was a flat ground plate suitably drilled for clamping bolts and locating dowels; it was levelled to within about 0.020 in by screw jacks. The laying up bed comprised 21 separate dies each approximately 3 in thick, 50 in long and 14 in wide. These dies were set up under the supervision of the inspection survey team. The method used was to set up the main datum points accurately (Fig. 8.4.5(i)). These points were the octant centre (an optical target securely fixed into the shop floor) and the main datum dowels. The datum radii and datum chord length were fixed by using accurate invar tapes. The chord length was checked by a theodolite set up on the octant centre. Intermediate dies were set up radially, relative to an accurate curved template located from the datum dies.

The horizontal plane of the dies was adjusted by the use of shims, fixed for level by spirit levels and fixed for height by the theodolite. Intermediate dies were set for height and level by checking the vertical step at the edges of adjacent tools. This step produced a step on the laminate and the maximum permitted step was

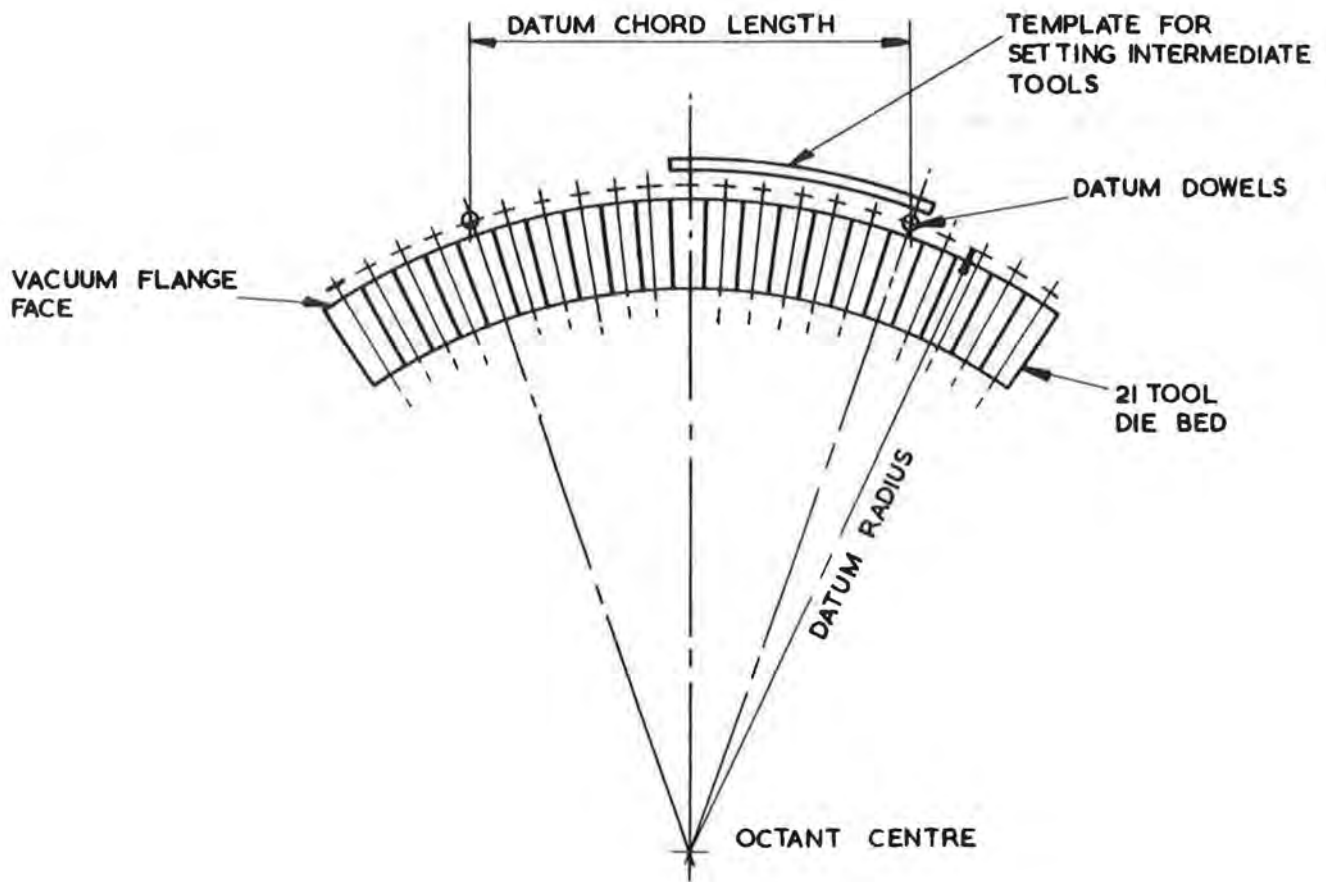


Fig. 8.4.5(i) Diagram of the Side Moulding Bed.

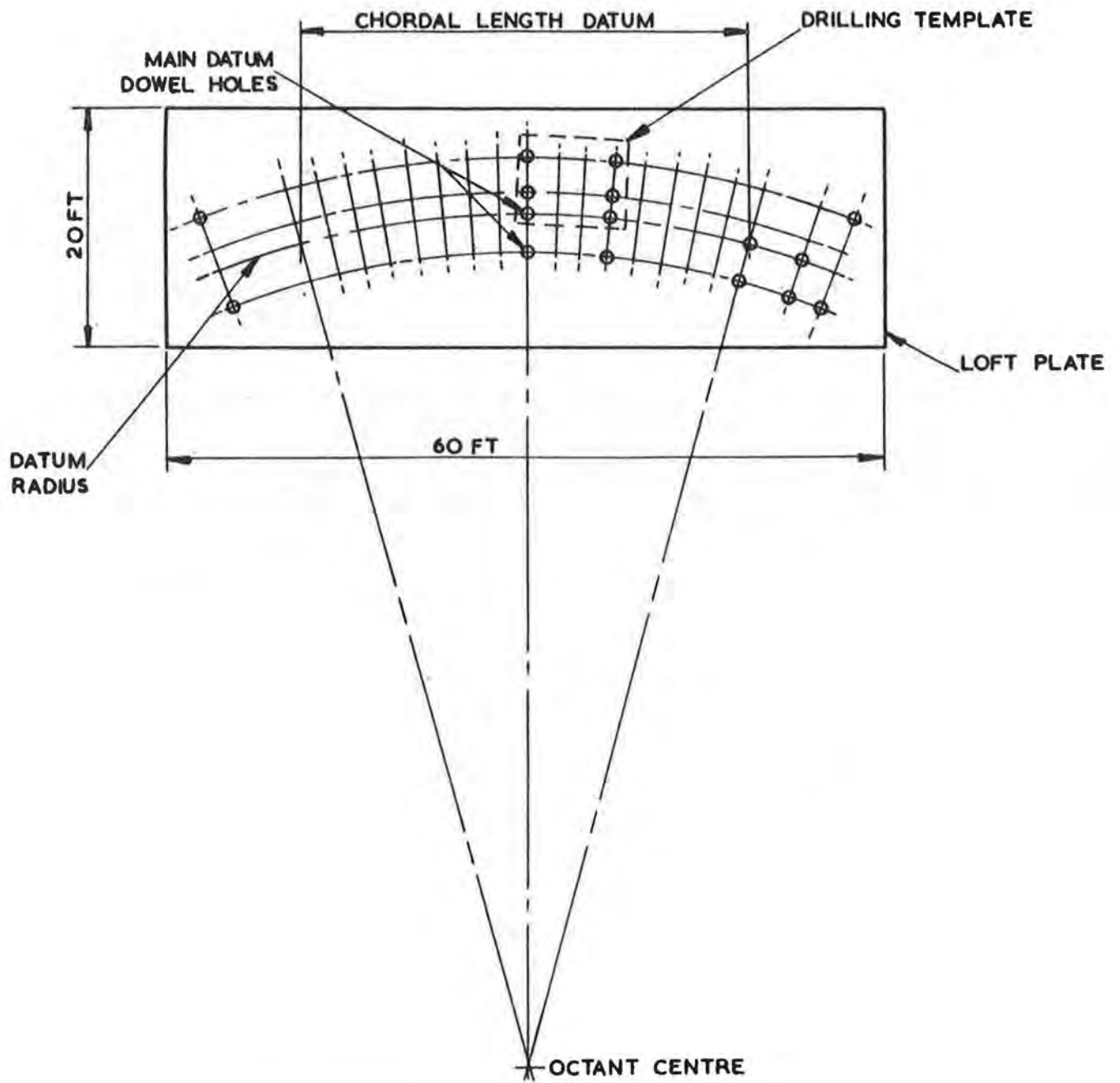


Fig. 8.4.7(i) Diagrammatic arrangement of the Loft Plate.

0.007 in. As the laminate step was found to be within 0.002 in of the die step, the maximum limit for the die step was set at 0.005 in.

Setting of the die bed then became the responsibility of the inspection department. The manufacturer's inspection staff were responsible for checking and for compiling suitable records. The U.K.A.E.A. team checked the records and did spot checks on the tools. The flatness of the die bed was checked after each heat cycle and the main datum points were checked periodically. All principal moulding beds were treated in the same manner.

8.4.6. Checking of Lay-Up

The majority of checks during lay-up were the responsibility of the process control team. They ensured, for example, that the correct numbers of pre-impregnated cloths were laid up, that the cloths did not overlap and were laid with the weft and the warp in the correct direction, and that the heating was switched on and off in the right sequence and at the right time.

One particularly important aspect at this stage is 'bulk factor' - the surplus resin which is forced out on closing the matched tools. This surplus resin ensures that the dies are completely filled and when it is pressed out it sweeps out the remaining air in the laminate. Too little excess bulk leaves air in the laminate; too much causes the cloths to move. A bulk factor of 10% was finally selected, which means 0.012 in excess thickness on the 0.125 in outer vessel panels. Thin plate aluminium templates were cut to simulate the top tool but with excessive gap, to allow the space between the laminate surface and the template edge to be measured. The melinex skin, which is laid on the wet laminate to facilitate rolling out, was left in place during this dimensional check and enabled the gap to be determined to within about 0.002 in. Pressure was not applied to the top tool (punch) until the tools were closed to within 0.010 in.

8.4.7. Laminate Inspection

The method of manufacture was to produce a piece of laminate cured over the bulk of its surface, with selected edges left uncured ('wet'). The wet ends of adjacent pieces were spliced together and cured until a complete vessel had been constructed. Each piece, therefore, needed to be checked, visually (for quality) and dimensionally after curing, before being married into the whole. Final vacuum testing was carried out at the Rutherford Laboratory.

The final arbiters on whether a piece of laminate should be rejected were a member of the Laboratory scientific staff for the vacuum properties and a member of the Laboratory Engineering Design staff for the mechanical and dimensional aspects. In general, however, the visual inspection was carried out by the senior member of the U.K.A.E.A. resident inspection team, who, by consultation and discussion with the Laboratory staff and by visiting the vacuum testing laboratory, had learned with a high degree of surety what was required.

All dimensional checking, whether of piece parts or of the whole, was carried out on the 'loft plate', (See Fig. 8.4.7(i)). The 'loft plate' was the centrepiece of the inspection equipment, and was highly successful in use. It served two principle functions:-

(i) As an accurate surface table for mounting inspection equipment to check dimensions.

(ii) As a drilled frame to hold drill jigs for the accurate drilling of all flange bolt holes.

The loft plate was constructed by setting up a steel structure mainly consisting of 15 in by 6 in steel joists each 20 ft long on which were mounted 4 ft by 2 ft plates (each 0.5 in thick) which were ground flat on one side to form a table top about 16 in above floor level. This table top measured 60 ft by 20 ft and the individual plates were levelled to lie in a flat plane to within 0.010 in. The level was checked from time to time and was so stable that by the completion date it was still within 0.020 in. The loft plate was in such demand that it became necessary to erect a second full size one and a third one measuring 20 ft by 20 ft.

The surface was drilled to accommodate dowelled drilling jigs and dial gauge checking jigs, the holes being located within 0.008 in. The octant centre was sited on the shop floor at approximately its final position and from this the location of the datum dowel holes were fixed and drilled from the jig-bored drilling template. The octant centre was then located accurately from these two holes and the fiduciary bolt locked firmly. The pitch of the dowel holes was a constant over the bulk of the length of the vessel which meant successive use of the drilling template around the arc. The extreme holes in the template were fitted with optical targets and checked relative to the octant centre with theodolite and invar tape before drilling commenced. The datum dowel holes in the template were fitted with eccentrics for any correction of the template position. Only three different templates were required for the drilling of about 250 holes in the loft plate.

Hollow cast iron cubes (9 ± 0.001 in) were used to support the bottom panel of the vessel. Aluminium plates $\frac{1}{4}$ in thick were cut accurately to the internal profile of the vessel and used to support the top panel and flange face at the correct aperture for dimension checking. The flange bolt hole drilling jig was fitted with accurately positioned locating faces and clamps to hold the flange square and firm during drilling.

8.4.8. Dimensional Accuracy

Some values are given here to illustrate the accuracies achieved:-

(i) Outer vessel top and bottom panels

The thickness tolerance specified was 0.125 ± 0.010 in. On ten vessels approximately 12000 readings were taken and in 98% of cases the specification was met. The other 2% were between + 0.010 in and + 0.016 in and occurred consistently on the same part of the panel. No action was taken to correct this because of its position.

Steps on the laminate caused by using press tools of approximately 14 in width along the 54 ft length of the vessel were specified as not to exceed 0.007 in. A total of about 5,000 readings were taken of which only 12 were outside tolerance and the maximum value was 0.009 in. A pair of thickness checks, one each side of a step, were made wherever a step check was performed. This permitted a direct check on the accuracy of the readings because one thickness plus step should equal second thickness plus second step. Four readings were involved and, if a discrepancy of more than 0.002 in occurred, the four readings were re-taken and checked.

(ii) Outer vessel front clamp bolt holes

To carry the atmospheric load on the outer vessel the magnet pole pieces are

clamped back to the magnet by jacks, at the back of the throat, and by bolts, which run from the polepieces through the vacuum vessel out to the magnet coil bracket, at the front. There are two bolts at the top and at the bottom for each magnet sector. 168 bolt holes per vessel were drilled on the loft plate. The distance between extreme holes was 50 ft, the tolerance on each hole was 0.030 in and only two holes out of 1344 needed to be opened out on assembly, and these by only 0.010 in.

(iii) Chordal height on all vessels

The chordal height of the 54 ft arc length of the main vacuum flanges was approximately 5 ft 6 in. These chordal heights were used for checking the effective radius. The tolerances specified were + 0.125 in, - 0.0625 in for the outer vessel; + 0.187 in, - 0.060 in for the inner vessel and \pm 0.030 in for the header vessel.

The outer vessel was subject to thermal stresses on final cooling of the back wall. The effect of this was difficult to predict with accuracy and the re-setting of tools to correct it would have been very expensive and time consuming. The tolerances were relaxed when it was found that the outer vessel could be strained by 0.25 in without danger and four of the ten vessels required this concession.

All inner vessels as measured on the loft plate were within tolerance.

It was found to be impractical to produce header vessel flanges by moulding methods to the extremely tight tolerances specified. Templates were bolted to the header vessel on the loft plate and located by reference to the dowel holes. The flange faces were then cut back to the template face, using a hand router. In this way the specification was met. Inner and header vessels proved to be individually interchangeable in every case examined.

8.4.9. Dimension Analysis

A further duty performed by the inspection staff, was the analysis of dimension trends in order to correct tools before tolerances were exceeded.

An example of this occurred during the manufacture of the prototype outer vessel. The steps on the flat panels caused by adjacent tools were found to be steadily increasing. A graph was drawn of all the steps on the tools, after each successive heat cycle, for three different positions across the tools. It showed that certain tools were climbing above their neighbours at an average rate of 0.002 in/cycle and that the middle of the tool was climbing more rapidly than the ends. The tools were re-layed with certain modifications to the assembly with the result stated in 8.4.8(i)

8.4.10. Repairs and Records

Scientific and engineering staff from the Rutherford Laboratory, together with the manufacturer's technical staff, developed a series of repair techniques which varied according to the repair position on the vessel and the thickness of the laminate. Before any repair was carried out a diagram of the proposed repair was presented to the U.K.A.E.A. inspection team for agreement.

The inspection team prepared a log book for each vessel delivered. They contain a full set of all the dimensional records taken during the manufacture of the vessel, a review of faults in the laminate and a full statement of the nature and location of all repairs.

8.5. Handling, Test Equipment and Installation

8.5.1. Transporting the Vessels

A special low level transporter was constructed to carry the vessels from the manufacturer's to the Rutherford Laboratory, a journey of 100 miles. To avoid wide load conditions the vessel was arranged to travel turned through 90° with the centre of the curved shape low in the centre of the transporter and the ends of vessel projecting vertically front and back of the transporter (Fig. 8.5.1(i)). The dimensions of the vehicle when loaded were 83 ft long, including traction unit, and 12 ft high. This meant special routing and police escort in 'built-up' areas. Even though some journeys were made in severe winter conditions all the vessels were delivered without mishap.

The vessel was supported during handling operations by a frame made as a welded structure from rolled mild steel sections, formed to follow the curvature of the vessel with cross bracing to produce a platform for the vessel to rest on. Felt pads were fitted to all frame members which would otherwise contact vessel surface. Collapsible wooden stiffening frames, tailored to the cross section of the vessel and upholstered to prevent damage, were inserted at approximately 2 ft intervals along the length of the vessel, with wooden spacers to hold the whole structure rigid. Cover plates were fitted to the open front face and end flanges.

Brackets were fitted to the front and back surfaces of the metal support frame. The front brackets aligned with bolts projecting from the centre of the front stiffening frame member so that when the vessel and support frame were turned through 90° the weight was suspended from the back wall of the vessel and supported by the frame. The brackets also acted as anchor points for a canvas strap which passed over the vessel, clamping it tight to the metal frame. The support frame had detachable structures which fitted to the outside curvature to act as feet when the whole assembly was turned through 90° so that the vessel and the frame could be arranged as a free standing assembly. All vacuum surfaces were protected by packing and the vessel was further protected by a clack valve to allow for barometric changes during the journey and a silica gel container to restrict water absorption by the vessel material. The whole assembly was then wrapped with PVC sheeting.

8.5.2. Test Equipment

On arrival at the Rutherford Laboratory the vessels were unloaded in the test bay. Four rigs were constructed, two for outer vessels (Fig. 8.5.2(i)) and two which could take either inner vessels separately or inner vessels combined with header vessels. The test area was a 'clean' area and special clothing was worn by all personnel. Cotton gloves, hats and overshoes were used when entering the vessels at any time.

The first vessels to arrive were outer vessels. All surfaces were inspected to identify areas in need of actual or possible repair. An oblique light was used to show up flaws and scores on vacuum joint surfaces. The transport frame formed part of the test rig and the vessel and frame were lifted on to the rig support members. When on its rig the vessel was 6 ft above floor level to enable the underside to be carefully probed with leak hunting gas and repairs to be carried out easily.

All transport equipment was removed with the exception of the internal stiffening frames which were later removed systematically, beginning from centre of vessel, and replaced by sets of aluminium frames to support the vessel walls against atmospheric

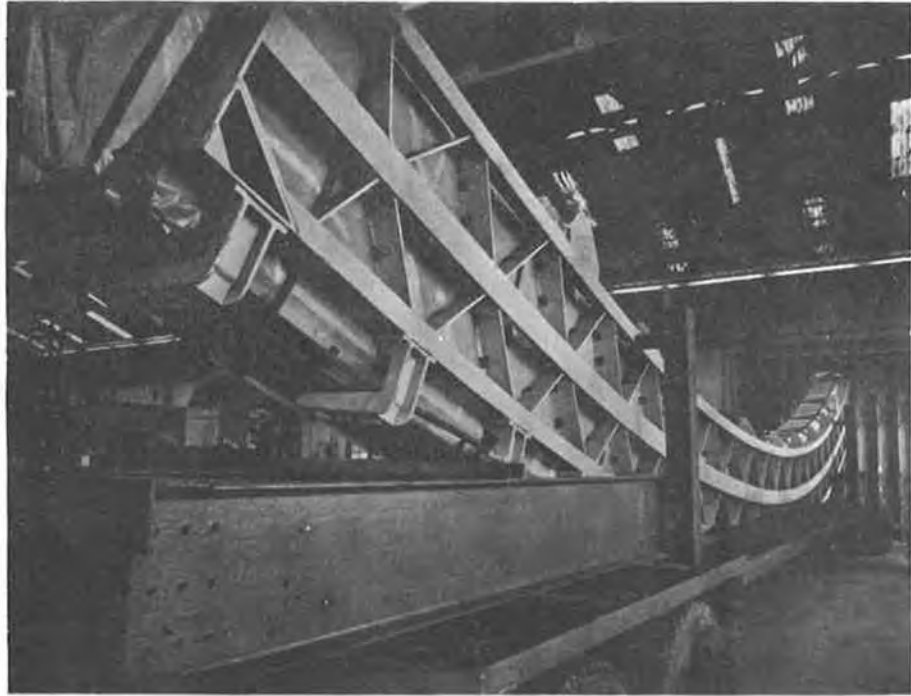


Fig. 8.5.1(i) View of a transporter carrying a vessel.

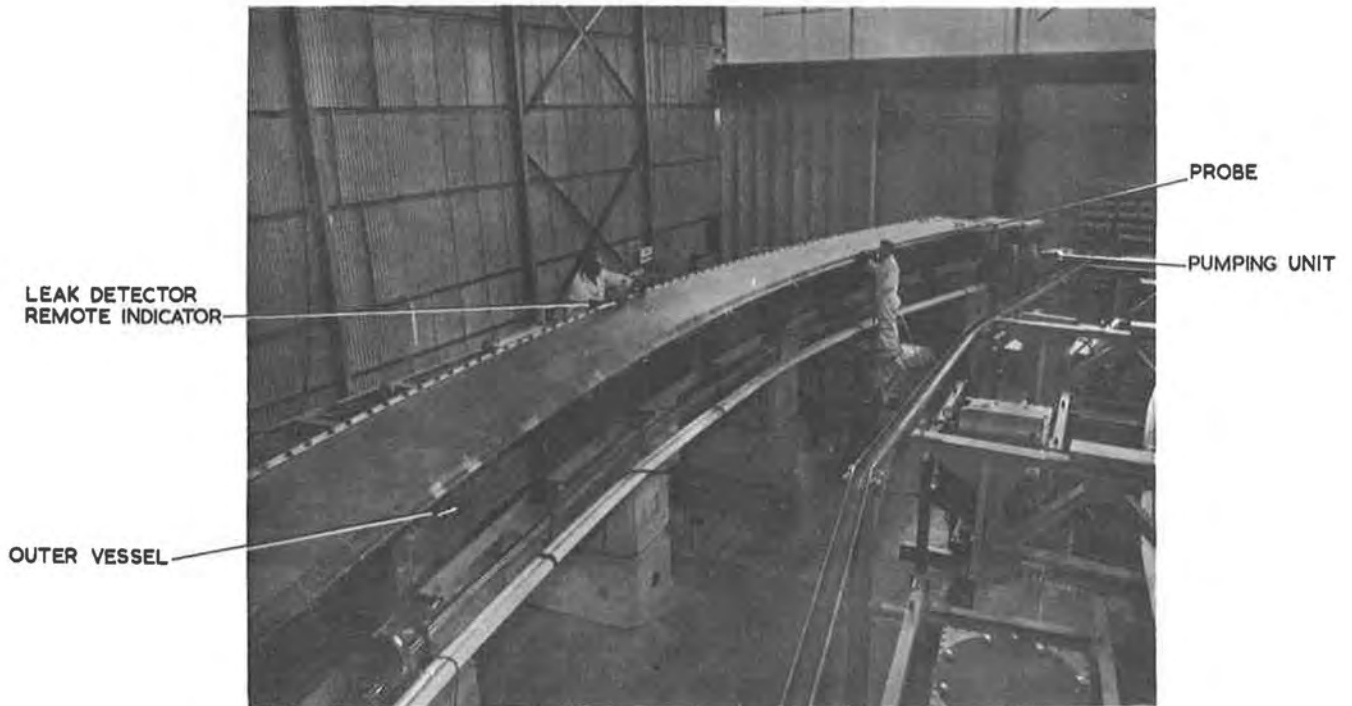


Fig. 8.5.2(i) Vessel test rig.

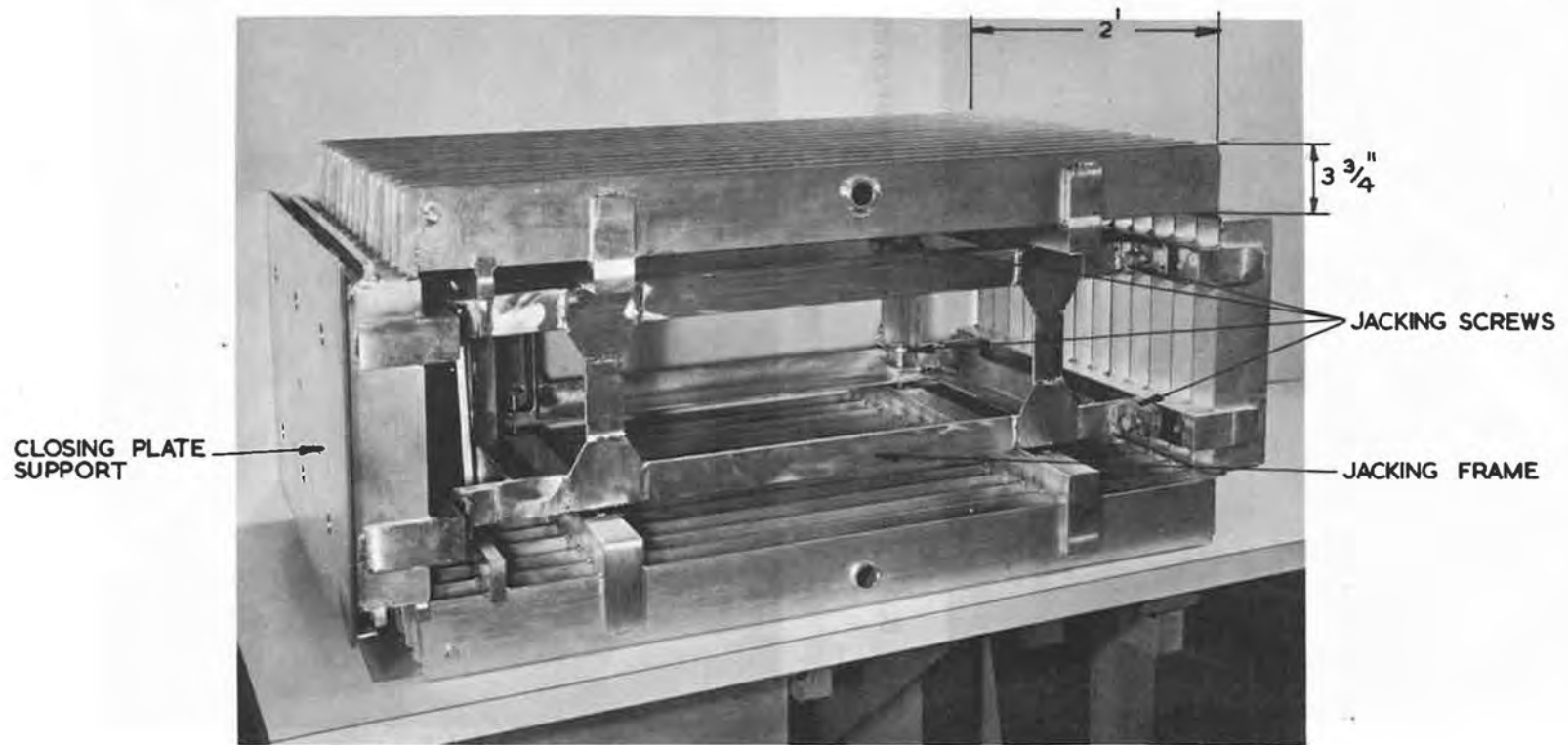


Fig. 8.5.2(ii) Outer vessel stiffening frame.

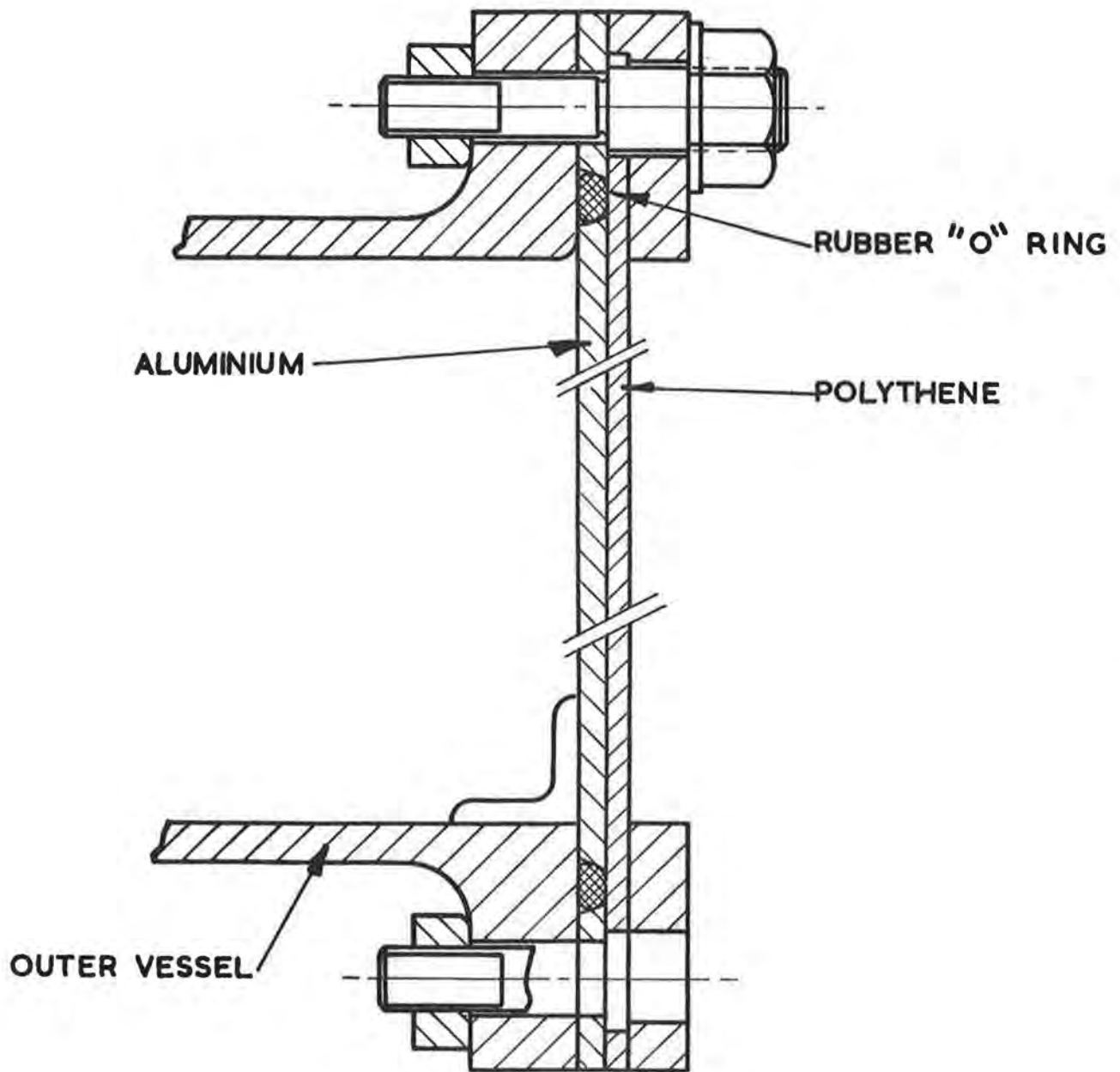


Fig. 8.5.2(iii) Typical Section through Test Seal on Front Flange.

pressure under 'pumped down' conditions.

The thickness of the vessel material, $\frac{1}{8}$ in, required a maximum unsupported span of $2\frac{1}{8}$ in if the design stress figures were not to be exceeded. During testing, support such as the machine components would have afforded would have been costly and undesirable, since most of the vessel surfaces would have been inaccessible making leak hunting impossible.

The aluminium frames (Fig. 8.5.2(ii)) were in sets, each set covering about 2 ft length of vessel and consisting of four members, supporting top, bottom and back walls of vessel with the fourth member bridging the gap between top and bottom flanges of the front open face of the vessel to support the closing plate. A jacking frame was used to jack the frames out to the profile of the vessel cross section. Each individual frame was constructed in a grille pattern with each grille member $\frac{3}{16}$ in wide by $3\frac{3}{4}$ in deep. The $\frac{3}{16}$ in face was in contact with the vessel surface and masked only a small section of the surface area without creating high bearing pressures which might damage the material. The span between adjacent frame members was kept to $2\frac{1}{8}$ in maximum. Care was taken when jacking out individual frame sets to use setting gauges across flange fixing holes to prevent irregular jacking which could cause steps along the vessel surfaces and create high stress points at the edges of frame sets, when atmospheric pressure was applied.

All frame sets were common except for the last two sets at each end of the vessel. The intermediate end frame was different to allow for projections on the inside of the vessel surfaces (end pole tip triple vacuum seal blocks) and the end frames were shorter as the vessel wall thickness was built up to 1 in on the inside surface. This section of the vessel projected beyond the magnet yoke and had to be capable of withstanding atmospheric pressure almost without support. It was, however, necessary to keep the outside top and bottom surfaces of the vessel flush, as the whole length of vessel, excluding about 3 in at each end, passed through the magnet throat in the method of assembly used.

Before any test equipment was inserted into the vessel, all inside surfaces were inspected and cleaned using dry lint - free cloths. All vacuum seal surfaces around the 330 bolt holes through the vessel wall, were checked and cleaned before plugs carrying seal rings were fitted. Each item of test equipment had previously been cleaned, degreased and packed in polythene bags until it was used.

The front open face of the vessel was closed by $\frac{1}{8}$ in thick aluminium plates, one per frame set, butting together along the vessel length and finally sealed over with $\frac{1}{8}$ in polythene closing plate continuous over the 54 ft length of the vessel. The closing plate sealed on to an uncemented, butt-jointed cord ring, held in a 'dovetail' groove formed by metal strips bolted to the vessel flanges (Fig. 8.5.2(iii)). The vessels were pumped by roughing pump unit and two 24 in diffusion pumps, one connected to each end flange.

At some stages of the construction programme it was necessary to store vessels before installation. In order to release the vessel support frame a special type of vessel lift was evolved to remove a vessel from its associated frame. Wooden internal stiffeners, spacers and outside cover plates were fitted and flat metal bars were inserted between the vessel and the frame in the space provided by the felt pads on the frame members. Bars were arranged to project over the back and front of the vessel. A second vessel support frame was lowered over the vessel and suspended just clear of the top surface. Bolts with spacer tubes were fitted between special brackets on back and front surfaces of top frame and metal bars under vessel

(Figs. 8.5.2(iv) and (v)). By hoisting the top frame, the vessel was removed from the bottom frame and held suspended and could be set down at any suitable position. This was called 'suspended lift'.

For manoeuvring vessels under the shield bridge or other areas not provided with crane coverage, four trollies mounted on castors were arranged in coupled pairs towards the front and back of the vessel. The span between the trollies could be varied to allow the vessel to sit on its frame on the trollies, as in the case of an outer vessel, or to allow the vessel to be suspended under a frame, as in case of inner and header vessels.

The equipment for testing inner vessels closely followed that used for the outer vessels. The height of the vessel, however, was much less than the outer and only two frame members were used per set, jacked apart to the top and bottom surfaces. The frames were of a different design and profiled to the 'crowned' shape of the vessel. After jacking out to the vessel shape, a further pad was jacked off a frame member on to the back wall of the vessel, the reaction being taken through the frame which was held by its fit into the crowned shape. These support frame members were made of mild steel coated in nylon for cleanliness and to protect the stainless steel foil lining of the vessel. During early vacuum test runs, the nylon caused considerable contamination due to out-gassing and it was removed and the frames electro-polished. To prevent damage to the vessel, the edges of the frames were covered with split polythene tube.

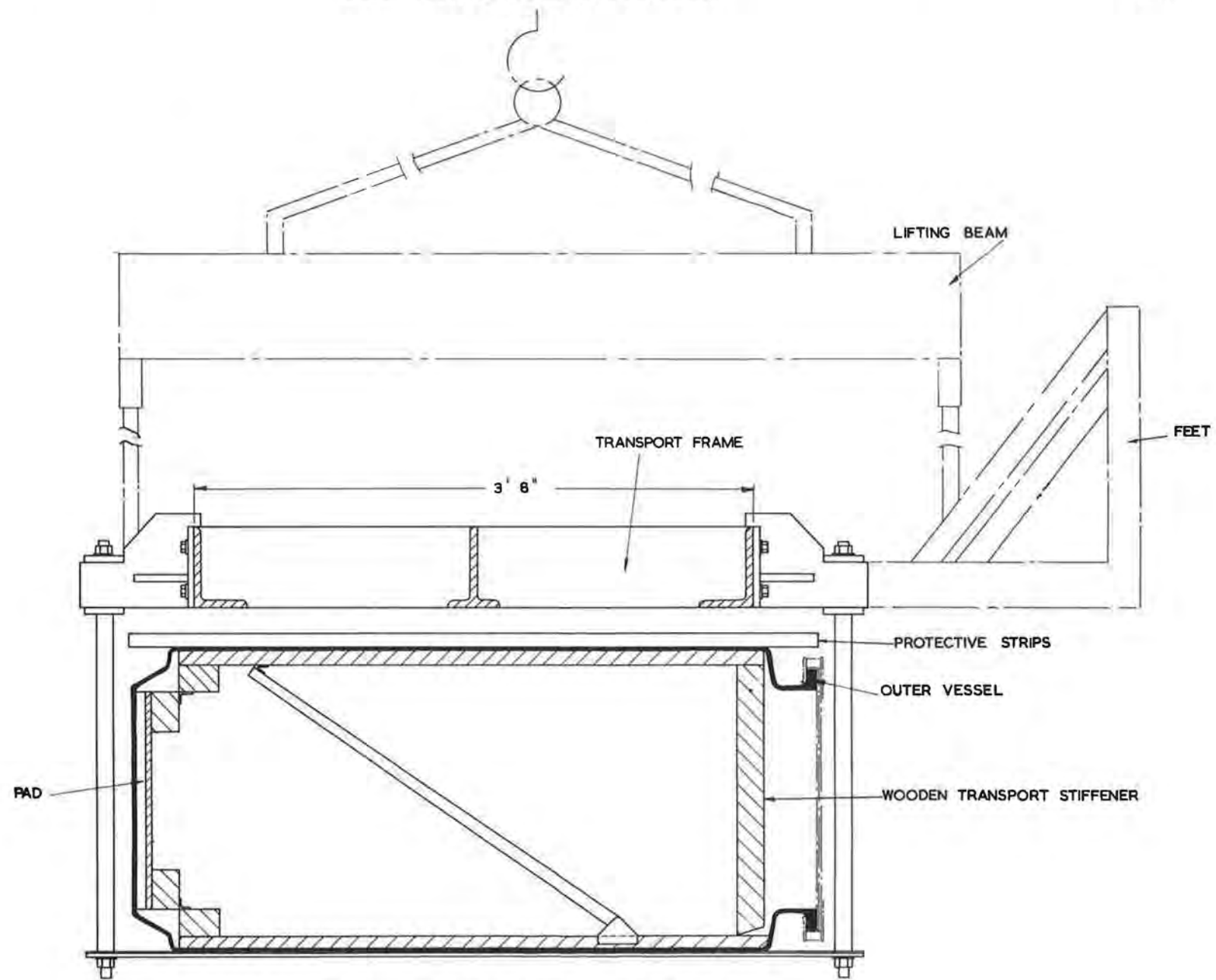
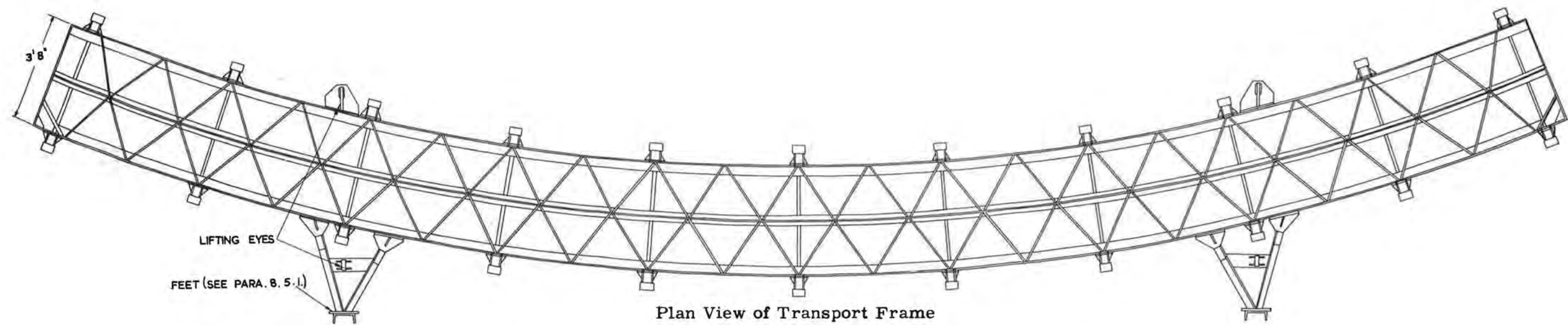
The header vessel, which was constructed to withstand atmospheric pressure between external attachment points, did not require the continuous frame support. Instead an internal jack was fitted to coincide with the position of external ties. No arrangement was made to test a header vessel separately and they were matched to a previously tested inner vessel.

During the test programme, some trouble was experienced on all vessels with leak paths around tapped metal insert positions and around metal ferrules lining holes in the flange. It was necessary in a number of cases to remove these to bond in new ones and it was desirable to do this while the vessel was pumped so that the resin would be drawn into the voids in the material. The test equipment proved very versatile during such operations, although some of these requirements were not consciously 'designed in'. Inserts on the front face of the header vessels were fixed parallel to the lay of the cloths and leaking inserts became so troublesome on the first and second header vessels that it was decided to remove all inserts on the front face and remake the surface as a vacuum seal surface only. Cover plate attachments were then arranged to fix to the top and bottom outside surfaces where inserts could be housed in the vessel material normal to the lay of the cloth.

8.5.3. Vessel Installation

Before the outer vessels were installed all magnet sector throat dimensions were taken and where steps between adjacent sectors exceeded 0.012 in cloth and resin shims were fixed to the throat surfaces. This ensured that sudden steps in the vessel walls were not created when the vessel was clamped between the magnet yoke and the pole tips. In the later stages of outer vessel manufacture, steps in adjacent vessel wall panels were found to exceed 0.012 in due to tooling faults and some shimming of the outside surface of the vessel was necessary.

To install an outer vessel, the frame with the vessel on it was placed on fabricated trestles which spanned the mechanical services trench in front of the



Typical Section of Suspended Lift.

Fig. 8.5.2(iv) Top Lifting Arrangement for Outer Vacuum Vessel.

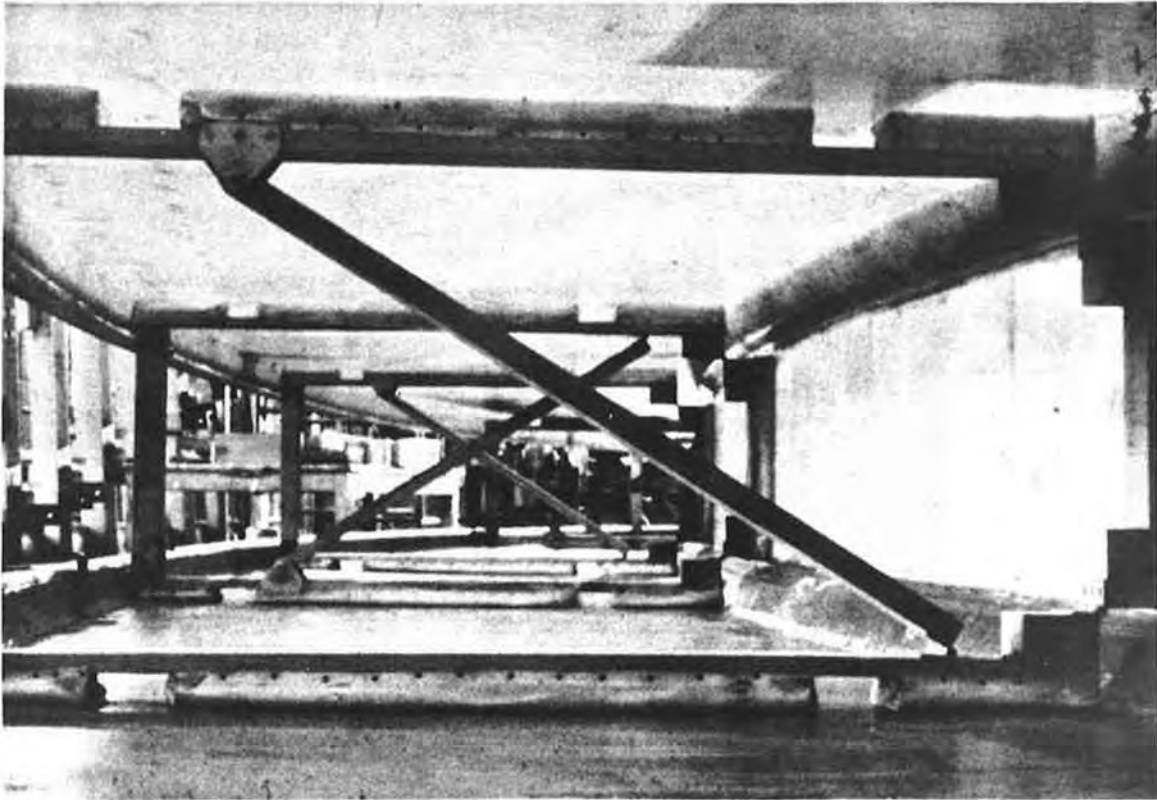


Fig. 8.5.2(v) View inside an outer vessel. (The wooden jigs are for packing purposes only).

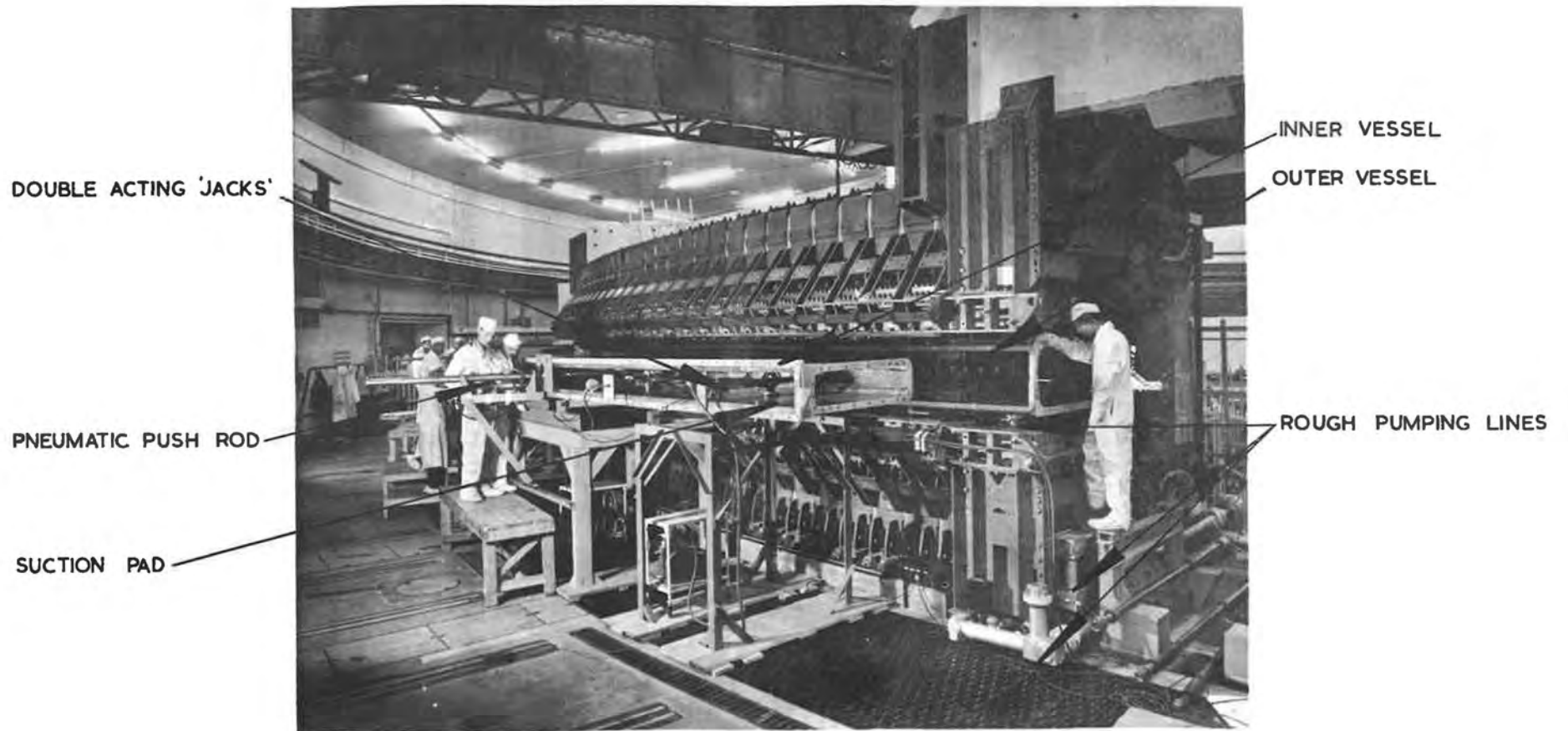


Fig. 8.5.3(i) Inner vessel assembly rig.

appropriate octant. The vessel was lifted clear of the felt pads on the frame by the insertion of 'drifts'. Initially the drifts had a PTFE top surface to allow the vessel to travel over them smoothly, but this was later removed in favour of a polished surface due to the PTFE tape 'picking up'. The vessel was adjusted to the correct height for feeding into the throat by means of jacking screws on the trestles and was pushed in, supported on the drifts, until it had entered 2/3rds of the way into the throat. The clearance between the height of the back wall of the vessel and the height of the magnet throat was increased by clamping the front flanges of the vessel closer together than their designed position. This 'bowed' the back wall slightly. It was not possible to do this near the ends of the vessel because of the stiffening effect of the end flanges and the end pole tip blocks, and careful dimensional checks and visual inspection for 'resin flash' were carried out before insertion.

The first outer vessels were pushed into the throat by man power; two men, at each of seven points equally spaced around the vessel, applied a load to a push rod which moved the vessel in, a stage each time, to a preset locking pin. The push rod was in contact with the back wall of the vessel and the load was spread on the material by means of a large pad. Although this method was successful it was later abandoned in favour of two pneumatically operated push rods which became available after the inner vessel assembly rig was designed. This gave much finer control of the process. After the vessel had been inserted to the correct depth into throat it was aligned circumferentially by equipment designed to pull the vessel sideways by attachments to the end flanges. The final position of the vessel was set as the best nominal alignment of the vertical pole piece bolt holes, gauged from the datum faces on the principle sectors (see section 4.5.2). When errors in curvature of the vessel were discovered, pairs of pole tips were assembled into the throat to clamp the vessel at the centre or the ends (depending on the direction of the error) and slight pressure was applied to the back wall of the vessel to move it on to the correct line of curvature. Further clamping pole tips were then assembled.

To install the inner vessels the same trestles were used with additional intermediate ones. No frame was involved except that used to bring the inner vessel into the magnet room in the 'suspended lift' condition. The vessel was then set down on slide rails assembled across the tops of the trestles (Fig. 8.5.3(i)). The crowned top and bottom surfaces of the vessel were designed to give a vessel height in excess of the gap between the pole tips in the throat. This was of such an order that the interference fit of these two items would give the vessel walls a thrust on to the pole tip faces, sufficient to resist the deflection of the vessel under its own weight and under the pressure due to the vacuum in the outer vessel. The crowning had, therefore, to be reduced in order to install the vessel in the throat.

When the vessel was placed on the trestles, the cover plates were removed and metal straps with a dimension slightly less than the designed span were bolted across the front flanges around the centre section. This reduced the height of the vessel over about 70% of its length. The ends, however, which are stiffened by the end flanges, remained almost at their 'free state' dimension. Three pneumatically operated, double acting jacks were inserted into the vessel at each end on the section of peak crowning. The jacks were spaced about 2 ft apart beginning 2 ft from the end flange; the end jack was larger than the other two. Rubber sucker caps, connected to a small roughing vacuum pump, were fitted at the top and bottom of each jack. The jacks were expanded pneumatically to a mechanical stop which gave sufficient pressure on to the inside surface of the vessel to effect a vacuum seal and the volume within the suckers was evacuated. The jacks were then retracted pneumatically to a mechanical stop, so pulling in the top and bottom surfaces of the vessel.

Two push rods, pneumatically operated, one positioned about 15 ft each side of the centre line of the vessel were arranged to push on the plate bolted across the front flanges of the vessel. The cylinders of both push rods were connected to a common control valve and the push rods travelled in stages to mechanical stops. This arrangement kept the push rods in phase by allowing for any lag occurring between the cylinder movements. The control valve was interlocked with the sucker caps to ensure that there was no movement into the magnet throat if the vacuum was lost on any sucker.

After insertion, the inner vessel was aligned to give the best nominal position of the front flange relative to the outer vessel front flange and an equal gap between the inner and outer flanges at the top, bottom and ends. When this had been achieved, the vacuum was released from all suckers and the vessel was allowed to expand to the pole tip faces.

The header vessel was transported to the appropriate octant by the 'suspended lift' method and was lowered on to small trollies mounted on support frames spanning the mechanical services trench. These were of a different construction to the frames used on outer and inner vessels because of the greater weight involved. There were seven trollies, two of which, placed at approximately 15 ft from the centre of the vessel, were attached to long lead screws. The vessel was gradually fed into the machine on the trollies, by means of the lead screws, until the inner and header flanges met. Flange bolts were then fitted and tightened by a torque wrench, commencing from the centre of the vessel and progressing out to the ends to gradually blend the flanges in together. Top and bottom support brackets and tie rods were fitted after careful shimming, to ensure the vessel was held in this position so that the weight of the vessel was kept off the matched flanges when the supports were removed.

8.6. Vacuum Testing

8.6.1. Introduction

10% of the total pumping speed of the high vacuum pumps was allowed to cover leakage into the system (Section 8.10.1). Based on the design specifications for the pumps, 5 pumps per octant would permit a leakage of 1.25×10^{-3} torr litres/s for each octant.

Most components in the vacuum system, other than the vacuum vessels, were likely to be of metal and individual leak rates for these items could be small. In fact for all such components, except straight section boxes, a tolerance of 10^{-7} torr litres/s was specified. The leak rate was to be established using palladium barrier gauge or mass spectrometer leak detectors in dynamic systems. In this way more than a thousand such components could be connected to each octant before any significant change in the total octant leak rate would occur. It was therefore reasonable to allow all of the permissible leak rate for the combination of inner and header vessel alone. In practice each inner vessel was individually tested and allowed 6×10^{-4} torr litres/s leakage and header vessels were tested with a previously proved inner vessel. Outer vessels had to meet a less stringent test but, since they were the first to be delivered, the opportunity was taken to try to achieve the lowest possible leak rates. Experience proved that leak rates of 5×10^{-3} torr litres/s could readily be attained.

Vessel leak rates were measured by pressure rise methods but were not continued long enough to eliminate the component due to outgassing. It was not practical to hood an entire vessel so that leak rates could be measured on the mass spectrometer by comparison with a reference leak.

Cleanliness was considered to be of prime importance in view of the tight leak rate tolerances. Since palladium barrier methods could be used for many of the tests, the use of solvents containing halogens was banned. If the use of such a solvent became necessary because of heavy contamination with oil or grease, a final rinse was always given using an approved solvent such as acetone or iso-propyl alcohol. In the case of the resin/glass laminates methylated spirits was the only approved cleaning solvent.

From the beginning of the testing programme, a final proof test took place at the Rutherford Laboratory before the component was installed, no matter what component testing had been carried out previously at the manufacturer's works. This protected against damage in transit and deterioration in storage. Strict control was maintained over tested items so that the test was not invalidated by subsequent modifications, etc.

Leak test facilities were required to be adaptable for large and small components. On large components particularly, the method of connecting the leak detector to the item for test could greatly affect the final sensitivity. For a system of volume V_1 , leak rate L , pressure p_1 and pumping speed S_1 using a particular test gas,

$$V_1 dp_1 = S_1 p_1 dt$$

Whence
$$p_1 = \frac{L}{S_1} \left[1 - \exp(-S_1 t/V_1) \right]$$

In the backing space of volume V_2 of this system, with the test gas partial pressure p_2 and pumping speed S_2 ,

$$V_2 dp_2 = S_1 p_1 dt - S_2 p_2 dt$$

Whence
$$p_2 = \frac{L}{S_2} \left[1 - \frac{1}{S_1/V_1 - S_2/V_2} \left\{ \frac{S_1}{V_1} \exp(-S_2 t/V_2) - \frac{S_2}{V_2} \exp(-S_1 t/V_1) \right\} \right]$$

Fig. 8.6.1(i) shows two curves plotted for a typical system and indicates the marked advantage of placing the leak detector in the backing space of the pumping system. All the pumping units were therefore provided with facilities for connecting a leak detector in the backing space and also with a throttle valve on the backing pump so that maximum advantage could be gained from the method.

For smaller components, static leak detection equipment consisted of a 9 in oil diffusion pump backed by a 2 in oil diffusion pump and rotary pump with a Palladium Barrier detector fitted in the interspace between the two diffusion pumps. Other versions of this equipment, but without the 9 in diffusion pump, were available for use with the 24 in pumping units on the synchrotron for vessel and octant testing. Mass spectrometer leak detectors could be used with any of the units.

8.6.2. Vacuum Vessels

(i) Outer vessel proof tests

A prototype vessel was the first to be tested. The vessel was known to be unfit for use in the machine because it was outside tolerance on several dimensions. It was also known to have many areas of laminate of inferior quality but it was considered very worthwhile to carry out the full test procedure in order to establish techniques and to attempt to specify the quality of laminate necessary to achieve the required leak rate.

This prototype vessel was estimated to have a leak rate in excess of 30 torr litres/s when it was first tested. Several large leaks existed and were fairly easily detected. There followed a long and tedious process of finding a large number of leaks, each of which was small in comparison with total throughput and often had a long time constant. Also, only the roughing pump was in use at this stage and the leaks were only just detectable, even with a mass spectrometer leak detector, due to the limitation of the sampling.

It was found, during vessel testing, that leaks in excess of 10^{-1} torr litres/s were readily detected on a Pirani gauge using hydrogen as the probe gas. Areas of the vessel were covered with anti-static rubber sheet (Fig. 8.6.2(i)), taped in position and the space between vessel and sheet filled with hydrogen. The sheet size was then reduced until the leaking area was localised. Further checks were then carried out using a hyperdermic needle attached to the probe with substantially reduced hydrogen pressure in order to determine the leak boundary of the porous area. The leaking area was then temporarily sealed using "twin pack" Araldite. The vessel pressure was noted before and after this operation. The process was repeated in successive passes over the vessel surfaces, successively smaller leaks being detected as the larger leaks were sealed.

This procedure was tedious and time consuming on the prototype vessels

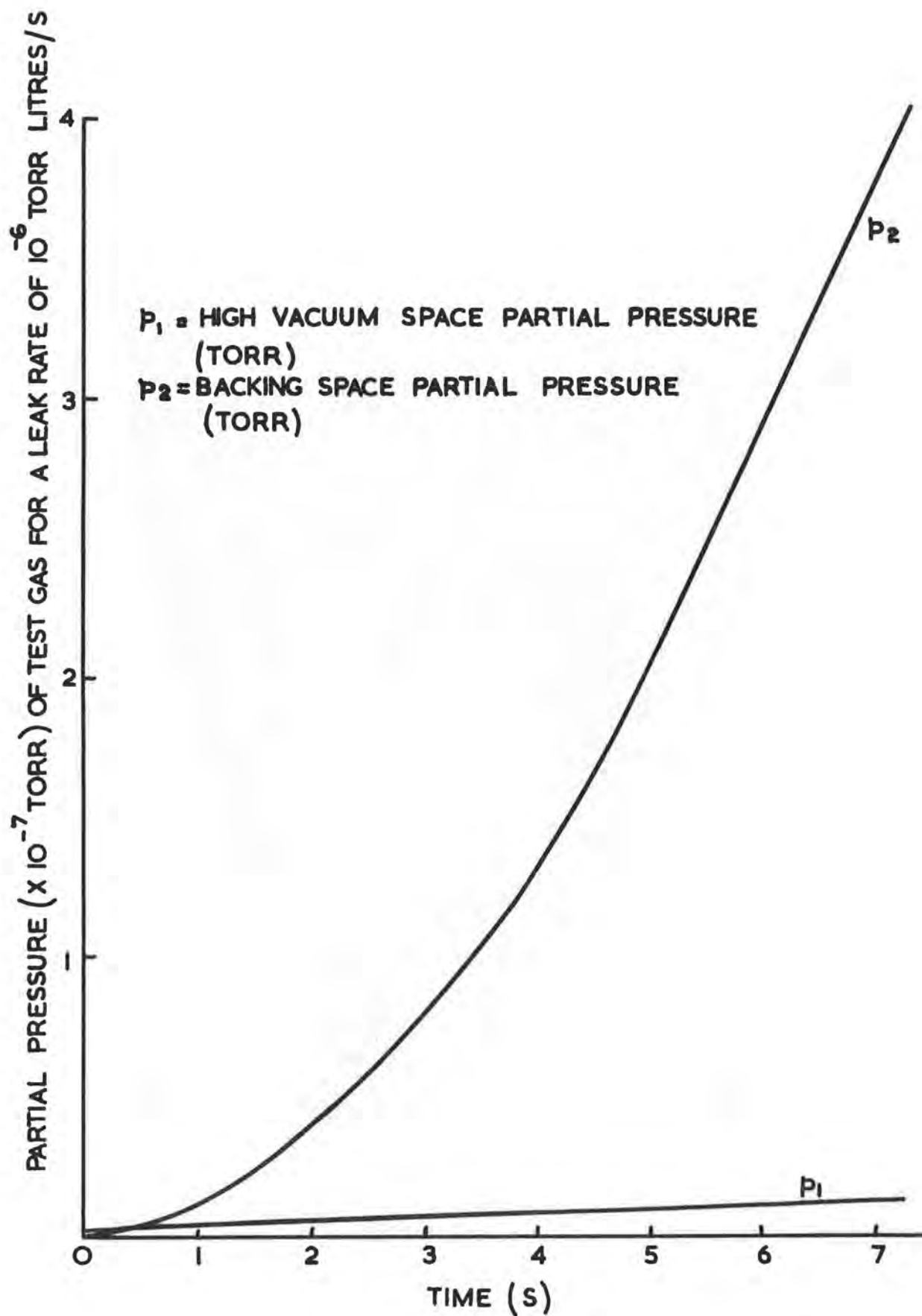


Fig. 8.6.1(i) Leak detection sensitivity

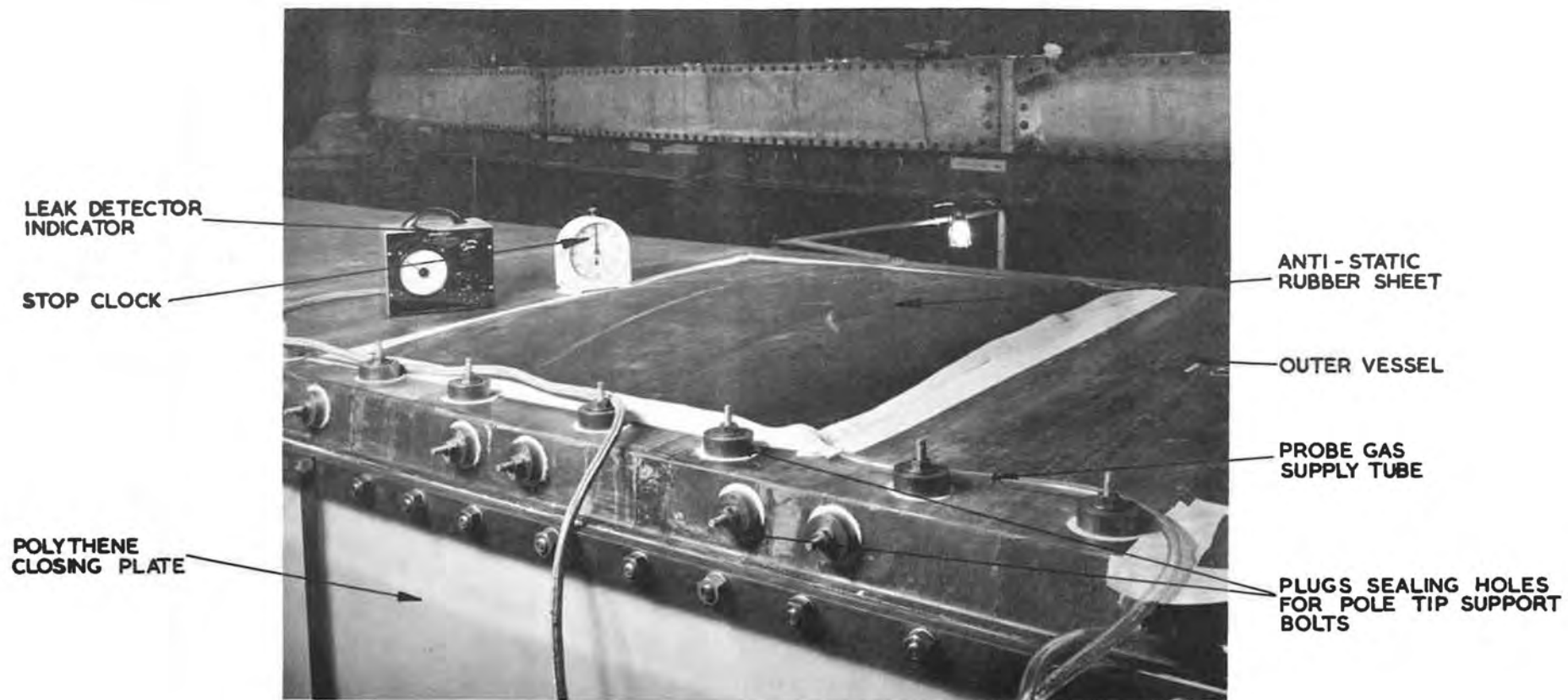


Fig. 8.6.2(i) An area of vessel shrouded for test.

(several months were spent on the outer vessel alone, including the repair time). Experience and a growing knowledge of the appearance of leaking areas, substantially reduced the time needed for testing until finally, vessels could be completed in two weeks.

When the pressure in the vessel was reduced to less than 10^{-4} torr, leak detection continued using a helium mass spectrometer connected to the backing line of one of the 24 in vacuum units. Sensitivity checks were made periodically by probing a calibrated reference leak attached to the vessel. Probing continued by shrouding areas as before and, as the vessel pressure was reduced by sealing leaks, it became more difficult to locate the remaining leaks. For leaks of 5×10^{-3} torr litres/s or less, the time constants were liable to increase as small porous areas with long leak paths were located. The test results are summarised in Table 8.6.2(I).

A major source of leakage was the large number of drilled holes in the vessel flanges. These had been coated with a thin film of resin in an attempt to seal the ends of any hollow glass fibres cut by the drill. Despite this treatment, many leaks were found and, even if the process of sealing was repeated, there was no guarantee of success. Subsequently it was discovered that damage could occur when the bolts were fitted. The resin coating was therefore replaced by thin walled brass ferrules bonded in position. This has eliminated this type of fault almost entirely.

Leakage was also troublesome in the region of whitened areas or white lines, usually where sections of the vessel had been spliced or where the laminate was starved of resin. A repair technique was evolved to overcome this problem (see section 8.7.).

A routine examination technique soon became established for the production vessels. The vessel was flexed to simulate the probable operating conditions in the machine by cycling the absolute pressures several times between 760 and 1 torr. The roughing pump then pumped the vessel down to 10^{-2} torr, at which pressure the roughing pump was isolated and the 24 in vacuum units were used to reduce the pressure further. Leaks in the range of pressures covered by the roughing pump were located by the Pirani/hydrogen technique and the mass spectrometer was used with the 24 in pumps as described above. The drill of locating and sealing leaks continued until the isolation pressure rise indicated a leak rate of less than 2×10^{-2} torr litres/s. The vessel was then isolated from the pumping system and the permanent repairs were carried out on the leaking areas with the vessel under vacuum. This allowed the resin mix used for the repair, to flow along the leak path and adequately seal the leak at depth. When the repairs were complete, the test sequence was repeated until all known leaks were permanently repaired. The vessel was considered acceptable if the indicated leak rate was less than 5×10^{-3} torr litres/s.

During the last phase of assembly on the test rig, the roughing pump and the two 24 in pumping units were checked for operational sequence and ultimate pressure.

TABLE 8.6.2(I)

Outer Vessel Proof Tests

Vessel Number	Number of Leaks	Final Leak Rate (10^{-3} torr litre/s)	Installed in Octant Number
1	3	4.1	5
2	5	1.8	4
3	10	2.6	1
4	10	1.6	8
5	7	2.2	2
6	6	2.8	3
7	3	1.9	6
8	14	2.0	7
9	5	3.8	Spare
10	2	1.1	Spare

(ii) Outer vessel installation test

During the installation of the outer vessels in the machine, the standards of cleanliness were maintained and all the vacuum faces and joint rings were inspected before assembly. On a number of occasions, damage occurred which necessitated a 'through' repair on the vessel as described in 8.7. These repairs were vacuum tested locally using a 'top hat' (Fig. 8.6.2(ii)) on the inside face of the vessel. The leak rate through the repair was ascertained by the isolation pressure rise method, with a tolerance of 10^{-5} torr litres /s/ft² surface area.

When the installation of the pole tips, pole face windings, roughing pumps and associated pipework was complete, the main polythene blank was again fitted and the system was pumped down using the permanent roughing pumps. Leak detection was carried out using the Pirani/hydrogen method until the leak rate of the system was less than $2 \cdot 10^{-1}$ torr litre/s. Before this leakage rate could be considered acceptable the pole face winding tubes were pressurised to 80 lb/in² before and during the measurement of the final pressure rise. If no additional leakage occurred the outer vessel was acceptable. Some 500 seals are introduced by the installation of the pole tips and pole face windings in each octant and these, together with the greatly increased surface area, account for the higher leak rates compared with the vessel proof tests.

(iii) Inner vessel proof tests

The inner vessels were treated in the same way as the outer vessels when they were received. It was found that the threaded inserts in the main and end vacuum flanges were susceptible to leakage at some stage of installation and after the first vessel was tested, it seemed advisable to pre-test these inserts before the overall proof test of the inner vessel began. Small 'top hats' (Fig. 8.6.2(iii)) were used with a threaded central projection which screwed into the insert. The circular ring in the base of the top hat was compressed against the vacuum face of the vessel flange and the top hat was evacuated using a small rotary pump. A leak rate of 1×10^{-5} torr litres/s. was acceptable. The biggest part of this indicated leakage was found, in practice, to be outgassing and it in no way influenced the ultimate leak

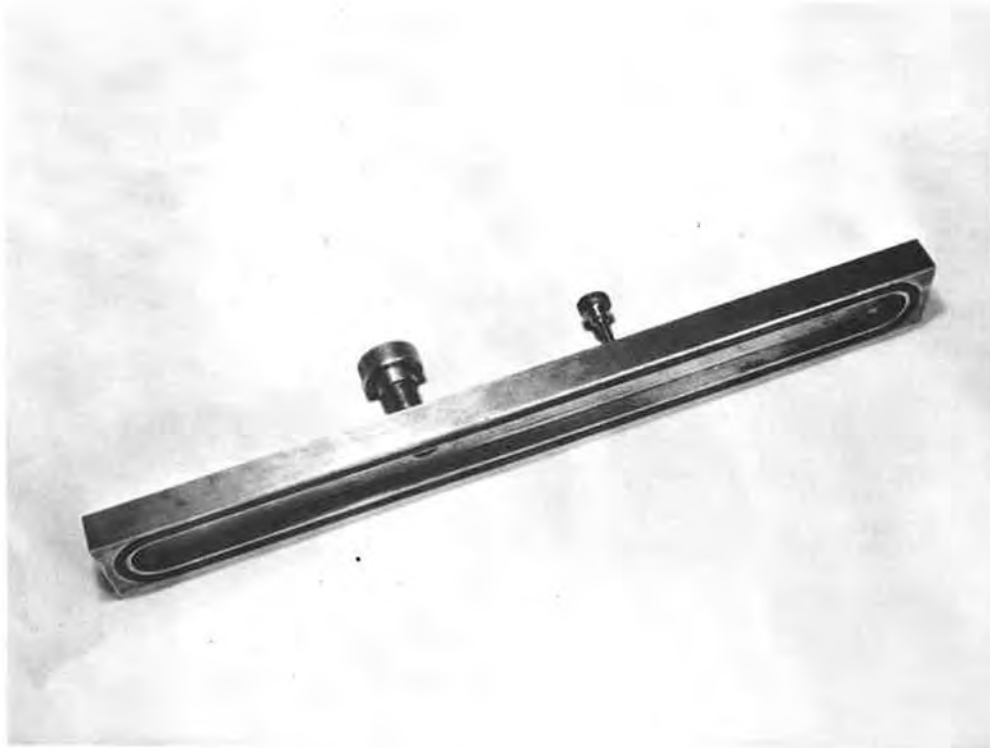


Fig. 8.6.2(ii) "Top hat" for local testing of a repaired area.



Fig. 8.6.2(iii) "Top hat" for vacuum testing inserts.

rate of the vessel. If an insert with an indicated leak rate in excess of 1×10^{-5} torr litres/s was found, an attempt was made to determine the leak path but if it could not be located it was assumed that excessive outgassing was occurring. This generally implied that the insert was badly located and steps were taken to remove and replace the insert.

On the first inner vessel tests it was found that the $\frac{1}{8}$ in thick polythene blank used to seal off the main flange was permeable to both air and helium causing an additional leakage into the system of 1.5×10^{-3} torr litres/s. This permeability caused difficulty for some time before it was finally traced. Probing around the vessel flanges gave reactions after some 20 min, reaching a peak after one hour, and considerable effort went into ensuring that the joint seals and the bolt holes were leak tight before eventually the polythene was suspected.

An aluminium blank of similar dimensions was substituted and enabled the vessels to be proof tested to a leak rate of less than 5×10^{-4} torr litres/s.

TABLE 8.6.2(II)
Inner Vessel Proof Tests

Vessel Number	Number of Leaks	Final Leak Rate (10^{-4} torr litre/s)	Installed in Octant Number
1	4	2.6	1
2	3	1.7	8
3	3	1.8	2
4	5	2.1	4
5	2	3.8	5
6	7	0.9	6
7	4	5.0	3
8	5	3.0	7
9	3	3.3	Spare
10	2	1.2	Spare

Header Vessel Tests

Only 4 header vessels have been provided and they are fitted to octants 3, 4, 5 and 6 to facilitate beam extraction. Great difficulty was experienced with the first vessels. Not only were there numerous leaks but they had long path lengths which made detection a tedious process. The leaks were eventually traced to tapped inserts bonded into the edge of the vessel on its larger radius. These inserts were provided for fixing the 'window' plates to the vessel and were positioned with their axes in the plane of the layers of glass cloth forming the laminate. By removing the inserts completely and making good the edge of the vessel by a wrap round repair after plugging the holes, more than 90% of the leaks were eliminated. This modification was incorporated in the third and fourth vessels by the manufacturers before delivery and on the first vessel (which was returned for rectification) but the second vessel was made acceptable by repair at the Rutherford Laboratory. Alternative means of fixing the window plates was provided by fixing aluminium clamp bars to the top and bottom of the vessels using inserts with their axes perpendicular to the plane of

the cloths. This method has now been satisfactorily proved.

TABLE 8.6.2(III)

Header Vessel Proof Tests

Vessel Number	Number of Leaks	Final Leak Rate * (10^{-3} torr litre/s)	Installed in Octant Number
1	96	30 (approx)	Returned for Rectification.
2	97	3.5 **	3
3	2	1.1	6
4	4	1.1	4
1	5	0.66	5

* Leak rate includes associated inner vessel leakage.

** Further repairs were carried out after installation in octant 3.

8.6.3. Straight Section Box Proof Tests

All straight section boxes were retested when they were received although they had been tested at the manufacturers. Of the seven boxes tested, all had leaks varying from 6 to 160 times tolerance. Vacuum testing was carried out using a 12 in pumping unit fitted to one vertical face of the box, with a separate roughing pump and connecting pipe. The prefabrication of the box conformed to normal vacuum practice with external welds intermittent, and internal welds continuous, but for magnetic reasons, each wall consisted of two mild steel plates separated by fibre glass insulation. With the box evacuated, leak detection was carried out by probing the gaps between the intermittent external welds. Having determined the leaking area approximately, the box was returned to atmospheric pressure. The inner weld leak was pinpointed by pumping the gap between the intermittent external weld and probing the inner continuous weld. All leak rates were indicated by isolation pressure rise and the acceptable leak rate was 1×10^{-4} torr litres/s.

TABLE 8.6.3(I)

Straight Section Box Proof Tests

Box Number	Number of Leaks	Final Leak Rate (10^{-5} torr litre/s)
1	2	15
2	2	42 *
3	2	6.2
4	4	5.1
5	8	13
6	1	8
7	1	6.7
8	-	18 **

* included some internal structures

** included epoxy resin insulators

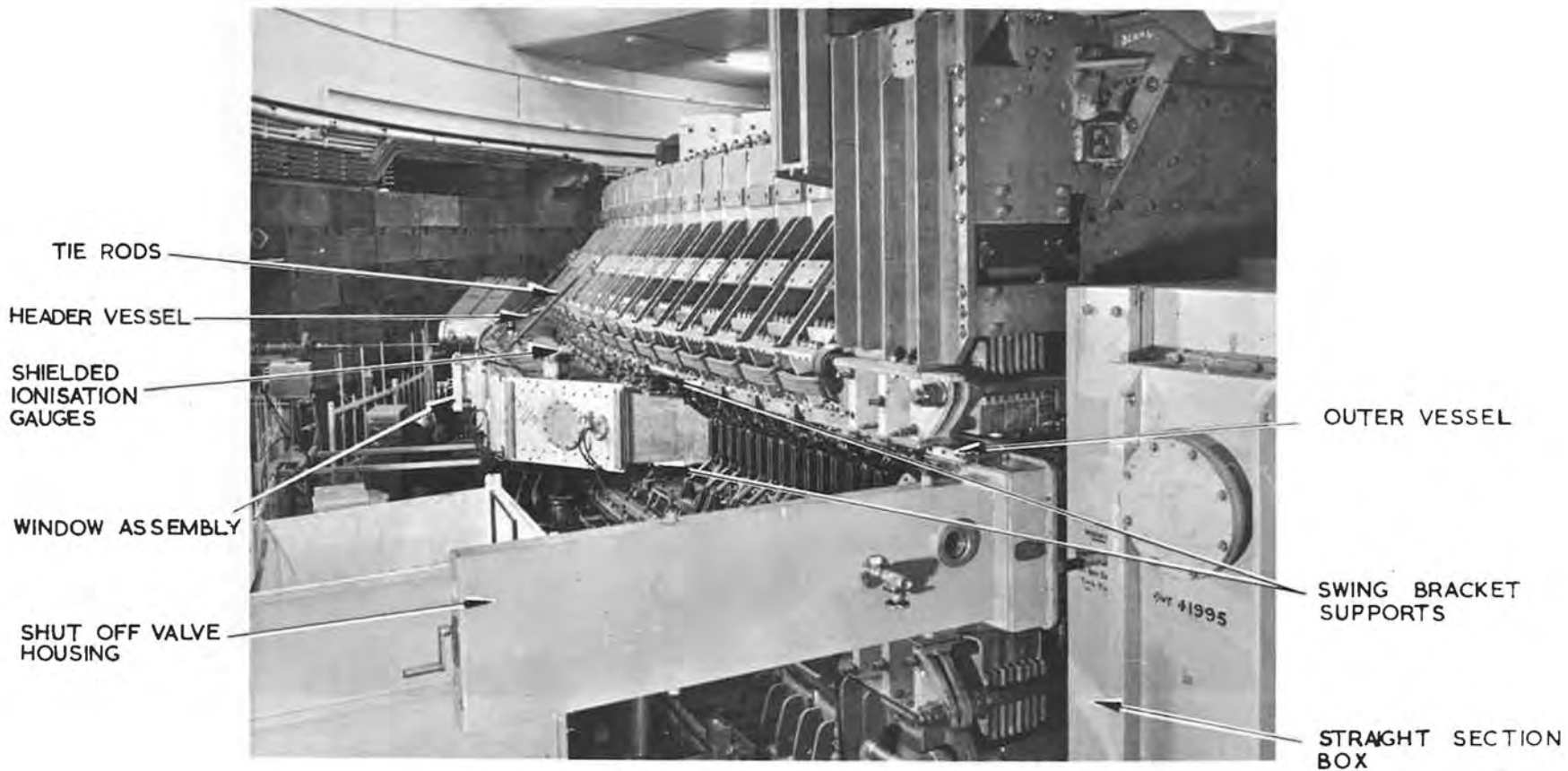


Fig. 8.6.4(i) An installed header vessel (octant 6).



Fig. 8.6.4(ii) An installed closure plate (octant 4).

8.6.4. Octant Testing

After proof testing, inner vessel was then moved adjacent to its final position in the machine. The inner and outer surfaces were cleaned and the vessel was immediately installed. After installation all vacuum faces were inspected and faults rectified before fitting the main vacuum seals. The closure plate or header vessel was then fitted in position, the main vacuum units and pump manifolds were permanently attached and, when ancillary items and roughing pipework was installed, the octant was handed over for vacuum test.

The octant was pumped down using the permanent pumping system and leak detection was carried out using a mass spectrometer connected to the backing line of one of the main units.

Inner vessels have been fitted to all octants, with four header vessels (Fig. 8.6.4(i)) and four polythene closing plates (Fig. 8.6.4(ii)). To date, one octant fitted with a closing plate has had a full vacuum test and a leak rate of about 10^{-3} torr litre/s was measured. The required machine operating pressure of 10^{-6} torr was achieved in 15 hours and after 60 hours the pressure was 4×10^{-7} torr (Fig. 8.6.4(iii)). Three other octants, which are not yet fully tested and have repairs still to be carried out, have indicated leak rates of less than 5×10^{-3} torr litres/s. A group of four octants recently coupled together by their associated straight section boxes was estimated to have a total leak rate of about 10^{-2} torr litre/s. The tests were carried out before diagnostic equipment was fitted to any of the octants.

The policy of pre-testing each component before installation paid handsome dividends. The vacuum system was so complicated, had so many seals and in some cases was so inaccessible after installation that tests would have been long drawn out, if in fact they were possible. This was particularly true of the outer and inner vessels the main surfaces of which are almost completely enclosed and the work entailed in removing an outer vessel for a major repair could have added three months to the Nimrod programme.

8.6.5. Leak Detectors

The programme of testing was frequently held up because of failure of the mass spectrometer leak detectors. Three types were in use, two of each type being available. Of these, one was never successfully used except in a permanent position where smaller components were brought for testing.

The second type could be moved around to a certain extent but this involved a loss of sensitivity by a factor of at least 10. These instruments were also subject to excessive background noise on their most sensitive ranges when connected to the larger systems, so that small leaks could not be detected.

The third type of mass spectrometer gave excellent service in comparison. It retained its sensitivity after being moved and was, therefore, the only instrument to be used for the final stages of vessel and octant testing.

8.7. Vessel Repairs

Techniques had to be developed to allow repairs to be carried out on the vacuum vessels either after initial fabrication to repair obvious mechanical defects, or during vacuum test, to cure leaks. The materials used for repair had to have the same properties as the vessel material (see section 8.1.) except in respect of manufacturing feasibility. Resin systems which complied with the requirements for gas evolution rate and mechanical properties had also to:

- (i) cure satisfactorily at a temperature below the heat distortion temperature of the parent material,
- (ii) have a minimum contraction on curing, to avoid introducing areas of high stress around the repair, and
- (iii) be compatible with the resin system of the parent material.

Other factors influencing the choice were the ease of 'wetting out' the fabric, the pot life at room temperature and the drainage which occurred when repairs were done on vertical surfaces.

Studies on available materials showed that a modified bisphenol A type resin system cured with a liquid aromatic hardener was the most satisfactory. This system required curing for 24 hours at room temperature (20°C) followed by 16 hours at 60°C (10°C below the heat distortion temperature of the parent material).

Suitable surfacing mediums for vacuum sealing faces were also investigated. At one time it was thought that the desired quality of finish could be obtained direct from the moulding tools. This proved impracticable for a number of reasons; for example, bad release, creases in release films, such as PTFE tape and damage caused in handling and transporting the vessels. The surfacing material must have similar properties to the parent laminate; in particular, it must cold cure and have a thermal coefficient of expansion close to that of the parent material, to prevent crazing of the sealing surface during operation.

Both solvent containing and solvent free formulations were considered. The most satisfactory was a solvent free proprietary material X83/44. It was whitened so that seal surfaces were readily identified. Later a formulation known as TSW 120 was developed at the Rutherford Laboratory, which contained silica flour and also bentone (which makes the material thixotropic). This formulation was very successful and its flow characteristics eased the problem of application considerably. In all cases vacuum sealing surfaces were dressed and polished to the required finish using 'wet and dry' Garnet paper.

Faults on the vacuum vessels may be classified into the following types:-

- (i) Crushed or insufficiently wetted fabric.

These areas were easily defined by a whitened appearance (Fig. 8.7(i)) and Fig. 8.7(ii)) and the complete removal of the faulty area was necessary. The faulty fabrics were removed singly using a sharp knife, or a wood chisel and a spatula. A half inch step was introduced every two layers of fabric (Fig. 8.7(iii)) and Fig. 8.7(iv)) to achieve the required mechanical strength in the finished repair.

When the desired profile had been achieved, fabric was pre-wetted with the

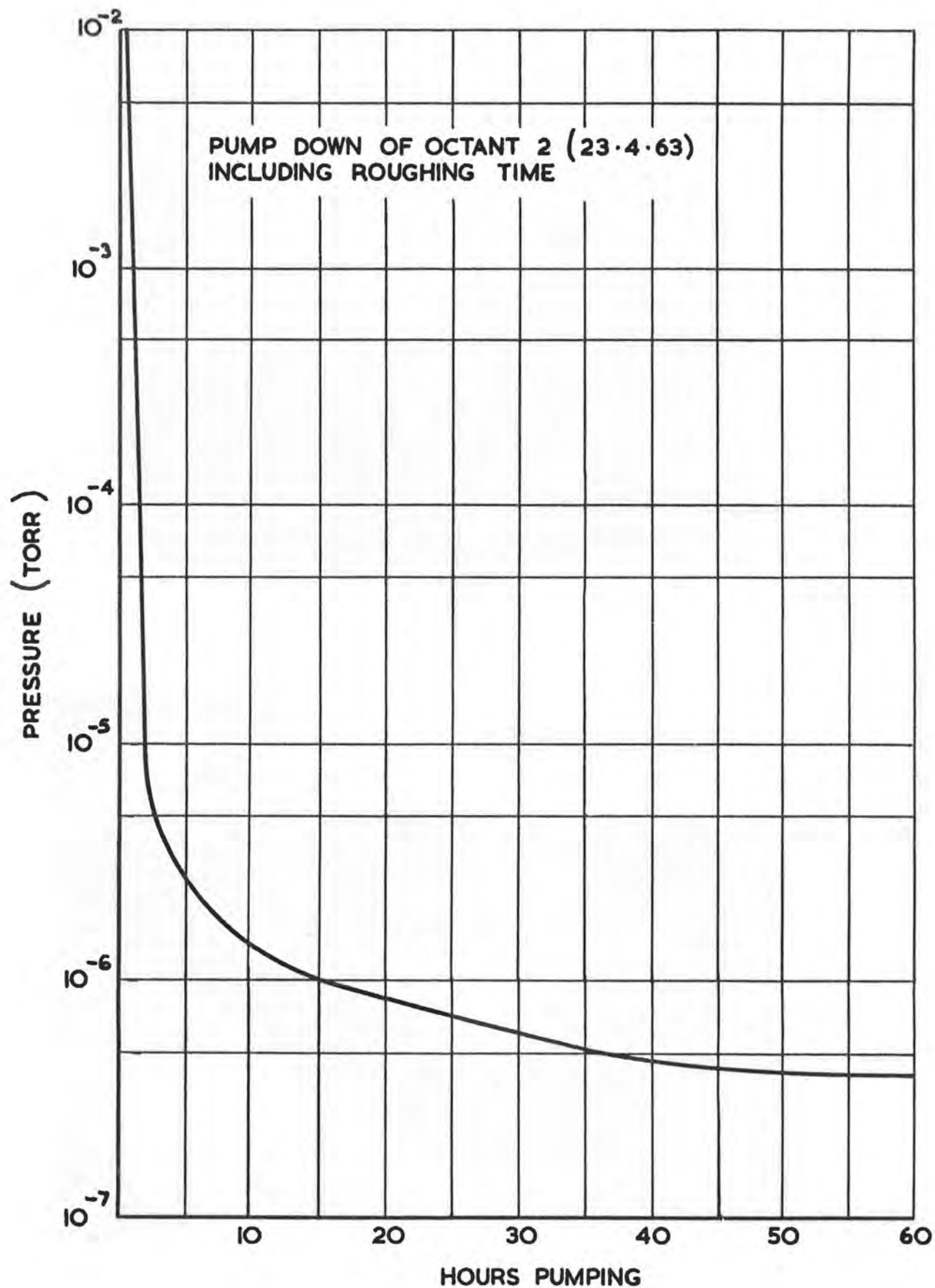


Fig. 8.6.4(iii) Pump down of octant 2.

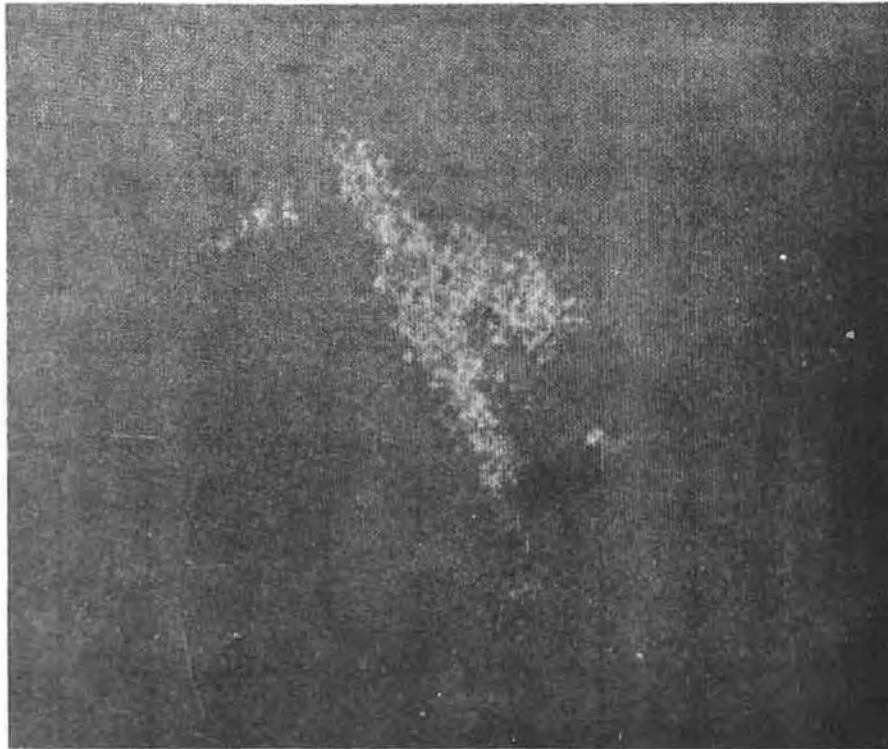


Fig. 8.7(i) An area of a vessel showing resin starvation.

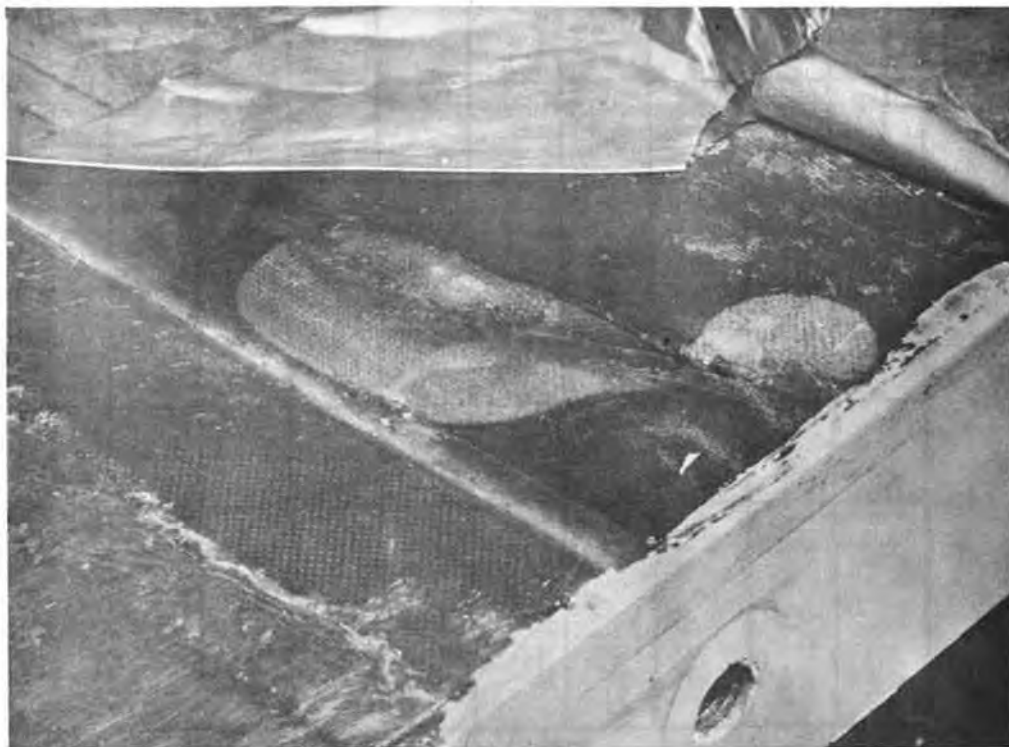


Fig. 8.7(ii) Crushing and voids on a vacuum vessel.

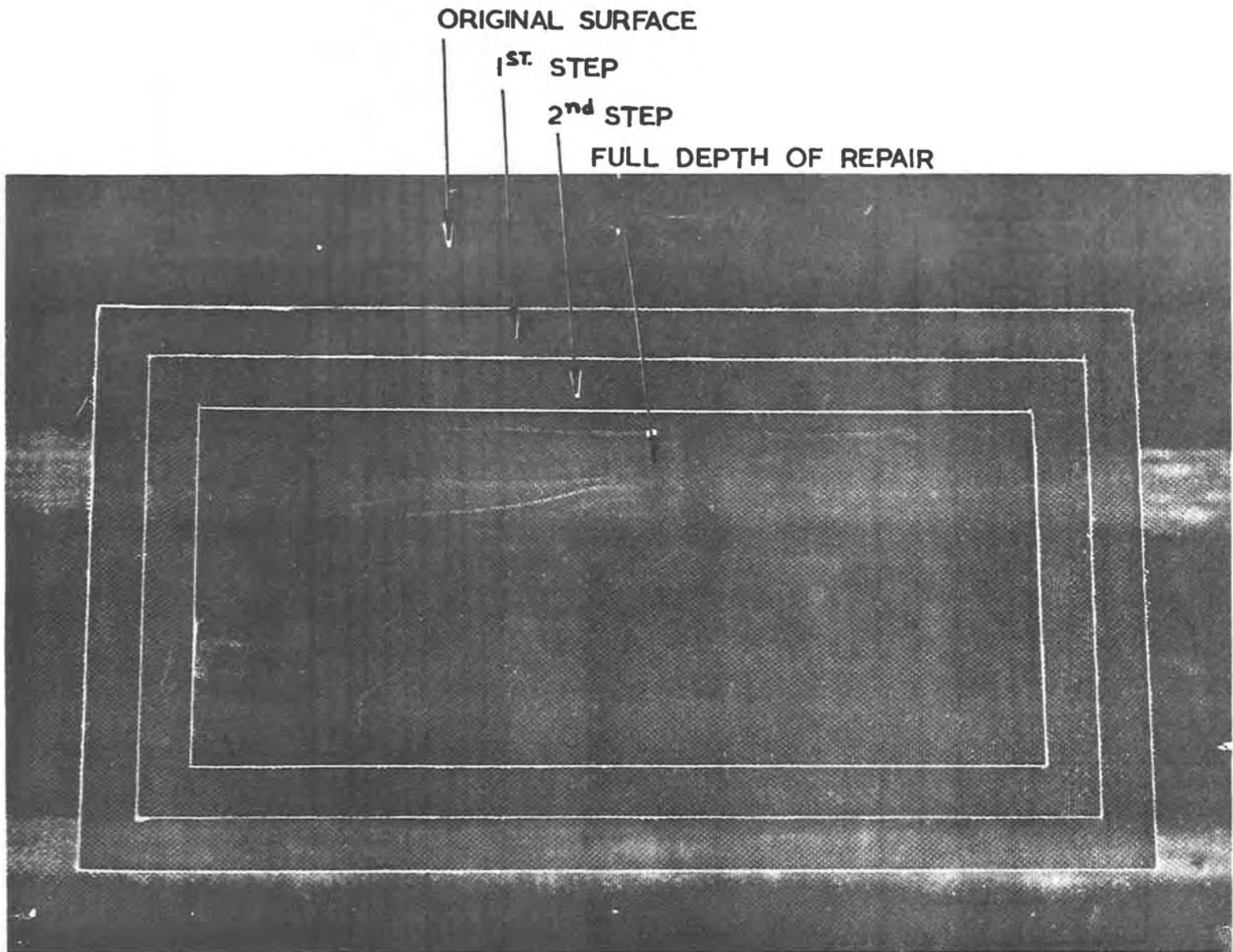
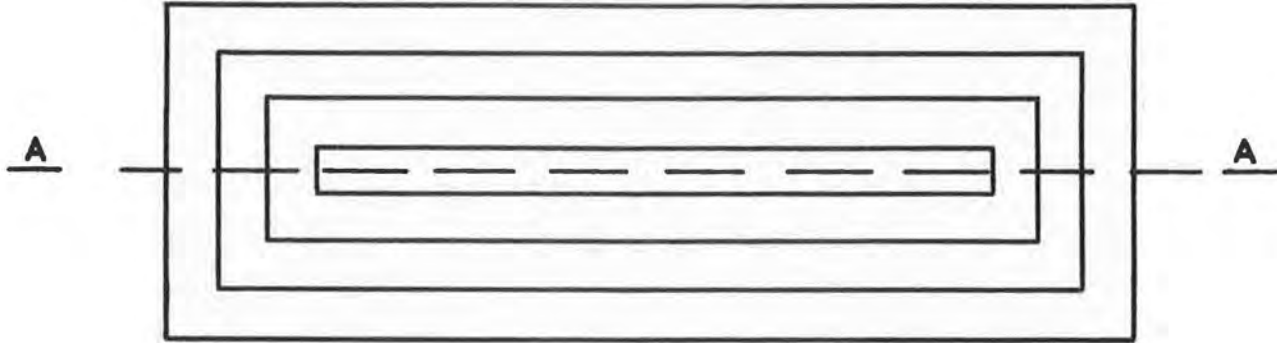
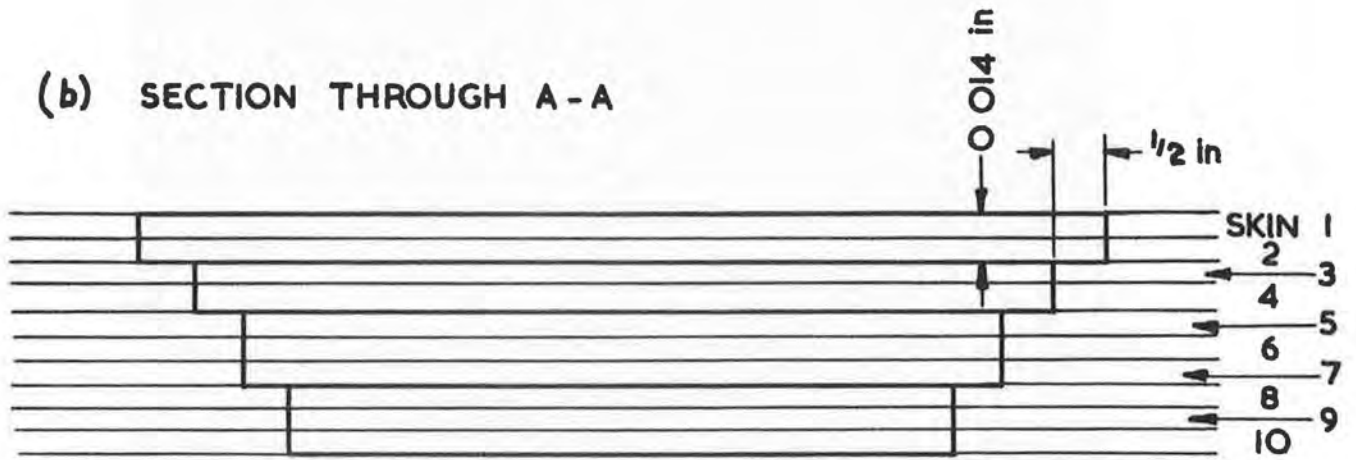


Fig. 8.7(iii) A cut out repair area showing the half inch steps

(a) PLAN VIEW OF PORTION OF VESSEL CUT FOR REPAIR



(b) SECTION THROUGH A - A



NOT TO SCALE

Fig. 8.7(iv) Typical repair profile

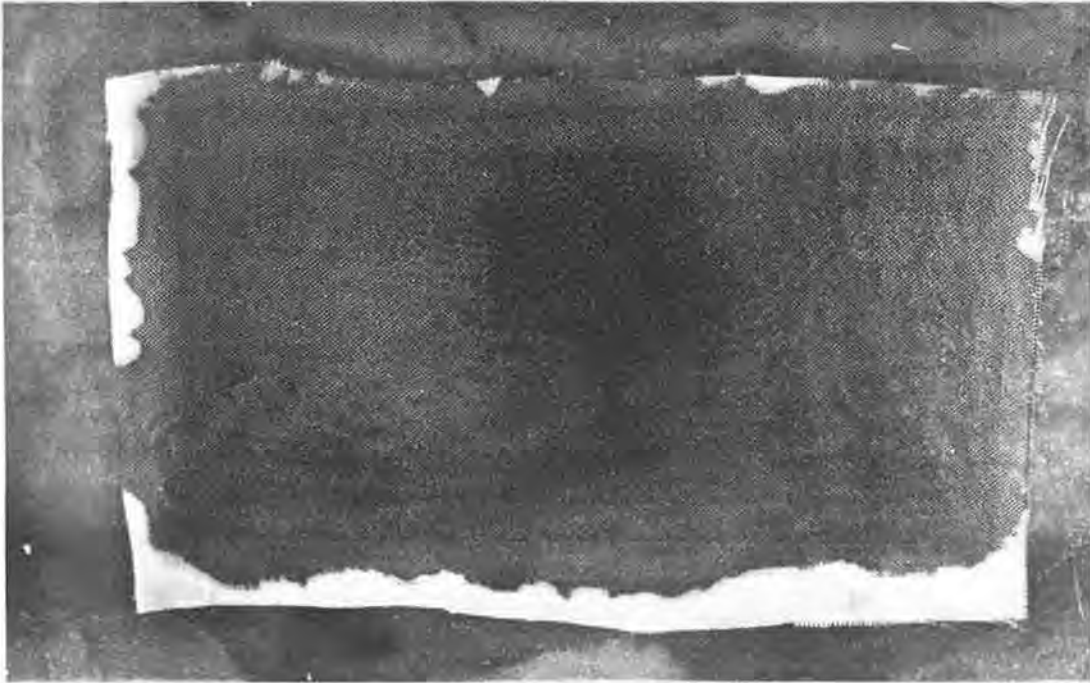


Fig. 8.7(v) Final stage of repair.

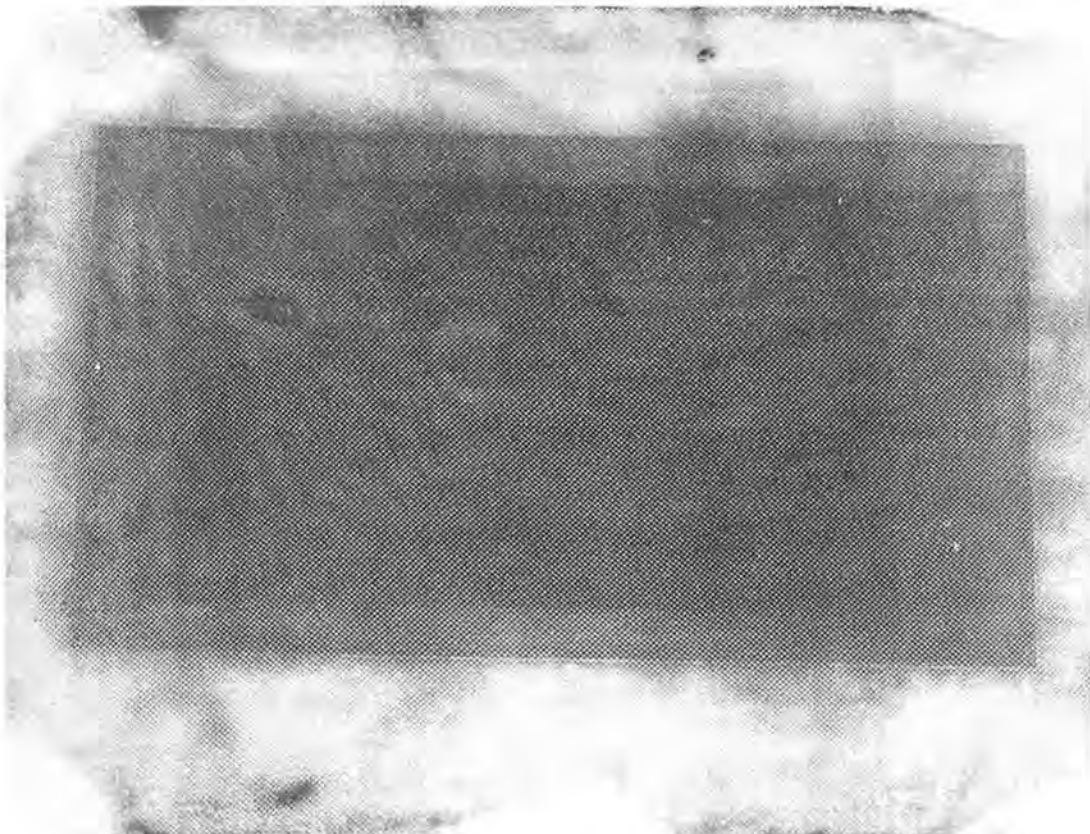


Fig. 8.7.(vi) A completed repair.

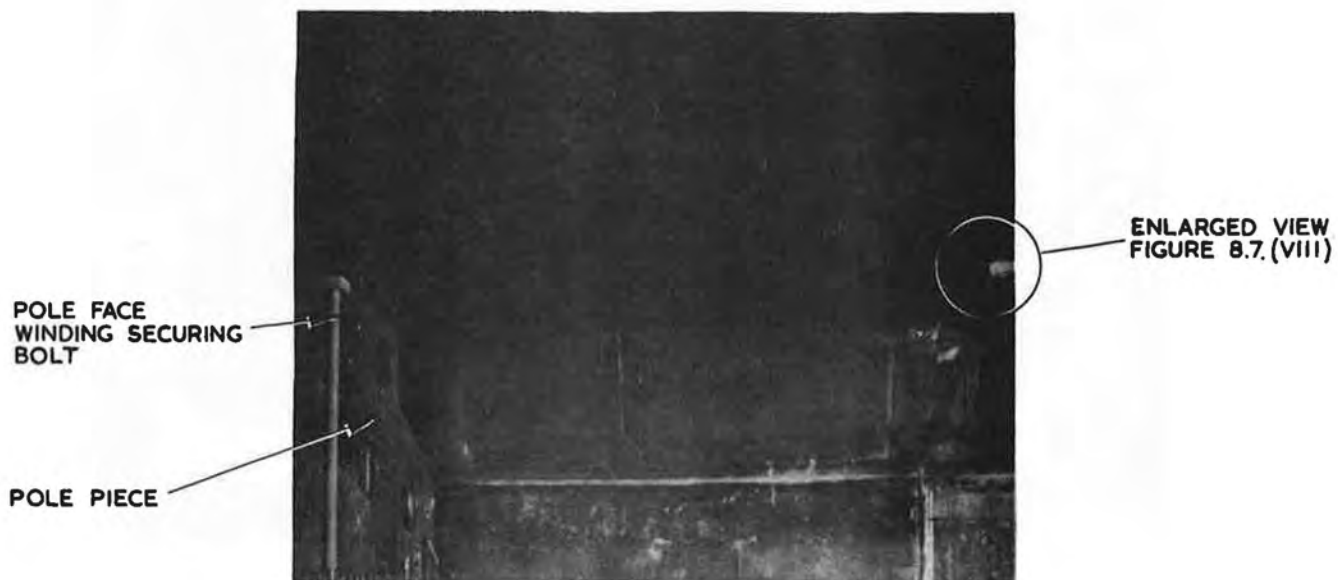


Fig. 8.7(vii) Accidental damage to an outer vessel.

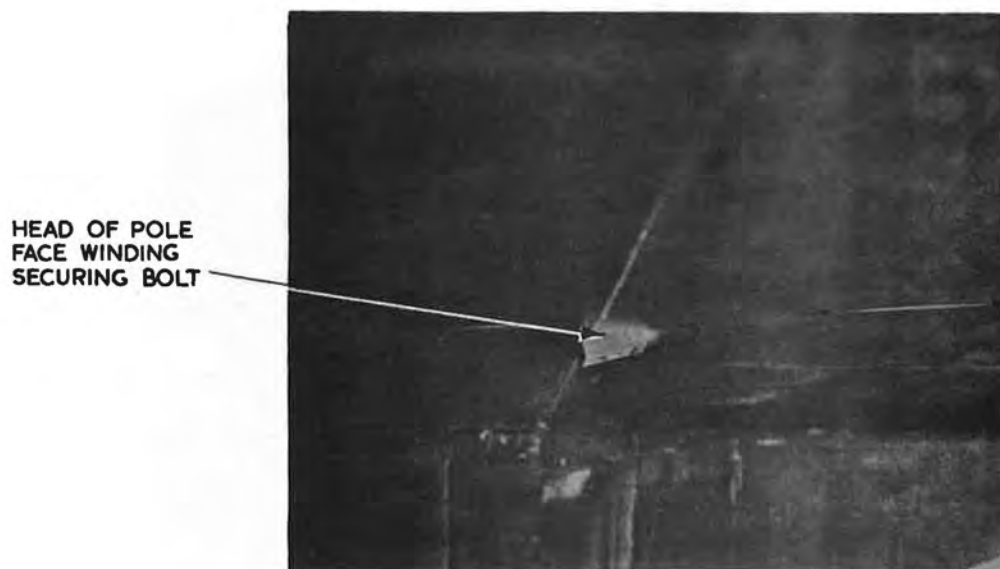


Fig. 8.7(viii) An enlarged view of the damage.

repair resin, fitted into the cut back area and tailored to size. Each layer was rolled to consolidate the repair and remove excess resin. This procedure was repeated until the area was built up to the level of the surrounding laminate. An additional skin larger than the repair was then added (Fig.8.7(v)) and was removed after curing (Fig.8.7(vi)). This gave an even finish and prevented drainage during the curing procedure. Temperature controlled electric blankets were used in curing the repairs.

(ii) Voids in laminate.

When no other fault was evident, voids were filled with the approved resin using a hypodermic needle or a grease gun.

(iii) Leakage round drilled holes due to hollow fibres.

Apart from flange bolt holes, where leaks were eliminated by fitting brass sleeves (see section 8.6.2), there were many larger diameter drilled or machined holes in the laminate where sleeves could not be used. Many of these holes were associated with vacuum seal surfaces and by using the surface coating material, thinned with 10% solvent, the leaks were dealt with satisfactorily.

To date about 130 repairs involving type (i) procedure have been carried out. Details are being published (15). A typical example of accidental damage is illustrated in Fig.8.7(vii) and Fig.8.7(viii). A pole face winding securing bolt was incorrectly placed between two pole tips (removed from the photograph for clarity). The rectangular head, with its long side at right angles, instead of parallel, to the pole tips was driven through the outer vessel laminate in the narrow gap between adjacent magnet sectors. It proved possible to slide a thin backing plate between the vessel and the sectors and a satisfactory repair was made without removing the vessel. This was extremely useful since the installation of pole tips in this octant was almost completed and to remove and replace the vessel with its 350 seals and 84 pole tips, positioned to an accuracy of a few thousandths of an inch would have lost a great deal of time.

8.8. Radiation Damage

A programme of high level radiation dosimetry has been instituted, to determine the rate of degradation of the vacuum vessels under radiation. Commercially available glass dosimeters do not register sufficiently high doses for our requirements and methods involving the change in the modulus of rubber and the change in optical behaviour of polystyrene, are being studied.

Samples of vacuum vessel material, suitable for mechanical testing, have been placed in the cavity between the inner and outer vessels during assembly and further samples, with stainless steel foil and aluminium foil on opposite surfaces, are being placed on the floor of the inner vessel.

Groups of rubber samples and strips of polystyrene are being placed at intervals on the floor of the inner vessel. They will be used to measure radiation doses up to at least 100 Mrad and will indicate when the properties of the vessel material dosimeters should be examined.

The mechanical properties of the vessel material samples will be determined at approximately 250 Mrad intervals, except for those placed within the pole piece cavity which will be examined as the opportunity arises. The outer vessel is substantially shielded by the pole pieces so that monitoring will be needed less frequently. To ensure maximum life from each vessel, targets and/or vessels may be rearranged if the dosimeter investigations show this to be necessary.

8.9. Main Vacuum Seals

8.9.1. Choice of Materials

The principal considerations in choosing the materials for the main vacuum seals were outgassing rate and irradiation stability. Outgassing rate was of greater importance than is usual for vacuum seals since the vacuum vessels are allowed wider engineering tolerances than metal fabrications and larger areas of the seals may be exposed to the vacuum.

Due to the complex nature of rubber formulations, an indication of their relative outgassing rates could only be obtained by examining the raw polymer forms. Outgassing measurements were therefore carried out on sheets of uncured polymer 3 mm thick. The following polymers were studied - isocyanate, butyl, neoprene, butadiene acrylonitrile, butadiene styrene, silicone, ethylene propylene and natural rubber. The results are shown in Fig.8.9.1(i). The silicone polymers were eliminated because of their high gaseous permeability and isocyanate polymer appeared to be the most satisfactory. The stability of this material under irradiation was determined and the results are shown in Fig.8.9.1(ii). The material still has adequate properties at integrated doses of 10^8 rad. However, it subsequently proved to be impracticable to manufacture the seals from this material, since the only method of fabrication was a casting technique. Difficulties were also experienced in producing satisfactory joints between the cast sections. Polyurethane materials, which can be moulded by standard rubber processing techniques, were therefore examined but did not have the required properties.

The material finally chosen was a polymer mixture known as PVC nitrile, which had the desired vacuum properties combined with satisfactory stability under irradiation (Fig.8.9.1(iii)) and could be processed by normal rubber moulding techniques.

8.9.2. Manufacturing Processes

The first manufacturing procedure considered was to extrude the profile and subsequently mould the ends, making four joints on each seal. Experiments with extrusion techniques indicated however, that the polymer would not have a satisfactory surface finish when produced by this method. It was necessary therefore, to mould the vacuum seal in 4 ft lengths and join these to produce the 50 ft sections. Preliminary mouldings suffered from severe mould corrosion due to the liberation of hydrochloric acid in the moulding process which gave a poor surface finish. All the tools used in the operation were chromium plated to reduce this effect. Changes were made in the plasticiser content and type and a better surface quality was produced. These changes did not materially affect the outgassing characteristics or the stability of the polymer under irradiation.

Experiments were carried out to determine the most satisfactory method of jointing. Various techniques were tried and a butt joint proved to have properties most near those of an unjoined seal. A joint strength 60% that of the parent material was regarded as acceptable (tensile strength of the parent material was 1900 lb/in²). Experiments with scarf joints experienced difficulty in the moulding process. The moulded sections were forced out of the mould, resulting in a low pressure area with entrained air at the joint, which was also outside dimensional tolerances.

The following technique was finally evolved and produced satisfactory joints in nearly all cases. The ends of the moulded sections were carefully cut at 90° and coated with a solution of uncured polymer in 50-50 acetone/tetrahydrofuran. They were left for 15 min to permit the solvent to evaporate before being placed in the mould at 150°C and pressed at 1,000 lb/in² for 8 min. The joint was then dressed down using 400 grade 'wet and dry' emery paper and water to give a satisfactory vacuum sealing surface. Experiments showed that the double cure in the area of the joint did not materially affect the properties of the finished product.

8.9.3. Properties of the Final Material

The material had a tensile strength of 1900 lb/in², an elongation at break of 450%, a hardness of 60° Shore and a compression set of 17%. Table 8.9.3(I) illustrates how the properties change with irradiation dose.

TABLE 8.9.3(I)

Dose (rad)	Hardness (°Shore)	Tensile strength (lb/in ²)	Elongation (%)
0	60	1900	456
5. 10 ⁷	85	1900	107
10 ⁸	100	3240	30
5. 10 ⁸	100	7856	75

Table 8.9.3(II) shows the effect on compression set of various cure times since, as indicated in 8.9.2, the seal will have a cure time of 16 min at 150°C in some cases.

TABLE 8.9.3(II)

Cure Time at 150°C (min)	Recovery after 25% compression for 24 hours at 80°C (%)
8	90
16	89.2
24	87.0

The recovery is significantly affected by irradiation as can be seen from Table 8.9.3(III)

TABLE 8.9.3(III)

Dose (rad)	Recovery after 25% compression (%)
0	90
5. 10 ⁷	81
10 ⁸	74
5. 10 ⁸	70

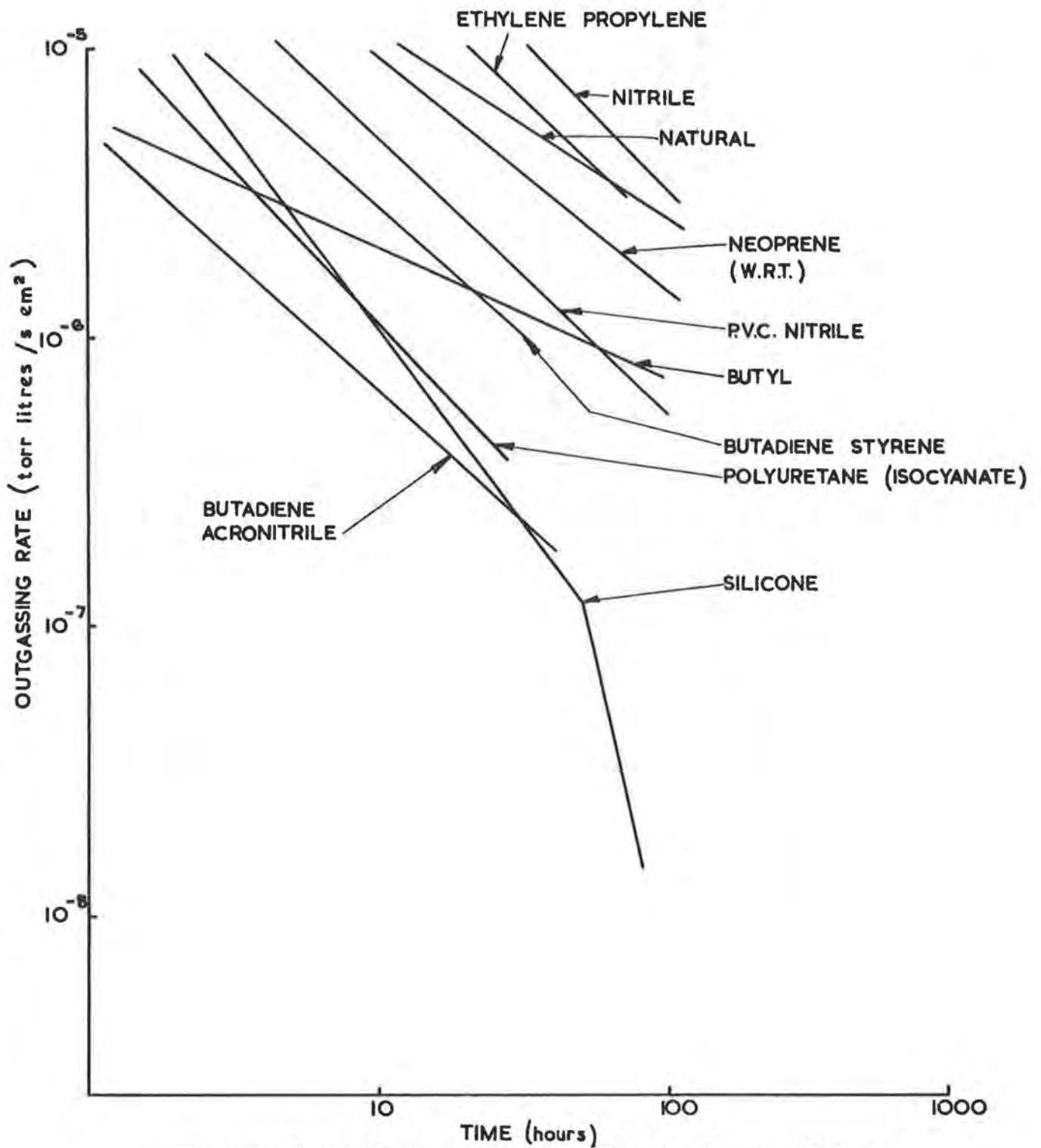


Fig. 8.9.1(i) Relative outgassing rates of Natural and Synthetic Rubbers.

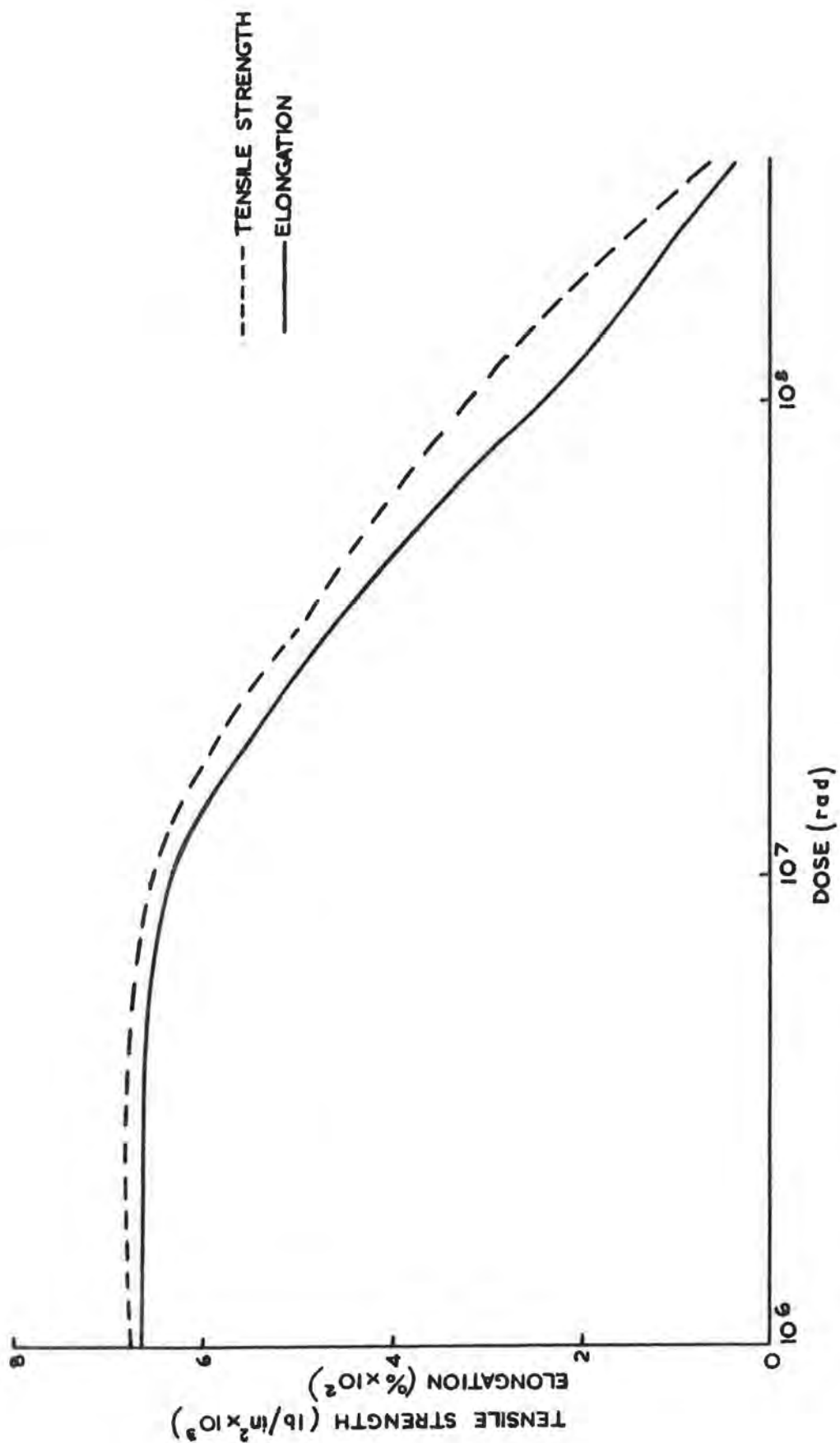


Fig. 8.9.1(ii) Stability of polyurethane rubber under irradiation.

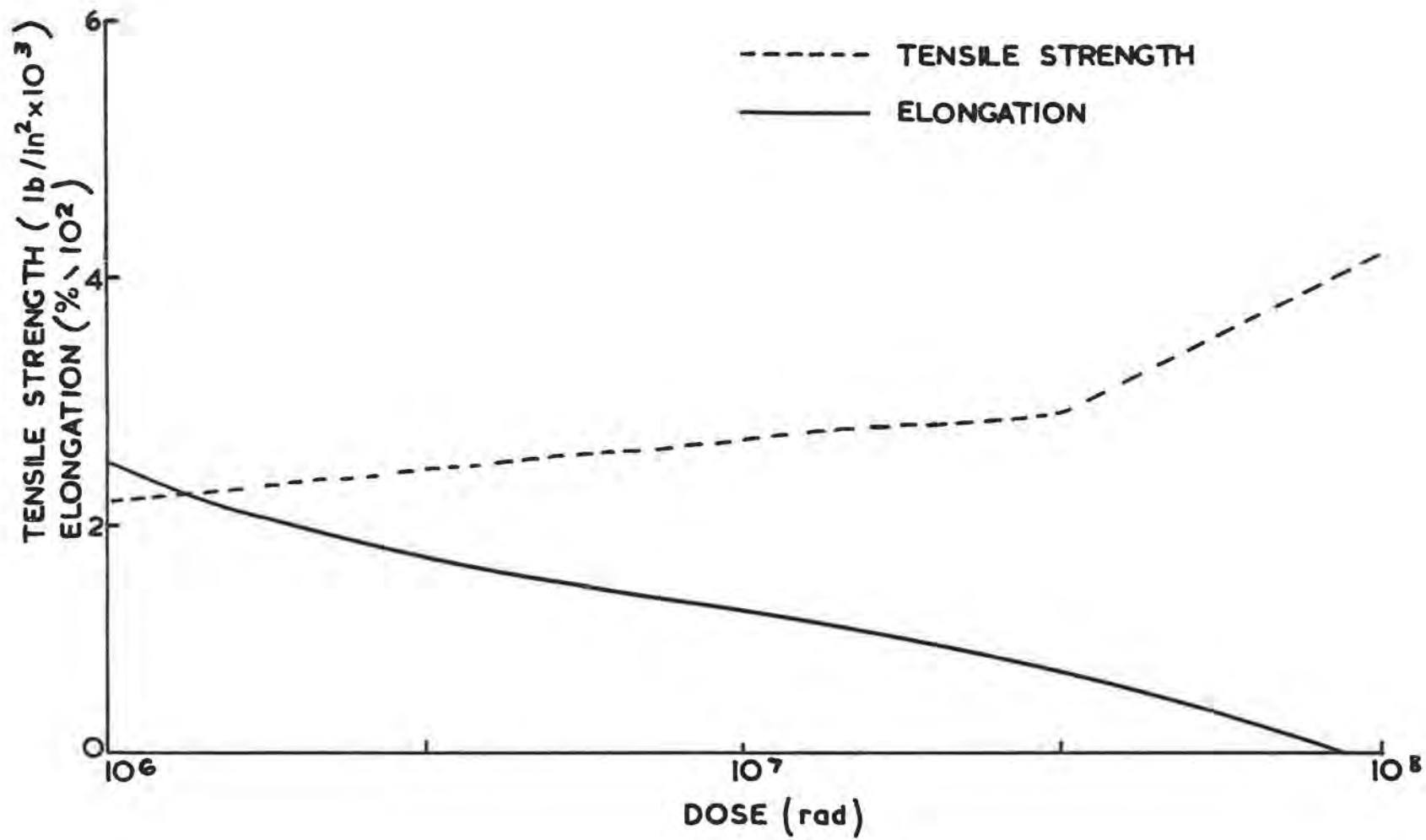


Fig. 8.9.1(iii) Stability of PVC nitrile under irradiation

Experiments have also been carried out on the compatibility of the vacuum seal material with the laminate of the vessels and the various surface coating materials used. The tests were done under 25% compression at 35°C and showed that no interaction takes place between the vacuum seal material and the various coating materials employed. Similar experiments with the material after irradiation showed that no migration of the plasticiser or other interactions takes place, even under these conditions.

8.9.4. Conclusions

The vacuum seals have now been manufactured and installed and have proved satisfactory in operation. One feature which has proved troublesome is the tendency of the material to creep during storage, sufficiently for the seals to be outside the dimensional tolerances after a relatively short period. It has been necessary to ensure that no stresses are introduced during storage.

8.10. Pumping System

8.10.1. Introduction

The theoretical considerations leading to the final choice of the main pumping units for the vacuum vessels have been discussed in reference 4.

Each of the 40 pumping units (Fig.8.10.1(i)) was specified to have a speed of at least 5000 litres/s for most of its pressure range, giving a total speed of 200,000 litres/s. However, at the machine operating pressure, 10^{-6} torr, the minimum overall speed of the system is only 100,000 litres/s which is equivalent to a throughput of 0.1 torr litre/s. The vacuum torus has a volume of about 100,000 litres and a general rule calling for 1 litre/s pumping speed for each litre of volume is therefore satisfied at the operating pressure.

Only 1% of the internal surface area of the inner and header vessels is epoxy resin laminate, not coated by stainless steel. Early work indicated that after 24 hours pumping most epoxy laminates had outgassing rates of the order of 10^{-6} torr litres/s cm^2 compared with 10^{-9} torr litres/s cm^2 for stainless steel. Calculations assuming that eight header vessels would be used gave the following results:

TABLE 8.10.1(I)

Material	Total Surface Area (cm^2)	24 Hour Outgassing Rate (torr litres/s cm^2)	Total Outgassing (torr litre/s)
Stainless Steel	6.4×10^6	10^{-9}	6.4×10^{-3}
Epoxy resin	6.4×10^4	10^{-6}	6.4×10^{-2}
			Total 7.0×10^{-2}

This total outgassing figure represents 70% of the available throughput at 10^{-6} torr. An allowance of 10% was arbitrarily made for leaks, leaving a 20% excess for future degradation. The final choice of epoxy resin showed a much better initial outgassing rate (almost 4×10^{-7} torr litres/s cm^2 after 24 hours) but a slightly higher rate (2×10^{-6} torr litres/s cm^2) after an irradiation dose of 10^9 rad. After this dose the mechanical properties of the laminate also became suspect so that the increase in pump down time would be a secondary consideration.

8.10.2. High Vacuum Pumps

Each pumping unit (16) consists of a 24 in bore sliding gate valve, a refrigerated chevron baffle, and a 24 in bore fractionating oil diffusion pump backed by a vapour booster pump and a rotary pump of 150 litres/min capacity. The gate valve is rigidly fixed to the header vessel by a two part header Fig.8.10.2(i), the part nearest the magnet being made of stainless steel and the lower part made of mild steel. Because of this rigid fixing, the pumping unit must be supported so that it is free to move with the header vessel under temperature variations. This is achieved by suspending the gate valve on four short wire ropes from cantilevers fixed to the magnet sectors and by supporting the frame of the pumping unit on four steel balls. The load on the steel balls can be adjusted to be a minimum by means of jacks which react with the outer part of a frame which is carried by four wheels. This carriage moves on rails fitted to the edges of the services trench encircling the magnet.

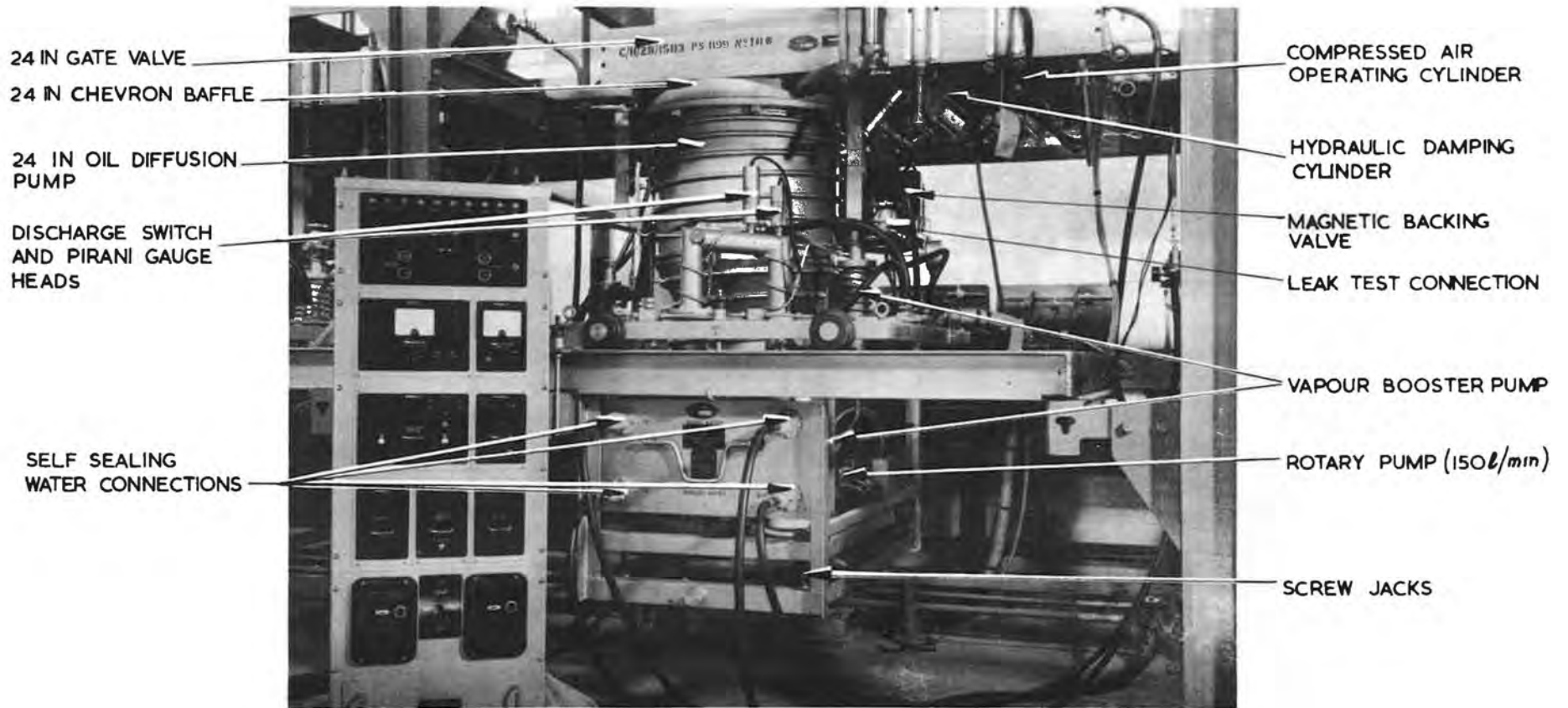


Fig. 8.10.1(i) 24 in oil diffusion pumping unit

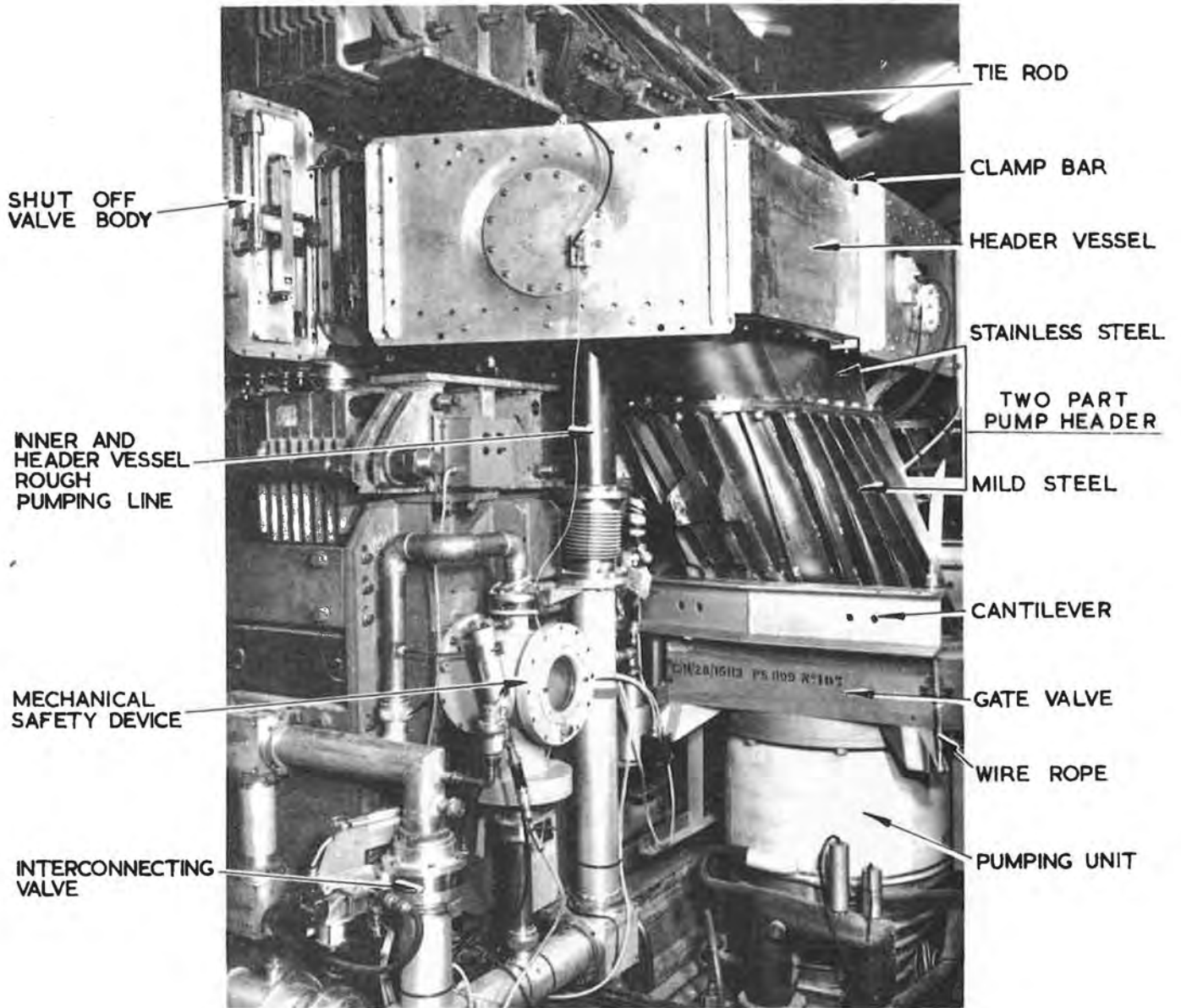


Fig. 8.10.2(i) Pump header and gate valve suspension

The backing system, employing a small rotary pump, was specially chosen to minimise the total weight of the pumping unit and to reduce substantially the vibration which would have been caused by a large rotary pump with no vapour booster pump.

The sliding gate valves can withstand a pressure differential of one atmosphere across the seat in either direction and are self sustaining in the closed position. This allows the valve to serve a dual role. The pumping unit may be isolated from the vacuum chamber and remain operating while the chamber is let up to atmospheric pressure and, alternatively, a faulty unit may be isolated from the system and subsequently removed and replaced. Services to the unit, such as water and compressed air, are provided with self sealing couplings and the jacks and wheeled carriages are used to free the unit from the gate valve and to move it to one side, where it can be hoisted from the services trench by crane.

The rates of opening and closing of the gate valve can be separately adjusted at the hydraulic damping cylinder so that fast closing (less than 10 s) and slow opening can be achieved. In order to limit the gas load on the pumping units during initial pumping of the vacuum chamber from the roughing pressure of 10^{-2} torr, the rate of opening of the valve was set such that the conductance of the aperture did not exceed 500 litres/s in the first minute, the valve taking about 30 min to open fully. In this way it was estimated that the maximum throughput of each unit (about 5 torr litres/s) would never be exceeded.

The four stage oil diffusion pump has an integral guard ring which gives a low backstreaming rate of about $5 \mu\text{g}/\text{min cm}^2$. This is further reduced by the chevron baffle which is cooled to -25°C . No measurement of the overall backstreaming rate has been attempted so far.

Each pumping unit is provided with a separate control console which houses the local operating controls and the power units for all the subsidiary items of pressure measurement and switching. The unit must be able to be controlled either locally or from the control room. The control system is therefore automatic and is arranged to follow a predetermined sequence of operations to avoid mal-operation. It is designed to 'fail-safe' wherever possible. A fuller description of the control system is given in section 9.2 and reference 16.

8.10.3. Roughing Pumps

Early thoughts on the rough pumping system centred on a scheme for a single walled vacuum vessel and employed only a single set of pumps. The pressure was required to be about 10^{-2} torr so that a small rotary pump could be used to meet the mechanical requirements of small vibration and weight in the high vacuum units when suspended from the header vessels. To achieve this pressure the use of mechanical booster pumps was necessary. These pumps were to be sited in the concrete monolith cavities and would therefore have pumping lines longer than 25 ft.

Based on the information available at that time, it was estimated that one 100 litres/s pump, situated at each straight section, would be sufficient to enable the required pressure to be maintained. The final choice fell on a Rootes type pump, backed by a 15 litre/s rotary piston pump (Fig.8.10.3(i)).

In order to limit oil contamination from the roughing pumps, a special refrigerated trap was designed (Fig.8.10.3(ii)). This operates at -50°C and serves

as a backstreaming baffle and stops the film of oil creeping along the surface of the roughing line.

When the design of the vessels and pole tips was finalised, a re-assessment of the rough pumping requirements was made. The pole tip laminations had many perforations exposing a larger area of the epoxy resin used for bonding the laminations. The pumping aperture circumferentially round an outer vessel was limited and pumping could only be allowed from the ends of each octant. Bearing in mind the early difficulties in testing the prototype outer vessel, it was thought that a reasonable pump down time could not be expected if the outer and inner vessels were pumped together to a pressure of 10^{-2} torr.

It was therefore decided to provide additional pumping units which would continually evacuate the outer vessels. No advantage could be seen in achieving a pressure lower than 1 torr since this was adequate for the mechanical protection of the inner vessel and inter-vessel leaks would not be substantially reduced by a lower outer vessel pressure. A rotating vane type pump (60 litres/s) was provided at each end of each outer vessel. These pumps were fitted with refrigerated traps similar to those on the inner vessel roughing pumps.

Fig.8.10.3(iii) shows the rough pumping pipe line layout indicating the valves and pressure switches provided. All roughing and equalising valves are solenoid controlled, pneumatically operated, 4 in nominal bore, quarter swing valves and the air admittance valve is 1 in, magnetic. Provision has been made for connecting the air admittance valves to a dry air supply (-40°C dew point) fed from a ring main.

Each pump has associated with it a capsule pressure switch, set at a relatively high pressure (15 torr) which simply ensures that the pump is working before the roughing valve can be opened. This pressure switch is then bypassed electrically. Each pump can be started locally from its own control panel but valves are only operated from a central marshalling kiosk in the magnet room.

8.10.4. Interlocks and Safety Devices

When the vessels are being pumped down, it is imperative that the separate pumping arrangements for outer and inner vessels are interconnected so that no pressure difference sufficient to cause damage to the inner vessel arises between the vessels. A specially developed thermistor type pressure switch (17) (Fig. 8.10.4(1)) has been fitted and interlocked so that the equalising valves remain open so long as any switch indicates a pressure greater than 1 torr. When this pressure is achieved the equalising valve closes automatically and the inner vessel can be pumped to 10^{-2} torr by its mechanical booster pumps.

Further pressure switches of the thermistor type then operate to complete an interlock circuit which allows the high vacuum valves on the main pumping units to be opened, provided that the inner roughing valves have closed. This sequence is assured by the use of a rotary switch to select 'Off', 'Rough Vacuum' or 'High Vacuum', all octants being controlled simultaneously from a marshalling kiosk in the Magnet room.

The thermistor switches were duplicated by providing switches performing the same function at each end of an octant and these, and other interlocks were connected in series chains so that every octant required to be in the same pressure state before the next stage of pump down could begin. It was thought advisable to arrange for all octants to operate together to safeguard the vacuum vessel,

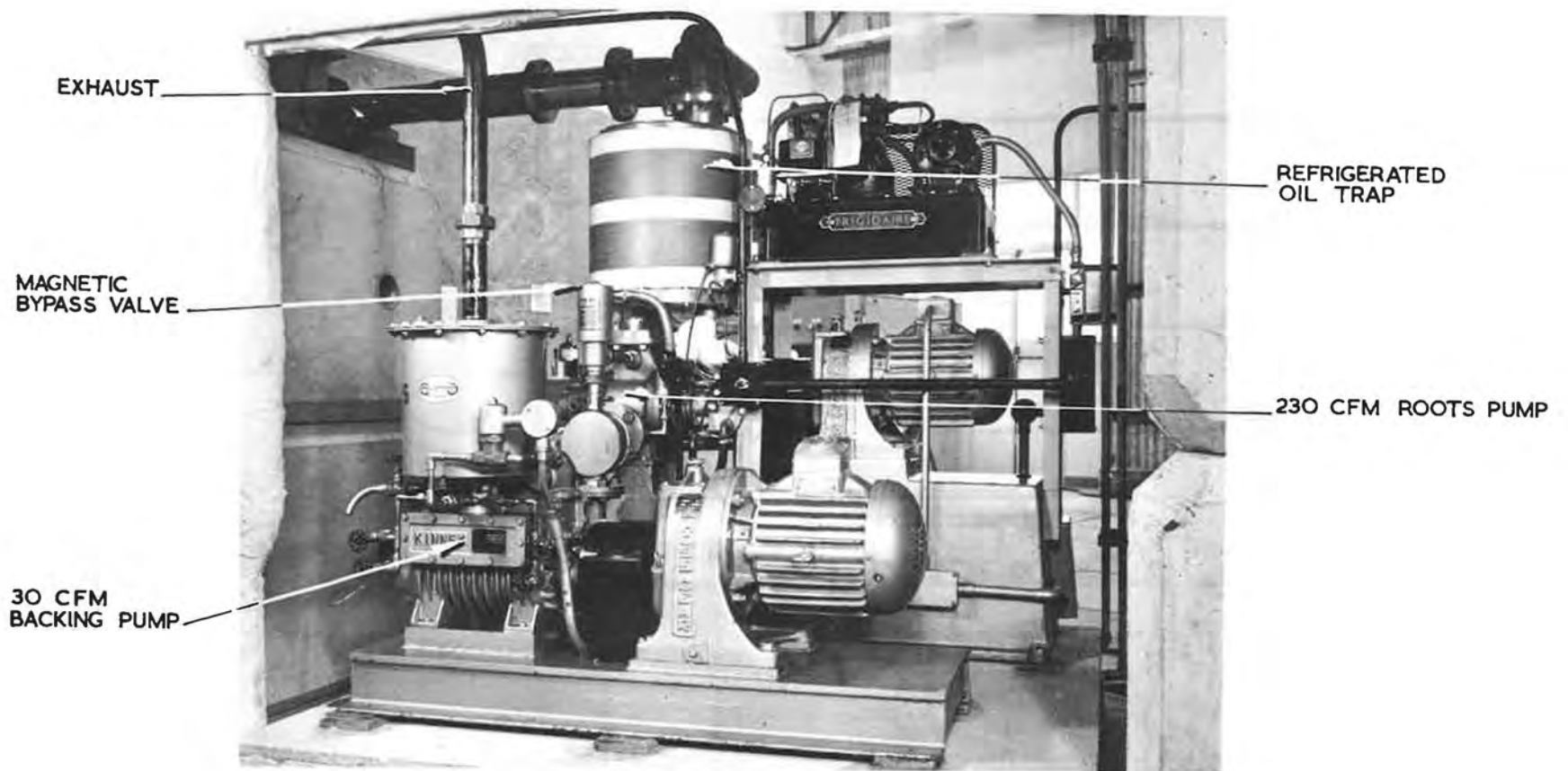


Fig. 8.10.3(i) Inner vessel roughing pump.

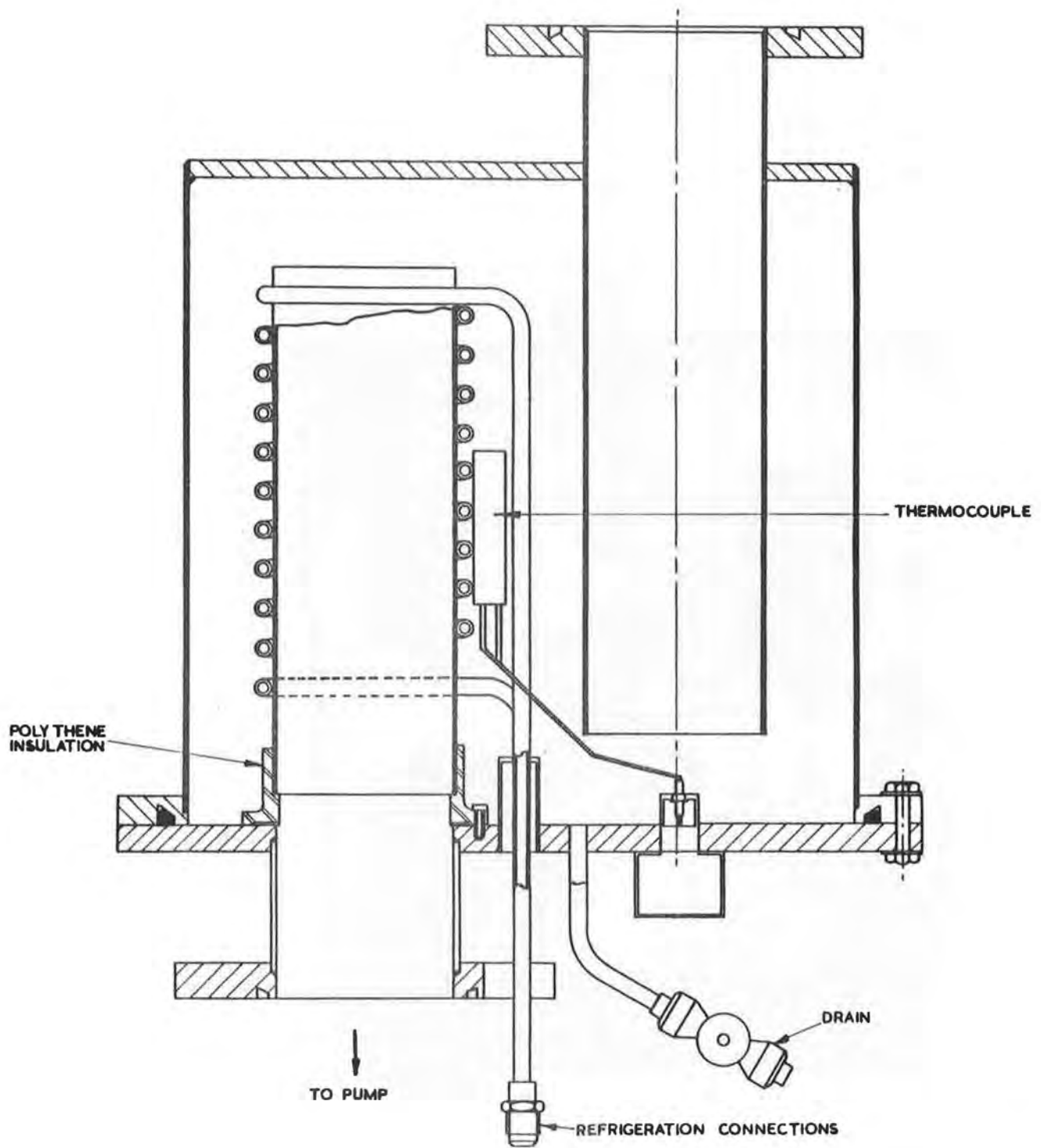
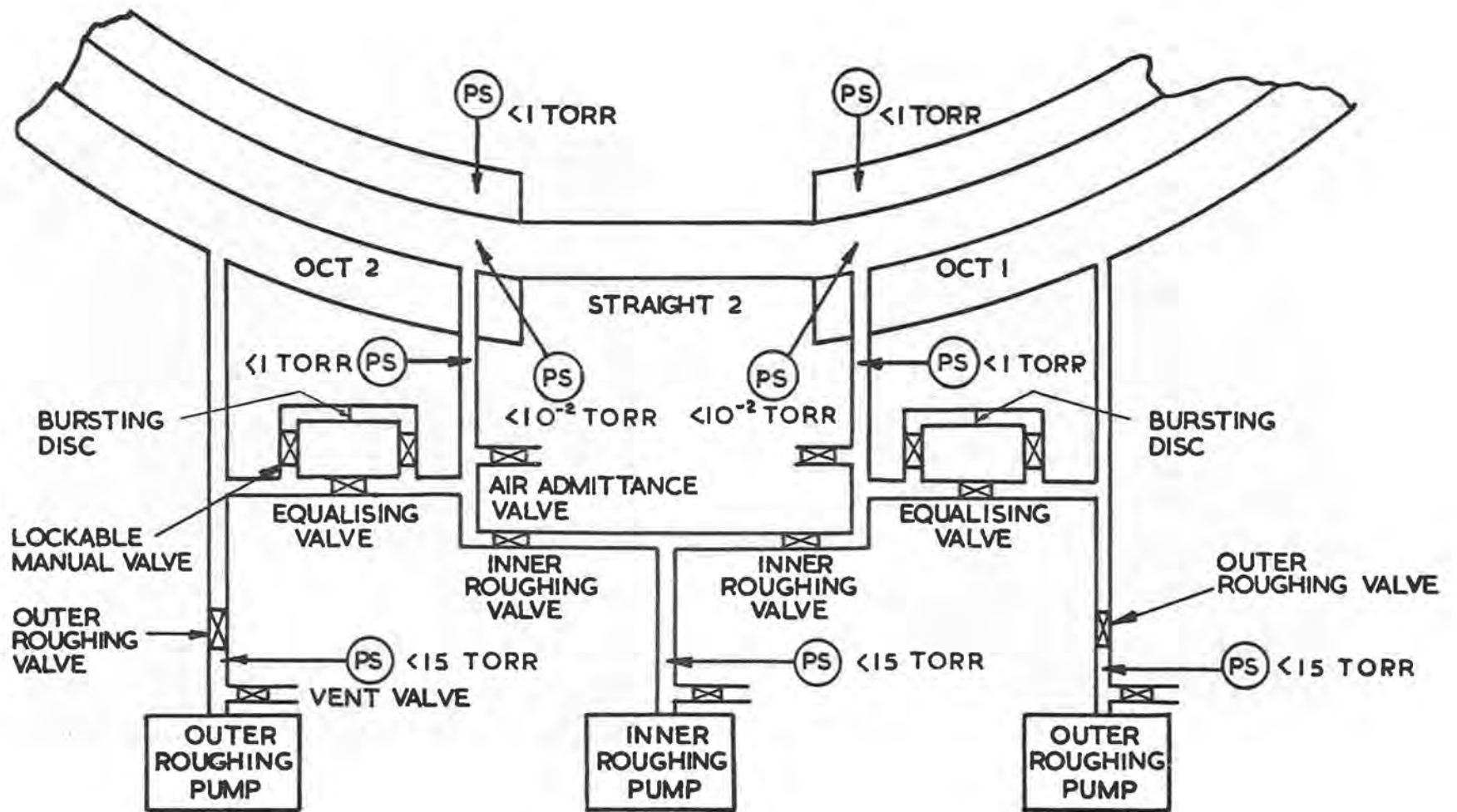


Fig. 8.10.3(ii) Refrigerated oil trap



PS = PRESSURE SWITCH

Fig. 8. 10. 3(iii) Layout of roughing system

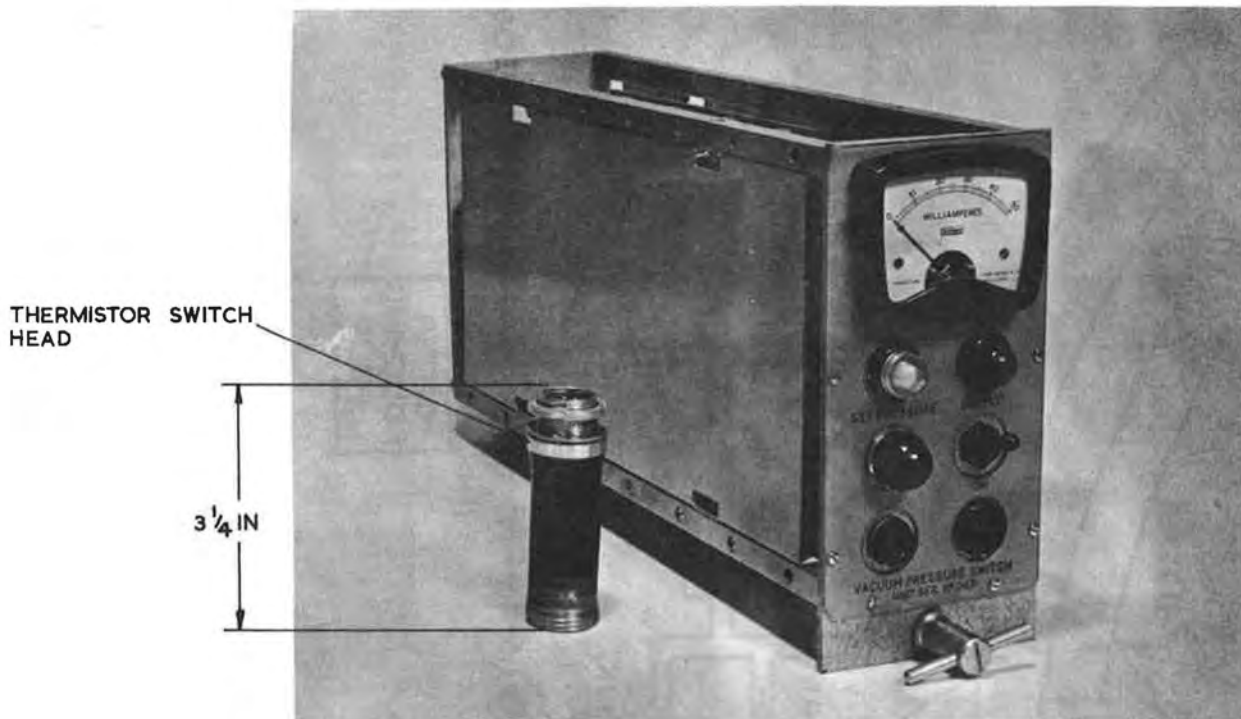


Fig. 8.10.4(i) Thermistor vacuum switch.

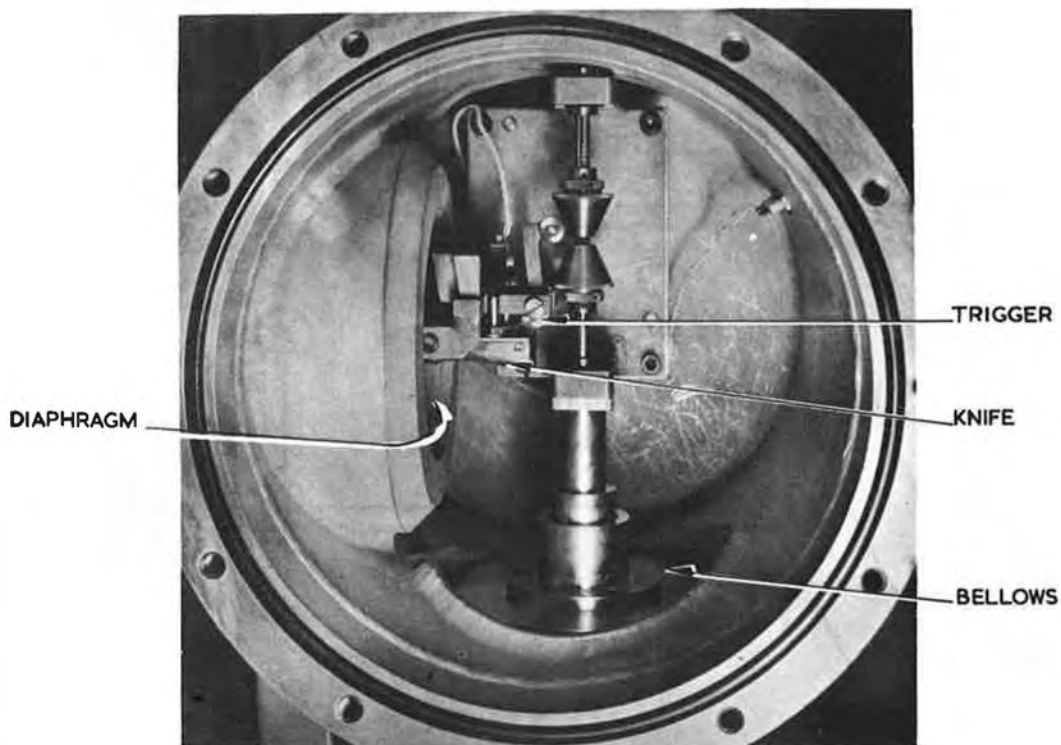


Fig. 8.10.4(ii) Mechanical safety device.

especially since the inner vessel, with the straight sections, form a continuous vacuum torus.

In the 'Off' position, air admittance valves are not automatically opened, final energising of the solenoids being controlled by a key operated switch. In the 'High Vacuum' position, each high vacuum valve is opened from the pumping unit, local control console.

If failure of the electricity supply occurs, all equipment 'fails safe' - high vacuum valves, roughing valves and air admittance valves close (or stay closed) and equalising valves open. Each roughing pump has a vent valve which opens after an electrical delay, to allow time for the roughing valves to close.

As a further safeguard for the inner vacuum vessel, a mechanical safety device was developed.⁽¹⁸⁾ This consists essentially of a copper diaphragm which can be ruptured by a spring loaded knife (Fig.8.10.4(ii)). The knife is released by a trigger which is actuated by movement of a bellows when subjected to high pressure difference between the inner and outer vessels. The device is calibrated to operate when the pressure in the outer vessel exceeds that in the inner by 6 torr and, in the reverse sense, when the pressure in the inner vessel exceeds that in the outer by 30 torr.

Two such devices are provided on each octant. They can be isolated from the octant only by unlocking manually operated valves. This will only occur on one device in an octant at any one time and then only for the purpose of replacing the copper diaphragm or so that a replacement device can be fitted while maintenance or recalibration is carried out.

During commissioning of the vacuum system it became necessary to evacuate individual octants to carry out the vacuum tests on the installed vessels and also to have octants 8, 1 and the inflector system **evacuated for machine experiments**. Originally it was thought that incomplete octants could be shorted out of the control system but this did not allow sufficient flexibility.

A temporary control panel was therefore set up which allowed Octants 8 and 1 to be controlled separately. The appropriate interlocks were detached from the main chain and operation of the vacuum valves was controlled by push button. The inner vessel roughing pumps were not used so that the control system could be kept simple. The interconnecting valves were kept open by isolating an appropriate pressure switch at a pressure above 1 torr and the inner vessel was pumped down by the outer vessel roughing pumps. Pressures of about 0.06 torr can be achieved in this way. When the high vacuum pumps are connected, the throughput soon becomes too high for individual pumps and the protective pressure switches close the gate valves, though some improvement in the vessel pressure occurs before they close. This process is then repeated until the valves remain open and the octants are pumped down.

This type of control has now been extended to allow any octant to be operated singly. A permanent system of control is under consideration which will allow work to be done on a single octant as well as providing the full ring control using all pumps.

8.10.5. Straight Section Box Pumping Arrangements

To allow for dimensional variations and thermal expansion, the inner and outer vessels are connected with the straight section boxes by specially designed stainless

steel bellows assemblies. These are essentially of two types (See Fig.8.10.5(i)). One type has a U section convolution joining the inner and outer vessels and the other with a double omega section convolution connecting the inner vessel to the straight section box. In the longer straight sections, shut off valves are interposed between the two bellows assemblies. In the shorter straight sections the two bellows types are integrated in one assembly.

The shut off valves consist of a body and a valve housing. The bodies are permanently fitted in the ring, two in each long straight making eight in all. The housing, which contains a valve plate and winding mechanism, can be attached to the body so that when the valve is closed it will withstand atmospheric pressure across its seat from one direction which can be chosen. The valve may be introduced into a body when it is under vacuum by using a vacuum lock principle, a flap on the body being controllable by a lever on the housing (Fig.8.10.5(ii)).

A reassessment of pumping requirements was made when the amount of experimental and diagnostic equipment to be fitted in the straight section boxes was known more accurately.

Electrodes with a large surface area, supported on insulators, are to be installed in several straights. On average, the total surface area (mainly of mild steel and aluminium) involved in one straight is about $5 \times 10^5 \text{ cm}^2$ and a typical outgassing rate for these materials, even after 48 hours, is 10^{-8} torr litres/s cm^2 . A straight section box could therefore contribute 5×10^{-3} torr litre/s to the gas load on the adjacent octant pumps. This represents 40% of the total pumping capacity of one octant at 10^{-6} torr and is a greater fraction of the capacity than could reasonably be allocated for this purpose, especially since the calculation is based on 48 hours pumping, which is at least twice as long as is desirable.

It was decided to obtain additional pumps to be mounted on the straight section boxes. The largest pumps which could be fitted without conflict with plunging mechanisms, beam outlet windows, etc., are of 12 in nominal bore. Two pumping units of this size have been obtained for each of six straights. Straight 8, which has the r.f. accelerating cavity, cannot be fitted with extra pumping but it has a relatively small vacuum chamber. Straight 1 had already been supplied with one 16 in pumping unit (2.250 litres/s at 10^{-6}) to replace a 24 in pumping unit which was displaced from octant 1 by a diagnostic probe assembly. All those units have similar control systems.

During proof tests of the 24 in units fitted on the octants, the pumping speeds were generally found to be higher by 20% than the specified minimum at 10^{-6} torr. This gives a useful margin and together with the additional pumps in the straight sections should allow the operating pressure to be achieved within 24 hours of the start of pumping.

Some pumping units have already been in almost continuous operation for 4 years and have performed remarkably well. A number of faults have occurred, mainly in the control equipment. The most important have been the unreliability of the cold cathode ion gauges and the hot wire switches used for pressure control. The ion gauges have been improved by modification and the switches require frequent re-calibration. Both devices may be replaced.

8.10.6. Arrangements for Diagnostic Equipment and Targets

Diagnostic probes and targets are introduced into the vacuum system through a

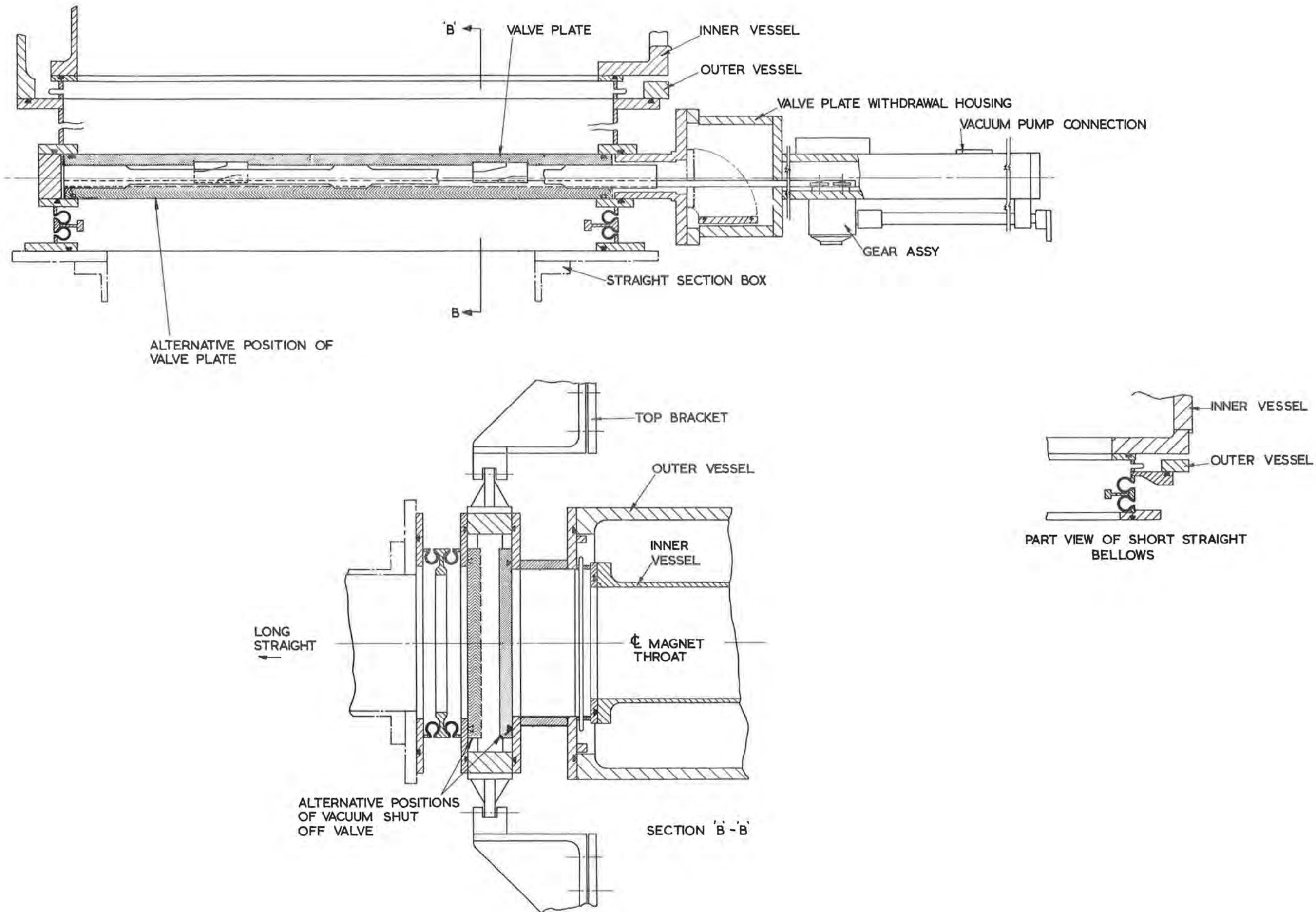


Fig. 8.10.5(i) Assembly of bellows, adaptors & vacuum shut-off valve to vacuum vessel in a long straight section.

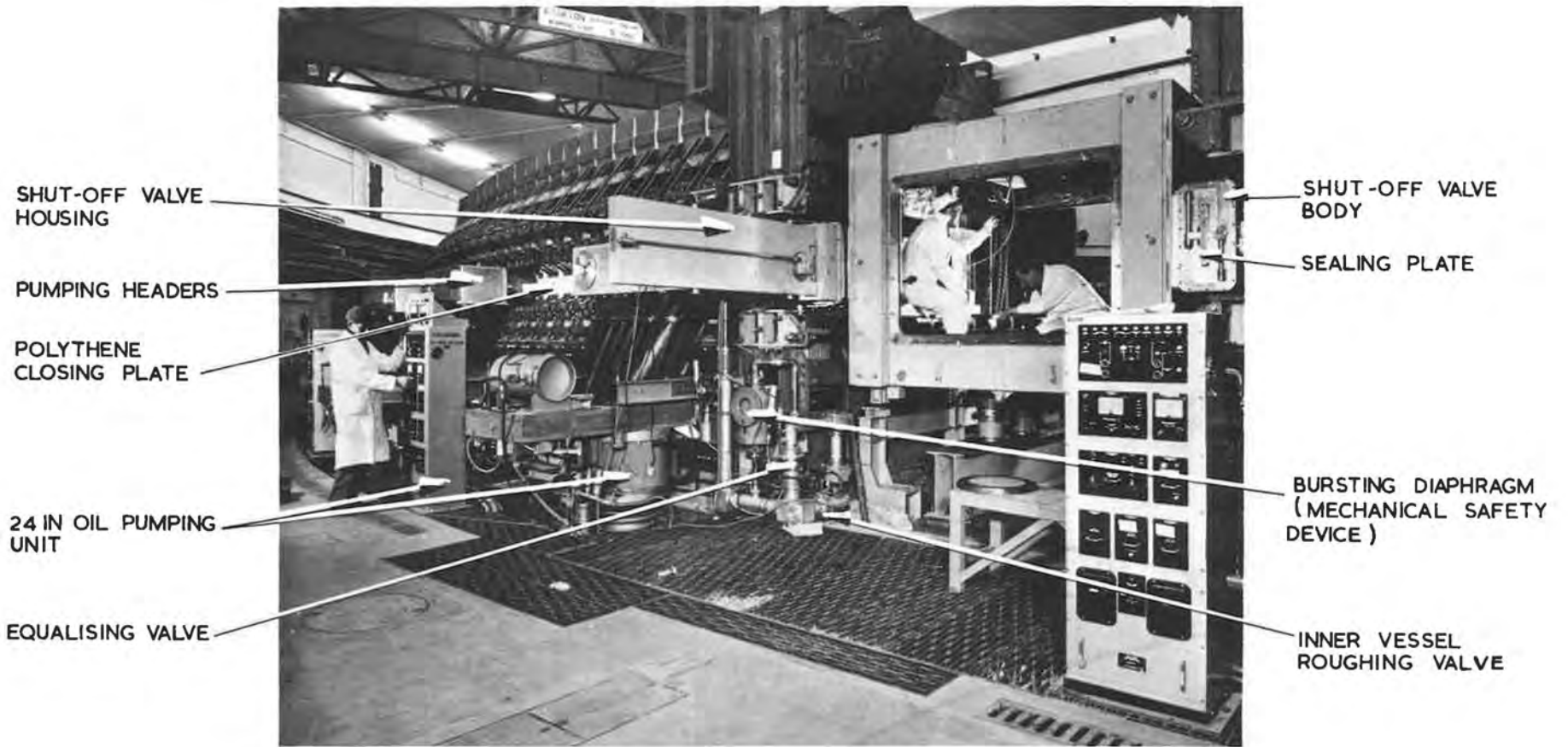


Fig. 8.10.5(ii) Shut off valve housing and body sealing plate.

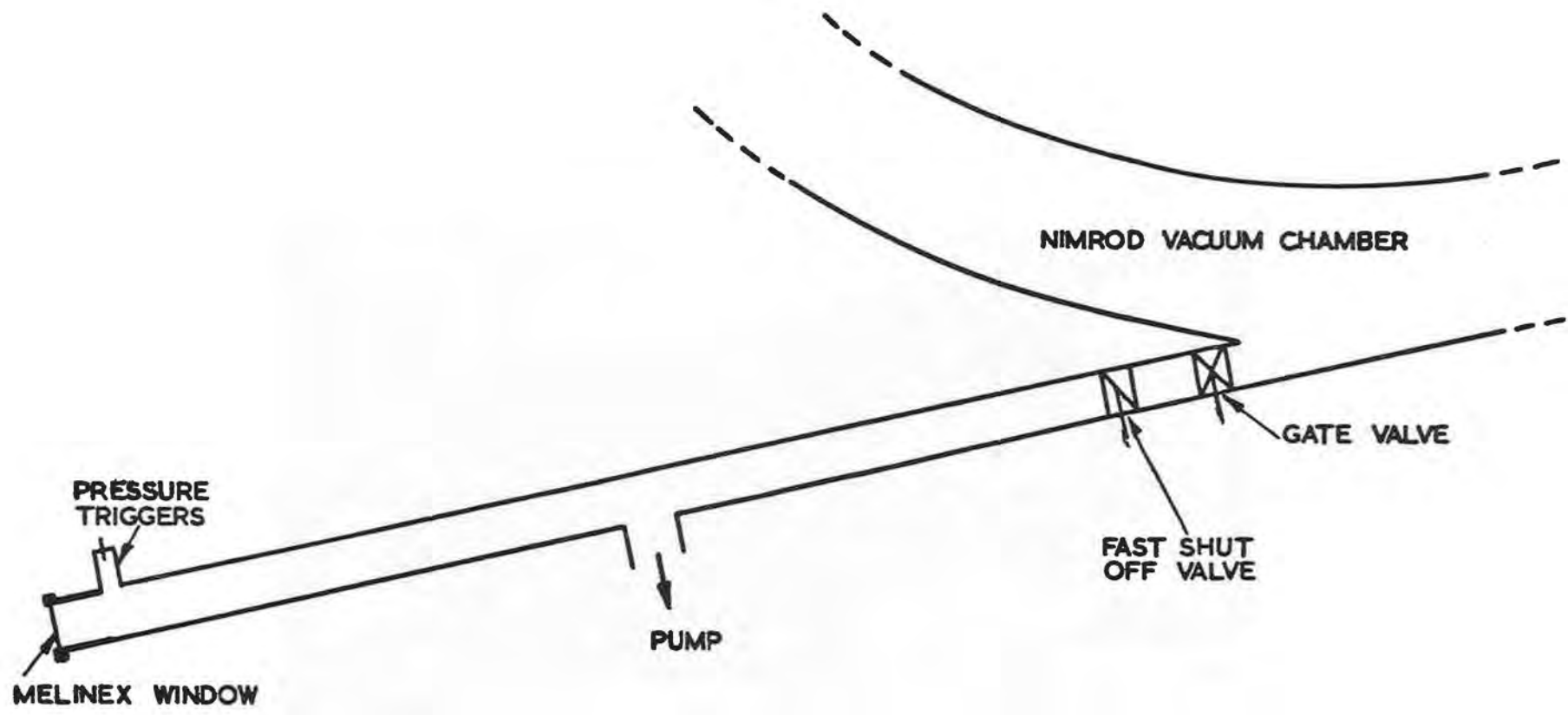


Fig. 8.10.7(i) Schematic layout of a typical beam line vacuum system

fully interlocked vacuum lock. A sliding gate valve separates a manifold from the torus and can only be opened when the manifold has been evacuated to a pressure of 10^{-1} torr by a portable pump. A probe can then be moved into the magnet aperture on the end of a tube which passes through a sliding seal on the manifold.

8.10.7. Beam Lines

Each beam line is terminated by a thin melinex window and if this is punctured or fails in any way, a sudden pressure rise would occur. To protect the vacuum vessels a fast shut off valve has been fitted on each beam line close to the machine and close to a normal isolation gate valve. The vacuum layout of a typical 8 in diameter beam line is shown in Fig.8.10.7(i).

The fast shut off valves (Fig.8.10.7(ii)) are designed to close before the "plug" of air from a burst melinex window reaches the valve. They take about 12 ms to close so that the total time from a window burst to the final closure of a valve is about 15 ms.

To give closure times of this order, the total weight of all moving parts is only 4 lb and the plate is driven by a piston which is propelled by nitrogen gas at a pressure of 1,000 lb/in². It is stopped at the end of its travel by an oil damper built into and around the piston rod. The valve is kept open by a system of rollers and levers which holds the plate by a 20 lb pull exerted by a solenoid. When the solenoid current is switched off the valve closes. The fast shut off valve, gate valve and pressure triggers operate on an integrated control system which is designed to fail safe under all circumstances; for example, trickle charged batteries are used to guard against mains failure. The pressure triggers consist of a Penning gauge head, a vacuum discharge switch head and a capsule switch.

The system is interlocked so that the machine gate valve can only be opened when

- (i) The beam pipe is pumped down to the required pressure.
- (ii) All electrical connections are made.
- (iii) The piston pressures of the fast shut off valve and the gate valve are at the operating value.
- (iv) The power is switched on.
- (v) The fast shut off valve is open.

The fast shut off valve is kept locked open until the beam pipe is pumped to the required pressure when it switches to the ready position. The gate valve closes if there is a slow pressure rise; the fast shut off valve closes if there is a fast pressure rise. The valve is triggered by a Penning gauge at about 10^{-4} torr, a vacuum discharge switch at about 0.2 torr, a capsule switch at about 5 - 10 torr. The vacuum discharge switch guards against any failure of the Penning gauge and the capsule switch covers both. With the capsule switch, the closure time goes up to around 40 ms.

The fast shut off valve has recently been modified so that it can be used on very short pipes; extra guide rails were needed to prevent the plate slicing its

way through the valve seat, since the plug of air would hit the fast moving plate before it is completely seated.

8.10.8. Pressure Measurement

The pressure in the torus is measured by double filament Bayard - Alpert type ionisation gauges using local control units with facility for remote switching and choice of filament. On the local units, several linear ranges and a logarithmic range cover pressures from 10^{-3} to 10^{-8} torr. The logarithmic indication is repeated in the control room on strip chart recorders.

Initially, ion gauge calibration proceeded along conventional lines using a manifold connected via liquid nitrogen traps to a commercial McLeod gauge and a pumping system. The gauges were calibrated with pure nitrogen. The calibrations obtained on the same gauge were inconsistent, showing a variation from day to day of, typically, 12%. This was investigated by taking a series of pressure readings on the same volume of trapped gas in the McLeod gauge, first by eye and then by reading the scale with a cathetometer. Readings were also taken with the mercury columns tapped mechanically and by hand. From these experiments the experimental error in the gauge calibration was estimated at $\pm 6\%$ when the reading were taken by eye and $\pm 2\%$ when the scale was read with the cathetometer. The 12% day to day variations in the calibration of a particular gauge could not therefore be due to experimental errors when using the cathetometer. The error must lie in the McLeod gauge or the ion gauges themselves and the latter were temporarily suspected.

A report(19) was published pointing out a serious error, due to the "vapour stream" effect, in the McLeod gauge when used in conjunction with a liquid nitrogen trap. The report tabulates the magnitude of the error to be expected for a particular system and several experiments were carried out to confirm this. The results agreed substantially with the predictions of the report. A more consistent way of calibrating ion gauges was therefore required and the methods of several American workers who used standard orifice techniques were followed. The pumping speed of a circular aperture in a diaphragm across a circular tube can be worked out theoretically. By knowing how much gas has been introduced into a system, and the speed at which it is being removed, the (absolute) pressure can be calculated. The results on the orifice system look promising. Two gauges calibrated at an interval of three weeks gave results which varied by only 3%, which is the order of the experimental accuracy. Batches of six gauges will be calibrated when a "bell jar" has been suitably modified.

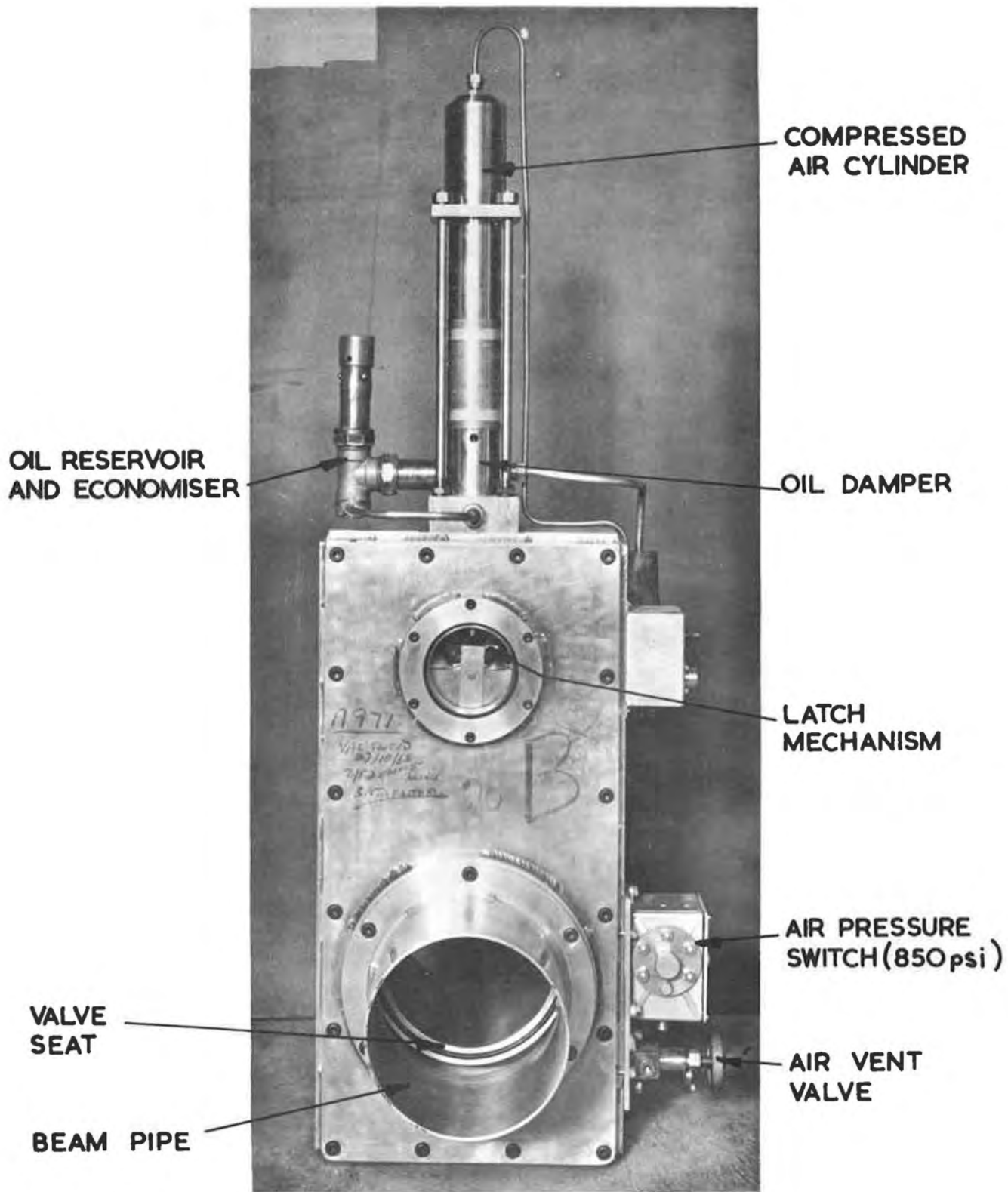


Fig. 8.10.7(ii) 8 in fast shut off valve.

8.11. Injector Vacuum System

8.11.1. Introduction

A comparison of the vacuum parameters of other linear accelerators established the optimum operating conditions for the injector (20) Pressures of less than 3×10^{-6} torr are generally considered necessary for reliable operation and it therefore seemed reasonable to aim at a pressure of 1 or 2×10^{-6} torr. The pumping speed was required to be proportional to surface area rather than to volume, since, at the lower pressures for a given speed, time for pump down would depend on total outgassing rate. On this basis a pumping speed of 8,000 litres/s was specified for the linac tank at a working pressure of 10^{-6} torr. The buncher and debuncher were rated proportionately for pumping speed. Operating conditions for the d.c. gun are quite different and the pumping capacity was determined according to the standard procedures for d.c. accelerators.

8.11.2. Linac Vacuum System

The most successful linacs have used mercury diffusion pumps. Oil contamination was known to increase X-ray production and the likelihood of multipactor phenomena occurring. Although it was thought possible that modern oil pumps could be provided with considerable improvement over previous oil systems, there seemed no reason to pass over a mercury system provided refrigeration equipment for the necessary traps was available in a reasonable time and at a reasonable cost.

As part of the development of the r.f. power system, a high-power test cavity was used equipped with a 24 in oil diffusion pump. The tests on the cavity were extremely successful. An ultimate pressure of 2×10^{-7} torr could be obtained in about 100 hours and the extent of back-streaming of the oil was very small. The opportunity was also taken in the construction of the cavity to test the proposed method of finishing the mild steel tank for the linac. The interior was scoured, using No. 120 grit emery discs, until the surface appeared uniformly marked and free from oxide inclusions. This type of surface proved very suitable and no deterioration has been noted over five years of life. The only necessary precaution was the use of cotton gloves to prevent oxidation by finger grease.

While tests on this unit were being carried out, examination of the refrigeration problem for mercury pumps suggested that there were no insuperable problems and mercury was chosen as the working fluid.

The main difficulty in the construction of the linac tank was the machining of the vacuum joint. The large flange of the D shaped cover and the face of the mating surface of the base plate had to accommodate a trapezoidal groove for a $\frac{1}{2}$ in diameter rubber cord seal. A tolerance of ± 0.005 in was required and presented a difficult task considering the length and width of the base plate. The only machine available to do this job was a long bed horizontal borer. The vertical head travel was insufficient to allow any of the machining to be completed at one setting and could not meet the tolerance at the upper limit of the travel. The machine was modified to fit a milling attachment and the components were set up on edge (Fig.8.11.2(i)). When the lower half of each component had been machined it was inverted and the milling head reset.

A form cutter was used to machine the groove. At each corner of the base plate special attention was required. The groove was formed at 45° across the corner and the metal outside this groove was then removed down to the bottom of the

groove already cut. A special corner piece was then manufactured and fitted to form a correct outer wall to the groove all round the corner (Fig.8.11.2(ii)) After this machining, the finish was not acceptable for vacuum seal surfaces and a certain amount of dressing (by hand and by machine) had to be performed. Tolerance was achieved over most of the length of the groove (110 ft) but was exceeded over about 20 ft near one corner. This was further aggravated by variations in diameter of the rubber cord. These difficulties were eventually overcome by using 0.01 in shims in the groove and by selecting lengths of rubber cord which met the required tolerance and accepting a greater number of butt joints, which were not cemented, in the cord seal. After installation, it was necessary to modify the base plate supports to eliminate sag and some straightening (by heating) was required before a satisfactory seal could be obtained.

The linac r.f. cavity presented a considerable vacuum problem. Large surface areas involved a high outgassing rate and practically every component in the cavity had to be water cooled, in many cases by electrically isolated cooling circuits with demountable joints. Tapped holes for screw fixings were provided with the usual pump out holes to eliminate virtual leaks. Outgassing was reduced as far as possible by maintaining strict cleanliness at all stages of manufacture, especially by eliminating all materials such as cutting oils and fluxes from surfaces before and after assembly. Slots with a total cross sectional area of 1250 in² (about one and a half times the area of the pumping ports to the linac tank) were provided in the cavity to ensure adequate pumping speed within the liner.

The equipment fitted inside the drift tubes is 'dirty' from a vacuum point of view and it was decided to connect these to a separate roughing system. This involved connecting each drift tube to a manifold which runs the full length of the copper liner and passes through the base plate to roughing pumps. To safeguard the drift tubes from mechanical damage in the event of failure of pumps and interlocks, a spring loaded ball valve was incorporated in the manifold. This valve opens when the pressure difference, in either direction, between the inside of the drift tubes and the main vacuum vessel exceeds a few torr. Each water circuit on the drift tubes had to be connected through a seal on the base plate to the appropriate water supply.

The water cooling pipes on the liner itself had all their brazed joints vacuum tested before the pipe was soldered to the copper cylinder. The test allowed for a pressure difference across each joint of the same order and direction as will prevail in operation. This involved the design of "outer space test sleeves" which could be clamped over a joint as shown in Fig.8.11.2(iii). The space between the sleeve and the joint under test was evacuated and connected to a leak detector. The pipe was pressurised with the probe gas. All water pipe joints throughout the system, whether permanent or demountable, were tested in this way.

Manufacture of the drift tubes (Fig.8.11.2(iv)) was arranged so that welds and brazed joints were tested before they became inaccessible in the next stage of production. In this way each drift tube was subjected to six intermediate tests before the final test was carried out. It was found after delivery that the side arm soldered joints were particularly susceptible to mechanical damage and additional tests were necessary. These were carried out after the electrical tests on each drift tube, after transportation to the injector room, and finally after installation in the liner.

266 such tests were carried out on the 50 drift tubes and 12 drift tubes with leaks in excess of tolerance were eventually accepted. Those with the larger leaks



Fig. 8. 11. 2(i) Machining of the linac vacuum vessel.

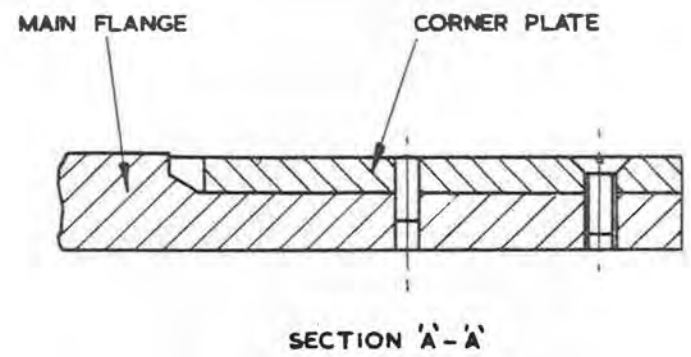
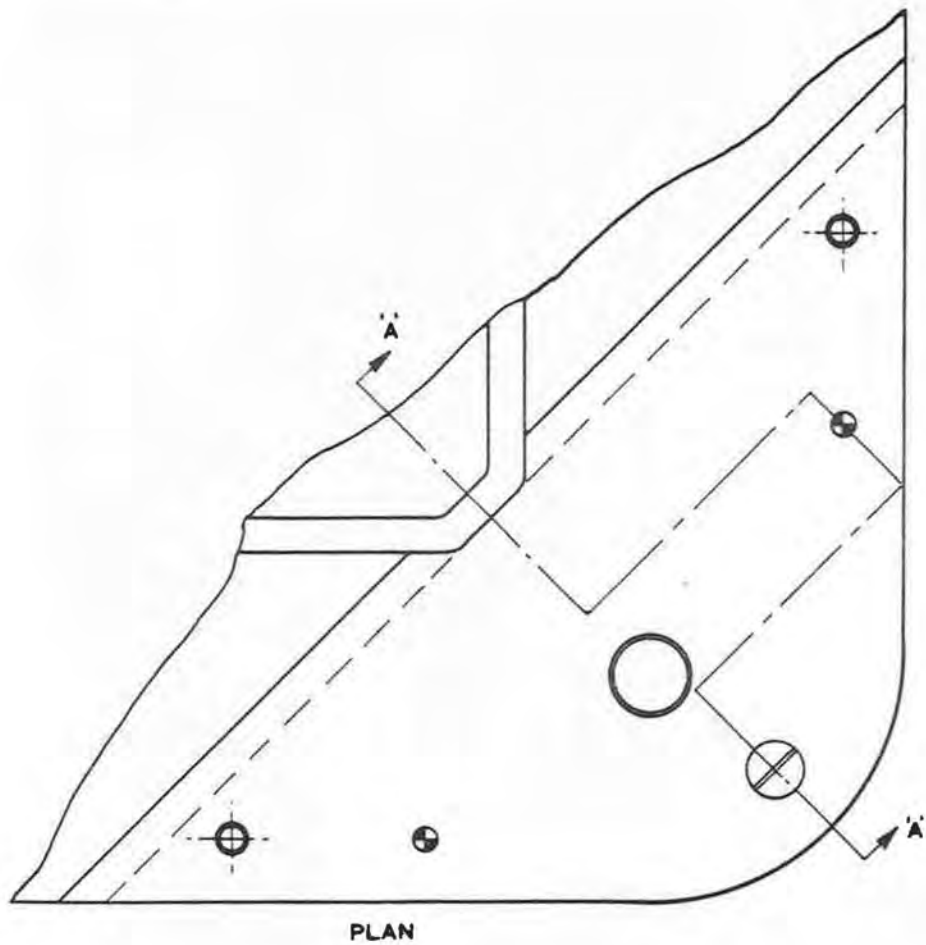


Fig. 8.11.2(ii) O-ring corner joint of the linac vacuum vessel

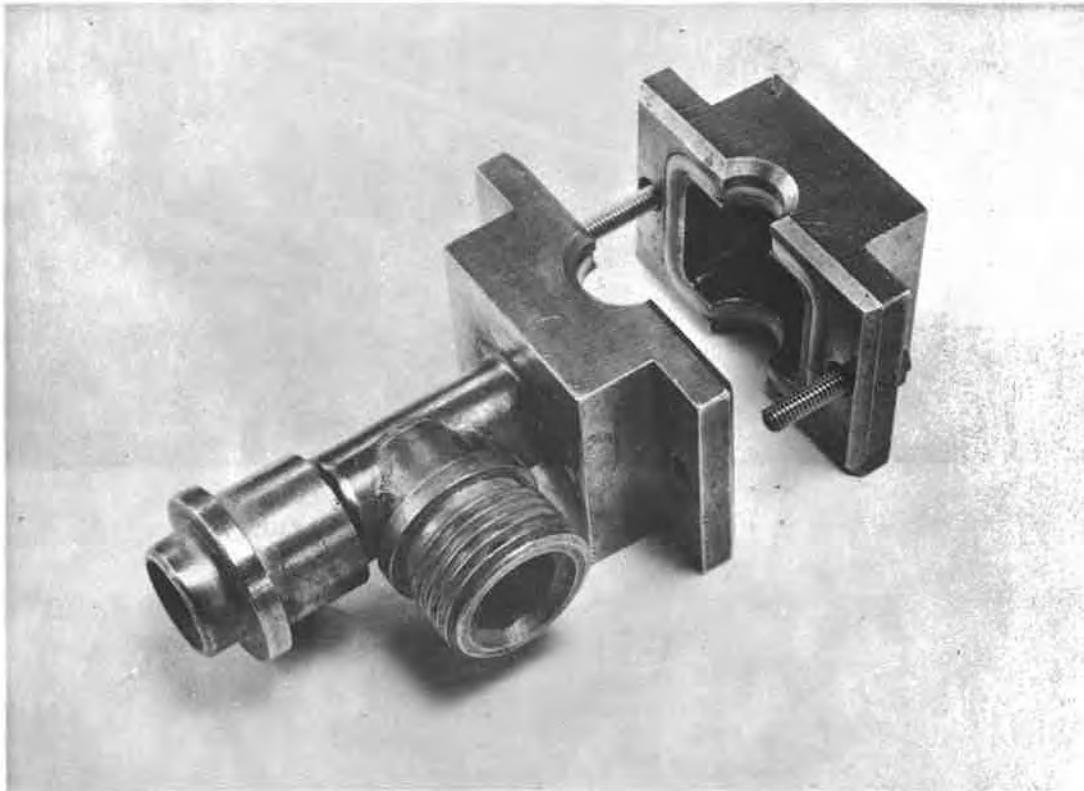


Fig. 8.11.2(iii) Outer space test sleeves.

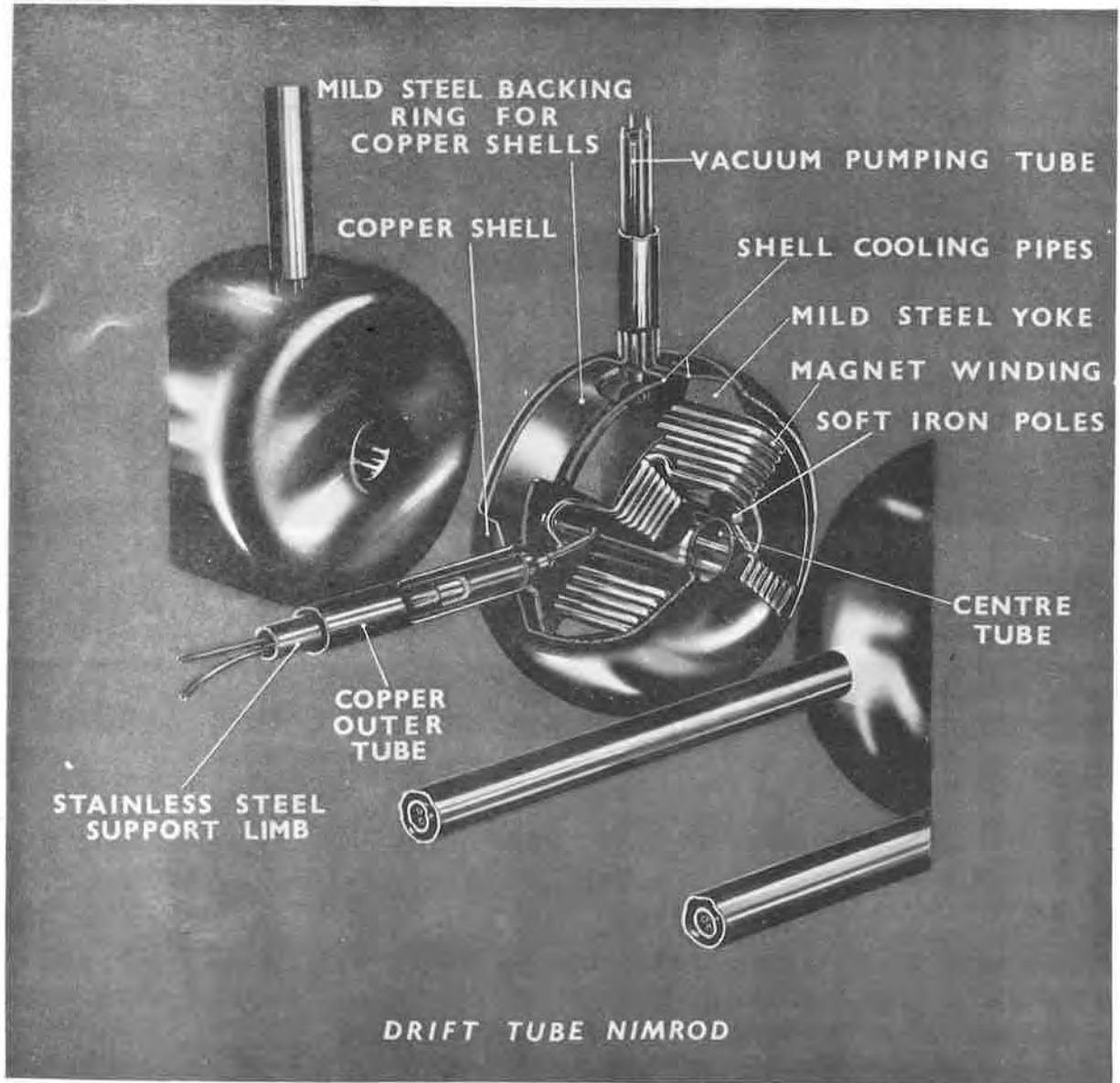


Fig. 8.11.2(iv) Linac drift tube.

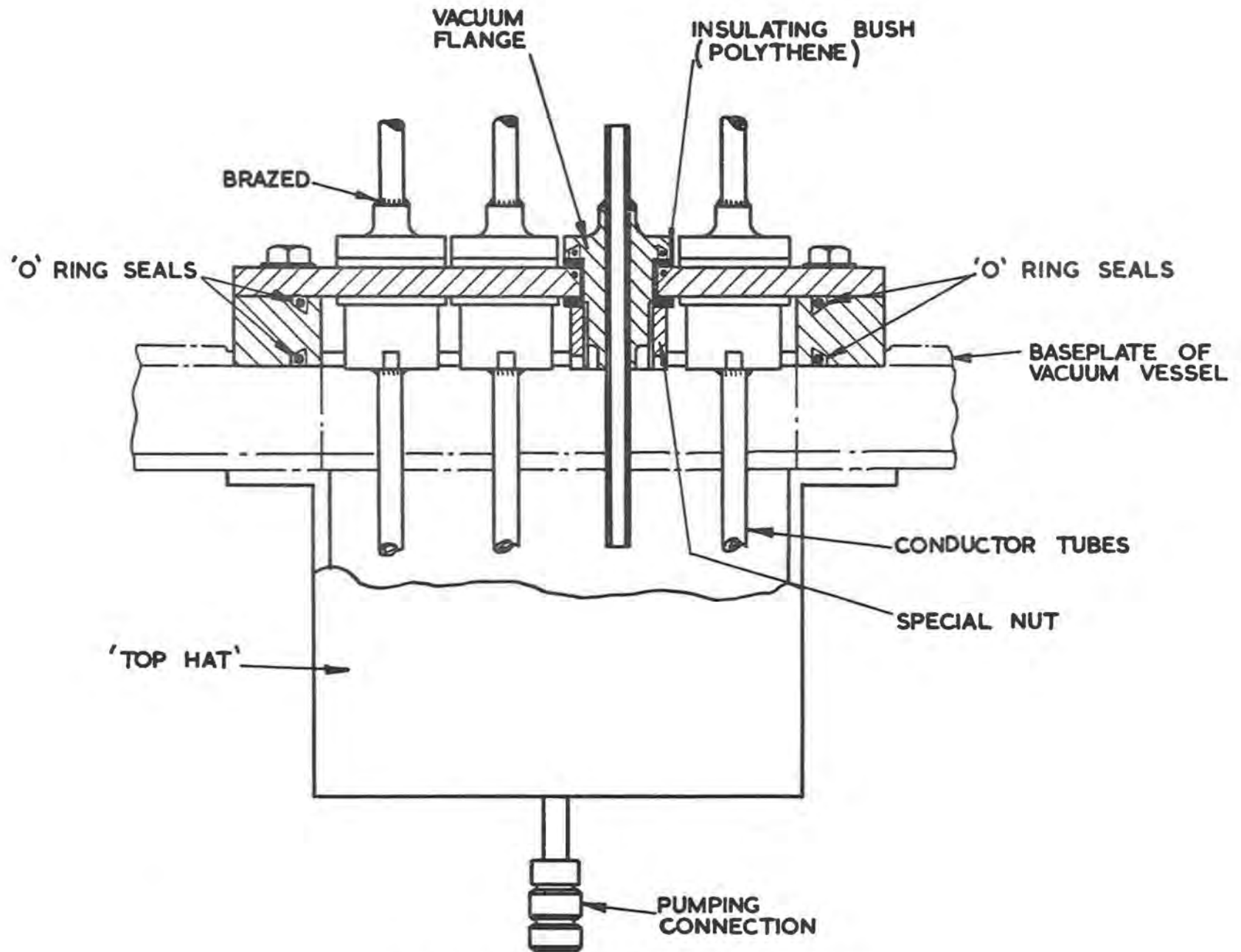


Fig. 8.11.2(v) 'Top hat' test on conductor tubes

were not connected to the roughing manifold since the outgassing of the interiors was less of a load on the high vacuum system than a continuous leak from the roughing system would be. A method of replacing the soft-soldered joint of the side arm by a braze could not be implemented because of the possibility of causing damage to the inner assembly of the drift tube.

Drift tube shell cooling pipes were connected, through the vertical support arm, to inlet and outlet manifolds running the length of the liner. Each branch of the manifold had only one demountable joint at the end of the drift tube support; any other necessary joints were brazed.

The quadrupole conductor windings on the other hand had to be insulated and, generally, four pairs of conductors were connected through a metal flange with an insulated polythene sleeve and were taken out through the base plate. The conductor pipes extended some 12 to 18 in below the base plate before being connected to flow switches. The same flanges had glass to metal seals carrying thermistor outputs for temperature monitoring of the liner. These seals have been very unsatisfactory and have virtually been 'potted' in epoxy resin to cure leaks. A more robust seal will be fitted when the opportunity arises. To test the whole installation it was necessary to provide a "top hat" (Fig.8.11.2(v)) on the under side of the base plate which could be evacuated to prove the base plate seal and the joint in the conductor pipes adjacent to the drift tube side support arm.

These cooling circuits introduced some three hundred demountable joints and approximately the same number of brazed joints, all of which are potential sources of water leaks into the vacuum system.

8.11.3. Preinjector and Drift Spaces

The other major parts of the injector vacuum system presented no great difficulty. The d.c. gun was the first section of the injector to be assembled and gave most trouble because personnel employed in the assembly work had not become accustomed to high vacuum techniques. Also the design incorporated types of 'O' ring groove which were subsequently discontinued in favour of fully trapped trapezoidal or, in certain instances, dovetail sections.

The flight tube between the d.c. gun and the linac (LEDS) and the linac and the inflector (HEDS) consists of lengths of aluminium pipe connected by probe boxes which take assemblies such as targets and probes. Gate valves were inserted at strategic positions so that the larger components could be isolated while alterations to the layout of the drift spaces proceeded or, alternatively, a particular component could receive attention without interfering with the remainder of the system (see Fig.3.1(i))

It was difficult to install more than two of the 6 in pumping units in the HEDS and it was intended to replace these with 75 litres/s ion pumps and to fit a 150 litres/s ion pump on the beam chopper. The ion pump on the chopper was installed first and has not proved very successful.

8.11.4. Pumping System

Four 24 in mercury pumps (Fig.8.11.4(i)), were provided to evacuate the linac tank and 9 in pumps for the other large cavities such as the buncher, debuncher and d.c. gun (Fig. 8.11.4(ii)). A number of 6 in pumps were provided for the flight tube. Each pumping unit consisted of a gate valve, a combined liquid air cooled spoon

trap and refrigerated chevron baffle and the mercury pump backed by a mechanical rotary pump. The chevron baffle serves to reduce the rate at which mercury collects on the spoon trap. On a 24 in unit without the chevron baffle the whole mercury charge of the pump could be transferred to the trap in one day but interposing the baffle at a temperature of -25°C , increases this time to more than 150 days.

The control system for the pumping units is essentially similar to that for the synchrotron oil pumps, the main differences being the absence of the vapour booster pump and the addition of the liquid air trap and its associated interlocks. The start up sequence required the mercury pump to be operating and the baffle chilled before liquid air was admitted to the trap otherwise it would collect unnecessary amounts of mercury vapour.

The liquid air system consists essentially of a number of direct condensation liquefying machines (Fig.8.11.4(iii)) supplying liquid air at atmospheric pressure to a depot collector which despatches batches of liquid into a reservoir which is pressurised to about 5 lb/in^2 gauge. Liquid from the reservoir is distributed to the traps via a vacuum insulated transfer line with a solenoid valve outlet to each trap. The solenoid is actuated by the pumping unit control system and by level sensing heads in the trap. A description of this system as originally conceived has been published (15). Much development work has been necessary and the system is not yet fully operational.

The rough pumping system for the injector comprises three 100 litres/s Rootes pump combinations identical to those used on the inner vessel of the main torus. The pumps are connected, via individual isolating valves, to a 10 in diameter roughing manifold from which a 9 in diameter branch is taken through a gate valve to the linac tank. The manifold is continued with reduced diameter to serve the other large cavities as well as individual sections of flight tube. In each case, electrically operated valves allow the items to be interlocked.

Individual pumping units of the injector vacuum system are started and run up to the ready condition locally and are then operated from the mimic panel in the injector hall. All the valves are operated by push buttons adjacent to the schematic position of the valve and there is indication of whether the valve is open or closed. When the appropriate pressures in the system, as determined by pressure switches, are achieved, they are indicated on the mimic panel and interlock the valves. For example: flight tube valves will not open unless the pressure on each side of the valve is less than 10^{-2} torr; roughing valves will not open unless air admittance valves in the same region are closed; high vacuum valves to pumping units will not open unless the volume to be connected to the pump is at a lower pressure than 10^{-2} torr and the appropriate roughing valve is closed; air admittance valves will not open unless a master key switch is operated and the appropriate high vacuum valves on pumping units together with flight tube valves for the particular sections are closed.

The leak rate tolerances were generally similar to those applying to the rest of the synchrotron. Exceptions included the linac tank, for which a leak rate of 2×10^{-3} torr litres/s was originally specified. There was considerable doubt that this standard could be achieved on a mild steel vessel of some 72,000 litres volume. Indeed the normal U.K.A.E.A. specification for vessels over one litre called for a pressure rise of less than 0.036 torr/hour (or a leak rate of 0.72 torr litres/s). However, calculation showed (Section 8.6.1), that using one 24 in oil pump for the tests, a leak rate of 10^{-4} torr litres/s would cause a partial pressure rise of

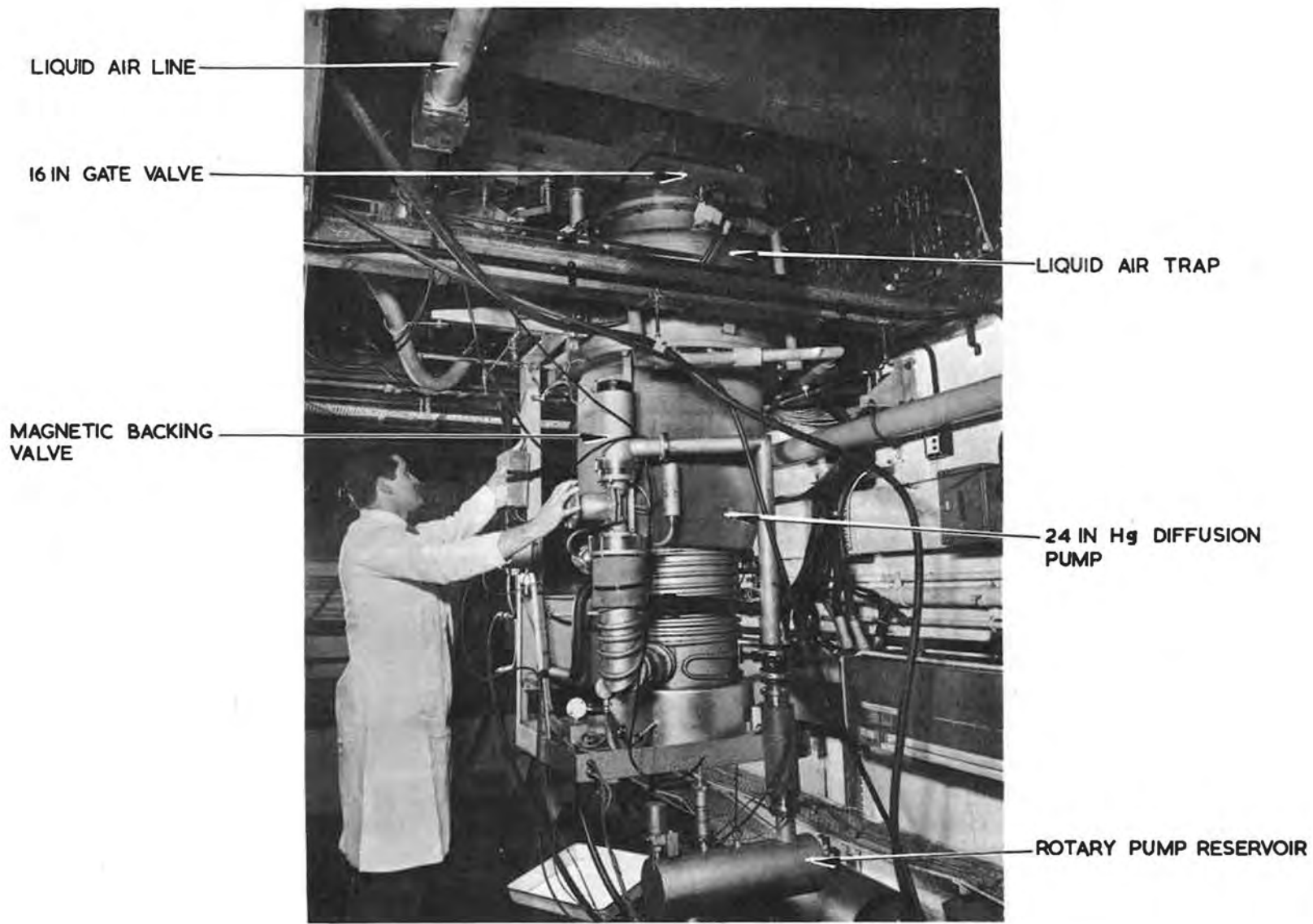


Fig. 8.11.4(i) An installed 24 in mercury pumping unit.

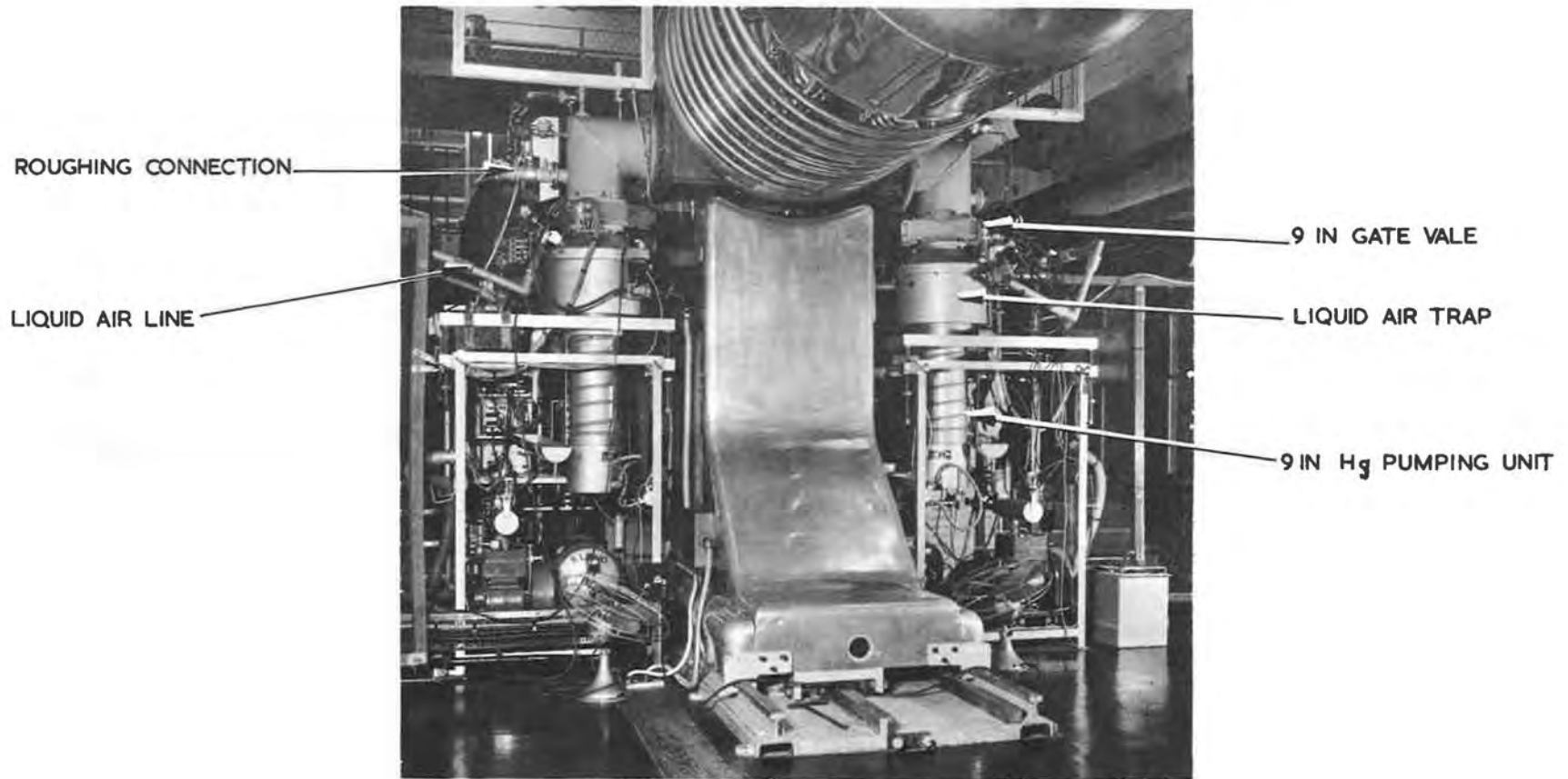


Fig. 8.11.4(ii) View of d.c. gun 9 in mercury pumping units.

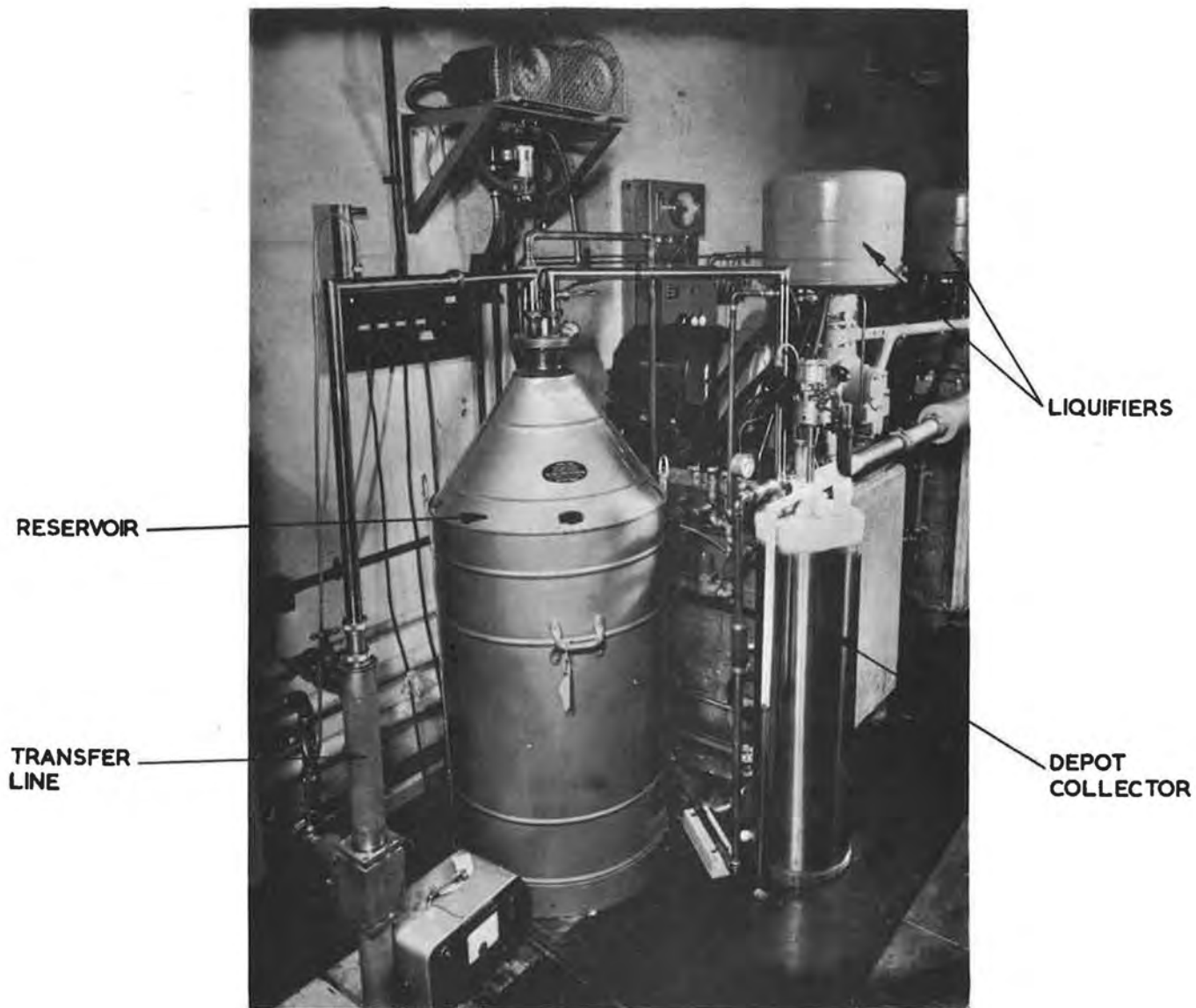


Fig. 8.11.4(iii) View of part of the liquid air system.

about 5×10^{-6} torr in the backing space after 5 s. This was at least four orders of magnitude greater than the minimum partial pressure detectable by a mass spectrometer leak detector in ideal conditions. Against a background due to other leaks and outgassing of the vessel walls this advantage might be reduced to one order of magnitude but it was still considered adequate for the specified leak rate to be attained. The doubt was soon dispelled for even on the first pump down before any leak detection was carried out the leak rate was 0.2 torr litres/s. No leaks were found in welded joints and after rectification of the main flange seal (as already described) and the replacement of many faulty 'O' ring seals on blank flanges and sight glasses, an overnight pressure rise equivalent to a leak rate of 2.5×10^{-4} torr litres/s was obtained.

The sensitivity of leak detection on the tank, using a mass spectrometer leak detector connected to the backing space of the prototype 24 in mercury pumping unit, was of the order of 2.5×10^{-3} torr litres/s for full scale deflection on the most sensitive range. The basic sensitivity of the mass spectrometer was 10^{-8} torr litres/s for the same deflection.

After assembly of the linac r.f. structure inside the tank, the initial leak rate was less than 2×10^{-3} torr litres/s. Using all the roughing and diffusion pumps a pressure of 2×10^{-6} torr was achieved in under 17 hours. After some pumping, the measured leak rate was 2.6×10^{-4} torr litres/s and under normal operating conditions, using only two of the four 24 in mercury pumps, a pressure of 2×10^{-6} torr was achieved in about 12 hours.

Since commissioning of the injector began, it has generally not been possible to use all four mercury pumps because of faulty spoon trap seals or because of the shortcomings of the liquid air system. Topping-up liquid air traps by hand or even using a semi-automatic system from a pressurised dewar, is tedious and time consuming and, while experimental work is in progress, is additionally troublesome because it is necessary to stop the injector operating every few hours while personnel are admitted to carry out the topping-up. It has involved carrying 6 to 10 dewars of 25 litres capacity into the injector hall at least three times in every 24 hours.

Plans are now being made to fit oil pumps on the linac tank in parallel with an experiment to determine the effect of oil pumps on the radio frequency cavities so that, in the event of continued difficulty with the liquid air system, information will be available to enable the choice between mercury and oil pumps to be re-assessed. There is some evidence to suggest that small amounts of oil vapour could assist in conditioning the surfaces of the drift tubes in the r.f. structure though it will probably result in a higher X-ray background.

REFERENCES FOR SECTION 8

1. R.J.B. Hadden. Gas Scattering in Proton Synchrotrons with variable rate of acceleration. AERE GP/R 2189.
2. A.J. Eggington and J.J. Wilkins. The ionisation produced by 7 GeV protons. Internal report HAG/EXP/8
3. A.J. Eggington and J.J. Wilkins. Estimates of ionisation dose in the 7 GeV synchrotron vacuum chamber. Internal report HAG/EXP/9
4. S.H. Cross. System Design and Choice of Materials for the Nimrod Vacuum System. Vacuum, Vol.10, No. 1/2, p.86.
5. Information supplied by C.I.B.A. (A.R.L.) Ltd.
6. R.J.B. Hadden and R. Sheldon. The Reinforced Resin Vacuum Envelope for the 7 GeV Proton Synchrotron. British Plastics Federation Symposium 1960, Paper 26.
7. I.D. Aitken, K. Ralph and R. Sheldon. Irradiation Studies on Anhydride Cured Epoxy Resins. AERE R 3339.
8. I.D. Aitken and R. Sheldon. The Significance of Phase Transition Effects in High Polymer Systems AERE L 134.
9. S.H. Cross. The vacuum chamber for the 7 GeV Proton Synchrotron. Internal report HAG/VAC/3.
10. R.J.B. Hadden and W. Spittle. The effects of proton and neutron irradiations on an epoxy resin vacuum chamber proposed for the Harwell 7 GeV Proton Synchrotron. AERE A/R 2690.
11. J.W. Burren and D. Morgan. High energy irradiation of the vacuum envelope of the 7 GeV Harwell synchrotron. AERE T/M 173
12. R.J.B. Hadden and G.J. Homer. Development Problems associated with the production of Nimrod Vacuum Chamber. NIRL/R/51
13. S.H. Lucas. The metalising of a glass reinforced epoxide vessel. I.C.I.Witton publication MD/RR/22/61.
14. I.D. Aitken, S.H. Cross and R. Sheldon. Quality Control on the Production of the 7 GeV Proton Synchrotron Vacuum Vessels. 17th Annual Meeting of the Reinforced Plastics Division, The Society of Plastics Industries, Inc. Section 15B.
15. C.E. Chapman, J. Langridge and R. Sheldon. The Repair of Reinforced Plastic Vacuum Envelopes for Nimrod. NIRL/R/61.
16. Special Nimrod Issue. Vacnique, Vol.2, No.7.
17. M.M. Cheshire and R.L. Redgrave. A Thermistor Vacuum Switch. NIRL/R/62.
18. R.J.B. Hadden and G.J. Homer. A Mechanical Safety Device for the Nimrod Vacuum System. NIRL/R/39.
19. H. Ishii and K. Nakayama. A fundamental defect in vacuum measurement with a McLeod vacuum gauge using a trap. AERE Trans. 949.
20. L.C.W. Hobbis. Thoughts on the Injector Vacuum System. Internal report HAG/INJ/8.

SECTION 9
CONTROL SYSTEM

The control system for the Nimrod machine is now almost completed with the installation entering its final stages. Almost all items of equipment have already operated under local control conditions and some large sections of the plant, such as the injector, have been remotely controlled from the main control room.

The control system embraces all the main items of plant such as the magnet and its power supply, the injector, the vacuum system, the radio-frequency accelerating cavity and its power supply, and the cooling plant, and integrates them into a common functioning machine, adding such interlocking and sequencing as may be required for personnel and equipment protection.

This report will take as examples for more complete description, the control aspects of the injector, vacuum system, coolant temperature and flow monitoring, personnel and safety interlocking and the main control room, these items being representative of the complete control system.

9.1. Injector.

9.1.1. Introduction.

Since the injector may be regarded as a linear accelerator which is complete in itself and is required to operate as such, especially in the early commissioning stages of Nimrod, it was necessary to design the control system so that it could either operate independently or be integrated at will into the main Nimrod control system. With this end in view, a local control room was provided and all control functions on the injector may be carried out from this position. When required the essential control functions can be extended to the main control room by the operation of changeover switches. The injector local control room can remain manned during the operation of the injector alone but when high energy beams are achieved in the synchrotron, the injector will need to be remotely controlled from the main control room.

Figs. 9.1.1(i) and 9.1.1(ii) show the layout and current appearance of the injector control room, which is situated in the injector hall adjacent to the H.T. platform and d.c. gun. Fig. 9.1.1(iii) shows a simplified block schematic of the injector control system.

The injector first operated successfully under local control in August 1961.

9.1.2. E.H.T. Supply, E.H.T. Platform and D.C. Gun.

A 600 kV d.c. supply is produced by an electrostatic generator. This supply feeds the d.c. gun which accelerates protons from the pulsed ion source into the linear accelerator. Since all the equipment associated with the ion source is at +600 kV with respect to earth, all control signals must be suitably isolated and accordingly compressed air is used to convey control signals through polythene tubes to the platform. Ion source trigger signals pass via light guides and photocells, and other control adjustments are carried out by reversible geared motor units with long insulated drive shafts. Electrical power to the equipment on the H.T. platform is provided by 115 V, 2000 c/s; 110 V, 50 c/s and 24 V d.c. generators mounted with their control equipment on the H.T. platform. The compressed air links provide control signals for sequence interlocking and

protection; other controls comprise E.H.T. voltage level, d.c. gun operating parameters and monitoring.

9.1.3. R.F. Drive.

More than 1 MW of r.f. power, at a frequency of 115 Mc/s and a pulse length of 2.5 ms is available to provide the r.f. drive for the linear accelerator. This power is obtained from a large triode valve, either driven from a crystal oscillator or run as a self oscillator by feedback, coupled directly from the linear accelerator resonant cavity. A pulse modulator provides 30 kV pulses of 2.5 ms duration to the power triode via a pulse transformer and ignitron from a delay line accurately charged by a grid-controlled rectifier system. All aspects of r.f. valve and modulator operation are sequence controlled and interlocked to ensure correct operation, and full remote operating and monitoring facilities are available.

R.F. drive for the buncher and debuncher is obtained via pick-up loops from the linac. Monitoring and remote motorised control are provided for drive and phase adjustments.

9.1.4. Tuners and Tilters.

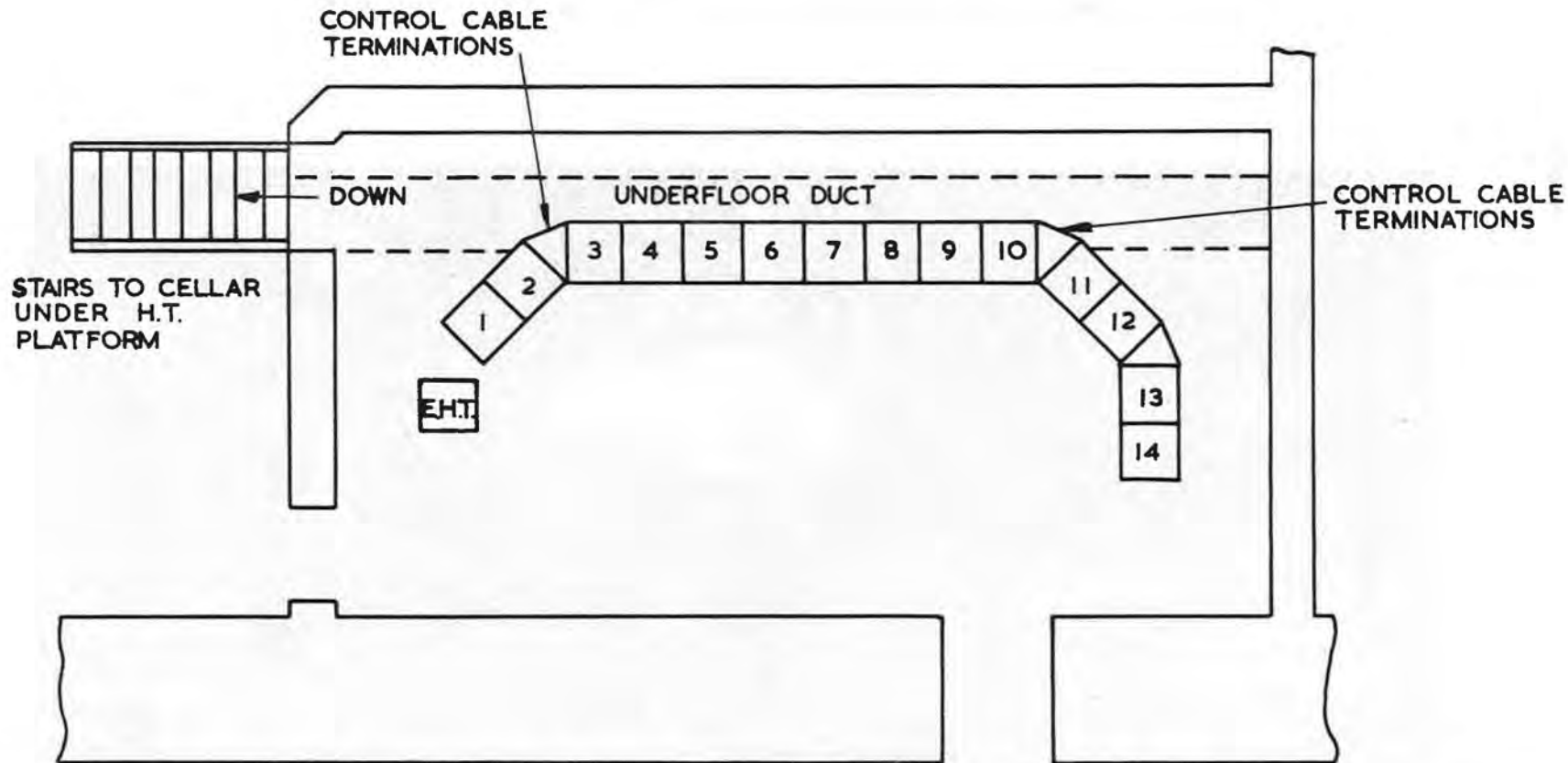
The buncher, linac and debuncher each form resonant cavities tuned to a frequency of 115 Mc/s. Sections of the r.f. liners of these vessels are arranged to incorporate flexibly mounted pads (tuners and tilters), movement of which modify the effective physical dimensions of the vessels and so the resonant frequency and the field configuration. In the case of the buncher this adjustment is made remotely by push button from the control room but for the linac and debuncher, motorised servo-controlled tuners are provided. Remote indication of pad movement, for both manual and servo tuners, is given by position indicators in the control room.

9.1.5. Quadrupoles and Steering Magnets.

The linac incorporates over 70 quadrupole focussing and beam steering magnets, the majority of which are water-cooled and contained within the vacuum space. The power requirements of these magnets varies according to their position and purpose, but in all cases the supply must be stabilised within close limits and the ripple voltage must be kept low. Voltage or current stabilisation via electronic regulators is employed for the control of the transducer-rectifier power units which vary in capacity from 2 kW to 150 kW. Fast response is attained in some cases by the use of flux-reset half-cycle transducer circuits, and stabilities vary from about $\pm 0.5\%$ in the case of the quadrupole magnets down to $\pm 0.03\%$ in the case of the inflector magnets. The voltage stabilised units employ precision potential dividers in the sensing circuits, while both shunts and d.c. current transformers have been used for the current stabilised power units. Most of the units incorporate some form of automatic current limiting or high speed short-circuit protection, and both selenium and silicon diodes are employed.

Where a number of magnets are grouped in series on to a common power unit, variable shunt resistor or transistorised networks are employed in conjunction with supply stabilisation in order to adjust the current in individual magnets.

Full remote control and monitoring of voltages and currents for the rectifier sets is available in the injector control room and main control room.



RACK	LAYOUT OF EQUIPMENT
1,2,3	H.T. PLATFORM & GUN
4	BEAM MONITORING
5,6	LINAC R.F. DRIVE
7,8	BUNCHER, LINAC & DE-BUNCHER
9	LINAC QUADRUPOLE POWER SUPPLY

RACK	LAYOUT OF EQUIPMENT
10	BEAM MONITORING OSCILLOSCOPES DELAY UNIT
11	DRIFT SPACE QUADRUPOLE POWER SUPPLIES
12	GUN, LINAC, BUNCHER, DE-BUNCHER, D.S. & VAC IND ^c .
13	LINAC & DRIFT SPACE TEMP. MONITORING
14	STEERING MAGNETS, INFLECTOR

SCALE = 0 1 2 3 4
FEET

Fig. 9.1.1 (i) Layout of Injector Control Room

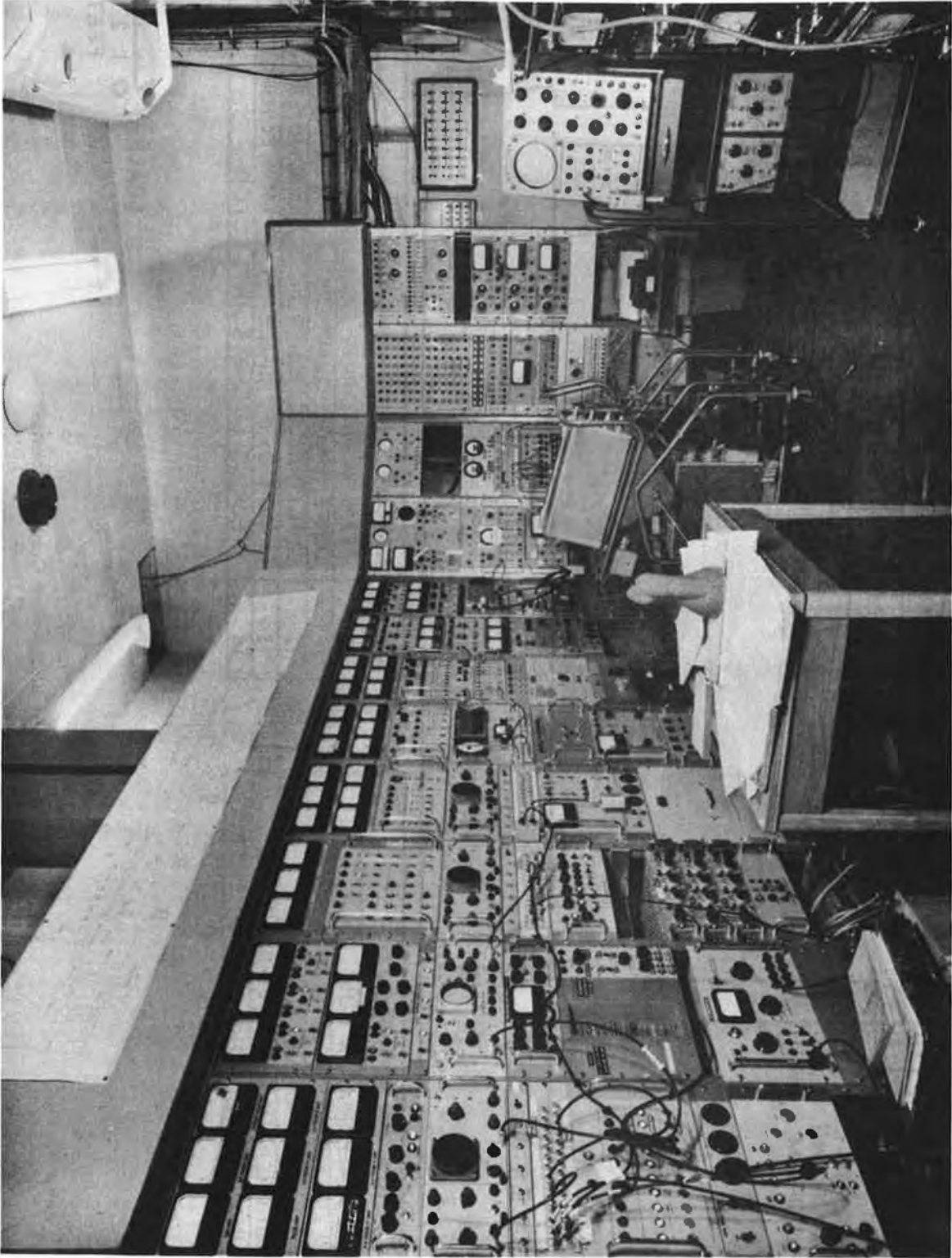


Fig. 9. 1. 1 (ii) General View of Injector Control Room

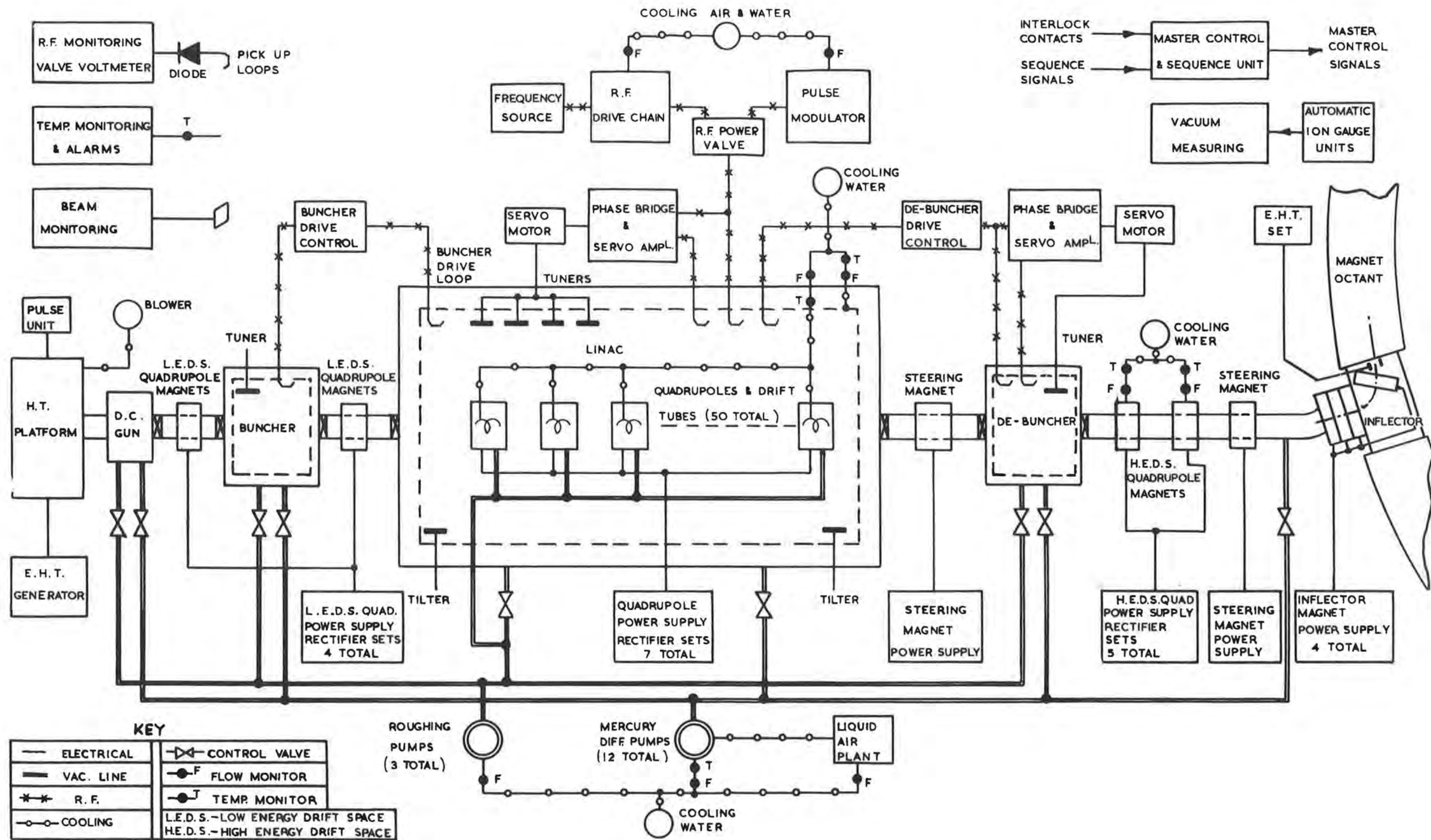


Fig. 9. 1. 1(iii) Block Diagram of Injector Control System.

9.1.6. Other Control Facilities.

Other facilities on the injector, such as vacuum, temperature control and monitoring and safety interlocking are dealt with below under these general headings.

9.2. Vacuum System.

9.2.1. Introduction.

The Nimrod vacuum system is a large and important part of the machine. The vacuum pressure required for operation is approximately 10^{-6} torr and this has to be achieved over the length of the injector and throughout the synchrotron inner vacuum vessel (150 ft dia.).

9.2.2. Injector Vacuum Controls.

The system is initially roughed by three two-stage mechanical pumping units, each comprising a Kinney pump, a Roots pump and refrigerated oil traps. These pumps are automatically controlled and pump the 45 ft long linac vacuum vessel and the auxiliary vessels down to a pressure of 10^{-2} torr. Twelve mercury diffusion pumps, mostly of 9 in and 24 in type, provide the high vacuum pumping capacity. Each pump has its own local control cubicle, with sequence interlocking, protective features and vacuum monitoring, which is capable of completely automatic remote operation. Fig. 9.2.2(i) is a schematic of the type of control circuit used for all the Nimrod diffusion pumps, there being only slight variations between mercury and oil pump circuits. In all cases, the equipment is so arranged that under a pump fault condition the respective gate valve is closed automatically, the pump is shut down and the appropriate fault indication is exhibited. The pumps are fitted with refrigerated baffles and traps cooled by liquid air. The liquid air is produced by four air liquefiers adapted for semi-automatic operation. The liquid air is dispensed to the traps on the diffusion pumps, via a reservoir and vacuum insulated distribution main, on a time-controlled basis and further controlled by liquid air level-switches on the pumps.

A combined "mimic diagram" and master control station in the injector room integrates the fifteen vacuum-pumping units, four air liquefiers, fifty solenoid-operated vacuum valves and numerous pressure switches into a single operational unit. This master control station indicates the status of the complete injector vacuum system at any time and gives control from a central position. Additionally, since both flexible and correct operation must be ensured, the entire system is selectively interlocked in such a way that only eventualities potentially detrimental to the prevailing operating conditions are prevented and a rigid operational sequence is not imposed. This gives the required flexibility.

Finally the injector vacuum system is integrated into the main synchrotron vacuum system, and control is extended to the main control room. Isolation of the two vacuum systems under fault conditions is achieved by incorporating a high speed shut-off valve in the linac high energy drift space.

9.2.3. Main Vacuum Vessel Controls.

The Nimrod main vacuum vessel is of double-walled construction. The vacuum required in the vessels for normal operation is about 10^{-6} torr for the inner vessel and < 1 torr for the outer vessel. The maximum differential pressure permissible at any time between inner and outer vessel is 2 torr.

Five 24 in oil diffusion pumps per octant and two 12 in oil diffusion pumps per straight section (i.e. a total of 56 pumps) comprise the high vacuum pumping capacity for the inner vessel which is initially roughed by eight two-stage roughing pumps of similar type to those employed on the injector. The outer vessel

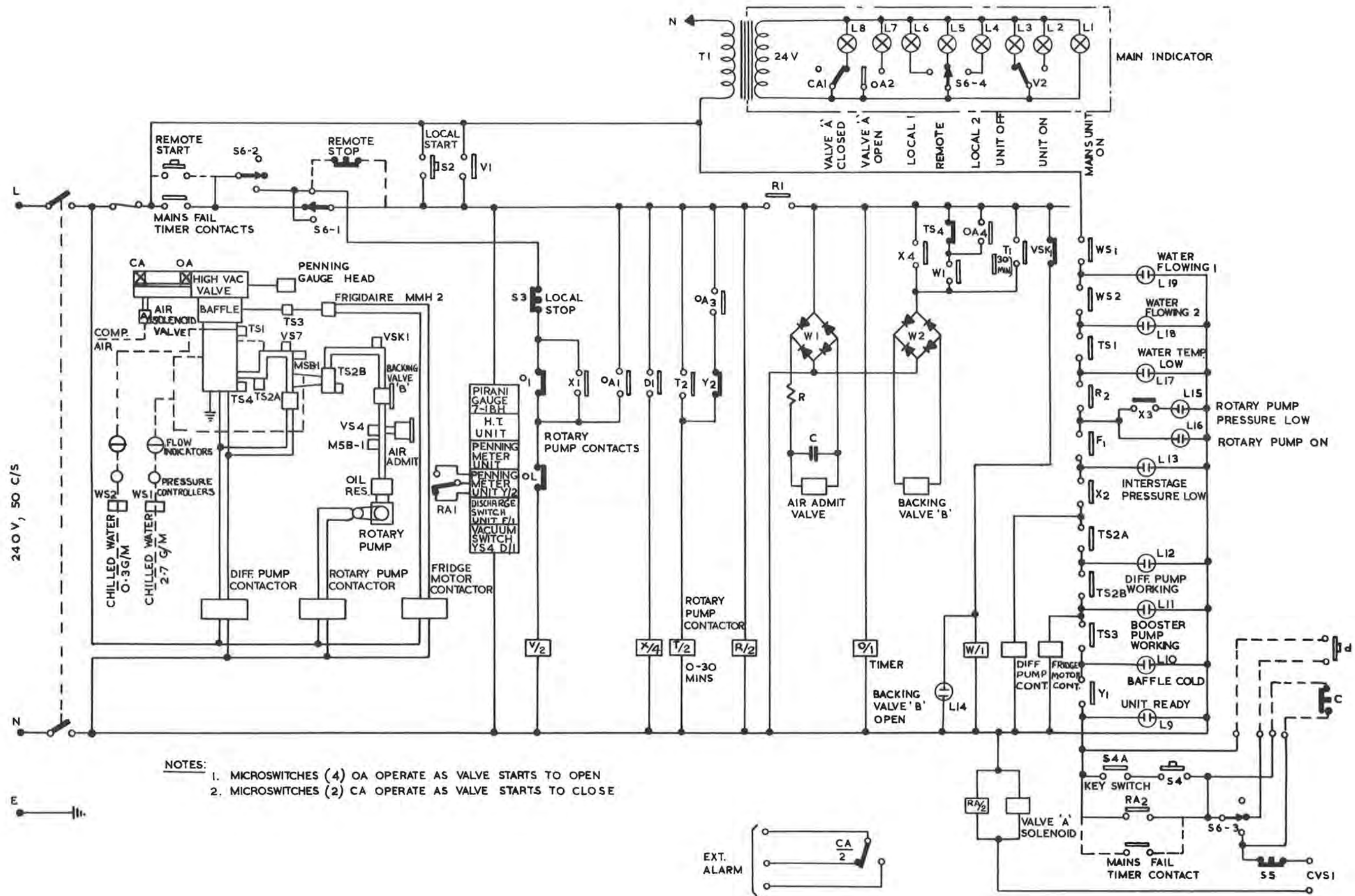


Fig. 9.2.2(i) Schematic Circuit Diagram of 24 in. Oil Diffusion Pump Unit.

MIMIC DIAGRAM

REMOTE CONTROL
PANELS

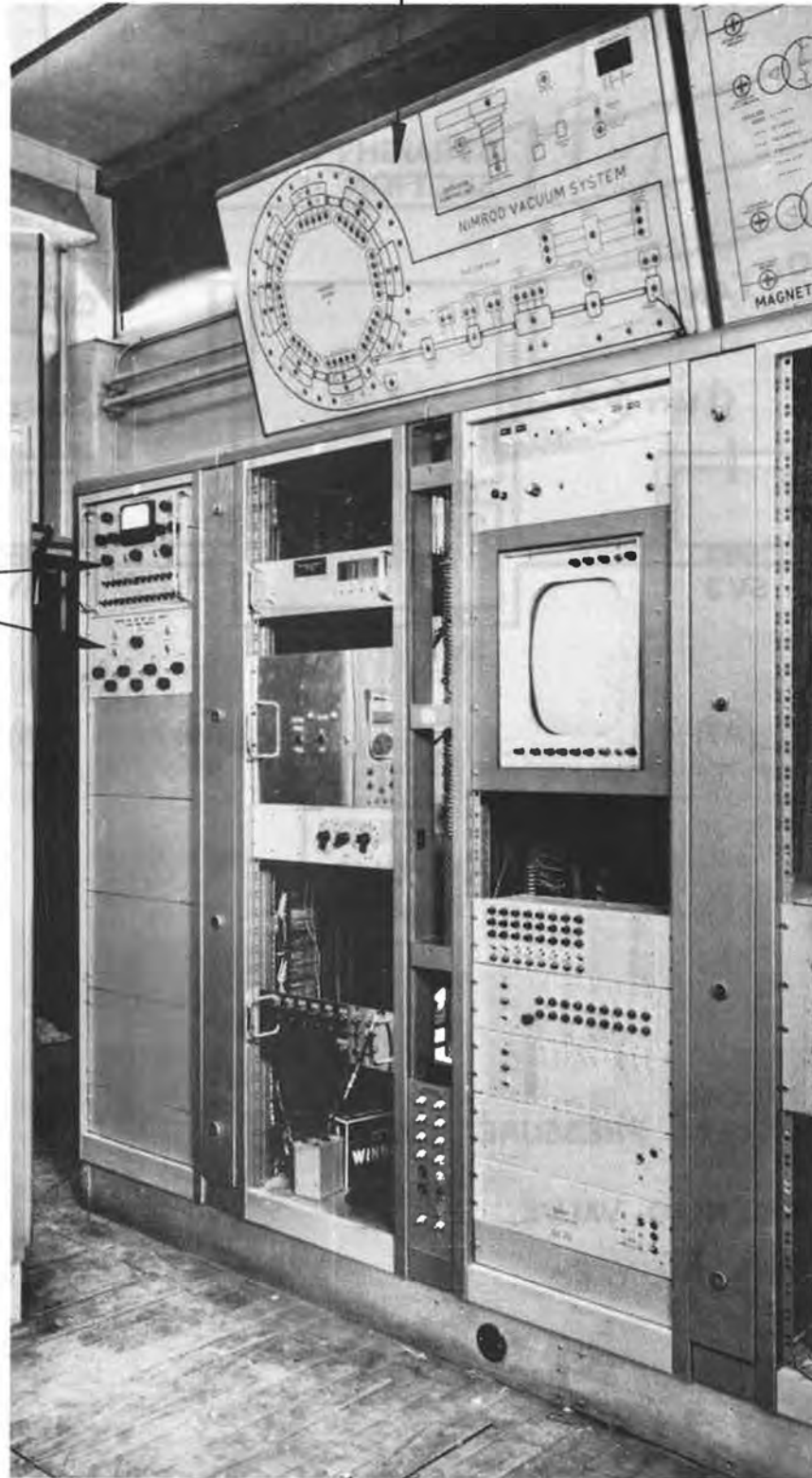
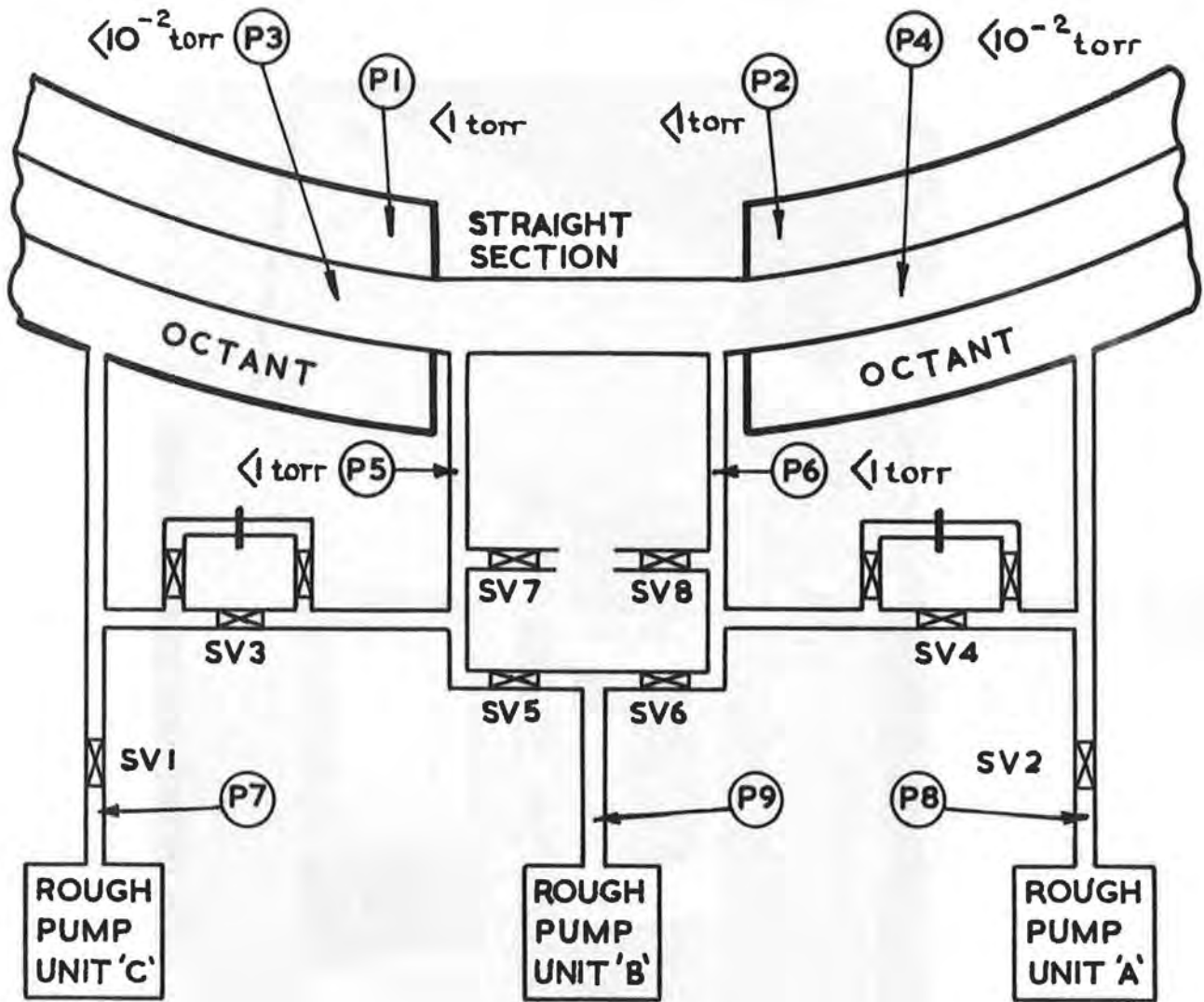


Fig. 9.2.3 (i) Vacuum System Mimic Diagram and Control Panels (in Main Control Room)



- (P) VACUUM PRESSURE SWITCH
- ☒ SOLENOID VALVE
- | BURSTING DISC

Fig. 9.2.3. (ii) Block Diagram of a Straight Section Interlock and Roughing System

is continually roughed by a maximum of two roughing pumps per octant.

All the pumping units are equipped with their own local control systems which are capable of monitoring and controlling operation in a manner similar to that already described for the injector pumps. These local controls are then grouped together in the magnet room to provide a single control and indicating point for the whole vacuum system. Finally, a minimum number of controls, for the diffusion pumps only, is taken back to the main control room where, in conjunction with a "mimic diagram" and associated selector switches, facilities are provided for stopping and starting any diffusion pump, opening or closing its gate valve, and displaying the working status of any selected pump in detail.

Fig. 9.2.3(i) is a photograph of the main control room "mimic diagram" and selector switches for the remote control of the entire Nimrod vacuum system.

Since it is essential to keep the differential pressure between inner and outer vessels to a minimum at all times considerable care is needed during pump down because of the different pumping speeds and impedances encountered. Fig. 9.2.3(ii) is a block diagram of the system employed at each straight section. It will be seen that inner and outer vessel pressures are continually monitored at many points and any excess differential pressure causes the opening of pressure equalising valves. During initial roughing the operation of the various valves is sequence controlled so that at this stage all the equalising valves are open and the inner and outer vessels are pumped together. When the pressure has reduced to 1 torr the equalising valves close and separate pumping continues under the monitoring of the pressure switches. The system is designed to fail-safe and in the event of any fault the equalising valves open. As a further safeguard bursting diaphragms are fitted across the equalising valves; these are designed to rupture with excessive differential pressure and so equalise the inner and outer vessel pressures.

Normally the inner vessel is a continuous vacuum space, while the outer vessel is effectively eight separate vessels since there is no double wall at the straight sections. This has involved considerable interlocking to ensure safe operation and the maintenance of minimum differential pressures at all times: it also dictated the early decision to operate the system as an integrated whole, rather than in sections which could be out-of-step in a vacuum sense. However, for the early commissioning of the vacuum system, single-octant working has been found necessary and temporary modifications have been carried out to achieve this. A more permanent system to permit sections to be pumped separately under certain closely controlled conditions has been worked out.

9.2.4. Vacuum Gauges and Switches.

In order to ensure effective control of a vacuum system as large as that for Nimrod, reliable methods are required for measuring a range of pressures. Each of the many diffusion pumps is equipped with pressure gauges and switches of the Penning, Pirani and hot wire type, operating over the range 10^{-6} torr to 10 torr. These instruments provide local indication of pressure and also interlock signals for the control circuits of the pumps.

Approximately 100 vacuum switches operating in the range 10^{-2} torr to 1 torr are used for the monitoring of the pressure in various positions in the injector and main vessel. These switches, which are of thermistor-transistor type, have been specially developed for this work and are fully described in Section 8.

The units give local indication of pressure and incorporate a relay coming into operation at a fixed pressure. Since the head amplifiers and switching units are transistorised, they are installed in the cellars under the magnet room to minimise radiation effects.

Indication of high vacuum in the range 10^{-3} torr to 10^{-8} torr is provided by specially developed ion gauges. These provide local indications of vacuum over a wide series of ranges chosen by selector switches. A further position on these switches provides a logarithmic output covering the range 10^{-4} torr to 10^{-7} torr. The outputs from the ion gauges are applied to three multi-channel recorders remotely situated in the main control room, so providing a continuous record of the vacuum conditions in the various parts of the machine. A further single-point recorder capable of being switched to any of the ion gauges and fitted with a repeater slide-wire is used to provide vacuum measuring facilities in the main control room, both at the control rack and on the main desk.

Provision is made, at the racks in the main control room, for remote switching to a standby ion gauge head.

9.3. Cooling Plant, Temperature Monitoring and Flow Monitoring.

9.3.1. Introduction.

Nimrod has many components, such as magnets and power supplies, which dissipate large quantities of heat. In most cases this heat is removed, via a closed-circuit cooling water system, to the main cooling towers. Advantage has been taken of this water cooling to reduce physical dimensions to a minimum and to increase current densities in conductors to a practical maximum. These factors indicate that if a complete or even partial water flow failure occurs, dangerous increases in temperature would probably result, causing damage to insulation or resulting in unacceptable changes in the length of magnet conductors.

Some impression of the scale of the problem is conveyed by the fact that on the main synchrotron magnet and associated pole face windings alone there are respectively 672 and 512 separate parallel water circuits and the peak pulse power dissipated in the main windings is about 12 MW, with a mean dissipation of a quarter of this.

Continuous temperature monitoring together with water flow monitoring is employed to ensure the detection of faulty conditions.

9.3.2. Temperature Monitoring.

There are two types of temperature monitoring currently in operation on the Nimrod cooling systems. The first of these is of the simple thermostat type which is employed on individual water circuits, especially where these are scattered. A high degree of accuracy is not required and the alarm condition is for a change in temperature in one direction only. Many hundreds of thermostats are used in this way, e.g. each of the 68 diffusion pumps is fitted with at least 4 thermostats for monitoring the operating temperature of various parts of the pump. The thermostats are fitted with contacts which perform interlocking and/or alarm and indication duties. No actual measurement of temperature is possible with this system.

The second type is considerably more sophisticated and permits sequential monitoring of large numbers of points for both high and low deviations of temperature, alarm and/or trip indications and local and remote measurement of temperature as required. It is installed in two separate designs: the earlier was installed about 4 years ago for the injector, and the later was recently installed for the synchrotron magnet and pole face windings. Both designs employ thermistors as the temperature sensing element.

Thermistors are available in a wide range of physical shapes (discs, rods, pellets, beads, etc.) and a range of resistances varying from less than 10 Ω to 1000 M Ω . The permissible temperature range is about -60°C to $+400^{\circ}\text{C}$ (reduced for some types). They were chosen in preference to thermocouples or resistance thermometers because of overall advantages when cost, size, robustness and performance for the particular duty (e.g. long leads with the risk of pick-up, etc.) were considered.

The chief disadvantage of thermistors is the non-linear relationship between the resistance R_T and the absolute temperature T , this being of the form $R_T = a \exp (b/T)$ where a and b are constants. However circuits can be designed which minimise the effects of this non-linearity and this has been done.

In the case of the injector temperature monitoring system the thermistors, many of which are inside the vacuum space and specially encapsulated, are sequentially scanned by uniselectors, which place each thermistor in turn across a Wheatstone Bridge circuit where they are compared with a standard resistor. The bridge is initially balanced for nominal temperature and any deviations, either high or low, cause resistance changes in a thermistor, creating unbalance conditions in the bridge. The unbalance of the bridge is detected in this design by a sensitive moving coil relay. This system has worked well over a period of several years, and its performance is limited only by the operating speed of the moving coil relay and the acceptable cycling rate for the uniselectors. The present cycling rate is 1 point/2s which is about the maximum rate for the moving coil relay. This is thought to be a little too slow and work is in hand to redesign the error detector circuit. The thermistors are individually trimmed for variations in resistance due to manufacturing tolerance and differing lead lengths, and the system is capable of an accuracy of $\pm 0.5^{\circ}\text{C}$ over the working range. Alarm and trip points operate at the nominal temperature $\pm 2^{\circ}\text{C}$ or $\pm 5^{\circ}\text{C}$ depending on the application. Fig. 9.3.2(i) is a photograph of this equipment.

The basic design used for the injector was reconsidered when the much larger systems required for the synchrotron magnet were being produced. The same basic thermistor sensing element was retained but the sequencing uniselectors were replaced by specially developed 100 way transistorised switching units. These switching units are completely static in nature and are driven by 10 way gas-tube counters of commercial design, and also provide indication (in the main control room) of the actual points being measured. This system is capable of an extremely high speed of operation (e.g. each 100 way unit could cycle, if required, at 2000 points/s) and is economical both in equipment cost and cabling. As with the previous scheme, facilities are provided for remote manual selection of thermistors and individual temperature measurement. During normal monitoring, any error signals detected by the bridges are fed to low-drift transistor amplifiers before operating alarm or trip relays. A cycling speed of 10 points/s has been adopted with sixteen 100 way units running in parallel, so that 1600 points can be completely surveyed every 10 s.

Owing to the large number of ways involved, it was decided to dispense with individual trimming for the thermistors, and accordingly types with a manufacturing tolerance of $\pm 2\%$ on resistance were chosen, together with circuit values sufficiently high to swamp variations due to different lead lengths. This has resulted in a minimum of components and has considerably reduced the setting-up time required, without increasing the maximum error over the operating range to greater than $\pm 1^{\circ}\text{C}$. This error could be reduced to about $\pm 0.5^{\circ}\text{C}$ if individual trimming of each point were added to the current design.

Figs. 9.3.2(ii), 9.3.2(iii) and 9.3.2(iv) show various elements of this transistorised version of the temperature monitoring system as applied to the synchrotron magnet and pole-face windings. It has been installed and is currently being commissioned. A report (NIRL/R/48) describes the system in greater detail.

9.3.3. Coolant Flow Monitoring.

In addition to temperature monitoring, continuous water flow monitoring is also carried out on all important circuits.



Fig. 9.3.2 (i) Temperature Monitoring Equipment for the Injector

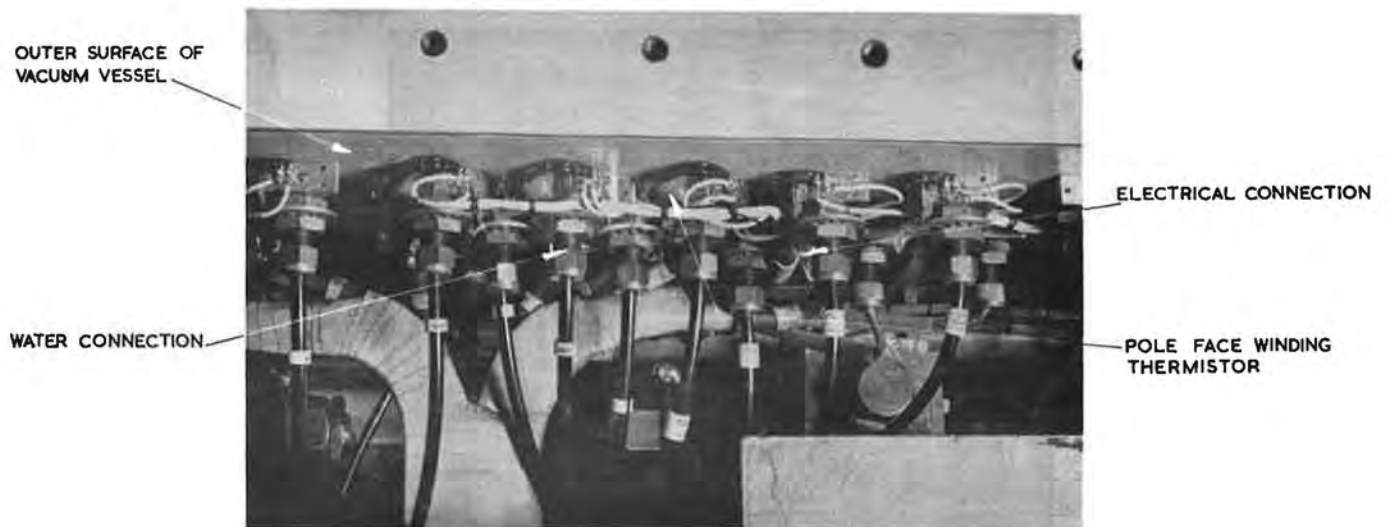


Fig. 9.3.2 (ii) Thermistors Mounted on Pole Face Winding Connections



Fig. 9.3.2 (iii) Transistorised Gating and Error Sensing Equipment for 1600 Way High Speed Temperature Monitoring System

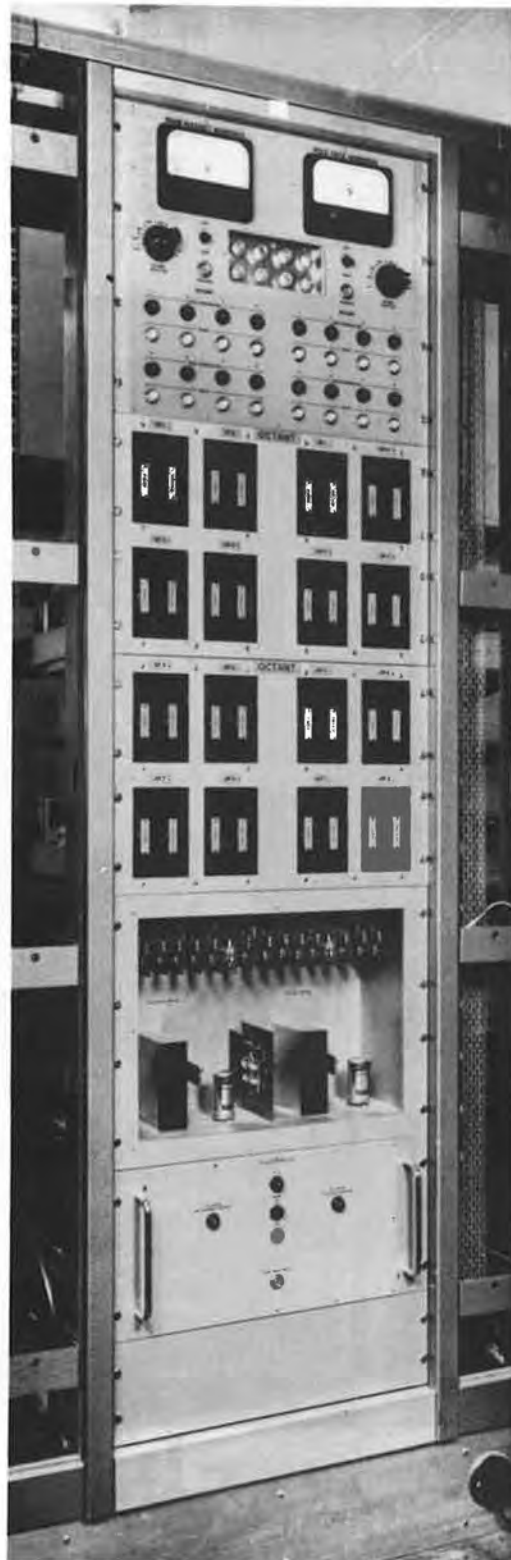


Fig. 9.3.2 (iv) Temperature Monitoring Control Panel (in Main Control Room)

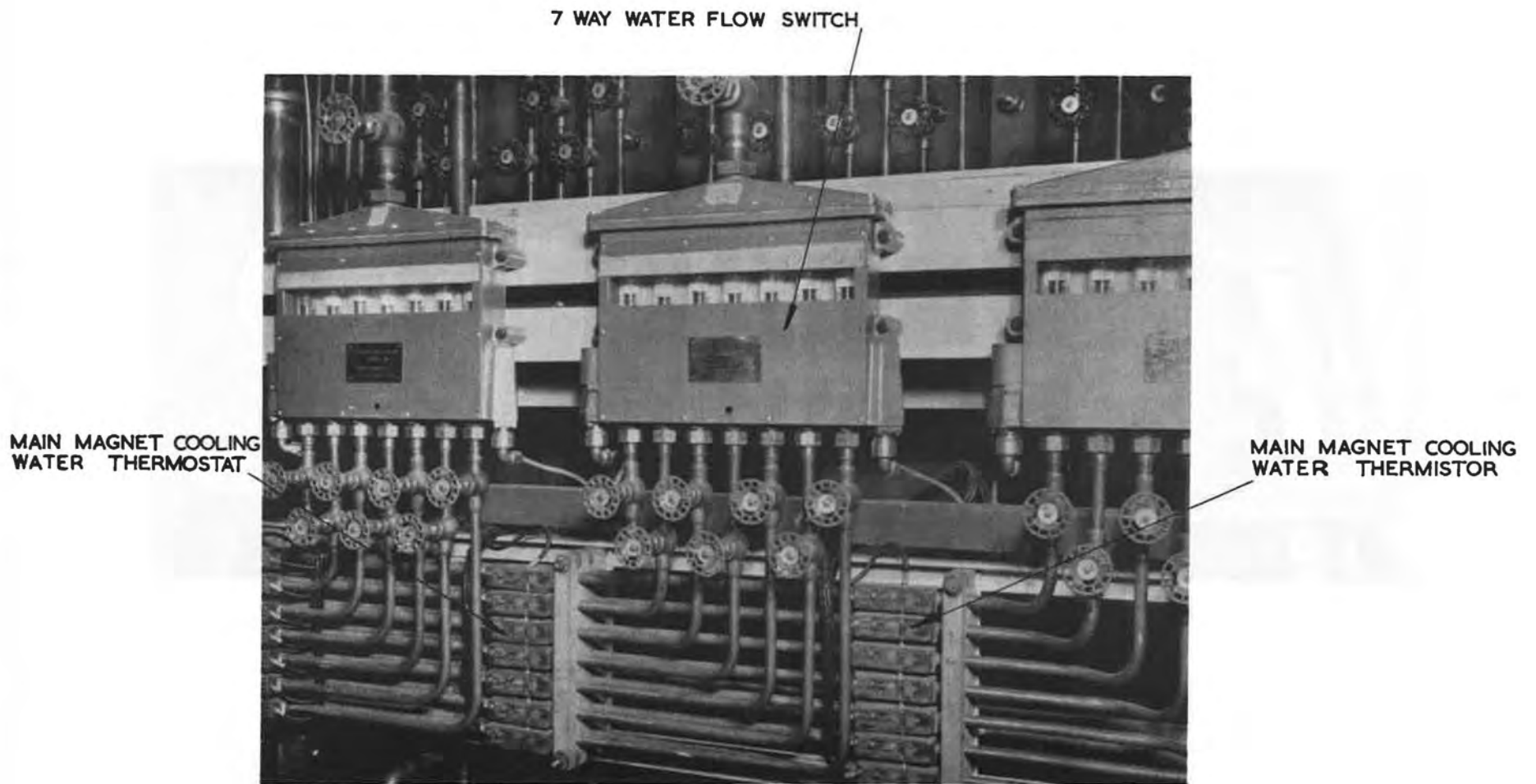


Fig. 9.3.3 (i) Seven-way Water Flow Monitor

Two main types of water flow relay have been used. The first of these, employed for the monitoring of single circuits, is of standard commercial design and is available in a wide range of flow rates. In this type a diaphragm communicates with the opposite sides of an orifice through which the cooling water flows. A reduction in flow causes the pressure differential across the orifice to fall and the diaphragm deflects, so operating a micro-switch.

A seven way flow switch, working on the stainless-steel float/tapered glass tube principle, has been especially developed for the magnet circuits, where large numbers of parallel water circuits are grouped together. The tapered part of the tube has flow graduations and the lower parallel portion of the tube corresponds to the trip setting. It is thus possible to match flows to accurate limits in adjacent conductors. Two different flow-rate settings are obtained by using floats of different weights.

Fig. 9.3.3(i) is a photograph of one of these units capable of monitoring seven flow circuits simultaneously. A flow rate above the set minimum raises the seven floats in the unit clear of a beam of light passing through all seven tapered glass tubes which are carrying the cooling water. The spacing of these tubes allows the light to refocus on adjacent tubes (i.e. each tube acts as a lens) thereby achieving maximum output from the cadmium sulphide photo-cell at the end of the unit. A number of such seven way units are grouped together in an alarm circuit. Water failure in one or more circuits causes a float to drop, so interrupting the beam of light in a unit and causing the alarm circuit to operate. Release of an alarm relay stops the magnet power supply pulsing and also raises an alarm and indication signal. This system has worked very reliably for about two years.

9.4. Main Control Room.

Fig. 9.4(i) shows a layout of the main control room and Figs. 9.4(ii) and 9.4(iii) are photographs taken during construction.

The control equipment is housed in about 70 racks which are of standard type except for minor modifications to the design of the top covers which provide a 5 in wide interspace between the racks when they are butted together. All incoming multi-core control cables are terminated in these interspaces, and then looped into the actual control panels mounted in the racks. All terminations in the interspaces are of the crimped ferrule type and the control room floor is of hollow construction to permit the control cables to be fed from the cable trenches into the bottom of each rack. The control racks accept panels of standard 19 in G.P.O. type.

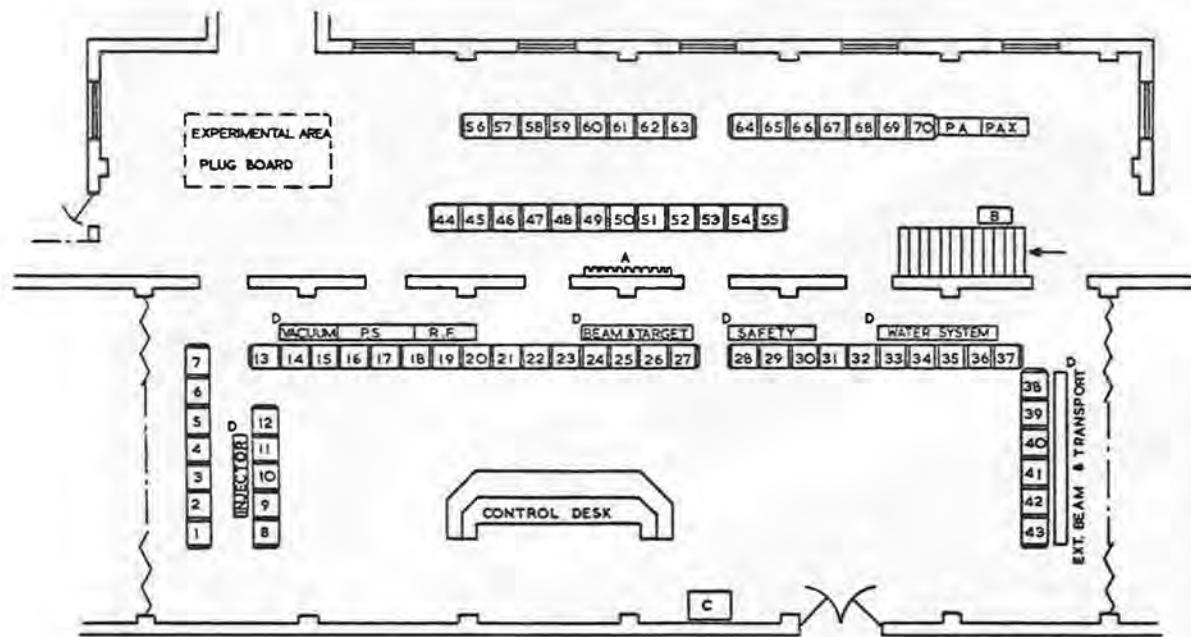
One of the main features of the Nimrod control system is the use of local control stations for almost every item of plant, with facilities for extension of control to the main control room. Thus nearly all plant can be run locally before being switched through to the main control room.

The main control room represents the focal point for operation of the machine and it is the only place where the operational status of all important parts of the machine are assembled and can be assimilated.

The quantity of information displayed is formidable since it is necessary to provide the operating staff with all the controls required to run the machine and adjust its important parameters, which in most cases must be done remotely since most of the machine is inaccessible during pulsing.

In order to assist staff to interpret the information displayed on the control panels, a number of "mimic diagrams" have been provided. These "mimic diagrams" are mounted on the top of the racks and display, by means of lamps, symbols and block diagrams, the state of various parts of the machine. In most cases these "mimic diagrams" operate in conjunction with an alarm annunciator equipment and take the place of the facia display units usually provided on these systems. In most cases the "mimics" are for display only but in the case of the vacuum system and personnel safety system the mimics form integral parts of the control equipment. "Mimics" have been completed for the vacuum system, the magnet and its power supply and the cooling water system. Others are to follow for the r.f. system, the personnel safety system, the extraction system and the beam handling system.

It is intended in the early commissioning stages of the machine to operate the necessary controls at the control racks and not to provide extensive facilities on the control desk. The framework of this desk has been installed, but only a minimum of controls, such as those for the public address system, are fitted. Further controls will be extended to the desk from the racks as dictated by operating experience.



RACK	LAYOUT OF EQUIPMENT
1	S.A.M.E.S. GUN AND H.T. PLATFORM
2-3	L.E.D.S. AND LINAC POWER SUPPLIES
4-7	MAGNET POLE FACE WINDINGS
8-10	DRIVE CHAIN, LINAC AND MASTER TIMER CONTROLS
11	BEAM MONITORING AND MEASURING
12	INFLECTOR AND H.E.D.S. POWER SUPPLIES
13	VACUUM MONITORING SYSTEM
14-15	BEAM MONITORING
16-17	MAGNET POWER SUPPLIES AND P.F.W.'S.
18-19	R.F. POWER AMPLIFIER AND CAVITY
20-22	R.F. BEAM SERVO
23	SPARE
24-27	BEAM EXTRACTION AND TARGETS
28	SAFETY INTERLOCKS
29-31	HEALTH MONITORS
32	RECORDERS, HYDROGEN AND AIR CONDITIONING
33-43	BEAM TRANSPORT
44-50	P.F.G.
51-53	BEAM CONTROL
54-55	DATA LOGGING
56-57	GENERAL PURPOSE CO-AX SYSTEM
58	GENERAL PURPOSE MULTI-CORES
59-62	SPARE
63	L.V. SUPPLY
64-66	ALARM ANNUNCIATORS
67-69	TEMPERATURE AND FLOW ALARMS AND MONITORING
70	SPARE
A	PATCHING LEAD HOLDER
B	P.A.X. BATTERY AND CHARGER
C	DATA LOGGING CONTROL
D	MIMIC DIAGRAM

SCALE 0 2 4 6 8
FEET

Fig. 9.4.(i) Layout of Main Control Room

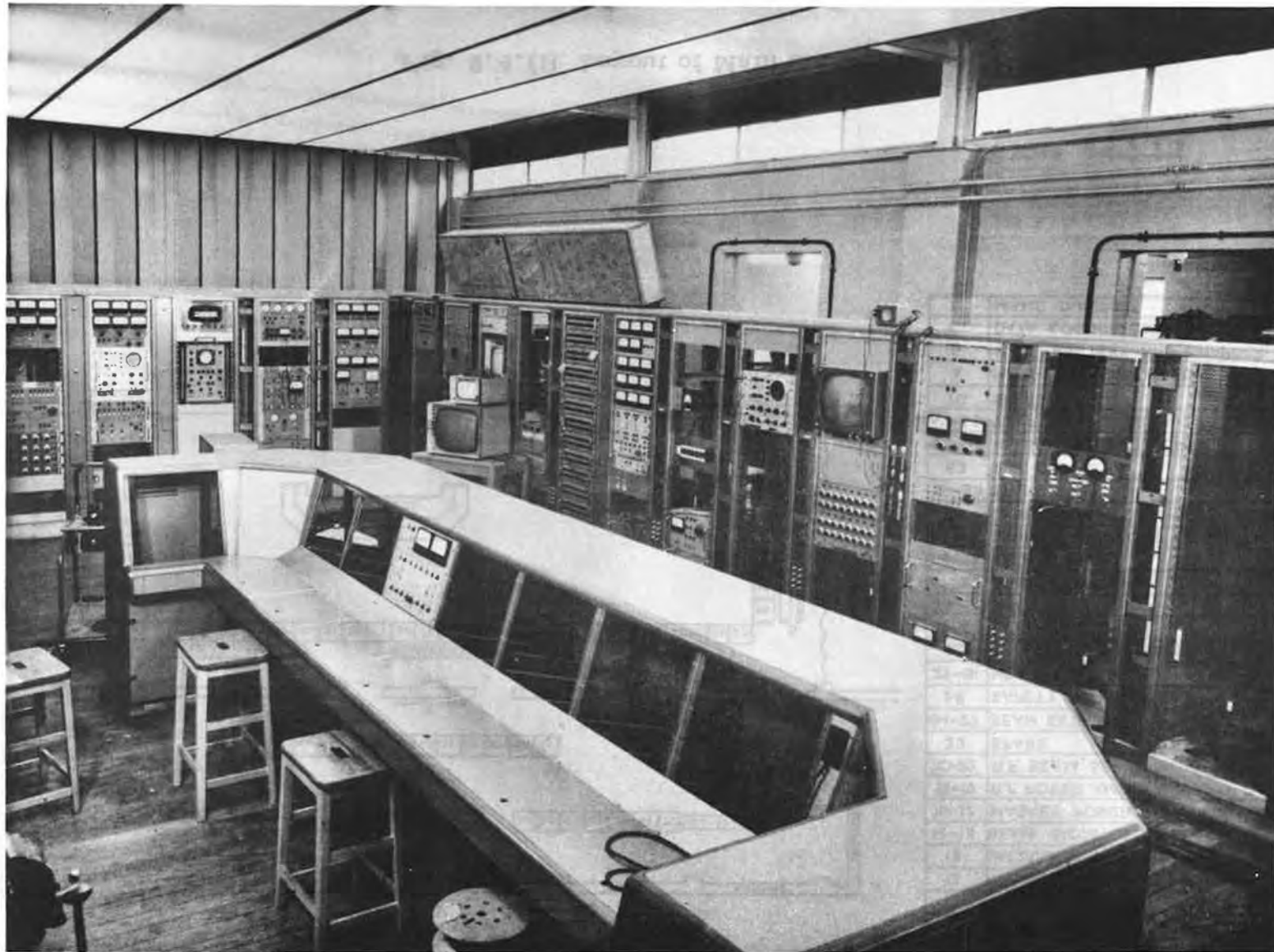


Fig. 9.4 (ii) General View of Main Control Room During Installation

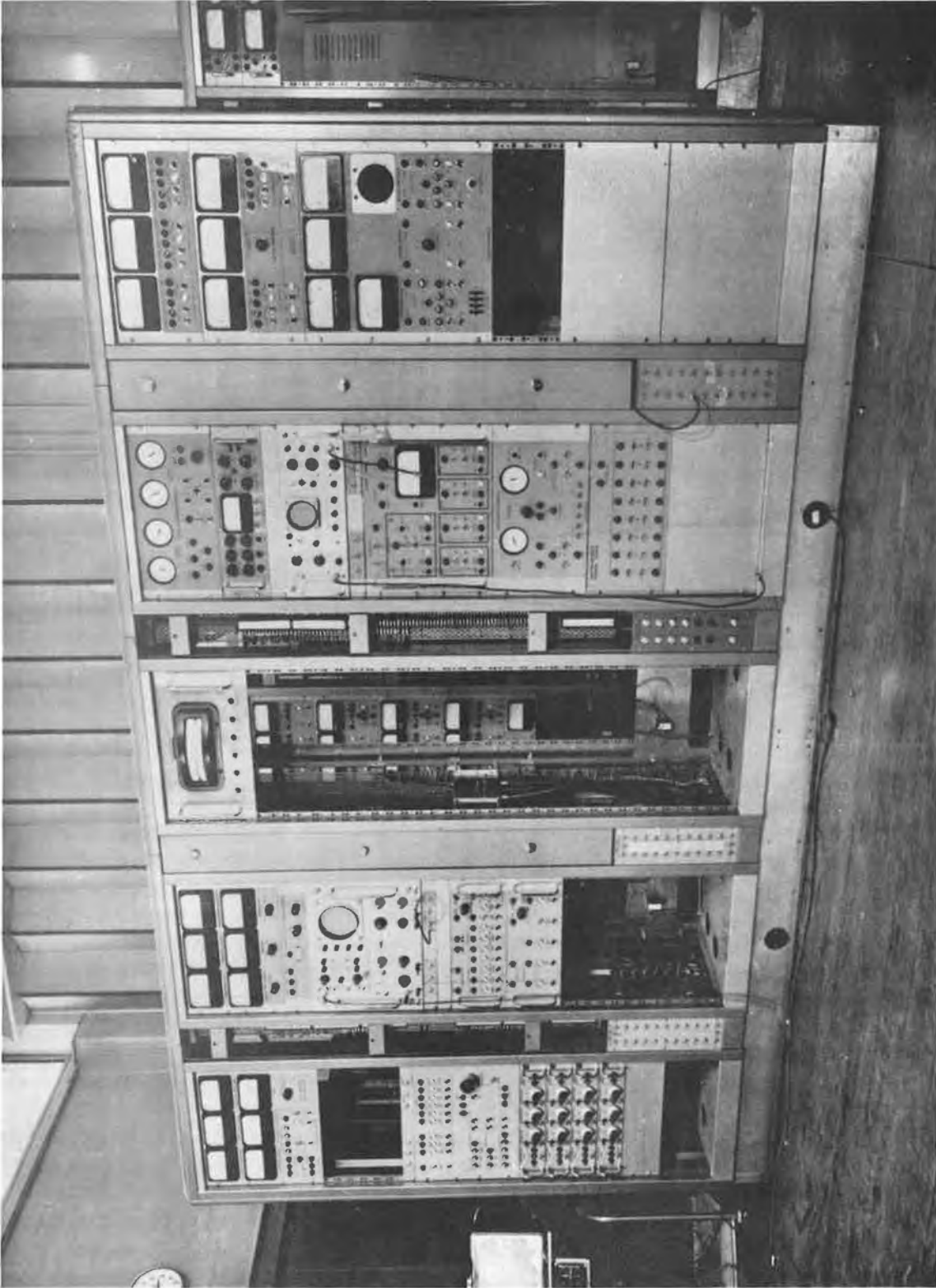


Fig. 9.4 (iii) Control Racks Installed in the Main Control Room

9.5. Personnel Control and Safety Interlocking.

When Nimrod is operating most of the machine and surrounding areas must be cleared of personnel because of radiation hazards; rigorous control procedures are required to ensure the necessary safety of staff and visitors. It is extremely difficult to devise a personnel control system which cannot fail under any combination of circumstances and yet still be sufficiently flexible to permit the effective commissioning and operation of the machine. All systems must rely to some extent on staff discipline and this is usually where the chief difficulties arise.

During the machine commissioning stages various temporary interlocking schemes have been employed. In the main these have been necessary to protect personnel in local areas, such as the injector room, where radiation and E.H.T. hazards have existed for several years prior to the completion of the magnet ring. These temporary systems have provided useful operating experience for the design of the permanent overall scheme, in addition to fulfilling their primary function.

The system chosen for the permanent personnel control installation will shortly be installed and it combines the simultaneous use of visual and audible warnings of impending machine operation with doors or barriers which are mechanically interlocked by a key system and electrically interlocked with door switches. Entrance is restricted by these systems but the doors are arranged so as to permit an easy exit at all times by any person trapped within an area. A closed-circuit television system covers certain of the access doors and large areas such as the magnet room so that temporary entrance to the machine by individuals and under closely controlled conditions can be permitted by the release of electric door locks remotely operated from the main control room.

The visual warnings are provided by a series of flashing indicators sited around the machine and associated with emergency beam-off push buttons, operation of any one of which stops machine pulsing. The level of lighting in the machine areas is also reduced (see below).

The audible warnings are provided by a public address system. The amplifier equipment for this is situated in the main control room and is operated from the main control desk. In addition to the normal public address facilities the system includes two tape machines for the transmission of repetitive pre-recorded warning announcements, four of which are normally available for selection. An oscillator produces three distinctive audible notes, any one of which may be selected for distribution over the loudspeaker network.

A possible way of using the facilities which are being provided is now described; the exact arrangement will be determined after experience in operating the machine. Machine start-up and running conditions are catered for in the interlocking and control procedure by four defined conditions or states of preparedness, namely: (a) Machine off (White), (b) Beam off (Green), (c) Beam temporarily off (Yellow), and (d) Beam on (Red).

In the "White" condition the machine is regarded as off for an extended period, certainly greater than 12 hours. During this period persons may enter at will, using a tally-board to indicate their presence.

In the "Green" condition the beam is off for a period exceeding half-an-hour but not exceeding 12 hours. Entrance to the area during this condition is normally restricted to authorised and semi-authorised persons only. Each person entering must take a key from a key-exchange box and return of all the keys is

necessary before the machine can operate again. When the "Green" period is within half-an-hour of the beam-on time, audible warning announcements will be made using the pre-recorded tapes and people will be told to leave. After a further 5 minutes those persons still outstanding (i.e. according to tally or key) will be warned over the loudspeaker system by name. As soon as all the keys and tallies have been recalled the machine condition will change to "Yellow".

The "Yellow" condition denotes that the beam is off but expected to come on within half-an-hour. During this period a thorough search will be made of all relevant areas and loudspeaker announcements and audible warning notes will be transmitted at frequent intervals. Entrance to the machine will be limited to a few doors and any semi-authorized person entering must be accompanied by an authorized person. This reduced number of doors will be controlled remotely from the main control room. After all the checks of the areas are complete, final warnings to leave the areas are given, all keys are returned to the key exchange boxes and all interlocks are closed. A "one-minute" warning is given over the public address system, followed by an interrupted 1000 c/s note. Half the main lights are turned off and the machine condition changes to "Red".

The "Red" condition does not necessarily signify that a beam is actually being produced but that all conditions and interlocks are correct for the production of a beam. The red flashing lights around the machine occur for 1 minute before the machine can be switched on and any person left in the area under these conditions must immediately operate an "Emergency Off" push button.

The safety interlocking and radiation protection system for Nimrod is more fully described in a Nimrod Design Note (NDN/600/1).

SECTION 10

ANCILLARY PLANT

10.1 Introduction

The Nimrod ancillary plant provides the services of water and air for Nimrod. Many of the main components of Nimrod generate heat and require cooling, for example, the heat generated in the magnet is dissipated by cooling the conductor coils with water and by passing air between the magnet sectors to give forced convection. The cooling water must, of necessity, be of low electrical conductivity and, before use, the raw water from the mains is treated in a special plant to demineralise it and give it a low oxygen content. For most items of Nimrod equipment, the cooling water also needs to be temperature controlled; in some instances this involves the use of refrigeration plant. Where low electrical conductivity is not important, the water used for cooling purposes is only softened to reduce scaling.

The magnet room temperature is controlled to ensure that the magnet does not tilt beyond the acceptable limit due to differential temperature gradients across the foundation monolith. The relative humidity is also controlled to reduce electrical breakdown and to minimise condensation. This is effected by means of a large air conditioning plant employing refrigeration units and steam heaters.

Commissioning and development of much of this ancillary plant has of necessity proceeded in parallel with the commissioning of the main machine, rather than preceding it. One reason was because of the impracticability of simulating the heat loads put out by Nimrod and associated experimental equipment. The ancillary equipment is now functioning reasonably well, but a full knowledge of component plant capacities and reliabilities is not yet known.

10.2 Cooling Towers

The four towers dissipate the whole of the heat output from Nimrod. There are three induced draught, evaporative units each of 320,000 Btu/min and 120,000 gal/h capacity, and one smaller unit of 160,000 Btu/min and 60,000 gal/h capacity. The cooled temperature of the water will depend on the heat input and climatic conditions but is not expected to exceed 79°F under the worst conditions. A schematic diagram of the water cooling system is shown in Fig. 10.2(i).

The geographical position of the towers is such that strong cross winds caused large amounts of water to be swept out of the towers against the air draught induced by the fans located above the cooling matrix. Under gusty conditions the waves formed on the ponds, lapped over the retaining walls. These troubles were overcome by detail modifications to the wooden air inlet louvres which improved air inlet flow conditions and by the addition of a vertical baffle across each pond normal to the direction of air inlet.

Considerable airborne debris is present in the locality of the Rutherford Laboratory; some is due to adjacent construction work but most is caused by the light soil conditions and at times the high insect population. The original pot type filters in the feed lines to the pumps were inadequate in area and necessitated a shut down and drainage of each pond in order to change a filter. Larger filters of 40 mesh (60 μ) have been fitted and no shut down is required to service them. A specific flow rate of 45 gal/min/ft² is satisfactory. A special washdown area has been constructed alongside the cooling towers to clean these filters.

The original design of the water system pipework did not allow the small cooling tower to be taken out of commission without shutting down all equipment served by it. As the small cooling tower distribution pump gives a slightly higher head than the other tower pumps, a pipework system was evolved which allowed the water to the small tower to be diverted to and from the other towers, thereby achieving the required maintenance facility. Various other similar modifications have been made to improve the operational flexibility.

Considerable work has been done to guard against frost damage to the cooling tower complex. This has included the application of heater tapes, controlled bleeds, repositioning of stop valves to eliminate dead legs and additional lagging. The main water stop valves to each tower are of the direct acting, hand operated type and require the effort of two men for operation. This is an extremely difficult job in very cold weather and geared drive units have been purchased but are not yet fitted.

Evaporation results in a steady increase in the total solid content of the water. An overflow and drain connection added to each tower will allow sufficient bleed off (about 1/40th of the system makeup water) to reduce the content to an acceptable level. At the present time, the need to clean the ponds of airborne and constructional debris (concrete dust, rust etc.) at least once a month renders this system inoperative.

Sodium pentachlorophenoxide (Algicide) was added to the towers at a concentration of 80 parts/million when algae was observed. To prevent a strain of algae developing resistance to Algicide, a shock dose of 100 parts/million is now added once a month. As Algicide is only effective in high concentrations, is toxic and does not protect against slimes, a more suitable material is being sought.

When magnet loading and ambient weather conditions have allowed, heat balance

trials have been performed on the towers. To date it has only been possible to check and confirm the performance at full heat load and fairly low ambient relative humidities.

10.3 Pump House

10.3.1 Pumps

The pump house contains the Kennicott softened water (raw water) plant, two 2500 gal/min pumps serving the three large cooling towers and two 500 gal/min pumps serving the small auxiliary cooling tower. An additional twin pump set has been installed to provide a raw water supply to laboratories. These are each of 800 gal/min capacity and the circuit is required to dissipate about 1200 kW. The two small pumps together provide the total flow from the auxiliary cooling tower to the air conditioning plant, injector and magnet room. One duplicate pump of 1000 gal/min capacity is being fitted to provide a maintenance facility and to guard against breakdown and loss of water supply.

The noise from the existing pumps was extremely high, over 100 dB at the worst azimuthal position. Sound absorber hoods were constructed and the level was reduced to 92 dB at the same position. The air cooling of the motors is now more directional and a lower running temperature is recorded.

The relative heights of the raw water pumps to the tower ponds is such that on pump start up there is insufficient head to give positive suction to start the pumps without cavitation. A priming system has been installed so that the raw water pump No. 1 of the Kennicott softening plant may be used to prime all raw water pumps. Rotameter flow indicators installed in the suction lines are inoperative due to air locks attributable to the low local suction pressures. No satisfactory alternative has yet been fitted.

10.3.2 Kennicott Plant

The Kennicott plant (shown schematically in Fig. 10.3.2(i)) is the treatment plant for the cooling tower water system. It consists first of an alkalinator section where the temporary hardness of the water is converted to carbonic acid. After passing through a scrubber tower, where the carbonic acid dissociates to form carbon dioxide, the water only contains permanent hardness. This is removed in the base exchange section where the calcium, magnesium, etc., is converted to sodium salts which (in solution) are non-scale forming. The difficulties associated with this plant were of a mechanical nature; chemically it fulfils its function.

The acid measure system gave considerable trouble. Initial leakage from the acid measure sight glass and the acid flow rotameter resulted in spillage of concentrated sulphuric acid. Sticking of the rotameter bobbin on the lower lead stop resulted in a low flow of the sulphuric acid to the primary dilution vessel, causing the water supply tank to be corroded through by dilute acid. The lower stop material was changed to P.T.F.E. (polytetrafluoroethylene), a spring buffer was fitted, and the lead lined steel tank was relined with Penton. Various rubber lined pipes were attacked by dilute acid; these were relined. A barometric loop, a non-return valve, a larger water trap and a larger air admittance solenoid valve were fitted to prevent water being sucked back into the primary acid measure tank. The vent for the acid secondary measure tank was altered so that if the tank is overfilled, acid flows into the acid storage tank bund and not outside the building. The lead bung for the drain from this bund is kept in position to allow acid spillage to be adequately diluted before release into the trade waste drain.

Failure of the constant level float valve on the caustic injection system flooded the plant room with a 5% caustic soda solution. The operation of the caustic dosing (before the base exchangers) became erratic due to coarse flow control and sticking of the solenoid valves. This resulted in resin being lost from the base exchanger due to high back wash flow. A high rate of corrosion of the base exchange tank was attributable to the erratic caustic dosing. The caustic injection system

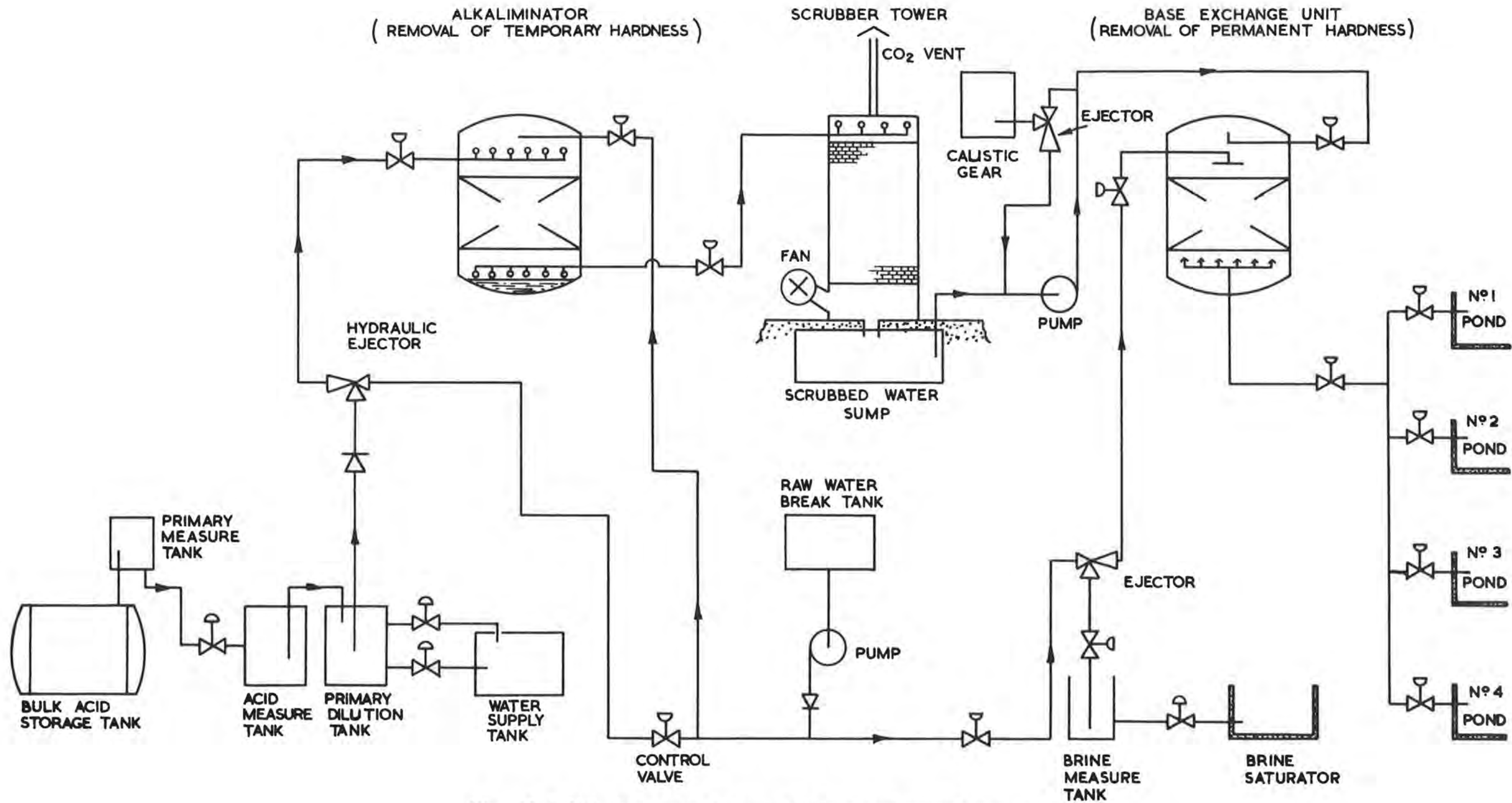


Fig. 10.3.2(i) Schematic diagram of Kennicott water treatment plant.

was re-designed and all other affected parts renewed. Solenoid valves now operate Saunders pneumatic diaphragm valves which have positive limit stops to prevent jamming at the end of the travel. One interesting failure occurred to the external diaphragm of a pneumatic valve by, presumably, the action of paint which had in error been applied to the diaphragm.

Compatibility of materials is always a problem on chemical plant. The bitumen paint on the degassed water sump and on the brine tank peeled off, exposing the concrete. The water sump was repainted successfully but the brine tank was coated with a glass fibre. The concrete bund of the acid storage tank was also lined with glass fibre but dilute acid broke this up and it had to be lined with glazed ceramic tiles. The use of incorrect grades of rubber on diaphragm valves has caused much trouble. To protect the concrete floor of the plant room a bund has been built around all acid measuring system equipment.

The cooling tower pond has capacitance type electrodes which control the plant. These were unsatisfactory due to excessive splashing from falling cooled water. They were repositioned and protected by splash covers and the electrodes were changed from mild steel to stainless steel because of corrosion.

The plant was originally intended for use with 80% B.O.V. acid. In order to minimise corrosion of the storage tank 96% C.O.V. acid is now being used.

The Neckar water hardness meter is troublesome mechanically. Regeneration is triggered off too frequently as the raw water hardness changes due to a change in the source of supply (Thames, deep well or local authority). A time switch is fitted to the control gear to control the frequency of regeneration of the alkalimeters to not less than once per hour.

10.4 Permutit Plant House

10.4.1 Heat Exchanger and Pump Systems

The Permutit plant house contains the Permutit water treatment plant, circulating water pumps and heat exchangers and all other equipment needed to supply the Magnet and associated equipment with demineralised water.

Four large and two small heat exchangers transfer heat from the demineralised water returning from the machine and experimental equipment, to raw water circulated back to the induced draught cooling towers. The demineralised water serving the magnet is kept substantially at a constant temperature of 90°F by passing the flow across two water/water coolers when the magnet is energised, and by heating a proportion of the flow by a subsidiary steam heater coil when the magnet is not energised. The demineralised water serving the experimental equipment, bubble chamber and vacuum system is not temperature controlled.

10.4.1(a) Magnet Circuit. Two pumps each delivering approximately 720 gal/min serve the magnet. Temperature transducers in the feed line to the magnet, pass a pneumatic signal to a controller where suitably amplified pneumatic signals are fed to three valves; one controlling the steam supply to a heat exchanger across which demineralised water is by-passed, one controlling the demineralised water through the demineralised raw water heat exchangers and the third controlling the water across the steam heater.

Considerable instability was experienced when this closed loop system was subjected to full magnet heat load conditions (it had been impractical to attempt to simulate such conditions). The system was stabilised by:-

- (i) repositioning the temperature transducer to such a position that it sensed a mean of the outlet water temperatures from the steam heater and main exchanger
- (ii) redesigning the valve trim of the three control valves to obtain a more linear flow characteristic
- (iii) increasing the proportional band of the positioners to counter instability (the positioners were changed for a new type to allow more latitude in control)
- (iv) reducing the speed of response of the control valves by heavily damping the air supply to the diaphragm motors
- (v) setting the response of the two valves controlling the water so that one valve always led another, thus ensuring that lags in the system did not result in the effective area for water flow being reduced.

The magnet is protected by thermistor temperature monitors set to shut down the pumps when the inlet water drops to 28°C. It is difficult to prevent small slugs of water at about this temperature being passed into the system due to the action of the control circuits. The very high speed of response of these thermistors caused frequent shut down of the plant and thermal damping (provided by mounting the thermistors on copper blocks) was necessary.

It was found that the pump installed to supply water to the experimental area delivered insufficient head to overcome adequately the losses in the system. A new pump has been installed.

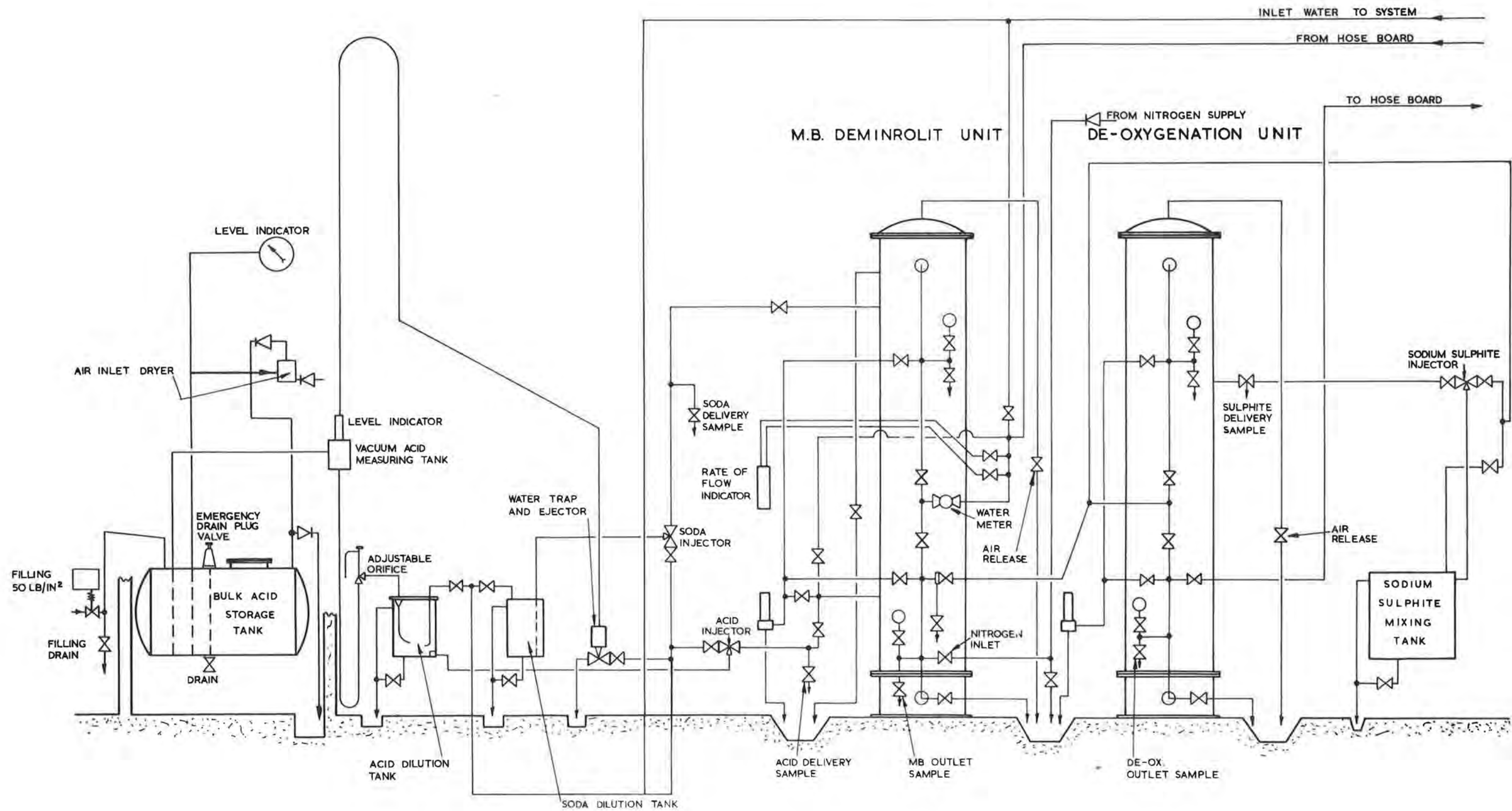


Fig. 10.4.2 (i) Permutit water treatment plant.

Each pump has a visual flow sight glass at its inlet but with the instrumentation necessary to run the plant (rotameters, pressure gauges and thermometers), such sight glasses are superfluous.

The pipework between the two small pumps and the double tube heat exchangers for the vacuum cooling circuit had to be modified to allow inspection of one exchanger nest without shutting down the other. This type of facility is most desirable to achieve efficient operation.

An additional pump and heat exchanger was installed to provide cooling for the ripple transformer amplifier in the magnet power supply plant.

10.4.1(b) Steam Heaters. These are of a double coiled tube design. Hydraulic vibration quickly fatigued the copper coils where they were braced to the main shell. A new design of 'U' tubes will be fitted since thicker coils and stiffer bracing have not completely cured the problem. It was also necessary to fit an automatic shut off valve in the steam supply line so that if a demineralised water circulating pump trips out, the steam supply is shut off.

10.4.2 Permutit Plant

This installation comprises three mixed bed demineralisation plants each associated with an ion-exchange de-oxygenation unit. Each pair of units (demineraliser and de-oxygenator) is capable of treating raw water for filling the circuits at a rate of 60 gal/h and 160 gal/h when operating on a recirculation basis. Fig.10.4.2(i) is a schematic diagram of the Permutit plant.

Initial tests on the mixed beds showed the plant capacity to be up to specification. When treating mains water the demineraliser produced water with a conductivity of $0.1 \mu\text{mho/cm}$ (specification $< 1.0 \mu\text{mho/cm}$) with a capacity measured over a regeneration-exhaustion-regeneration cycle of 1700 gal (specification 1400 gal). Two de-oxygenator columns met the specification in delivering water at 0.2 parts/million O_2 after a throughput of about 2800 gal. One column needed modification to the sodium-sulphite regenerant injector dilution system before it met the specification.

Low capacities experienced at one time, were rectified by cleaning the caustic injection system which was partially blocked by wood pulp from a wood stick used for mixing the caustic solution. Operating instructions were issued to prevent a recurrence.

Strainers were fitted to the mixed bed air release lines to avoid loss of resin when backflowing the beds with nitrogen during the regeneration cycle. The resin bed of one demineraliser unit, which is used for continuous circulation of the magnet system water, was found to be compacted when it became exhausted after being in use for three months. Regeneration once a month is now necessary to avoid this trouble.

The capacity of the mixed bed units was often only 50% of that specified. The cation resin usually exhausts first. The acid measure was dismantled and found to contain a quantity of ferrous sulphate which decreased the volume available in the measure of sulphuric acid. This is partly due to attack on mild steel by sulphuric acid which has become diluted by water vapour from the acid vacuum injector. Poor separation of the resins for regeneration will reduce the efficiency of regeneration and the backwash flow rate is being increased in easy stages to find an optimum condition.

Ceramic and cloth bag filters were fitted at the inlet to the mixed bed columns

to prevent the resins acting as filters for system debris.

A secondary system of conductivity checks was installed, using a cell and standard meter. Existing conductivity cells were extremely unreliable due to faulty internal sealing against water. They have since been modified and now give no trouble.

A dissolved oxygen meter for monitoring the mixed bed units and the main demineralised water circuits was constructed in the Laboratory. This meter is based on an existing dissolved oxygen meter and has an electrolytic calibration unit.

10.4.3 Demineralised Water Storage Header Tanks

Five 1000 gal and one 500 gal mild steel tanks provide a static head of some 18 lb/in² on the whole demineralised water system. After a few months of operation three tanks were opened up because of leakage at the inspection hole flanges between the mild steel shell and the P.V.C. lining. The linings were found to be badly split, several sections having fallen away. It was considered that failure was due to physical, not chemical causes - bad bonding and operational thermal stress. The water temperature at no time exceeded 100°F but the coefficient of linear expansion of P.V.C. is some eight times that of mild steel. The strength of the P.V.C. welds on the lining was high and no failure occurred on them. This failure resulted in a large rise in the demineralised water conductivity.

Investigation of suitable tank linings led to the adoption of a vulcanised neoprene. After the tanks were lined, they were acid treated with boiling 5% sulphuric acid followed by alkali treatment with boiling 5% sodium hydroxide. The 500 gal tank was filled with water from the Permutit plant at a conductivity of 0.8 μmho/cm and after standing for four days, this increased to 1.4 μmho/cm. Subsequent inspection after six months use showed that the linings were in good condition but inspection of two tanks after twelve months revealed defects. Repairs were effected and inspection will again be necessary after a further nine months.

Modifications to the method of filling and control of level in these tanks were necessary. The original design was based on constant topping up and overflow but for better use of the Permutit plant, the tanks are now filled through the mixed bed units to a set level; the Permutit column is then available for other duties. A simple visual sight glass has been installed on each tank and it is an operator's responsibility to observe the level a few times a day to check against system leaks. An alarm system was fitted, using a bellows switch, to warn of a leak occurring in any demineralised system by registering the rate at which tank levels dropped compared with a predetermined maximum. With the differential heads available to register a small flow, the setting of this switch was difficult and, since it was possible to damage the bellows by excess pressure on filling the tanks if certain isolating valves were not closed, the use of this device was discontinued. Experience will dictate whether an automatic alarm system should be reconsidered.

10.5 Water Distribution System

All water systems are commissioned but modifications are continually being made to suit various experimental conditions. The greatest trouble, and not an uncommon one with these systems, has been the filtration of constructional debris. To counter this, all new pipework is fitted under scrupulously clean conditions with careful supervision. It takes many months to clean up a new closed loop circuit, which has been installed under normal constructional conditions, to a standard where in-line filters are little needed. Debris in the system (concrete dust, spelter, bitumen, metal chips, etc.) does not necessarily worsen the conductivity of the water.

One problem has arisen because the whole demineralised water system is made from copper pipe. On the machine itself only pure aluminium is used for the water systems because of radiation problems. The copper ions in the water can react unfavourably with the aluminium and sacrificial aluminium pipes have been fitted in the external feed pipes to the machine in the hope that this pipework will bear the brunt of corrosion. As corrosion can occur in a random manner consideration is now being given to the fitting of small ion exchange columns in place of the sacrificial pipes, to take out the copper ions from the water entering the machine.

With the raw water distribution system it is physically impracticable to filter out the fine debris that is deposited by the scrubbing action of the cooling towers. The raw water to the magnet and injector rooms is fine filtered to about 80 mesh and individual items of equipment are fitted with individual filters if necessary. Too low a margin on circulating water pump heads, limits the standard of filtration on raw and demineralised systems to the minimum necessary.

Corrosion problems exist in the water distribution systems due to differences in the anti-corrosion treatment of the pipe bores. Some sections of mild steel pipework containing cooling tower water are unprotected, much is bitumen coated and sections that have been welded 'in situ' are painted. The cooling tower pond water is slightly corrosive due to sulphates and chlorides from the make-up water and the high chloride content may attack the small section galvanized pipework. The use of inhibitors is not practical in this installation and a large bleed-off of pond water to reduce chloride levels would be too much for the effluent disposal facilities and the site water supply. Corrosion of pipework is being carefully watched.

The ebonite foam insulation for the pole face winding chilled water system was found to be releasing hydrogen sulphide. Since concentrations of 50 parts/million were measured in the magnet room, the insulation was encased with impermeable material, to prevent possible effects on personnel and electrical contacts.

Chilling units are used for various systems on the machine. The steel tanks containing demineralised water were painted with an epoxy paint which blistered. The relative inaccessibility of some of these units for repair work led to their rubber lining being scrapped and the tanks were reconstructed in copper. Corrosion of the tinned copper refrigerant coils was experienced on one unit and the cause attributed to attack by cement dust before the unit was put into commission. After thorough mechanical cleaning no further corrosion has occurred.

10.6 Air Conditioning Plant House

10.6.1 Air conditioning Plant

This plant, shown schematically in Fig.10.6.1(i), provides conditioned air for the magnet and injector rooms; nominally at $65^{\circ}\text{F} \pm 2^{\circ}\text{F}$ and at a specified relative humidity of 60%. It consists of two self-contained air conditioning sets, one acting as a master to the other. Each set has a refrigerator plant with a refrigerant capacity of 120 ton and a flow and extract fan capable of $51,000 \text{ ft}^3/\text{min}$ air flow. The two sets can be run together or singly and, with reservations, at half capacity. The refrigerator plant chills demineralised water to about 40°F which is stored in an insulated steel tank. Chilled water is supplied from this tank to the injector room subsidiary air conditioning plant and to the cooling batteries of the main air conditioning plant.

Air is extracted from the magnet room by an extract fan discharging 10% of the air and taking in 10% fresh air as make-up. The air then passes over a heat exchanger where chilled water precipitates moisture. The required temperature is then re-established by passing the air over a steam heater. Filters are installed to filter the incoming air and the re-circulated air.

Slight instability of the temperature control system occurred on commissioning, which adjustment of the control equipment did not eliminate. The fault was traced to excessive backlash and lost motion in the steam control valves giving rise to a relatively long delay in response between the two sets.

Vibration is often a problem on reciprocating and rotary plant. On the compressors in the refrigerator plant repeated failures of small bore copper pipes forming part of the system unloading the cylinder heads, occurred on change from full to half load, or vice versa. Changing to thicker gauge Tungum cured the problem. (It is pertinent to report that a large number of failures of small pipes have occurred due to the use of copper which is often insufficiently annealed. Tungum is a much better substitute). Flutter of a metal dividing plate in the steel air ducting to the fans necessitated some stiffening. Vibration also caused the pipework from one compressor set to crack at the weld neck of an oil separator when the compressor was on half load. A change of pipe support has lessened the severity of vibration but further investigation may be necessary.

10.6.1(a) Capacity of the Plant. Two full scale heat balance trials have been conducted to check that the plant meets the specification. It is reasonably clear that the heater bank and fans are satisfactory but the cooler bank is of insufficient capacity. It is possible to hold 65°F air inlet temperature for the relatively short time that the magnet has been pulsed at maximum load but it has, as yet, been impossible to check for a long period. The specified relative humidity of 60% is not met. Although this may not in itself be important at the higher air inlet temperatures, it is hoped to achieve an inlet temperature of 60°F (63°F has been achieved) when the margin between the wet bulb temperature and the dew point will be much smaller. It is relatively easy to increase the performance of the cooler bank but if the refrigerator plant proves incapable of meeting a high sustained load, it may be difficult to improve its performance. The matter is now being considered by outside consultants.

10.6.1(b) Temperature control. An investigation has been made into what parameters could practicably be used to control the air inlet temperature to the magnet room under various load conditions. Calculations relating the differential temperature gradient between the top and bottom surfaces of the magnet room concrete monolith with tilt of the magnets have established the required relationship between air inlet temperature and magnet load to restrict the tilt to acceptable

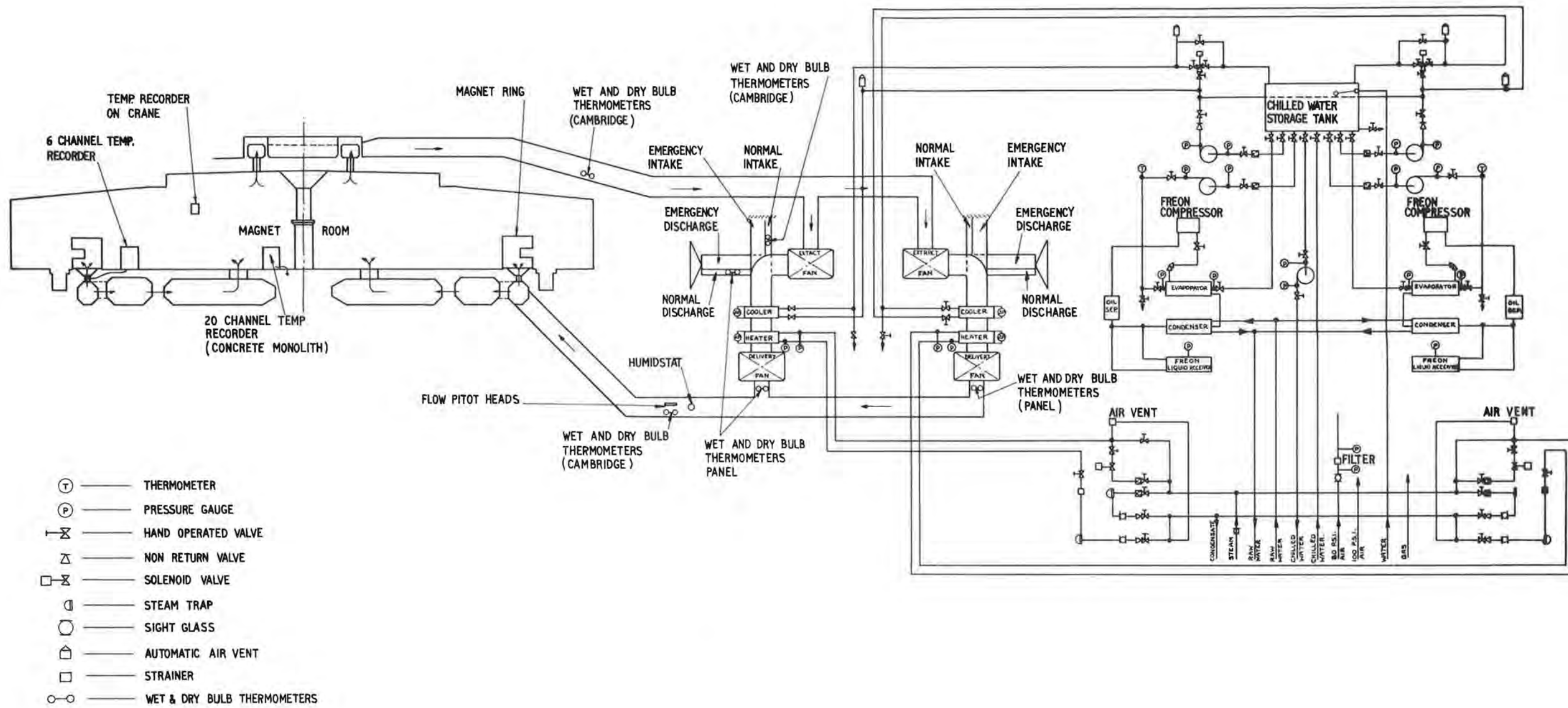


Fig. 10.6.1(i) Air Conditioning System.

limits (0.0035 in over the 120 in width of the magnet). Remote recording tilt meters positioned on top of the magnets have been considered but as these would require considerable development, simple spirit levels will be used. The thermal inertias of the magnet room structure are large, therefore periodic visual checks of these levels will be adequate.

10.6.2 Chilled Water Storage Tank

This galvanised steel tank was initially filled with untreated mains water. The tank carries mild steel pipework and heat exchangers of brass and copper. Considerable corrosion of the mild steel parts of the tank resulted in filter blockage.

Tests conducted to find the most suitable corrosion inhibitor included adding: (i) 10 parts/million calgon (ii) an alkali (iii) 0.5% sodium chromate at pH 8. After thoroughly cleaning the system, the circuit was flushed and filled with mains water containing 0.25% sodium chromate at pH 8.5-9.0, and the suspended solid content reduced from 8 to 1 part/million by the use of 7 thou. filters in circuit.

The inhibitor has reduced corrosion but to reduce it further it is intended to provide means of filling the system with demineralised water.

10.7 Air Distribution System

Air from the air conditioning plant is supplied to the magnet room via an underground tunnel to an annular space which is located underneath the magnet ring. A proportion of the air is then passed through stack pipes and carried up in between the magnet sectors where it absorbs heat. The remaining air is distributed into the cavities within the magnet monolith, the mass flow of air to each cavity being proportioned according to the heat output of the installed equipment. This air then passes into the magnet room via 4 ft diameter holes in the ceiling of each inner cavity. Air is returned to the plant room via a tunnel running from an annular duct in the roof of the magnet room.

Attention has been given to the cleanliness of these air ducts in which a considerable amount of dust was precipitated, particularly where a thin cement had been floated on the base concrete, and was carried into the magnet room. The concrete was treated with 'Lithurin' and the ducts are periodically cleaned with a vacuum cleaner. Water leaks at subsidence joints required attention.

The return duct from the magnet room roof has a steep slope of about 1 in 4, which requires a 'life-line' rope to assist ascent and descent, particularly when air is flowing.

The design of the ducts gives rise to relatively high aerodynamic losses since large areas of re-circulation occur, reducing the effective flow area. It is considered, as with the water systems, that the capacity of the air conditioning plant may be marginal and therefore some attention will be given to simple streamlining in certain parts of these ducts to improve, however little, the total head pressure delivered and hence the volumetric flow.

The proportion of air fed to the magnets and to the cavities has been determined experimentally, using anemometers to measure flow. More equipment has been installed in the cavities since this work was done, which has increased resistance to flow and, more significantly, requires the flow in the cavities to be reapportioned to suit the new heat loads. Some doubt exists as to the validity of the early measurement because of strong circulations in the cable ducts between the cavities and the magnet room. The magnet room pressure will also change when the shielding bridge is completed. To assist in circulating air through the cavities and out into the magnet room, all ducts not required for air flow have been blanked off and extract fans installed in the 4 ft outlet holes. As might be expected recirculation occurred around these fans and they now are being adequately ducted. A recheck of the air distribution and a re-setting of controlling dampers will be done at the first available opportunity.

10.8 Injector Room

10.8.1 Injector Cooling System

Heat is transferred from injector components to demineralised water and then, via a local cooling plant within the injector room, to the Nimrod raw water system. The raw water plant incorporates the cooling towers and the water softening plant. The raw water is fed back to the local cooling plant at 80°F maximum.

The major portion of the injector cooling plant is situated in the south east area of the injector room, and occupies a floor area of about 260 ft². A platform over this area is provided for non-rotating components of the plant and flush panelling with an entry door forms a neat screen around the area. The components to be cooled are grouped into one of four circuits according to the operating temperature as follows:-

Circuit 1: vacuum diffusion pumps (upper circuit) and liquid air machines. (See Fig.10.8.1(i))

A total of 26 kW of heat can be extracted, raising the demineralised water temperature to 50°F. This is then cooled and returned by the plant at 40°F ± 3°F and 15 gal/min flow (89,000 Btu/h).

Circuit 2: r.f. liner, drift tube shells, buncher, debuncher, S.A.M.E.S. EHT set and r.f. modulator. (See Fig.10.8.1(ii))

A total of 8 kW of heat can be extracted, raising the demineralised water temperature to 70°F. This is then cooled and returned by the plant at 68°F ± 1°F and 23 gal/min flow (27,360 Btu/h).

Circuit 3: drift tube quadrupole magnets, external quadrupole magnets, steering magnets and inflector system magnets.

A total of 270 kW of heat can be extracted, raising the demineralised water temperature to 108°F. This is then cooled and returned by the plant at 90°F ± 2°F and 85 gal/min flow (920,000 Btu/h).

Circuit 4: high vacuum pump (lower half circuit), targets, roughing pumps and four - jaw boxes.

A total of 30 kW of heat can be extracted, raising the demineralised water temperature to 100°F. This is then cooled and returned by the plant at 90°F maximum, and 17 gal/min flow (102,500 Btu/h).

Circuits 1 and 2 are provided with refrigerated circuits between the demineralised water and raw water circuits. Circuits 1 and 2 are functioning correctly and were up to specification, but an increase in the number of liquid air units on Circuit 1 increased the load above the capacity of the plant. A Thames Valley Unit was installed to cope with the liquid air units and the vacuum pump circuit left on the existing plant.

Circuit 2 is controlled to 68°F ± 1°F. The control of the refrigeration plant is as close as possible and, although the tolerance of ±1°F is achieved, there is too high a frequency of oscillation of temperature within this tolerance band. It is intended to increase the thermal inertia of the temperature controlled water system by installing a heat sink in the form of a large sealed tank in the supply line. Lack of thermal inertia is a fault common to all circuits of the plant: it

results in frequent stop and start conditions and has made the optimum setting of the control systems difficult. To protect the plant the installation of similar heat sinks will be considered.

Circuits 3 and 4 use one heat exchanger between the demineralised water and raw water circuits, with a temperature controlled mixing valve to by-pass the heat exchanger (on the demineralised water side) as necessary. The heat exchanger for circuits 3 and 4 is of sufficient capacity for a 30% increase in duty.

When tested, the water/water heat exchanger serving both circuits 3 & 4 cooled the demineralised water to within $\frac{1}{2}^{\circ}\text{F}$ of 90°F . If fouling resistance of the heat exchangers was taken into account this was 3°F from design point and did not allow for the specified 30% overload capacity. The low performance was attributed to the fact that the drainage notches at the bottom of internal baffles in the heat exchanger were machined too large and hence too much water was by-passed along the internal nest of tubes instead of across them. An additional heat exchanger was installed in parallel with the existing one to make good this 30% deficiency.

All circuits have water pumps for recirculating the demineralised water. A stand-by pump is provided in parallel, with suitable valves, so that maintenance does not interfere with the use of the plant. Similarly, refrigerator compressors and motors are duplicated. Materials throughout the demineralised water circuits are substantially zinc-free.

Copper pipework from the circuits of the cooling plant is run in the floor services trenches, and terminates in valves at appropriate points near the items to be cooled. Flow switches and thermistors are also included, and these, together with automatic monitoring equipment installed in the local control room, permit continuous observation of flows and temperatures in the various cooling circuits. High pressure hoses and fittings and self sealing couplings make the final connections between the copper pipes and the equipment to be cooled.

R.F. Valve Cooling Circuit A separate, free standing cooling unit is used to supply very high purity demineralised cooling water to the last two r.f. valves in the power drive chain, removing about 20 kW (70,000 Btu/h). An insulated, copper tank of 400 gal capacity contains demineralised water and immersed evaporator coils. Refrigerator compressors, condensers and control gear are mounted over the lid of the tank; valves, motors, pumps, level alarm units, etc., are attached to the tank side. Two motor-pump sets for the circulation of demineralised water to the r.f. valve circuits are provided in parallel, one set being used as standby during maintenance periods. Each pump is capable of delivering 8 gal/min against 52 ft head and the temperature of the cooling water supplied to the r.f. valves is closely maintained at 68°F . Raw water from the Nimrod circuit is supplied to a manifold connected to the condensers of the refrigerating system. Two full flow ion exchange columns (in parallel) are interposed in the demineralised water circuit between the circulating pumps and the r.f. valve lines, with stop valves, flowmeter, sampling points, purity indicator, flow switches and temperature and pressure measuring devices. Indication of purity and of absolute temperature of the cooling water is available in the injector control room. For maintenance and for recharge of resin, one ion exchange column can be removed at a time without interrupting the use of the circuit. Typical analysis results show a conductivity of $1.2\ \mu\text{mho/cm}$ and 6.8 pH value.

One problem (occurring far too frequently on the cooling circuits) was the inadequacy of instrumentation, or provision for instrumentation, to display local

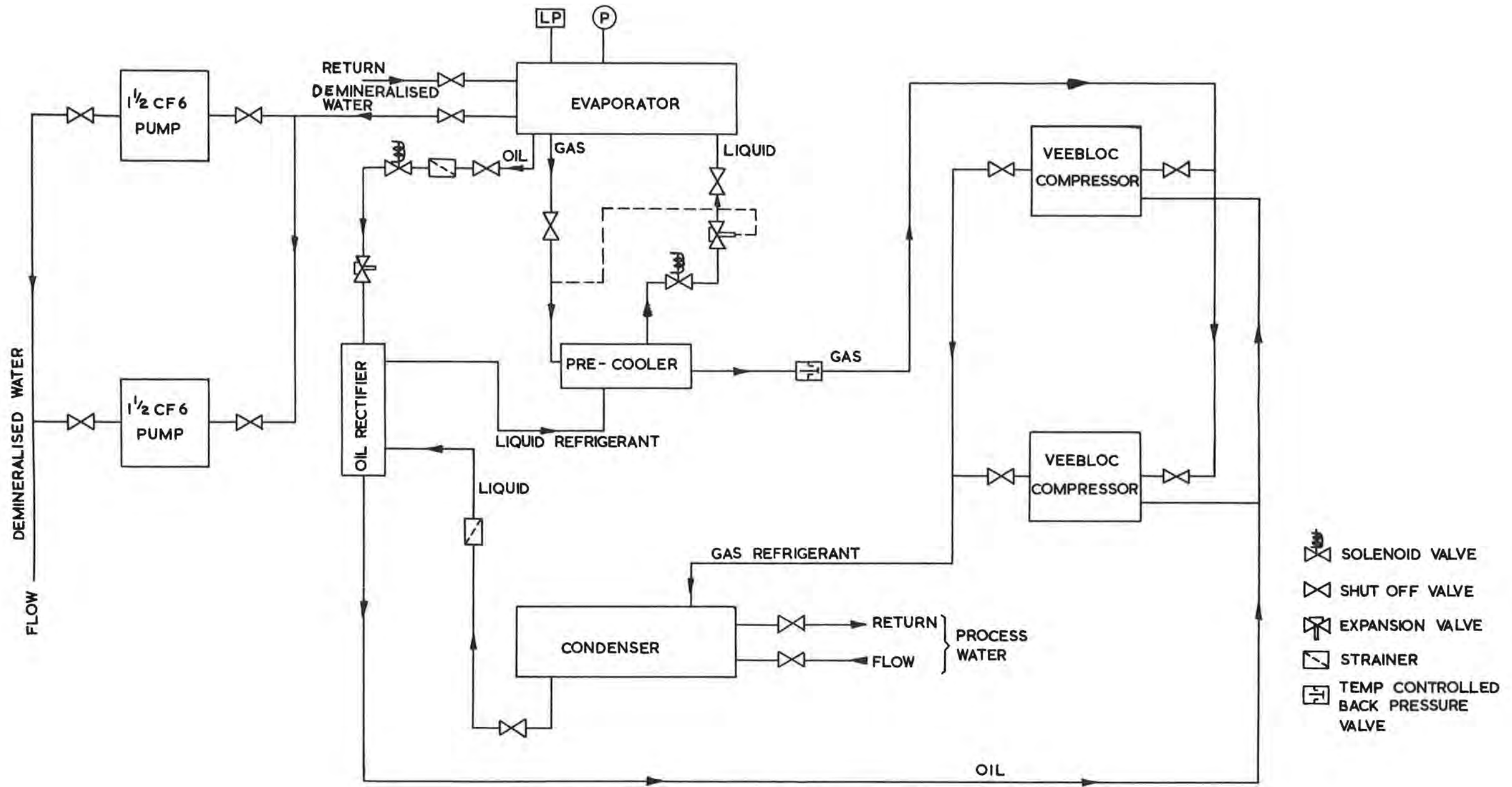


Fig. 10.8.1(i) Chilled demineralised water system; Circuit No. 1.

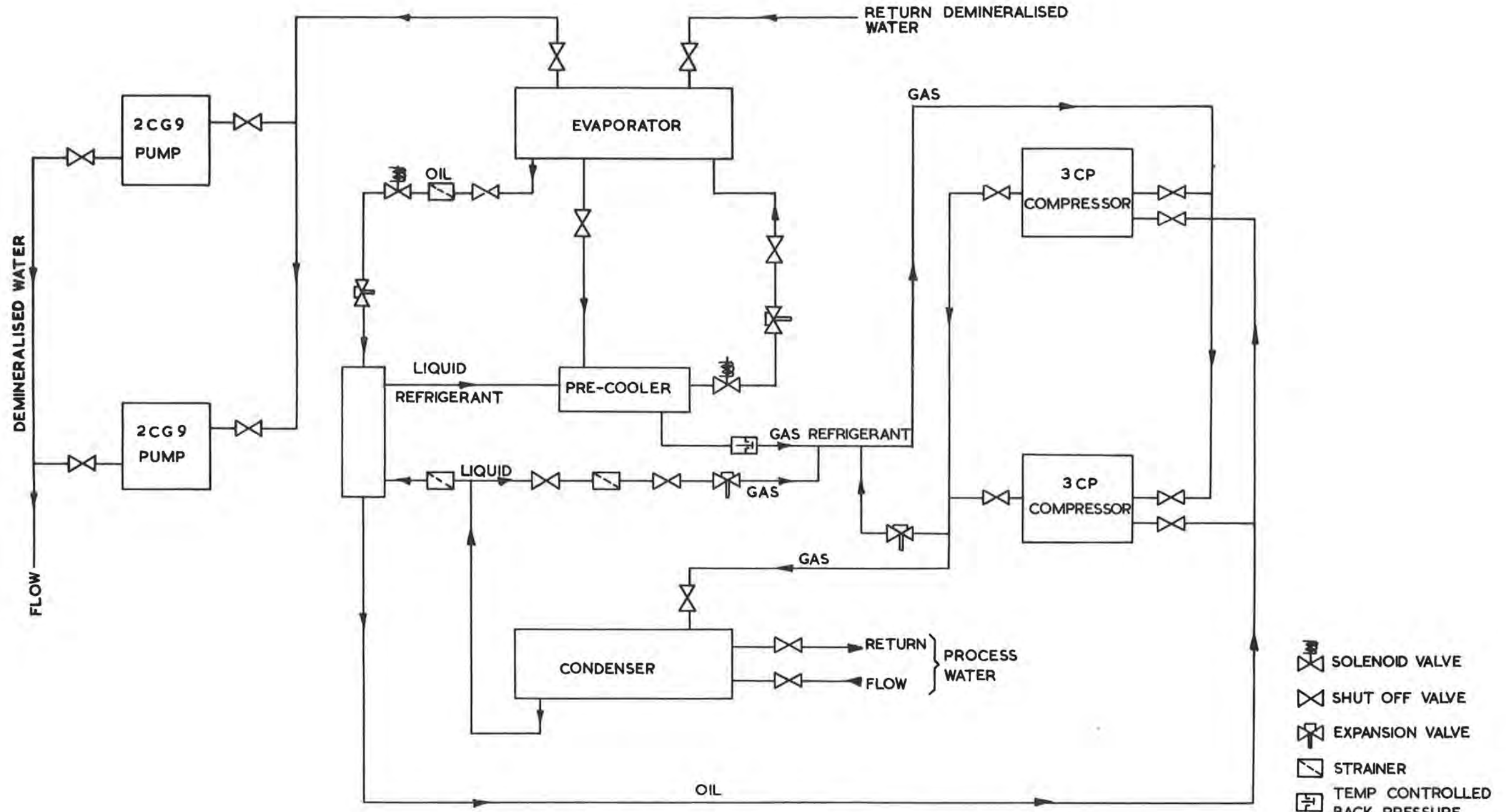


Fig. 10.8.1(ii) Chilled demineralised water system; Circuit No. 2.

conditions and assist in assessing performance or in fault finding. Once equipment is in operation it is often difficult to find time to fit missing instrumentation. It must be strongly emphasised that provision for instrumentation, by T pieces, bosses, etc., should be generous.

The conductivity of each circuit was designed to be controlled by a proportional flow through the Permutit plant. Experience has shown that in attempting this operation, temperature control of each circuit becomes impossible due to the large input of water at an uncontrolled temperature. Small ion exchange columns are being fitted to each circuit and the Permutit plant will only normally be used for topping up.

10.8.2 Injector Room Ventilation

Two similar sets of equipment are provided for ventilation purposes, one mounted on the north wall and the other on the south wall of the injector room. The total amount of heat to be extracted is estimated as 130 kW maximum. On each circuit, heat is removed from the injector room by means of an axial flow fan drawing air over an air-to-water heat exchanger which is connected to the Nimrod chilled water supply (50°F at the injector room). This air (5,500 ft³/min on each circuit) is mixed with a proportion of warmed air 2,500 ft³/min each circuit) drawn from the magnet room and is blown down an aluminium distribution duct mounted beneath the crane corbel and running the full length of the injector room. A supporting platform for each set is provided at high level, close to the curtain wall between the magnet room and injector room, so that air from the magnet room can be conveniently drawn in through holes in the wall. A small proportion of air returns to the magnet room through the large opening under the curtain wall.

No commissioning problems have arisen on this plant, other than the need to fit felt filters to the air inlet of the air to water heat exchangers. The installation of a shield wall between the magnet and injector rooms has seriously impeded the flow of air from the injector room and hence the mean temperature tends to rise.

10.9 R.F. Chilling Equipment

This plant is designed to control the temperature of the ferrite in the accelerator unit of the r.f. cavity to a mean temperature of 77°F. The equipment comprises a triple compressor refrigerator unit capable of handling 218,000 Btu/h. The refrigerant is Freon 12 and the primary coolant is transformer oil. The condensers are water cooled. A schematic diagram of the equipment is shown in Fig.10.9(i).

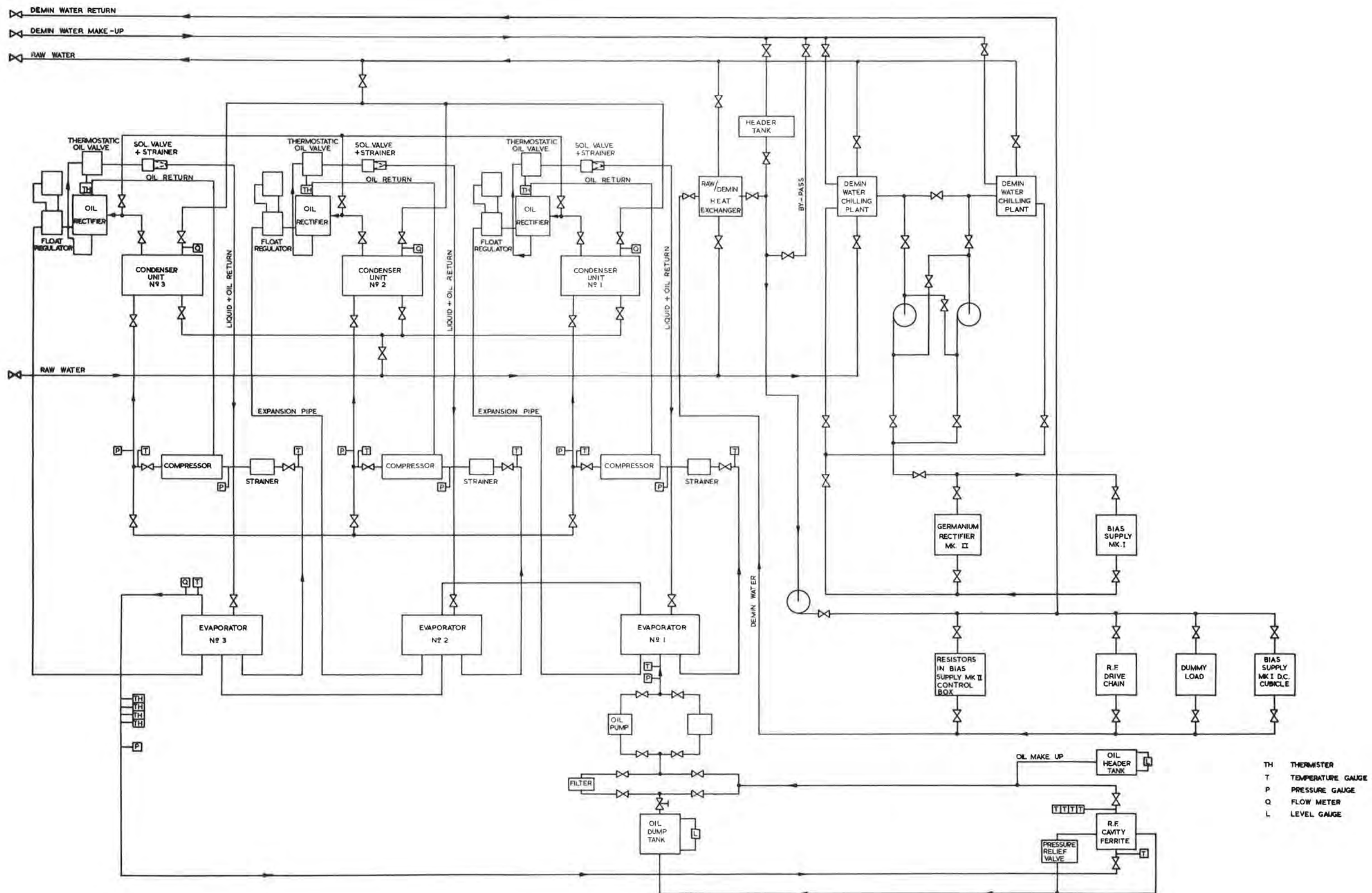
The refrigeration plant was commissioned with little trouble. Minor modifications have been made to both water and oil systems to obviate the need for venting these systems of air on start up. The main changes have been raising the make-up header tanks of each system, increasing the size of the main oil sump and providing means whereby oil from the sump can be pumped to the header tank (this provides a facility for priming the main circulating pump).

The oil pumps, dump tank, and evaporators are housed in a fire proof box within outer cavern No. 8. Since a CO₂ fire extinguishing system is installed it is imperative that, if it is used, no CO₂ should be allowed to seep indiscriminately into other caverns or service ducts. With a sealed box a complete discharge of CO₂ will raise the internal pressure one atmosphere; therefore a vent system is required to allow a displacement of the encased air. A scheme for this is in hand.

10.10 Sumps and Tunnels

The main problem here has been to provide automatic priming of the sump pumps. For various reasons, such as faulty foot valves and header tanks of insufficient capacity, no pumps installed were completely satisfactory. In two instances it was possible to fit fully submersible pumps but elsewhere work continues on improving the automatic pumping systems.

With the exception of one cable tunnel, all service tunnels are vented naturally. With the future use of heavy gases for experimental work (e.g. propane) the ventilation of these tunnels is being reconsidered since they are all at the same height as, or lower than, the experimental area.



- TH THERMISTER
- T TEMPERATURE GAUGE
- P PRESSURE GAUGE
- Q FLOW METER
- L LEVEL GAUGE

Fig. 10.9(i) R. F. Chilling Equipment.

10.11 Miscellaneous Work

A considerable amount of detailed development of a mechanical nature has been carried out on Nimrod during the constructional and commissioning phase. This has been partly on equipment designed as part of the diagnostic system but mainly on work aimed at easy assembly, easy maintenance and improved reliability. Further modifications may be necessary to assist mechanical handling, due to limited access into the machine area when the shield wall is closed and due to the future need for remote handling of certain equipment.

10.11.1 General Access

Access is important since it is undesirable to dismantle experimental installations in order to service the machine. A 5 ton hoist and crab is being fitted to the 30 ton radial crane in the magnet room to enable bulky equipment to be passed over the magnet by utilizing the space between the crane girder frames. Spare inner vacuum vessels and poleface windings are stored within the magnet ring for ready access. A study is in hand to rationalise the equipment used for handling and assembly of major machine components by making as many items as possible common and by making the equipment demountable.

10.11.2 Injector

One piece of equipment requiring development is the 'four-jaw box', a device designed to provide variable dimension slits that can be traversed horizontally or vertically over the cross section of the beam. It is used to set up the beam and consists of two plates located edge on in a common slide, each actuated by a hydraulic ram. At present it is not possible to inch these plates across an aperture with acceptable accuracy and repeatability. The control system is open loop and it has been established that error is caused by hysteresis effects due to the flexibility of rubber hose, strain energy imparted to rubber piston seals and leaks across solenoid valves. Some significant improvement is possible without resorting to the complication of a closed loop system.

A beam stop is under development which is designed to plunge a plate across the beam aperture at a predetermined repetition rate. This has led to an investigation into suitable vacuum seals for reciprocating motion. Although a reasonably satisfactory seal has evolved, wear may reduce its effectiveness too rapidly for it to be of much use; therefore an alternative scheme for a rotary beam stop is in hand.

A number of items of equipment have been modified to make them work, if only for a limited period of time. As an example, one or two vacuum gate valves are designed so that a beryllium copper, leaf spring biases the valve gate away from the sealing 'O' ring when the valve is being actuated. Fatigue of this spring will gradually diminish the clearance between the gate and 'O' ring and damage will eventually ensue. Such designs are being critically examined to obviate as far as possible the effects of fatigue or wear.

10.11.3 Diagnostic Equipment

Mechanical design was undertaken within the Laboratory on most of this equipment. It has led to development work on three aspects - glass windows to allow scintillating grids in the vacuum vessel to be observed, thin diaphragms to withstand vacuum in the beam lines, and reciprocating seals. Windows, $11\frac{1}{2}$ in by $38\frac{1}{2}$ in were necessary in order to obtain an adequate field of view when observing the scintillating grids. The stress levels set up by the differential pressure of 14.7 lb/in^2 necessitated the use of two $\frac{1}{2}$ in thick layers of toughened glass bonded together by polyvinyl butyral. Each layer is capable of taking the load imposed, but

prudence dictated two layers in case one became damaged. These windows were thoroughly tested in single and double layer form up to 75 lb/in². When the window was bolted into its carrier frame stress concentrations were found to be satisfactory by subjecting the assembly to photo-elastic stress analysis. The lifetime of these windows will be limited due to radiation and consideration is being given to the possibility of using a cerium stabilised glass.

Thin "windows" are required in certain beam lines to maintain vacuum when the line downstream is at atmospheric pressure. The material used must conform to certain physical requirements, three materials being suitable; aluminium, stainless steel and terylene (Melenix or Mylar). Investigation of the bursting pressure, fatigue and creep properties is being made with various thicknesses of window. A suitable method of supporting the windows has been evolved and tests on Melenix materials has progressed to the stage when installation of 4½ in diameter windows in beam pipes is now possible with some degree of confidence when using 0.015 in thick material. Testing of rectangular windows is now in hand and a report will be issued to cover this work.

A reasonably satisfactory seal has been developed for the plunging mechanisms which employ vacuum seals subjected to reciprocating motion. The mechanism reciprocates at the rate of 0.7 s per stroke for 7 GeV conditions. At the higher rate of 0.2 s per stroke for 2 GeV conditions the seal may not hold vacuum and in both cases it is considered that wear will be unacceptably high. The same conditions apply to the plunging beam stop used in the injector HEDS. A small rig is being used to develop this type of seal and it is hoped that by use of a suitable labyrinth seal, a reasonable life can be obtained without the need for inter-space vacuum pumping. A larger rig is being planned for further development.

10.11.4 Remote Handling

Work is in hand on the design of equipment for handling radioactive equipment. A mechanism has been manufactured that will allow the installation of a target into the machine without letting up the vacuum and a simple test rig is being constructed to prove this equipment without using the machine itself. An investigation is in hand on the methods of transporting this target from the machine to a 'hot' store yet to be designed. A suitable lead coffin has been designed.

A critical investigation is necessary throughout the machine to ascertain what equipment can be modified in detail to allow rapid installation or withdrawal, what materials need be changed to reduce the effect of radiation and what assemblies require duplicating to reduce the time taken for component replacement.

Methods of checking the radiation dosage for oils have been reported in private communication from the Research Department of Castrol Ltd. A check will be kept of the radiation dose received by the lubricating oils actuating plunging and target mechanisms since tests have shown that relatively low doses will cause the evolution of hydrogen in the oil, giving rise to spongy or erratic control.

10.12 Records Office, Storage and Workshop

10.12.1 Records Office

Operationally, much importance must be placed on the need for an efficient Records Office. Such an office has been set up for Nimrod to deal with planning and progressing of work, acquisition of equipment and spares, planned maintenance, running plant store and clerical duties of a technical nature.

The build, and change of build, of Nimrod is being controlled by collating in index form all relevant information, such as construction schedules, drawings, build instructions, test instructions etc. into log books covering various specified parts of the machine. From this information it is possible to rationalise the acquisition and storage of spares and miscellaneous equipment and it serves to record for posterity various build standards of the machine or associated equipment.

10.12.2 Storage

Some 7,000 ft² of heated store has been allocated for storage of equipment for Nimrod. It is essential to know exactly what spares and equipment exist and where they are available. It must also be made easy to obtain such equipment at all hours of the day and a suitable system has been devised so that, in emergency, relevant equipment can be obtained promptly. Equipment that is stored in unheated premises, is suitable treated against corrosion and then put on a care and maintenance basis. Some equipment is cocooned and some held in zip-up moisture proof containers. The value of certain materials and the difficulty of obtaining some materials for Nimrod has made necessary a small bonded store. A scheme is in hand for building a small 'hot' store to take targets and machine parts that become radio-active.

10.12.3 Test Area

A small area has been set aside as a mechanical test laboratory. Much ancillary equipment requires a brief functional check after overhauling before it is re-installed, and there is always a steady load of this work applicable to the machine. One item of equipment that has been constructed is a water flow test rig capable of dealing with up to 30 gal/min at pressures up to 150 lb/in² and with a variable temperature control of the circulating water. Another rig that has been constructed and found most valuable, is a portable unit designed for cleaning up any demineralised water system or equipment so that the conductivity of the treated water is brought down to an acceptable level before the main circulating demineralised water system is connected.

10.12.4 Workshop

A local workshop has been set up to deal with day to day maintenance and with the development work for Nimrod. General purpose machine tools have been installed but no equipment requiring specialised skills has been bought, since it is considered more appropriate to do such work in the main Laboratory workshop or by external contractor. It is, however, essential for the class of work required in the Laboratory, that welding equipment of high quality, capable of dealing with stainless steels and aluminium be readily available.

The potential work load of such a local workshop is high and care must be taken at all times to provide the capacity to deal with any emergency.

SECTION 11

OPERATION

The Nimrod Operating Staff has been built up gradually during the past two years. Engineers and technicians were occupied in the installation, commissioning and operation of equipment, with the long term aim of developing balanced crews, the members of which should be able to operate the accelerator and, in addition, provide a steadily improving coverage for fault diagnosis and first line repair. Experience has now been gained on equipment in all parts of the machine and has necessitated the development of safety, interlocking and operational procedures.

Various items of plant have been running for a considerable time: in particular, the main magnet has been pulsed for many hundreds of hours during periods of magnet and main power plant testing, and also for the magnetic survey. The administration of the magnet room to allow a maximum amount of installation and commissioning work to proceed safely during these periods has been a major problem since hundreds of personnel (staff and contractors) are involved.

Shift work has been adopted as required since the autumn of 1961 and the present staffing position is such that Nimrod could be crewed operationally from the main control room for about 60% of the available time.

Experience in accelerator operation has been gained in the injector room, where 15 MeV beams have been run on 86 days between 1st August, 1961 and 31st December, 1962. Initially, installation work was carried out during the day-time and a team consisting of a Duty Officer, Assistant Duty Officer and Duty Technician (with extra support when required) supervised beam operation in the evening. When more reliable beam operation was achieved, it was found necessary to allocate alternate periods to installation and experimental or commissioning work. These periods were not in general of identical length but were based on a weekly module. The injector was manned for 15 hours a day and during an experimental week 12 hours a day for 5 days was scheduled for beam operation. Whenever possible, all other time was used for maintenance, installation or commissioning of plant.

At the end of 1962 the injector was not yet complete as a fully operational machine and close co-operation and liaison was still maintained between Construction and Injector Groups. Generally, all experimental work was carried out using the permanently installed systems if possible but some of the planned facilities were not then available. The machine is expected to increase in reliability when all the designed equipment is in use.

Present experience shows that the percentage of the scheduled hours during which actual running is obtained, increases substantially the longer the machine is kept running - by the end of 1962 the running time had reached 75%. With most equipment on the injector few faults have recurred, having once been rectified, and running time should increase still further as the faults encountered during commissioning are eliminated.

Up to the end of 1962 the injector was operated from the local control room only. Considerable operation experience has been gained which it is anticipated will be of great value when full commissioning and operation take place from the main control room. Some equipment has in fact already been tested and operated from the main control room and installation of the remainder of the control system will proceed steadily to provide operational facilities from either control position.

In an accelerator as large and complex as Nimrod many troubles must arise during construction and commissioning; details of some and how they were overcome are recorded elsewhere in this report. The following general points may be worth mentioning from an operational point of view:-

- (a) The cooling water circuits throughout the machine have been a frequent source of trouble. If plant of greater capacity had been installed, with more complete standby and isolating facilities, many of these troubles would have been eliminated.
- (b) Since it has often proved difficult for the designer to forecast control cabling requirements well enough in advance to allow the job to be engineered as a whole, it would have helped considerably if main control cable marshalling points had been established in the early stages near the injector control room, in the magnet room and adjacent to the main control room. The installation of the main cable runs could then have been carried out well in advance of the machine requirements.

GENERAL ARTICLES AND RUTHERFORD LABORATORY REPORTS

AND MEMOS ON THE NIMROD PROJECT

GENERAL ARTICLES

- Brown Boveri Review, Vol.45 No.9, September 1958, p.426. "Equipment for Feeding the Magnet of the 7 GeV P.S. at Harwell, England". A. Danz.
- Nuclear Engineering, April 1959, pp.151-169. "The 7 GeV Proton Synchrotron"- (Theoretical Aspects; Engineering Design; Buildings, Civil Engineering and Services). T.G. Pickavance, P. Bowles, G.W. Dixon and A.G. Entwistle.
- The Engineer, 29th March 1959, p.838. "7000 ton Magnet for 7 GeV Proton Synchrotron".
- Nuclear Energy, February 1960, p.57. "Nimrod- Britain's 7 GeV Proton Synchrotron". J.J. Wilkins and A.J. Egginton.
- Vacuum, Vol.10, February/April 1960, p.86. "System design and choice of materials for the Nimrod vacuum system". S.H. Cross.
- Journal of the British Nuclear Energy Society, January 1962, p.51. "The Main Buildings for the 7 GeV Proton Synchrotron at Harwell". S.A. Rossiter and J.E. Brown.
- Vacnique, July 1962, p.4. "Pumping Equipment for Nimrod". N.T.M. Dennis. "Control Units for the Nimrod Proton Synchrotron High Vacuum System". W. Steckelmacher. "Liquid Air Supply for Mercury Diffusion Pumping Stations for Nimrod". T.A. Heppel.
- The Engineer, 3rd September 1962, p.194. "Vacuum Chamber for Nimrod".
- Electrical Times, 8th November 1962, p.675. "Analogue Study of Automatic Voltage Regulations for Nimrod". J. Switzman.
- Electrical Review, 29th March 1963. "7 GeV Proton Synchrotron Power Supply for the Nimrod Magnet". H. Hadley.

REPORTS

- NIRL/R/3 "24-anode pulsed power supply for magnet model VI". A.J. Holt and J.D. Milne. February 1961.
- NIRL/R/4 "Measuring Apparatus and methods used during the design and commissioning of the Nimrod magnet". D.A. Gray, M.R. Harold, P.F. Jones, R.H.C. Morgan, Miss J.E. Partington and I.C. Pyle. January 1963.

NIRL/R/5 "Ferrite for the accelerating cavity of Nimrod; its electrical properties and their measurements". D.J. Thompson. February 1961.

NIRL/R/6 "Design of fringing shims for magnet poles". J.J. Wilkins and A.H. Spurway. May 1961.

NIRL/R/12 "Design Studies for the Nimrod external proton beam". J.E. Gardner, N.M. King & D. Whiteside. January 1962.

NIRL/R/17 "Some high-current circuits using transistors". J.T. Hyman. January 1962.

NIRL/R/30 "Toroidal transformers and pre-amplifiers for transparent beam-current monitors". J.T. Hyman. March 1963.

NIRL/R/31 "The measurement of accelerator produced neutron flux using the $S^{32}(n,p)P^{32}$ reaction". K.B. Shaw. March 1963.

NIRL/R/33 "The Nimrod magnet saturable-fin polepieces". J.J. Wilkins and D.A. Gray. April 1963.

NIRL/R/39 "A mechanical safety device for the Nimrod vacuum system". R.J.B. Hadden and G.J. Homer. Beams Group. September 1963.

NIRL/R/43 "R.F. beam loading in Nimrod". G.H. Rees. August 1963.

NIRL/R/46 "Computer program for particle tracking in Nimrod". D. Whiteside. August 1963.

NIRL/R/47 "Particle trajectories from a Nimrod octant". D. Whiteside. July 1963.

NIRL/R/48 "A high-speed temperature monitoring system". J.H. Major. June 1963.

NIRL/R/52 "Movement of 3,000 tons of concrete shielding blocks adjacent to the Nimrod magnet foundations". J.T. Delury, E.G. Higgins and J.B. Mucklow. October 1963.

NIRL/R/58 "A guide to the irradiation stability of plastics and rubbers". R. Sheldon. September 1963.

NIRL/R/61 "The repair of the reinforced plastic vacuum envelope for Nimrod". C.E. Chapman, J.D. Langridge and R. Sheldon. January 1964.

MEMOS

NIRL/M/10 "Rough estimates of shielding requirements in the Nimrod Experimental Area". R.H. Thomas. December 1960.

NIRL/M/14 "Some properties of beams and transport systems". R. Billinge. March 1961.

NIRL/M/18 "500 kW modulator for Nimrod Injector". R.C. Fowler.
April 1961.

NIRL/M/22 "The performance of an injection trigger pulse generator".
L.J.C. Appleby, R.C. Hazell, R. Kur and P. Wilde.
July 1961.

NIRL/M/25 "The Nimrod injector buncher and debuncher cavities".
N.D. West. September 1961.

NIRL/M/26 "A capillary tube gas flowmeter using automatic timing".
H.E. Walford. November 1961.

NIRL/M/27 "A line charge approximation to quadruple fields".
R. Billinge. January 1962.

NIRL/M/29 "Response characteristics of a balanced ion-chamber system".
K.B. Shaw and D. Laws. April 1962.

NIRL/M/46 "Investigation of energy spread in the beam from the
Nimrod injector linac". N.D. West. February 1963.

NIRL/M/49 "'O' ring joints for rectangular and other non-circular
vacuum flanges". W.T. Smith. May 1963.

NIRL/M/50 "Nimrod targetting". R.G.T. Bennett. February 1963.

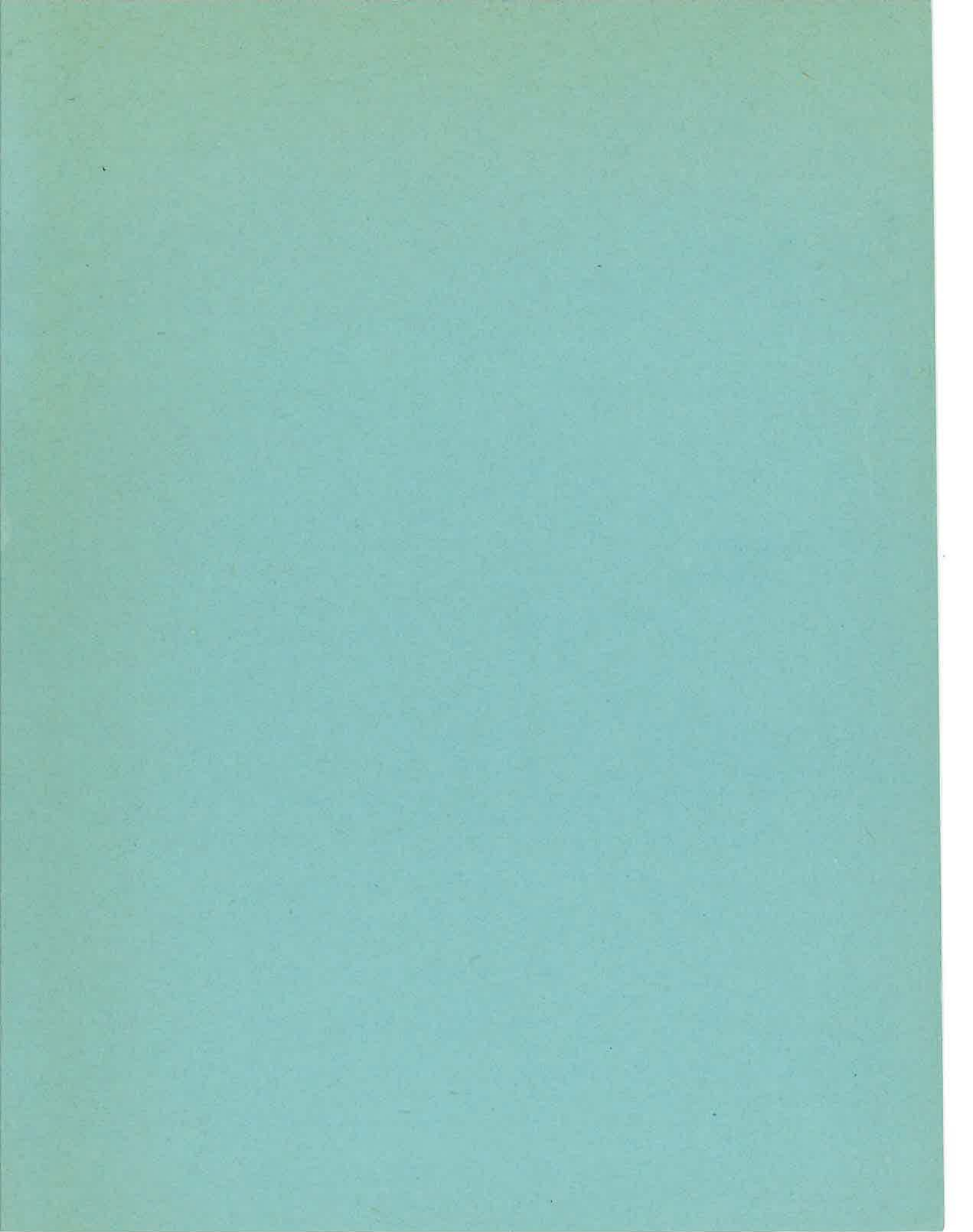
NIRL/M/52 "PROFILE 1. A computer program to produce a direct
graphical output of the beam profile through any triplet
system". J.V. Hoare. June 1963.

NIRL/M/53 "Experiments on the Nimrod inflector magnets".
P.P. Starling. June 1963.

NIRL/M/57 "Tests on triplex toughened glass windows". D.R. Moore
and R. Malton. October 1963.

NIRL/M/58 "A numerical method for solving the general profile
equation". P. Starling and J.V. Hoare. November 1963.

1. The first part of the document is a list of names and addresses of the members of the committee.	1. 10/1/19
2. The second part is a list of the names of the members of the committee who have been elected to the office of Chairman.	2. 10/1/19
3. The third part is a list of the names of the members of the committee who have been elected to the office of Secretary.	3. 10/1/19
4. The fourth part is a list of the names of the members of the committee who have been elected to the office of Treasurer.	4. 10/1/19
5. The fifth part is a list of the names of the members of the committee who have been elected to the office of Auditor.	5. 10/1/19
6. The sixth part is a list of the names of the members of the committee who have been elected to the office of Librarian.	6. 10/1/19
7. The seventh part is a list of the names of the members of the committee who have been elected to the office of Corresponding Secretary.	7. 10/1/19
8. The eighth part is a list of the names of the members of the committee who have been elected to the office of Reading Room Librarian.	8. 10/1/19
9. The ninth part is a list of the names of the members of the committee who have been elected to the office of Bookkeeper.	9. 10/1/19
10. The tenth part is a list of the names of the members of the committee who have been elected to the office of Steward.	10. 10/1/19



Available from
HER MAJESTY'S STATIONERY OFFICE

York House, Kingsway, London W.C.2
423 Oxford Street, London W.1
13a Castle Street, Edinburgh 2
109 St. Mary Street, Cardiff
39 King Street, Manchester 2
50 Fairfax Street, Bristol 1
35 Smallbrook, Ringway, Birmingham 5
80 Chichester Street, Belfast
or through any bookseller.

Printed in England